



THE UNIVERSITY
of ADELAIDE

Calibration of alkaline earth metal isotope tracers in semi-arid coastal environments

Yuexiao Shao

Department of Earth Sciences
School of Physical Sciences
University of Adelaide

This thesis is submitted in fulfilment of the requirements
for the degree of Doctor of Philosophy

July 2021

Table of Contents

Abstract	1
Declaration	3
Acknowledgements	4
Publications arising from this Ph.D. research	5
Chapter 1	7
1.1 Coastal systems and isotope tracer studies	8
1.2 Study area	11
1.3 Thesis aims	11
1.4 Thesis outline	12
<i>Chapter 2: Calcium and strontium isotope systematics in the lagoon-estuarine environments of South Australia: Implications for water source mixing, carbonate fluxes and fish migration</i>	13
<i>Chapter 3: Impact of salinity and carbonate saturation on stable Sr isotopes ($\delta^{88/86}\text{Sr}$) in a lagoon-estuarine system</i>	13
<i>Chapter 4: Seasonal carbonate cycling and water source mixing in a semi-arid coastal lagoon-estuarine system: Insights from stable Sr isotopes ($\delta^{88/86}\text{Sr}$)</i>	14
<i>Chapter 5: Reconstructing palaeo-hydrology and salinity of the Coorong lagoon in South Australia based on multi-tracer analyses ($^{87}\text{Sr}/^{86}\text{Sr}$, $\delta^{88/86}\text{Sr}$ and Mg/Sr) of fossil carbonate shells</i>	15
References	15
Chapter 2	21
Abstract	26
2.1 Introduction	27
2.2 Study area	28
2.3 Methods	30
2.3.1 Sample collection and preparation	30
2.3.2 Elemental and isotope analyses	32

Table of Contents

2.3.3 Geochemical modeling of mineral saturations in waters using PHREEQC	34
2.4 Results	34
2.4.1 Spatial variations of salinity in the Coorong	34
2.4.2 $^{87}\text{Sr}/^{86}\text{Sr}$ and $\delta^{44/40}\text{Ca}$ variations in waters, sediments and otoliths	35
2.4.3 XRD analysis of the sediment crust sample	36
2.4.4 Mineral saturation (SI) of lagoon waters	37
2.5 Discussion	38
2.5.1 Constraints on water source mixing and evaporation effects	39
2.5.2 Carbonate fluxes in the Coorong	44
2.5.3 Fish migration and otoliths biomineralisation: Insights from Ca and Sr isotopes	49
2.5.4 Implications for palaeo-salinity reconstructions of lagoon-estuarine environments based on coupled $^{87}\text{Sr}/^{86}\text{Sr}$ and $\delta^{44/40}\text{Ca}$	50
2.6 Conclusions	51
Acknowledgments	52
References	53
Chapter 3	59
Abstract	63
3.1 Introduction	63
3.2 Study area	66
3.3 Material and methods	67
3.3.1 Sample description	67
3.3.2 Field measurements and sample preparation of waters and carbonates	68
3.3.3 Coupled $^{87}\text{Sr}/^{86}\text{Sr}$ and $\delta^{88/86}\text{Sr}$ analyses via TIMS	69
3.3.4 Geochemical / PHREEQC modelling of mineral saturation state in waters	70
3.4 Results	71

3.5 Discussion	74
3.5.1 <i>Water source mixing and local carbonate cycling: Insights from $^{87}\text{Sr}/^{86}\text{Sr}$ and $\delta^{88/86}\text{Sr}$</i>	74
3.5.2 <i>Links between $\delta^{88/86}\text{Sr}$ and salinity/carbonate saturation of waters in the CLLMM</i>	77
3.5.3 <i>Coupling between $\delta^{88/86}\text{Sr}$ and $\delta^{44/40}\text{Ca}$ in the CLLMM water samples</i>	79
3.5.4 <i>Quantifying carbonate removal in the Coorong via $\delta^{88/86}\text{Sr}$ and Rayleigh modelling</i>	81
3.5.5 <i>Coupled $^{87}\text{Sr}/^{86}\text{Sr}$ and $\delta^{88/86}\text{Sr}$ approach for palaeo-hydrology and salinity reconstructions</i>	82
3.6 Conclusions	83
Acknowledgements	84
References	85
Chapter 4	91
Abstract	94
4.1 Introduction	94
4.2 Study area	96
4.3 Material and methods	99
4.3.1 <i>Sample description</i>	99
4.3.2 <i>Field collection measurements and sample preparation of waters</i>	99
4.3.3 <i>Elemental concentrations analyses of water samples</i>	100
4.3.4 <i>Alkalinity and pH analyses of water samples</i>	101
4.3.5 <i>Coupled $^{87}\text{Sr}/^{86}\text{Sr}$ and $\delta^{88/86}\text{Sr}$ analyses via TIMS</i>	101
4.3.6 <i>Geochemical / PHREEQC modelling of mineral saturation state in waters</i>	102
4.4 Results	102
4.5 Discussion	105
4.5.1 <i>Influence of seasonal variations of water source mixing on the Coorong lagoon chemistry</i>	105

Table of Contents

4.5.2 Seasonal variation of Sr fluxes and carbonate dynamics in the Coorong	108
4.5.3 The controls of $\delta^{88/86}\text{Sr}$ in the Coorong lagoon waters	110
4.5.4 Quantifying seasonal changes in carbonate output in the South Lagoon via $\delta^{88/86}\text{Sr}$ tracer	113
4.6 Conclusions	114
Acknowledgements	115
References	116
Chapter 5	122
Abstract	126
5.1 Introduction	126
5.2 Material and methods	129
5.2.1 Modern sample collection and field measurements	129
5.2.2 Sediment core collection	129
5.2.3 Water and shell sample preparation	131
5.2.4 Geochronological methods	131
5.2.5 Elemental concentration analyses of water and shell samples	132
5.2.6 $^{87}\text{Sr}/^{86}\text{Sr}$ and $\delta^{88/86}\text{Sr}$ analyses via thermal ionisation mass spectrometry	133
5.3 Results and discussion	134
5.3.1 $^{87}\text{Sr}/^{86}\text{Sr}$ and $\delta^{88/86}\text{Sr}$ variations in modern shells and water samples	134
5.3.2 Geochronology, $^{87}\text{Sr}/^{86}\text{Sr}$ and $\delta^{88/86}\text{Sr}$ evolution of the South Lagoon waters	136
5.3.3 Water source mixing and palaeo-salinity reconstruction of the South Lagoon waters via a coupled $^{87}\text{Sr}/^{86}\text{Sr}$ and Mg/Sr approach	138
5.3.4 Evolution of $^{87}\text{Sr}/^{86}\text{Sr}$ and $\delta^{88/86}\text{Sr}$ in palaeo-waters of the South Lagoon: Evidence for temporal changes in water source mixing and local carbonate cycling	140
5.3.5 Quantifying local carbonate output through time in the Coorong South Lagoon	141
5.4 Conclusions	143

Table of Contents

Acknowledgements	144
References	144
Chapter 6	149
6.1 Calibrating $\delta^{44/40}\text{Ca}$ and $\delta^{88/86}\text{Sr}$ tracers in a semi-arid coastal system with respect to water salinity and carbonate saturation	150
6.2 Water source mixing and local carbonate cycling in the present-day Coorong Lagoons	151
6.3 Reconstructions of palaeo-hydrology, salinity and water source mixing history in the Coorong South Lagoon	152
6.4 Future recommendations	153
References	153
Appendices	155
Appendix 1	156
Appendix 2	192
Appendix A: Tables of Results	193
Appendix B: Details of research protocols and supplementary modeling	197
<i>B.1. Chromatographic purification – semi-automatic sample purification method for Sr via prepFAST</i>	<i>197</i>
<i>B.2. Further Details on TIMS analyses for Sr isotopes</i>	<i>198</i>
<i>B.3. PHREEQC Modelling</i>	<i>198</i>
<i>B.4. Additional constraints to the magnitudes of Ca removal in the South Lagoon</i>	<i>203</i>
Appendix C: Supplementary Tables and Figures	205
Appendix 3	216
Appendix A. Sampling site information	217
Appendix B. Elemental and cation/anion compositions of waters and carbonates	220
<i>B.1 Elemental concentrations analyses of water samples</i>	<i>220</i>
<i>B.2 Elemental concentration analyses of shell samples (A. helmsi)</i>	<i>225</i>

Table of Contents

<i>B.3 Alkalinity and pH of waters</i>	225
<i>B.4 Mineralogical XRD analysis of the tubeworm carbonate sample</i>	227
Appendix C. Sr isotope analysis – Sample preparation and TIMS measurements	229
<i>C.1 Column chemistry – Purification of Sr prior to the isotope analysis</i>	229
<i>C.2 Mass Spectrometry and TIMS analytical procedures</i>	229
<i>C.3 Procedural Sr blank analyses</i>	230
<i>C.4 The Sr double-spike method</i>	231
Appendix D. Supporting models using Sr isotopes and elemental concentrations	236
<i>D.1 Apportioning water sources through $^{87}\text{Sr}/^{86}\text{Sr}$ and elemental ratio tracers</i>	236
<i>D.2 Evidence of CaCO_3 precipitation through $\delta^{88/86}\text{Sr}$ and elemental concentrations</i> ..	237
<i>D.3 Constraints on $\delta^{88/86}\text{Sr}_{\text{INI}}$ parameter from the Sr isotope mass balance calculations</i>	238
<i>D.4 $\delta^{88/86}\text{Sr}$ values of carbonate samples</i>	240
Appendix E. PHREEQC modelling and analyses of waters for the calculation of mineral saturation states	241
<i>E.1 Source data for PHREEQC modelling</i>	241
<i>E.2 Saturation Indices (SI) based on laboratory-based (lab pH) and field-based pH (probe pH) measurements</i>	243
<i>E.3 Saturation Indices (SI) calculated via PHREEQC vs. CO2SYS</i>	245
References	248
Appendix 4	250
Appendix A. Sampling site information	251
Appendix B. Supplementary results	254
<i>B.1 Elemental concentrations of waters</i>	254
<i>B.2 Alkalinity and pH of waters</i>	260
<i>B.3 Results of Sr isotope ratios ($^{87}\text{Sr}/^{86}\text{Sr}$ and $\delta^{88/86}\text{Sr}$) of all water samples</i>	261

Appendix C. Supporting evidence of water chemistry in the Coorong	263
<i>C.1. Influence of storm events, barrage outflows and Salt Creek discharges on Coorong water salinities and levels</i>	<i>263</i>
<i>C.2. The driving mechanisms of the aragonite saturation indices in the Coorong</i>	<i>268</i>
<i>C.3. The driving mechanisms of $\delta^{88/86}\text{Sr}$ in the Coorong water samples</i>	<i>271</i>
Appendix D. Elemental concentrations vs. salinity in the CLLMM	272
Appendix E. $\delta^{88/86}\text{Sr}$ and Rayleigh and equilibrium modelling	274
References	275
Appendix 5	276
Appendix A. Sampling site information	277
<i>A.1 Modern samples and sediment cores</i>	<i>277</i>
Appendix B. Supplementary results	278
<i>B.1 Elemental concentrations</i>	<i>278</i>
<i>B.2 Chronological age data and model</i>	<i>284</i>
<i>B.3 Results of Sr isotope ratios ($^{87}\text{Sr}/^{86}\text{Sr}$ and $\delta^{88/86}\text{Sr}$) of all water and shell samples ..</i>	<i>285</i>
<i>B.4 Distribution coefficients between shell and water samples</i>	<i>287</i>
Appendix C. Supporting evidence of palaeo-hydrology of the South Lagoon	288
<i>C.1. Elemental concentrations</i>	<i>288</i>
Appendix D. Details of ^{14}C dating and pollen age	289
<i>D.1 Pollen age</i>	<i>289</i>
<i>D.2 ^{14}C dating</i>	<i>289</i>
<i>D.3 Bacon age model code in R program</i>	<i>290</i>
References	291
Appendix 6	293
<i>Calibration of marine Ca and Sr isotope proxies against ‘salinity’ in fresh-to-hypersaline coastal lagoon-estuarine settings of South Australia</i>	<i>294</i>

Table of Contents

Stable and radiogenic strontium isotope systematics in hypersaline coastal environments: constraints for paleo-hydrology in the Coorong, South Australia. 295

Calibration of stable strontium isotopes ($\delta^{88/86}\text{Sr}$) with respect to salinity and carbonate saturation in lagoon-estuarine environments 295

Insights into palaeo-hydrology of the Coorong Lagoon, South Australia, based on Strontium Isotope Tracers ($^{87}\text{Sr}/^{86}\text{Sr}$ and $\delta^{88/86}\text{Sr}$) in fossil carbonates 297

Abstract

Coastal systems in semi-arid areas are characterised by complex physico-chemical processes involving mixing of marine and continental water sources as well as precipitation of evaporitic and carbonate minerals. The latter processes involving carbonate cycling also represent an important but currently poorly constrained component of the coastal carbon budget. This thesis fills important knowledge gaps in our understanding of water source mixing and local carbonate cycling in a semi-arid coastal system in South Australia – the Coorong, Lower Lakes and Murray Mouth (CLLMM) estuary, using selected alkaline earth metals (Ca and Sr) and their isotopes with the following research components:

1. Application of radiogenic Sr isotopes ($^{87}\text{Sr}/^{86}\text{Sr}$), stable Ca isotopes ($\delta^{44/40}\text{Ca}$) and elemental ratios, complemented by mineralogical analysis of top-sediment samples and geochemical (PHREEQC) modelling of carbonate saturations in the CLLMM waters to constrain the water source apportionment and local carbonate output in the Coorong lagoon.
2. Development and validation of high-precision stable Sr isotope analysis ($\delta^{88/86}\text{Sr}$) using thermal ionisation mass spectrometry (TIMS) and follow up calibration of $\delta^{88/86}\text{Sr}$ in the CLLMM waters with respect to changing salinity and carbonate saturation states.
3. Application of $^{87}\text{Sr}/^{86}\text{Sr}$ and $\delta^{88/86}\text{Sr}$ tracers, along with elemental concentration data, to monitor seasonal variations (i.e., every 3 months) in water source mixing and carbonate dynamics (i.e., dissolution vs precipitation) in the CLLMM.
4. Reconstruction of palaeo-hydrology and salinity in the Coorong South Lagoon throughout the past ~2400 years, based on $^{87}\text{Sr}/^{86}\text{Sr}$, $\delta^{88/86}\text{Sr}$ and Mg/Sr analysed in fossil bivalve shell species (*Arthritica helmsi*) collected from sediment cores. The above data were complemented by radiocarbon (^{14}C) and pollen-based geochronological models.

Overall, the results from the thesis showed that the modern North Lagoon waters are mainly sourced from the Southern Ocean, with transient freshwater inputs sourced from the River Murray and Lower Lakes and/or local groundwater discharge. In contrast, the hypersaline South Lagoon waters are basically highly evaporated ‘brackish waters’ with significant contribution of Sr from continental water sources. Importantly, stable Ca and Sr isotope tracers and water chemistry data indicate that the South Lagoon acts as a net sink for dissolved inorganic carbon (DIC) in the form of precipitated carbonate minerals (mostly aragonite). Both $\delta^{44/40}\text{Ca}$ and $\delta^{88/86}\text{Sr}$ in the CLLMM waters seem to be controlled by mass-dependent isotope fractionation, most likely related to carbonate dissolution and precipitation. Despite the current uncertainty regarding the role of local groundwater discharge on the chemistry of Coorong waters, the results indicate that an increased alkalinity supply (mainly from the Salt Creek) may locally promote CaCO_3 precipitation and increase in $\delta^{88/86}\text{Sr}$ of waters in the South Lagoon. Finally, the multi-proxy analysis ($^{87}\text{Sr}/^{86}\text{Sr}$, $\delta^{88/86}\text{Sr}$ and Mg/Sr) of fossil shells revealed that over the

past two millennia the South Lagoon waters were never purely marine but originally rather comprised brackish waters (estimated minimum salinities of ~6-23 PSU) with at least 60% contribution from continental water. Overall, the findings of this thesis improved our understanding of modern and past water source mixing and carbonate cycling in the CLLMM system and can hopefully benefit future water management strategies and plans.

Declaration

I certify that this work contains no material which has been accepted for the award of any other degree or diploma in my name, in any university or other tertiary institution and, to the best of my knowledge and belief, contains no material previously published or written by another person, except where due reference has been made in the text. In addition, I certify that no part of this work will, in the future, be used in a submission in my name, for any other degree or diploma in any university or other tertiary institution without the prior approval of the University of Adelaide and where applicable, any partner institution responsible for the joint-award of this degree.

I acknowledge that copyright of published works contained within this thesis resides with the copyright holder(s) of those works.

I also give permission for the digital version of my thesis to be made available on the web, via the University's digital research repository, the Library Search and also through web search engines, unless permission has been granted by the University to restrict access for a period of time.

I acknowledge the support I have received for my research through the provision of an Adelaide Graduate Research Scholarship (AGRS).

Acknowledgements

I would like to acknowledge several people who contributed to completion of this thesis in multiple ways. Above all, I would like to thank my partner Michael Curtis for his company, understanding and support. I feel lucky to have the guidance from my supervisors Juraj Farkaš, Jonathan Tyler and Bronwyn Gillanders, as all three of them are inspirational to me. First, none of this could have been achieved without Juraj's support. Juraj inspired me with the structures of the projects and sharing valuable knowledge and provided funding. He also helped multiple times with my fieldwork, data analyses and interpretation. Juraj had been greatly supporting my publications by advising on my manuscripts and encouraging me when I made mistakes or had to deal with harsh comments from reviewers. I thank Jonathan for providing me with grant opportunities (e.g., ANSTO), useful advices on improving my models, revising my manuscripts, giving mental support and advising on my time arrangement, especially when Juraj was busy. I also thank Bronwyn on the overall guidance of the structure of my research, sharing cross-discipline knowledge, revising my manuscripts and guidance on scientific writing. I sincerely thank Luke Mosley as we collaborated multiple projects and especially his patient guidance on the PHREEQC software and fieldwork, as well as his contribution on my publications.

I gratefully acknowledge David Bruce's help in the laboratory as he kept instruments maintained and provided maximum amount of help when I needed, which greatly improved the efficiency and quality of this research. I also thank Robert Klæbe and Tony Hall for being helpful with technique and laboratory difficulties, and Sarah Gilbert who helped data acquiring in Adelaide Microscopy.

I greatly appreciate the financial and analytical support from Australian Nuclear Science and Technology Organisation (ANSTO) and funding from the CRC LEME Regolith Science Scholarship via Cooperative Research Centre for Landscape Environments and Mineral Exploration. I am honoured to be a recipient of the Adelaide Graduate Research Scholarship from University of Adelaide, as it provided major financial support to my daily life.

Many thanks also go to my co-authors who contributed to my projects and publications, as well as my friends and colleagues at University of Adelaide who showed great mental support and keep my work and life balanced.

Last but not least, I would like to thank my parents and close family for their mental support and love, although they were not physically being with me.

Publications arising from this Ph.D. research

Journal articles

Shao, Y., Farkaš, J., Holmden, C., Mosley, L., Kell-Duivesteyn, I., Izzo, C., Reis-Santos, P., Tyler, J., Törber, P., Frýda, J., Taylor, H., Haynes, D., Tibby, J. and Gillanders, B.M. (2018) Calcium and strontium isotope systematics in the lagoon-estuarine environments of South Australia: Implications for water source mixing, carbonate fluxes and fish migration, *Geochimica et Cosmochimica Acta* **239**, 90-108. <https://doi.org/10.1016/j.gca.2018.07.036>

Shao, Y., Farkaš, J., Mosley, L., Tyler, J., Wong, H., Chamberlayne, B., Raven, M., Samanta, M., Holmden, C., Gillanders, B.M., Kolevica, A., Eisenhauer, A. (2021) Impact of salinity and carbonate saturation on stable Sr isotopes ($\delta^{88/86}\text{Sr}$) in a lagoon-estuarine system. *Geochimica et Cosmochimica Acta* **293**, 461-476. doi: <https://doi.org/10.1016/j.gca.2020.11.014>

Conference abstracts

Shao, Y., Woolston, Z., Farkaš, J., Chamberlayne, B., Tibby, J., Haynes, D., Tyler, J. (2021) Insights into palaeo-hydrology of the Coorong Lagoon, South Australia, based on Strontium Isotope Tracers ($^{87}\text{Sr}/^{86}\text{Sr}$ and $\delta^{88/86}\text{Sr}$) in fossil carbonates. AESC 2021, virtual conference.

Shao, Y., Farkaš, J., Tibby, J., Haynes, D., Wong, H. and Tyler, J. (2020) Insights of modern- and palaeo-hydrology of the Coorong based on Strontium Isotope Tracers: $^{87}\text{Sr}/^{86}\text{Sr}$ and $\delta^{88/86}\text{Sr}$. Goldschmidt2020, virtual conference.

Shao, Y., Farkaš, J., Mosley, L., Wong, H., Samanta, M., Tyler, J., Holmden, C., Gillanders, B.M., Kolevica, A. and Eisenhauer, A. (2019) Alkaline earth metal isotopes as a novel tool to constrain water sources and changes in carbonate precipitation in the lagoon-estuarine environments. South Australian Coastal Conference, Adelaide, Australia.

Shao, Y., Farkaš, J., Mosley, L., Wong, H., Samanta, M., Tyler, J., Holmden, C., Gillanders, B.M., Kolevica, A. and Eisenhauer, A. (2019) Calibration of stable strontium isotopes ($\delta^{88/86}\text{Sr}$) with respect to salinity and carbonate saturation in lagoon-estuarine environments. Goldschmidt2019, Barcelona, Spain.

Shao, Y., Farkaš, J., Tyler, J., Gillanders, B.M., Chamberlayne B. and Haynes, D. (2019) Stable strontium isotopes ($\delta^{88/86}\text{Sr}$) as a salinity proxy in the lagoon-estuarine environments. INQUA, Dublin, Ireland.

Shao, Y., Farkaš, J., Tyler, J., Gillanders, B.M., Chamberlayne B. and Haynes, D. (2018) Stable and

radiogenic strontium isotope systematics in hypersaline coastal environments: constraints for palaeo-hydrology in the Coorong, South Australia. Australasian Quaternary Association biennial meeting, Canberra, Australia.

Shao, Y., Farkaš, J., Tyler, J., Gillanders, B.M., Chamberlayne B. and Haynes, D. (2018) Stable and radiogenic strontium isotope systematics in hypersaline coastal environments: constraints for palaeo-hydrology in the Coorong, South Australia. GSA Earth Science Student Symposium – South Australia, Adelaide, Australia.

Shao, Y., Farkaš, J., Tyler, J., Gillanders, B.M., Chamberlayne B. and Haynes, D. (2018) Stable and radiogenic strontium isotope systematics in hypersaline coastal environments: constraints for palaeo-hydrology in the Coorong, South Australia. Australian Geoscience Council Convention, Adelaide, Australia.

Shao, Y., Farkaš, J., Holmden, C., Mosley, L., Kell-Duiveststein, I., Izzo, C., Reis-Santos, P., Tyler, J., Törber, P., Frýda, J., Taylor, H., Haynes, D., Tibby, J. and Gillanders, B.M. (2018) Strontium isotopes in coastal environments: Applications for water source mixing, carbon cycle and palaeo-hydrology in the Coorong, South Australia. ECSA 57, Perth, Australia.

Shao, Y., Farkaš, J., Holmden, C., Mosley, L., Kell-Duiveststein, I., Izzo, C., Reis-Santos, P., Tyler, J., Törber, P., Frýda, J., Taylor, H., Haynes, D., Tibby, J. and Gillanders, B.M. (2018) Calcium and strontium isotope cycling in coastal lagoon-estuarine environments, South Australia: Implications for water mixing, carbonate fluxes and fish migration. Natural Resources Management Science Conference, Adelaide, Australia.

Shao, Y., Farkaš, J., Holmden, C., Mosley, L., Kell-Duiveststein, I., Izzo, C., Reis-Santos, P., Tyler, J., Törber, P., Frýda, J., Taylor, H., Haynes, D., Tibby, J. and Gillanders, B.M. (2017) Calcium and strontium isotope cycling in coastal lagoon-estuarine environments, South Australia: Implications for water mixing, carbonate fluxes and fish migration. GSA Earth Science Student Symposium – South Australia, Adelaide, Australia.

Shao, Y., Farkaš, J., Holmden, C., Mosley, L., Kell-Duiveststein, I., Izzo, C., Reis-Santos, P., Tyler, J., Haynes, D., Tibby, J. and Gillanders, B. (2017) Calibration of marine Ca and Sr isotope proxies against ‘salinity’ in fresh-to-hypersaline coastal lagoon-estuarine settings of South Australia. Goldschmidt, Paris, France.

CHAPTER 1

Introduction and thesis outline

Chapter 1.

Introduction and thesis outline

1.1 Coastal systems and isotope tracer studies

Coastal lagoons and estuaries, which represent the most productive ecosystems on Earth, are dynamic hydrological systems that typically involve complex processes such as the mixing of continental and marine water sources with various impacts of local biogeochemical cycles on the elemental and isotope compositions of coastal waters. The latter are in turn sensitive indicators of the ongoing environmental changes occurring at these ocean-land interface environments. Anthropogenic perturbation had caused a number of water quality and contamination issues in coastal environments, including eutrophication, hypersalinity, and changing carbonate saturation state of coastal waters, which together impact local nutrient and carbon cycling as well as coastal carbon budgets (Bennett et al., 2001; Halpern et al., 2008; Bauer et al., 2013; Regnier et al., 2013), with implications for ecosystem conservation strategies and water management solutions (Warwick et al., 2018, and references therein). Furthermore, coastal marine environments are also associated with the formation, deposition and/or dissolution of evaporitic and carbonate minerals that have a major impact on the local elemental fluxes of calcium (Ca^{2+}), sulphur (SO_4^{2-} , HS^-) and carbon (HCO_3^- , CO_3^{2-}) ionic species, and thus the net removal of dissolved inorganic carbon (DIC) from the coastal waters (Ware et al., 1992; Elderfield, 2006), representing an important but currently poorly constrained component of the coastal carbon cycle and the ‘blue carbon’ budget quantification (Macreadie et al., 2017).

To face the present-day and future challenges related to management of coastal environments and sustainable ecosystems in semi-arid regions such as South Australia, it is required to advance our knowledge on declining and everchanging water sources and controlling mechanisms that impact water quality and local elemental cycling, including the sources of salts and other dissolved ions contributing to salinity in these coastal systems. A better understanding of these complex processes in modern coastal environments is also critical for reliable paleoenvironmental and hydrological reconstructions of ancient lagoon-estuarine depositional systems and key controlling factors on long-term variations in their biogeochemistry and local carbon cycling (Velez et al., 2018). A number of isotope tracers exhibits strong and systematic variations across the biogeochemical gradients in coastal systems (e.g., salinity, redox, nutrient levels), and are therefore excellent tools to understand the controlling mechanisms behind spatial and temporal changes in quality and chemical/isotope composition of coastal waters (Fry, 2002). Briefly, “traditional” stable isotope tracers of lighter elements such as H, C, N, O and S, are commonly used in coastal systems and analysed by gas-source isotope ratio mass spectrometry (IRMS) techniques (Valley and Cole, 2001; Hoefs, 2009) with applications to trace the

sources and biogeochemical pathways of the above life-essential elements and nutrients in response to degree of evaporation, temperature and salinity changes in modern coastal environments as well as paleoenvironmental studies (Patterson et al., 1994; Ostrom et al., 1997; Coplen et al., 2008; Matsubaya and Kawaraya, 2014; Petersen et al., 2016; Caschetto et al., 2017). However, the signals of these traditional isotope tracers in fossil biogenic carbonates and sedimentary archives is often overridden by biological processes, also called “vital effects”, which thus complicate their interpretation in terms of past environmental conditions and/or water source signals (Smith et al., 2000; Shirai et al., 2005).

Since early 2000s, and with the advent of new generation multi-collector mass spectrometers, more elements in the periodic table including alkali, alkaline earth and redox-sensitive metals and their isotope systems, have been explored and applied as novel tracers for various bio-geochemical processes (e.g., oxidation/reduction, precipitation/dissolution of minerals, water-rock interactions, biological uptake and cycling of metals, etc), (Wiederhold, 2015; Teng et al., 2017 and references therein).

This thesis focuses on the application of selected alkaline earth metals and their isotope systems, specifically stable calcium (Ca) and radiogenic and stable strontium (Sr) isotopes, to provide insights and constraints on water source mixing and carbonate dynamics in semi-arid lagoon and estuarine environments in South Australia. The stable Ca isotope tracer ($^{44}\text{Ca}/^{40}\text{Ca}$, denoted as $\delta^{44/40}\text{Ca}$) is broadly applied in environmental and biological studies to elucidate the biogeochemistry of marine, terrestrial and coastal Ca cycling due to its particular sensitivity to ‘kinetic’ or biological and rate-controlled processes (i.e., mass-dependent fractionation effects) (Fantle and Tipper, 2014; Griffith and Fantle, 2020 and references therein). The key biogeochemical processes in these environments, which also impact the global carbon cycle, are inorganic and biogenic formation of calcium carbonate minerals and their subsequent dissolution/recrystallisation which consume dissolved Ca^{2+} ions (Tang et al., 2008; Fantle and Tipper, 2014; Farkaš et al., 2011 and 2016). Strontium isotopes, and particularly the radiogenic $^{87}\text{Sr}/^{86}\text{Sr}$ ratio, has been used frequently as a sensitive geochemical and isotope tracer in a number of geological, ecosystem and hydrological studies (Capo et al., 1998; Holmden and Belanger, 2010; Dickin, 2018). Due to the radioactive decay of ^{87}Rb to ^{87}Sr , the isotope ratio of $^{87}\text{Sr}/^{86}\text{Sr}$ varies significantly in different geological and biological reservoirs (Kuznetsov et al., 2012). Weathering and leaching of these reservoirs impart $^{87}\text{Sr}/^{86}\text{Sr}$ of waters and fluids, which can thus be used to trace or ‘fingerprint’ different water sources and their provenance (e.g., seawater, continental waters, saline brines, etc). In addition, the applications of $^{87}\text{Sr}/^{86}\text{Sr}$ tracer to hydrogeology can help to quantify the relative contributions and mixing proportions of different water sources in complex hydrological and geological environments such as coastal lagoon-estuarine systems. Related to that, the $^{87}\text{Sr}/^{86}\text{Sr}$ record of fossil carbonate archives such as shells, corals, micro-fossils, and/or carbonate cements (micrite, sparite etc.) from marine, terrestrial and coastal systems can be also used to infer past changes in the water sources and thus palaeo-hydrological regimes (Elderfield, 1986; Åberg, 1995; Rüggeberg et al., 2008).

Importantly, over the last decade or so, the stable Sr isotopes (i.e., $^{88}\text{Sr}/^{86}\text{Sr}$ ratios, denoted as $\delta^{88/86}\text{Sr}$) have emerged as a complementary tracer for the Sr isotope studies applied to marine and terrestrial systems, with particularly promising research potential relevant to problems of marine carbonate cycling (i.e., precipitations vs dissolution of calcite/aragonite), which are processes that could not be quantified properly via the traditional radiogenic $^{87}\text{Sr}/^{86}\text{Sr}$ tracer (Krabbenhöft et al., 2009 and 2010; Raddatz et al. 2013; Stevenson et al. 2014; Vollstaedt et al. 2014; Pearce et al., 2015; Fruchter et al., 2016; Shalev et al., 2017). Also, due to the similarities in ionic radii and charge (+2) of alkaline earth metals such as Sr and Ca, these two elements can substitute each other in minerals like carbonates and sulphates (Finch and Allison, 2007; Doubleday et al., 2014). This in turn causes that both Ca and Sr and their isotope fractionation in nature commonly follows similar trends and pathways, thus causing a coupling between $\delta^{88/86}\text{Sr}$ and $\delta^{44/40}\text{Ca}$ data as documented by some pioneering studies focusing on marine environments and/or laboratory-controlled experiments (Böhm et al., 2012; AlKhatib and Eisenhauer, 2017b; Wang et al., 2021). Therefore, the $\delta^{88/86}\text{Sr}$ tracer can potentially be used as an alternative proxy for $\delta^{44/40}\text{Ca}$, with the advantage of being analysed simultaneously with the radiogenic $^{87}\text{Sr}/^{86}\text{Sr}$ ratios, thus improving the ‘discrimination potential’ or application range for isotope tracing studies. Furthermore, recent pioneering studies (Raddatz et al., 2013; Vollstaedt et al., 2014; Fruchter et al., 2016 and 2017) also documented relatively constant Sr isotope offset ($\Delta^{88/86}\text{Sr} = \delta^{88/86}\text{Sr}_{\text{carb}} - \delta^{88/86}\text{Sr}_{\text{water}}$) between the inorganic and biogenic aragonites (e.g., bivalves, brachiopods, belemnites and corals) and ambient fluids (i.e., seawater, calcifying fluids). Although, the $\Delta^{88/86}\text{Sr}$ is species-dependent, its value is mostly around -0.2‰ and seems to be relatively independent of environmental conditions such as temperature, saturation states and pH (Raddatz et al., 2013; Vollstaedt et al., 2014; Fruchter et al., 2016). However, it is argued that $\Delta^{88/86}\text{Sr}$ between inorganic carbonates (calcite, aragonite) and the ambient fluid is controlled by temperature and precipitation rates, as documented in laboratory experiments by AlKhatib and Eisenhauer (2017a and b), which may thus also be relevant to biogenic carbonates (Wang et al., 2021) thus contradicts with the above mentioned study by Fruchter et al. (2016). Keeping in mind these complexities, and if verified by future studies, this presumably ‘constant’ stable Sr isotope fractionation ($\Delta^{88/86}\text{Sr}$) between carbonate minerals and a fluid might open doors for applications where the $\delta^{88/86}\text{Sr}$ proxy could be used to reconstruct the stable Sr isotope composition of palaeo-waters and/or calcifying fluids based on the analysis of well-preserved carbonate archives. So far, most of the pioneering studies on stable Sr and Ca isotopes were conducted primarily in marine or coastal systems where water salinities were typically close to ‘normal’ seawater (~35 PSU. Practical Salinity Units), and basically no systematic studies have been done in hypersaline coastal environments. Hence, this thesis aims to fill such knowledge gap, by providing new insights and analytical data on stable Sr and Ca isotopes in a semi-arid coastal system in South Australia – the Coorong Lagoon and Murray Mouth estuary.

1.2 Study area

The Coorong is an elongated coastal lagoon that is located within the Coorong, Lower Lakes and Murray Mouth (CLLMM) estuary in South Australia at the terminus of the River Murray and Murray-Darling Basin – Australia’s largest river system and catchment area. The Coorong region is also one of the most important wetlands in Australia listed under the Ramsar Convention list (Reeves et al., 2015) and thus of and international importance. The Coorong is home to various water birds, fish, plant communities and invertebrates, and is of high cultural importance for the indigenous Ngarindjeri people (Stone et al., 2016). Additionally, the Coorong provides important resources for local fisheries and tourism, which largely supports the local economy (Sloan, 2005; Ferguson et al., 2019). However, due to continued extraction of freshwater from the upper parts of the Murray Darling Basin over the past several decades, as well as the reduction in the connectivity of the lagoon to the Southern Ocean due to increased sediment deposition at the Murray Mouth region, the Coorong has experienced a severe decline in ecological conditions, long-term decreases in freshwater inflow from the River Murray, and markedly reduced water levels (Brookes et al., 2018). In response, the south part of the Coorong (i.e., the South Lagoon) has become hypersaline and experienced widespread algal blooms, which leads to water eutrophication and generally anoxic or oxygen-depleted top-sediment conditions (Brookes et al., 2018; Paton et al., 2018).

Despite of these deteriorating ecological conditions, the Coorong is also a ‘natural laboratory’ where these processes can be studied and used for the calibration of traditional and novel isotope proxies, such as Sr and Ca isotopes, with respect to salinity, water mixing and carbonate precipitation/dissolution processes. Due to the unique geomorphology and hydrology facilitating lagoon’s restriction, the Coorong has a wide range of salinity from brackish and marine to hypersaline (>100 PSU) (Gillanders and Munro, 2012), accompanied by a similarly large range in CaCO_3 mineral saturation (Fernandes and Tanner, 2009). A combination of natural and anthropogenic processes operating within the Coorong region control a number of parameters of the Coorong, including (i) inputs and mixing between seawater and continental waters, (ii) water evaporation, and (iii) carbonate precipitation rates and modes of CaCO_3 formation (Fernandes and Tanner, 2009; Gillanders and Munro, 2012; Brookes et al., 2018; Mosley et al., 2020). Specifically, biogenic or skeletal carbonates produced by organisms such as bivalves, foraminifera and tubeworm species are commonly found in the brackish/marine part of the Coorong part (Dittmann et al., 2009; Chamberlayne et al., 2019), while in the hypersaline areas, there is mainly ‘inorganic’ or authigenic aragonite and calcite precipitation (von der Borch et al., 1975), forming distinctive spatial variation in carbonate dynamics along the Coorong.

1.3 Thesis aims

Based on the analyses of radiogenic and stable Sr isotopes, stable Ca isotopes and elemental con-

centrations in modern waters, biogenic/inorganic carbonates, and fossil carbonate shells in sediment cores from the CLLMM, the main research aims of this thesis are (i) to understand and quantify the water source mixing and carbonate dynamics (dissolution vs precipitation) in this semi-arid coastal system, including the hypersaline Coorong lagoon waters, with implications for the local coastal carbon cycle, and (ii) to reconstruct a long-term evolution of palaeo-hydrology and salinity of the Coorong, with implications for past climate changes.

To achieve these goals, the following aims or research modules were addressed and accomplished in this thesis:

(i) to develop and validate a high precision (< 0.05 per mil) method for the analysis of stable Sr isotope variations ($\delta^{88/86}\text{Sr}$) in waters and carbonates, using TIMS and double-spike approach.

(ii) to observe how $\delta^{88/86}\text{Sr}$ in the CLLMM waters respond to changing salinity and carbonate saturation in this semi-arid coastal system, and especially in hypersaline conditions of the Coorong; and to compare links between stable Ca ($\delta^{44/40}\text{Ca}$) and $\delta^{88/86}\text{Sr}$ variations observed in the CLLMM system and what are their plausible controlling mechanisms.

(iii) to monitor and quantify seasonal variations in water source mixing (seawater, continental water, and local groundwaters) as well as carbonate dynamics in the CLLMM, and particularly the Coorong, using stable and radiogenic Sr isotopes and elemental mass balance, complemented also by other conservative tracers (e.g. Mg/Na ratios) for water source mixing.

(iv) to identify and applied suitable carbonate archives (i.e., calcite/aragonite shells) present in both modern lagoon system but also in local sediment cores (i.e., fossil shells) to reconstruct palaeo-hydrology, salinity and water source mixing in the Coorong based on the stable and radiogenic Sr isotope analysis and trace element concentrations.

Overall, the findings of this thesis thus provide an advanced knowledge in our understanding of present-day and past water source mixing phenomena and hydrological changes in the CLLMM and particularly the Coorong, which in turn might be useful also for future water management strategies for the sustainable restoration of suitable environmental condition in the Coorong region.

1.4 Thesis outline

Based on the above aims, four major research modules or components (Chapters 2 to 5) were completed in this thesis (see below), while Chapter 1 is 'Introduction' and Chapter 6 summarises the key findings of this thesis and also provides some recommendations or ideas for future research directions.

Chapter 2: Calcium and strontium isotope systematics in the lagoon-estuarine environments of South Australia: Implications for water source mixing, carbonate fluxes and fish migration

This chapter presents both stable Ca and radiogenic Sr isotopes ($\delta^{44/40}\text{Ca}$ and $^{87}\text{Sr}/^{86}\text{Sr}$) in waters and fish otoliths (i.e., aragonitic ear-stones) of smallmouth hardyhead fish species (*Atherinosoma microstoma*) across the CLLMM estuary collected in May 2015 and May 2016. The majority of analyses were completed during my honours degree in 2016, but major modification or addition was done as part of PhD (to form this chapter and publication) and that additional work included: (i) X-Ray Diffraction (XRD), $\delta^{44/40}\text{Ca}$ and $^{87}\text{Sr}/^{86}\text{Sr}$ analyses of authigenic carbonate sample from the South Lagoon, (ii) revision of Sr isotope mass balance models using $^{87}\text{Sr}/^{86}\text{Sr}$ and elemental ratios and apportionment of continental water sources, (iii) geochemical modelling of mineral saturations in waters using PHREEQC and (iv) exploration of relationship between $\delta^{44/40}\text{Ca}$ and carbonate saturation. To the best of our knowledge, this study is the first one to calibrate the above Ca and Sr isotope proxies with respect to (i) a large salinity gradient ranging from fresh to hypersaline (i.e., 0 to ~120 PSU), as well as (ii) changes in the carbonate saturation of local waters. Water source mixing models based on salinity, $\delta^{44/40}\text{Ca}$, $^{87}\text{Sr}/^{86}\text{Sr}$ and Ca, Sr and Na elemental concentrations were established to apportion freshwater inputs into the Coorong and quantify local carbonate deposition in the lagoon via Rayleigh and equilibrium modelling and $\delta^{44/40}\text{Ca}$ data. Finally, the fish otoliths were also examined as potential carbonate archives for $\delta^{44/40}\text{Ca}$ and $^{87}\text{Sr}/^{86}\text{Sr}$ of the ambient lagoon waters.

This chapter is published as: Shao, Y., Farkaš, J., Holmden, C., Mosley, L., Kell-Duivesteyn, I., Izzo, C., Reis-Santos, P., Tyler, J., Törber, P., Frýda, J., Taylor, H., Haynes, D., Tibby, J. and Gillanders, B.M. (2018) Calcium and strontium isotope systematics in the lagoon-estuarine environments of South Australia: Implications for water source mixing, carbonate fluxes and fish migration, *Geochimica et Cosmochimica Acta* **239**, 90-108. <https://doi.org/10.1016/j.gca.2018.07.036>

Chapter 3: Impact of salinity and carbonate saturation on stable Sr isotopes ($\delta^{88/86}\text{Sr}$) in a lagoon-estuarine system

The main aim of this chapter was to investigate the sensitivity of stable Sr isotope tracer ($\delta^{88/86}\text{Sr}$) with respect to carbonate saturation and salinity of local waters in the CLLMM system in South Australia, utilising the same sample set as the one used in Chapter 2. Importantly, a high-precision stable Sr isotope ($^{88}\text{Sr}/^{86}\text{Sr}$, noted as $\delta^{88/86}\text{Sr}$) analytical method via thermal ionisation mass spectrometry (TIMS) was developed and validated at the University of Adelaide with the aid of the ^{87}Sr - ^{84}Sr double spike technique, resulting a long-term reproducibility for $\delta^{88/86}\text{Sr}$ data of $\pm 0.03\text{‰}$ (2SD). This in turn, allows simultaneous analyses of the novel stable Sr isotope tracer ($\delta^{88/86}\text{Sr}$) and the radiogenic Sr isotope tracer ($^{87}\text{Sr}/^{86}\text{Sr}$), which was the first time developed in Australia. In addition, modified PHREEQC models of carbonate saturations across the CLLMM estuary were made using high precision spectro-

photometric pH and alkalinity measurements. Furthermore, in order to confirm whether stable Sr and Ca isotope fractionation in the CLLMM were controlled by similar mechanisms (i.e., carbonate dissolution vs precipitation processes), the $\delta^{88/86}\text{Sr}$ data were compared with available $\delta^{44/40}\text{Ca}$ data from chapter 2. Finally, the novel $\delta^{88/86}\text{Sr}$ tracer was used in tandem with the more established radiogenic Sr isotope ratio ($^{87}\text{Sr}/^{86}\text{Sr}$) to quantify the carbonate fluxes and water source mixing in the South Lagoon.

This chapter is published as: Shao, Y., Farkaš, J., Mosley, L., Tyler, J., Wong, H., Chamberlayne, B., Raven, M., Samanta, M., Holmden, C., Gillanders, B.M., Kolečica, A., Eisenhauer, A. (2020) Impact of salinity and carbonate saturation on stable Sr isotopes ($\delta^{88/86}\text{Sr}$) in a lagoon-estuarine system. *Geochimica et Cosmochimica Acta* **293**, 461-476. doi: <https://doi.org/10.1016/j.gca.2020.11.014>

Chapter 4: Seasonal carbonate cycling and water source mixing in a semi-arid coastal lagoon-estuarine system: Insights from stable Sr isotopes ($\delta^{88/86}\text{Sr}$)

This chapter aims to constrain the seasonal variations (~3-month sampling period) in water source mixing and carbonate dynamics in the CLLMM and particularly the Coorong, with results providing better understanding of (i) the possible impact of groundwater on the lagoon water chemistry, and (ii) controlling mechanisms (i.e., salinity, saturation state, alkalinity, temperature, etc.) on the local carbonate formation/dissolution with implications also for the local carbon cycling in the Coorong. The main data sets presented in this chapter include radiogenic and stable Sr isotope ($^{87}\text{Sr}/^{86}\text{Sr}$ and $\delta^{88/86}\text{Sr}$) measurements, calculated carbonate saturation indices (SI) of waters collected during four seasons in 2018-2019, coupled with elemental concentration data, to constrain the seasonal and spatial variations of water sources and CaCO_3 dynamics in the CLLMM. Although the methodology and research approach is similar to that used in chapter 3, this study is the first one that systematically investigates the impact of seasonal changes on stable and radiogenic Sr isotope composition of coastal waters, and the impact of salinity, temperature and SI changes on the elemental and isotope composition of lagoon and estuarine waters from the CLLMM system, and particularly the Coorong.

This chapter is formatted for publication and submission to the journal of *Science of The Total Environment*, with the following authors and title of the manuscript: Shao, Y., Farkaš, J., Mosley, L., Tyler, J., Wong, H., Priestley, S., Gillanders, B.M. (2021) Seasonal carbonate cycling and water source mixing in a semi-arid coastal system: Insights from stable Sr isotopes ($\delta^{88/86}\text{Sr}$).

Chapter 5: Reconstructing palaeo-hydrology and salinity of the Coorong lagoon in South Australia based on multi-tracer analyses ($^{87}\text{Sr}/^{86}\text{Sr}$, $\delta^{88/86}\text{Sr}$ and Mg/Sr) of fossil carbonate shells

This chapter tested the fidelity of the aragonite shells of bivalve species *Arthritica helmsi* in the modern Coorong lagoon environment as archives for reconstruction of stable and radiogenic Sr isotope composition of palaeo-lagoon waters. Accordingly, a multi-proxy approach based on Sr isotopes ($^{87}\text{Sr}/^{86}\text{Sr}$ and $\delta^{88/86}\text{Sr}$) and trace element ratios (Mg/Sr) analysed in fossil *A. helmsi* shells collected from the two sediment cores (C18 and CSC) in the South Lagoon of the Coorong was used to reconstruct the local palaeo-hydrology, water mixing history and palaeo-salinity changes in the past ~2400 years. These Sr isotope and elemental concentration data acquired from fossil shells were also complemented by carbon (^{14}C) dating of shells and pollen age data to construct plausible geochronological models for the studied sediment cores. Altogether, the results generated in this chapter helped to constrain (i) temporal changes in the water source mixing and plausible palaeo-salinity changes, as well as (ii) associated variations in local carbonate cycling in the Coorong South Lagoon over the last two millennia.

This chapter is formatted for publication in the journal of *Limnology and Oceanography*, with the following authors: Shao, Y., Woolston, Z., Chamberlayne, B., Foster, N., Haynes, D., Gilbert., S., Jacobsen., G., Tyler, J., Gillanders, B.M., Farkaš, J.; and a title: Reconstructing palaeo-hydrology and salinity of the Coorong lagoon in South Australia based on multi-tracer analyses ($^{87}\text{Sr}/^{86}\text{Sr}$, $\delta^{88/86}\text{Sr}$ and Mg/Sr) of fossil carbonate shells.

References

- Åberg, G. (1995) The use of natural strontium isotopes as tracers in environmental studies. *Water, Air, and Soil Pollution* **79**, 309-322.
- AlKhatib, M. and Eisenhauer, A. (2017a) Calcium and strontium isotope fractionation in aqueous solutions as a function of temperature and reaction rate; I. Calcite. *Geochimica et Cosmochimica Acta* **209**, 296-319.
- AlKhatib, M. and Eisenhauer, A. (2017b) Calcium and strontium isotope fractionation during precipitation from aqueous solutions as a function of temperature and reaction rate; II. Aragonite. *Geochimica et Cosmochimica Acta* **209**, 320-342.
- Bauer, J. E., Cai, W. J., Raymond, P. A., Bianchi, T. S., Hopkinson, C. S. and Regnier, P. A. (2013) The changing carbon cycle of the coastal ocean. *Nature* **504**, 61-70.
- Bennett, E. M., Carpenter, S. R. and Caraco, N. F. (2001) Human impact on erodable phosphorus and

eutrophication: a global perspective: increasing accumulation of phosphorus in soil threatens rivers, lakes, and coastal oceans with eutrophication. *BioScience* **51**, 227-234.

Böhm, F., Eisenhauer, A., Tang, J., Dietzel, M., Krabbenhöft, A., Kisakürek, B. and Horn, C. (2012) Strontium isotope fractionation of planktic foraminifera and inorganic calcite. *Geochimica et Cosmochimica Acta* **93**, 300-314.

Brookes, J., Dalby, P., Dittmann, S., O'Connor, J., Paton, D., Quin, R., & Ye, Q. (2018). Recommended actions for resorting the ecological character of the South Lagoon of the Coorong. *Goyder Institute for Water Research Technical Report Series*, (18/04).

Caschetto, M., Colombani, N., Mastrocicco, M., Petitta, M. and Aravena, R. (2017) Nitrogen and sulphur cycling in the saline coastal aquifer of Ferrara, Italy. A multi-isotope approach. *Applied Geochemistry* **76**, 88-98.

Capo, R. C., Stewart, B. W. and Chadwick, O. A. (1998) Strontium isotopes as tracers of ecosystem processes: theory and methods. *Geoderma* **82**, 197-225.

Chamberlayne, B. K., Tyler, J. J. and Gillanders, B. M. (2019) Environmental Controls on the Geochemistry of a Short-Lived Bivalve in Southeastern Australian Estuaries. *Estuaries and Coasts*, 1-16.

Coplen, T. B., Neiman, P. J., White, A. B., Landwehr, J. M., Ralph, F. M. and Dettinger, M. D. (2008) Extreme changes in stable hydrogen isotopes and precipitation characteristics in a landfalling Pacific storm. *Geophysical Research Letters* **35**.

Dickin A. (2018) Radiogenic Isotope Geology, Cambridge University Press, The Third Edition. ISBN 9781316163009.

Dittmann, S., Rolston, A., Bengler, S. N. and Kupriyanova, E. K. (2009) *Habitat requirements, distribution and colonisation of the tubeworm Ficopomatus enigmaticus in the Lower Lakes and Coorong*. Report for the South Australian Murray-Darling Basin Natural Resources Management Board, Adelaide, 99.

Doubleday, Z. A., Harris, H. H., Izzo, C. and Gillanders, B. M. (2014) Strontium randomly substituting for calcium in fish otolith aragonite. *Analytical chemistry* **86**, 865-869.

Elderfield, H. (1986) Strontium isotope stratigraphy. *Palaeogeography, palaeoclimatology, palaeoecology* **57**, 71-90.

Elderfield, H. (2006) The oceans and Marine Geochemistry, Vol. 6., Treatise on Geochemistry (eds. H.D. Holland and K.K. Turekian), Elsevier-Pergamon, Oxford.

Fantle, M. S. and Tipper, E. T. (2014) Calcium isotopes in the global biogeochemical Ca cycle: Impli-

cations for development of a Ca isotope proxy. *Earth-Science Reviews* **129**, 148-177.

Farkaš, J., Déjeant, A., Novák, M., and Jacobsen, S. B. (2011) Calcium isotope constraints on the uptake and sources of Ca²⁺ in a base-poor forest: a new concept of combining stable ($\delta^{44/42}\text{Ca}$) and radiogenic (ϵCa) signals. *Geochimica et Cosmochimica Acta*, **75**, 7031–7046.

Farkaš, J., Frýda, J., and Holmden, C. (2016) Calcium isotope constraints on the marine carbon cycle and CaCO₃ deposition during the late Silurian (Ludfordian) positive $\delta^{13}\text{C}$ excursion. *Earth and Planetary Science Letters* **451**, 31-40.

Ferguson, G. J., Earl, J. and Ye, Q. (2019) The History of Fisheries in the Lower Lakes and Coorong. In *Natural history of the Coorong, Lower Lakes, and Murray Mouth region (Yarluwar-Ruwe)* (eds. L. M. Mosley, Q. Ye, S. Shepherd, S. Hemming, and R. Fitzpatrick) University of Adelaide Press on behalf of the Royal Society of South Australia, Adelaide. pp. 452-476.

Fernandes, M. and Tanner, J. E. (2009) Hypersalinity and phosphorus availability: the role of mineral precipitation in the Coorong lagoons of South Australia. CSIRO: Water for a Healthy Country National Research Flagship and South Australian Research and Development Institute (Aquatic Sciences).

Finch, A. A. and Allison, N. (2007) Coordination of Sr and Mg in calcite and aragonite. *Mineralogical Magazine* **71**, 539-552.

Fruchter, N., Eisenhauer, A., Dietzel, M., Fietzke, J., Böhm, F., Montagna, P., Stein, M., Lazar, B., Rodolfo-Metalpa, R. and Erez, J. (2016) ⁸⁸Sr/⁸⁶Sr fractionation in inorganic aragonite and in corals. *Geochimica et cosmochimica acta* **178**, 268-280.

Fry, B. (2002) Conservative mixing of stable isotopes across estuarine salinity gradients: a conceptual framework for monitoring watershed influences on downstream fisheries production. *Estuaries* **25**, 264-271.

Gillanders, B. M. and Munro, A. R. (2012) Hypersaline waters pose new challenges for reconstructing environmental histories of fish based on otolith chemistry. *Limnology and Oceanography* **57**, 1136.

Griffith E. and Fantle M. (2020) Calcium Isotopes. Book chapter in ‘Elements in Geochemical Tracers in Earth System Science, Cambridge University Press, ISBN 9781108853972.

Halpern, B. S., Walbridge, S., Selkoe, K. A., Kappel, C. V., Micheli, F., D’Agrosa, C., Bruno, J. F., Casey, K. S., Ebert, C., Fox, H. E., Fujita, R., Heinemann, D., Lenihan, H. S., Madin, E. M. P., Perry, M. T., Selig, E. R., Spalding, M., Steneck, R. and Watson, R. (2008). A global map of human impact on marine ecosystems. *science* **319**, 948-952.

Hoefs, J. (2009) *Stable isotope geochemistry* (Vol. 285). Berlin: springer.

Holmden, C. and Bélanger, N. (2010) Ca isotope cycling in a forested ecosystem. *Geochimica et cosmochimica acta* **74**, 995-1015.

Krabbenhöft, A., Fietzke, J., Eisenhauer, A., Liebetrau, V., Böhm, F. and Vollstaedt, H. (2009) Determination of radiogenic and stable strontium isotope ratios ($^{87}\text{Sr}/^{86}\text{Sr}$; $\delta^{88/86}\text{Sr}$) by thermal ionization mass spectrometry applying an $^{87}\text{Sr}/^{84}\text{Sr}$ double spike. *Journal of Analytical Atomic Spectrometry* **24**, 1267-1271.

Krabbenhöft, A., Eisenhauer, A., Böhm, F., Vollstaedt, H., Fietzke, J., Liebetrau, V., Augustin, N., Peucker-Ehrenbrink, B., Müller, M. N., Horn, C., Hansen, B. T., Nolte, N. and Wallmann, K. (2010) Constraining the marine strontium budget with natural strontium isotope fractionations ($^{87}\text{Sr}/^{86}\text{Sr}^*$, $\delta^{88/86}\text{Sr}$) of carbonates, hydrothermal solutions and river waters. *Geochimica et cosmochimica acta* **74**, 4097-4109.

Kuznetsov, A. B., Semikhatov, M. A. and Gorokhov, I. M. (2012) The Sr isotope composition of the world ocean, marginal and inland seas: Implications for the Sr isotope stratigraphy. *Stratigraphy and Geological Correlation* **20**, 501-515.

Macreadie, P. I., Serrano, O., Maher, D. T., Duarte, C. M. and Beardall, J. (2017) Addressing calcium carbonate cycling in blue carbon accounting. *Limnology and Oceanography Letters* **2**, 195-201.

Matsubaya, O. and Kawaraya, H. (2014) Hydrogen and oxygen isotopic characteristics of precipitation in coastal areas of Japan determined by observations for 23 years at Akita and for 1-2 years at other several localities. *Geochemical Journal* **48**, 397-408.

Mosley, L. M., Priestley, S., Brookes, J., Dittmann, S., Farkaš, J., Farrell, M., Ferguson, A. J., Gibbs, M., Hipsey, M., Huang, J., Lam-Gordillo, O., Simpson, S. L., Teasdale, P. R., Tyler, J. J., Waycott, M., Welsh, D. T. (2020) Coorong water quality synthesis with a focus on the drivers of eutrophication. Goyder Institute for Water Research Technical Report Series No. 20/10, Adelaide, South Australia. ISSN: 1839-2725.

Ostrom, N. E., Macko, S. A., Deibel, D. and Thompson, R. J. (1997) Seasonal variation in the stable carbon and nitrogen isotope biogeochemistry of a coastal cold ocean environment. *Geochimica et Cosmochimica Acta* **61**, 2929-2942.

Patterson W. P. and Walter L. M. (1994) Depletion of ^{13}C in seawater ΣCO_2 on modern carbonate platforms: Significance for the carbon isotopic record of carbonates. *Geology* **22**, 885– 888.

Paton D.C., Paton F.L. and Bailey C.P. (2018). Monitoring of *Ruppia tuberosa* in the southern Coorong, summer 2017-18. The University of Adelaide, Adelaide.

Pearce, C. R., Parkinson, I. J., Gaillardet, J., Charlier, B. L., Mokadem, F. and Burton, K. W. (2015)

Reassessing the stable ($\delta^{88/86}\text{Sr}$) and radiogenic ($^{87}\text{Sr}/^{86}\text{Sr}$) strontium isotopic composition of marine inputs. *Geochimica et Cosmochimica Acta* **157**, 125-146.

Petersen S. V., Tabor C. R., Lohmann K. C., Poulsen C. J., Meyer K. W., Carpenter S. J., Erickson J. M., Matsunaga K. K., Smith S. Y. and Sheldon N. D. (2016) Temperature and salinity of the Late Cretaceous Western Interior Seaway. *Geology* **44**, 903–906.

Raddatz, J., Liebetrau, V., Rüggeberg, A., Hathorne, E., Krabbenhöft, A., Eisenhauer, A., Böhm, F., Vollstaedt, H., Fietzke, J., López Correa, M., Freiwald, A. and -Chr.Dullo, W., (2013) Stable Sr-isotope, Sr/Ca, Mg/Ca, Li/Ca and Mg/Li ratios in the scleractinian cold-water coral *Lophelia pertusa*. *Chemical geology* **352**, 143-152.

Regnier, P., Friedlingstein, P., Ciais, P., Mackenzie, F. T., Gruber, N., Janssens, I. A., Laruelle, G. G., Lauerwald, R., Luysaert, S., Andersson, A. J., Arndt, S., Arnosti, C., Borges, A. V., Dale, A. W., Gallego-Sala, A., Goddérís, Y., Goossens, N., Hartmann, J., Heinze, C., Ilyina, T., Joos, F., LaRowe, D. E., Leifeld, J., Meysman, F. J. R., Munhoven, G., Raymond, P. A., Spahni, R., Suntharalingam, P. and Thullner, Martin. (2013) Anthropogenic perturbation of the carbon fluxes from land to ocean. *Nature geoscience* **6**, 597-607.

Reeves, J. M., Haynes, D., García, A. and Gell, P. A. (2015) Hydrological change in the Coorong Estuary, Australia, past and present: Evidence from fossil invertebrate and algal assemblages. *Estuaries and coasts* **38**, 2101-2116.

Rüggeberg, A., Fietzke, J., Liebetrau, V., Eisenhauer, A., Dullo, W. C. and Freiwald, A. (2008) Stable strontium isotopes ($\delta^{88/86}\text{Sr}$) in cold-water corals—a new proxy for reconstruction of intermediate ocean water temperatures. *Earth and Planetary Science Letters* **269**, 570-575.

Shalev, N., Gavrieli, I., Halicz, L., Sandler, A., Stein, M. and Lazar, B. (2017) Enrichment of ^{88}Sr in continental waters due to calcium carbonate precipitation. *Earth and Planetary Science Letters* **459**, 381-393.

Shirai, K., Kusakabe, M., Nakai, S., Ishii, T., Watanabe, T., Hiyagon, H. and Sano, Y. (2005). Deep-sea coral geochemistry: Implication for the vital effect. *Chemical Geology* **224**, 212-222.

Smith, J. E., Schwarcz, H. P., Risk, M. J., McConnaughey, T. A. and Keller, N. (2000) Paleotemperatures from deep-sea corals: overcoming ‘vital effects’. *Palaios* **15**, 25-32.

Sloan, S. (2005) *Management Plan for the South Australian lakes and Coorong fishery*. Agriculture, Food and Fisheries, Primary Industries and Resources SA.

Stevenson, E. I., Hermoso, M., Rickaby, R. E., Tyler, J. J., Minoletti, F., Parkinson, I. J., Mokadem, F. and Burton, K. W. (2014) Controls on stable strontium isotope fractionation in coccolithophores with

implications for the marine Sr cycle. *Geochimica et Cosmochimica Acta* **128**, 225-235.

Stone, D., Palmer, D., Hamilton, B., Cooney, C. and Mosley, L., (2016) Coorong, Lower Lakes and Murray Mouth water quality monitoring program 2009-2016 Summary report. *Environmental Protection Authority, South Australia*.

Tang, J., Dietzel, M., Böhm, F., Köhler, S. J., Eisenhauer, A. (2008) Sr²⁺/Ca²⁺ and ⁴⁴Ca/⁴⁰Ca fractionation during inorganic calcite formation: II. Ca isotopes. *Geochim. Cosmochim. Acta* **72**, 3733–3745.

Teng, F. Z., Dauphas, N. and Watkins, J. M. (2017) Non-traditional stable isotopes: retrospective and prospective. *Reviews in mineralogy and geochemistry* **82**, 1-26.

Valley, J. W., Cole, D. R. E. (Eds.) (2001) Stable Isotope Geochemistry. Rev Mineral Geochem 43, Mineralogical Society of America and the Geochemical Society, Washington DC.

Velez, M. I., Conde, D., Lozoya, J. P., Rusak, J. A., García-Rodríguez, F., Seitz, C., Harmon, T., Perillo, G. M. E., Escobar, J. and Vilardy, S. P. (2018) Paleoenvironmental reconstructions improve ecosystem services risk assessment: case studies from two coastal lagoons in South America. *Water* **10**, 1350.

Vollstaedt, H., Eisenhauer, A., Wallmann, K., Böhm, F., Fietzke, J., Liebetrau, V., Krabbenhöft, A., Farkaš, J., Tomašových, A., Raddatz, J. and Veizer, J. (2014) The Phanerozoic δ^{88/86}Sr record of seawater: New constraints on past changes in oceanic carbonate fluxes. *Geochimica et cosmochimica acta* **128**, 249-265.

von der Borch, C. C., Lock, D. E. and Schwebel, D. (1975) Ground-water formation of dolomite in the Coorong region of South Australia. *Geology* **3**, 283-285.

Wang, J., Jacobson, A. D., Sageman, B. B. and Hurtgen, M. T. (2021) Stable Ca and Sr isotopes support volcanically triggered biocalcification crisis during Oceanic Anoxic Event 1a. *Geology* **49**, 515–519.

Ware, J. R., Smith, S. V. and Reaka-Kudla, M. L. (1992) Coral reefs: sources and sinks of atmospheric CO₂? *Coral Reefs* **11**, 127-130.

Warwick R. M., Tweedley J. R. and Potter I. C. (2018) Microtidal estuaries warrant special management measures that recognise their critical vulnerability to pollution and climate change. *Mar. Pollut. Bull.* **135**, 41–46.

Wiederhold, J. (2015) Metal Stable Isotope Signatures as Tracers in Environmental Geochemistry, *Environmental Science and Technology* **49**, 2606-2624.

CHAPTER 2

Calcium and strontium isotope systematics in the lagoon-estuarine environments of South Australia: Implications for water source mixing, carbonate fluxes and fish migration

Published as

Shao, Y., Farkaš, J., Holmden, C., Mosley, L., Kell-Duivestein, I., Izzo, C., Reis-Santos, P., Tyler, J., Törber, P., Frýda, J., Taylor, H., Haynes, D., Tibby, J. and Gillanders, B.M. (2018) Calcium and strontium isotope systematics in the lagoon-estuarine environments of South Australia: Implications for water source mixing, carbonate fluxes and fish migration, *Geochimica et Cosmochimica Acta* 239, 90-108. doi: <https://doi.org/10.1016/j.gca.2018.07.036>

This chapter was reformatted from the published article to match the rest of the thesis, the text remains the same except for section numbers, which are prefaced with the chapter number e.g. 1. Introduction is now 2.1 Introduction.

The published version is in Appendix 1.

Statement of Authorship

Title of Paper	Calcium and strontium isotope systematics in the lagoon-estuarine environments of South Australia: Implications for water source mixing, carbonate fluxes and fish migration
Publication Status	<input checked="" type="checkbox"/> Published <input type="checkbox"/> Accepted for Publication <input type="checkbox"/> Submitted for Publication <input type="checkbox"/> Unpublished and Unsubmitted work written in manuscript style
Publication Details	Shao, Y., Farkaš, J., Holmden, C., Mosley, L., Kell-Duivesteyn, I., Izzo, C., Reis-Santos, P., Tyler, J., Törber, P., Frýda, J., Taylor, H., Haynes, D., Tibby, J. and Gillanders, B.M. (2018) Calcium and strontium isotope systematics in the lagoon-estuarine environments of South Australia: Implications for water source mixing, carbonate fluxes and fish migration, <i>Geochimica et Cosmochimica Acta</i> 239 , 90-108. doi: https://doi.org/10.1016/j.gca.2018.07.036

Principal Author

Name of Principal Author (Candidate)	Yuexiao Shao		
Contribution to the Paper	Field sample collection and measurements, sample preparation, $^{87}\text{Sr}/^{86}\text{Sr}$ analyses and data collection, data interpretation and modelling, manuscript writing, acting as the corresponding author.		
Overall percentage (%)	65		
Certification:	This paper reports on original research I conducted during the period of my Higher Degree by Research candidature and is not subject to any obligations or contractual agreements with a third party that would constrain its inclusion in this thesis. I am the primary author of this paper.		
Signature		Date	2/2/2021

Co-Author Contributions

By signing the Statement of Authorship, each author certifies that:

- i. the candidate's stated contribution to the publication is accurate (as detailed above);
- ii. permission is granted for the candidate to include the publication in the thesis; and
- iii. the sum of all co-author contributions is equal to 100% less the candidate's stated contribution.

Name of Co-Author	Juraj Farkaš		
Contribution to the Paper	Conceptual development, funding supply, field work assistance, guidance on data interpretation and modelling, manuscript evaluation and review.		
Signature		Date	15/03/2021

Name of Co-Author	Chris Holmden		
Contribution to the Paper	Conceptual development, Ca isotope ($\delta^{44}\text{Ca}$) analyses, assistance on data interpretation and modelling, manuscript evaluation and review.		

Signature		Date	January 31, 2021
-----------	--	------	------------------

Name of Co-Author	Luke Mosley		
Contribution to the Paper	Conceptual development, Guidance on PHREEQC mineral saturation modelling, manuscript review.		
Signature		Date	2/2/21

Name of Co-Author	Isaac Kell-Duivesteyn		
Contribution to the Paper	Provided preliminary data of ⁸⁷ Sr/ ⁸⁶ Sr and in the Coorong and groundwater samples.		
Signature		Date	15/03/2021 (on behalf of I. Kell-Duivesteyn)

Name of Co-Author	Christopher Izzo		
Contribution to the Paper	Assistance on field work, guidance on extraction of fish otoliths, manuscript review.		
Signature		Date	03/02/2021

Name of Co-Author	Patrick Reis-Santos		
Contribution to the Paper	Assistance on field work, guidance on extraction of fish otoliths, manuscript review.		
Signature		Date	02/02/2021

Name of Co-Author	Jonathan Tyler		
-------------------	----------------	--	--

Contribution to the Paper	Conceptual development, assistance on data interpretation, reviewed and improved the structure language of the manuscript.		
Signature		Date	2/2/2021

Name of Co-Author	Philip Törber		
Contribution to the Paper	Provided carbonate crust sample, and assistance on XRD analysis.		
Signature		Date	10/3/21

Name of Co-Author	Jiří Fryda		
Contribution to the Paper	XRD analysis on the carbonate sample.		
Signature		Date	01/03/2021

Name of Co-Author	Holly Taylor		
Contribution to the Paper	XRD analysis on the carbonate sample.		
Signature		Date	03/02/2021

Name of Co-Author	Deborah Haynes		
Contribution to the Paper	Manuscript review.		
Signature		Date	03/02/2021

Name of Co-Author	John Tibby		
-------------------	------------	--	--

Contribution to the Paper	Manuscript review.		
Signature		Date	2/2/2021

Name of Co-Author	Bronwyn M. Gillanders		
Contribution to the Paper	Conceptual development, funding supply, guidance on manuscript structure and review process.		
Signature		Date	3 March 2021

Chapter 2.

Calcium and strontium isotope systematics in the lagoon-estuarine environments of South Australia: Implications for water source mixing, carbonate fluxes and fish migration

Abstract

This study uses Ca and Sr isotopes ($\delta^{44/40}\text{Ca}$ and $^{87}\text{Sr}/^{86}\text{Sr}$), coupled with elemental ratios, to better understand the water source apportionment and carbonate output in the Coorong, Lower Lakes and Murray Mouth Estuary, which represents the term

Abstract
This study uses Ca and Sr isotopes ($\delta^{44/40}\text{Ca}$ and $^{87}\text{Sr}/^{86}\text{Sr}$), coupled with elemental ratios, to better understand the water source apportionment and carbonate output in the Coorong, Lower Lakes and Murray Mouth Estuary, which represents the terminus of Australia's longest river system. The geochemistry of waters in the Coorong (i.e., North and South Lagoon) can be explained by mixing of three major components, including: (i) the Southern Ocean seawater, (ii) local freshwaters, and (iii) hypersaline lagoon waters, the latter significantly modified by ongoing evaporation and carbonate formation. The Sr and Ca isotope composition of the North Lagoon is indistinguishable from that of the Southern Ocean (i.e., normal salinity of ~ 35 PSU), with the exception of transient freshwater input events that can temporarily lower the salinity to brackish levels. Interestingly, our results from the hypersaline South Lagoon (salinity up to ~ 120 PSU) confirmed that the latter is highly evaporated brackish water (with $\geq 40\%$ contribution from continent-derived waters), which has been additionally modified by in-situ carbonate precipitation. Importantly, our Ca isotope and elemental constraints showed that about 15 to 17% of the dissolved Ca^{2+} in the South Lagoon has been removed as CaCO_3 (primarily as aragonite). This in turn has implications for the local carbonate cycle and blue carbon studies, suggesting that the South Lagoon acts as a net sink for the dissolved inorganic carbon (DIC).

Ca isotope data from the otoliths of smallmouth hardyhead fish species (*Atherinosoma microstoma*) collected in the Coorong indicate that $\delta^{44/40}\text{Ca}$ is primarily controlled by biological processes (i.e., kinetic isotope fractionation effects related to growth rate), rather than by the Ca isotope composition of local lagoon waters. As to $^{87}\text{Sr}/^{86}\text{Sr}$ in otoliths, the latter confirmed the importance of continent-derived water sources in the Coorong, recorded over the life span of the fish.

Overall, with suitable fossil carbonate archives (e.g., bivalve shells, foraminifera), our calibration of $^{87}\text{Sr}/^{86}\text{Sr}$ and $\delta^{44/40}\text{Ca}$ in the modern hydrological system, with respect to a large salinity gradient (ranging from fresh to hypersaline, i.e., 0 to ~ 120 PSU), implies potential future applications of these

isotope tracers in carbonate-producing coastal systems, which include (i) tracing and apportioning different water sources, (ii) quantifying local carbonate outputs, and (iii) reconstructing palaeo-salinity changes.

2.1 Introduction

Coastal systems such as lagoons and estuaries represent a dynamic interface between terrestrial and marine environments, which provides an essential link between bio-geochemical processes operating on the continents and in the oceans. Isotopes have not only been applied as natural tracers in a variety of coastal environments to infer fluxes and biogeochemical pathways of elements, but also used as proxies to reconstruct the recent and past environmental changes in these hydrological systems through studies of local sediment archives and included fossils (e.g., carbonate shells).

Traditionally, stable isotope tracers of light elements, such as $\delta^{13}\text{C}$, $\delta^{18}\text{O}$ and δD , have been used to trace carbon and water sources and understand the degree of water evaporation and palaeo-salinity in coastal environments (Tan and Hudson, 1974; Hendry and Kalin, 1997; Patterson and Walter, 1994; Patterson, 1999; Holmden and Hudson, 2003; Wierzbowski and Joachimski, 2007; McKirdy et al., 2010; Gemitzi et al., 2014; Petersen et al., 2016). However, these approaches are often hampered by non-conservative mixing of the above light elements related to gas exchange reactions at the air-water interface, involving water vapor and carbon dioxide. In contrast, traditional radiogenic isotope tracers of heavier metals (e.g., $^{87}\text{Sr}/^{86}\text{Sr}$, $^{143}\text{Nd}/^{144}\text{Nd}$, $^{206}\text{Pb}/^{207}\text{Pb}$) are not sensitive to water-gas exchange processes, but they are still susceptible to non-conservative mixing effects related to local water-sediment interactions (Holmden et al., 1997; Anadón et al., 2002; Holmden and Hudson, 2003; Dickin, 2005; Frank, 2011; Elderfield, 2006). More recent studies have seen increasing applications of stable isotope systems of redox-sensitive elements (Cr, Mo, U), and/or alkali and alkaline earth metals (Li, Mg, Ca, Sr, Ba) as natural tracers of metals and water sources in both marine and terrestrial settings (Baskaran, 2012; Holmden et al., 2012; Fantle and Tipper, 2014; Scheiderich et al., 2015; Wiederhold, 2015; Cao et al., 2016; Teng et al., 2017).

Of particular interest are the isotope studies of geochemically similar alkaline earth metals, such as Sr and Ca, which are the primary focus of this study. These metal isotope tracers (i) are highly abundant and readily soluble in natural waters forming divalent cations, (ii) exhibit both stable and radiogenic isotope variations, and (iii) have biogeochemical pathways closely linked to the global carbon cycle via processes involving precipitation and weathering of carbonate minerals. Hence, Sr and Ca isotopes are valuable tracers of carbonate weathering/precipitation, water source mixing, as well as biological uptake of these elements by plants and organisms in coastal systems (Holmden et al., 1997; Fantle and DePaolo, 2007; Tang et al., 2008; Holmden and Bélanger, 2010; Holmden et

al., 2012; Fantle and Tipper 2014; Fantle, 2015; Farkaš et al., 2011 and 2016; Harouaka et al., 2014 and 2016). Importantly, the calcium carbonate (CaCO_3) cycle in coastal systems plays an important role in quantifying the blue carbon budget (i.e., carbon storage capacity) in coastal ecosystems. This in turn is essential for better assessment of global CO_2 input and output fluxes. However, most studies have been only focused on brackish and marine salinities, the hypersaline coastal environments, which receive much more significant effects from water evaporation and induced mineral precipitation, are poorly understood.

Here we illustrate how a novel approach with coupled Sr and Ca isotopes could be used in the carbonate-producing Coorong lagoon system, which has a salinity range from fresh to hypersaline, to distinguish and apportion different water sources, and better constrain the local CaCO_3 cycle, which is currently a poorly constrained component in the global blue carbon studies (Macreadie et al, 2017). Additionally, the Sr and Ca isotope data of fish otoliths (i.e., aragonitic ear-stones) from Coorong are used to infer potential short-term changes in the isotope signatures of local water masses (Gillanders and Munro, 2012). Finally, a broader objective of this study is to explore the possibility of using these isotope tracers, calibrated with respect to salinity in modern settings, to reconstruct palaeo-salinity changes in the studied area and/or other carbonate-producing coastal environments from suitable fossil carbonates (e.g., bivalve shells or foraminifera) in local sediment archives.

2.2 Study area

The Coorong, Lower Lakes and Murray Mouth Estuary, located on the southeast coast of Australia (Fig. 1), represents a unique mixing zone where continental-sourced freshwaters interact with seawater from the Southern Ocean in the circulation-restricted Coorong, which is a 130-km-long lagoon formed behind a complex of Quaternary- and Holocene-age sand barrier islands and beach dunes (i.e., Younghusband Peninsula, see Fig. 1) (Kjerfve, 1986; Knoppers, 1994). This coastal area is of particular ecological and environmental importance, being a conservation park for many local species, has also been listed in the Ramsar Convention of wetlands of international importance since 1985 (Webster, 2010).

The Coorong lagoon system acts as a natural ‘reservoir’ for mixing of different water sources, and it is divided into two sub-lagoons – the North and South Lagoons, with a narrow and shallow (< 1 m depth) connection at Parnka Point (Fig. 1). The two lagoons have average water levels of ~1.2 m and ~1.4 m respectively, fluctuating seasonally with an amplitude of approximately 0.8 m to 1 m (Webster, 2010). The North Lagoon receives water inputs from the Southern Ocean via the Murray Mouth at its northern end and occasionally also from the release of freshwater through barrages. The latter separate the Coorong from the Lower Lakes (i.e., Lake Alexandrina and Lake Albert), which

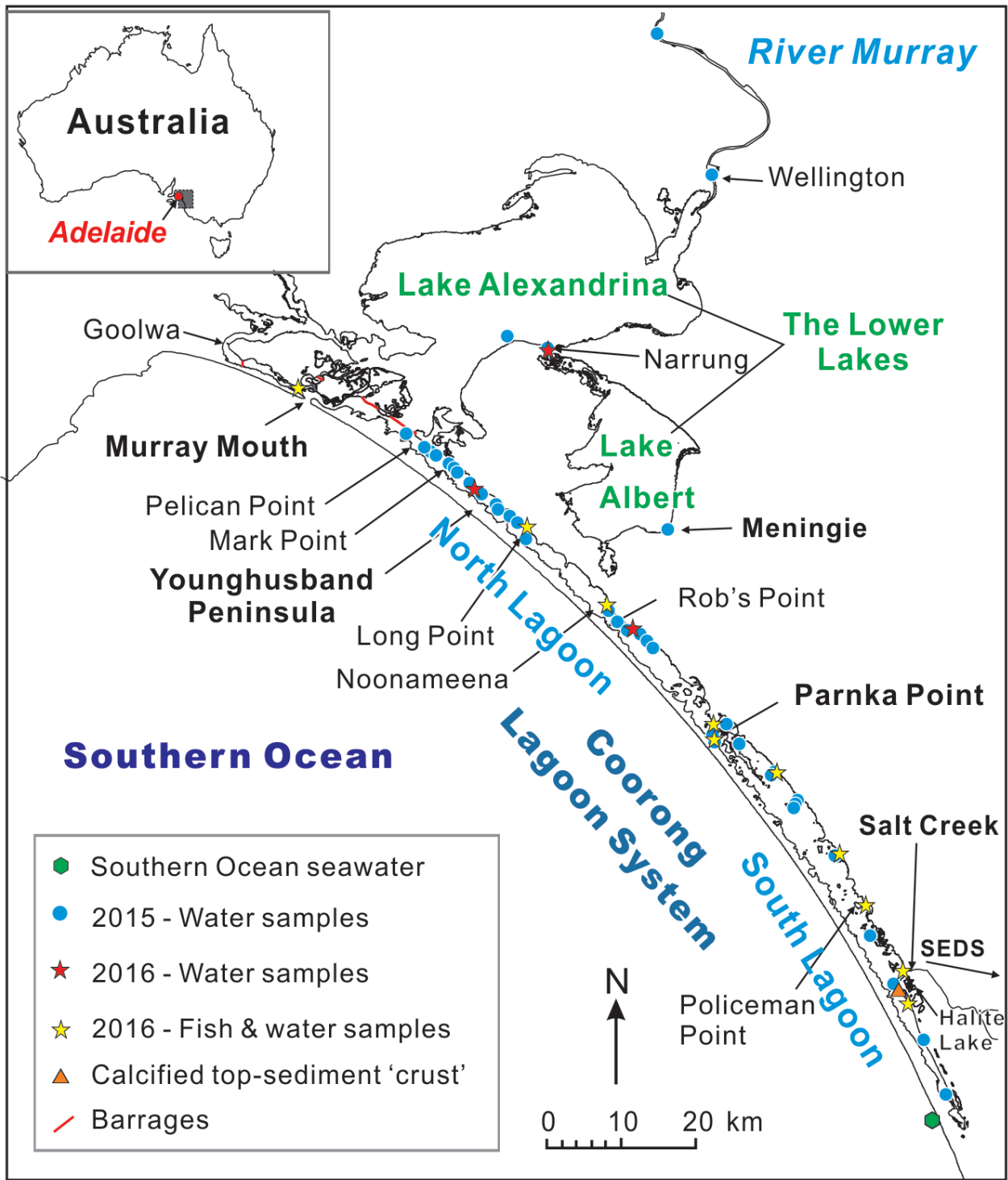


Figure 1: A map showing the Coorong and Lower Lakes at the terminus of the River Murray in South Australia. Sampling locations for this study are color and symbol coded for sampling years of 2015 (circles) and 2016 (stars). Red bars in North Lagoon between Pelican Point and Goolwa show the locations of barrages. SEDS = the South East drainage system. Note that the Coorong refers to the narrow back-barrier lagoon separated from the Southern Ocean by the Younghusband Peninsula; the Lower Lakes refer to Lake Alexandrina and Albert; and the Murray Mouth refers to the connection of the Coorong to the ocean, locating at the northern end of the lagoon (cf., Webster, 2010).

are fed by the River Murray (see Fig. 1). Prior to the construction of barrages between 1935 and 1940, water exchange between the Coorong, Lake Alexandrina and the Southern Ocean occurred naturally through the Murray Mouth. Thus, the construction of the barrages effectively isolated the Lower Lakes from the saline waters of the Coorong. This, along with increased extraction of river water for upstream irrigation, has gradually reduced freshwater inputs to the Coorong over the past seven decades (Phillips and Muller, 2006). In addition, the South Lagoon is hydrologically more restricted compared to North Lagoon, and the supply of waters is facilitated either via Parnka Point (i.e., a connection to the North Lagoon), or via Salt Creek that receives freshwater from the South East drainage system (Fig. 1) constructed over the last 150 years (Mosley et al., 2017; Reid and Mosley, 2016). Limited flushing by river outflows and reduced connectivity with the open ocean through the mouth have caused the South Lagoon to become progressively more hypersaline over the last five decades, which is of significant environmental and ecological concern (Haese et al., 2008; Mckirdy et al., 2010; Webster, 2010).

The mean annual rainfall in the studied area is ~390 mm with the average annual pan evaporation approximately 1500 mm according to Bureau of Meteorology (Station 023894 on Hindmarsh Island), based on data from 2003-2018. In addition, there is evidence for ongoing and past local groundwater discharge through numerous seeps exposed in the lagoon and along its shorelines. These groundwater inputs are sourced from the Murray Group limestone aquifer, and are manifested by *in situ* carbonate precipitation occurring at the sites of local groundwater discharge in the form of carbonate tufa structures (Von der Borch et al., 1975; Haese et al., 2008; Webster, 2010; Gillanders and Munro, 2012). Proximal to the Coorong, especially the South Lagoon, are a series of shallow in-land ephemeral lakes (0.5 m - 1 m deep) that are fed by seawater intrusions, rainfall and local groundwater seepage. These lakes contain waters and brines modified by extreme evaporation and freshwater-seawater mixing, which has led to formation of in-situ primary dolomite (\pm magnesite), high-Mg calcite, aragonite and halite (Von der Borch et al., 1975). However, these ephemeral lakes are currently not directly connected to the Coorong lagoons. The abovementioned groundwater discharge is likely not limited only to the Coorong, but the overall impact of groundwater on water quality in this coastal system remains unconstrained. Better knowledge of these processes and local groundwater inputs is of considerable interest and concern, especially with respect to future sustainable water management strategies (Haese et al., 2008; Barnett, 2015).

2.3 Methods

2.3.1 Sample collection and preparation

In total, we collected 31 water samples in 2015, including river water from the channel of the River Murray near Wellington, waters from the Lower Lakes and the Coorong, two samples of local

groundwater, as well as a reference ‘seawater’ collected from the Southern Ocean. In 2016/2017, we collected 42 samples in the Coorong area, including 13 water samples from the Coorong and Lower Lakes, 4 rainwater samples in Adelaide area (not shown in Fig. 1), one cemented top-sediment ‘crust’ in the Coorong South Lagoon, and 24 fish specimens across the lagoon. The coordinates of the sampling sites and dates are listed in the Appendix (Table C.1), and see also Fig. 1 for our sampling locations.

2.3.1.1 Waters and sediment

Representative water samples were collected from the surface of the water bodies by wading, using pre-cleaned 500 mL polypropylene bottles washed with 10% HNO₃. Water temperature, pH, conductivity/salinity, and total dissolved solids (TDS) were measured directly at the sampling sites using a Hanna Instrument HI-98194 multiparameter probe. In addition, two samples of local groundwater were collected via a 12V Whale inline pump from two separate private wells located near Noonameena. Water samples were filtered through 0.45 µm cellulose nitrate filters and stored in acid-cleaned 15 mL polypropylene test tubes. All Teflon labware for isotope and elemental analysis was cleaned in 6M HNO₃ at 170 °C on a hotplate for 48 hours, rinsed with deionised water, and then further cleaned in 6M HCl at 170 °C for 24 hours and dried.

Additionally, four rainwater samples were collected about 150 km north of the Coorong in the Adelaide area to determine the representative isotope composition of South Australian atmospheric precipitation, and its possible impact on the isotope signatures observed in the Coorong. Rainwaters were collected from polyethylene (Rain-PT) and a galvanised iron (Rain-IT) tanks, respectively. These ‘bulk’ samples thus represent the long-term average of local rainwaters that accumulated in the tanks over a period of several years. Two more rainwater samples (Rain-A and Rain-B) were collected in August 2016 during storm events using 2L pre-cleaned polypropylene bottles, which thus represent more recent and ‘snap-shot’ samples of the local atmospheric deposition.

A carbonate-cemented top sediment ‘crust’ (ca. 0.5 to 1 cm thick), which is commonly formed in the Coorong lagoons, was collected from the South Lagoon on March 2017 at a site south of Salt Creek near Halite Lake.

2.3.1.2 Fish species and otoliths

The smallmouth hardyhead (*Atherinosoma microstoma*, Fig. C.1B, Appendix C), belonging to the Atherinidae family, generally have a total length of less than 110 mm and an annual life cycle (Gillanders and Munro, 2012; Wedderburn et al., 2014). This species lives usually in shallow estuarine and marine environments (within 2 m of water depth) and feeds on small invertebrates and plankton. The major advantage of using *A. microstoma* in this study is that the species has limited migration patterns (Molsher et al., 1994; Wedderburn et al., 2007 and 2008) and also extremely high salinity

tolerance (i.e., from 3.3 to 108 PSU; Lui, 1969), which allows sampling of this fish across the entire Coorong and the Murray Mouth (Fig. 1).

Specimens of smallmouth hardyheads were collected by wading in shallow waters using a fine-meshed seine net. Two or three large specimens were selected from each sampling site, weighed and measured for length. Sagittal otoliths were removed under a dissecting microscope, cleaned of adhering tissue in ultrapure water, dried, weighed and transferred to individual 1.5 mL centrifuge tubes. Additionally, two otoliths from the North and South Lagoons (samples C03-03 and C10-03, respectively) were embedded in epoxy resins and polished using fine grit lapping paper until the core was exposed (see also Fig. C.1A, Appendix C), then subsampled using a computer operated micromilling device (Merchantek Micromill Sampler). Each sample comprised the core of the otolith, which represents the early life of the fish, while the edge comprised material laid down shortly before capture and should be representative of the area where fish were collected.

2.3.2 Elemental and isotope analyses

2.3.2.1 Elemental concentrations

Elemental concentrations of Ca, Sr, Mg, Ba, Mn, Fe, Na, Zn and Cu in filtered water samples were measured with an Agilent 7500cs solution ICP-MS at Adelaide Microscopy, University of Adelaide. A multi-element standard was used for calibration. The uncertainty for all analyses is $\pm 3\%$ (2s). The measured elemental concentrations are listed in Table C.3 in the Appendix (see also plots of concentrations against salinity in Fig. C.2, Appendix C).

2.3.2.2 XRD mineralogical composition analysis

The mineralogical composition of the sediment ‘crust’ from the South Lagoon was determined using X-Ray diffraction (XRD) adapted from Schreiner (1995) and Martin et al. (2015), performed at the School of Earth and Environmental Sciences, University of Wollongong. The sediment ‘crust’ sample was dried at 50–60 °C and crushed to $<4 \mu\text{m}$ by hand using an agate mortar and pestle prior to analysis. The sample was then mounted in aluminum holders and placed in a Phillips 1130/90 diffractometer with Spellman DF3 generator set to 1 kW. The mounted sample was loaded and analysed through an automatic sample holder. The 1 kW energy was achieved by setting the diffractometer to 35 kV and 28.8 mA. Then the sample was analysed between 4° and 70° 2-theta at 2° per minute with a step size of 0.02° . Diffraction patterns were produced through a GBC 122 control system and analysed using Traces, UPDSM and SIROQUANT software. The XRD diffraction patterns were calibrated using the quartz peak at 26.66° 2-theta. The areas between 3.5 to 5.7° 2-theta were excluded as these were subject to background radiation. Peaks within 44.4 and 44.9° 2-theta were removed as they resemble the aluminum peak from the sample holder. The error on the XRD diffraction pattern was assessed by

the chi-squared value (χ^2). A χ^2 of 3.52 was obtained. When $\chi^2 = 1$ it is statistically a perfect fit of the observed data to the model, therefore a χ^2 value of 1-5 is acceptable (Schreiner, 1995).

2.3.2.3 $^{87}\text{Sr}/^{86}\text{Sr}$ and $\delta^{44/40}\text{Ca}$

A total of 76 samples were measured for $^{87}\text{Sr}/^{86}\text{Sr}$, including 48 waters and 28 whole otoliths samples or micro-drilled sections of otoliths. The isotopic measurements were performed by thermal ionisation mass spectrometry (TIMS) using a Phoenix Isotopx instrument at the University of Adelaide. Prior to TIMS analyses, all samples were processed through a chromatographic column to separate the Sr fraction at the University of Adelaide using a semi-automated prepFAST-MC system, with the method adapted from Romaniello et al. (2015). See section B.1 in Appendix for detailed procedures. Procedural Sr blanks were run in parallel with samples for each batch of samples, and the ^{84}Sr -enriched single spike was used to determine the Sr blanks via an isotope dilution (Lamberty and Pauwels, 1991). These tests confirm that most of the Sr blank was sourced from the chromatographic columns. The total procedural Sr blanks of our method ranged from ~ 60 to 200 ng, and considering that these represent only $\sim 0.1\%$ of our sample Sr signal, these blanks are negligible. The typical external precision of the $^{87}\text{Sr}/^{86}\text{Sr}$ analyses is better than ± 0.00001 (2s), and the long-term reproducibility of IAPSO (OSIL) standard is 0.709171 ± 0.00001 (2s, n=13). Whereas the long-term reproducibility of SRM 987 (NIST) standard is 0.710246 ± 0.000018 (2s, n=36), which was used to monitor the stability and overall performance of TIMS measurements. For smaller sample sizes (~ 100 ng), the reproducibility of SRM 987 standard is 0.710247 ± 0.000011 (2s, n=16), giving a typical external precision of < 0.00003 (2s). Detailed information on sample loading, filament ionisation, and measurement uncertainties is provided in section B.2 in Appendix B.

A total of 26 samples were analysed for $\delta^{44/40}\text{Ca}$, including 15 water samples, the sediment sample from the South Lagoon and 10 whole otolith samples. Prior to the Ca isotope analysis, all samples were mixed with a ^{43}Ca - ^{42}Ca double-spike and passed through cation exchange columns to purify Ca (Holmden, 2005; Lehn et al., 2013). The isotopic measurements were performed using a double-spike TIMS technique using a Thermo Elemental Triton instrument in the Saskatchewan Isotope Laboratory at the University of Saskatchewan, adapted from Holmden and Bélanger (2010) and Farkaš et al. (2016). The total procedure Ca blank was 80 – 130 ng, and represents less than 0.1% of Ca originating from a sample (for detailed procedures, refer to Holmden and Bélanger, 2010). The Ca isotope variations presented in this study are expressed in the conventional delta notation (as $\delta^{44/40}\text{Ca}$ values) relative to IAPSO, according to the following relationship: $\delta^{44/40}\text{Ca} = [({}^{44}\text{Ca}/{}^{40}\text{Ca}_{\text{Sample}} / {}^{44}\text{Ca}/{}^{40}\text{Ca}_{\text{IAPSO}} - 1)] \times 1000$. The typical external precision of the $\delta^{44/40}\text{Ca}$ values is better than ± 0.05 ‰ (2s) (see Table A.1, Appendix A), and the long-term reproducibility of SRM 915b (NIST) standard is -1.13 ± 0.03 ‰ (2s, n=3).

2.3.3 Geochemical modeling of mineral saturations in waters using PHREEQC

The saturation states or indices (SI) of calcite, aragonite, gypsum and dolomite in the Coorong waters were calculated via PHREEQC (Parkhurst and Appelo, 2013), using concentrations of the major cations (Na^+ , Ca^{2+} , Mg^{2+} , K^+) and anions (Cl^- , SO_4^{2-} , DIC), as well as alkalinity, pH and temperature from representative water samples from five different locations across the Coorong (i.e., C02, C03, C06, C10 and C11). However, because the concentrations of Cl^- , SO_4^{2-} , and alkalinity were not measured in our water samples, these parameters had to be inferred indirectly from available historical geochemical data collected in the Coorong from 1998 to 2010 (provided by the Department for Environment, Water and Natural Resources South Australia), using sodium (Na^+) concentrations as a reference element. Based on the local long-term correlation trends between the concentrations of Na and the above ions of interest from historical data (i.e., 1998-2010), we were able to infer the corresponding concentrations of K^+ , Cl^- , SO_4^{2-} , and alkalinity for our water samples (for details see the Appendix, section B.3.1, Table B.2 and Fig. B.1). For PHREEQC modeling, Cl^- was used as the sole anion for charge balancing, with calculated charge balance errors typically $< 5\%$ (2s). The activity coefficients and Saturation Indices (SI) were calculated using the *Pitzer database* (Parkhurst and Appelo, 2013). To examine potential uncertainty in saturation index (SI) calculations, several simulations were performed varying pH (± 0.2), Ca ($\pm 10\%$), alkalinity ($\pm 10\%$) from measured values. This was based on estimated analytical errors in this range and a lot of the correlations being around 0.9 for derivation of the missing major ion concentrations.

2.4 Results

All analytical data, including measured $^{87}\text{Sr}/^{86}\text{Sr}$, $\delta^{44/40}\text{Ca}$, and selected elemental concentrations are compiled in Tables A.1 and A.2, in Appendix A. Salinity, $^{87}\text{Sr}/^{86}\text{Sr}$ and $\delta^{44/40}\text{Ca}$ data across the north-south trend of the Coorong, Lower Lakes and River Murray are plotted in Fig. 2 against the latitude of sampling locations to illustrate their spatial variability.

2.4.1 Spatial variations of salinity in the Coorong

The salinity of the North Lagoon was similar to the adjacent Southern Ocean (~ 35 PSU, i.e., normal seawater). In contrast, the salinity of the South Lagoon increased from ~ 60 PSU around Parnka Point to high values of ~ 120 PSU approaching the southern end (Fig. 2A), reflecting the geomorphological restriction of the lagoon towards the south. The most obvious difference between 2015 and 2016 data is the decrease in water salinity (from marine to brackish) in 2015 in the central part of the North Lagoon (near Noonameena and extending towards Rob's Point). This brackish event reflects increased freshwater inputs either via barrage outflow from the Lower Lakes or local groundwater seepage, which are scenarios evaluated in the discussion section.

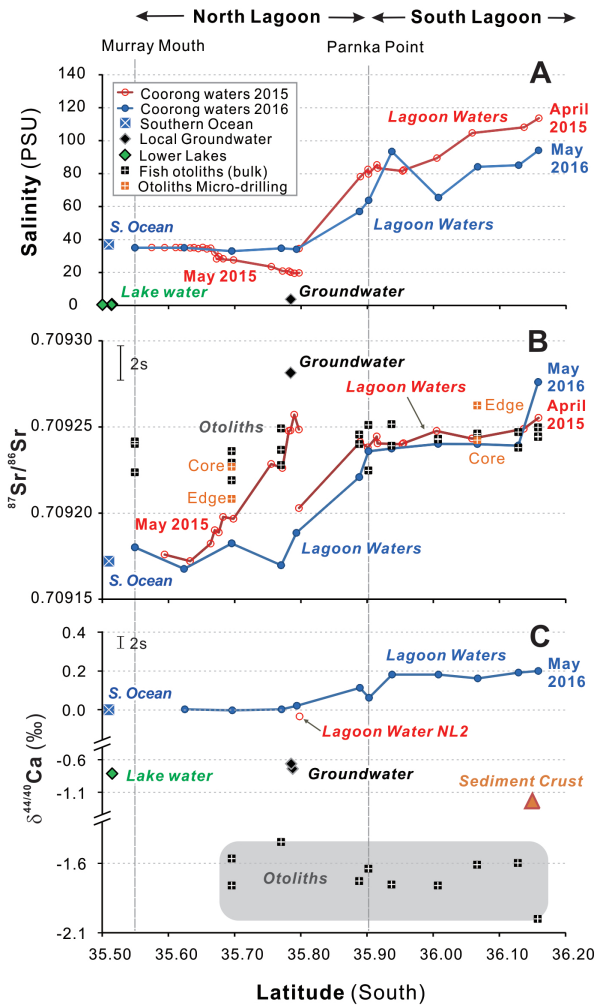


Figure 2: (A) Salinity profile across the Coorong and Lower Lakes, measured in 2015 and 2016. (B) $^{87}\text{Sr}/^{86}\text{Sr}$ variability in the Coorong, based on samples of waters and otoliths. Note that fish samples (i.e., the otolith providers) were collected only in 2016. Black squares with white cross represent whole otolith $^{87}\text{Sr}/^{86}\text{Sr}$, whereas orange squares with white cross represent $^{87}\text{Sr}/^{86}\text{Sr}$ measured in core and edge material of a single otolith. The Lower Lakes and River Murray samples are too high to be plotted on the scale (see Table A.1 in Appendix). (C) The $\delta^{44/40}\text{Ca}$ in the Coorong and Lower Lakes, based on the water samples (circles), carbonate-cemented top sediment (triangle) and fish otoliths (black squares with white cross). All data were plotted as a function of the geographic latitude for corresponding sampling sites.

2.4.2 $^{87}\text{Sr}/^{86}\text{Sr}$ and $\delta^{44/40}\text{Ca}$ variations in waters, sediments and otoliths

2.4.2.1 Coorong lagoon waters and local groundwater

Excluding the brackish water samples measured in 2015, the average $^{87}\text{Sr}/^{86}\text{Sr}$ of the North Lagoon water was 0.70918 ± 0.00001 (2s), which is indistinguishable from the average $^{87}\text{Sr}/^{86}\text{Sr}$ of global seawater, 0.70917 ± 0.00002 (2s, $n = 7$) (see Krabbenhöft et al., 2009, and references therein). In contrast, the brackish waters (Table A.1, Appendix A) yielded 0.70925 ± 0.00001 (2s), indicating continental water inputs with higher $^{87}\text{Sr}/^{86}\text{Sr}$ than seawater. The groundwater samples yielded an average $^{87}\text{Sr}/^{86}\text{Sr}$ of 0.70930 ± 0.00001 (2s), which is higher than the brackish water and seawater. The average $^{87}\text{Sr}/^{86}\text{Sr}$ of the hypersaline South Lagoon was $\sim 0.70924 \pm 0.00001$ (2s) (Fig. 2B), similar to the North Lagoon brackish water, despite their contrasting salinities.

Other continental waters yielded much higher $^{87}\text{Sr}/^{86}\text{Sr}$ values than those illustrated above. Specifically, the River Murray water had a $^{87}\text{Sr}/^{86}\text{Sr}$ of ~ 0.71212 – the highest among waters analysed in this study. Following are the Lower Lakes waters with $^{87}\text{Sr}/^{86}\text{Sr}$ of ~ 0.71094 (Table 3, and Fig. 3A). Samples of local atmospheric precipitation or rainwaters yielded $^{87}\text{Sr}/^{86}\text{Sr}$ ratios ranging between ~ 0.71008 to 0.71154 (Table A.1, Appendix A), indicating a continental influence in the rainwater, most likely due to the presence of dissolved Sr from mineral dust.

The $\delta^{44/40}\text{Ca}$ of lagoon waters generally increased with increasing water salinity (Fig. 2C), with the

exception of brackish water (i.e., sample NL2 with salinity ~20 PSU) collected from the North Lagoon in 2015. Overall, North Lagoon waters with normal seawater salinities (~35 PSU), yielded $\delta^{44/40}\text{Ca}$ values close to 0‰. In contrast, freshwater samples yielded systematically lower $\delta^{44/40}\text{Ca}$ values, with groundwater at -0.73‰, and water from the Lower Lakes as low as -0.84‰. Finally, hypersaline waters from the South Lagoon yielded much higher $\delta^{44/40}\text{Ca}$ values of about +0.20‰, which is thus higher than typical seawater, the latter uniform at ~0‰.

2.4.2.2 Sediment crust from Coorong Lagoon

The carbonate fraction of the sediment crust in the South Lagoon (sample CLS-1, see also XRD data in Table 1) yielded $\delta^{44/40}\text{Ca}$ of $-1.16 \pm 0.03\text{‰}$, which is approximately 1.4‰ lower than the $\delta^{44/40}\text{Ca}$ in the South Lagoon waters. Note that this sample was not analysed for $^{87}\text{Sr}/^{86}\text{Sr}$.

2.4.2.3 Fish otoliths

The $^{87}\text{Sr}/^{86}\text{Sr}$ of whole fish otoliths vary from ~0.70922 in the North Lagoon to up to ~0.70925 in the South Lagoon (Fig. 2B; see also data in Table A.1, Appendix A). Otolith $^{87}\text{Sr}/^{86}\text{Sr}$ ratios of fish collected from the South Lagoon are very close to the average $^{87}\text{Sr}/^{86}\text{Sr}$ of local lagoon waters. In contrast, $^{87}\text{Sr}/^{86}\text{Sr}$ ratios of otoliths from fish collected in the North Lagoon are higher than the local lagoon waters.

The measured $^{87}\text{Sr}/^{86}\text{Sr}$ from the micro-drilled sections of selected otoliths (orange squares in Fig. 2B, Table A.2 and Fig. C.1 in Appendix) represent early (juvenile = core) and older or more recent (i.e., edge) growth increments, and by inference fish migration patterns and/or changes in $^{87}\text{Sr}/^{86}\text{Sr}$ of local lagoon waters over the lifespan of the fish. Specifically, a sample C03-03 from the North Lagoon shows that the recent $^{87}\text{Sr}/^{86}\text{Sr}$ value (i.e., edge) is lower than the one recorded during fish's early life (i.e., core). In contrast, sample C10-03 from the South Lagoon shows that the recent $^{87}\text{Sr}/^{86}\text{Sr}$ value in otolith (i.e., edge) is higher (~0.70926), while the juvenile $^{87}\text{Sr}/^{86}\text{Sr}$ parts of this otolith (i.e., core) yielded $^{87}\text{Sr}/^{86}\text{Sr}$ that is similar to the ambient lagoon waters (~0.70924) (Table A.1, Appendix A).

Whole otolith samples yielded $\delta^{44/40}\text{Ca}$ values ranging between -1.46 and -2.00‰ (Fig. 2C and data in Table A.1, Appendix A). There is no obvious correlation between the $\delta^{44/40}\text{Ca}$ values of otoliths and those of local lagoon waters where the fish were captured (Fig. C.4, Appendix C). There is, however, a correlation between fish/otolith size and $\delta^{44/40}\text{Ca}$ ($R^2 \approx 0.4$, $p < 0.08$, $n = 10$). Specifically, smaller otoliths (i.e., smaller fish) tend to have lower $\delta^{44/40}\text{Ca}$ values (see data in Table A.1, Appendix A).

2.4.3 XRD analysis of the sediment crust sample

The mineralogy of the sediment 'crust' from the South Lagoon is given in Table 1. Approximately 75% of the sediment crust is composed of carbonate minerals, the latter being mostly aragonite

Table 1. Relative abundances of mineral phases (determined by XRD) in the top-sediment cemented ‘crust’, sampled in the South Lagoon (south of Salt Creek, near Halite Lake). The CaCO_3 phases, i.e. calcite and aragonite, are highlighted.

Sample ID	CSL-1 (top sediment crust) Depth: 0.5 – 1 cm	
Mineral Phase	% Abundance	% Error
Quartz	18.7	0.3
Dolomite	0.3	0.4
Gypsum	1.1	0.4
Halite	2.9	0.2
Aragonite	64.7	0.7
Calcite	8.9	0.3
Magnesite	1.5	0.6
Ankerite	2.0	0.4

(~65%), with smaller amounts of calcite (~9%), ankerite (~2%) and magnesite (~1%). The non-carbonate component of the sediment is mostly quartz (~19%), with minor amounts of halite (~3%) and gypsum (~1%).

2.4.4 Mineral saturation (SI) of lagoon waters

PHREEQC modeling shows increasing saturation indices (SI) in the Coorong lagoon waters from north to south with respect to calcite, aragonite, dolomite, and gypsum (Table 2, see also Fig. B2 in Appendix B). Carbonate minerals (CaCO_3 and $\text{CaMg}(\text{CO}_3)_2$) are systematically oversaturated ($\text{SI} > 0$) in waters across the entire Coorong, whereas gypsum ($\text{CaSO}_4 \cdot 2\text{H}_2\text{O}$) is mostly undersaturated ($\text{SI} < 0$) except in the most circulation restricted portions of the South Lagoon where SI is close to 0. The typical uncertainty associated with calculated SI values is ± 0.2 SI (2s), which is based on propagation of analytical uncertainties (Table 2).

These PHREEQC modeling results, and predicted minerals formed from local waters, are consistent with the mineralogical data acquired using XRD from the sediment ‘crust’ sample collected in the

Table 2. A summary with calculated SI values for selected minerals, based on the PHREEQC modelling

Sample IDs and 2016 sampling sites*	Mineral Saturation Index (SI)			
	Calcite	Aragonite	Dolomite	Gypsum
C02 - Mark Point	0.82	0.67	2.49	-0.69
C03 - Long Point	0.87	0.72	2.6	-0.76
C06 - Parnka Point	1.41	1.26	3.74	-0.38
C10 - Policemans Point	1.44	1.29	3.82	-0.24
C11 - Salt Creek	1.4	1.25	3.75	-0.23

*The locations of these sampling sites are available in Fig. 1, and for more accurate coordinates see also Table C.1, Appendix C. Note that the estimated error on individual SI values is about ± 0.2 SI-unit.

Table 3. The Sr, Ca and Na concentrations and isotope compositions of possible end-members for water sources used in our isotope mixing models (data extracted from Table A.1, A.2, and Table C.4, in Appendix). The data presented for the mixtures are the average values, specific sample IDs refer to Table A.1, Appendix A.

	Sample ID	Salinity (PSU)	Sr (ppm)	Ca (ppm)	Na (ppm)	$^{87}\text{Sr}/^{86}\text{Sr}$	$\delta^{44/40}\text{Ca}$ (‰)
End-members*							
Seawater/S. Ocean (SW)	SL11	36.9	8.0	414	10800	0.70917	0.00
Groundwater (GW)	JWP2	1.2	1.3	101	148	0.70932	-0.77
Continental surface freshwater/The Lower Lakes (LL)	C01	0.8	0.5	33	181	0.71088	-0.84
Mixtures							
Brackish North Lagoon waters	–	~20	4.9	301	6223	0.70925	-0.04 [#]
The South Lagoon	–	~100	23.6	980 ^s	26769	0.70924	+0.2

* The possible freshwater (FW) end-members for water source apportioning models are the GW and LL.

[#] The $\delta^{44/40}\text{Ca}$ value for the brackish North Lagoon water is from sample NL2, since this is the only one analysed for $\delta^{44/40}\text{Ca}$.

^s Inferred from the cross plots of Ca concentration versus salinity in the Coorong from Gillanders and Munro (2012).

South Lagoon (Table 1). The only exception is dolomite, which was not present in the XRD scans, but is predicted to occur. This discrepancy, also referred to as ‘dolomite problem’, is discussed in more details in the Appendix B.3.2.

2.5 Discussion

Previous studies (Haese et al., 2008 and 2009; Webster 2010; Gillanders and Munro, 2012; Mosley et al., 2017) have documented and modeled the spatially and temporally variable character of the surface waters and hydrology of the Coorong, Lower Lakes and Murray Mouth Estuary. This complexity is evident also from the range of salinities in this hydrological system, and further supported by systematic variations observed in our $^{87}\text{Sr}/^{86}\text{Sr}$ and $\delta^{44/40}\text{Ca}$ water data. In this section, we aim to use these two isotope tracers to understand the water source mixing, evaporation and carbonate precipitation in this modern lagoon estuary system, especially the North and South Lagoons. Furthermore, we also discuss here the potential of Sr and Ca isotope proxies to reconstruct the hydrology and palaeo-salinity of this lagoon-estuarine system based on the $^{87}\text{Sr}/^{86}\text{Sr}$ and $\delta^{44/40}\text{Ca}$ analysis of suitable carbonate archives.

In order to distinguish between surface and groundwater sources of freshwater in the studied lagoon system, two mixing scenarios – *groundwater-seawater* (GW-SW) and *continental surface freshwater-seawater* (LL-SW) are considered in our models. Specifically, the continental surface freshwaters are represented here by the Lower Lakes water sample (labeled as LL, see Table 3), which has average geochemical characteristics and isotopic compositions of all freshwater samples analysed (i.e., the River Murray, the Lower Lakes and the rainwater). A local groundwater is labeled as GW, and the Southern Ocean seawater is labeled as SW in our models. The elemental concentrations and isotope compositions of these individual water sources (i.e., end-members) and mixtures used in our calculations are listed in Table 3.

2.5.1 Constraints on water source mixing and evaporation effects

2.5.1.1 Sr isotope systematics

As obvious from Fig. 2, the similarities in salinities and $^{87}\text{Sr}/^{86}\text{Sr}$ of the North Lagoon waters (~35 PSU and ~0.70918, respectively) and the Southern Ocean seawater (37 PSU and 0.70917) indicate that the primary source of water in the North Lagoon is typical seawater. However, samples from May 2015 show brackish salinity (~20 PSU) and higher $^{87}\text{Sr}/^{86}\text{Sr}$ in the central part of the North Lagoon (~0.70925), pointing to inputs of continentally derived freshwater either from the Lower Lakes (0.71094), and/or local groundwater sources (~0.70932) (Table 3). As to the South Lagoon, these waters are systematically more radiogenic ($^{87}\text{Sr}/^{86}\text{Sr}$ ~0.70924) than typical seawater, indicating inputs of continentally derived Sr and by inference freshwaters. The hypersaline waters of the South Lagoon are thus a product of highly evaporated brackish waters present in this semi-restricted environment.

2.5.1.2 Evaluation of the water evaporation effects in the Coorong

Before resolving the water source mixing in the studied hydrological system with the aid of Sr and Ca isotopes, it is important to understand the net effect of water evaporation on the chemical and isotope composition of the Coorong waters, since the latter can be significantly altered by these processes. These evaporation effects on Coorong waters are shown in plots of $^{87}\text{Sr}/^{86}\text{Sr}$ ratios against Sr concentrations and salinity (Fig. 3). The theoretical LL-SW and GW-SW mixing trends (i.e., dashed curves in Fig. 3), not affected by water evaporation, were calculated using the end-member values listed Table 3, and the following elemental and isotopes mass balance equations:

$$(^{87}\text{Sr}/^{86}\text{Sr})_{\text{MIX}} M_{\text{MIX}} C_{\text{MIX}} = (^{87}\text{Sr}/^{86}\text{Sr})_{\text{FW}} M_{\text{FW}} C_{\text{FW}} + (^{87}\text{Sr}/^{86}\text{Sr})_{\text{SW}} M_{\text{SW}} C_{\text{SW}} \quad (\text{Eq. 1})$$

where M is the mass of water, such that $M_{\text{MIX}} = M_{\text{FW}} + M_{\text{SW}}$ and C is the Sr concentration or salinity of individual end-members and the mixture. The subscripts SW and FW denote seawater and freshwater (i.e., LL or GW for each mixing scenario) respectively, and MIX denotes the theoretical mixture of

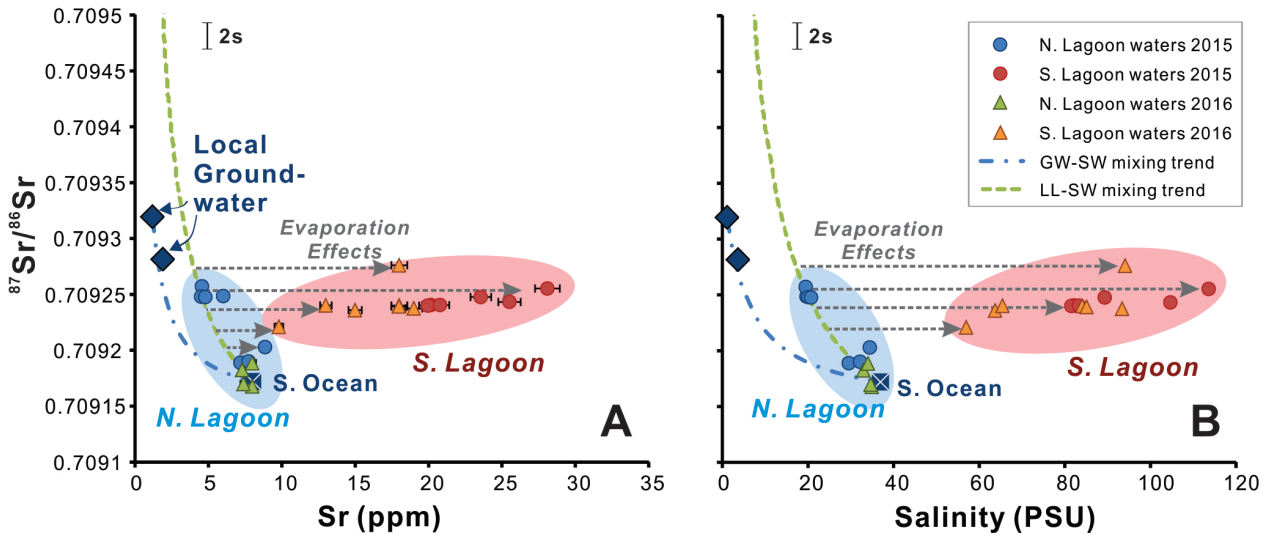


Figure 3: (A) The theoretical mixing trends for $^{87}\text{Sr}/^{86}\text{Sr}$ versus Sr concentration data, constructed for the mixing of the following end-members: a local groundwater (GW), seawater (SW), and the continental surface freshwaters represented by the Lower Lakes water (noted as LL); plotted along with data acquired from the Coorong water samples. (B) The modeled mixing trends and water data for $^{87}\text{Sr}/^{86}\text{Sr}$ versus Salinity cross-plot. Note that the continental surface freshwaters - seawater (LL-SW) mixing trends were truncated due to a very high $^{87}\text{Sr}/^{86}\text{Sr}$ of the continental surface freshwater (represented as 0.710880, see Table 3), which is out of scale. As neither water evaporation nor carbonate precipitation is expected to change the $^{87}\text{Sr}/^{86}\text{Sr}$ of the lagoon waters, the original Sr concentration and salinity can be estimated by projecting the back-projection) of the measured data onto the theoretical mixing trends.

the two water sources.

$$C_{\text{MIX}} = C_{\text{FW}} X_{\text{FW}} + C_{\text{SW}} (1 - X_{\text{FW}}) \quad (\text{Eq. 2})$$

where X_{FW} is the mass fraction of freshwater, assigned from 0 to 1.

Accordingly, if the mixtures were formed only by mixing of the above water sources with no impact from evaporation, they should all plot along those theoretical mixing trends.

Overall, Fig. 3 confirmed that the South Lagoon experienced water geochemistry exhibited much higher effects of water evaporation, as the data plot away from theoretical mixing trends, while the North Lagoon was under very limited water evaporation effect. This difference can be explained the specific hydrology of the Coorong, where – the North Lagoon readily exchanges water with the Southern Ocean, thus the evaporation effect is barely accumulates. In contrast, the South Lagoon is highly restricted with limited connectivity to the North Lagoon via Parnka Point (Fig. 1). Furthermore, the brackish North Lagoon water from 2015 plot along the LL-SW mixing trend (Fig. 3), indicating that the primary source of freshwater during this transient brackish event was most likely sourced from the Lower Lakes rather than from local groundwater sources.

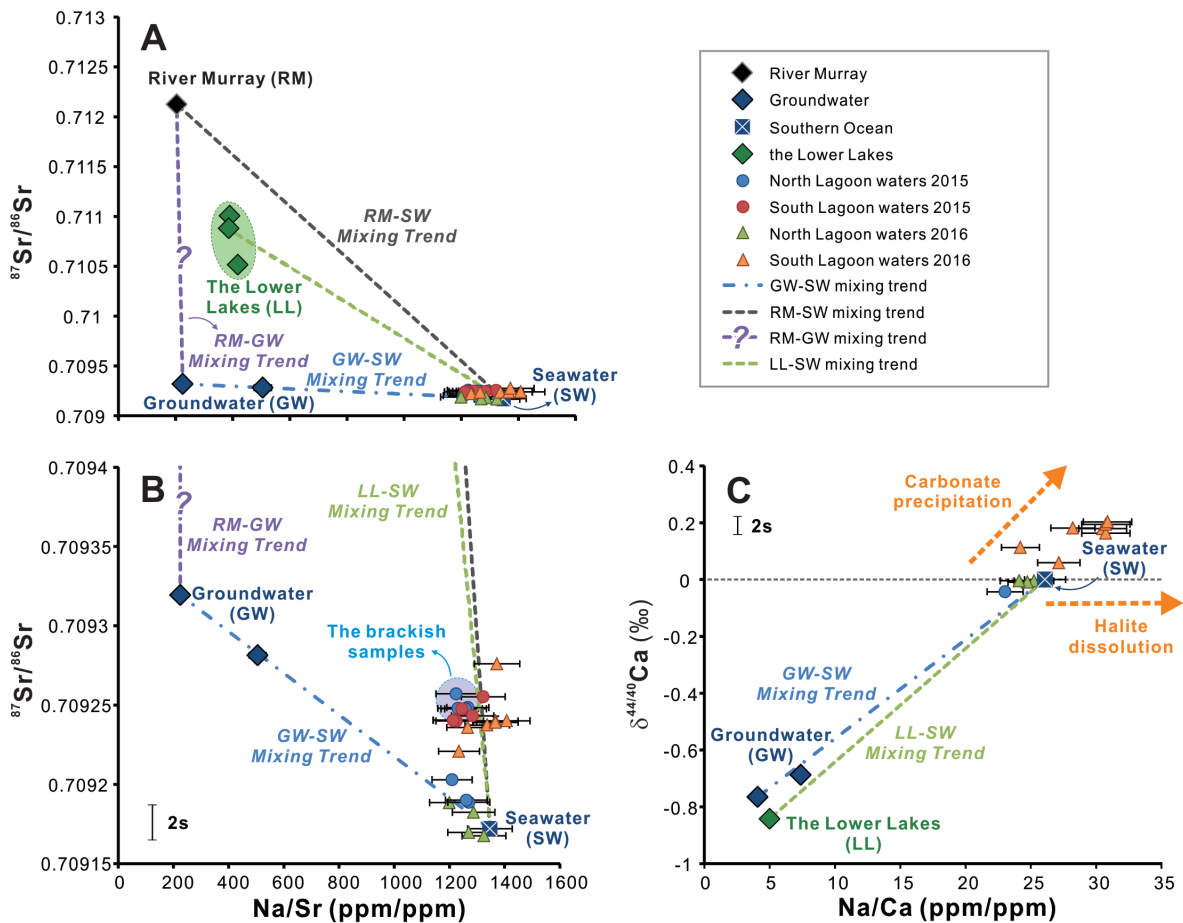


Figure 4: (A) The modeled mixing lines for $^{87}\text{Sr}/^{86}\text{Sr}$ versus Na/Sr ratio, defined by simple two-component mixings of (i) local groundwater (GW, presumably sourced from the surrounding limestone aquifers) and seawater (SW, i.e., the Southern Ocean), (ii) the Lower Lakes (LL) and seawater (SW), (iii) the River Murray (RM) and seawater (SW), and (iii) the River Murray (RM) and groundwater (GW); plotted together with the Coorong water data. The question mark on the RM-GW mixing trend is added because groundwaters around the Lower Lakes might have different $^{87}\text{Sr}/^{86}\text{Sr}$ to the ones sampled at the Coorong. (B) Truncated Y-axis to a $^{87}\text{Sr}/^{86}\text{Sr}$ value of 0.7094 from (A) to better visualise the water mixing scenarios. (C) The modeled mixing trends for $\delta^{44/40}\text{Ca}$ versus Na/Ca ratio, defined by simple two-component mixings of (i) local groundwater (GW) versus seawater (SW, i.e., the Southern Ocean), and (ii) the Lower Lakes (LL) versus seawater (SW). Dashed arrows indicate anticipated directions/trends for progressive (i) aragonite precipitation, and (ii) halite dissolution, and their expected impact on water chemistry and Ca isotope composition.

2.5.1.3 Multi-proxy constraints ($\delta^{44/40}\text{Ca}$, $^{87}\text{Sr}/^{86}\text{Sr}$, element/Na) on water source mixing

In order to visualise the water source mixing in the studied hydrological system in a bigger picture while eliminating the cumulative effects of water evaporation, we plot $^{87}\text{Sr}/^{86}\text{Sr}$ and $\delta^{44/40}\text{Ca}$ acquired from the water samples against their element/Na ratios, along with the calculated theoretical mixing trends in Fig. 4.

A close-up view on the data (Fig. 4B) confirms the North Lagoon waters were predominantly derived from the Southern Ocean, with the exception of the ‘brackish event’ from 2015, which reflects temporary freshwater input from the Lower Lakes water over the barrages during a period of high water

levels in the River Murray (Mosley, 2016, and reference therein).

Interestingly, the South Lagoon waters also plots along the LL-SW mixing trend (Fig. 4B), suggesting that a continental surface freshwater source with similar chemistry to the Lower Lakes water plays an important role in the water mixing in the South Lagoon. Considering the distance from the barrages and the narrow constriction at Parnka Point, the only way for the Lower Lakes water to enter the South Lagoon is during periods of increased barrage outflow in the North Lagoon, driving increased flow of brackish waters to the South Lagoon. This scenario is consistent with the hydrodynamic study of the Coorong by Webster (2010), showing that water levels and salinity in the North and South Lagoons are closely tied to the barrage outflow regime. However, this does not preclude that other contributions of local sources of freshwater to the South Lagoon are not important, and these might include groundwater seeps and/or surface drainage water inputs from the South East drainage system (Mosley, 2016, see also Fig. 1). More work is needed to identify and quantify the impact of these alternative freshwater sources, and their $^{87}\text{Sr}/^{86}\text{Sr}$, $\delta^{44/40}\text{Ca}$ and elemental concentrations must be measured.

Additionally, the $\delta^{44/40}\text{Ca}$ vs. Na/Ca diagram (i.e., Fig. 4C) also shows that the South Lagoon waters yielded consistently higher $\delta^{44/40}\text{Ca}$ and Na/Ca ratios than other samples. We interpret this as evidence for ongoing carbonate precipitation in the South Lagoon, mainly in the form of aragonite as suggested by the XRD data (Table 1). Alternatively, the high Na/Ca ratios can be caused by the dissolution of halite (NaCl) transported from nearby ephemeral lakes (e.g., Halite Lake) via runoff during rainfall events or lifted by wind and deposited as halite dust. However, the processes of halite dissolution/addition versus carbonate precipitation will follow different trajectories in the $\delta^{44/40}\text{Ca}$ vs. Na/Ca plot (see dashed arrows in Fig. 4C). Specifically, halite dissolution only adds Na to the lagoon waters, but does not affect Ca concentrations or $\delta^{44/40}\text{Ca}$ values, which is thus at odds with our data. In contrast, carbonate precipitation is expected to change both parameters, i.e., increasing Na/Ca and $\delta^{44/40}\text{Ca}$, due to removal of Ca^{2+} and light ^{40}Ca isotopes from the lagoon waters, which is a trend that agrees with our water data from the South Lagoon (Fig. 4C).

Interestingly, our results also showed that the Lower Lakes are not a simple mixture of seawater and the River Murray water, as the lake water plot away from a theoretical mixing line for a river water and seawater end-members (RM-SW) (Fig. 4A). The lake waters must thus receive Sr also from additional freshwater source, which could be local groundwater as shown in Fig. 4A, in agreement with observed physical evidence for local groundwater discharge in the Coorong and Lower Lakes (Haese et al., 2008), and/or other small tributary sources from the Eastern Mount Lofty Ranges (Australian Water Environments, Ecological Associates and GHD Pty Ltd., 2011).

2.5.1.4 Water source mixing and apportionment

Below we use both salinity and elemental/isotope mass balance constraints to quantify the water

Table 4. The mass fractions of freshwater (X_{FW}) in the brackish North Lagoon waters observed in May 2015, using (i) salinity constraints, (ii) $^{87}\text{Sr}/^{86}\text{Sr}$ and Sr concentration, and (iii) $\delta^{44/40}\text{Ca}$ and Ca concentration.

The mass fraction of freshwater (X_{FW}) ¹		Based on Salinity constraints	Based on $^{87}\text{Sr}/^{86}\text{Sr}$ and Sr	Based on $\delta^{44/40}\text{Ca}$ and Ca
Mixing Scenarios	LL-SW	47%	44%	39%
	GW-SW	46%	88%	18%

¹ the FW components are LL and GW in both mixing scenarios, respectively.

source mixing and apportionment in the brackish North Lagoon (samples from 2015) and also in typical hypersaline South Lagoon waters. .

The mass fraction of freshwater in the brackish North Lagoon can be calculated from the decrease in salinity, using a salinity of 36.9 PSU for seawater (SW), 0.8 PSU for the Lower Lakes water (LL), and 1.2 PSU for groundwater (GW) (Table 3). The LL-SW mixing scenario yields a freshwater fraction of 47% (Table 4), suggesting that seawater was diluted with approximately equal amount of lake water in the North Lagoon in May 2015. A very similar freshwater fraction of 46% is calculated based on salinity data for the alternative GW-SW mixing scenario (Table 4).

To resolve which one of the above scenarios (LL-SW versus GW-SW) is more realistic, and to better quantify the amount and origin of freshwater in the Coorong, one can also use isotope mass balance constraints. These allow to calculate the mass fraction of freshwater (X_{FW}) in the mixture ($X_{FW} = M_{FW}/M_{MIX}$), based on the rearranged Eqs. 1 and 2:

$$X_{FW} = M_{FW}/M_{MIX} = C_{SW} [(^{87}\text{Sr}/^{86}\text{Sr})_{MIX} - (^{87}\text{Sr}/^{86}\text{Sr})_{SW}] / \{C_{FW} [(^{87}\text{Sr}/^{86}\text{Sr})_{FW} - (^{87}\text{Sr}/^{86}\text{Sr})_{MIX}] + C_{SW} [(^{87}\text{Sr}/^{86}\text{Sr})_{MIX} - (^{87}\text{Sr}/^{86}\text{Sr})_{SW}]\} \quad (\text{Eq. 3})$$

Similar approach can be used also for $\delta^{44/40}\text{Ca}$ and Ca concentration data to calculate the mass fractions of freshwater (X_{FW}) in the Coorong.

Importantly, these three different approaches give very similar fractions of freshwater derived from the Lower Lakes, and we therefore conclude that the barrage outflow from the lakes is the major source of freshwater during 2015 brackish event (in agreement with data plotted in Fig. 4B). In contrast, the calculated freshwater fractions for the GW-SW mixing scenario disagree with each other (Table 4), further corroborating that this mixing scenario is not realistic for our data set.

As for the restricted and hypersaline South Lagoon, we cannot use the salinity and $\delta^{44/40}\text{Ca}$ constraints for the calculation of in local lagoon waters due to the impacts from water evaporation and carbonate precipitation processes. Nevertheless, one can use Sr isotope constraints that are not sensitive to these processes, and this approach yields freshwater mass fractions of 41% and 85%, for LL-SW and GW-SW scenarios respectively.

2.5.2 Carbonate fluxes in the Coorong

2.5.2.1 Ca isotope systematics

The carbonate fluxes in the Coorong are mainly addressed by the $\delta^{44/40}\text{Ca}$, which is a sensitive indicator of carbonate precipitation, as the latter preferentially incorporates light Ca isotopes in CaCO_3 minerals (Gussone et al., 2005; Fantle and Tipper, 2014; Farkas et al. 2016). The process of carbonate precipitation can thus explain the systematically higher $\delta^{44/40}\text{Ca}$ values (+0.2 ‰) relative to Southern Ocean, observed in the hypersaline South Lagoon (Fig. 4C). There might be also minor impact from gypsum formation in the highly evaporated lagoon waters (Von der Borch, 1962; Fernandes and Tanner, 2009; Harouaka et al., 2014), since these Ca-bearing sulfate minerals also preferentially sequester lighter Ca isotopes (Gussone et al., 2005; Harouaka et al., 2014)

In addition, Ca isotopes in coastal waters are also sensitive to freshwater-seawater mixing due to the expected differences in $\delta^{44/40}\text{Ca}$ signatures for these isotopically contrasting water sources (Holmden et al., 2012; Fantle and Tipper, 2014). Such salinity- and water source-controlled behavior of the $\delta^{44/40}\text{Ca}$ is also confirmed by our data (Fig. 5), and a similar pattern has been observed in the published data from the coastal waters of the Florida Bay (Holmden et al., 2012, see cross-symbols in Fig. 5).

A comparison between $\delta^{44/40}\text{Ca}$ and salinity (PSU) in the Coorong waters suggests a systematic coupling between these two variables, expressed as statistically significant positive correlation ($R^2 = 0.974$, $p < 0.05$) (Fig. 5). Taking into account the characteristic $\delta^{44/40}\text{Ca}$ values of different water sources in earth surface environments (cf., Fantle and Tipper, 2014), the observed $\delta^{44/40}\text{Ca}$ variability in the North Lagoon waters (Fig. 5), including the brackish sample NL2 from 2015 with slightly lower $\delta^{44/40}\text{Ca}$, can be explained by a mixing between seawater (0.0‰) and continentally derived freshwaters (−0.77 to −0.84‰) (Fig. 5), see also data and the water apportionment calculation in Table 4.

2.5.2.2 Quantifying the fraction of Ca^{2+} removal in the South Lagoon due to CaCO_3 formation

To further quantify the plausible magnitudes of Ca removal in the South Lagoon, due to local carbonate precipitation, we explore here two approaches or fractionation models that rely on Ca concentration and isotope data measured in the lagoon waters and precipitated CaCO_3 minerals based on data from Table 3.

Rayleigh and Equilibrium Ca isotope fractionation models

Ca isotopes can be used to estimate the fraction of Ca^{2+} removed in the South Lagoon by CaCO_3 precipitation using *Rayleigh* and/or *equilibrium* models. These models assume a closed-system behavior of Ca isotopes in a reservoir, which is a reasonable approximation for the highly restricted hydrological setting of the South Lagoon.

To apply these models, one has to constrain the initial $\delta^{44/40}\text{Ca}$ value of the South Lagoon water, which

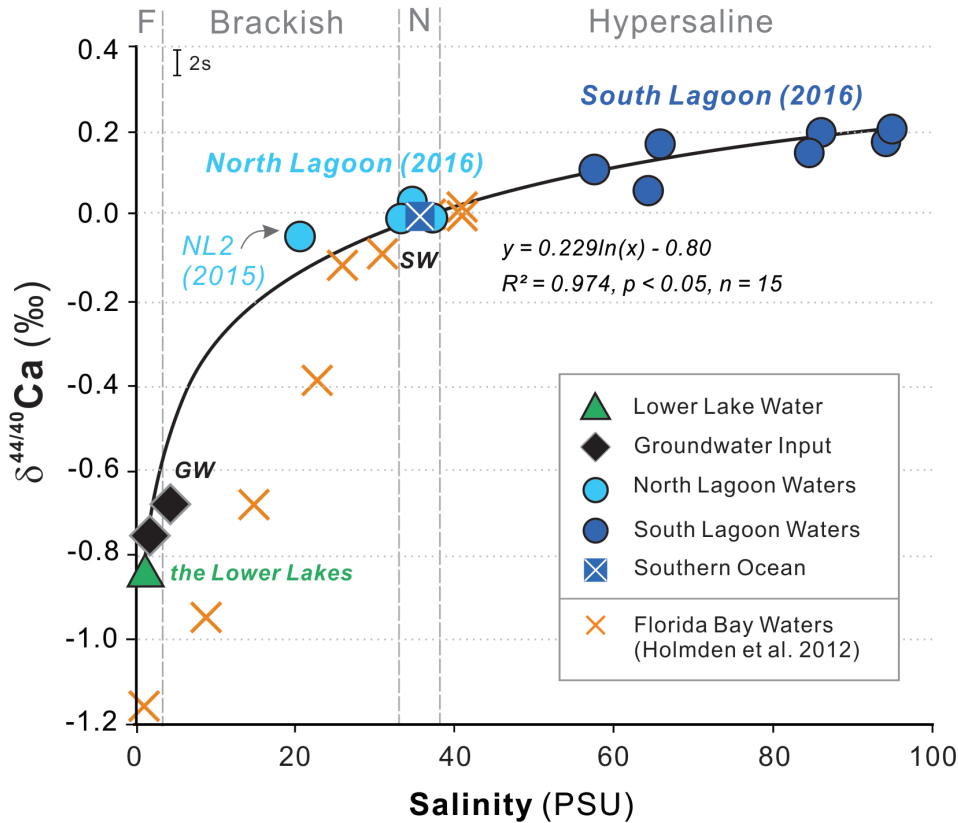


Figure 5: $\delta^{44/40}\text{Ca}$ of waters from the Coorong, Lower Lakes, and Murray Mouth hydrological system, which cover a wide range of water salinities (i.e., fresh, brackish, marine and hypersaline) and show a logarithmic correlation pattern; complemented by the published data from waters collected in the Florida Bay (Holmden et al., 2012). The following abbreviations are used: F = Freshwater; N = Normal Marine; SW = Seawater; and GW = Groundwater.

assume no precipitation of CaCO_3 minerals, as a hypothetical starting point for the models. Such initial $\delta^{44/40}\text{Ca}$ can be calculated from theoretical mixing trends for Sr and Ca isotopes in South Lagoon, and the corresponding $^{87}\text{Sr}/^{86}\text{Sr}$ signature measured in the South Lagoon waters, as the latter is not expected to be impacted by carbonate precipitation (for details see Fig. 6). The two hypothetical mixing scenarios, LL-SW and GW-SW, are shown in Fig. 6, each yields very different initial $\delta^{44/40}\text{Ca}$ values: -0.05‰ for the LL-SW, and -0.44‰ for the GW-SW mixing scenario. In the following calculations, we use both of these initial $\delta^{44/40}\text{Ca}$ values, to illustrate the range of plausible Ca^{2+} removal fractions in the South Lagoon.

The *Rayleigh* model assumes a finite pool of Ca in the South Lagoon where precipitated carbonate minerals (i.e., product) once formed would not interact with the seawater or lagoon water (i.e., reactant). In such a system, the fractionation of Ca isotopes between the reactant and product can be described by the *Rayleigh distillation* (Frings et al., 2016), according to the following equation:

$$\delta^{44/40}\text{Ca} = [(\delta^{44/40}\text{Ca}_{\text{INI}} + 10^3) (1 - f_{\text{CC}})^{(\alpha_{\text{CC/SW}} - 1)}] - 10^3 \quad (\text{Eq. 4})$$

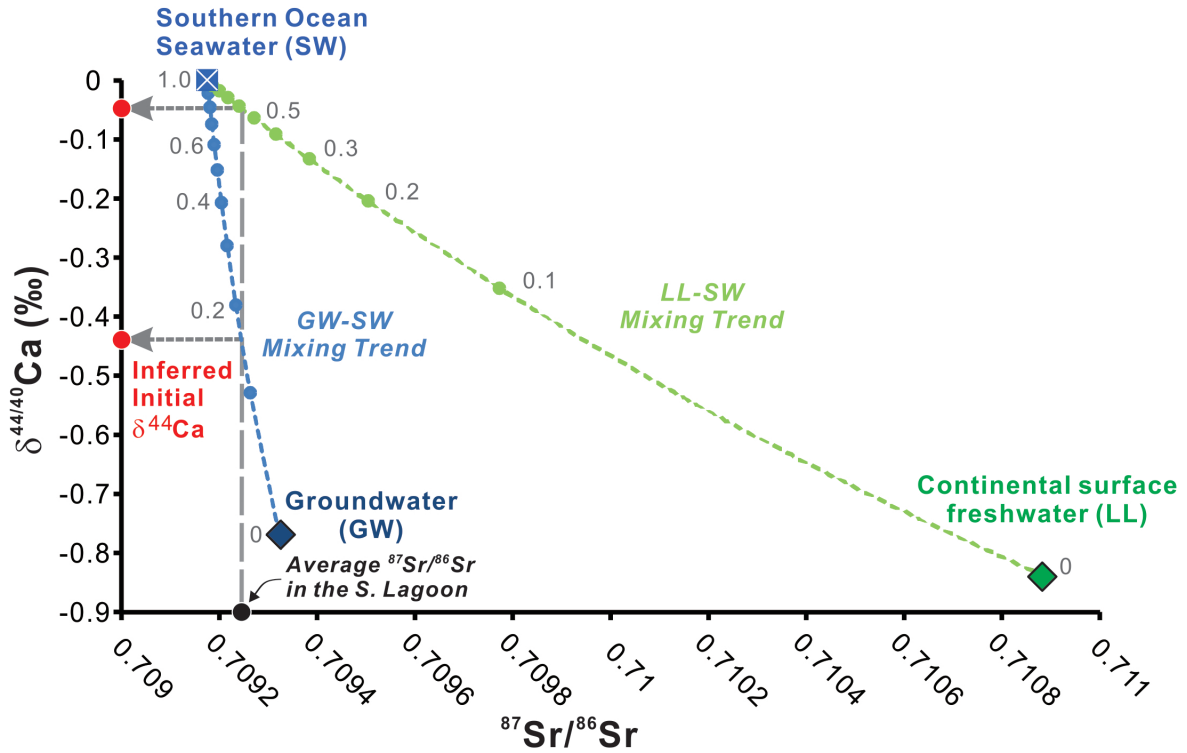


Figure 6: Theoretical mixing trends for $\delta^{44/40}\text{Ca}$ and $^{87}\text{Sr}/^{86}\text{Sr}$ tracers in the Coorong, calculated for the following end-members: normal seawater (SW), groundwater (GW), and the continental surface freshwater represented by the Lower Lakes water (LL), assuming no evaporation and/or additional carbonate formation in the system. Note that the numbers next to circles represent the calculated fractions of seawater (FSW) in the mixtures; and red circles illustrate the expected ‘initial’ $\delta^{44/40}\text{Ca}$ of the South Lagoon waters for GW-SW and LL-SW scenarios (based on $^{87}\text{Sr}/^{86}\text{Sr}$ constraints), not impacted by additional carbonate precipitation in the lagoon.

where $\delta^{44/40}\text{Ca}$ represents the isotope value of a residual unreacted Ca^{2+} pool in the lagoon waters; $\delta^{44/40}\text{Ca}_{\text{INI}}$ is the *initial* $\delta^{44/40}\text{Ca}$ value derived from Fig. 6; and f_{CC} represents the fraction of Ca that was removed from the measured lagoon waters (i.e., reactant) as CaCO_3 minerals (i.e., product), and solving Eq. 4 gives:

$$f_{\text{CC}} = 1 - (\alpha_{\text{CC/SW}}^{-1}) \sqrt{(\delta^{44/40}\text{Ca} + 10^3) / (\delta^{44/40}\text{Ca}_{\text{INI}} + 10^3)} \quad (\text{Eq. 5})$$

finally, the parameter $\alpha_{\text{CC/SW}}$ is the Ca isotope fractionation factor between carbonate minerals (CC) and lagoon waters or seawaters (SW) (Frings et al., 2016), calculated by:

$$\alpha_{\text{CC/SW}} = (1 + \delta^{44/40}\text{Ca}_{\text{CC}}/1000) / (1 + \delta^{44/40}\text{Ca}_{\text{MIX}}/1000) = (1000 + \delta^{44/40}\text{Ca}_{\text{CC}}) / (1000 + \delta^{44/40}\text{Ca}_{\text{MIX}}) \quad (\text{Eq. 6})$$

where $\delta^{44/40}\text{Ca}_{\text{CC}}$ is the Ca isotope value of the precipitated CaCO_3 mineral, and $\delta^{44/40}\text{Ca}_{\text{MIX}}$ refers to the lagoon water (+0.2‰). According to Gussone et al. (2005), and taking into account the average water temperature in Coorong lagoons of $\sim 17.5^\circ\text{C}$, the $\delta^{44/40}\text{Ca}_{\text{CC}}$ for two CaCO_3 polymorphs of *aragonite* and *calcite* would be -1.65‰ and -0.75‰ , respectively. These give the $\delta^{44/40}\text{Ca}_{\text{MIX}}$ values of ~ -0.9984 for *aragonite* and ~ -0.9993 for *calcite*. Based on our isotope measurements of the sediment

crust sample (CLS-1) from the South Lagoon, the difference between $\delta^{44/40}\text{Ca}$ of the sediment sample (-1.16‰) and the lagoon waters ($+0.20\text{‰}$) is -1.36‰ . This in turn, corresponds to an $\alpha_{\text{CC/SW}}$ value of ~ 0.9986 , in agreement with the predominant aragonite precipitation.

The *equilibrium* model, on the other hand, describes a system with a finite pool of Ca in which the reactant and products interact and exchange Ca isotopes as carbonates are precipitated (Frings et al., 2016). In this case, the following expression applies for the calculation of the $\delta^{44/40}\text{Ca}$ value in lagoon water as a function of changing f_{CC} parameter (cf., Sigman et al., 2009; Frings et al., 2016):

$$\delta^{44/40}\text{Ca} = \delta^{44/40}\text{Ca}_{\text{INI}} + \varepsilon f_{\text{CC}} \quad (\text{Eq. 7})$$

where ε is the fractionation *isotope effect*, which is related to the abovementioned $\alpha_{\text{CC/SW}}$ based on the following equation:

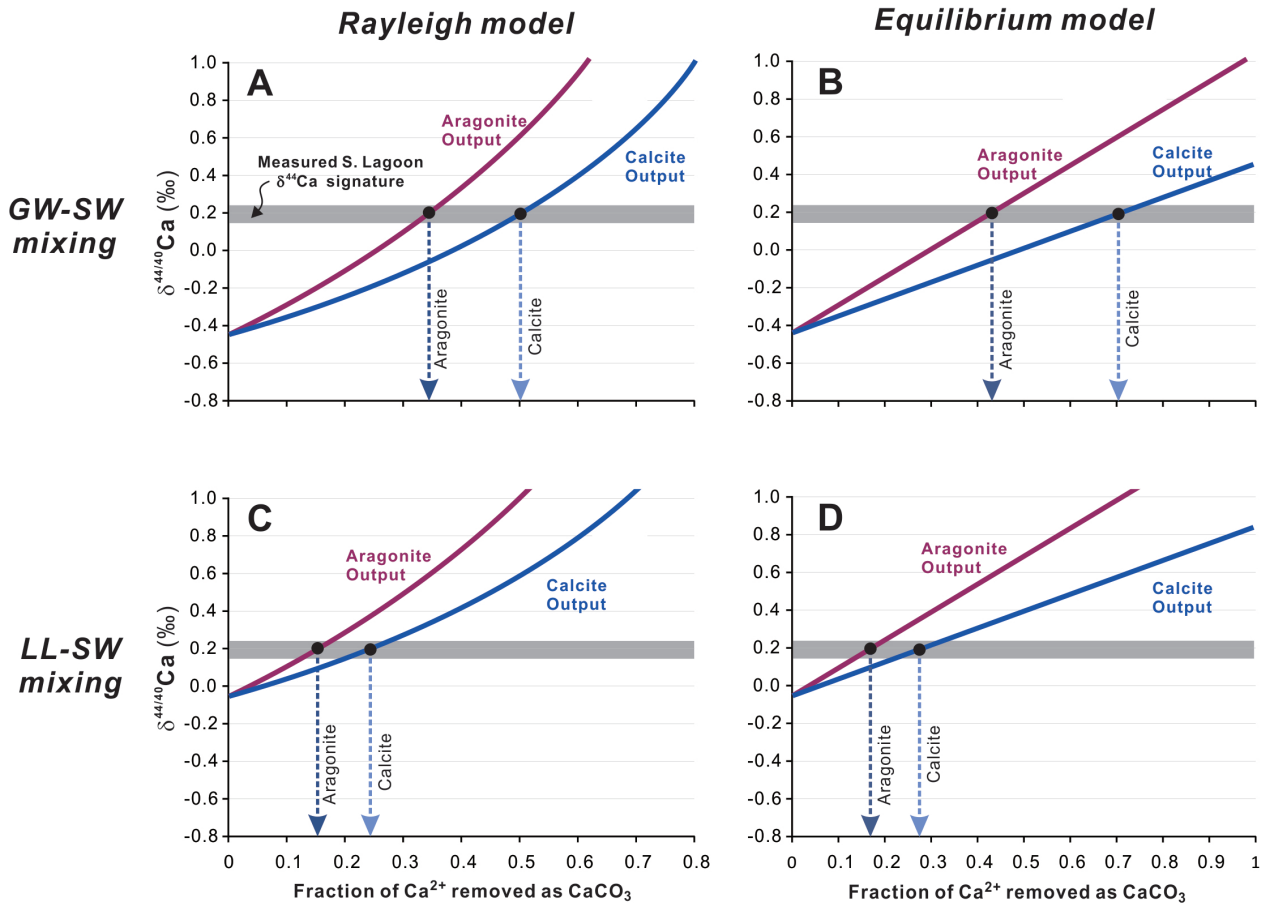


Figure 7: The groundwater-seawater (GW-SW) and continental surface freshwater-seawater (LL-SW) mixing scenarios for the quantification of Ca^{2+} removal and carbonate output in the South Lagoon: (A) (C) The *Rayleigh* model for Ca isotopes in lagoon waters, driven by increasing carbonate precipitation in the South Lagoon, assuming no interaction between precipitated carbonate (i.e. product) and lagoon waters (i.e., reactant), modeled for *aragonite* and *calcite* carbonate outputs. (B) (D) The *equilibrium* model for the South Lagoon, assuming an exchange and interactions between the product (CaCO_3) and reactant (lagoon waters), modeled for both *aragonite* and *calcite* scenarios. The gray band represents the observed $\delta^{44/40}\text{Ca}$ in the South Lagoon waters.

$$\varepsilon = -10^3 (\alpha_{\text{CC/SW}} - 1) \quad (\text{Eq. 8})$$

Accordingly, the f_{CC} can be calculated based on:

$$f_{\text{CC}} = (\delta^{44/40}\text{Ca} - \delta^{44/40}\text{Ca}_{\text{INI}}) / [-10^3 (\alpha_{\text{CC/SW}} - 1)] \quad (\text{Eq. 9})$$

Considering the GW-SW and LL-SW mixing scenarios, the modeled evolution curves for $\delta^{44/40}\text{Ca}$ in the South Lagoon waters based on the two Ca isotope fractionation models above are illustrated in Fig. 7. Based on the measured $\delta^{44/40}\text{Ca}$ of the hypersaline South Lagoon waters (+0.2‰) and the fact that aragonite is the major carbonate precipitate, the calculated fractions of Ca^{2+} removed in the South Lagoon as CaCO_3 (as aragonite) range from ~15% and ~45% (Fig. 7). These estimates are also in general agreement with mass balance calculations based on Ca concentration and salinity and constraints from the carbonate alkalinity of local lagoon waters (see Appendix, section B.4). Importantly, these supplementary calculations suggest that a more realistic fraction is actually closer to ~15% (rather than 45%), thus points to the importance of LL-SW mixing, or continental freshwater inputs into the South Lagoon.

2.5.2.3 The local carbon cycling in the Coorong

The quantification of Ca^{2+} removal in the Coorong has also implications for the local carbon cycling, as our data suggest that the hypersaline South Lagoon acts as a sink for the dissolved inorganic carbon (DIC) present in the lagoon waters, based on the simplified equation for the marine carbonate formation:



Taking the buffering capacity of seawater or seawater-like solutions (Zeebe and Wolf-Gladrow, 2001) into consideration, a large proportion of this liberated CO_2 is actually converted to bicarbonate (HCO_3^-). Specifically, under typical surface ocean conditions that are in contact with the present-day atmospheric CO_2 pressure, the precipitation of 1 mol of CaCO_3 yields only about 0.6 mol of CO_2 (Ware et al., 1992; Elderfield, 2006), with remaining C being converted to dissolved C species (0.4 mol as HCO_3^-), and therefore not released into the atmosphere. Thus, if applicable to the Coorong, this would suggest that with each mole of dissolved Ca^{2+} that is removed as aragonite and/or calcite approximately 1.4 mols of carbon is also fixed in the system (i.e., 1 mol of C in CaCO_3 mineral, and ~0.4 mol of C in the produced HCO_3^- species), with remaining ~0.6 mol being outgassed as CO_2 from the lagoon into the atmosphere. Overall, these theoretical constraints coupled with our Ca isotope data suggest that the South Lagoon acts as a net sink for the dissolved inorganic carbon due to the locally enhanced precipitation of CaCO_3 minerals in the hypersaline and carbonate-oversaturated lagoon waters.

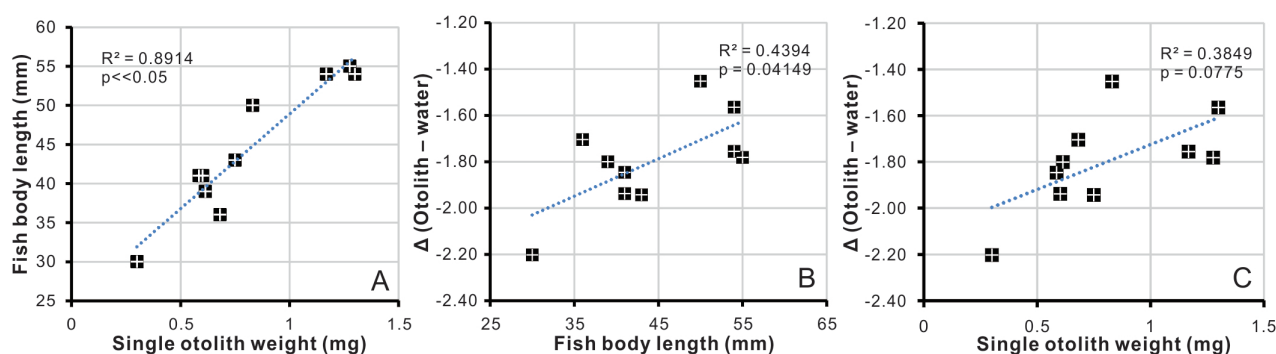


Figure 8: Correlations of fish size parameters (i.e. fish body length and single otoliths weight) with otoliths $\delta^{44/40}\text{Ca}$ values: (A) Fish body length vs. single otoliths weight; (B) Fractionation factor Δ of $\delta^{44/40}\text{Ca}$ between otoliths and lagoon water of the same sampling site vs. fish body lengths; (C) Fractionation factor Δ vs. single otoliths weight. In chart (B) and (C), $\delta^{44/40}\text{Ca}$ for sites C07, C08 and C09 in South Lagoon were estimated by linear interpolation of $\delta^{44/40}\text{Ca}$ values measured in waters from the most proximal sites, and Δ values were then calculated.

2.5.3 Fish migration and otoliths biomineralisation: Insights from Ca and Sr isotopes

2.5.3.1 $^{87}\text{Sr}/^{86}\text{Sr}$ in otoliths: A time-integrated signature of local water masses?

$^{87}\text{Sr}/^{86}\text{Sr}$ in fish otoliths of migratory species are interpreted as historical records of the movement of individual fish (Chesney et al., 1998; Brennan et al., 2015a, b). As for less mobile species such as *A. microstoma* in the Coorong, the observed $^{87}\text{Sr}/^{86}\text{Sr}$ in otoliths relative to those measured in ambient lagoon waters (Fig. 2B) could be viewed as an integrated signal of the environmental history of local water masses over the entire lifespan of a fish (ca. 1 year period; see Gillanders and Munro, 2012; Wedderburn et al., 2014, and references therein). Accordingly, otolith data indicate that there is an overall higher input of continent-derived freshwater sources with higher $^{87}\text{Sr}/^{86}\text{Sr}$ into the North Lagoon, compared to our estimates that are based only on ‘snap-shot’ sampling of waters performed in 2015 and 2016. Alternatively, our otolith $^{87}\text{Sr}/^{86}\text{Sr}$ data might suggest that fish collected in the North Lagoon have spent a significant portion of their life in the hypersaline South Lagoon with higher $^{87}\text{Sr}/^{86}\text{Sr}$, and moved to the North Lagoon waters where they were caught and sampled.

We tried to address these questions via micro-drilling selected otoliths for the Sr isotope analysis along the growth increments (i.e., core and edge $^{87}\text{Sr}/^{86}\text{Sr}$ record). Theoretically, the $^{87}\text{Sr}/^{86}\text{Sr}$ of core (i.e., juvenile part) and edge (i.e., more recent) of an otolith should reflect the local water composition of the years 2015 and 2016, respectively, given the fish sampled was large and old enough. However, the core and edge $^{87}\text{Sr}/^{86}\text{Sr}$ of the North Lagoon otolith is constantly higher than the local water, this points to some of the complexities of interpreting otolith $^{87}\text{Sr}/^{86}\text{Sr}$ records in terms of fish migration patterns. Nevertheless, the North Lagoon otolith shows a lower edge $^{87}\text{Sr}/^{86}\text{Sr}$ value than that of the otolith core, this trend matches the observed temporal decline in local water $^{87}\text{Sr}/^{86}\text{Sr}$ over one year (from 2015 to 2016). On the other hand, the core and edge $^{87}\text{Sr}/^{86}\text{Sr}$ pattern acquired from another larger otolith (sample C10-03), collected from the South Lagoon, showed an opposite trend where the

$^{87}\text{Sr}/^{86}\text{Sr}$ value from the edge is higher than the core (see Fig 2B), perhaps suggesting that the former was inherited from the highly radiogenic waters present at the southern-most end of the lagoon.

2.5.3.2 $\delta^{44/40}\text{Ca}$ in otoliths: The role of 'kinetics' and biomineralisation

The lack of correlation between the $\delta^{44/40}\text{Ca}$ of otoliths and local lagoon waters indicates that biomineralisation processes rather than water mixing and/or fish migration are primarily responsible for the otoliths' Ca isotope composition. However, as light Ca isotopes are preferentially incorporated during otolith biomineralisation, the $\delta^{44/40}\text{Ca}$ of otoliths might be potentially used to infer changes in otoliths growth rates. To better visualise the fractionation of Ca isotopes in the otoliths relative to ambient lagoon waters, the fractionation factor Δ is used here, and this parameter reflects the difference between $\delta^{44/40}\text{Ca}$ of otolith and local waters at the same sampling site. In Fig. 8, we plot the Ca isotope fractionation factor, Δ (otolith-water), as a function of the fish size parameters, including (i) fish body length, and (ii) the otolith's weight.

Otolith size is proportional to fish body length ($R^2 = 0.8914$, $p < 0.05$) (Fig. 8A), but data also indicate the large (more mature) fish yield smaller fractionations (i.e. less negative Δ) in otoliths. In contrast, small (juvenile) fish yielded larger fractionations (i.e. more negative Δ) ($R^2 = 0.44$, $p < 0.08$, $n = 10$) (Fig. 8B, C). This correlation between the fish/otolith size (or weight) and the Δ values likely reflect kinetic Ca isotope fractionation effects, where juvenile fish otoliths grows at faster rates during early life stages, thus preferentially incorporating lighter Ca isotopes, therefore producing larger isotope fractionations (Tang et al., 2008; Fantle and Tipper, 2014; AlKhatib and Eisenhauer, 2017).

Although further validation is required, our $\delta^{44/40}\text{Ca}$ data from otoliths suggest an overall strong biological control related to growth rate effects. As elemental/Ca concentration patterns in fish otoliths are also related to the latter biological processes (Grønkvær, 2016; Izzo et al., 2018), future Ca isotopes studies coupled with elemental proxies might help to differentiate signals originating from (i) biological processes (i.e., changes in growth or precipitation rates of otoliths), and those imparted by (ii) distinct water masses with unique elemental and isotope signatures (i.e., fish migration signal).

2.5.4 Implications for palaeo-salinity reconstructions of lagoon-estuarine environments based on coupled $^{87}\text{Sr}/^{86}\text{Sr}$ and $\delta^{44/40}\text{Ca}$

To illustrate the potential of the above isotope proxies for palaeo-studies, we plot here $^{87}\text{Sr}/^{86}\text{Sr}$ and $\delta^{44/40}\text{Ca}$ of waters against their respective salinities (from 0 to ~120 PSU, Fig. 9). This approach shows the potential and limitations of these isotope proxies for palaeo-salinity studies of the Coorong, Lower Lakes, and Murray Mouth Estuary.

As shown in Fig. 9A, the Coorong have three major water components, which are (i) normal marine waters, (ii) fresh/brackish waters, and (iii) the chemically/isotopically evolved hypersaline lagoon waters, the last type was present primarily in the South Lagoon. Solely based on $^{87}\text{Sr}/^{86}\text{Sr}$, one can dis-

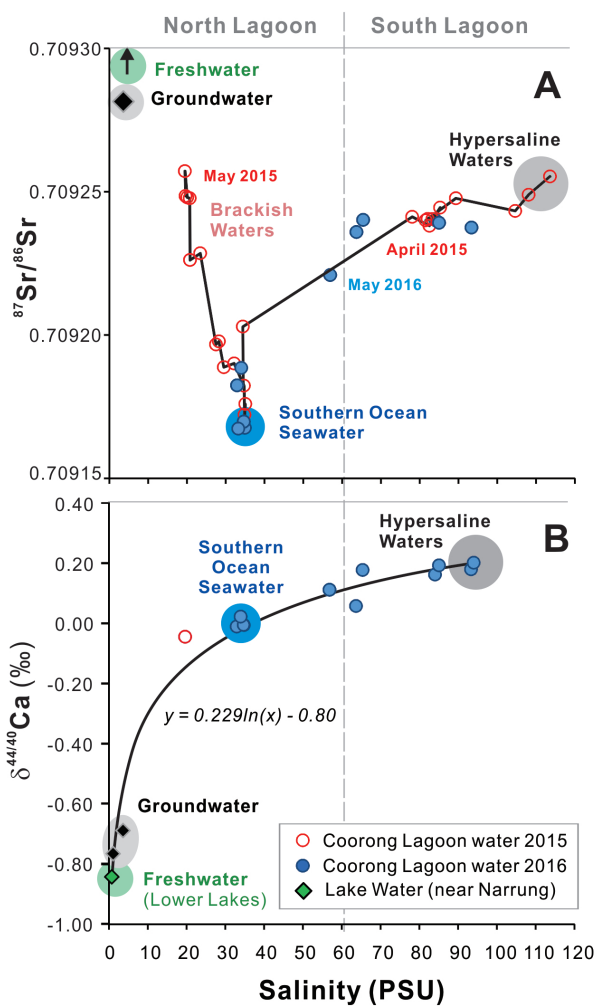


Figure 9: Summary charts illustrating water mixing trends in the Coorong hydrological system: (A) $^{87}\text{Sr}/^{86}\text{Sr}$ versus salinity plot showing the main end-members and water sources; note that the Lower Lake and River Murray samples were too high to be plotted on the scale. (B) $\delta^{44/40}\text{Ca}$ versus salinity plot for the main end-members and studied water samples. The three colored circles represent the main end-member or water sources: (i) the local groundwater, (ii) normal seawater, and (iii) hypersaline lagoon waters.

tinguish less radiogenic ‘normal marine waters’ from more radiogenic waters impacted by continental water sources. However, the Sr isotope data cannot distinguish between the brackish and the hypersaline lagoon waters, as both yielded equally high $^{87}\text{Sr}/^{86}\text{Sr}$, plot above the typical Southern Ocean seawater (Fig. 9A). Importantly, this inability of Sr isotopes, can be resolved with

the application of $\delta^{44/40}\text{Ca}$ (Fig. 9B), because the hypersaline waters have systematically positive $\delta^{44/40}\text{Ca}$ of up to $+0.20\text{‰}$, compared to normal seawater ($0.00 \pm 0.05\text{‰}$), while the freshwater sources yielded very negative $\delta^{44/40}\text{Ca}$ as low as $-0.84 \pm 0.03\text{‰}$ (Fig. 9B).

Thus, with analyses in suitable carbonate archives, a multi-proxy approach combining both $^{87}\text{Sr}/^{86}\text{Sr}$ and $\delta^{44/40}\text{Ca}$ tracers can be used to reconstruct palaeo-salinity changes in the Coorong over geological time. Moreover, this approach should be generally applicable to other carbonate-producing coastal lagoon-estuarine environments and their salinity reconstructions.

2.6 Conclusions

The Sr and Ca isotopes applied in this study illustrate that the Coorong hydrological system has three major water components, including: (i) local freshwaters (i.e., River Murray and groundwater), (ii) the Southern Ocean seawater, and (iii) hypersaline lagoon waters, the latter additionally modified by ongoing evaporation, and in-situ carbonate precipitation.

The $\delta^{44/40}\text{Ca}$, $^{87}\text{Sr}/^{86}\text{Sr}$ and salinity data from the North Lagoon waters are basically indistinguishable from those in the Southern Ocean (i.e., normal seawater), with the exception of transient freshwater input events, such as the one documented in May 2015. The latter had caused a shift to more brackish salinity (~ 20 PSU) in parts of the lagoon, which based on our isotope constraints was a consequence of ‘trapped’ barrage outflow sourced from the Lower Lakes, with some although minor contributions from local

groundwater. Interestingly, the South Lagoon hypersaline waters are much more complex in terms of their origins and mixing histories, and our mass balance constraints showed that they are basically highly evaporated brackish waters (with $\geq 40\%$ contribution from originally continent-derived waters), and their chemistries have been additionally modified via ongoing carbonate precipitation. These processes, i.e., the CaCO_3 formation and inputs of continent-derived Sr, have led to a systematic shift of the South Lagoon waters to higher $\delta^{44/40}\text{Ca}$ and $^{87}\text{Sr}/^{86}\text{Sr}$ values relative to the Southern Ocean seawater. Based on the Ca isotope constraints (i.e., *Rayleigh* and *equilibrium* models), the plausible fraction of the Ca removed in the South Lagoon due to in-situ carbonate precipitation (mostly as aragonite) is about 15 to 17% of the original Ca pool present in the lagoon. This in turn has implications for the blue carbon studies and local C cycling in the South Lagoon, suggesting that the latter acts as a net sink for the dissolved inorganic carbon (DIC), due to the ongoing CaCO_3 formation.

Ca isotope data from smallmouth hardyhead (*Atherinosoma microstoma*), indicate that $\delta^{44/40}\text{Ca}$ in otoliths is primarily controlled by biological process (i.e., the kinetic growth rate effects). Thus future Ca isotopes studies on otoliths coupled with trace-element data might help to differentiate ‘signals’ originating from (i) biological processes (i.e., changes in growth rates of otoliths), and those imparted by (ii) distinct water masses with unique elemental and isotope signatures (i.e., fish migration signal). Additionally, the $^{87}\text{Sr}/^{86}\text{Sr}$ record of otoliths confirmed the importance of continent-derived water sources to the Coorong over the life span of the fish.

Overall, our calibration of $^{87}\text{Sr}/^{86}\text{Sr}$ and $\delta^{44/40}\text{Ca}$ based on two sets of data mainly from 2015 and 2016 proxies provides spatial variations of water chemistry in the modern Coorong hydrological system, with respect to salinity and CaCO_3 saturation. Further studies focusing on temporal variations are necessary for a more complete understanding of the modern hydrology of Coorong. Nevertheless, such multi-proxy approach combining Sr and Ca isotopes measured in suitable fossil carbonate archives (e.g., bivalve shells, foraminifera) could potentially be used to (i) trace and apportion different water sources, (ii) quantify local carbonate output, and/or (ii) to reconstruct palaeo-salinity changes at our study site, or other carbonate-producing lagoon-estuarine environments.

Acknowledgments

This project was supported by the Czech Science Foundation (GACR grant No. 17-18120S), the Environment Institute and a start-up grant of the University of Adelaide to JF; and via the ARC research support to BMG. Additional support from the Base-Line Earth project (ITN MC Horizon 2020, grant agreement No. 643084), and the ARC Linkage project LP160101353 are also acknowledged. Fundação para a Ciência e Tecnologia via UID/MAR/04292/2013 and the SFRH/BPD/95784/2013 grant awarded to PRS also supported this work. This study is part of the Ph.D. research of YS, supported by Adelaide Graduate Research Scholarships.

The sampling in the Coorong National Park was performed under the Department for Environment, Water and Natural Resources (DEWNR) research permit No. Q26018-5. The water quality data provided by the DEWNR is gratefully acknowledged. Technical and laboratory assistance of David Bruce and Tony Hall at University of Adelaide is greatly appreciated, especially regarding the training sessions, and the maintenance of TIMS and clean laboratory facilities. We also thank Aoife McFadden for her assistance with the elemental analyses by ICP-MS at the Adelaide Microscopy Centre. Finally, Prof. Justin Brookes at the University of Adelaide is acknowledged for his assistance with obtaining water samples in the North Lagoon.

References

- AlKhatib, M. and Eisenhauer, A. (2017) Calcium and strontium isotope fractionation during precipitation from aqueous solutions as a function of temperature and reaction rate; II. Aragonite. *Geochimica et Cosmochimica Acta* **209**, 320-342.
- Anadón, P., Gliozzi, E. and Mazzini, I. (2002) Paleoenvironmental reconstruction of marginal marine environments from combined paleoecological and geochemical analyses on ostracods. *GEOPHYSICAL MONOGRAPH-AMERICAN GEOPHYSICAL UNION* **131**, 227-248.
- Australian Water Environments, Ecological Associates and GHD Pty Ltd. (2011). *Environmental water delivery: River Murray—Coorong, Lower Lakes and main channel below Lock 1*. Prepared for Commonwealth Environmental Water, Department of Sustainability, Environment, Water, Population and Communities. ISBN: 978-1-921733-37-6.
- Barnett, S. (2015) Assessment of the groundwater resources in the non-prescribed areas of the South Australian Murray-Darling Basin, DEWNR Technical report 2015/09, Government of South Australia, Department of Environment, Water and Natural Resources, Adelaide. ISBN: 978-1-922255-47-1.
- Baskaran, M. (2012) Handbook of Environmental Isotope Geochemistry, Springer, Heidelberg. pp. 951. Springer-Verlag, Berlin. ISBN: 3642106366.
- Brennan, S. R., Fernandez, D. P., Zimmerman, C. E., Cerling, T. E., Brown, R. J. and Wooller, M. J. (2015a) Strontium isotopes in otoliths of a non-migratory fish (slimy sculpin): Implications for provenance studies. *Geochimica et Cosmochimica Acta* **149**, 32-45.
- Brennan, S. R., Zimmerman, C. E., Fernandez, D. P., Cerling, T. E., McPhee, M. V. and Wooller, M. J. (2015b) Strontium isotopes delineate fine-scale natal origins and migration histories of Pacific salmon. *Science advances* **1**, e1400124.
- Cao, Z., Siebert, C., Hathorne, E. C., Dai, M. and Frank, M. (2016) Constraining the oceanic barium

cycle with stable barium isotopes. *Earth and Planetary Science Letters* **434**, 1-9.

Chesney, E. J., McKee, B. M., Blanchard, T. and Chan, L. H. (1998) Chemistry of otoliths from juvenile menhaden *Brevoortia patronus*: evaluating strontium, strontium: calcium and strontium isotope ratios as environmental indicators. *Marine Ecology Progress Series*, 261-273.

Dickin, A. P. (2005) *Radiogenic Isotope Geology*. Cambridge University Press. pp. 508. ISBN 0521823161.

Elderfield, H. (2006) *The oceans and Marine Geochemistry*, Vol. 6., *Treatise on Geochemistry* (eds. H.D. Holland and K.K. Turekian), Elsevier-Pergamon, Oxford.

Fantle, M. S. and DePaolo, D. J. (2007) Ca isotopes in carbonate sediment and pore fluid from ODP Site 807A: the Ca²⁺(aq)-calcite equilibrium fractionation factor and calcite recrystallization rates in Pleistocene sediments. *Geochimica et Cosmochimica Acta* **71**, 2524-2546.

Fantle, M. S. and Tipper, E. T. (2014) Calcium isotopes in the global biogeochemical Ca cycle: Implications for development of a Ca isotope proxy. *Earth-Science Reviews* **129**, 148-177.

Fantle, M. S. (2015) Calcium isotopic evidence for rapid recrystallization of bulk marine carbonates and implications for geochemical proxies. *Geochimica et Cosmochimica Acta* **148**, 378-401.

Farkaš, J., Déjeant, A., Novák, M., and Jacobsen, S. B. (2011) Calcium isotope constraints on the uptake and sources of Ca²⁺ in a base-poor forest: a new concept of combining stable ($\delta^{44/42}\text{Ca}$) and radiogenic (ϵCa) signals. *Geochimica et Cosmochimica Acta*, **75**, 7031–7046.

Farkaš, J., Frýda, J., and Holmden, C. (2016) Calcium isotope constraints on the marine carbon cycle and CaCO₃ deposition during the late Silurian (Ludfordian) positive $\delta^{13}\text{C}$ excursion. *Earth and Planetary Science Letters* **451**, 31-40.

Fernandes, M. and Tanner, J. E. (2009) *Hypersalinity and phosphorus availability: the role of mineral precipitation in the Coorong lagoons of South Australia*. CSIRO Water for a Healthy Country.

Frank, M. (2011) Geochemical proxies for ocean circulation and weathering inputs: Radiogenic isotopes of Nd, Pb, Sr, Hf, and Os. *IOP Conf, Series: Earth and Environmental Science* **14**, 1-7. IOP Publishing. DOI: 10.1088/1755-1315/14/1/012010.

Frings, P. J., Clymans, W., Fontorbe, G., Christina, L. and Conley, D. (2016) The continental Si cycle and its impact on the ocean Si isotope budget. *Chemical Geology* **425**, 12-36.

Gemitzi, A., Stefanopoulos, K., Schmidt, M. and Richnow, H. H. (2014) Seawater intrusion into groundwater aquifer through a coastal lake-complex interaction characterised by water isotopes ²H and ¹⁸O. *Isotopes in environmental and health studies* **50**, 74-87.

- Gillanders, B. M. and Munro, A. R. (2012) Hypersaline waters pose new challenges for reconstructing environmental histories of fish based on otolith chemistry. *Limnology and Oceanography* **57**, 1136.
- Grønkjær, P. (2016) Otoliths as individual indicators: a reappraisal of the link between fish physiology and otolith characteristics. *Marine and Freshwater Research* **67**, 881-888.
- Gussone, N., Boehm, F., Eisenhauer, A., Dietzel, M., Heuser, A., Teichert, B.M. and Dullo, W.C. (2005) Calcium isotope fractionation in calcite and aragonite. *Geochimica et cosmochimica acta* **69**, 4485-4494.
- Haese, R. R., Gow, L., Wallace, L. and Brodie, R. S. (2008) Identifying groundwater discharge in the Coorong (South Australia). *AUSGEO news* **91**, 1-6.
- Haese, R. R., Wallace, L. and Murray, E. J. (2009) *Nutrient sources, water quality, and biogeochemical processes in the Coorong, South Australia*. Geoscience Australia.
- Harouaka, K., Eisenhauer, A., and Fantle, M. (2014) Experimental investigation of Ca isotope fractionation during abiotic gypsum precipitation. *Geochimica et Cosmochimica Acta*, **129**, 157-176.
- Harouaka, K., Mansor, M., Macalady, J. L. and Fantle, M. S. (2016) Calcium isotopic fractionation in microbially mediated gypsum precipitates. *Geochimica et Cosmochimica Acta* **184**, 114-131.
- Hendry, J. P. and Kalin, R. M. (1997) Are oxygen and carbon isotopes of mollusc shells reliable palaeosalinity indicators in marginal marine environments? A case study from the Middle Jurassic of England. *Journal of the Geological Society* **154**, 321-333.
- Holmden, C., Creaser, R.A. and Muehlenbachs, K. (1997) Paleosalinities in ancient brackish water systems determined by $^{87}\text{Sr}/^{86}\text{Sr}$ ratios in carbonate fossils: A case study from the Western Canada Sedimentary Basin. *Geochimica et Cosmochimica Acta* **61**, 2105-2118.
- Holmden, C., and Hudson J. D. (2003) $^{87}\text{Sr}/^{86}\text{Sr}$ and Sr/Ca investigation of Jurassic molluscs from Scotland: Implications for paleosalinities and the Sr/Ca ratio of seawater. *Geological Society of America Bulletin* **115**, 1249–1264.
- Holmden, C. (2005) Measurement of $\delta^{44}\text{Ca}$ using a ^{43}Ca - ^{42}Ca double-spike TIMS technique. In *Summary of Investigations 2005*, Vol. 1, Saskatchewan Geological Survey, Sask. Industry Resources, Misc. Rep. 2005-1, CD-ROM, Paper A-4, 7p.
- Holmden, C. and Bélanger, N. (2010) Ca isotope cycling in a forested ecosystem. *Geochimica et cosmochimica acta* **74**, 995-1015.
- Holmden, C., Papanastassiou, D. A., Blanchon, P., Evans, S. (2012) $\delta^{44/40}\text{Ca}$ variability in shallow water carbonates and the impact of submarine groundwater discharge on Ca-cycling in marine environments. *Geochim. Cosmochim. Acta* **83**, 179–194.

- Izzo, C., Reis-Santos, P. and Gillanders, B. M. (2018) Otolith chemistry does not just reflect environmental conditions: A meta-analytic evaluation. *Fish and Fisheries*, 1–14. <https://doi.org/10.1111/faf.12264>.
- Kjerfve, B. (1986) Comparative oceanography of coastal lagoons. In: *Estuarine variability* (ed. D. A. Wolf) Academic Press, New York, USA, p. 63-81.
- Knoppers, B. (1994) Aquatic primary production in coastal lagoons. *Elsevier Oceanography Series* **60**, 243-286.
- Krabbenhöft, A., Fietzke, J., Eisenhauer, A., Liebetrau, V., Böhm, F. and Vollstaedt, H. (2009) Determination of radiogenic and stable strontium isotope ratios ($^{87}\text{Sr}/^{86}\text{Sr}$; $\delta^{88/86}\text{Sr}$) by thermal ionization mass spectrometry applying an $^{87}\text{Sr}/^{84}\text{Sr}$ double spike. *Journal of Analytical Atomic Spectrometry* **24**, 1267-1271.
- Lamberty, A. and Pauwels, J. (1991) How to correct for blanks in isotope dilution mass spectrometry. *International Journal of Mass Spectrometry and Ion Processes* **104**, 45-48.
- Lehn, G. O., Jacobson, A. D. and Holmden, C. (2013). Precise analysis of Ca isotope ratios ($\delta^{44/40}\text{Ca}$) using an optimized ^{43}Ca – ^{42}Ca double-spike MC-TIMS method. *International Journal of Mass Spectrometry* **351**, 69-75.
- Lui, L. C. (1969) Salinity tolerance and osmoregulation of *Taeniomembris microstomus* (Gunther, 1861), (Pisces: Mugiliformes: Atherinidae) from Australian salt lakes. *Marine and Freshwater Research* **20**, 157-162.
- Macreadie, P. I., Serrano, O., Maher, D. T., Duarte, C. M. and Beardall, J. (2017) Addressing calcium carbonate cycling in blue carbon accounting. *Limnology and Oceanography Letters* **2**, 195-201.
- Martin, A. N., Dosseto, A. and Kinsley, L. P. (2015) Evaluating the removal of non-detrital matter from soils and sediment using uranium isotopes. *Chemical Geology* **396**, 124-133.
- McKirdy, D. M., Thorpe, C. S., Haynes, D. E., Grice, K., Krull, E. S., Halverson, G. P. and Webster, L. J. (2010) The biogeochemical evolution of the Coorong during the mid-to late Holocene: an elemental, isotopic and biomarker perspective. *Organic Geochemistry* **41**, 96-110.
- Molsher, R. L., Geddes, M. C., and Paton, D. C. (1994) Population and reproductive ecology of the small-mouthed hardyhead *Atherinosoma microstoma* (Günther) (Pisces: Atherinidae) along a salinity gradient in the Coorong, South Australia. *Transactions of the Royal Society of South Australia* **118**, 207–216.
- Mosley, L. M. (2016) Barrage release optimisation trial August 2015: assessment of environmental outcomes and achievement of management objectives. University of Adelaide, South Australia.

Mosley, L. M., Hamilton B., Busch B., Hipsey M., and Taylor B. (2017) Assessment and modelling of the effects of the 2013–2016 Morella Basin releases on Coorong water quality. Report to the Department of Environment, Water and Natural Resources (DEWNR). University of Adelaide, South Australia.

Parkhurst, D. L. and Appelo, C. A. J. (2013) Description of input and examples for PHREEQC version 3: a computer program for speciation, batch-reaction, one-dimensional transport, and inverse geochemical calculations. *U.S. Geological Survey Techniques and Methods*, book 6, chap. A43, p. 497; Available at <http://pubs.usgs.gov/tm/06/a43>.

Patterson, W. P. and Walter L. M. (1994) Depletion of ^{13}C in seawater ΣCO_2 on modern carbonate platforms: Significance for the carbon isotopic record of carbonates. *Geology* **22**, 885-888.

Patterson, W. P. (1999) Oldest isotopically characterized fish otoliths provide insight to Jurassic continental climate of Europe. *Geology* **27**, 199-202.

Petersen, S. V., Tabor, C. R., Lohmann, K. C., Poulsen, C. J., Meyer, K. W., Carpenter, S. J., Erickson, J.M., Matsunaga, K.K., Smith, S.Y. and Sheldon, N. D. (2016) Temperature and salinity of the Late Cretaceous Western Interior Seaway. *Geology* **44**, 903-906.

Phillips, B. and Muller, K. (2006) *Ecological character of the Coorong, Lakes Alexandrina and Albert wetland of international importance*. Department for Environment and Heritage.

Reid, R. J. and Mosley, L. M. (2016) Comparative contributions of solution geochemistry, microbial metabolism and aquatic photosynthesis to the development of high pH in ephemeral wetlands in South East Australia. *Science of The Total Environment* **542**, 334-343.

Romaniello, S., Field, M., Smith, H., Gordon, G., Kim, M. and Anbar, A. D. (2015) Fully automated chromatographic purification of Sr and Ca for isotopic analysis. *Journal of Analytical Atomic Spectrometry* **30**, 1906-1912.

Scheiderich, K., Amini, M., Holmden, C. and Francois, R. (2015) Global variability of chromium isotopes in seawater demonstrated by Pacific, Atlantic, and Arctic Ocean samples. *Earth and Planetary Science Letters* **423**, 87-97.

Schreiner, W. N. (1995) A standard test method for the determination of RIR values by X-ray diffraction. *Powder Diffraction* **10**, 25-33.

Sigman, D. M., Karsh, K.L. and Casciotti, K. L. (2009) Ocean process tracers: nitrogen Isotopes in the Ocean. *In Encyclopedia of Ocean Sciences 2nd Ed* (eds. J. H. Steele, K. K. Turekian and S. A. Thorpe). Elsevier ScienceDirect, Amsterdam. <https://doi.org/10.1016/B978-012374473-9.00632-9>

Tan, F. C. and Hudson, J. D. (1974) Isotopic studies on the palaeoecology and diagenesis of the Great

- Estuarine Series (Jurassic) of Scotland. *Scottish Journal of Geology* **10**, 91-128.
- Tang, J., Dietzel, M., Böhm, F., Köhler, S. J., Eisenhauer, A. (2008) Sr²⁺/Ca²⁺ and ⁴⁴Ca/⁴⁰Ca fractionation during inorganic calcite formation: II. Ca isotopes. *Geochim. Cosmochim. Acta* **72**, 3733–3745.
- Teng, F. Z., Dauphas, N., and Watkins, J. M. (2017) Non-Traditional Stable Isotopes: Retrospective and Prospective. *Reviews in Mineralogy and Geochemistry* **82**, 1-26.
- Von der Borch, C. C. (1962) Sedimentary carbonate deposits of the Coorong area, South Australia (Doctoral dissertation).
- Von der Borch, C. C., Lock, D. E. and Schwebel, D. (1975) Ground-water formation of dolomite in the Coorong region of South Australia. *Geology* **3**, 283-285.
- Ware, J. R., Smith, S. V. and Reaka-Kudla, M. L. (1992) Coral reefs: sources and sinks of atmospheric CO₂? *Coral Reefs* **11**, 127-130.
- Webster, I. T. (2010) The hydrodynamics and salinity regime of a coastal lagoon—The Coorong, Australia—Seasonal to multi-decadal timescales. *Estuarine, Coastal and Shelf Science* **90**, 264-274.
- Wedderburn, S. D., Walker, K. F. and Zampatti, B. P. (2007) Habitat separation of Craterocephalus (Atherinidae) species and populations in off-channel areas of the lower River Murray, Australia. *Ecology of Freshwater Fish* **16**, 442-449.
- Wedderburn, S. D., Walker, K. F. and Zampatti, B. P. (2008) Salinity may cause fragmentation of hardyhead (Teleostei: Atherinidae) populations in the River Murray, Australia. *Marine and Freshwater Research* **59**, 254-258.
- Wedderburn, S. D., Barnes, T. C. and Hillyard, K. A. (2014) Shifts in fish assemblages indicate failed recovery of threatened species following prolonged drought in terminating lakes of the Murray–Darling Basin, Australia, *Hydrobiologica* **730**, 179-190.
- Wiederhold, J. (2015) Metal Stable Isotope Signatures as Tracers in Environmental Geochemistry, *Environmental Science and Technology* **49**, 2606-2624.
- Wierzbowski, H. and Joachimski, M. (2007). Reconstruction of late Bajocian–Bathonian marine palaeoenvironments using carbon and oxygen isotope ratios of calcareous fossils from the Polish Jura Chain (central Poland). *Palaeogeography, Palaeoclimatology, Palaeoecology* **254**, 523-540.
- Zeebe, R. and Wolf-Gladrow, D. (2001) CO₂ in Seawater: Equilibrium, Kinetics, Isotopes. *Elsevier Oceanography Series* **65** Amsterdam, 346.

CHAPTER 3

Impact of salinity and carbonate saturation on stable Sr isotopes ($\delta^{88/86}\text{Sr}$) in a lagoon-estuarine system

Published as

Shao, Y., Farkaš, J., Mosley, L., Tyler, J., Wong, H., Chamberlayne, B., Raven, M., Samanta, M., Holmden, C., Gillanders, B.M., Kolevica, A., Eisenhauer, A. (2021) Impact of salinity and carbonate saturation on stable Sr isotopes ($\delta^{88/86}\text{Sr}$) in a lagoon-estuarine system. *Geochimica et Cosmochimica Acta* 293, 461-476. doi: <https://doi.org/10.1016/j.gca.2020.11.014>

This chapter was reformatted from the published article to match the rest of the thesis, the text remains the same except for section numbers, which are prefaced with the chapter number e.g. 1. Introduction is now 3.1 Introduction.

The published version is in Appendix 1.

Statement of Authorship

Title of Paper	Impact of salinity and carbonate saturation on stable Sr isotopes ($\delta^{88/86}\text{Sr}$) in a lagoon-estuarine system
Publication Status	<input checked="" type="checkbox"/> Published <input type="checkbox"/> Accepted for Publication <input type="checkbox"/> Submitted for Publication <input type="checkbox"/> Unpublished and Unsubmitted work written in manuscript style
Publication Details	Shao, Y., Farkaš, J., Mosley, L., Tyler, J., Wong, H., Chamberlayne, B., Raven, M., Samanta, M., Holmden, C., Gillanders, B.M., Kolevica, A., Eisenhauer, A. (2021) Impact of salinity and carbonate saturation on stable Sr isotopes ($\delta^{88/86}\text{Sr}$) in a lagoon-estuarine system. <i>Geochimica et Cosmochimica Acta</i> 293 , 461-476. doi: https://doi.org/10.1016/j.gca.2020.11.014

Principal Author

Name of Principal Author (Candidate)	Yuexiao Shao		
Contribution to the Paper	Field sample collection and measurements, sample preparation, development of Sr isotope analyses routine, pH and alkalinity analyses, data collection, data interpretation and modelling, manuscript writing, acting as the corresponding author.		
Overall percentage (%)	75		
Certification:	This paper reports on original research I conducted during the period of my Higher Degree by Research candidature and is not subject to any obligations or contractual agreements with a third party that would constrain its inclusion in this thesis. I am the primary author of this paper.		
Signature		Date	2/2/2021

Co-Author Contributions

By signing the Statement of Authorship, each author certifies that:

- i. the candidate's stated contribution to the publication is accurate (as detailed above);
- ii. permission is granted for the candidate to include the publication in the thesis; and
- iii. the sum of all co-author contributions is equal to 100% less the candidate's stated contribution.

Name of Co-Author	Juraj Farkaš		
Contribution to the Paper	Conceptual development, funding supply, field work assistance, guidance of development of $\delta^{88/86}\text{Sr}$ analytical method, guidance on data interpretation and modelling, manuscript evaluation and review.		
Signature		Date	15/03/2021

Name of Co-Author	Luke Mosley		
Contribution to the Paper	Conceptual development, field work assistance, guidance on pH and alkalinity analyses, guidance on PHREEQC mineral saturation modelling, manuscript review.		

Signature		Date	2/2/21
-----------	--	------	--------

Name of Co-Author	Jonathan Tyler		
Contribution to the Paper	Conceptual development, assistance on data interpretation, reviewed and improved the structure language of the manuscript.		
Signature		Date	2/2/2021

Name of Co-Author	Henri Wong		
Contribution to the Paper	Elemental concentration analyses.		
Signature		Date	2/2/2021

Name of Co-Author	Briony Chamberlayne		
Contribution to the Paper	Provided shell samples and species information, manuscript review.		
Signature		Date	03/02/2021

Name of Co-Author	Mark Raven		
Contribution to the Paper	XRD analyses of carbonate sample.		
Signature		Date	2/03/2021

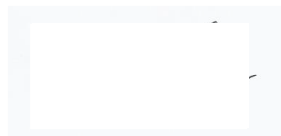
Name of Co-Author	Moneesha Samanta		
-------------------	------------------	--	--

Contribution to the Paper	Development of $\delta^{88/86}\text{Sr}$ double spike correction algorithm.		
Signature		Date	5/2/21

Name of Co-Author	Chris Holmden		
Contribution to the Paper	Conceptual development, manuscript evaluation and review.		
Signature		Date	January 31, 2021

Name of Co-Author	Bronwyn M. Gillanders		
Contribution to the Paper	Conceptual development, guidance on manuscript structure, manuscript evaluation and review.		
Signature		Date	3 March 2021

Name of Co-Author	Ana Kolevica		
Contribution to the Paper	Making and providing ^{87}Sr - ^{84}Sr double spike solution.		
Signature		Date	03.02.2021

Name of Co-Author	Anton Eisenhauer		
Contribution to the Paper	Making and providing ^{87}Sr - ^{84}Sr double spike solution.		
Signature		Date	2/3/2021

Chapter 3.

Impact of salinity and carbonate saturation on stable Sr isotopes ($\delta^{88/86}\text{Sr}$) in a lagoon-estuarine system

Abstract

Local carbonate cycling in lagoon-estuarine systems, involving processes such as inorganic and biogenic carbonate precipitation/dissolution, represents an important but poorly constrained component of the coastal carbon budget. This study investigates the sensitivity of stable Sr isotope tracer ($\delta^{88/86}\text{Sr}$) with respect to carbonate saturation and salinity of local waters in the Coorong, Lower Lakes and Murray Mouth (CLLMM) estuary in South Australia. The CLLMM has an extensive range of salinity from fresh to hypersaline (from ~ 0 to over 100 PSU), with corresponding variations in water chemistry and major ion composition that in turn controls mineral saturation states, and thus CaCO_3 precipitation/dissolution in local waters. Here we use the novel $\delta^{88/86}\text{Sr}$ tracer in tandem with the more established radiogenic Sr isotope ratio ($^{87}\text{Sr}/^{86}\text{Sr}$), where the latter is a robust proxy for Sr sources and thus water provenance. We also produced a geochemical (PHREEQC) model of calcium carbonate (CaCO_3) saturation changes across this unique lagoon-estuarine system.

The results indicate a systematically increasing trend of $\delta^{88/86}\text{Sr}$ (from $\sim 0.25\text{‰}$ to $\sim 0.45\text{‰}$) with increasing salinity and CaCO_3 (aragonite, calcite) saturation indices of the coastal waters, which in turn suggest an overall control of carbonate dissolution/precipitation processes on the stable Sr isotope composition in the CLLMM system. This was further corroborated by Ca isotope data ($\delta^{44/40}\text{Ca}$) published previously on the same samples from the Coorong, as well as a quantitative simulation of local carbonate removal in the lagoon based on Rayleigh modelling and Sr isotope data.

Overall, our results confirm that a coupled Sr isotope approach (combining $^{87}\text{Sr}/^{86}\text{Sr}$ and $\delta^{88/86}\text{Sr}$) can be used to constrain not only the main water sources (continental versus marine Sr) but also local CaCO_3 dissolution/precipitation processes, and thus inorganic carbon and coastal carbonate cycling in the CLLMM system. Finally, this coupled $\delta^{88/86}\text{Sr}$ and $^{87}\text{Sr}/^{86}\text{Sr}$ approach can be potentially applied to fossil carbonate archives to reconstruct palaeo-hydrology and salinity changes in the CLLMM and/or other carbonate-producing coastal systems.

3.1 Introduction

Lagoon-estuarine systems represent unique coastal environments at the land-ocean interface that are ecologically important and highly productive, in particular for fisheries. Moreover, temperate and arid lagoon-estuarine systems are regarded as some of the most degraded ecosystems due to their

susceptibility to salinisation and eutrophication from anthropogenic effects, as well as their sensitivity to climate change induced perturbations (Anthony et al., 2009; Glamore et al., 2016; Warwick et al., 2018). These dynamic environments typically involve complex interactions of hydrological, geochemical, and biological processes and water source mixing phenomena, resulting in variable salinities, mineral saturation states and chemical/isotopic composition. These in turn are critical parameters for the calcium carbonate (CaCO_3) cycling in marine and coastal regions, representing an important but currently poorly constrained component of the global carbon cycle, including the coastal ‘blue carbon’ budget (i.e., the carbon storage capacity of vegetated coastal systems, Macreadie et al., 2017). For instance, inorganic carbonate precipitation due to evaporation releases CO_2 to the atmosphere and increasing atmospheric CO_2 levels and exchange with surface waters leads to coastal ocean acidification and affects the local carbon storage (Zeebe and Wolf-Gladrow, 2001). Thus, detailed studies into C and CaCO_3 cycling in lagoon-estuarine systems, especially in arid environments, is of high importance and remains a priority.

Stable isotopes of elements such as H, C, N, O and S in the oceans, continental waters and/or sediment archives have been used successfully to trace the Earth’s surface processes and to reconstruct palaeo-environmental conditions in both marine and terrestrial systems (Hoefs, 2018 and references therein). However, to constrain the local CaCO_3 budget and carbonate precipitation/dissolution processes in coastal systems, more robust and direct tracers for inorganic C cycling are needed. Novel isotope tracers of alkali and alkaline earth metals such as stable calcium ($\delta^{44/40}\text{Ca}$) and magnesium ($\delta^{26}\text{Mg}$) isotopes have the potential to resolve and quantify some aspects of the marine carbonate cycle, and implications for the present and past Ca, Mg, and C budgets and elemental cycling in the oceans (Tipper et al., 2006; Farkaš et al., 2007 and 2016; Holmden et al., 2012; de Souza et al., 2010; Chao et al., 2013 and 2015; Chao et al., 2015; Shalev et al. 2018).

Strontium (Sr) is geochemically similar to calcium (Ca) with an identical charge (+2) and similar ionic radius (Finch and Allison, 2007; Menadakis et al., 2009; de Souza et al., 2010). As an indirect tracer of the oceanic Ca cycling and marine carbonate budget, the Sr isotopes offer a perspective that is different but complementary to that of Ca isotope studies. The most notable difference is the larger (and thus easier to measure) range in variations of the radiogenic Sr isotope (^{87}Sr) abundance in most terrestrial materials, compared to fairly limited radiogenic ^{40}Ca excess observed in natural waters and carbonates (Caro et al., 2010). Applications of the $^{87}\text{Sr}/^{86}\text{Sr}$ tracer for hydrological and ecosystem studies have thus been established for decades as a sensitive tool for investigations of Sr provenance in both terrestrial and marine environments (Holmden et al., 1997; Capo et al., 1998; Bullen and Bailey, 2005; de Souza et al., 2010; Farkaš et al., 2011; Chao et al., 2013 and 2015; Pearce et al., 2015). Modern seawater has a relatively homogeneous $^{87}\text{Sr}/^{86}\text{Sr}$ ratio (~ 0.7092) due to the long oceanic residence time of Sr in global oceans compared with the mixing time of seawater ($\sim 1\text{ka}$) (2.5 Ma, Hodell et al., 1990; Vollstaedt et al., 2014). However, at the interface between continental and marine en-

vironments, which is the subject of this study, the variation in seawater $^{87}\text{Sr}/^{86}\text{Sr}$ can be considerably larger, due to the release of radiogenic ^{87}Sr into coastal waters from the weathering of the continental crust (Kuznestov et al., 2012).

Variations of stable Sr isotopes (expressed as $\delta^{88/86}\text{Sr}$) in marine and terrestrial Earth-surface environments can be used as a complementary isotope tracer to better constrain the global Sr cycle and its main input and output fluxes (Krabbenhöft et al., 2010; de Souza et al., 2010; Raddatz et al., 2013; Chao et al., 2013 and 2015; Stevenson et al., 2014; Vollstaedt et al., 2014; Pearce et al., 2015; Fruchter et al., 2016). Carbonate minerals such as calcite and aragonite preferentially incorporate light isotopes of Sr and thus, their $\delta^{88/86}\text{Sr}$ values are lower than the dissolved Sr in the waters from which they formed (Krabbenhöft et al., 2009; Vollstaedt et al., 2014). Thus, carbonate precipitation in the oceans, coastal marine environments and/or lakes drives the $\delta^{88/86}\text{Sr}$ of seawater or local lagoon/lake waters to higher values, while carbonate dissolution has an opposite effect (Krabbenhöft et al., 2009; Fruchter et al., 2017). The stable Sr isotope variations resulting from these processes are quite small in nature, on the order of about 0.1–0.2 per mil (‰), which thus requires precise and accurate measurement of $\delta^{88/86}\text{Sr}$ (Andrews et al., 2016; Shalev et al. 2017; Fruchter et al., 2016 and 2017).

Reconnaissance studies show that the stable Sr isotopes are fractionated by similar processes to those that fractionate Ca isotopes (Böhm et al., 2012; Stevenson et al. 2014; Vollstaedt et al. 2014; Fruchter et al. 2016 and 2017). Therefore $\delta^{88/86}\text{Sr}$, similar to $\delta^{44/40}\text{Ca}$, can be also used to identify water sources, carbonate precipitation/dissolution or chemical kinetics of CaCO_3 formation in natural waters (cf., Krabbenhöft et al., 2009; AlKhatib and Eisenhauer, 2017), but with the advantage of simultaneously analysing the radiogenic ^{87}Sr component (i.e., $^{87}\text{Sr}/^{86}\text{Sr}$).

In this study, we present high-precision $\delta^{88/86}\text{Sr}$ measurements ($\pm 0.03\text{‰}$, 2SD) of waters and carbonates from a lagoon-estuarine system in South Australia – the Coorong, Lower Lakes and Murray Mouth (CLLMM) estuary (Fig. 1). In the CLLMM system, a wide variation in: (i) water salinity (from fresh to hypersaline), (ii) carbonate saturation states and (iii) redox conditions (from oxic to sub-oxic/anoxic) combine to create a ‘natural laboratory’ for testing the behaviour and sensitivity of geochemical and isotopic tracers to the above physico-chemical parameters of coastal waters. The main objective of this study is to calibrate and assess the sensitivity of the $\delta^{88/86}\text{Sr}$ tracer in the CLLMM to changes in salinity, carbonate saturation state, and CaCO_3 precipitation/dissolution; and to compare these findings to previous work done on stable Ca isotopes ($\delta^{44/40}\text{Ca}$) analysed in the same samples (see Shao et al., 2018). We also discuss the potential of a coupled $^{87}\text{Sr}/^{86}\text{Sr}$ and $\delta^{88/86}\text{Sr}$ approach for palaeo-hydrological and salinity reconstructions in the CLLMM and/or other coastal marine, lagoon and freshwater systems based on Sr isotope analysis of fossil carbonate archives.

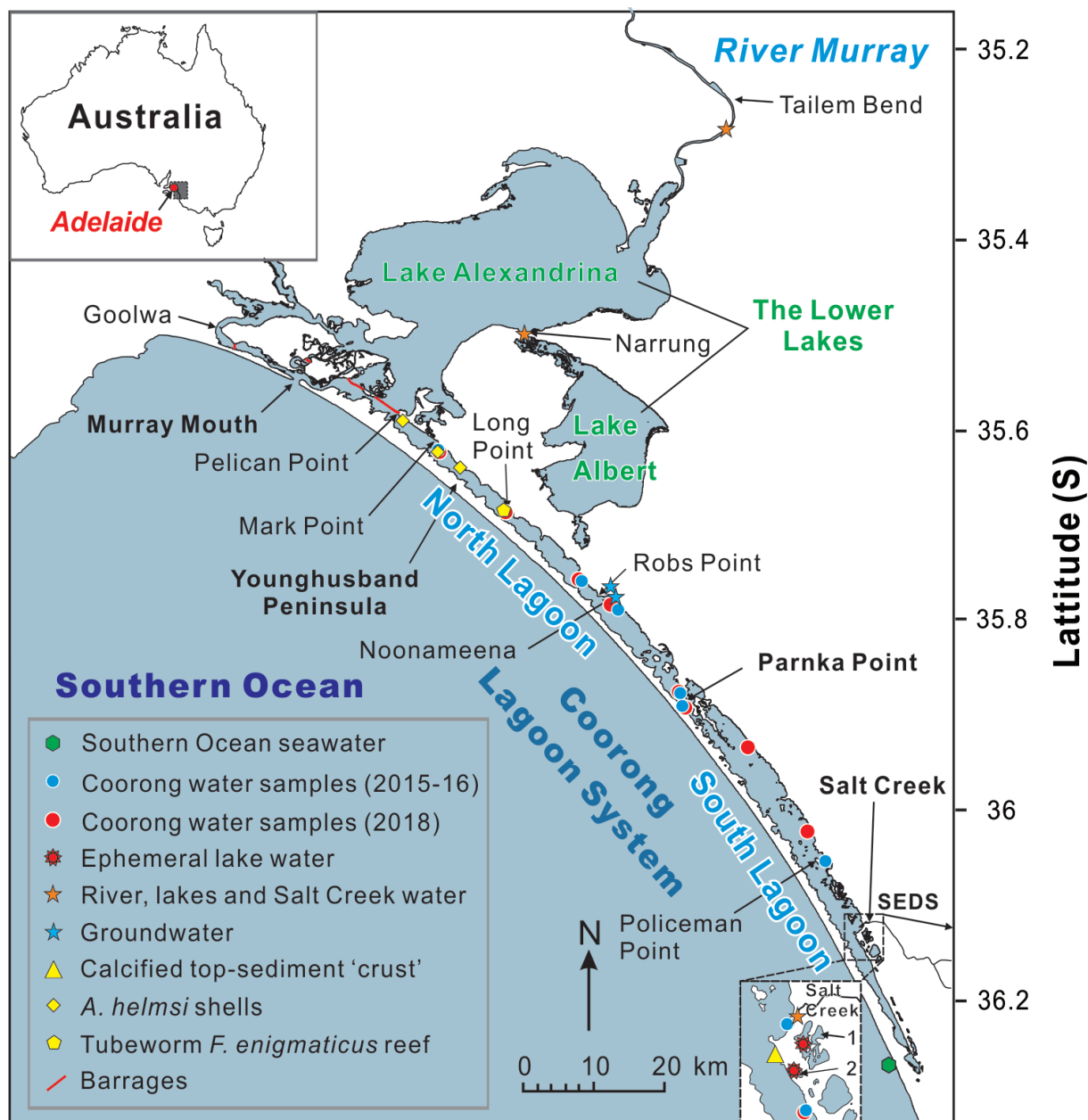


Figure 1: Map of the Coorong, Lower Lakes and Murray Mouth (CLLMM) estuary with the representative sampling sites for waters and carbonates. The inset represents a magnified view near Salt Creek. Note that “1” = Milne Lake, and “2” = Halite Lake; coordinates and sampling dates for all samples analysed are listed in the Appendix (Tables A.1 and 2). SEDS = South East Drainage System.

3.2 Study area

The CLLMM forms a unique coastal system in South Australia (Fig. 1), located at the terminus of the River Murray and Murray-Darling Basin, which is Australia’s largest river system. Due to its specific geomorphology and hydrology, waters of the CLLMM range from freshwater (~0 PSU) to hypersaline (>100 PSU) (Gillanders and Munro, 2012), accompanied by ongoing CaCO_3 precipitation and seasonal groundwater discharge events (Haese et al., 2008; Fernandes and Tanner, 2009). These phenomena are particularly prominent in the Coorong, which is a semi-restricted and elongat-

ed lagoon that runs parallel to the coast of the Southern Ocean, divided at a narrow connection (i.e., Parnka Point) that separates the North and South Lagoons (Fig. 1). The North Lagoon receives water inputs from the Southern Ocean via the Murray Mouth and occasionally also from the River Murray via the Lower Lakes, from which discharge is regulated by a series of barrages (Fig. 1). The South Lagoon is hydrologically more restricted compared to the North Lagoon, and in recent decades, the lagoon water has become increasingly hypersaline, ecologically impoverished, and locally anoxic due to reduced flow of freshwater from the South East Drainage System (SEDS) via Salt Creek (see Fig. 1) (Reeves et al., 2015; Brookes et al., 2018; Mosley et al., 2019). These environmental changes and habitat deterioration have hampered the establishment of benthic calcifying communities, such as bivalves and foraminifera that would normally produce biogenic carbonates in the South Lagoon. At present, it is more common to find biogenic carbonates in the North Lagoon where the salinity is lower (close to typical seawater), including bivalves, foraminifera and tubeworm species (Dittmann et al., 2009; Chamberlayne et al., 2019). In contrast, inorganic carbonate precipitates in the form of crusts and carbonate tufa are now commonly forming in the hypersaline South Lagoon (Haese et al., 2008), and these are predominantly composed of aragonite (~87%) and calcite (~12%), complemented by minor occurrences of gypsum (~1%) (Von der Borch et al., 1975; Shao et al., 2018). Unlike abundant carbonate precipitation, the impact of gypsum formation on the Coorong water chemistry and its isotope composition is believed to be minor and transient, as gypsum precipitation in the South Lagoon is only evident during summer (i.e., December to February, in S. Hemisphere) when salinity is > 3.5 times that of normal seawater (i.e., >120 PSU, see Lazar et al., 1983; Fernandes and Tanner, 2009).

3.3 Material and methods

3.3.1 Sample description

In this study, samples were divided into groups 1 to 3 according to time of collection and analytical purposes (Fig. 1).

Group 1 originates from the previous study of Shao et al. (2018), including Coorong lagoon waters (n = 8), Lower Lakes waters (n = 1) and local groundwaters (n = 2) all collected in 2015 and 2016, and a sample of calcified aragonitic top-sediment crust collected in 2017. All these water samples were previously measured for major/trace element concentrations and stable Ca isotopes ($\delta^{44/40}\text{Ca}$), and the sediment crust sample was analysed for mineralogy via X-ray diffraction (XRD), (data from Shao et al., 2018).

Group 2 consists of newly collected samples, including waters from the River Murray (n = 1), Salt Creek (n = 1) and two ephemeral lakes (Milne Lake and Halite Lake; n = 2), which were all collected in August 2018 (for details see Fig. 1). Biogenic carbonate samples from the North Lagoon include

(i) *Arthritica helmsi* bivalve shell samples (n = 3) collected alive in January and May 2018 (Fig. B.2 in the Appendix), and (ii) a sample of carbonate precipitates produced by the tubeworm *Ficopomatus enigmaticus*, which typically forms small ‘reefs’ or colonies, collected near Long Point in August 2018 (Fig. B.3 in the Appendix). *A. helmsi* is an aragonitic micro bivalve that is short-lived with a lifespan of ca. 1 year (Dittmann et al., 2009; Chamberlayne et al., 2019). The Serpulid tubeworms (*F. enigmaticus*), which produces calcitic skeletal carbonates (see XRD analysis in Table B.5, Appendix B.3), is believed to be an invasive species that is currently found in the North Lagoon all year round with a natural lifespan of ca. 20-24 months (Dittmann et al., 2009).

Group 3 consists of water samples (n = 12) collected from the CLLMM in May 2018; data from these water samples were used for PHREEQC modelling of mineral saturation states. Sample site information and locations for all the above samples of waters and carbonates are listed in Appendix A (see Tables A.1 and 2).

3.3.2 Field measurements and sample preparation of waters and carbonates

For water samples collected in 2018 (i.e., Groups 2 and 3), temperature and salinity were measured in the field using a YSI ProDSS multi-parameter water quality meter, with location recorded by GPS at each sampling site (Tables A.1 and 2, Appendix A). The water samples were filtered through 0.45 µm cellulose nitrate membrane filters to remove particulate matter and other impurities, and the filtered waters were refrigerated at 4°C and stored in acid-cleaned HDPE bottles before alkalinity, elemental concentrations and isotopic analyses were undertaken. For pH measurements, unfiltered water samples were collected simultaneously in acid-cleaned HDPE bottles with minimum headspace to avoid creation of air bubbles and loss of CO₂, and samples were stored and refrigerated at 4°C before pH measurements.

The dried, powdered and homogenised calcified sediment crust (CLS-1) and tubeworm carbonate reef (CW2w) were analysed for mineralogy via XRD with a PANalytical X’Pert Pro Multi-purpose Diffractometer as described in Appendix B.4. Afterwards, the powdered samples were reacted with 0.5M acetic acid in a Teflon vial on a hotplate at 45°C for 24 hours to dissolve the carbonate fraction (Palchan et al., 2013), which was used for subsequent elemental and isotope analyses after centrifugation. A total of 5 to 10 shells from living specimens of *A. helmsi* (Sample IDs: 122s, 149s and 151s) were collected and extracted from top sediments from the North Lagoon (see Table A.1 in the Appendix for sample locations). Shells were then rinsed with DI water, cleaned in 10% H₂O₂ overnight, rinsed in an ultrasonic bath, leached in 0.27 M HCl for ~1 minute (to remove attached clays and coatings), dried and weighed, and then completely dissolved in 5% HNO₃ in preparation for elemental concentration analysis (described in Appendix B.2), and follow up ⁸⁷Sr/⁸⁶Sr and δ^{88/86}Sr analyses.

3.3.3 Coupled $^{87}\text{Sr}/^{86}\text{Sr}$ and $\delta^{88/86}\text{Sr}$ analyses via TIMS

Samples of filtered waters, dissolved biogenic carbonates, and a sediment crust (i.e., groups 1 and 2) were all analysed for $^{87}\text{Sr}/^{86}\text{Sr}$ and $\delta^{88/86}\text{Sr}$ by thermal ionisation mass spectrometry (TIMS) using a Phoenix Isotopx instrument at the Metal Isotope Group (MIG) facility at the University of Adelaide. In order to apply the ^{87}Sr - ^{84}Sr double spike method to analyse the $\delta^{88/86}\text{Sr}$ in an unknown sample, two aliquots each containing about 500 ng of Sr were taken from a stock sample solution, where one aliquot was spiked with the ^{87}Sr - ^{84}Sr double spike solution, resulting ‘spike to sample’ ratios (i.e., $^{84}\text{Sr}_{\text{sp}}/^{84}\text{Sr}_{\text{sa}}$) ranging from ~10 to ~32 (details in Appendix C.4). Afterwards, the Sr fraction from each sample was purified from the sample ‘matrix’ using a 600 μL Micro Bio-Spin separation columns filled with Sr-specific resin (Eichrom Sr-SPS) following procedures in Appendix C.1. The pure Sr fractions were then loaded on single non-zone-refined rhenium filaments before TIMS analyses. For each ‘batch’ of TIMS analyses (i.e., one analytical session), which contain both spiked and unspiked samples, these were run in parallel with two SRM987 standards (one at the beginning and one at the end of analytical session). In addition, an IAPSO seawater or JCP-1 carbonate standard were analysed in each ‘batch’, depending on whether waters or carbonate samples were analysed (i.e., IAPSO was used for the former and JCP-1 for the latter).

For stable Sr isotopes, all data measured in this study are reported as a conventional delta notation ($\delta^{88/86}\text{Sr}$), expressed in per mil (‰), where $^{88}\text{Sr}/^{86}\text{Sr}$ ratio of an unknown sample is normalised relative to SRM987 standard, according to the following equation:

$$\delta^{88/86}\text{Sr} = \left[\left(\frac{^{88}\text{Sr}/^{86}\text{Sr}}{^{88}\text{Sr}/^{86}\text{Sr}} \right)_{\text{sample}} / \left(\frac{^{88}\text{Sr}/^{86}\text{Sr}}{^{88}\text{Sr}/^{86}\text{Sr}} \right)_{\text{SRM987}} - 1 \right] \times 1000 \quad (\text{Eq. 1})$$

Specifically, $\delta^{88/86}\text{Sr}$ values of unknown samples (and IAPSO and JCP-1 standards) were normalised to the average of two SRM987 standards analysed in the same ‘batch’ or analytical session. This approach was used to correct any session-to-session drifts, which were quantified by monitoring SRM987 (see Appendix, Fig C.2B), following the approach adopted by previous studies focused on high-precision Sr isotope analyses (Krabbenhöft et al., 2009; Andrews et al., 2016 and 2017, Shalev et al., 2017).

The total procedural Sr blanks (details in Appendix C.3) ranged from 19 to 211 pictograms (pg) Sr, with an average value of 72 pg (2SEM = 20 pg, n=30), determined by an isotope dilution (ID) technique using an ^{84}Sr -enriched single spike, amounting to less than 0.1% of Sr from the analysed samples (see below). In addition, the ^{85}Rb ion beam during TIMS analyses was lower than 1×10^{-4} V for all analysed samples, and therefore the isobaric interference from ^{87}Rb was negligible, but an on-line correction for Rb on mass 87 was performed for all samples.

To determine $\delta^{88/86}\text{Sr}$, both spiked and unspiked samples were analysed by TIMS using a static multicollection routine. Typically, a ^{88}Sr beam with a magnitude of about 5-6 V was attained, and ^{84}Sr , ^{85}Rb , ^{86}Sr , ^{87}Sr , and ^{88}Sr isotope beams were collected over 200 cycles (10 cycles for 20 blocks, with 30s baseline and 8s peak integrations), with a total analytical time of ca. 1 hour. From these collected data, the following isotope ratios were calculated: $^{88}\text{Sr}/^{84}\text{Sr}$, $^{86}\text{Sr}/^{84}\text{Sr}$, $^{87}\text{Sr}/^{84}\text{Sr}$ and $^{88}\text{Sr}/^{86}\text{Sr}$, which in turn were used to calculate the ‘double-spike corrected’ $^{88}\text{Sr}/^{86}\text{Sr}$ ratios, and thus $\delta^{88/86}\text{Sr}$ (see Eq. 1). Any procedural and/or instrumental isotope fractionation effects were corrected using an iterative ^{87}Sr - ^{84}Sr double spike correction algorithm (i.e., double-spike correction) adapted from Heuser et al. (2002) and Samanta et al. (2016) using the Sr isotopic ratios measured above.

To obtain high-precision $^{87}\text{Sr}/^{86}\text{Sr}$ ratios, unspiked sample aliquots were re-run on the TIMS using a multi-dynamic peak-hopping method (details see Appendix C.2). In this approach, a typical ^{88}Sr beam of 5-6 V was attained, and the following isotope ratios were collected: $^{87}\text{Sr}/^{86}\text{Sr}$, $^{86}\text{Sr}/^{88}\text{Sr}$ and $^{84}\text{Sr}/^{86}\text{Sr}$, using a method consisting of 100 cycles (20 cycles for 5 blocks), with 30 s of baseline and 10 s peak integrations. Instrumental mass-dependent fractionation effects were corrected via an internal normalisation, using an exponential law and assuming $^{86}\text{Sr}/^{88}\text{Sr}$ of 0.1194 as a normalising ratio (Nier, 1938), which allowed calculation of the corrected $^{87}\text{Sr}/^{86}\text{Sr}$ ratios.

Following the analytical procedures described above, the long-term average $^{87}\text{Sr}/^{86}\text{Sr}$ and $\delta^{88/86}\text{Sr}$ values and uncertainties of standards in this study were 0.709248 ± 0.000004 (2SEM, n=30) and $0.000 \pm 0.005\text{‰}$ (2SEM, n=29) for SRM987 (Fig. C.2, Appendix), 0.709172 ± 0.000005 (2SEM, n=8) and $0.395 \pm 0.009\text{‰}$ (2SEM, n=10) for IAPSO seawater (Fig. C.3, Appendix), and 0.709174 ± 0.000006 (2SEM, n=7) and $0.198 \pm 0.014\text{‰}$ (2SEM, n=7) for JCP-1 carbonate (Fig. C.3, Appendix). These $^{87}\text{Sr}/^{86}\text{Sr}$ and $\delta^{88/86}\text{Sr}$ results of the above standards (SRM987, IAPSO, JCP-1) acquired during the course of this study agree well with the published data from these standards, where the SRM987 reported $^{87}\text{Sr}/^{86}\text{Sr} = 0.710252 \pm 0.000001$ (2SEM, n=94) and $\delta^{88/86}\text{Sr} = 0.000 \pm 0.004\text{‰}$ (2SEM, n=77) (Andrews et al., 2016), the IAPSO reported $^{87}\text{Sr}/^{86}\text{Sr} = 0.709168 \pm 0.000007$ (2SEM, n=10) (Krabbenhöft et al., 2009) and $\delta^{88/86}\text{Sr} = 0.396 \pm 0.005\text{‰}$ (2SEM, n=54) (Andrews et al., 2016), and the JCP-1 reported $^{87}\text{Sr}/^{86}\text{Sr} = 0.709172 \pm 0.000004$ (2SEM, n=32) and $\delta^{88/86}\text{Sr} = 0.193 \pm 0.004\text{‰}$ (2SEM, n=32) (Vollstaedt et al., 2014). In this study, $^{87}\text{Sr}/^{86}\text{Sr}$ and $\delta^{88/86}\text{Sr}$ analyses of unknown samples were performed only once, if the measurements of standards (SRM987, IAPSO and JCP-1) within the same batch were within 2SD of their long-term values. Detailed discussion on the accuracy and precision of $^{87}\text{Sr}/^{86}\text{Sr}$ and $\delta^{88/86}\text{Sr}$ data on standards is available in Appendix C.4 (see Figs C.2 and C.3).

3.3.4 Geochemical / PHREEQC modelling of mineral saturation state in waters

The saturation indices (SI) for calcite and aragonite in waters from the CLLMM hydrological system,

sampled in May 2018 (Group 3), were calculated using the geochemical model PHREEQC (available at <https://www.usgs.gov/software/phreeqc-version-3>), following the approach detailed in Shao et al. (2018). To ensure that the May 2018 samples represent the water chemistry of May 2016 samples, where the latter account for the majority of the key analyses ($^{87}\text{Sr}/^{86}\text{Sr}$ and $\delta^{88/86}\text{Sr}$), comparison of salinity and major cations between the two sets of samples were made in Appendix E.1. Briefly, the following parameters were used as input data for PHREEQC modelling: temperature, concentrations of the main cations and anions (Tables A.2, B.1 and 2 in Appendix) and high-precision laboratory alkalinity and pH measurements (described in Appendix B.3). The Pitzer database was used since it is suited for high salinity solutions (Parkhurst and Appelo, 2013). As a comparison to the water samples, the SI values of these carbonates in typical seawater were also calculated based on data from Nordstrom et al. (1979). According to the PHREEQC manual by Parkhurst and Appelo (2013), when modelling with PHREEQC, individual element concentrations can be adjusted within their uncertainty limits to achieve charge balance or equilibrium with a pure phase. Such an approach was thus used in this study, where Cl^- concentration data were used as a reference element for charge balance calculations.

Additionally, alternative calculation of SI values for calcite and aragonite were estimated using the CO2SYS program (Lewis and Wallace, 1998). The comparison of these two modelling methods PHREEQC and CO2SYS showed good agreement (Appendix E.3).

3.4 Results

The salinity, $^{87}\text{Sr}/^{86}\text{Sr}$ and $\delta^{88/86}\text{Sr}$ values of the Coorong waters all displayed systematically increasing trends from the North to the South Lagoon (Figs. 2A-C). The salinity and $^{87}\text{Sr}/^{86}\text{Sr}$ of North Lagoon waters were similar to that in typical seawater (35 PSU and ~ 0.70917 , respectively). However, $\delta^{88/86}\text{Sr}$ of the North Lagoon waters yielded slightly lower values (0.35‰) than typical seawater that is homogenous at $0.395 \pm 0.016\text{‰}$ (Krabbenhöft et al., 2010; and data from this study). In contrast, hypersaline waters (~ 90 PSU) in the more restricted South Lagoon yielded higher $^{87}\text{Sr}/^{86}\text{Sr}$ of ~ 0.70924 ; and their $\delta^{88/86}\text{Sr}$ values were quite variable, ranging from 0.40 to 0.45‰, with an average of $\sim 0.42\text{‰}$. The latter were slightly but systematically higher than the $\delta^{88/86}\text{Sr}$ of present-day seawater (Figs. 2A-C). The analysis of the continental waters (i.e., River Murray, Lower Lakes, and Salt Creek) with fresh to brackish salinities, yielded $^{87}\text{Sr}/^{86}\text{Sr}$ ratios ranging from ~ 0.70925 in Salt Creek up to ~ 0.71206 in the River Murray (Fig. 2B), and their $\delta^{88/86}\text{Sr}$ were systematically lower than those of the lagoon waters and/or seawater, ranging from 0.25 to 0.30‰ with an average of $\sim 0.27\text{‰}$ (Fig. 2C).

All carbonate samples including carbonate crust and biogenic skeletal carbonates, yielded variable $^{87}\text{Sr}/^{86}\text{Sr}$ ranging from ~ 0.70919 to ~ 0.70935 , which were higher than typical seawater (0.70917).

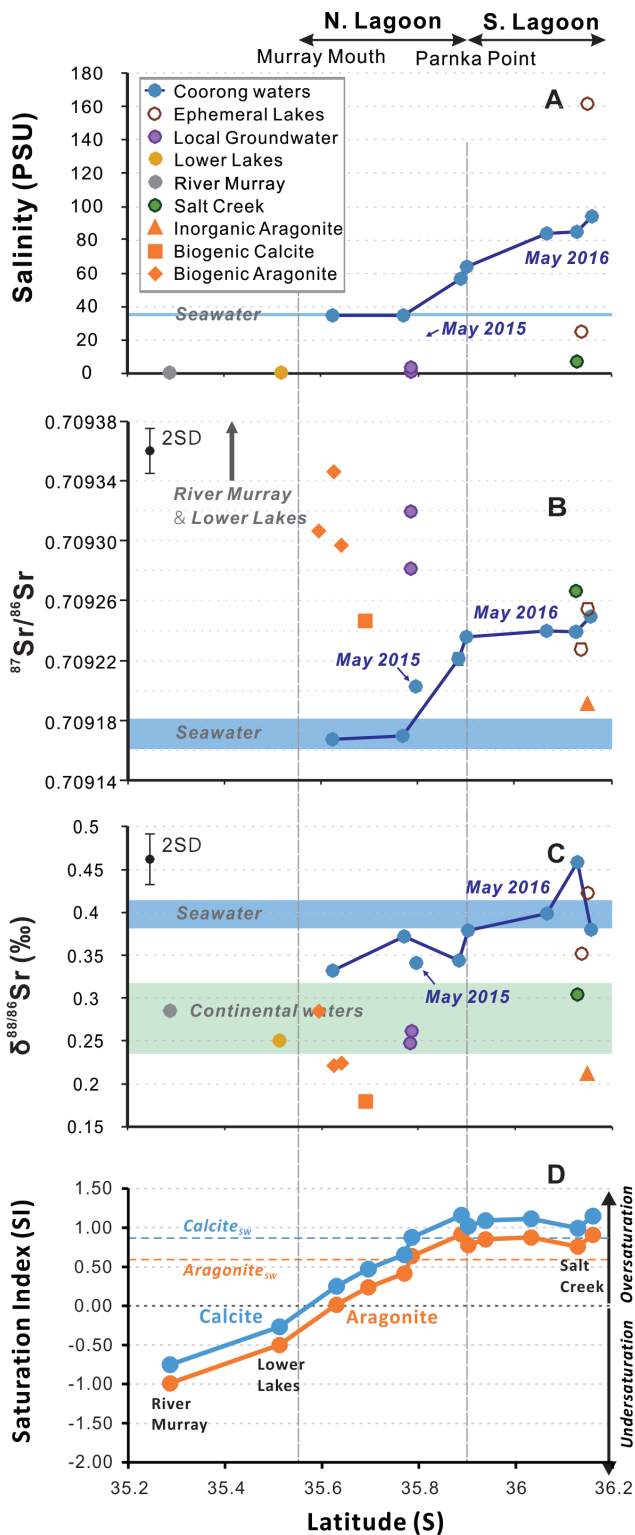


Figure 2: (A) Salinity profile across the CLLMM hydrological system, plotted as a function of latitude (adopted from Shao et al., 2018). (B) Radiogenic Sr isotope ratios ($^{87}\text{Sr}/^{86}\text{Sr}$) of local waters and carbonates. Note that water samples from River Murray (RM) and Lower Lakes (LL) plot out of scale and thus are not shown, and their $^{87}\text{Sr}/^{86}\text{Sr}$ were 0.712055 and

0.710880 respectively. (C) Stable Sr isotope values ($\delta^{88/86}\text{Sr}$) of local waters and carbonates normalised to SRM987 standard. Blue rectangles illustrate typical seawater salinity and Sr isotope compositions, based on the long-term analyses of IAPSO seawater standard (for details see Table 1). (D) The saturation indices (SI) of calcite (blue) and aragonite (orange) in waters from the CLLMM, modelled by PHREEQC for water samples collected in May 2018. The SI values of calcite and aragonite in typical surface seawater (Nordstrom et al., 1979) are shown as blue and orange dashed lines, respectively.

Biogenic calcite and aragonite samples from the North Lagoon (i.e., tubeworm and bivalve skeletal carbonates, respectively) yielded higher $^{87}\text{Sr}/^{86}\text{Sr}$ (>0.70924) than the local lagoon waters (~ 0.70917); while the inorganic aragonite sample (i.e., carbonate crust) collected in the South Lagoon had a lower $^{87}\text{Sr}/^{86}\text{Sr}$ (0.709192) than the local lagoon waters (~ 0.70924) (Fig. 2B). In contrast, $\delta^{88/86}\text{Sr}$ of all carbonate samples including inorganic and biogenic carbonates were relatively less variable, ranging from $\sim 0.18\text{‰}$ to $\sim 0.28\text{‰}$ (Fig. 2C). Also, these $\delta^{88/86}\text{Sr}$ values overlapped with each other within 2SD error (Fig. D.5 in Appendix D.4). These $\delta^{88/86}\text{Sr}$ values are thus all lower than the local lagoon waters, corresponding to Sr isotope difference between the $\delta^{88/86}\text{Sr}$ of local waters and carbonate minerals of 0.1 to 0.20‰ (see Fig. 2C).

Waters from two ephemeral lakes in the Coorong region with very different salinities (i.e., brackish Milne Lake and hypersaline Halite Lake; Fig. 2A) yielded $^{87}\text{Sr}/^{86}\text{Sr}$ ratios similar to the South Lagoon waters (~ 0.70924). The $\delta^{88/86}\text{Sr}$ value of the brackish Milne Lake (salinity = 25 PSU) was similar to the North Lagoon waters ($\sim 0.35\text{‰}$), while the hypersaline Halite Lake (162 PSU) yielded a much higher $\delta^{88/86}\text{Sr}$ value that was

Table 1. Stable and radiogenic Sr isotope composition ($\delta^{88/86}\text{Sr}$ and $^{87}\text{Sr}/^{86}\text{Sr}$), and stable Ca isotope variations ($\delta^{44/40}\text{Ca}$), in the samples, with associated sampling location/area, date and water salinity. Note that reported $\delta^{44/40}\text{Ca}$ data are from Shao et al. (2018). 2SEM is the external precision for repeated analyses with size n; but when n is not given, 2SEM is internal precision of a single analysis of the sample through 200 cycles for $\delta^{88/86}\text{Sr}$, and 100 cycles for $^{87}\text{Sr}/^{86}\text{Sr}$.

	Area	Sampling date	Salinity (PSU)	$\delta^{88/86}\text{Sr}$ (‰_{SRM987})	2SEM	$\delta^{44/40}\text{Ca}$ (‰_{IAPSO})	2SEM	$^{87}\text{Sr}/^{86}\text{Sr}$	2SEM
Samples									
RMW	River Murray	Aug 31, 2019	0.22	0.286	0.016			0.712055	0.000004
C01	Lower Lakes	May 16, 2016	0.80	0.250	0.011	-0.84	0.03	0.710880	0.000009
JWP2	North Lagoon (Groundwater)	June 25, 2015	1.15	0.261	0.017	-0.77	0.03	0.709319	0.000003
BWP2	North Lagoon (Groundwater)	June 25, 2015	3.66	0.247	0.012	-0.69	0.03	0.709281	0.000003
SCW	Salt Creek	Aug 31, 2019	7.18	0.304	0.013	N/A	N/A	0.709253	0.000004
ELW1	Milne Lake/ Pipe Clay Lake	Aug 31, 2019	24.99	0.352	0.018	N/A	N/A	0.709236	0.000004
ELW2	Halite Lake	Aug 31, 2019	161.86	0.423	0.016	N/A	N/A	0.709248	0.000004
C02	North Lagoon	May 16, 2016	34.98	0.332	0.017	0.00	0.03	0.709168	0.000003
C04	North Lagoon	May 16, 2016	34.67	0.372	0.016	0.00	0.05	0.709170	0.000003
NL2	North Lagoon	May 15, 2015	19.69	0.341	0.019	-0.04	0.03	0.709203	0.000003
C06	NL-SL connection	May 16, 2016	63.73	0.378	0.018	0.06	0.03	0.709236	0.000003
C07	NL-SL connection	May 16, 2016	56.97	0.397	0.012	0.11	0.03	0.709221	0.000004
C10	South Lagoon	May 16, 2016	84.10	0.399	0.019	0.16	0.03	0.709240	0.000003
C11	South Lagoon	May 16, 2016	85.10	0.458	0.017	0.19	0.03	0.709239	0.000003
C12	South Lagoon	May 16, 2016	94.10	0.428	0.012	0.20	0.03	0.709245	0.000004
SL11	Southern Ocean	April 10, 2015	36.97	N/A	N/A	N/A	N/A	0.709172	0.000003
122s	North Lagoon	Jan 18, 2018	N/A	0.222	0.012	N/A	N/A	0.709346	0.000004
149s	North Lagoon	May 5, 2018	N/A	0.224	0.012	N/A	N/A	0.709297	0.000004
151s	North Lagoon	May 5, 2018	N/A	0.285	0.012	N/A	N/A	0.709307	0.000004
CW2w	North Lagoon	Aug 31, 2018	N/A	0.181	0.014	N/A	N/A	0.709246	0.000003
CLS-1 ¹	South Lagoon	Mar 5, 2017	N/A	0.211	0.011 (n=3)	-1.16	0.03	0.709192	0.000009 (n=3)
Standards									
IAPSO	N/A	N/A	35.00	0.395	0.009 (n=10)	0.00	N/A	0.709172	0.000005 (n=8)
JCP-1	N/A	N/A	N/A	0.198	0.014 (n=7)	N/A	N/A	0.709174	0.000006 (n=7)

¹ The $\delta^{88/86}\text{Sr}$ and $^{87}\text{Sr}/^{86}\text{Sr}$ of CLS-1 was the average of 3 analyses with different double spike to sample ratios (Appendix C.4, Table C.4). The $\delta^{44/40}\text{Ca}$ of CLS-1 was from Shao et al. (2018).

close to the South Lagoon waters ($\sim 0.42\text{‰}$).

The results from PHREEQC modelling showed that the saturation indices (SI) of aragonite and calcite in the Coorong lagoon waters increased from just saturated ($SI \approx 0$) in the north part of the lagoon, to slightly oversaturated conditions ($SI > 0$) near Parnka Point (see data in Fig. 2D). In the hypersaline South Lagoon, the SI values showed systematic oversaturation with relatively stable SI values of ~ 1 , which were slightly higher than those found in the typical surface seawater of the nearby Southern Ocean (Fig. 2D). In contrast, continental waters including the Murray River and Lower Lakes, both yielded systematically undersaturated SI values of -0.25 to -1 (Fig. 2D), apart from the Salt Creek fresh/brackish waters that were oversaturated ($SI \approx 0.7$) with respect to calcium carbonate.

3.5 Discussion

The Coorong lagoon waters are natural mixtures of different water sources including Southern Ocean seawater (SW), local groundwater (GW), River Murray (RM) and Lower Lakes (LL) freshwaters, and the fresh-to-brackish Salt Creek water (SC). These water sources also represent theoretical end-members for isotope mass balance calculations of the local Sr cycle in the lagoon, and water mixing and carbonate precipitation/dissolution processes in the Coorong. Specifically, the GW-SW and LL-SW mixing scenarios were discussed in Shao et al. (2018) using $^{87}\text{Sr}/^{86}\text{Sr}$, $\delta^{44/40}\text{Ca}$ data and elemental concentrations (e.g., Sr, Na/Sr and Na/Ca ratios). In Appendix D.1, similar mixing models were established using $^{87}\text{Sr}/^{86}\text{Sr}$, Mg/Ca and Mg/Na ratios of waters from the CLLMM, with the addition of Salt Creek. Interestingly, Salt Creek can be explained by GW-SW mixing (see Fig. D1 in Appendix), and the latter input (Salt Creek) was also considered a direct source of freshwater/brackish water input into the Coorong by previous studies (Mosley, 2016). Moreover, based on $^{87}\text{Sr}/^{86}\text{Sr}$ and Mg/Na tracers, the latter mixing scenario (GW-SW) was also observed as dominant mixing scenario for the Coorong lagoon water samples, in contrast to LL-SW mixing (Fig. D1B in Appendix). Nevertheless, the analysed water samples are only ‘snapshots’ of the CLLMM’s hydrological system, and more systematic and seasonal studies are needed to validate the above observations and interpretations.

Unlike $^{87}\text{Sr}/^{86}\text{Sr}$ tracer, the $\delta^{88/86}\text{Sr}$ can be used as an index for carbonate precipitation vs. dissolution, similar to the way $\delta^{44/40}\text{Ca}$ tracer has been used in the CLLMM system by Shao et al. (2018), to provide more advanced understanding of (i) local carbonate fluxes, and (ii) water source mixing in the Coorong.

3.5.1 Water source mixing and local carbonate cycling: Insights from $^{87}\text{Sr}/^{86}\text{Sr}$ and $\delta^{88/86}\text{Sr}$

$^{87}\text{Sr}/^{86}\text{Sr}$ and $\delta^{88/86}\text{Sr}$ of the samples from CLLMM (Fig. 3) confirmed that the North Lagoon wa-

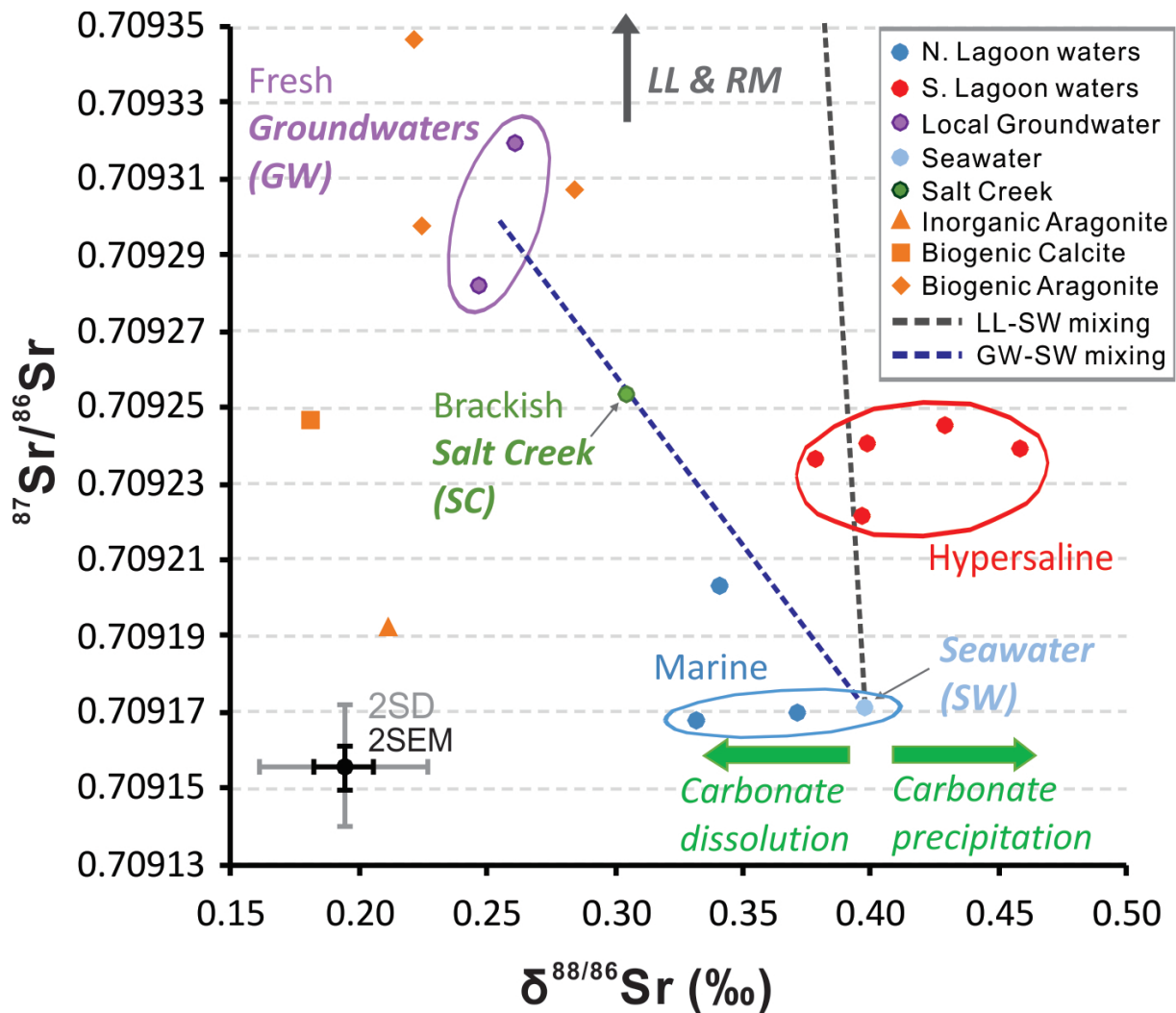


Figure 3: A cross-plot of $^{87}\text{Sr}/^{86}\text{Sr}$ vs. $\delta^{88/86}\text{Sr}$ values of waters and carbonates from the CLLMM. Note that the following abbreviations are used: LL = the Lower Lakes, RM = River Murray, GW = Groundwater, and SW = seawater). The dashed lines represent theoretical mixing lines for two water-source mixing scenarios (LL-SW and GW-SW). Green arrows illustrate expected shifts in $\delta^{88/86}\text{Sr}$ of local waters due to possible carbonate dissolution or precipitation in the Coorong. The 2SD and 2SEM errors were based on long-term IAPSO and JCP-1 standard measurements (see Appendix C.4).

ters with typical marine salinities of about 35 PSU were primarily sourced from seawater/Southern Ocean, as indicated by their marine $^{87}\text{Sr}/^{86}\text{Sr}$ ratios (~ 0.70917 , Fig. 2B). However, the generally lower $\delta^{88/86}\text{Sr}$ in North Lagoon waters indicates possible carbonate dissolution in comparison to seawater (Fig. 3), which is in agreement with the lower SI values for calcite/aragonite documented in the North Lagoon waters compared to typical seawater (Fig. 2D). This is possibly caused by occasional input of continental waters such as Murray River and Lower Lakes, which yielded highly undersaturated SI values of -0.25 to -1 (Fig. 2D), as expected for typical freshwaters, but such inputs are not detectable in $^{87}\text{Sr}/^{86}\text{Sr}$ data.

The influence of continental waters and seawater mixing in the South Lagoon was confirmed by their generally higher and non-marine $^{87}\text{Sr}/^{86}\text{Sr}$ values of ~ 0.70924 . In terms of $\delta^{88/86}\text{Sr}$, the South Lagoon

waters yielded 0.1 to 0.15‰ higher $\delta^{88/86}\text{Sr}$ than expected from a theoretical GW-SW mixing line (i.e., the interception of the horizontal line indicating the average $^{87}\text{Sr}/^{86}\text{Sr}$ in the South Lagoon and the GW-SW mixing line, Fig. 3). Although, these South Lagoon waters plot along the LL-SW mixing line (Fig. 3), it was not likely that the lake water was a major source as discussed in Appendix D.1. The Salt Creek water plots on the GW-SW mixing line, gave $^{87}\text{Sr}/^{86}\text{Sr}$ similar to the hypersaline South Lagoon, but its $\delta^{88/86}\text{Sr}$ was detectably lower ($\sim 0.1\%$) than ambient South Lagoon waters (Fig. 3), which was likely impacted by groundwater sourced from carbonate aquifers (Reid and Mosley, 2016), thus inherited low $\delta^{88/86}\text{Sr}$ from these carbonates. The importance of groundwater to Salt Creek water chemistry was also confirmed in Appendix D.1.

Overall, these data and observations led to several possible explanations with respect to plausible water sources and internal CaCO_3 cycling in the South Lagoon. One explanation is that the lagoon waters could be a mixture of local groundwater (GW) and seawater (SW), which is in agreement with purportedly significant local groundwater discharges to the Coorong proposed by Haese et al. (2008) and Barnett (2015). Alternatively, the brackish Salt Creek input could be the main source of water and Sr into the South Lagoon. In this case, we propose that high degree of water evaporation has caused oversaturation with respect to calcium carbonates, leading to progressive shifts to higher $\delta^{88/86}\text{Sr}$ in South lagoon waters (Fig. 3) due to carbonate precipitation (Shao et al., 2018). According to Reid and Mosley (2016), the waters in Salt Creek are supplied mostly from a local carbonate aquifer, with waters that are high in carbonate ions/alkalinity and pH (≥ 8.5), which was also confirmed by our data (see Table B.4, Appendix). This is consistent with the observed carbonate oversaturation in the Salt Creek waters (SI between 0.5 and 1, Fig. 2D). Consequently, the inflow of such alkalinity-charged waters might further promote the precipitation of carbonates in the South Lagoon, and thus its shifts to higher $\delta^{88/86}\text{Sr}$, especially near the inflow of Salt Creek waters into the lagoon (see the sample C11, $\delta^{88/86}\text{Sr} = \sim 0.45\%$, Figs. 2C and 3).

With respect to the carbonate samples (e.g., aragonitic shells and the crust), instead of providing an instant ‘snap shot’ of $^{87}\text{Sr}/^{86}\text{Sr}$ and $\delta^{88/86}\text{Sr}$ signals, which is the case for the local lagoon waters, the Sr isotope composition of carbonates rather reflects a long-term integrated signal of Sr inputs and local processes over a period of shell growth and/or formation of the inorganic carbonate crust. The $^{87}\text{Sr}/^{86}\text{Sr}$ recorded in the samples of biogenic skeletal carbonates (bivalves and tubeworm reef) yielded ratios ranging from ~ 0.70925 to ~ 0.70935 , which are higher than local North Lagoon waters (~ 0.70917) and closer to (i) South Lagoon waters and/or (ii) local continent-derived water sources (e.g., groundwater, Salt Creek waters). These observations thus suggest that the formation of the above biogenic minerals was affected by increased inputs from the River Murray and Lower Lakes due to higher barrage release to the North Lagoon, e.g. during 2016 (Mosley, 2016), increased groundwater recharge, or accompanied by potential overflow of the South Lagoon waters into the North Lagoon.

In contrast, in the South Lagoon, the closer-to-marine $^{87}\text{Sr}/^{86}\text{Sr}$ ratios of a local inorganic carbonate

precipitate (i.e., aragonite-rich crust) suggests that the South Lagoon has been receiving higher inputs of marine Sr in the past, likely via infiltration of seawater from the Southern Ocean into the Coorong. Importantly, the $\delta^{88/86}\text{Sr}$ of the inorganic aragonite crust, which was considered the main carbonate precipitate formed in the South Lagoon, yielded a value that is $\sim 0.2\%$ lower than the present day lagoon waters or typical seawater (Fig. 2C). This agrees with a typical stable Sr isotope fractionation between aragonite and a solution from laboratory experiments and/or natural systems (cf., Fruchter et al., 2016; Vollstaedt et al., 2014; AlKhatib and Eisenhauer, 2017). However, the difference in $\delta^{88/86}\text{Sr}$ values between biogenic carbonate (i.e., bivalve shells and tubeworm reefs) and local brackish waters in the North Lagoon is smaller, ranging between 0.10 and 0.15‰ (Fig. 2C), thus less than that observed in typical marine environments ($\sim 0.2\%$, Fruchter et al., 2016 and references therein). Nevertheless, due to the limited number of carbonate samples analysed in this study, and potential short term variability in $\delta^{88/86}\text{Sr}$ of local lagoon waters, the magnitude and exact mechanisms responsible for the stable Sr isotope fractionation between waters and biogenic/inorganic carbonates in the Coorong lagoon is difficult to assess and quantify at this stage. In summary, our limited data suggest that the difference between $\delta^{88/86}\text{Sr}$ of local carbonate minerals and lagoon waters in the Coorong is approximately 0.1 to 0.2‰.

3.5.2 Links between $\delta^{88/86}\text{Sr}$ and salinity/carbonate saturation of waters in the CLLMM

According to Von der Borch et al. (1975) and Fernandes and Tanner (2009), aragonite and calcite are the major carbonate precipitates in the Coorong, while gypsum precipitation occurs only seasonally (in summer season) but is generally insignificant. Moreover, our data suggest that carbonate precipitation (aragonite, calcite), rather than gypsum formation is the main control of $\delta^{88/86}\text{Sr}$ fractionation in the Coorong (see also Appendix D.2). Therefore, the following discussion and modelling only involves processes related to carbonates.

Overall, our data from the CLLMM support a general coupling between $\delta^{88/86}\text{Sr}$ and salinity (Fig. 4A), as well as aragonite/calcite saturation index (SI) of the waters (Fig. 4, see also SI data in Fig. 2D). In detail, CaCO_3 undersaturated freshwaters yielded $\delta^{88/86}\text{Sr}$ as low as $\sim 0.25\%$, brackish/marine waters plot around 0.35‰, and the oversaturated hypersaline lagoon waters gave positively fractionated $\delta^{88/86}\text{Sr}$ values up to $\sim 0.45\%$, thus higher than a normal seawater that is homogeneous at 0.40‰.

Among these lower salinity continental waters, the Salt Creek brackish water was exceptionally oversaturated with respect to CaCO_3 with SI about 0.7 (Fig. 4B), which may explain its slightly higher $\delta^{88/86}\text{Sr}$ of 0.30‰ compared to the rest of freshwaters (Fig. 4A); likely linked to the high alkalinity of the Salt Creek waters that should promote in-situ carbonate precipitation (Reid and Mosley, 2016; Shalev et al., 2017). A similar process involving ongoing carbonate formation can also explain sig-

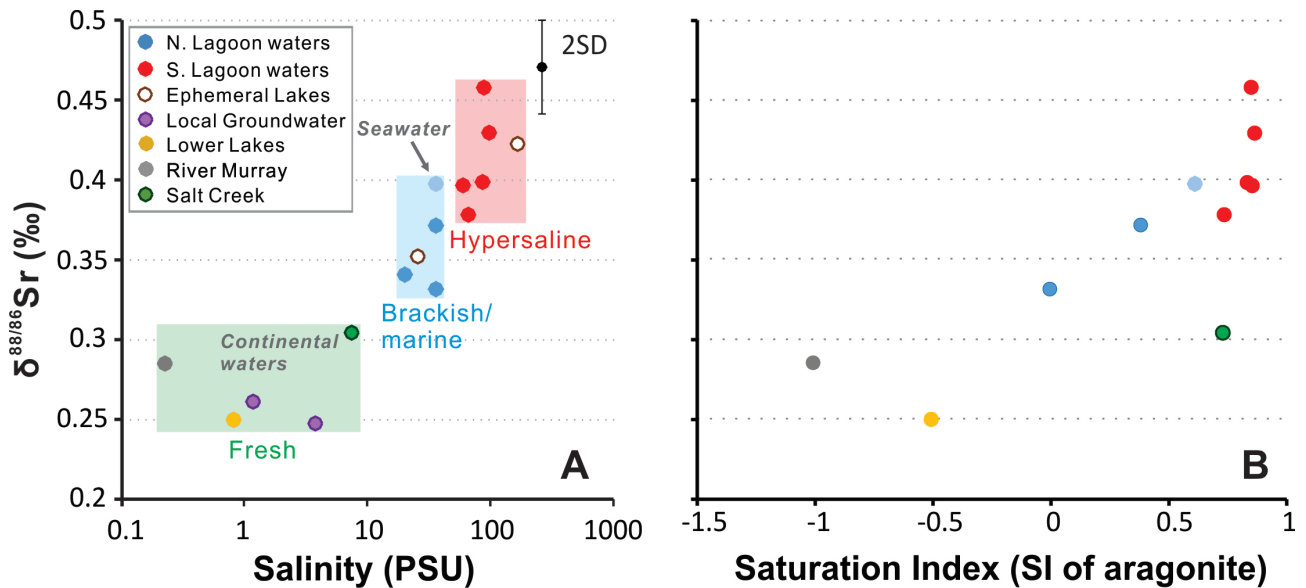


Figure 4: (A) $\delta^{88/86}\text{Sr}$ values of water samples from the CLLMM, plotted against their respective salinities, ranging from fresh to hypersaline, with source data listed in Table 1. (B) $\delta^{88/86}\text{Sr}$ values of water samples from the CLLMM plotted against their respective aragonite saturation indices (SI values) based on PHREEQC modelling of water data collected in May 2018. Note that based on XRD analysis of local sediments, inorganic aragonite precipitates (i.e., carbonate crusts) represent the main carbonate mineralogy in the South Lagoon.

nificantly high $\delta^{88/86}\text{Sr}$ values (in excess of 0.4‰ and thus higher than normal seawater) observed in the hypersaline waters of the South Lagoon (90 PSU), and/or in the ephemeral Halite Lake waters with salinity of about 160 PSU (Fig. 4A). In summary, our results and previous studies (Krabbenhöft et al., 2010; Fruchter et al., 2016; Shalev et al., 2017) suggest that carbonate formation/dissolution processes are the main drivers of the stable Sr isotope composition in natural waters, and the observed $\delta^{88/86}\text{Sr}$ variations in the CLLMM.

Interestingly, the results also suggest that the carbonate saturation in South lagoon waters reached a ‘plateau’ with aragonite SI values of ~ 0.7 (slightly higher than that of typical surface seawater), but the $\delta^{88/86}\text{Sr}$ values of local hypersaline waters is more variable. To further understand this spatial variation of $\delta^{88/86}\text{Sr}$ in the South Lagoon waters (ranging from $\sim 0.38\text{‰}$ to $\sim 0.45\text{‰}$, Fig. 4), which seems to scatter at SI of around ~ 1 , one should bear in mind that there are also numerous other factors such as (i) temperature, (ii) precipitation rate, (iii) biological Sr removal, and (iv) local water chemistry that may additionally affect stable Sr isotope fractionation in the lagoon or other near-surface environments, as documented by previous studies (Rüggeberg et al., 2008; Raddatz et al., 2013; Stevenson et al., 2014; AlKhatib and Eisenhauer, 2017).

Although carbonate saturation, rather than water salinity, seems to be the main driver of stable Sr isotope composition observed in the CLLMM waters, the tight link between these two parameters in the studied hydrological system suggests that there is potential to use $\delta^{88/86}\text{Sr}$ (complemented by $^{87}\text{Sr}/^{86}\text{Sr}$) to distinguish among (i) fresh/brackish, (ii) marine, and (iii) hypersaline waters in the CLLMM (Fig. 3).

3.5.3 Coupling between $\delta^{88/86}\text{Sr}$ and $\delta^{44/40}\text{Ca}$ in the CLLMM water samples

Shao et al. (2018) showed the sensitivity of stable Ca isotopes ($\delta^{44/40}\text{Ca}$) to local carbonate saturation of waters in the CLLMM, which can be simulated via a Rayleigh fractionation model. Similar properties were observed for $\delta^{88/86}\text{Sr}$ in this study as illustrated by data in Fig. 4 and discussed in the section 5.2. Moreover, the $\delta^{88/86}\text{Sr}$ and $\delta^{44/40}\text{Ca}$ data from the same waters and carbonates collected in the CLLMM hydrological system exhibit a statistically significant positive correlation ($R^2 = 0.90$, P value $\ll 0.05$, $n = 13$) (Fig. 5). This further corroborates common causative mechanism(s) for stable Sr and Ca isotope fractionation in the CLLMM linked to the dissolution/precipitation of carbonates.

Specifically, we discuss three common fractionation mechanisms – equilibrium (eq), chemical kinetic (kin), and diffusional kinetic (diff) fractionation, and their influence on $^{88}\text{Sr}/^{86}\text{Sr}$ and $^{44}\text{Ca}/^{40}\text{Ca}$ isotope fractionation. Following the studies of Young et al. (2002) and Böhm et al. (2012), one can calculate the slope or a ratio (β) for the $\Delta^{88/86}\text{Sr}_{(\text{carb-aq})}$ vs. $\Delta^{44/40}\text{Ca}_{(\text{carb-aq})}$ relationship for the above three main fractionation mechanisms (equilibrium, kinetic, and diffusional) using the equations below:

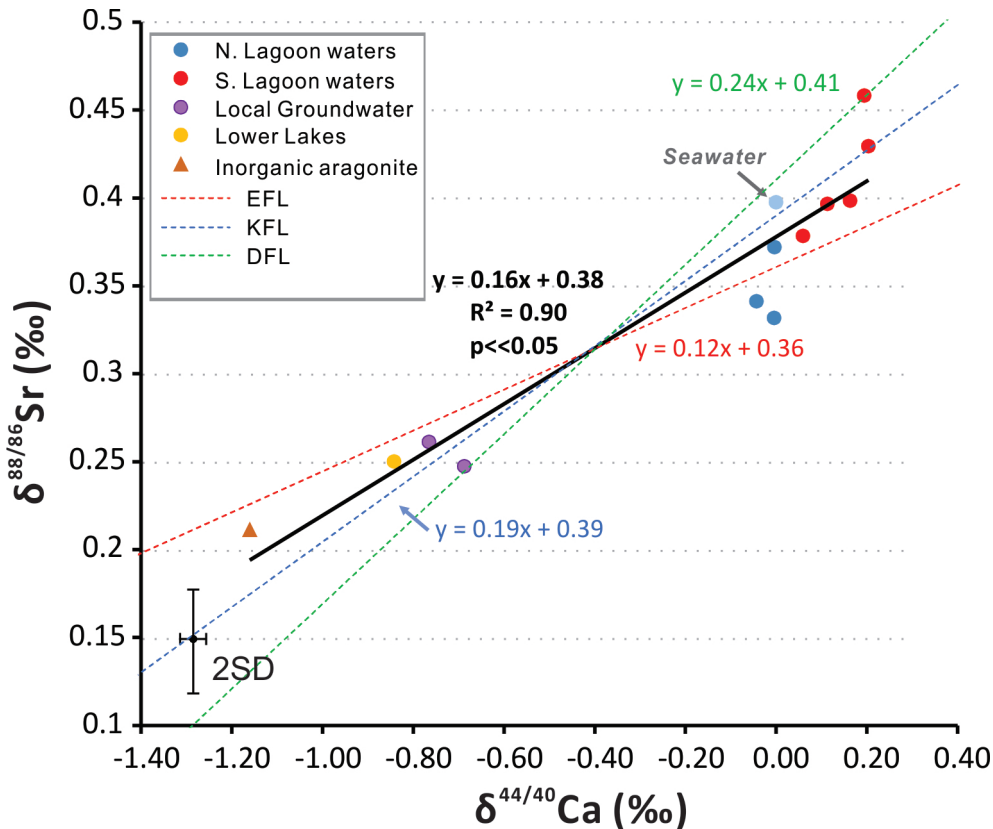


Figure 5: A cross-plot of $\delta^{88/86}\text{Sr}$ vs. $\delta^{44/40}\text{Ca}$ (normalised to IAPSO seawater) values in waters and the inorganic aragonitic carbonate crust (CLS-1) from the CLLMM hydrological system. The straight black line represents a line of best fit for the data, which can be written as a linear function. Note that $\delta^{44/40}\text{Ca}$ data are from Shao et al. (2018). The three dashed lines represent theoretical fractionation lines for equilibrium (EFL), chemical kinetic (KFL), and diffusional kinetic (DFL) fractionation mechanisms.

$$\beta_{\text{eq}} = (87.906^{-1} - 85.909^{-1}) / (43.955^{-1} - 39.963^{-1}) = 0.12 \quad (\text{Eq. 2})$$

$$\beta_{\text{kin}} = \log(\mu_{\text{Sr(h)}} / \mu_{\text{Sr(l)}}) / \log(\mu_{\text{Ca(h)}} / \mu_{\text{Ca(l)}}) \quad (\text{Eq. 3})$$

where $\mu_{i(\text{h})}$ and $\mu_{i(\text{l})}$ represent reduced masses for the heavy and light isotopes of element i , respectively, calculated as $\mu_i = M * m_i / (M + m_i)$, and M is the mass of the molecules contributing to the reacting complex bonded to the element of interest. The equation was calculated with $M = 108.1$ amu for $(\text{H}_2\text{O})_6$, $M = 144.1$ amu for $(\text{H}_2\text{O})_8$ and the respective atomic strontium and calcium isotope masses. Based on these values and parametrisation, the $\beta_{\text{kin}} = 0.19$

Finally, the slope or β_{diff} for the diffusional kinetic fractionation for stable Sr and Ca isotopes is calculated based on:

$$\beta_{\text{diff}} = \log(87.906/85.909) / \log(43.955/39.963) = 0.24 \quad (\text{Eq. 4})$$

These β values, reflecting the slopes for theoretical mass-dependent fractionation lines (EFL, KFL and DFL) are illustrated in Fig. 5, and plotted along with $\delta^{88/86}\text{Sr}$ and $\delta^{44/40}\text{Ca}$ data from the CLLMM. Interestingly, the slope for the latter data yielded a value of 0.16, thus plotting between KFL (slope = 0.19) and EFL (slope = 0.12), suggesting that both chemical kinetic and equilibrium fractionation processes were responsible for the observed stable Sr and Ca isotope variations measured in the CLLMM data.

Nevertheless, there are also some differences between stable Sr and Ca isotope data from the CLLMM. Specifically, the $\delta^{88/86}\text{Sr}$ of certain North Lagoon waters were slightly lower than that of the seawater (see also section 5.1, Figs. 3 and 2D), while $\delta^{44/40}\text{Ca}$ data did not show such discrepancy (Fig. 5 and Shao et al., 2018). In addition, $\delta^{88/86}\text{Sr}$ of hypersaline South Lagoon waters varied from close to seawater values of ca. 0.38‰ up to ~0.45‰ (see Fig. 2C), but the $\delta^{44/40}\text{Ca}$ of these samples were consistently higher than that of a typical seawater (i.e. Southern Ocean and/or North Lagoon waters). These slight differences in the behaviour of $\delta^{88/86}\text{Sr}$ and $\delta^{44/40}\text{Ca}$ tracers in the Coorong lagoon might be a result of (i) different concentrations and thus residence times of Sr and Ca in the lagoon, impacting the response of their isotope tracers to perturbations, (ii) higher uptake of Sr into aragonite relative to calcite and associated isotope effects, and different solubilities of these carbonate minerals in water, and finally also perhaps due to (iii) variable precipitation rates of carbonates in the lagoon and their comparably different influence on stable Ca and Sr isotopes (Fruchter et al., 2016 and 2017; AlKhatib and Eisenhauer, 2017). Overall, both isotope tracers, $\delta^{88/86}\text{Sr}$ and $\delta^{44/40}\text{Ca}$, suggest that the most saline and oversaturated lagoon waters had experienced highest net removal of light Sr and Ca isotopes from lagoon waters into precipitating carbonates (Figs. 3, 5 and Shao et al., 2018).

3.5.4 Quantifying carbonate removal in the Coorong via $\delta^{88/86}\text{Sr}$ and Rayleigh modelling

Given that both $\delta^{88/86}\text{Sr}$ and $\delta^{44/40}\text{Ca}$ tracers are controlled by similar fractionation processes, one should be able to quantify the net removal of Sr^{2+} from waters in the South Lagoon driven by ongoing carbonate (mainly aragonite) precipitation using stable Sr isotopes (as done previously for Ca isotopes, Shao et al., 2018). These processes can be quantified via Rayleigh and equilibrium isotope fractionation models (Frings et al., 2016; and Shao et al., 2018), which allow simulation of $\delta^{88/86}\text{Sr}$ variations in lagoon waters as a function of carbonate precipitation. In this case, only the GW/SC-SW (groundwater/Salt Creek-seawater) mixing scenario is shown in the models, since it is dominant in the Coorong for our samples as discussed in the beginning of section 5 and Appendix D.1.

The Rayleigh model assumes no interaction between precipitated carbonate (i.e. product) and lagoon waters (i.e., reactant). In this case, the stable Sr isotope fractionation (α) between a local lagoon water (i.e., reactant) and precipitated carbonate mineral (i.e., product) controls the $\delta^{88/86}\text{Sr}$ signature of the water based on the following equation:

$$\delta^{88/86}\text{Sr} = [(\delta^{88/86}\text{Sr}_{\text{INI}} + 10^3) (1 - f_{\text{CC}})^{(\alpha_{\text{CC}} - 1)}] - 10^3 \quad (\text{Eq. 5})$$

where $\delta^{88/86}\text{Sr}$ represents the Sr isotope composition of a residual unreacted Sr pool in the lagoon; f_{CC} represents the fraction of Sr^{2+} that was removed as aragonite (i.e., product); the $\delta^{88/86}\text{Sr}_{\text{INI}}$ or the initial Sr isotope composition of lagoon water (with no carbonate precipitation, i.e., $f_{\text{CC}} = 0$) is set at different values in our models for different scenarios. Specifically, the expected $\delta^{88/86}\text{Sr}_{\text{INI}}$ value (equals 0.32‰) can be inferred from the theoretical mixing lines as shown in Fig. D.4, Appendix D.3 using the $^{87}\text{Sr}/^{86}\text{Sr}$ of lagoon water.

The parameter α is the Sr isotope fractionation factor between the lagoon water and precipitated CaCO_3 ,

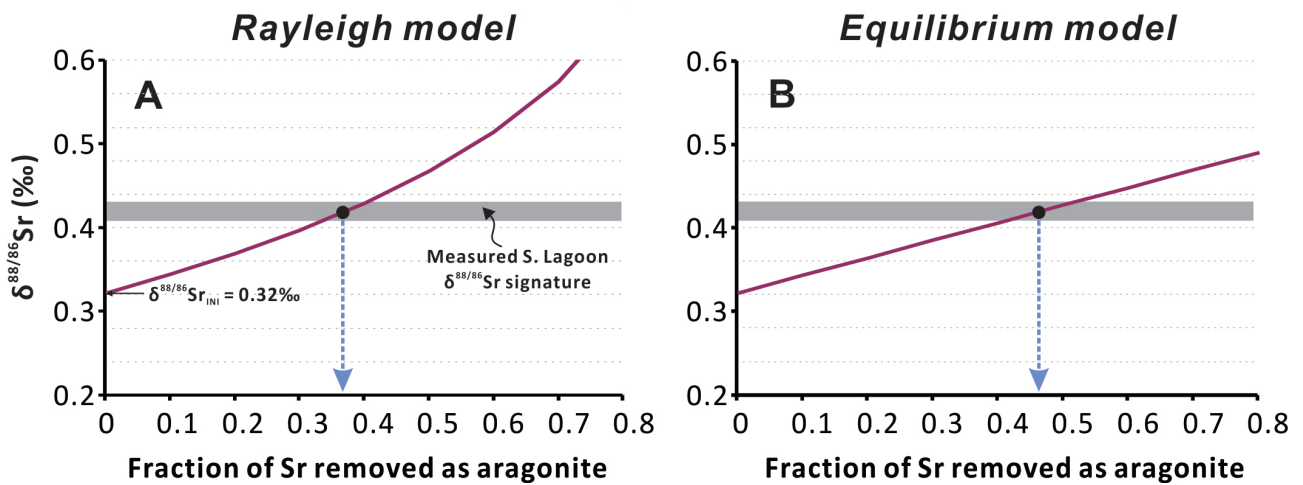


Figure 6: Plots showing modelled $\delta^{88/86}\text{Sr}$ trends in the South Lagoon waters as a function of Sr fraction removed from the lagoon waters as aragonite. (A) The Rayleigh model; (B) the equilibrium model. The grey band represents the measured $\delta^{88/86}\text{Sr}$ variations in the South Lagoon waters, and coloured line illustrate GW/SC-SW (groundwater/Salt Creek-seawater) mixing scenario for $\delta^{88/86}\text{Sr}_{\text{INI}}$ of 0.32‰.

(i.e., aragonite, denoted as subscript CC), the latter calculated by:

$$\alpha_{CC} = (1 + \delta^{88/86}\text{Sr}_{CC}/1000)/(1 + \delta^{88/86}\text{Sr}_{MIX}/1000) = (1000 + \delta^{88/86}\text{Sr}_{CC})/(1000 + \delta^{88/86}\text{Sr}_{MIX}) \quad (\text{Eq. 6})$$

where $\delta^{88/86}\text{Sr}_{CC}$ is the stable Sr isotope signature of the precipitated CaCO_3 mineral (0.21‰), and $\delta^{88/86}\text{Sr}_{MIX}$ refers to the lagoon water (0.42‰), based on data from the studied CLLMM system (see Fig. 3). Accordingly, the specific α_{CC} (i.e., stable Sr isotope fractionation factor) calculated for the Coorong water-carbonate system has a value of 0.9998.

In contrast with the Rayleigh model, the equilibrium model considers interactions and an isotope exchange (i.e., equilibration) between the product and reactant (Frings et al., 2016); and the evolution of $\delta^{88/86}\text{Sr}$ in lagoon waters due to aragonite precipitation based on this model can be calculated using the following equation (Frings et al., 2016; Shao et al., 2018):

$$\delta^{88/86}\text{Sr} = \delta^{88/86}\text{Sr}_{INI} + \varepsilon f_{CC} \quad (\text{Eq. 7})$$

where $\delta^{88/86}\text{Sr}_{INI}$ is the same as that mentioned above; and ε is the fractionation isotope effect, which is related to the abovementioned α_{CC} based on:

$$\varepsilon = -10^3 (\alpha_{CC} - 1) \quad (\text{Eq. 8})$$

Results of both models (Fig. 6) suggest that the fraction of Sr removed from the South Lagoon as aragonite, ranges from 35% to 45% (for Rayleigh and Equilibrium models, respectively). Given that the Sr/Ca ratio of the South Lagoon waters (and precipitated aragonite) is relatively constant (see Table B.1, Fig. B.1 in Appendix, and data in Shao et al., 2018), and the typical Sr partition coefficient K_d of marine aragonite, defined as $K_d^{ar} = (\text{Sr}/\text{Ca})_{ar}/(\text{Sr}/\text{Ca})_{fluid}$, is ~ 1 (Gaetani and Cohen, 2006), it is reasonable to assume that the fraction of Sr removed from the lagoon is proportional to the fraction of Ca that has been removed into CaCO_3 . Indeed, our $\delta^{88/86}\text{Sr}$ data and modelling suggest that the South Lagoon acts as a net sink for CaCO_3 , which is in agreement with Shao et al. (2018) who used $\delta^{44/40}\text{Ca}$ to generate a similar estimate of 35 to 45% Ca removal by aragonite precipitation in the South Lagoon.

3.5.5 Coupled $^{87}\text{Sr}/^{86}\text{Sr}$ and $\delta^{88/86}\text{Sr}$ approach for palaeo-hydrology and salinity reconstructions

Plotting the main water sources in $^{87}\text{Sr}/^{86}\text{Sr}$ vs. salinity plots (see data and legend in Fig. 7A) revealed that the traditional $^{87}\text{Sr}/^{86}\text{Sr}$ tracer can help to distinguish (i) a normal seawater (with typical marine $^{87}\text{Sr}/^{86}\text{Sr}$ of ~ 0.70917) from (ii) non-marine water sources impacted by continental weathering and thus higher and more radiogenic $^{87}\text{Sr}/^{86}\text{Sr}$ (typically > 0.7092), the latter originating from surficial freshwaters (rivers, streams) and/or subsurface groundwaters. However, as illustrated in Fig. 7A, the $^{87}\text{Sr}/^{86}\text{Sr}$ tracer cannot faithfully distinguish between (i) fresh and (ii) hypersaline water sources in the

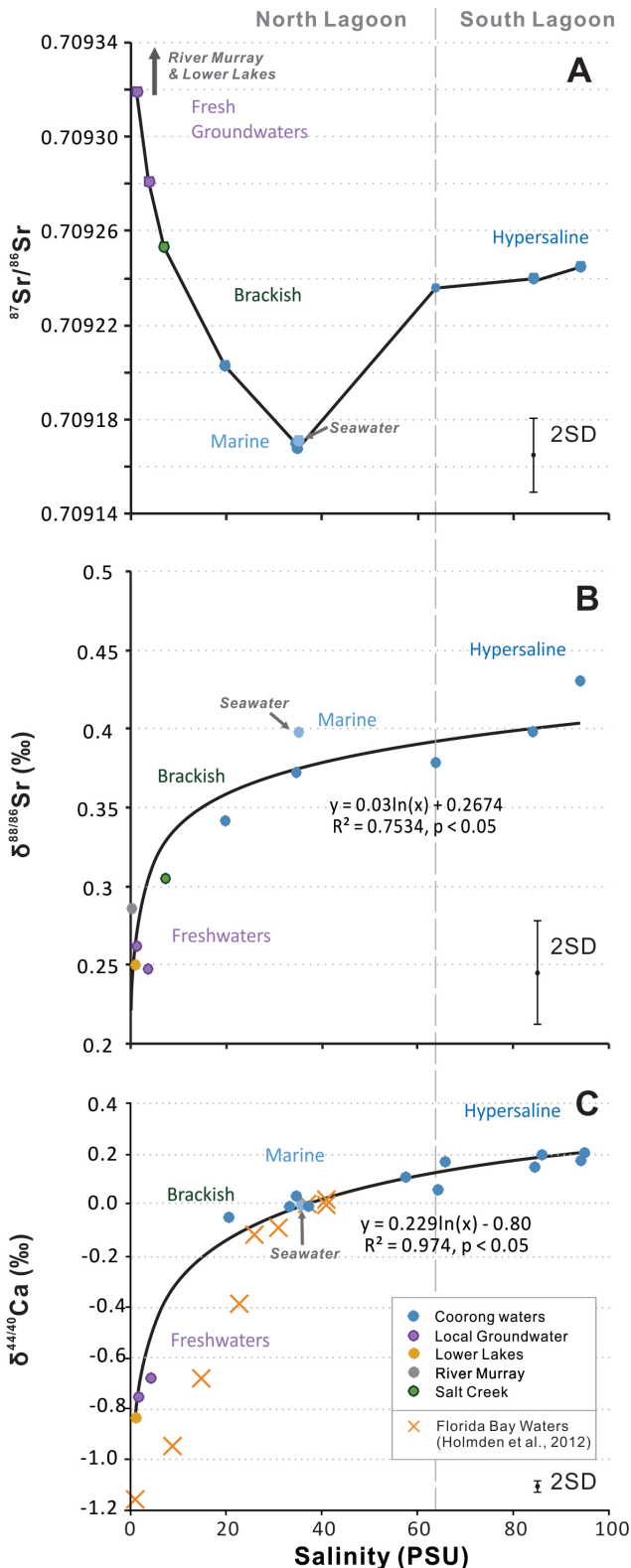


Figure 7: (A) $^{87}\text{Sr}/^{86}\text{Sr}$ of main water sources in the CLLMM, plotted against their water salinities (in PSU). (B) $\delta^{88/86}\text{Sr}$ vs. salinity of main water sources in the CLLMM. (C) $\delta^{44/40}\text{Ca}$ vs. salinity of main water sources in the CLLMM (data from Shao et al., 2018) and Florida Bay (data from Holmden et al., 2012). The dashed lines represent theoretical mixing trends for two water-source mixing scenarios (LL-SW and GW-SW) calculated by isotope mass balance.

studied CLLMM system, as both have been affected by continental waters and thus have overlapping and non-marine $^{87}\text{Sr}/^{86}\text{Sr}$ ratios. In contrast, $\delta^{88/86}\text{Sr}$ values of CLLMM waters, impacted by carbonate dissolution/precipitation processes, correlate strongly with the salinity (Fig. 7B) and to some degree also with calcite/aragonite saturation (SI) of CLLMM waters (Fig. 4B). Based on these observations, fresh and undersaturated CLLMM waters yielded low $\delta^{88/86}\text{Sr}$, while hypersaline and oversaturated waters have systematically higher $\delta^{88/86}\text{Sr}$ values. Accordingly, a coupled Sr isotope approach that combines $\delta^{88/86}\text{Sr}$ and $^{87}\text{Sr}/^{86}\text{Sr}$ traces could be applied to other carbonate-producing lagoon-estuarine systems or coastal settings worldwide, such as the Florida Bay (Fig. 7C, Holmden et al., 2012). Moreover, if the observed difference between $\delta^{88/86}\text{Sr}$ of local carbonate minerals and present-day lagoon water in the Coorong has been constant through time, then such a coupled approach combining $^{87}\text{Sr}/^{86}\text{Sr}$ and $\delta^{88/86}\text{Sr}$ analysis of fossil carbonates can be used to reconstruct palaeo-hydrology and water source mixing, and by inference palaeo-salinity, in the past CLLMM system.

3.6 Conclusions

This study shows that $\delta^{88/86}\text{Sr}$ of the waters from the Coorong, Lower Lakes and Murray Mouth estuary in South Australia exhibit a general-

ly increasing trend with increasing carbonate saturation and salinity of local waters. Specifically, the hypersaline waters in the Coorong lagoon have the highest $\delta^{88/86}\text{Sr}$ up to 0.45‰ due to ongoing carbonate formation (i.e., higher than typical seawater at $0.40 \pm 0.016\text{‰}$), while freshwaters (river, groundwater, and lake water) yielded systematically lower $\delta^{88/86}\text{Sr}$ values (as low as 0.25‰), likely linked to carbonate dissolution that supplies light Sr from continental weathering of carbonate rocks. This study also revealed a statistically significant positive correlation between stable Sr and Ca isotope data in waters across the CLLMM, where both tracers $\delta^{88/86}\text{Sr}$ (this study) and $\delta^{44/40}\text{Ca}$ (Shao et al., 2018) seem to be controlled by common underlying mechanisms, following equilibrium and kinetic fractionation linked to carbonate dissolution/precipitation processes. The latter process was further quantified by PHREEQC modelling of carbonate saturation in local CLLMM waters. The estimates of Sr removal in the Coorong using Rayleigh and equilibrium models based on $\delta^{88/86}\text{Sr}$ data is 35-45%, which provided similar results as the Ca removal calculated based on $\delta^{44/40}\text{Ca}$ data (Shao et al., 2018). Both $\delta^{88/86}\text{Sr}$ and $\delta^{44/40}\text{Ca}$ tracers indicate that the South Lagoon acts as a net sink for dissolved inorganic C due to ongoing CaCO_3 precipitation, mostly as aragonite, which readily forms in hypersaline and oversaturated local lagoon waters. Thus, the results of this study suggest that $\delta^{88/86}\text{Sr}$ can be used as an alternative or complementary proxy to $\delta^{44/40}\text{Ca}$ to constrain the local carbon cycling and CaCO_3 dissolution/precipitation processes in coastal systems, with potential application in studying ocean acidification and coastal carbon cycling. Finally, the coupled approach based on stable and radiogenic Sr isotopes ($^{87}\text{Sr}/^{86}\text{Sr}$ and $\delta^{88/86}\text{Sr}$), presented in this study, can be also applied to ancient carbonates, with potential for palaeo-hydrology and salinity reconstructions of the CLLMM and/or other carbonate producing coastal and lagoon-estuarine systems.

Acknowledgements

This work was supported by the Project Coorong (HCHB – Healthy Coorong Healthy Basin program) and the Czech Science Foundation (GACR grant No. 17-18120S), and additional support from the Environment Institute of the University of Adelaide as well as an ARC Linkage project (LP160101353) are also acknowledged. This study is part of the Ph.D. research of YS, supported by an Adelaide Graduate Research Scholarship, ANSTO research portal (No. 11642), and funding from the CRC LEME Regolith Science Scholarship via Cooperative Research Centre for Landscape Environments and Mineral Exploration (CRC LEME) Regolith Science Scholarship.

The sampling in the Coorong National Park was performed under the Department for Environment and Water (DEW) research permit No. U26745-1. The living bivalve shell samples were collected under the Primary Industries and Regions South Australia Ministerial Exemption number 9902844. The water quality data provided by the DEW is gratefully acknowledged. Technical and laboratory assistance provided by David Bruce at University of Adelaide is greatly appreciated, especially re-

garding the training sessions, and the maintenance of TIMS and clean laboratory facilities. We also thank Sima Bargrizan and Flynn Watson for their assistance with pH and alkalinity analyses at the University of Adelaide.

References

AlKhatib, M. and Eisenhauer, A. (2017) Calcium and strontium isotope fractionation during precipitation from aqueous solutions as a function of temperature and reaction rate; II. Aragonite. *Geochimica et Cosmochimica Acta* **209**, 320-342.

Andrews, M. G., Jacobson, A. D., Lehn, G. O., Horton, T. W. and Craw, D. (2016) Radiogenic and stable Sr isotope ratios ($^{87}\text{Sr}/^{86}\text{Sr}$, $\delta^{88/86}\text{Sr}$) as tracers of riverine cation sources and biogeochemical cycling in the Milford Sound region of Fiordland, New Zealand. *Geochimica et Cosmochimica Acta* **173**, 284-303.

Andrews, M. G. and Jacobson, A. D. (2017) The radiogenic and stable Sr isotope geochemistry of basalt weathering in Iceland: role of hydrothermal calcite and implications for long-term climate regulation. *Geochimica et Cosmochimica Acta* **215**, 247-262.

Anthony, A., Atwood, J., August, P., Byron, C., Cobb, S., Foster, C., Fry, C., Gold, A., Hagos, K., Heffner, L., Kellogg, D. Q., Lellis-Dibble, K., Opaluch, J. J., Oviatt, C., Pfeiffer-Herbert, A., Rohr, N., Smith, L., Smythe, T., Swift, J. and Vinhateiro, N. (2009) Coastal lagoons and climate change: ecological and social ramifications in U.S. Atlantic and Gulf coast ecosystems. *Ecology and Society* **14**, 8.

Barnett, S. (2015) Assessment of the groundwater resources in the non-prescribed areas of the South Australian Murray-Darling Basin, DEWNR Technical report 2015/09, Government of South Australia, Department of Environment, Water and Natural Resources, Adelaide. ISBN: 978-1-922255-47-1.

Brookes, J., Dalby, P., Dittmann, S., O'Connor, J., Paton, D., Quin, R., Rogers, D., Waycott, M. and Ye, Q. (2018) *Recommended actions for restoring the ecological character of the South Lagoon of the Coorong*. Goyder Institute for Water Research Technical Report Series No. 18/04, Adelaide, South Australia. ISSN: 1839-2725.

Bullen T. D. and Bailey S. W. (2005) Identifying calcium sources at an acid deposition-impacted spruce forest: a strontium isotope, alkaline earth element multi-tracer approach. *Biogeochemistry* **74**, 63-99.

Böhm, F., Eisenhauer, A., Tang, J., Dietzel, M., Krabbenhöft, A., Kisakürek, B. and Horn, C. (2012) Strontium isotope fractionation of planktic foraminifera and inorganic calcite. *Geochimica et Cosmo-*

chimica Acta **93**, 300-314.

Capo, R. C., Stewart, B. W. and Chadwick, O. A. (1998) Strontium isotopes as tracers of ecosystem processes: theory and methods. *Geoderma* **82**, 197-225.

Caro, G., Papanastassiou, D.A., Wasserburg, G.J. (2010) ^{40}K - ^{40}Ca isotopic constrains on oceanic calcium cycle. *Earth and Planetary Science Letters* **296**, 124-132.

Chamberlayne, B. K., Tyler, J. J. and Gillanders, B. M. (2019) Environmental Controls on the Geochemistry of a Short-Lived Bivalve in Southeastern Australian Estuaries. *Estuaries and Coasts*, 1-16.

Chao, H. C., You, C. F., Liu, H. C. and Chung, C. H. (2013) The origin and migration of mud volcano fluids in Taiwan: Evidence from hydrogen, oxygen, and strontium isotopic compositions. *Geochimica et Cosmochimica Acta* **114**, 29-51.

Chao, H. C., You, C. F., Liu, H. C. and Chung, C. H. (2015) Evidence for stable Sr isotope fractionation by silicate weathering in a small sedimentary watershed in southwestern Taiwan. *Geochimica et Cosmochimica Acta* **165**, 324-341.

de Souza, G. F., Reynolds, B. C., Kiczka, M. and Bourdon, B. (2010) Evidence for mass-dependent isotopic fractionation of strontium in a glaciated granitic watershed. *Geochimica et Cosmochimica Acta* **74**, 2596-2614.

Dittmann, S., Rolston, A., Bengler, S. N. and Kupriyanova, E. K. (2009) *Habitat requirements, distribution and colonisation of the tubeworm *Ficopomatus enigmaticus* in the Lower Lakes and Coorong*. Report for the South Australian Murray-Darling Basin Natural Resources Management Board, Adelaide, 99.

Farkaš, J., Böhm, F., Wallmann, K., Blenkinsop, J., Eisenhauer, A., Van Geldern, R., Munnecke, A., Voigt, S. and Veizer, J. (2007) Calcium isotope record of Phanerozoic oceans: Implications for chemical evolution of seawater and its causative mechanisms. *Geochimica et Cosmochimica Acta* **71**, 5117-5134.

Farkaš, J., Déjeant, A., Novák, M. and Jacobsen, S. B. (2011) Calcium isotope constraints on the uptake and sources of Ca^{2+} in a base-poor forest: a new concept of combining stable ($\delta^{44/42}\text{Ca}$) and radiogenic (ϵ_{Ca}) signals. *Geochimica et Cosmochimica Acta* **75**, 7031-7046.

Farkaš, J., Frýda, J. and Holmden, C. (2016) Calcium isotope constraints on the marine carbon cycle and CaCO_3 deposition during the late Silurian (Ludfordian) positive $\delta^{13}\text{C}$ excursion. *Earth and Planetary Science Letters* **451**, 31-40.

Fernandes, M. and Tanner, J. E. (2009) Hypersalinity and phosphorus availability: the role of mineral

precipitation in the Coorong lagoons of South Australia. CSIRO: Water for a Healthy Country National Research Flagship and South Australian Research and Development Institute (Aquatic Sciences).

Finch, A. A. and Allison, N. (2007) Coordination of Sr and Mg in calcite and aragonite. *Mineralogical Magazine* **71**, 539-552.

Frings, P. J., Clymans, W., Fontorbe, G., Christina, L. and Conley, D. (2016) The continental Si cycle and its impact on the ocean Si isotope budget. *Chemical Geology* **425**, 12-36.

Fruchter, N., Eisenhauer, A., Dietzel, M., Fietzke, J., Böhm, F., Montagna, P., Stein, M., Lazar, B., Rodolfo-Metalpa, R. and Erez, J. (2016) $^{88}\text{Sr}/^{86}\text{Sr}$ fractionation in inorganic aragonite and in corals. *Geochimica et cosmochimica acta* **178**, 268-280.

Fruchter, N., Lazar, B., Nishri, A., Almogi-Labin, A., Eisenhauer, A., Shlevin, Y. B. E. and Stein, M. (2017) $^{88}\text{Sr}/^{86}\text{Sr}$ fractionation and calcite accumulation rate in the Sea of Galilee. *Geochimica et Cosmochimica Acta* **215**, 17-32.

Gaetani, G. A. and Cohen, A. L. (2006) Element partitioning during precipitation of aragonite from seawater: a framework for understanding paleoproxies. *Geochimica et Cosmochimica Acta* **70**, 4617-4634.

Gillanders, B. M. and Munro, A. R. (2012) Hypersaline waters pose new challenges for reconstructing environmental histories of fish based on otolith chemistry. *Limnology and Oceanography* **57**, 1136.

Glamore, W. C., Rayner, D. S. and Rahman, P. F. (2016) Estuaries and climate change. Technical Monograph prepared for the National Climate Change Adaptation Research Facility. Water Research Laboratory of the School of Civil and Environmental Engineering, UNSW.

Haese, R. R., Gow, L., Wallace, L. and Brodie, R. S. (2008) Identifying groundwater discharge in the Coorong (South Australia). *AUSGEO news* **91**, 1-6.

Heuser, A., Eisenhauer, A., Gussone, N., Bock, B., Hansen, B. T. and Nægler, T. F. (2002) Measurement of calcium isotopes ($\delta^{44}\text{Ca}$) using a multicollector TIMS technique. *International Journal of Mass Spectrometry* **220**, 385-397.

Hodell, D. A., Mead, G. A. and Mueller, P. A. (1990) Variation in the strontium isotopic composition of seawater (8 Ma to present): Implications for chemical weathering rates and dissolved fluxes to the oceans. *Chemical Geology: Isotope Geoscience section* **80**, 291-307.

Hoefs, J. (2018) Isotope fractionation processes of selected elements. In *Stable Isotope Geochemistry*. Springer, Cham. pp. 53-227.

Holmden, C., Creaser, R. A. and Muehlenbachs, K. (1997) Paleosalinities in ancient brackish water

systems determined by $^{87}\text{Sr}/^{86}\text{Sr}$ ratios in carbonate fossils: a case study from the Western Canada Sedimentary Basin. *Geochimica et Cosmochimica Acta* **61**, 2105-2118.

Holmden, C., Papanastassiou, D. A., Blanchon, P. and Evans, S. (2012) $\delta^{44/40}\text{Ca}$ variability in shallow water carbonates and the impact of submarine groundwater discharge on Ca-cycling in marine environments. *Geochimica et Cosmochimica Acta* **83**, 179-194.

Krabbenhöft, A., Fietzke, J., Eisenhauer, A., Liebetrau, V., Böhm, F. and Vollstaedt, H. (2009) Determination of radiogenic and stable strontium isotope ratios ($^{87}\text{Sr}/^{86}\text{Sr}$; $\delta^{88/86}\text{Sr}$) by thermal ionization mass spectrometry applying an $^{87}\text{Sr}/^{84}\text{Sr}$ double spike. *Journal of Analytical Atomic Spectrometry* **24**, 1267-1271.

Krabbenhöft, A., Eisenhauer, A., Böhm, F., Vollstaedt, H., Fietzke, J., Liebetrau, V., Augustin, N., Peucker-Ehrenbrink, B., Müller, M. N., Horn, C., Hansen, B. T., Nolte, N. and Wallmann, K. (2010) Constraining the marine strontium budget with natural strontium isotope fractionations ($^{87}\text{Sr}/^{86}\text{Sr}^*$, $\delta^{88/86}\text{Sr}$) of carbonates, hydrothermal solutions and river waters. *Geochimica et cosmochimica acta* **74**, 4097-4109.

Kuznetsov, A.B., Semikhatov, M.A., Gorokhov, I.M. (2012) The Sr isotope composition of the world ocean, marginal and inland seas: Implications for the Sr isotope stratigraphy. In: *Stratigraphy and Geological Correlation*, Vol. 20, p. 501-515. Pleiades Publishing Ltd. ISSN 086-5938.

Lazar, B., Starinsky, A., Katz, A., Sass, E. and Ben-Yaakov, S (1983). The carbonate system in hypersaline solutions: alkalinity and CaCO_3 solubility of evaporated seawater. *Limnology and Oceanography* **28**, 978-986.

Lewis, E. and Wallace, D. (1998) *Program developed for CO_2 system calculations* (No. ORNL/CDI-AC-105). Brookhaven National Lab., Dept. of Applied Science, Upton, NY (United States); Oak Ridge National Lab., Carbon Dioxide Information Analysis Center, TN (United States).

Macreadie, P. I., Serrano, O., Maher, D. T., Duarte, C. M. and Beardall, J. (2017) Addressing calcium carbonate cycling in blue carbon accounting. *Limnology and Oceanography Letters* **2**, 195-201.

Menadakis, M., Maroulis, G. and Koutsoukos, P. G. (2009) Incorporation of Mg^{2+} , Sr^{2+} , Ba^{2+} and Zn^{2+} into aragonite and comparison with calcite. *Journal of mathematical chemistry* **46**, 484.

Mosley, L. M. (2016) Barrage release optimisation trial August 2015: assessment of environmental outcomes and achievement of management objectives. University of Adelaide, South Australia.

Mosley, L. M., Ye, Q., Shepherd, S., Hemming, S. and Fitzpatrick, R. (2019) *Natural history of the Coorong, Lower Lakes, and Murray Mouth region (Yarluwar-Ruwe)*. University of Adelaide Press on behalf of the Royal Society of South Australia.

Nier, A.O. (1938) The isotopic constitution of strontium, barium, bismuth, thallium and mercury. *Phys. Rev.* **5**, 275–278.

Nordstrom, D. K., Plummer, L. N., Wigley, T. M. L., Wolery, T. J., Ball, J. W., Jenne, E. A., Bassett, R. L., Crerar, D. A., Florence, T. M., Fritz, B., Hoffman, M., Holdren, Jr., G. R., Lafon, G. M., Mattigod, S. V., McDuff, R. E., Morel, F., Reddy, M. M., Sposito, G. and Thraillkill, J. (1979) A comparison of computerized chemical models for equilibrium calculations in aqueous systems. In *Chemical Modeling in Aqueous Systems* (ed. E.A Jenne). American Chemical Society, Washington, pp. 857-892.

Palchan, D., Stein, M., Almogi-Labin, A., Erel, Y. and Goldstein, S. L. (2013) Dust transport and synoptic conditions over the Sahara–Arabia deserts during the MIS6/5 and 2/1 transitions from grain-size, chemical and isotopic properties of Red Sea cores. *Earth and Planetary Science Letters* **382**, 125-139.

Parkhurst, D. L. and Appelo, C. A. J. (2013) *Description of input and examples for PHREEQC version 3: a computer program for speciation, batch-reaction, one-dimensional transport, and inverse geochemical calculations* (No. 6-A43). US Geological Survey.

Pearce, C. R., Parkinson, I. J., Gaillardet, J., Charlier, B. L., Mokadem, F. and Burton, K. W. (2015) Reassessing the stable ($\delta^{88/86}\text{Sr}$) and radiogenic ($^{87}\text{Sr}/^{86}\text{Sr}$) strontium isotopic composition of marine inputs. *Geochimica et Cosmochimica Acta* **157**, 125-146.

Raddatz, J., Liebetrau, V., Rüggeberg, A., Hathorne, E., Krabbenhöft, A., Eisenhauer, A., Böhm, F., Vollstaedt, H., Fietzke, J., López Correa, M., Freiwald, A. and -Chr.Dullo, W., (2013) Stable Sr-isotope, Sr/Ca, Mg/Ca, Li/Ca and Mg/Li ratios in the scleractinian cold-water coral *Lophelia pertusa*. *Chemical geology* **352**, 143-152.

Reeves, J. M., Haynes, D., García, A. and Gell, P. A. (2015) Hydrological change in the Coorong Estuary, Australia, past and present: Evidence from fossil invertebrate and algal assemblages. *Estuaries and coasts* **38**, 2101-2116.

Reid, R. J. and Mosley, L. M. (2016) Comparative contributions of solution geochemistry, microbial metabolism and aquatic photosynthesis to the development of high pH in ephemeral wetlands in South East Australia. *Science of the Total Environment* **542**, 334-343.

Rüggeberg, A., Fietzke, J., Liebetrau, V., Eisenhauer, A., Dullo, W. C. and Freiwald, A. (2008) Stable strontium isotopes ($\delta^{88/86}\text{Sr}$) in cold-water corals—a new proxy for reconstruction of intermediate ocean water temperatures. *Earth and Planetary Science Letters* **269**, 570-575.

Samanta, M., Ellwood, M. J. and Mortimer, G. E. (2016). A method for determining the isotopic composition of dissolved zinc in seawater by MC-ICP-MS with a ^{67}Zn – ^{68}Zn double spike. *Microchemical*

Journal **126**, 530-537.

Shalev, N., Gavrieli, I., Halicz, L., Sandler, A., Stein, M. and Lazar, B. (2017) Enrichment of ^{88}Sr in continental waters due to calcium carbonate precipitation. *Earth and Planetary Science Letters* **459**, 381-393.

Shalev, N., Farkaš, J., Fietzke, J., Novak, M., Schuessler, J., Pogge von Strandmann, P., and Torber P. (2018) Mg isotope interlaboratory comparison of reference materials from earth-surface low-temperature environments. *Geostandards and Geoanalytical Research* **42**, 205-221.

Shao, Y., Farkaš, J., Holmden, C., Mosley, L., Kell-Duiveststein, I., Izzo, C., Reis-Santos, P., Tyler, J., Törber, P., Frýda, J., Taylor, H., Haynes, D., Tibby, J. and Gillanders, B.M. (2018) Calcium and strontium isotope systematics in the lagoon-estuarine environments of South Australia: Implications for water source mixing, carbonate fluxes and fish migration, *Geochimica et Cosmochimica Acta* **239**, 90-108.

Stevenson, E. I., Hermoso, M., Rickaby, R. E., Tyler, J. J., Minoletti, F., Parkinson, I. J., Mokadem, F. and Burton, K. W. (2014) Controls on stable strontium isotope fractionation in coccolithophores with implications for the marine Sr cycle. *Geochimica et Cosmochimica Acta* **128**, 225-235.

Tipper, E.T., Galy, A., Gaillardet, J., Bickle, M.J., Elderfield, H., Carder, E.A. (2006) The magnesium isotope budget of the modern ocean: Constraints from riverine magnesium isotope ratios. *Earth and Planetary Science Letters* **250**, 241-253.

Vollstaedt, H., Eisenhauer, A., Wallmann, K., Böhm, F., Fietzke, J., Liebetrau, V., Krabbenhöft, A., Farkaš, J., Tomašových, A., Raddatz, J. and Veizer, J. (2014) The Phanerozoic $\delta^{88/86}\text{Sr}$ record of seawater: New constraints on past changes in oceanic carbonate fluxes. *Geochimica et cosmochimica acta* **128**, 249-265.

Von der Borch, C. C., Lock, D. E. and Schwebel, D. (1975) Ground-water formation of dolomite in the Coorong region of South Australia. *Geology* **3**, 283-285.

Warwick, R. M., Tweedley, J. R. and Potter, I. C. (2018) Microtidal estuaries warrant special management measures that recognise their critical vulnerability to pollution and climate change. *Marine pollution bulletin* **135**, 41-46.

Young, E. D., Galy, A. and Nagahara, H. (2002) Kinetic and equilibrium mass-dependent isotope fractionation laws in nature and their geochemical and cosmochemical significance. *Geochimica et Cosmochimica Acta* **66**, 1095-1104.

Zeebe, R. E. and Wolf-Gladrow, D. (2001) *CO₂ in seawater: equilibrium, kinetics, isotopes* (No. 65). Gulf Professional Publishing.

CHAPTER 4

Seasonal carbonate cycling and water source mixing in a semi-arid coastal lagoon-estuarine system: Insights from stable strontium isotopes ($\delta^{88/86}\text{Sr}$)

This chapter is formatted for publication and submission to the journal of Science of The Total Environment, with the following authors and title of the manuscript: Shao, Y., Farkaš, J., Mosley, L., Tyler, J., Wong, H., Priestley, S., Gillanders, B.M. (2021) Seasonal carbonate cycling and water source mixing in a semi-arid coastal system: Insights from stable Sr isotopes ($\delta^{88/86}\text{Sr}$).

Statement of Authorship

Title of Paper	Seasonal carbonate cycling in coastal systems constrained by stable Sr isotopes ($\delta^{88/86}\text{Sr}$): Insights from a lagoon-estuarine environment
Publication Status	<input type="checkbox"/> Published <input type="checkbox"/> Accepted for Publication <input type="checkbox"/> Submitted for Publication <input checked="" type="checkbox"/> Unpublished and Unsubmitted work written in manuscript style
Publication Details	Shao, Y., Farkaš, J., Mosley, L., Tyler, J., Wong, H., Priestley, S., Gillanders, B.M. (2021) Seasonal carbonate cycling and water source mixing in a semi-arid coastal lagoon-estuarine system: Insights from stable strontium isotopes ($\delta^{88/86}\text{Sr}$). <i>Science of The Total Environment in prep.</i>

Principal Author

Name of Principal Author (Candidate)	Yuexiao Shao		
Contribution to the Paper	Field sample collection and measurements, sample preparation, Sr isotope analyses, pH and alkalinity analyses, data collection, data interpretation and modelling, manuscript writing, acting as the corresponding author.		
Overall percentage (%)	80		
Certification:	This paper reports on original research I conducted during the period of my Higher Degree by Research candidature and is not subject to any obligations or contractual agreements with a third party that would constrain its inclusion in this thesis. I am the primary author of this paper.		
Signature		Date	2/2/2021

Co-Author Contributions

By signing the Statement of Authorship, each author certifies that:

- i. the candidate's stated contribution to the publication is accurate (as detailed above);
- ii. permission is granted for the candidate to include the publication in the thesis; and
- iii. the sum of all co-author contributions is equal to 100% less the candidate's stated contribution.

Name of Co-Author	Juraj Farkaš		
Contribution to the Paper	Conceptual development, funding supply, field work assistance, guidance on data interpretation and modelling, manuscript evaluation and review.		
Signature		Date	15/03/2021

Name of Co-Author	Luke Mosley		
Contribution to the Paper	Conceptual development, field work assistance, guidance on pH and alkalinity analyses, guidance on PHREEQC mineral saturation modelling, manuscript review.		

Signature		Date	2/2/21
-----------	--	------	--------

Name of Co-Author	Jonathan Tyler		
Contribution to the Paper	Conceptual development, assistance on data interpretation, reviewed and improved the structure language of the manuscript.		
Signature		Date	2/2/2021

Name of Co-Author	Henri Wong		
Contribution to the Paper	Elemental concentration analyses.		
Signature		Date	2/2/2021

Name of Co-Author	Stacey Priestley		
Contribution to the Paper	Conceptual development, manuscript evaluation and review.		
Signature		Date	3/2/21

Name of Co-Author	Bronwyn M. Gillanders		
Contribution to the Paper	Conceptual development, guidance on manuscript structure, manuscript evaluation and review.		
Signature		Date	3 March 2021

Chapter 4.

Seasonal carbonate cycling and water source mixing in a semi-arid coastal lagoon-estuarine system: Insights from stable strontium isotopes ($\delta^{88/86}\text{Sr}$)

Abstract

Seasonal variations in water sources and carbonate dynamics provide challenges to understanding the controlling mechanisms of the local carbon cycle in coastal systems. The Coorong region in South Australia, located at the end of River Murray system, provides a lagoon-estuarine environment that exhibits extensive ranges in salinity, mineral saturation states, and thus CaCO_3 dynamics, forming a unique natural geochemical laboratory. This study presents radiogenic and stable Sr isotope data ($^{87}\text{Sr}/^{86}\text{Sr}$ and $\delta^{88/86}\text{Sr}$) from water samples collected seasonally (every 3 months) from the Coorong, Lower Lakes and Murray Mouth (CLLMM) region during a period from 2018 to 2019. These Sr isotope time-series data are complemented by elemental concentration data and carbonate saturation states to constrain the seasonal and spatial variations of water sources and CaCO_3 dynamics in the Coorong lagoon. Overall, $^{87}\text{Sr}/^{86}\text{Sr}$ and ratios of conservative tracers such as Mg/Na indicate that most of the Coorong lagoon water samples were mixtures of Southern Ocean seawater, Salt Creek continental drainage water and/or local groundwater, while the influence of river and lake input still needs to be assessed through samples during major barrage release events. Coupled $^{87}\text{Sr}/^{86}\text{Sr}$ and $\delta^{88/86}\text{Sr}$ data suggest that the South Lagoon of the Coorong acts as a sink of dissolved inorganic carbon (DIC) in forms of CaCO_3 precipitate. Salinity showed the strongest positive correlation to $\delta^{88/86}\text{Sr}$ in the Coorong lagoon waters, along with alkalinity, controlling net carbonate formation in the lagoon. The combined effects of increased alkalinity and high salinity is believed to cause the largest increase of $\delta^{88/86}\text{Sr}$ in lagoon waters (from 0.41‰ to 0.48‰) observed South Lagoon sites from August (winter) to December (Spring) 2018. This increase in $\delta^{88/86}\text{Sr}$ can be explained by Rayleigh and equilibrium models in which up to ~25-30% of Sr in the South Lagoon was removed via CaCO_3 (mostly aragonite) formation.

4.1 Introduction

Carbon cycling in coastal systems, which represents an interface between the land and ocean, account for a significant part of global carbon cycles and budgets (Cole et al., 2007; Bauer et al., 2013). Modern human activities have caused a significant imbalance of the global carbon cycle, therefore an improved mechanistic understanding and better quantification of local carbon budgets and cycling in

coastal systems is of a high priority (Regnier et al., 2013). Lagoons and estuaries are unique coastal systems that typically display large gradients in parameters such as salinity, redox and mineral saturation state of local waters resulting from the effects of mixing between oceanic and continental waters as well as local biogeochemical processes. These parameters are thus critical for better understanding local calcium carbonate (CaCO_3) cycling, which are linked to the inorganic carbon cycle that needs to be addressed and better quantified in coastal ‘blue carbon’ studies (i.e., the question of carbon storage capacity in vegetated coastal systems), (Macreadie et al., 2017). Moreover, additional challenges in quantifying the local carbon budget and cycling in estuarine environments are related to unique geomorphologies and hydrological dynamics of these complex systems, thus causing temporal, seasonal and spatial heterogeneities (Bauer et al., 2013).

Hence, to better constrain the CaCO_3 budget and inorganic carbon cycling in these environments, two issues need to be addressed: (i) the water sources and mixing, and (ii) local carbonate precipitation/dissolution processes. Due to the geochemical similarity of alkaline earth metals such as strontium (Sr) and calcium (Ca), with their identical charge (+2) and similar ionic radius, Sr isotopes have been often used as a tracer for Ca sources and cycling, as these two elements substitute and follow each other in many geological and biological systems (Finch and Allison, 2007; Menadakis et al., 2009; Drouet et al., 2005; de Souza et al., 2010; Doubleday et al., 2014). The radiogenic Sr isotope ratio ($^{87}\text{Sr}/^{86}\text{Sr}$) of minerals and rocks is dependent on their initial Rb content and age, controlled through the process of ^{87}Rb decay to ^{87}Sr over geological time. The $^{87}\text{Sr}/^{86}\text{Sr}$ has been thus used for several decades as a sensitive and valuable tool for tracing the sources and geochemical pathways of Sr in both terrestrial and marine environments (Fisher and Stueber, 1976; Hodell et al., 1990; Holmden et al., 1997; Capo et al., 1998; Bullen and Bailey, 2005; Drouet et al., 2005; de Souza et al., 2010; Chao et al., 2013). For instance, modern seawater exposed to weathering of basaltic oceanic crust has a relatively less radiogenic and globally homogeneous $^{87}\text{Sr}/^{86}\text{Sr}$ ratio of ~ 0.70917 , while surface waters on continents draining granitic and sedimentary rocks have more radiogenic although highly variable in $^{87}\text{Sr}/^{86}\text{Sr}$ signatures. The latter is due to large variations of local bedrock geology, age of weathered terrains and subsequent water source mixing in these continental and/or coastal settings (Kuznetsov et al., 2012).

The stable Sr isotope ratio (i.e., a variation in $^{88}\text{Sr}/^{86}\text{Sr}$ expressed as $\delta^{88/86}\text{Sr}$) is an emerging tracer that has been recently used to complement the more established $^{87}\text{Sr}/^{86}\text{Sr}$ tracer to further refine and constrain the global Sr cycle and its sources and fluxes, including marine carbonate dissolution/precipitation processes (Krabbenhöft et al., 2009, 2010; de Souza et al., 2010; Vollstaedt et al., 2014; Pearce et al., 2015; Fruchter et al., 2016; Shao et al. 2021). In addition, as shown by Shao et al. (2021), stable Sr and Ca isotope tracers ($\delta^{88/86}\text{Sr}$ and $\delta^{44/40}\text{Ca}$) correlate with each other in the Coorong coastal lagoon, due to equilibrium and kinetic fractionation processes related to carbonate dissolution and precipitation. One advantage of $\delta^{88/86}\text{Sr}$ is that it can be measured simultaneously with $^{87}\text{Sr}/^{86}\text{Sr}$

from the same sample aliquots (i.e., purified Sr fractions), thus complementing the more established $\delta^{44/40}\text{Ca}$ tracer (Stevenson et al. 2014; Shao et al., 2021), which has been used more frequently to constrain marine carbonate cycling (Farkaš et al., 2007a, b, and 2016; Holmden et al., 2012; Fantle and Tipper, 2014).

This study aims to use a coupled stable and radiogenic strontium isotope ($\delta^{88/86}\text{Sr}$ and $^{87}\text{Sr}/^{86}\text{Sr}$) approach, complemented also by elemental ratios, as tools to investigate the temporal/seasonal changes and spatial differences in (i) water source mixing and (ii) carbonate cycling in the Coorong, Lower Lakes and Murray Mouth estuary in South Australia. In addition, this study also quantifies the seasonal changes in carbonate budget in the Coorong lagoon using Rayleigh models based on stable Sr isotopes and associated fractionation effects linked to carbonate (mainly aragonite) formation. Overall, these results improve our knowledge of links and effects of different factors (e.g., salinity, saturation state, alkalinity inputs, lagoon restriction) on the fractionation of stable Sr isotopes in lagoon-estuary environments, with implications for local carbonate cycling and its seasonal dynamics.

4.2 Study area

The Coorong, Lower Lakes and Murray Mouth (CLLMM) hydrological system is located ~110 km southeast to the city of Adelaide, South Australia, at the terminus of the longest river in Australia – the River Murray (Fig. 1). In the CLLMM system, the Southern Ocean and various continental waters flow into the Coorong lagoon, forming a ‘mixture’ of marine and continental waters (see Fig. 2). This unique and elongated lagoon-estuarine hydrological system spans more than 100 km along the coastline, separated from the Southern Ocean by a narrow (<3 km wide) eolian sand barrier called Youngusband Peninsula (Fig. 1). The Coorong is divided into two parts – the North and South Lagoons, separated by a narrow channel at Parnka Point (Figs. 1-2). Due to wind action the lagoon waters are typically well mixed and homogenised locally and vertically across the water column (Gibbs et al., 2019), but because of the restricted water-flow at Parnka Point, the chemistry and salinity of North and South Lagoon waters are very different. As illustrated in Fig. 1, the North Lagoon receives seawater inflow from the Southern Ocean via Murray Mouth, and continental waters are supplied to the North Lagoon from the River Murray as well as Lower Lakes via a series of barrages constructed in 1930s. The South Lagoon is geomorphologically more restricted from the Southern Ocean and mainly receives fresh to brackish continental waters from the South East Drainage System (SEDS) via Salt Creek (Figs. 1-2; see also Gibbs et al., 2019). Atmospheric deposition and/or surface drainage of freshwater into the lagoon is limited due to low annual rainfall (400-500 mm) in the Coorong region, impacted also by generally very porous and permeable sandy soils (Barnett, 2015). However, there are reports of localised groundwater discharge into the Coorong with fresh to brackish salinities (Haese et al., 2008), but the actual magnitude and importance of such groundwater discharge is cur-

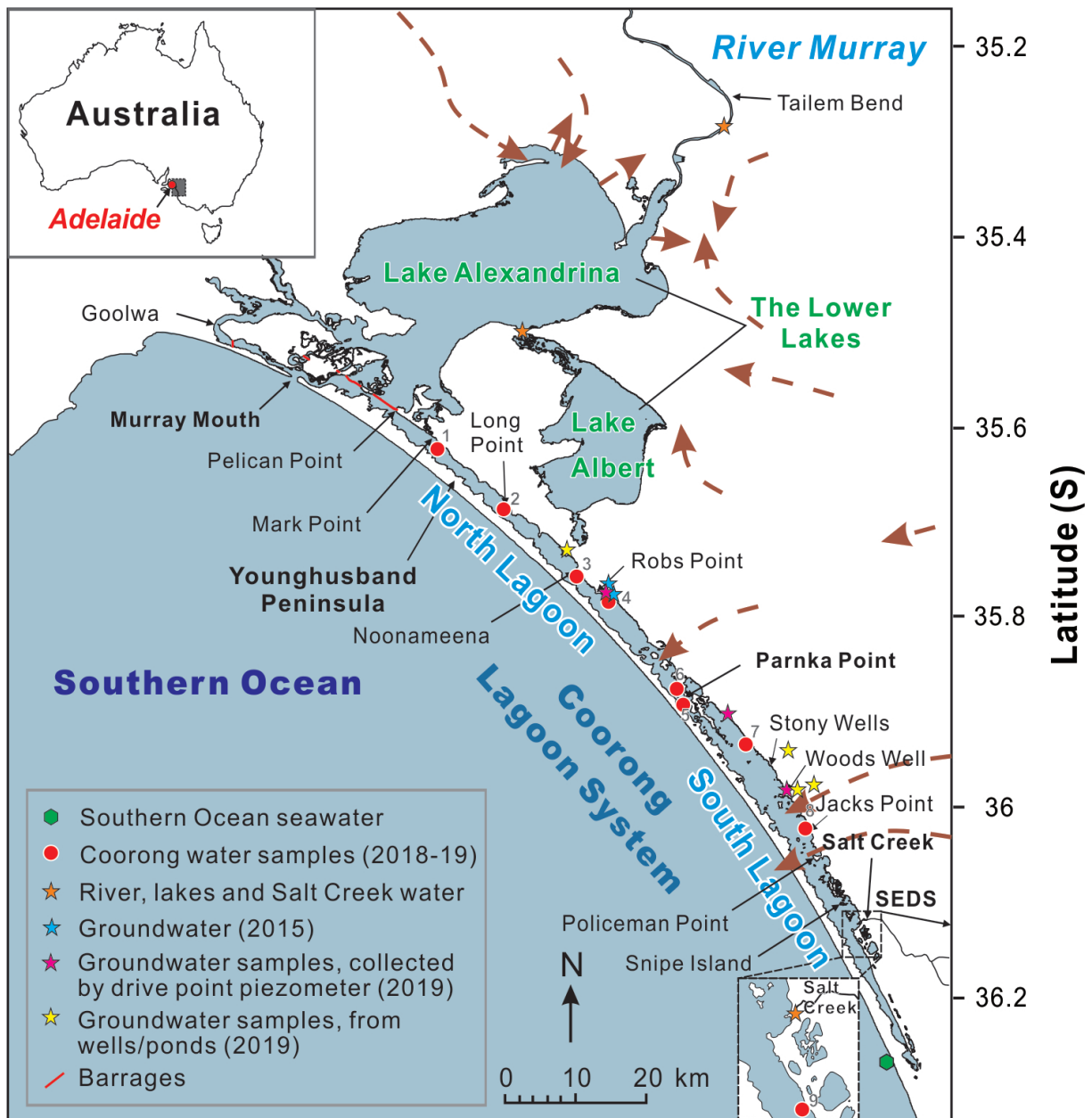


Figure 1: Map of the Coorong, Lower Lakes and Murray Mouth (CLLMM) estuary with the representative sampling sites for waters and carbonates. The solid red lines represent the five barrages. The brown dashed arrows represent shallow groundwater flow direction (Haese et al., 2008). Note that the numbers next to the 2018-19 Coorong water samples are site numbers corresponding to the last code of their sample IDs, which are listed together with their coordinates and sampling dates in the Appendix (Table A.1).

rently poorly constrained, including its potential impact on water quality in the Coorong (see Haese et al., 2008; Haynes et al., 2019). Previous studies suggested that the shallow subsurface groundwaters are mainly sourced from the Quaternary Limestone aquifer, and deeper ones are from the Murray Group and Renmark Group aquifer systems (Haese et al., 2008; Barnett, 2015). These occasional but poorly constrained groundwater inflows could thus impact water salinity along the Coorong which varies markedly between 20 and 35 PSU (practical salinity unit) in the North Lagoon, and 40 to >100

PSU in the South Lagoon, respectively (DEWNR, 2011).

As to precipitation and formation of carbonates in the Coorong, biogenic carbonates such as bivalves, foraminifera and tubeworm species are commonly found in the North Lagoon (Fig. 2) (Dittmann et al., 2009; Chamberlayne et al., 2020). In the South Lagoon, biogenic carbonates were present historically (and remain visible in the sediment) (Cann and Lower, 2019) but now their formation is very limited due to the hypersalinity and impoverished ecology, and instead inorganic carbonate precipitation in the form of aragonitic crusts and/or carbonate tufa are commonly observed (Fig. 2) (Haese et al., 2008; Dittmann, et al., 2009; Reeves et al., 2015; Brookes et al., 2018; Shao et al., 2018; Gibbs et al., 2019). Specifically, these carbonate precipitates are predominantly composed of aragonite (~87%) and minor calcite (~12%), complemented by trace amounts of gypsum (~1%) (von der Borch et al., 1975; Shao et al., 2018). Interestingly, even though the water salinity is much higher in dry summer seasons (due to evaporation under elevated temperatures), Fernandes and Tanner (2009) observed lower carbonate precipitation rates in summer compared to more wet winter seasons. These authors suggested that the precipitation of CaCO_3 in summer is hampered by high concentration of Mg^{2+} and dissolved organic carbon (DOC) in local lagoon waters, regardless of the fact of carbonate supersaturation in the South Lagoon (Fernandes and Tanner, 2009). These observations and hypotheses raise the questions what controls the local carbonate dynamics and CaCO_3 precipitation in the Coorong Lagoon, and what is the importance and role of biogenic versus inorganic carbonate precipitation.

Apart from differences in modes of carbonate production in the Coorong, other parameters such as salinity, nutrients, and water levels also vary spatially and seasonally across the North and South Lagoons (Aldridge et al., 2010; Webster, 2010; Gibbs et al., 2019; Mosley et al., 2020). Specifically, in spring, high volumes of freshwaters from barrage outflows enter the Coorong (up to ~20 gigalitres (GL) per day) causing a transient ‘freshening’ of the system for several days to weeks (Mosley, 2016). However, during other times of the year, these barrage flows are generally limited and thus affecting or ‘flushing’ only localised areas of the Coorong predominantly between the barrages and Murray Mouth (Webster, 2010; Mosley, 2016). Finally, the Salt Creek input of fresh-to-brackish waters into the South Lagoon usually peaks at winter-spring times, reaching up to ~500 megalitres (ML) per day

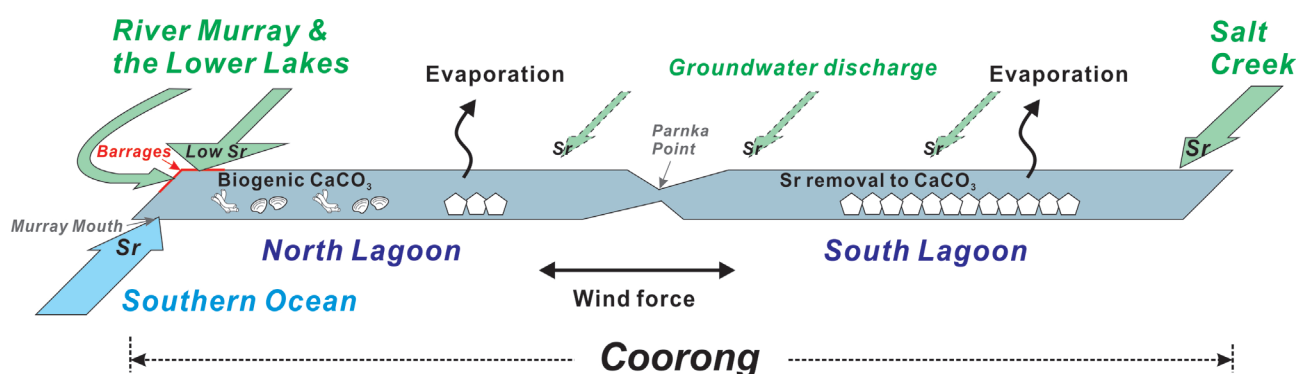


Figure 2: Schematic diagram of strontium fluxes from the CLLMM water sources to the Coorong.

which typically last during most of the ‘wet’ or rainy seasons (Mosley et al., 2017).

4.3 Material and methods

4.3.1 Sample description

In this study, 53 water samples from the CLLMM estuary were collected in 2018-2019. Four sets of water samples were collected through four different seasons, specifically on 24th May (n=12), 31st August (n=10), 7th December (n=12) 2018 and 7-8th March 2019 (n=11), and a sample of Southern Ocean seawater was collected on the 7-8th March 2019 trip. A set of groundwater samples (n=7) were collected along the Coorong Lagoons on 11-12th April 2019. Additionally, data from two more local groundwater samples collected on 25th June 2015 from private wells near Noonamena presented in Shao et al., (2018 and 2021) were used in the discussion.

Note that the CLLMM estuary was located in the Southern Hemisphere, which means the seasons are opposite to the Northern Hemisphere. Specifically, the seasons for this study are defined by grouping the calendar months in the following way:

- Spring - the transition months September, October and November.
- Summer - the high temperature and dry months December, January and February.
- Autumn - the transition months March, April and May.
- Winter - the low temperature and relatively wet months June, July and August.

In this study, CLLMM water samples were collected subsequently at the end of each season, starting from autumn 2018. Specifically, autumn samples were collected in May 2018, winter samples in August 2018, spring samples in December 2019, and summer samples in March 2019.

4.3.2 Field collection measurements and sample preparation of waters

Temperature and salinity were measured at sampling site in the field using a YSI ProDSS multi-parameter water quality meter, with location recorded by GPS at each sampling site (Table A.1, Appendix A). The water samples were filtered through 0.45 μm cellulose nitrate membrane filters in acid-cleaned HDPE bottles and refrigerated at 4°C in the dark before alkalinity, elemental concentrations and isotopic analyses were undertaken. For pH measurements, unfiltered water samples were collected simultaneously in acid-cleaned HDPE bottles with minimum headspace to avoid creation of air bubbles and loss of CO₂, and samples were stored and refrigerated at 4°C in the dark.

Groundwater samples were collected at selected locations adjacent to the lagoon (a) using a drive point piezometer (Solinst 615) installed at approximately 1 m depth, and (b) from existing groundwater wells near Noomanema and Robs Point (Fig. 1). The piezometer outlet was connected to a peristaltic pump and in line flow cell containing the above water quality meter. Prior to sample collection the piezometer was purged for several minutes until clear was obtained and water quality readings were stable.

4.3.3 Elemental concentrations analyses of water samples

The concentrations of selected dissolved cations (Al, B, Ca, Fe, K, Mg, Mn, Na, P, S, Si and Sr) in the filtered water samples were measured using a Thermo Fisher iCAP 7600 ICP-AES at the Australian Nuclear Science and Technology Organisation (ANSTO). All elemental concentrations were determined against calibration standards with element concentrations ranging from 0.01 - 10 ppm and up to 500 ppm for Ca, K, Mg and Na. All standards were prepared from certified 1000 ± 3 ppm single element National Institute of Standards and Technology (NIST) standards in 3% v/v Merck Suprapure Nitric acid. A certified 'cocktail' of multi-element NIST standard from another supplier was run at the beginning of each analytical session as another independent quality control. A set of standards was added after every 20th sample throughout the analysis session to monitor instrument drift. All samples and standards were spiked with 1 ppm of In and Rh for internal standard correction. Samples with concentrations over the instrument calibration range were diluted with 3% v/v HNO₃ and reanalysed. A separate rinse containing 0.25 ml of 1% v/v Triton X-100 in 5 L of 1% HNO₃ was used for rinsing between standards and samples. The typical uncertainty for all analyses was $\pm 5\%$ (2SD).

The concentrations of dissolved anions (F⁻, Cl⁻, NO₂⁻, Br⁻, NO₃⁻, SO₄²⁻, I⁻ and PO₄³⁻) in the filtered water samples, diluted with Type I ultra-pure water, were measured using a Dionex ICS-2100 Ion Chromatograph (IC) with a KOH eluant generator, an auto-suppressor and temperature controlled conductivity detector coupled to a 4 mm AS19 guard and AS19 analytical column at ANSTO.

Concentrations were determined against calibration standards ranging from 0.01 ppm to 100 ppm for F⁻, NO₂⁻, Br⁻, NO₃⁻, I⁻, PO₄³⁻ and up to 500ppm for Cl⁻ and SO₄²⁻. All standards were prepared from certified 1000 ± 3 ppm (except for NO₂⁻, which is certified for 1000 ± 12 ppm) single element NIST traceable standards with type I ultra-pure water. A certified 'cocktail' or multi-element NIST standard from HPS (High Purity Standards) was run at the beginning of each analytical session as another independent quality control. The typical uncertainty for all analyses was $\pm 5\%$. The measured elemental concentrations in waters, including main cations and anions, are listed in Tables B.1 and B.2, Appendix B.

4.3.4 Alkalinity and pH analyses of water samples

The alkalinity and pH measurements were completed using the spectrophotometric method detailed in Appendix B.3 from Shao et al. (2021). Briefly, for alkalinity, water samples were acidified to pH of 3.5 with 0.1M HCl, then measured using a spectrophotometric method of Nand and Ellwood (2018). pH of samples were measured from unfiltered samples shortly after collection following the addition of m-Cresol purple and using the indicator dye dissociation constants from Loucaides et al. (2017). The measured alkalinity and pH values in waters, acquired using the above spectrophotometric methods, are listed in Table B.3, Appendix B.

4.3.5 Coupled $^{87}\text{Sr}/^{86}\text{Sr}$ and $\delta^{88/86}\text{Sr}$ analyses via TIMS

Samples of filtered waters were analysed for $^{87}\text{Sr}/^{86}\text{Sr}$ and $\delta^{88/86}\text{Sr}$ by thermal ionisation mass spectrometry (TIMS) using a Phoenix Isotopx instrument at the Metal Isotope Group (MIG) facility at the University of Adelaide. The analyses followed the procedures described in Shao et al. (2021). To apply the ^{87}Sr - ^{84}Sr double spike method to analyse the $\delta^{88/86}\text{Sr}$ in an unknown sample, two aliquots each containing about 500 ng of Sr were taken from a stock sample solution, where one aliquot was spiked with the ^{87}Sr - ^{84}Sr double spike solution (composition described in Shao et al., 2021), resulting in $^{84}\text{Sr}_{\text{sp}}/^{84}\text{Sr}_{\text{sa}}$ ratios (i.e., spike to sample ratios) close to 20 (mean = 20.5, 2SEM = 0.4, n=53). Prior to TIMS analyses, the Sr fraction from each sample and standard was purified from the sample ‘matrix’ using a 600 μL Micro Bio-Spin separation column filled with Sr-specific resin (Eichrom Sr-SPS), then the pure Sr fractions were loaded on single non-zone-refined rhenium filaments.

For stable Sr isotopes, all data measured in this study are reported as $\delta^{88/86}\text{Sr}$, expressed in per mil (‰), where $^{88}\text{Sr}/^{86}\text{Sr}$ ratio of an unknown sample is normalised relative to SRM987 standard, according to the following equation:

$$\delta^{88/86}\text{Sr} = \left[\left(\frac{^{88}\text{Sr}/^{86}\text{Sr}}{\text{sample}} \right) / \left(\frac{^{88}\text{Sr}/^{86}\text{Sr}}{\text{SRM987}} \right) - 1 \right] \times 1000 \quad (\text{Eq. 1})$$

The total procedural Sr blanks determined via ^{84}Sr isotope dilution ranged from 16 to 138 picograms (pg), with an average value of 63 pg (2SEM = 21 pg, n=13), corresponding to less than 0.1% of total Sr (~500 ng) sourced from an analysed sample.

The long-term average $^{87}\text{Sr}/^{86}\text{Sr}$ and $\delta^{88/86}\text{Sr}$ values and uncertainties of standards in this study were, respectively, 0.709256 ± 0.000004 (2SEM, n=23) and $0.000 \pm 0.008\text{‰}$ (2SEM, n=22) for SRM987 standard; and 0.709186 ± 0.000004 (2SEM, n=11) and $0.399 \pm 0.012\text{‰}$ (2SEM, n=13) for IAPSO seawater. The analysed $^{87}\text{Sr}/^{86}\text{Sr}$ and $\delta^{88/86}\text{Sr}$ values in waters from the CLLMM hydrological system are listed in Table B.4, Appendix B.

4.3.6 Geochemical / PHREEQC modelling of mineral saturation state in waters

The saturation indices (SI) for calcite and aragonite in the CLLMM water samples were calculated using the geochemical model PHREEQC, following the approach detailed in Shao et al. (2018 and 2021), and using the following source data for the modelling: the temperature, concentrations of the main cations and anions (Tables B.1 and B.2, Appendix B) and laboratory alkalinity and pH measurements (Table B.3, Appendix B).

4.4 Results

Water salinities in the Coorong lagoons generally increased from north to south, as documented throughout our seasonal sampling period (see data in Fig. 3A, B). The only exception was observed during December 2018 sampling when the highest salinity was at Parnka Point (86 PSU), higher than that in the South Lagoon (Fig. 3A and B). In the North Lagoon, Mark Point sampling site (labelled as #1 in Fig. 1), located close to the barrages, had salinities consistently around 30 PSU, slightly below that of the seawater (36 PSU). Other locations in the North Lagoon (e.g. Noonamena and Robs Point; #3 and 4 in Fig. 1) had more variable salinities throughout the seasons (Fig. 3B), reaching up to 60 and 70 PSU respectively, in the warmer December 2018 and March 2019 sampling periods. The hypersaline South Lagoon had a larger salinity ranges between seasons compared to that of the North Lagoon (Fig. 3B). Specifically, the samples from March (summer) 2019 yielded the highest salinities in the South Lagoon (>100 PSU), which are significantly higher compared to salinities observed in the South Lagoon for the winter (August 2018) sampling period that reached only up to 61 PSU (Fig. 3A). River Murray and Lower Lakes samples had freshwater salinities of no more than ~0.5 PSU with very little seasonal variability. In contrast, Salt Creek water samples collected near its inflow into the South Lagoon (see the 'inset' in Fig. 1) had slightly more variable but overall brackish salinities of about 7 to 8 PSU in the colder May and August 2018 sampling periods, and reaching up to ~15 PSU in March 2019 summer samples (see also data in Fig. 3A). The groundwater samples collected along the Coorong (see 'star' symbols in Fig. 1) yielded the most variable salinities among all the continental waters sampled, which ranged from about 1 PSU up to 20 PSU (see Fig. 3A, B). Remarkably, the fresher groundwater samples (<5 PSU) were all collected from wells near Noonamena and Robs Point, with the exception of one groundwater sample that was collected using a drive point piezometer (marked as magenta star near site #4 in Fig. 1) that yielded much higher salinity (~17 PSU). In contrast, the groundwater samples collected further south near the South Lagoon (i.e., south-east from Parnka Point), were all generally more saline (~10 to 20 PSU), as illustrated in Fig. 3A.

As to Sr isotope variations, the radiogenic $^{87}\text{Sr}/^{86}\text{Sr}$ values also showed distinctive temporal and spatial

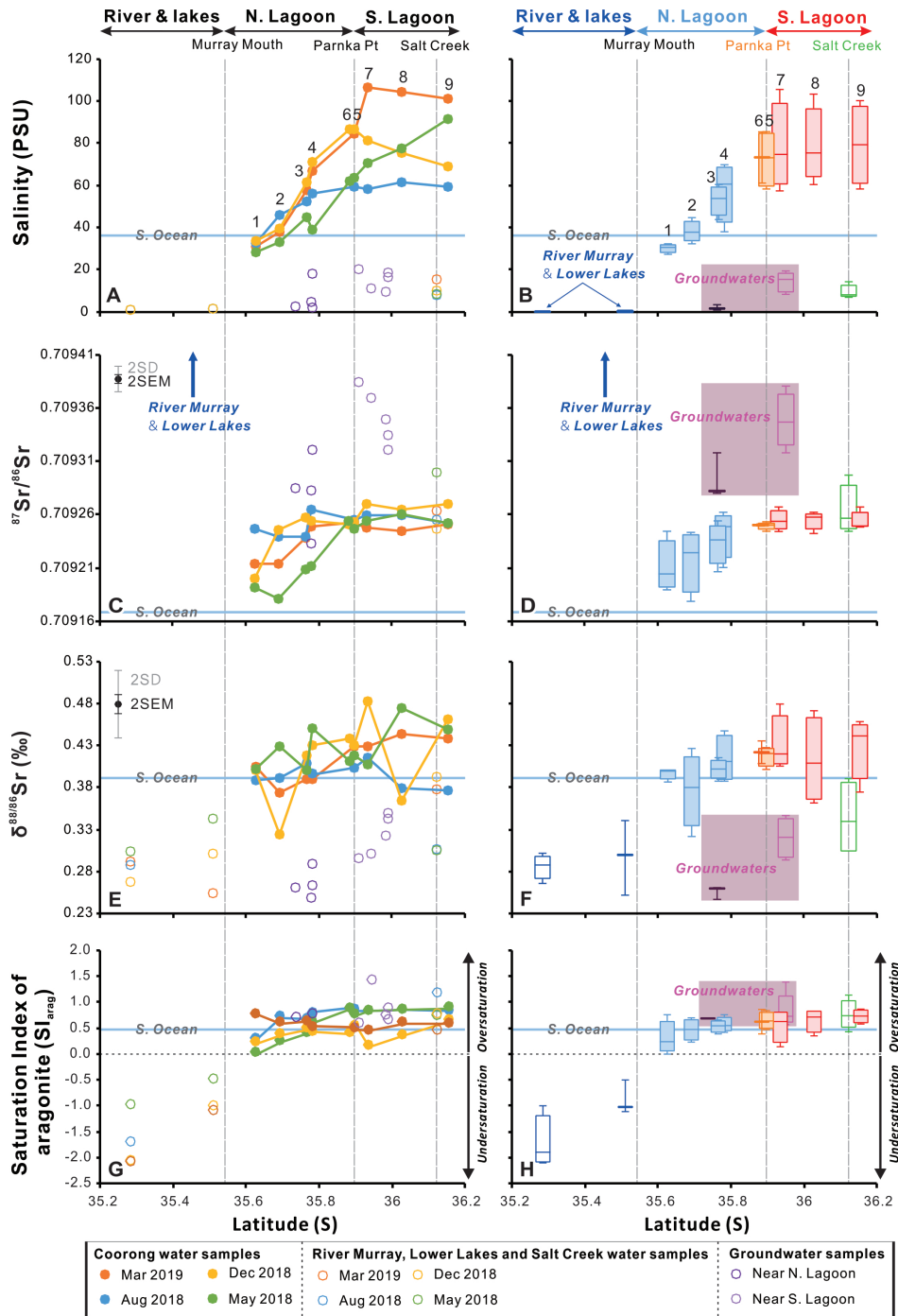


Figure 3: Analytical results of all water samples by latitude (degree south). (A) Salinity. (C) radiogenic Sr isotope ratios ($^{87}\text{Sr}/^{86}\text{Sr}$). Note that water samples from River Murray (RM) and Lower Lakes (LL) plot out of scale and thus are not shown, and their average $^{87}\text{Sr}/^{86}\text{Sr}$ were 0.71199 (2SD = 0.00015, $n = 4$) and 0.71136 (2SD = 0.00011, $n = 3$) respectively; individual values are in Table B.4, Appendix B. (D) Stable Sr isotope values ($\delta^{88/86}\text{Sr}$) normalised to SRM987 standard. (E) The saturation indices (SI) of aragonite modelled by PHREEQC. Plots (B, D, F, H) are box and whisker plots of the same results presented in (A, C, E, G) for the purpose of visualising the seasonal variations of these results. The blue horizontal line illustrate Southern Ocean seawater value based on analyses of the sample “SWSu” (for details see Table A.1 and B.4 in Appendix). Groundwater values are encompassed within the magenta box. Numbers 1-9 are the Coorong water samples are sites labelled in Fig. 1. Note that the error bars related to Y-axis represent 2SD and 2SEM uncertainties of long term and repeat IAPSO seawater standard measurements.

characteristics throughout the Coorong (Fig. 3C and D). Generally, the North Lagoon water samples had more variable but relatively less radiogenic $^{87}\text{Sr}/^{86}\text{Sr}$ compared to data from the South Lagoon (Fig. 3D), with May 2018 and March 2019 samples yielding values closest to that of seawater from the Southern Ocean (0.70917). In contrast, August and December 2018 samples from North Lagoon exhibit generally higher values, especially at Noonamena and Robs Point, yielding $^{87}\text{Sr}/^{86}\text{Sr}$ values up to 0.70926 (Fig. 3C). The $^{87}\text{Sr}/^{86}\text{Sr}$ values of the South Lagoon were relatively constant, with values scattering around 0.70926 ± 0.00002 , 2SD (Fig. 3D). Interestingly, overall our data point to more similar $^{87}\text{Sr}/^{86}\text{Sr}$ values in both the North and South Lagoons during August and December 2018 periods, and generally much larger differences between the lagoons in May 2018 and March 2019 (Fig. 3C). Among all water samples, River Murray and Lower Lakes constantly yielded the highest $^{87}\text{Sr}/^{86}\text{Sr}$ values between 0.711 and 0.712, which are consistent with the weathering of ‘old’ and generally felsic and thus more radiogenic bedrocks of the surrounding catchment areas (cf., Rippon et al., 2020). Salt Creek water samples had $^{87}\text{Sr}/^{86}\text{Sr}$ values of 0.70925 – 0.70930, similar or slightly higher than those of the South Lagoon samples (Fig. 3D). Finally, the groundwater (GW) samples yielded rather variable $^{87}\text{Sr}/^{86}\text{Sr}$ signatures, where the GW sampled along the North Lagoon showing comparable values to the Salt Creek, while the ones collected near the South Lagoon had slightly higher values reaching up to 0.70938 (see Fig. 3C, D).

As to stable Sr isotope variations, the $\delta^{88/86}\text{Sr}$ values of the North Lagoon water samples yielded values close to the seawater value of $\sim 0.395 \pm 0.025\%$, but some sites also exhibit values as low as 0.32‰ (site #2 in Fig. 1) and as high as 0.45‰ (site #4 in Fig. 1) (Fig. 3F). Note that the highest $\delta^{88/86}\text{Sr}$ in the North Lagoon were always found at Robs Point (#4 in Fig. 1), followed by Noonamena (#3 in Fig. 1) for most of the seasons, except in May 2018 where Long Point (#2 in Fig. 1) had the second highest $\delta^{88/86}\text{Sr}$ (Fig. 3E). The $\delta^{88/86}\text{Sr}$ values of the South Lagoon waters were generally and systematically higher than that of typical seawater (Fig 3E, F), but varied also seasonally from $\sim 0.36\%$ up to $\sim 0.48\%$, where the latter (i.e., the highest $\delta^{88/86}\text{Sr}$ value) was documented at Stony Wells site (#7 in Fig. 1) in December 2018 (Fig. 3E). In contrast, continental waters generally yielded $\delta^{88/86}\text{Sr}$ values that were lower than that of the seawater. Specifically, River Murray and Lower Lakes water samples show $\delta^{88/86}\text{Sr}$ values ranging from 0.25 to 0.34‰, which are thus the lowest among all samples in this study (Fig. 3E, F). Salt Creek samples, on the other hand, had the highest $\delta^{88/86}\text{Sr}$ values of continental water samples in this study, with values ranging seasonally from 0.30 to 0.39‰. Finally, the groundwater (GW) samples yielded similar $\delta^{88/86}\text{Sr}$ as the river and lake waters (0.25-0.35‰), however the groundwater samples collected along the South Lagoon exhibit generally higher $\delta^{88/86}\text{Sr}$ values compared to ones collected near the North Lagoon (Fig. 3F).

As to CaCO_3 dynamics and water carbonate chemistry, the saturation indices of aragonite (SI_{arag}) in both North and South Lagoons were consistently supersaturated (i.e., $\text{SI}_{\text{arag}} > 0$), and generally higher than in ‘normal’ seawater ($\text{SI}_{\text{arag}} = 0.4$) (Fig. 3G, H). Exceptions came from May 2018 in the North

Lagoon and December 2018 in both North and South Lagoons where lagoon water samples had lower SI_{arag} than that of seawater. In general, the South Lagoon had slightly higher SI_{arag} than the North Lagoon, with the highest values of 0.8 and 0.9 recorded in August and May 2018, respectively (Fig. 3H). As to continental waters, the River Murray and Lower Lakes samples were always undersaturated with respect to aragonite ($SI_{arag} < 0$) with SI_{arag} values ranging between -2.1 and -0.5 (Fig. 3G, H). Finally, Salt Creek brackish waters yielded highly oversaturated SI_{arag} values of 0.4 to 1.1 (Fig. 3H); similarly, groundwaters collected along the Coorong also showed significantly oversaturated and highest SI_{arag} values ranging from 0.6 to up to 1.4 (Fig. 3H). These high SI_{arag} values of Salt Creek and groundwaters were likely linked to the high alkalinity content of these continental waters (Reid and Mosley, 2016).

4.5 Discussion

In order to improve the knowledge of seasonal changes in the water source mixing and carbonate cycling in the CLLMM throughout the sampling period of 2018-2019, Sr isotope mass balance equations (Shao et al., 2018) were used in the following sections to calculate theoretical mixing trends between Southern Ocean seawater (SW) and continental water sources. The latter include the following end-members: the River Murray (RM), Lower Lakes (LL) waters, fresh-to-brackish groundwater (GW) and Salt Creek (SC). Also, due to long residence time of Sr in the global ocean, including the South Ocean, the Sr concentration and isotope composition of seawater can be assumed to be homogeneous (Krabbenhöft, 2010), while the compositions of continental water sources in the CLLMM are expected to vary seasonally.

4.5.1 Influence of seasonal variations of water source mixing on the Coorong lagoon chemistry

Both Mg and Na concentrations in the CLLMM waters are considered to be conservative tracers (Fig. D.1, Appendix D), due to lack of dolomite and halite formation (i.e., major sinks for Mg and Na, respectively) in the CLLMM system; with the exception of ‘ephemeral lakes’ (located more inland and SE from Salt Creek) (von der Borch et al., 1975; Haese et al., 2008) which were not investigated in this study. Thus, the elemental Mg/Na ratio can be used as a conservative tracer in the CLLMM waters collected in this study, which would not be sensitive to evaporation effects and mineral formation. Accordingly, plotting Mg/Na ratios of waters against their $^{87}\text{Sr}/^{86}\text{Sr}$ data (another conservative tracer not sensitive to evaporation and mineral formation) allows (i) identification of different water sources and also (ii) quantification of their relative mixing in the Coorong Lagoons (Fig. 4) via elemental and isotope mass balance calculations.

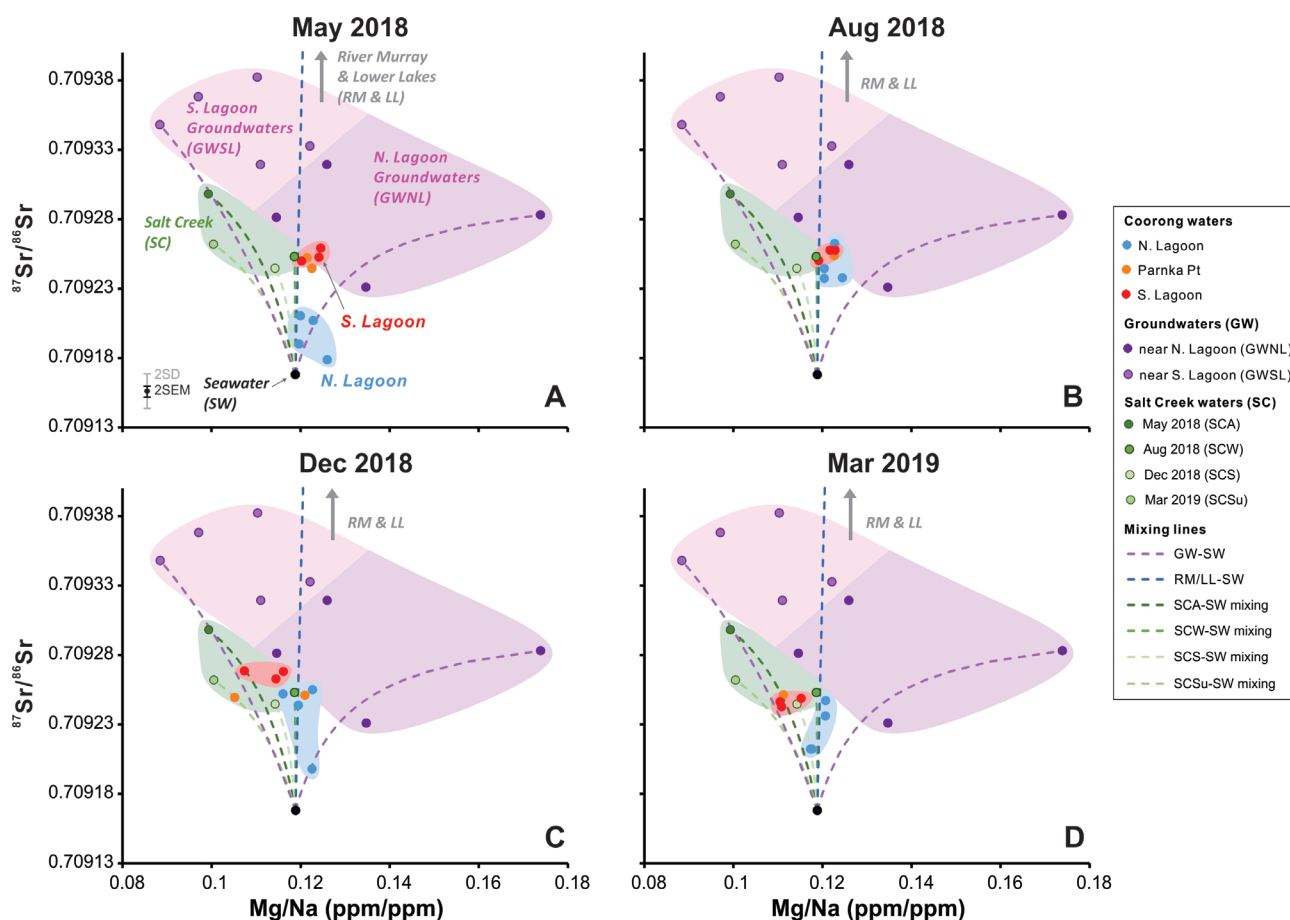


Figure 4: Cross-plots of $^{87}\text{Sr}/^{86}\text{Sr}$ vs. Mg/Na of water samples from the CLLMM for each sampling period. (A) May 2018 autumn samples; (B) August 2018 winter samples; (C) December 2018 spring samples and (D) March 2019 summer samples. Note that the error bars related to Y-axis represent 2SD and 2SEM uncertainties of long term and repeat IAPSO seawater standard measurements.

The River Murray (RM) and Lower Lakes (LL) waters exhibit different but relatively constant $^{87}\text{Sr}/^{86}\text{Sr}$ and Mg/Na ratios, illustrated also by RM/LL-SW mixing lines that do not show much variations over the seasonal sampling period (see Fig. 4). In contrast, Salt Creek (SC) water input had more seasonal variations in both $^{87}\text{Sr}/^{86}\text{Sr}$ and Mg/Na data and was illustrated as a ‘cloud’ in the data (Fig. 4). Specifically, the SC input had lower Mg/Na (~ 0.10) in May 2018 and March 2019, compared to August and December 2018 when Mg/Na systematically higher and close to ~ 0.12 . As to $^{87}\text{Sr}/^{86}\text{Sr}$ variations, SC waters yielded the highest values of 0.70930 in May 2018, followed by the other sampling times or seasons with $^{87}\text{Sr}/^{86}\text{Sr}$ scattering between 0.70925 and 0.70926 (see data in Fig. 4).

Interestingly, among all studied continental water sources from the CLLMM, the groundwaters (GW) showed the most spatial variations in both $^{87}\text{Sr}/^{86}\text{Sr}$ and Mg/Na ratios (Fig. 4). In general, the GW collected along the North Lagoon yielded lower $^{87}\text{Sr}/^{86}\text{Sr}$ but higher Mg/Na ratios, compared to GW collected along the South Lagoon. These spatial differences in the GW isotopic and chemical composition, as well as salinity, suggest that the GW from the Coorong region might be influenced by local

geomorphology and evaporation effects, or specific water-rock interactions due to different subsurface flow-paths and water residence times (Haese et al., 2008; Barnett, 2015).

To illustrate some of the complexities, the fresher GW with salinity of 1.5 to 3 PSU were sampled south of Lake Albert where a nearby small Ordovician granite intrusion (which is part of larger basement rocks) might have elevated local water table and hence increased the local hydraulic gradient. In contrast, low-lying or deeper groundwaters with higher salinities (up to ~20 PSU) were found along the South Lagoon, thus likely reflecting their relatively longer residence times and associated evaporative enrichments (Barnett, 2015 and 2019). These more saline GW samples also likely experienced enhanced ‘water-rock’ interaction histories, i.e., being exposed not only to the carbonate aquifer but possibly also to local granitic intrusions for a longer period of time, as suggested by their higher $^{87}\text{Sr}/^{86}\text{Sr}$ signatures (see GWSL data in Fig. 4). However, the reason why groundwater samples from the North Lagoon area (GWNL) exhibit systematically higher Mg/Na ratios compared to GW from the South Lagoon region (GWSL) is yet unclear and not understood. One possibility could be that dolomite formation in ephemeral lakes near the South Lagoon region consumed Mg from the groundwater sources nearby through cyanobacterial activities (Von der Borch et al., 1975; Wacey et al.; 2007), but this scenario still needs to be tested and validated by future studies.

Based on observations provided by the government monitoring sites in the Coorong region (Appendix C.1), the major ‘water source input’ events into the lagoons identified in the CLLMM during our sampling period were: (i) a major storm in mid-February 2018, complemented by intermittent storms in May-August, and November-December 2018; and (ii) a significant barrage release of freshwater in late July to mid-August 2018, and finally also (iii) a major input of brackish water from Salt Creek discharge event documented from late July to late November 2018, plus smaller ones from mid-December 2018 to mid-January 2019 (see data in Appendix, Fig. C1). Importantly, these individual ‘events’ are also reflected in the $^{87}\text{Sr}/^{86}\text{Sr}$, and Mg/Na data of the Coorong waters analysed in this study (Fig. 4).

Overall, data indicate that the North Lagoon waters are primarily sourced from the Southern Ocean or seawater, with the exception of major storm events and barrage outflows events (i.e., in August 2018) when the North Lagoon waters show ‘non-marine’ character with higher $^{87}\text{Sr}/^{86}\text{Sr}$ signatures (see Fig 4B). Interestingly, although the North Lagoon waters plot along the RM/LL-SW mixing trend in the $^{87}\text{Sr}/^{86}\text{Sr}$ vs. Mg/Na cross-plot (see blue dashed lines in Fig. 4), no detectable decrease in lagoon water salinity was observed even after the biggest barrage release event (i.e., August 2018 samples, Fig. C.1 in Appendix), indicating that impact of such freshwater inputs to the North Lagoon water salinity was negligible, but still detectable in $^{87}\text{Sr}/^{86}\text{Sr}$ data.

Based on the government monitoring records and observations, these freshwater barrage outflows seem to impact and lower the salinity of lagoon waters only in the vicinity of barrages (Webster,

2010), except during very high flows as recorded in (Geddes and Butler, 1984) and Mosley (2016) when the middle of the North Lagoon was also freshened. Given that (i) our samples did not catch the time of maximum barrage releases (C.1A, Appendix C.1), and (ii) during 2018-2019, the barrage outflows (maximum of <15000 ML/day, Fig. C.1A, Appendix C.1) were much lower compared to previous years (e.g., maximum ~80000 ML/day around 2012 and 2017, recorded in Mosley et al., 2020), it is possible that our samples were not representative to interpret the impact of river/lake water through barrage releases on the Sr isotope signatures of the Coorong water. An alternative ‘continental water’ component reflected in the elevated North Lagoon $^{87}\text{Sr}/^{86}\text{Sr}$ data since August 2018 could originate from either groundwater (GW) inputs, and/or water exchange from the South Lagoon via Parnka Point (see Fig. 1). In contrast, the South Lagoon waters exhibit much more consistent and homogeneous $^{87}\text{Sr}/^{86}\text{Sr}$ vs. Mg/Na signatures, which were less seasonally variable, and generally overlap with the composition of Salt Creek (see data in Fig. 4), showing limited influence from seawater and Southern Ocean compared to in the North Lagoon. Overall, these results suggest that the semi-restricted South Lagoon represents a well-mixed reservoir of highly evaporated and evolved ‘water mixture’ that are dominated by the SC water sources, at least during the period of our sampling.

Additionally, it is also possible that the presented SC-SW and RM/LL-SW mixing scenarios for the CLLMM system (see dashed lines in Fig. 4), and the Coorong lagoon water samples that plot along these theoretical mixing trends, can be also to some degrees influenced by local groundwater (GW) inputs, although the latter was not yet considered in previous studies to be a significant component due to low hydraulic gradients of groundwaters in the Coorong region (Barnett, 2019). Overall, due to the limited data and the complexity related to differences in local groundwater (GW) sources in the South and North Lagoons, and their specific chemical/isotope compositions and salinities (see GWSL and GWNL data in Fig. 4), it is currently problematic to properly assess and quantify the overall effect of GW inputs on the chemical and isotope composition of the Coorong waters.

4.5.2 Seasonal variation of Sr fluxes and carbonate dynamics in the Coorong

The elemental and isotope Sr budget in the Coorong Lagoons is controlled by (i) water source inputs and (ii) carbonate precipitation/dissolution, where the former increases the total amount of Sr in the Coorong lagoon waters and is reflected in changing radiogenic $^{87}\text{Sr}/^{86}\text{Sr}$ ratios (i.e., plotted along the theoretical mixing lines, Fig. 5). In contrast, the latter processes can either remove (i.e., carbonate precipitation) or add (i.e., dissolution) Sr within the Coorong, and are reflected as changes or variations in stable $\delta^{88/86}\text{Sr}$ values (i.e., horizontal ‘shifts’ from the theoretical mixing lines, illustrated in Fig. 5 as green arrows). To better understand and quantify temporal changes in water source mixing and local carbonate cycling (i.e., precipitation vs dissolution) in the Coorong and the entire CLMMM system, one can interrogate the data using a 3-isotope plot, with $^{87}\text{Sr}/^{86}\text{Sr}$ vs. $\delta^{88/86}\text{Sr}$ (Fig. 5).

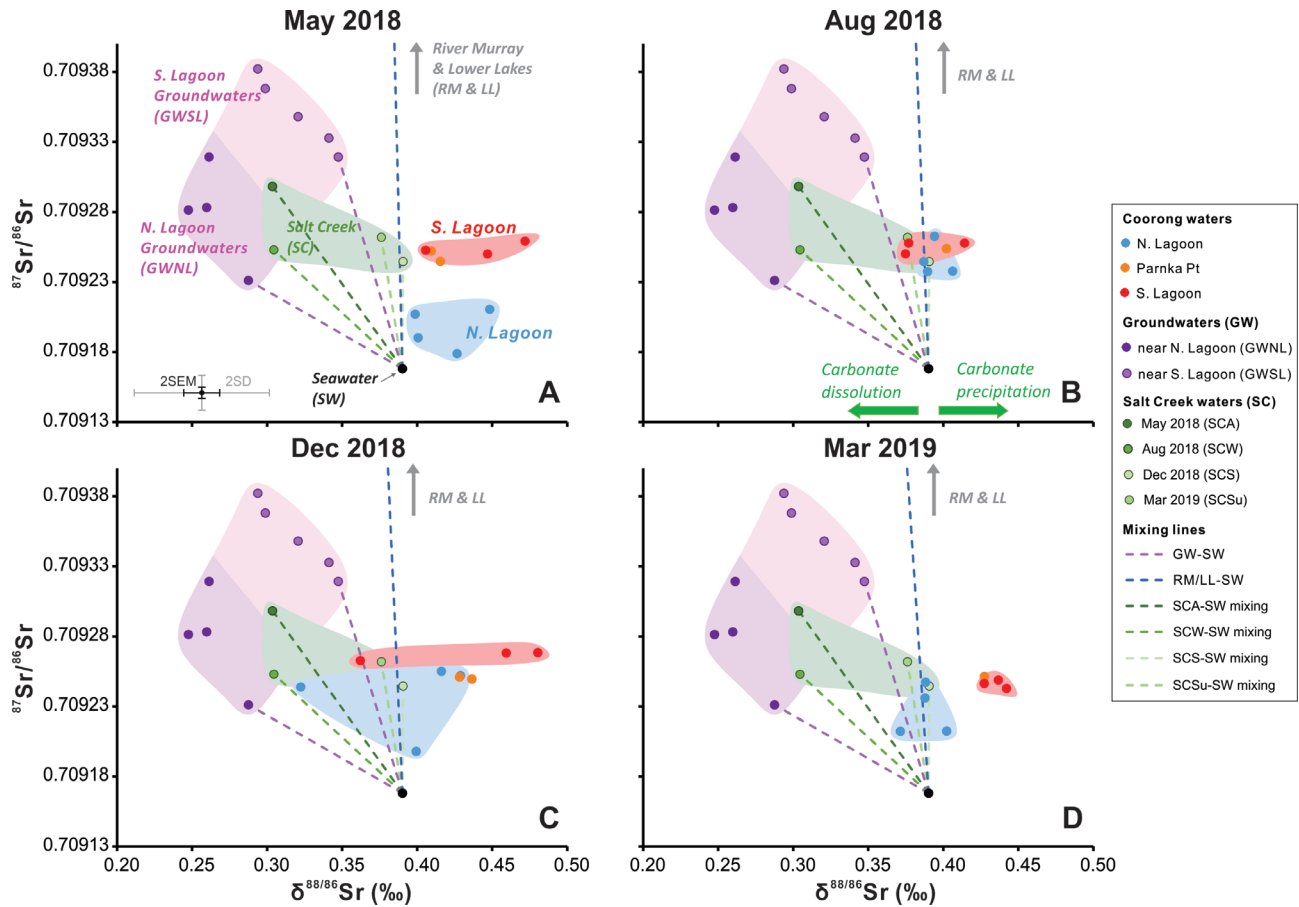


Figure 5: Cross-plots of $^{87}\text{Sr}/^{86}\text{Sr}$ vs. $\delta^{88/86}\text{Sr}$ of water samples from the CLLMM for each sampling period. (A) May 2018 Autumn samples; (B) August 2018 Winter samples; (C) December 2018 Spring samples and (D) March 2019 Summer samples. Note that the error bars represent 2SD and 2SEM uncertainties of long term and repeat IAPSO seawater standard measurements.

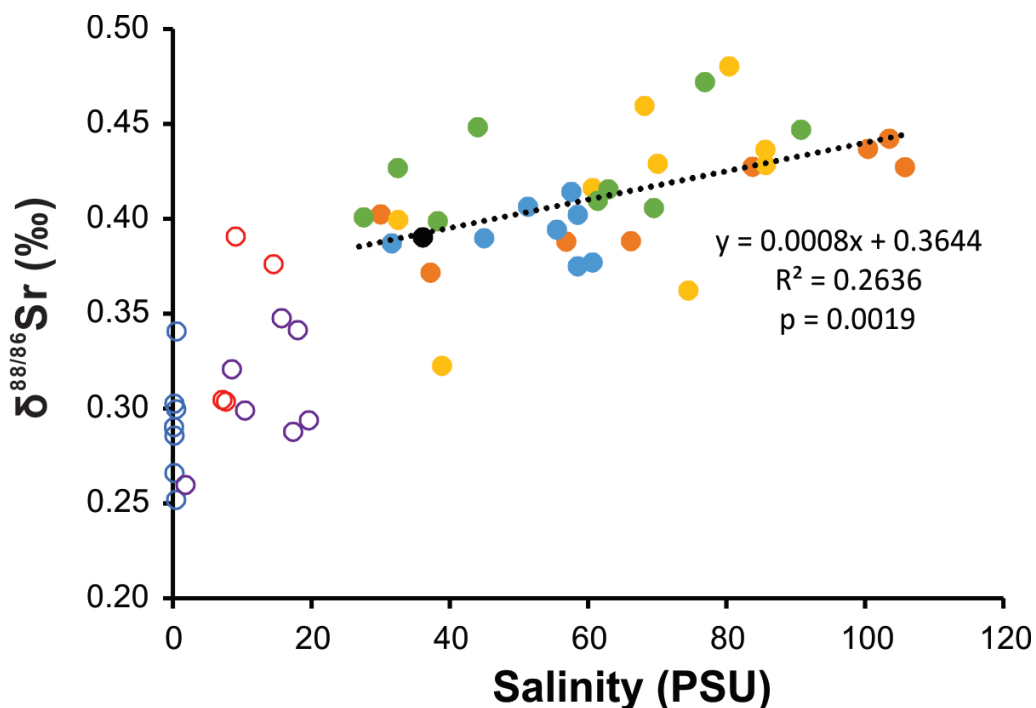
As already pointed out in the previous section discussing the $^{87}\text{Sr}/^{86}\text{Sr}$ data, the North and South Lagoons behave differently in terms of Sr fluxes throughout all seasons. These differences between the lagoons and their local Sr cycling are also reflected in $\delta^{88/86}\text{Sr}$ data (Fig. 5). Specifically, in the North Lagoon, (NL), there were considerable variations in both $^{87}\text{Sr}/^{86}\text{Sr}$ and $\delta^{88/86}\text{Sr}$ data (see blue data in Fig. 5), with $\delta^{88/86}\text{Sr}$ scattering around the seawater value (0.39‰) throughout most of the seasons, except in May 2018 where data yielded the highest $\delta^{88/86}\text{Sr}$ values measured in the NL (up to 0.45‰ see Fig. 5, observed at Robs Point, see #4 in Fig. 1). In contrast, the South Lagoon (SL) water samples (red data in Fig. 5) showed very limited variations in $^{87}\text{Sr}/^{86}\text{Sr}$ but considerable changes in $\delta^{88/86}\text{Sr}$ data, thus pointing to a relatively more dynamic carbonate cycling (i.e., active carbonate precipitation), which however, occurs in a relatively well-mixed ‘reservoir’ or water source.

Apart from the general comparison of variations in the $^{87}\text{Sr}/^{86}\text{Sr}$ and $\delta^{88/86}\text{Sr}$ between the NL and SL, it is also noticeable that specific sites or sampling locations in the Coorong also showed more complex and variable seasonal changes in $^{87}\text{Sr}/^{86}\text{Sr}$ vs. $\delta^{88/86}\text{Sr}$ data compared to other sites (see Fig. 3E, F). As an example, Long Point (#2 in Fig. 1, $\delta^{88/86}\text{Sr} = 0.32\text{‰}$) from the North Lagoon and Jacks Point (#8 in

Fig. 1, $\delta^{88/86}\text{Sr} = 0.36\text{‰}$) from the South Lagoon, plotted very close to GW-SW mixing lines (see Figs. 4C and 5C), but had significantly lower $\delta^{88/86}\text{Sr}$ values compared to other Coorong sites in December 2018. This might suggest that some local inputs of light Sr, likely from continental sources with low $\delta^{88/86}\text{Sr}$, such as the groundwater discharge sourced from carbonate aquifers, and/or alternatively local carbonate dissolution, could explain these data and observations.

4.5.3 The controls of $\delta^{88/86}\text{Sr}$ in the Coorong lagoon waters

According to Shao et al. (2021), the fractionation of stable Sr isotopes in the Coorong is mainly controlled by the combination of ‘kinetic’ and ‘equilibrium’ isotope fractionation effects, the latter linked to processes such as dissolution and/or precipitation of carbonates in the CLLMM system. Therefore, $\delta^{88/86}\text{Sr}$ can be used as a tracer or index for the local carbonate cycling, and corresponding input and output fluxes in the CLLMM system. However, such mass-dependent fractionation processes of Sr isotopes in the lagoon-estuarine systems can be also affected by multiple environmental factors, such as salinity, temperature, mineral saturation, the latter linked to supply of Ca, Sr and alkalinity. As de-



Coorong waters	R ²	p value	Others
● Mar 2019	0.7152	0.0079	○ River and lakes
● Dec 2018	0.3439	0.0967	○ Groundwater
● Aug 2018	0.0042	0.8840	● S. Ocean
● May 2018	0.2439	0.1800	○ Salt Creek

Figure 6: $\delta^{88/86}\text{Sr}$ of the CLLMM water samples vs. salinity (PSU), with linear correlation of two parameters in the Coorong water samples.

tailed in the previous sections, the chemistry and isotope composition of the Coorong waters is highly variable both temporally and spatially. This raises the question of what predominantly controls the $\delta^{88/86}\text{Sr}$ variations in the Coorong, and how these processes control the local carbonate fluxes.

In order to answer these questions, the $\delta^{88/86}\text{Sr}$ data from the CLLMM water samples were plotted against their salinity (Fig. 6), water temperature, carbonate saturation (SI_{arag}) and alkalinity (Fig. C.8, Appendix C.3). The results indicate that the $\delta^{88/86}\text{Sr}$ of the Coorong waters exhibit the strongest correlation with water salinity ($R^2 = 0.26$, $p < 0.05$; Fig. 6), which agrees with previous findings of Shao et al. (2021). Especially, March 2019 Coorong samples, collected at the end of summer season, showed the strongest statistical correlation ($R^2 = 0.72$, $p < 0.05$; Fig. 6 legend); while in the opposite season (i.e., winter, August 2018), data showed no correlation ($R^2 = 0.00$, $p = 0.88$; Fig. 6 legend) between $\delta^{88/86}\text{Sr}$ and salinity. This means the influence of salinity on $\delta^{88/86}\text{Sr}$ fractionation in water had strong seasonality and played a much more important role in dry and hot summer seasons than wetter and colder seasons. Interestingly, no statistically significant correlations were found for $\delta^{88/86}\text{Sr}$ plotted against the other parameters (Fig. C.8, Appendix C.3). Overall, these observations suggest that water salinity has some control on the $\delta^{88/86}\text{Sr}$ of the Coorong waters, likely due to the fact that higher salinity is generally associated with more evaporation and hence carbonate oversaturation and thus calcite/aragonite formation; and the opposite (i.e., carbonate dissolution) is expected for fresh and undersaturated continental waters such as Murray River and Lower Lakes waters (see also data in Fig. 3G, H).

Due to the specific geomorphology of the Coorong, and their relative restriction with respect to the Southern Ocean (which is progressively increasing from the North to South Lagoon), the $\delta^{88/86}\text{Sr}$ in lagoon waters reflect the local and site-specific conditions, water quality and environmental factors. These site-specific complexities and their seasonal impacts on the local $\delta^{88/86}\text{Sr}$ signatures of lagoon waters is illustrated in Fig. 7, where the effects of four parameters or water properties (i.e., salinity, temperature, alkalinity and carbonate (aragonite) saturation index SI_{arag}) were investigated and assessed. For example, at the site Stony Wells (#7 in Fig. 1) in the South Lagoon, $\delta^{88/86}\text{Sr}$ values are positively correlated with a moderate statistical significance to ambient water temperatures ($R^2 = 0.77$, $p = 0.13$), and negatively correlated to both alkalinity ($R^2 = 0.78$, $p = 0.12$) and SI_{arag} ($R^2 = 0.88$, $p = 0.06$), see Fig. 7. Such trends and correlation patterns seem to suggest that high supply of carbonate alkalinity, likely sourced from Salt Creek discharge during cool and more rainy seasons (e.g., late July to the end of November 2018) can lead to transient changes in SI_{arag} (as explained in Appendix C.2) and lower $\delta^{88/86}\text{Sr}$ in waters due to mixing of local 'lagoon water' with Salt Creek input, as the latter has low $\delta^{88/86}\text{Sr}$ values of about 0.30 to 0.39‰ (as discussed in the section 5.1). Also, as the temperature increased in a drier and hotter season (December 2018), accompanied by a simultaneous decrease in the Salt Creek water input (see also Fig. C.1B in Appendix), the $\delta^{88/86}\text{Sr}$ of lagoon waters at Stony Wells site increased, likely as a result of ongoing carbonate precipitation driven by evapora-

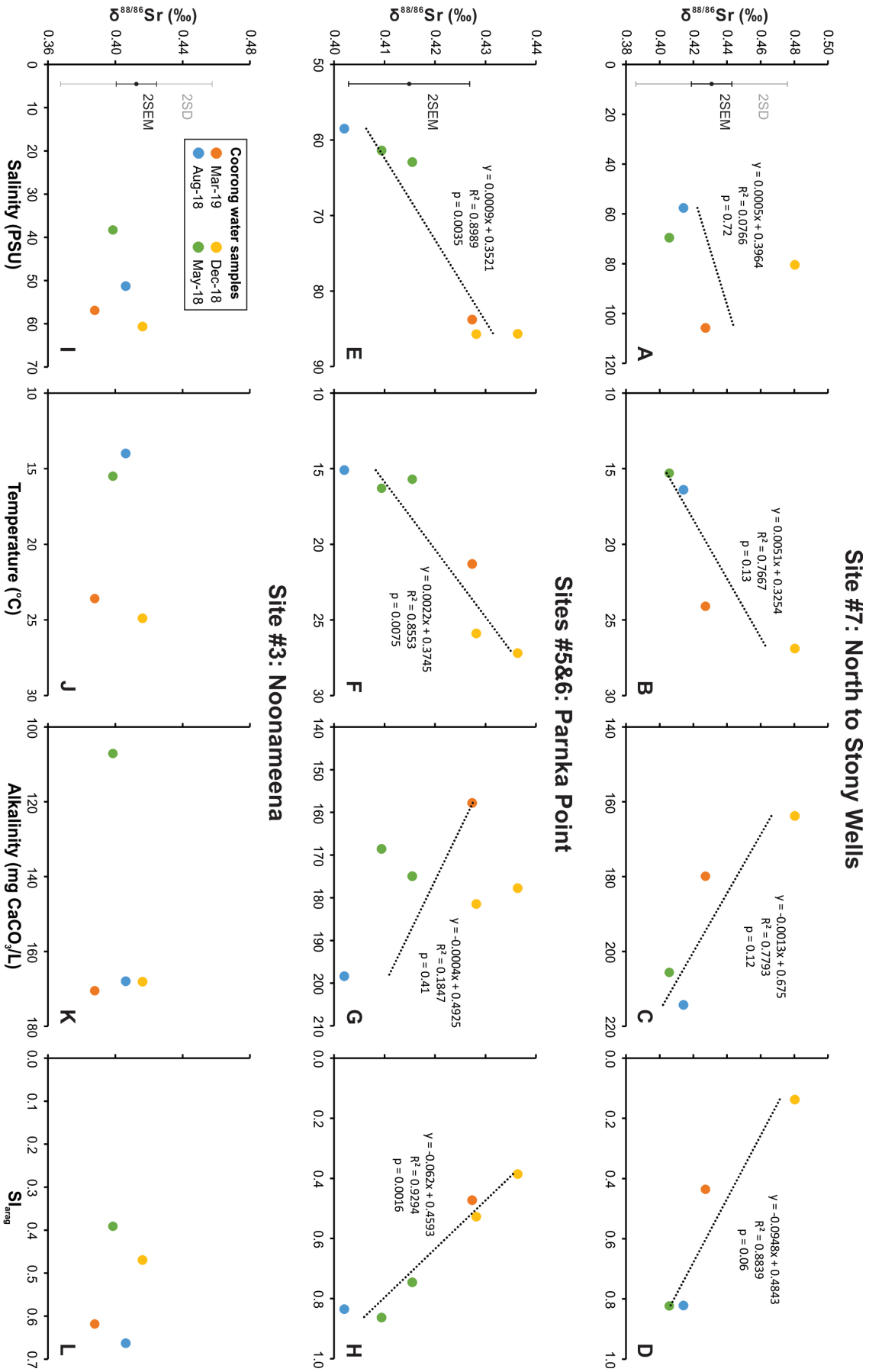


Figure 7: $\delta^{88/86}\text{Sr}$ of North of Stony Wells (#7 in Fig. 1, South Lagoon) water samples vs. (A) water salinity (PSU), (B) water temperature ($^{\circ}\text{C}$), (C) alkalinity ($\text{mg CaCO}_3/\text{L}$) and (D) S_{1avg}; same plots for sampling sites at Parnka Point (#5 and 6 in Fig. 1) (E-H) and Noonameena (#3 in Fig. 1, North Lagoon) (I-L). Note that the Y-axis error bars represent 2SD and 2SEM uncertainties of long term and repeat IAPSO seawater standard measurements.

tion and local carbonate oversaturation. Finally, in March 2019 when the summer season ended, the $\delta^{88/86}\text{Sr}$ of the lagoon waters at this particular site decreased again, accompanied by consumption of alkalinity, and therefore lower SI_{arag} (Fig. 7C and D).

In the shallowest area in the Coorong – the Parnka Point, the situation was much less complicated. As demonstrated in Appendix C.1 based on salinity, water level and temperature data from government monitoring sites, the salinity of this site was predominantly temperature/evaporation controlled, apart from the minor storm effects. This is also reflected in the changes in $\delta^{88/86}\text{Sr}$ of water samples at the Parnka Point sites (#5 and 6 in Fig. 1) as they were strongly and positively correlated to salinity and temperature (Fig. 7E and F). Also, as the local carbonate precipitation increased (reflected by lower or ‘consumed’ alkalinity), SI_{arag} temporarily decreased accompanied by higher $\delta^{88/86}\text{Sr}$ values in local lagoon waters (Fig. 7G and H). That said, it needs to be also pointed out that higher precision $\delta^{88/86}\text{Sr}$ measurements would be needed to further confirm and validate these tentative trends and correlation patterns, as the overall $\delta^{88/86}\text{Sr}$ variations are less than 0.1‰ at Stony Well site, and even smaller (<0.05‰) at Parnka Point (see data in Fig. 7).

Finally, the $\delta^{88/86}\text{Sr}$ values in North Lagoon water samples, for instance at Noonameena site (#3 in Fig. 1), seem to be insensitive to above water parameters and conditions, as $\delta^{88/86}\text{Sr}$ water data at this site stayed ‘constant’ at around 0.40‰ throughout all seasons (see data in Fig. 7). Given that the water source inputs to the North Lagoon (traced via $^{87}\text{Sr}/^{86}\text{Sr}$, and discussed in 5.1) were quite variable throughout the year, these $\delta^{88/86}\text{Sr}$ results are rather surprising, as one would expect some variability also in $\delta^{88/86}\text{Sr}$ data. Nevertheless, the remaining $\delta^{88/86}\text{Sr}$ data from other sites in the North Lagoon (Fig. 3E, F) revealed significant variability in $\delta^{88/86}\text{Sr}$ data throughout four seasons sampled during 2018-2019, thus pointing to a highly dynamic carbonate cycling also in the North Lagoon.

Overall, our results suggest that water salinity (and thus seasonal temperature and water discharge changes) seem to be the most dominant factors controlling the local carbonate cycling and formation in the Coorong and the associated $\delta^{88/86}\text{Sr}$ fractionation effects, which was especially obvious in summer season. Moreover, the $\delta^{88/86}\text{Sr}$ of lagoon waters at some sites (e.g., Stony Wells) seems to be also sensitive to local alkalinity supply versus consumption, impacting the saturation state (SI_{arag}) of waters and their stable Sr isotope composition.

4.5.4 Quantifying seasonal changes in carbonate output in the South Lagoon via $\delta^{88/86}\text{Sr}$ tracer

Given that the stable Sr isotope composition ($\delta^{88/86}\text{Sr}$) of natural waters is a sensitive indicator of the carbonate formation vs dissolution, and the fact that there are detectable seasonal changes in $\delta^{88/86}\text{Sr}$ of the most CLLMM waters (see Figs. 5 and 7), it is possible to provide first order estimates or quanti-

fications of temporal and spatial changes in local carbonate formation (i.e., Sr output) in the Coorong Lagoons using a Rayleigh modelling approach, following Shao et al. (2021) and Frings et al. (2016). An example of such application or approach can be illustrated on seasonally variable $\delta^{88/86}\text{Sr}$ data from the North of Stony Well (#7 in Fig. 1) site, e.g. for a period from August (winter) to December (spring) 2018 when $\delta^{88/86}\text{Sr}$ in local waters increased systematically from $\sim 0.41\text{‰}$ to $\sim 0.48\text{‰}$ (Fig. 7A-D), likely due to the abovementioned increase in alkalinity supply from a major Salt Creek discharge event (late July - end of November 2018) accompanied also by an increase in water's temperature and evaporation (i.e., salinity), (Fig. 7). Assuming that the Coorong is a 'closed system', and using the 'August 2018' water $\delta^{88/86}\text{Sr}$ signature (0.41‰) from this site as an 'initial' or starting value and 'December 2018' water $\delta^{88/86}\text{Sr}$ data (0.48‰) as the 'final' value, the Rayleigh modelling suggests that 25-30% of Sr present initially in the lagoon water was removed via carbonate (aragonite) formation during this period (for details see also results and calculations in Appendix, and Fig. E.1). A similar approach and modelling could be applied to other sampling sites and seasonal and spatial $\delta^{88/86}\text{Sr}$ data across the Coorong. Finally, considering that (i) the Sr/Ca ratio of waters across the Coorong is rather constant at ~ 0.02 (ppm/ppm) (Fig. D. 2A, Appendix D), and (ii) similar fractionation processes (i.e., carbonate formations vs. dissolution) control both stable Sr and Ca isotopes ($\delta^{88/86}\text{Sr}$ and $\delta^{44/40}\text{Ca}$) in the Coorong (Shao et al., 2021), the calculated fraction of Sr removal via carbonate formation can be also translated to approximate fraction of local Ca removal in the lagoon. This in turn allows to quantify also expected removal of dissolved inorganic carbon (DIC) or bicarbonate ions (HCO_3^-) from the Coorong Lagoons via in-situ carbonate formation based on the following equation:



According to the above equation, and present-day conditions of marine carbonate system in equilibrium with atmospheric CO_2 , each mol of Ca^{2+} removed as CaCO_3 , should be accompanied by 1.4 mols of carbon (C) fixed in the lagoon as carbonate mineral (cf., Shao et al., 2018), with remaining 0.6 mol of carbon released via CO_2 outgassing. Thus, overall, our evidence for seasonally high $\delta^{88/86}\text{Sr}$ values documented especially in the South Lagoon (Fig. 5), suggest that this part of the Coorong acts as a net sink for dissolved inorganic carbon, facilitated via an in-situ carbonate formation.

4.6 Conclusions

Tracers for water source mixing such as $^{87}\text{Sr}/^{86}\text{Sr}$ and Mg/Na ratios revealed that during the sampling period of 2018-2019, most of the Coorong lagoon waters represent 'complex mixtures' of water sources originating from the Southern Ocean seawater, Salt Creek brackish water and/or local groundwater, with potential influence (i.e., near the barrages) also from River Murray and Lower Lakes freshwaters. However, samples during major barrage release events are still needed to quan-

tify their effects on the Sr isotope signatures in the Coorong water. Overall, the North Lagoon seems to have more variable sources of waters compared to the South Lagoon, where the latter seems to be dominated primarily by Salt Creek and seawater sources, with superimposed effects of local CaCO_3 (mainly aragonite) formation on $\delta^{88/86}\text{Sr}$ of the lagoon waters. Interestingly, water salinity seems to be the most dominant factor controlling the carbonate formation and thus stable Sr isotope fractionation ($\delta^{88/86}\text{Sr}$ variations) in the Coorong, but alkalinity supply and ambient water temperature (i.e., degree of evaporation and thus carbonate oversaturation) also playing an important role at some sites. Apart from the regularly occurring tides bringing seawater and thus alkalinity into the Coorong, Salt Creek was another important source of alkalinity into the system, especially in the hypersaline and CaCO_3 supersaturated South Lagoon. Overall, these results suggest that high alkalinity accompanied by rising salinity and hence evaporation, is the predominant driver of local carbonate dynamics and CaCO_3 formation in the Coorong, which can be quantified via Rayleigh modelling of $\delta^{88/86}\text{Sr}$ data especially from the South Lagoon, suggesting that the latter acts as a net sink for dissolved inorganic carbon.

In addition, the groundwater (GW) samples collected along the Coorong showed clear spatial patterns, where GW from the North Lagoon are generally fresher and lower $^{87}\text{Sr}/^{86}\text{Sr}$, while those collected near the South Lagoon tend to be more saline and with higher $^{87}\text{Sr}/^{86}\text{Sr}$. Future systematic studies and complementary tracers (e.g., radium and radon isotopes, Duque et al., 2019) are needed to further evaluate and quantify the role of groundwaters on the Coorong water chemistry, salinity and Sr isotope composition, which will also further advance our understanding of the local carbonate cycling and carbon removal in this unique coastal lagoon system.

Acknowledgements

This study was primarily supported by the ‘Project Coorong’ and the ‘HCHB – Healthy Coorong Healthy Basin’ initiative funded by the Commonwealth and South Australian Government, and partial support from the Environment Institute of the University of Adelaide and ARC Linkage project (LP160101353) is also acknowledged. This study is part of the Ph.D. research of YS, supported by an Adelaide Graduate Research Scholarship (AGRS), ANSTO research portal (No. 11642), and funding from the CRC LEME Regolith Science Scholarship via Cooperative Research Centre for Landscape Environments and Mineral Exploration (CRC LEME).

The sampling in the Coorong National Park was performed under the Department for Environment and Water (DEW) research permit No. U26745-1. The water quality data provided by the DEW is gratefully acknowledged. Technical and laboratory assistance provided by David Bruce at University of Adelaide is greatly appreciated, especially regarding the maintenance of TIMS and clean laboratory facilities. We also thank Sima Bargrizan and Flynn Watson for their assistance with pH and

alkalinity analyses on some of the samples at the University of Adelaide.

References

Aldridge, K., Payne, A. and Brookes, J. (2010). Literature Review: nutrient cycling and phytoplankton communities of the Lower River Murray, Lower Lakes and Coorong. *Report to the Department of Environment and Heritage, the Government of South Australia*.

Barnett, S. (2015) Assessment of the groundwater resources in the non-prescribed areas of the South Australian Murray-Darling Basin, DEWNR Technical report 2015/09, Government of South Australia, Department of Environment, Water and Natural Resources, Adelaide. ISBN: 978-1-922255-47-1.

Barnett, S. (2019) Hydrogeology of the Lower Lakes and Coorong Region. In *Natural history of the Coorong, Lower Lakes, and Murray Mouth region (Yarluwar-Ruwe)* (eds. L. M. Mosley, Q. Ye, S. Shepherd, S. Hemming, and R. Fitzpatrick) University of Adelaide Press on behalf of the Royal Society of South Australia, Adelaide. pp. 217-226.

Bauer, J. E., Cai, W. J., Raymond, P. A., Bianchi, T. S., Hopkinson, C. S. and Regnier, P. A. (2013) The changing carbon cycle of the coastal ocean. *Nature* **504**, 61-70.

Brookes, J., Dalby, P., Dittmann, S., O'Connor, J., Paton, D., Quin, R., Rogers, D., Waycott, M. and Ye, Q. (2018) *Recommended actions for restoring the ecological character of the South Lagoon of the Coorong*. Goyder Institute for Water Research Technical Report Series No. 18/04, Adelaide, South Australia. ISSN: 1839-2725.

Bullen T. D. and Bailey S. W. (2005) Identifying calcium sources at an acid deposition-impacted spruce forest: a strontium isotope, alkaline earth element multi-tracer approach. *Biogeochemistry* **74**, 63–99.

Cann, J. and Lower, C. (2019) Fossil Molluscs, Foraminifera, Ostracods and Oogonia Record a Coorong History. In *Natural history of the Coorong, Lower Lakes, and Murray Mouth region (Yarluwar-Ruwe)* (eds. L. M. Mosley, Q. Ye, S. Shepherd, S. Hemming, and R. Fitzpatrick) University of Adelaide Press on behalf of the Royal Society of South Australia, Adelaide. pp. 144-166.

Capo, R. C., Stewart, B. W. and Chadwick, O. A. (1998) Strontium isotopes as tracers of ecosystem processes: theory and methods. *Geoderma* **82**, 197-225.

Chamberlayne, B. K., Tyler, J. J. and Gillanders, B. M. (2020) Environmental Controls on the Geochemistry of a Short-Lived Bivalve in Southeastern Australian Estuaries. *Estuaries and Coasts*, 1-16.

Chao, H. C., You, C. F., Liu, H. C. and Chung, C. H. (2013) The origin and migration of mud volcano

fluids in Taiwan: Evidence from hydrogen, oxygen, and strontium isotopic compositions. *Geochimica et Cosmochimica Acta* **114**, 29-51.

Cole, J. J., Prairie, Y. T., Caraco, N. F., McDowell, W. H., Tranvik, L. J., Striegl, R. G., Duarte, C. M., Kortelainen, P., Downing, J. A., Middelburg, J. J. and Melack, J. (2007). Plumbing the global carbon cycle: integrating inland waters into the terrestrial carbon budget. *Ecosystems* **10**, 172-185.

de Souza, G. F., Reynolds, B. C., Kiczka, M. and Bourdon, B. (2010) Evidence for mass-dependent isotopic fractionation of strontium in a glaciated granitic watershed. *Geochimica et Cosmochimica Acta* **74**, 2596-2614.

DEWNR (2011) Determining the environmental water requirements for the Coorong, Lower Lakes and Murray Mouth region. Technical Report by the Coorong, Lower Lakes and Murray Mouth (CLL-MM) Research Group for the Department of Environment, Water and Natural Resources (DEWNR, Adelaide).

Dittmann, S., Rolston, A., Bengler, S. N. and Kupriyanova, E. K. (2009) *Habitat requirements, distribution and colonisation of the tubeworm *Ficopomatus enigmaticus* in the Lower Lakes and Coorong*. Report for the South Australian Murray-Darling Basin Natural Resources Management Board, Adelaide, 99.

Doubleday, Z. A., Harris, H. H., Izzo, C. and Gillanders, B. M. (2014) Strontium randomly substituting for calcium in fish otolith aragonite. *Analytical chemistry* **86**, 865-869.

Drouet, T., Herbauts, J., Gruber, W. and Demaiffe, D. (2005). Strontium isotope composition as a tracer of calcium sources in two forest ecosystems in Belgium. *Geoderma* **126**, 203-223.

Duque, C., Knee, K. L., Russoniello, C. J., Sherif, M., Risha, U. A. A., Sturchio, N. C. and Michael, H. A. (2019) Hydrogeological processes and near shore spatial variability of radium and radon isotopes for the characterization of submarine groundwater discharge. *Journal of Hydrology* **579**, 124192.

Fantle, M. S. and Tipper, E. T. (2014) Calcium isotopes in the global biogeochemical Ca cycle: implications for development of a Ca isotope proxy. *Earth-Science Reviews* **129**, 148-177.

Farkaš, J., Buhl, D., Blenkinsop, J. and Veizer, J. (2007) Evolution of the oceanic calcium cycle during the late Mesozoic: evidence from $\delta^{44/40}\text{Ca}$ of marine skeletal carbonates. *Earth and Planetary Science Letters* **253**, 96-111.

Farkaš, J., Böhm, F., Wallmann, K., Blenkinsop, J., Eisenhauer, A., Van Geldern, R., Munnecke, A., Voigt, S. and Veizer, J. (2007b) Calcium isotope record of Phanerozoic oceans: Implications for chemical evolution of seawater and its causative mechanisms. *Geochimica et Cosmochimica Acta* **71**, 5117-5134.

Farkaš, J., Frýda, J. and Holmden, C. (2016) Calcium isotope constraints on the marine carbon cycle and CaCO₃ deposition during the late Silurian (Ludfordian) positive δ¹³C excursion. *Earth and Planetary Science Letters* **451**, 31–40.

Fernandes, M. and Tanner, J. E. (2009) Hypersalinity and phosphorus availability: the role of mineral precipitation in the Coorong lagoons of South Australia. CSIRO: Water for a Healthy Country National Research Flagship and South Australian Research and Development Institute (Aquatic Sciences).

Finch, A. A. and Allison, N. (2007) Coordination of Sr and Mg in calcite and aragonite. *Mineralogical Magazine* **71**, 539-552.

Fisher R. S. and Stueber A. M. (1976) Strontium isotopes in selected streams within the Susquehanna River Basin. *Water Resour. Res.* **12**, 1061–1068.

Frings, P. J., Clymans, W., Fontorbe, G., Christina, L. and Conley, D. (2016) The continental Si cycle and its impact on the ocean Si isotope budget. *Chemical Geology* **425**, 12-36.

Fruchter, N., Eisenhauer, A., Dietzel, M., Fietzke, J., Böhm, F., Montagna, P., Stein, M., Lazar, B., Rodolfo-Metalpa, R. and Erez, J. (2016) ⁸⁸Sr/⁸⁶Sr fractionation in inorganic aragonite and in corals. *Geochimica et cosmochimica acta* **178**, 268-280.

Fruchter, N., Lazar, B., Nishri, A., Almogi-Labin, A., Eisenhauer, A., Shlevin, Y. B. E. and Stein, M. (2017) ⁸⁸Sr/⁸⁶Sr fractionation and calcite accumulation rate in the Sea of Galilee. *Geochimica et Cosmochimica Acta* **215**, 17-32.

Geddes, M. C. and Butler, A. J. (1984) Physicochemical and biological studies on the Coorong lagoons, South Australia, and the effect of salinity on the distribution of the macrobenthos. *Transactions of the Royal Society of South Australia. Adelaide* **108**, 51-62.

Gibbs, M., Joehnk, K., Webster, I. and Heneker, T. (2019) Hydrology and Hydrodynamics of the Lower Lakes, Coorong and Murray Mouth. In *Natural history of the Coorong, Lower Lakes, and Murray Mouth region (Yarluwar-Ruwe)* (eds. L. M. Mosley, Q. Ye, S. Shepherd, S. Hemming, and R. Fitzpatrick) University of Adelaide Press on behalf of the Royal Society of South Australia, Adelaide. pp. 197-216.

Haese, R. R., Gow, L., Wallace, L. and Brodie, R. S. (2008) Identifying groundwater discharge in the Coorong (South Australia). *AUSGEO news* **91**, 1-6.

Haynes, D., Tibby, J., Fluin, J. and Skinner, R. (2019) Palaeolimnology of the Lower Lakes and Coorong Lagoon. In *Natural history of the Coorong, Lower Lakes, and Murray Mouth region (Yarluwar-Ruwe)* (eds. L. M. Mosley, Q. Ye, S. Shepherd, S. Hemming, and R. Fitzpatrick) University of Adelaide Press on behalf of the Royal Society of South Australia, Adelaide. pp. 122-143.

Hodell, D. A., Mead, G. A. and Mueller, P. A. (1990) Variation in the strontium isotopic composition of seawater (8 Ma to present): Implications for chemical weathering rates and dissolved fluxes to the oceans. *Chemical Geology: Isotope Geoscience section* **80**, 291-307.

Holmden, C., Creaser, R. A. and Muehlenbachs, K. (1997) Paleosalinities in ancient brackish water systems determined by $^{87}\text{Sr}/^{86}\text{Sr}$ ratios in carbonate fossils: a case study from the Western Canada Sedimentary Basin. *Geochimica et Cosmochimica Acta* **61**, 2105-2118.

Holmden, C., Papanastassiou, D. A., Blanchon, P. and Evans, S. (2012) $\delta^{44/40}\text{Ca}$ variability in shallow water carbonates and the impact of submarine groundwater discharge on Ca-cycling in marine environments. *Geochimica et Cosmochimica Acta* **83**, 179-194.

Krabbenhöft, A., Fietzke, J., Eisenhauer, A., Liebetrau, V., Böhm, F. and Vollstaedt, H. (2009) Determination of radiogenic and stable strontium isotope ratios ($^{87}\text{Sr}/^{86}\text{Sr}$; $\delta^{88/86}\text{Sr}$) by thermal ionization mass spectrometry applying an $^{87}\text{Sr}/^{84}\text{Sr}$ double spike. *Journal of Analytical Atomic Spectrometry* **24**, 1267-1271.

Krabbenhöft, A., Eisenhauer, A., Böhm, F., Vollstaedt, H., Fietzke, J., Liebetrau, V., Augustin, N., Peucker-Ehrenbrink, B., Müller, M. N., Horn, C., Hansen, B. T., Nolte, N. and Wallmann, K. (2010) Constraining the marine strontium budget with natural strontium isotope fractionations ($^{87}\text{Sr}/^{86}\text{Sr}^*$, $\delta^{88/86}\text{Sr}$) of carbonates, hydrothermal solutions and river waters. *Geochimica et cosmochimica acta* **74**, 4097-4109.

Kuznetsov, A. B., Semikhatov, M. A., Gorokhov, I. M. (2012) The Sr isotope composition of the world ocean, marginal and inland seas: Implications for the Sr isotope stratigraphy. In: *Stratigraphy and Geological Correlation*, Vol. 20, p. 501-515. Pleiades Publishing Ltd. ISSN 086-5938.

Loucaides, S., Rèrolle, V. M., Papadimitriou, S., Kennedy, H., Mowlem, M. C., Dickson, A. G., Gledhill, M. and Achterberg, E. P. (2017) Characterization of meta-Cresol Purple for spectrophotometric pH measurements in saline and hypersaline media at sub-zero temperatures. *Scientific reports* **7**, 2481.

Macreadie, P. I., Serrano, O., Maher, D. T., Duarte, C. M. and Beardall, J. (2017) Addressing calcium carbonate cycling in blue carbon accounting. *Limnology and Oceanography Letters* **2**, 195-201.

Menadakis, M., Maroulis, G. and Koutsoukos, P. G. (2009) Incorporation of Mg^{2+} , Sr^{2+} , Ba^{2+} and Zn^{2+} into aragonite and comparison with calcite. *Journal of mathematical chemistry* **46**, 484-491.

Mosley, L. M. (2016) Barrage release optimisation trial August 2015: assessment of environmental outcomes and achievement of management objectives. Report to SA Water. University of Adelaide, 23rd March, 2016.

Mosley, L. M., Hamilton, B., Busch, B., Hipsey, M., and Taylor, B. (2017) Assessment and model-

ling of the effects of the 2013-2016 Morella Basin releases on Coorong water quality. Report to the Department of Environment, Water and Natural Resources (DEWNR). University of Adelaide, South Australia.

Mosley, L. M., Priestley, S., Brookes, J., Dittmann, S., Farkaš, J., Farrell, M., Ferguson, A. J., Gibbs, M., Hipsey, M., Huang, J., Lam-Gordillo, O., Simpson, S. L., Teasdale, P. R., Tyler, J. J., Waycott, M., Welsh, D. T. (2020) *Coorong water quality synthesis with a focus on the drivers of eutrophication*. Goyder Institute for Water Research Technical Report Series No. 20/xx.

Nand, V. and Ellwood, M. J. (2018) A simple colorimetric method for determining seawater alkalinity using bromophenol blue. *Limnology and Oceanography: Methods* **16**, 401-410.

Regnier, P., Friedlingstein, P., Ciais, P., Mackenzie, F. T., Gruber, N., Janssens, I. A., Laruelle, G. G., Lauerwald, R., Luysaert, S., Andersson, A. J., Arndt, S., Arnosti, C., Borges, A. V., Dale, A. W., Gallego-Sala, A., Godd ris, Y., Goossens, N., Hartmann, J., Heinze, C., Ilyina, T., Joos, F., LaRowe, D. E., Leifeld, J., Meysman, F. J. R., Munhoven, G., Raymond, P. A., Spahni, R., Suntharalingam, P. and Thullner, Martin. (2013) Anthropogenic perturbation of the carbon fluxes from land to ocean. *Nature geoscience* **6**, 597-607.

Reeves, J. M., Haynes, D., Garc a, A. and Gell, P. A. (2015) Hydrological change in the Coorong Estuary, Australia, past and present: Evidence from fossil invertebrate and algal assemblages. *Estuaries and coasts* **38**, 2101-2116.

Reid, R. J. and Mosley, L. M. (2016) Comparative contributions of solution geochemistry, microbial metabolism and aquatic photosynthesis to the development of high pH in ephemeral wetlands in South East Australia. *Science of the Total Environment* **542**, 334-343.

Rippon, L., Rollog, M., Bruce, D., Farkas, J., Pate, F. D., Owen, T., Moffat, I. (2020). Baseline bio-available strontium and oxygen isotope mapping of the Adelaide Region, South Australia. *Journal of Archaeological Science: Reports*, **34**, 102614.

Shao, Y., Farkaš, J., Holmden, C., Mosley, L., Kell-Duivesteyn, I., Izzo, C., Reis-Santos, P., Tyler, J., T rber, P., Fr yda, J., Taylor, H., Haynes, D., Tibby, J. and Gillanders, B.M. (2018) Calcium and strontium isotope systematics in the lagoon-estuarine environments of South Australia: Implications for water source mixing, carbonate fluxes and fish migration. *Geochimica et Cosmochimica Acta* **239**, 90-108.

Shao, Y., Farkaš, J., Mosley, L., Tyler, J., Wong, H., Chamberlayne, B., Raven, M., Samanta, M., Holmden, C., Gillanders, B.M., Kolevica, A., Eisenhauer, A. (2021) Impact of salinity and carbonate saturation on stable Sr isotopes ($\delta^{88/86}\text{Sr}$) in a lagoon-estuarine system. *Geochimica et Cosmochimica Acta* **293**, 461-476. doi: <https://doi.org/10.1016/j.gca.2020.11.014>

Stevenson, E. I., Hermoso, M., Rickaby, R. E., Tyler, J. J., Minoletti, F., Parkinson, I. J., Mokadem, F. and Burton, K. W. (2014) Controls on stable strontium isotope fractionation in coccolithophores with implications for the marine Sr cycle. *Geochimica et Cosmochimica Acta* **128**, 225-235.

Vollstaedt, H., Eisenhauer, A., Wallmann, K., Böhm, F., Fietzke, J., Liebetrau, V., Krabbenhöft, A., Farkaš, J., Tomašových, A., Raddatz, J. and Veizer, J. (2014) The Phanerozoic $\delta^{88/86}\text{Sr}$ record of seawater: New constraints on past changes in oceanic carbonate fluxes. *Geochimica et Cosmochimica Acta* **128**, 249-265.

Von der Borch, C. C., Lock, D. E. and Schwebel, D. (1975) Ground-water formation of dolomite in the Coorong region of South Australia. *Geology* **3**, 283-285.

Wacey, D., Wright, D. T. and Boyce, A. J. (2007) A stable isotope study of microbial dolomite formation in the Coorong Region, South Australia. *Chemical Geology* **244**, 155-174.

Webster, I. T. (2010) The hydrodynamics and salinity regime of a coastal lagoon—The Coorong, Australia—Seasonal to multi-decadal timescales. *Estuarine, Coastal and Shelf Science* **90**, 264-274.

CHAPTER 5

Reconstructing the palaeo-hydrology and salinity of the Coorong lagoon in South Australia using multi-tracer analyses ($^{87}\text{Sr}/^{86}\text{Sr}$, $\delta^{88/86}\text{Sr}$ and Mg/Sr) of fossil carbonate shells

This chapter is formatted for publication in the journal of Limnology and Oceanography, with the following authors: Shao, Y., Woolston, Z., Chamberlayne, B., Foster, N., Haynes, D., Gilbert, S., Jacobsen, G., Tyler, J., Gillanders, B.M., Farkaš, J.; and a title: Reconstructing the palaeo-hydrology and salinity of the Coorong lagoon in South Australia based on multi-tracer analyses ($^{87}\text{Sr}/^{86}\text{Sr}$, $\delta^{88/86}\text{Sr}$ and Mg/Sr) of fossil carbonate shells.

Statement of Authorship

Title of Paper	Reconstructing paleo-hydrology and salinity of the Coorong lagoon in South Australia based on multi-tracer analyses ($^{87}\text{Sr}/^{86}\text{Sr}$, $\delta^{88/86}\text{Sr}$ and Mg/Sr) of fossil carbonates
Publication Status	<input type="checkbox"/> Published <input type="checkbox"/> Accepted for Publication <input type="checkbox"/> Submitted for Publication <input checked="" type="checkbox"/> Unpublished and Unsubmitted work written in manuscript style
Publication Details	Shao, Y., Woolston, Z., Chamberlayne, B., Foster, N., Haynes, D., Gilbert, S., Jacobsen., G., Tyler, J., Mosley, L., Gillanders, B.M., Farkaš, J. (2021) Reconstructing the palaeo-hydrology and salinity of the Coorong lagoon in South Australia using multi-tracer analyses ($^{87}\text{Sr}/^{86}\text{Sr}$, $\delta^{88/86}\text{Sr}$ and Mg/Sr) of fossil carbonate shells. <i>Limnology and Oceanography in prep.</i>

Principal Author

Name of Principal Author (Candidate)	Yuexiao Shao		
Contribution to the Paper	Sample preparation, sample preparation, Sr isotope analyses, data collection, data interpretation and modelling, making radiocarbon age model of core CSC, manuscript writing, acting as the corresponding author.		
Overall percentage (%)	65		
Certification:	This paper reports on original research I conducted during the period of my Higher Degree by Research candidature and is not subject to any obligations or contractual agreements with a third party that would constrain its inclusion in this thesis. I am the primary author of this paper.		
Signature		Date	2/2/2021

Co-Author Contributions

By signing the Statement of Authorship, each author certifies that:

- i. the candidate's stated contribution to the publication is accurate (as detailed above);
- ii. permission is granted for the candidate to include the publication in the thesis; and
- iii. the sum of all co-author contributions is equal to 100% less the candidate's stated contribution.

Name of Co-Author	Zara Woolston		
Contribution to the Paper	Water and shell sample collection, provided Sr isotope and concentration data on (i) a water and two shell samples and (ii) sedimentary core CSC, data collection and interpretation.		
Signature		Date	19/02/2021

Name of Co-Author	Briony Chamberlayne		
Contribution to the Paper	Water and shell sample collection, provided concentration data on collected samples, making radiocarbon age model of core C18.		

Signature		Date	03/02/2021
-----------	--	------	------------

Name of Co-Author	Nicole Foster		
Contribution to the Paper	Collection of core CSC, provided core observation, preparation of core CSC for radiocarbon dating.		
Signature		Date	02/02/21

Name of Co-Author	Deborah Haynes		
Contribution to the Paper	Collection of core C18, provided lithological diagrams for both core C18 and CSC.		
Signature		Date	03/02/2021

Name of Co-Author	Sarah Gilbert		
Contribution to the Paper	Elemental concentration analyses.		
Signature		Date	24/02/2021

Name of Co-Author	Geraldine Jacobsen		
Contribution to the Paper	Radiocarbon dating of cores C18 and CSC.		
Signature		Date	05/02/2021

Name of Co-Author	Jonathan Tyler		
Contribution to the Paper	Conceptual development, assistance on lab work, assistance on data interpretation and modelling, manuscript review.		

Signature		Date	2/2/2021
-----------	--	------	----------

Name of Co-Author	Luke Mosley		
Contribution to the Paper	Assistance on data interpretation, manuscript review.		
Signature		Date	6/3/21

Name of Co-Author	Bronwyn M. Gillanders		
Contribution to the Paper	Conceptual development, guidance on manuscript structure, manuscript evaluation and review.		
Signature		Date	3 March 2021

Name of Co-Author	Juraj Farkaš		
Contribution to the Paper	Conceptual development, assistance on data interpretation and modelling, manuscript review.		
Signature		Date	15/03/2021

Chapter 5.

Reconstructing the palaeo-hydrology and salinity of the Coorong lagoon in South Australia based on multi-tracer analyses ($^{87}\text{Sr}/^{86}\text{Sr}$, $\delta^{88/86}\text{Sr}$ and Mg/Sr) of fossil carbonate shells

Abstract

To address the environmental problems of the Ramsar-listed Coorong coastal lagoon, especially in the hypersaline South Lagoon of the Coorong, an advanced understanding of the long-term hydrological history of the local hydrology, including knowledge of the water source mixing and changes in salinity and water evaporation is essential. To reconstruct the paleo-hydrology and salinity of the South Lagoon over the past two millennia (i.e., last ~2400 years), we first analysed and compared the Sr isotope compositions ($^{87}\text{Sr}/^{86}\text{Sr}$ and $\delta^{88/86}\text{Sr}$) in the aragonitic short-lived bivalve *Arthritica helmsi* (about 1-year life span) and ambient lagoon waters where the shells were living and collected. These results confirmed a relatively constant or consistent isotope offset ($\Delta^{88/86}\text{Sr}$) of -0.104‰ between $\delta^{88/86}\text{Sr}$ values of modern shells and local lagoon waters ($\delta^{88/86}\text{Sr}_{\text{shell}} - \delta^{88/86}\text{Sr}_{\text{water}}$). Consequently, this offset was applied to $\delta^{88/86}\text{Sr}$ data of fossil *A. helmsi* shells collected from two sediment cores to reconstruct the Sr isotope composition and temporal evolution of $\delta^{88/86}\text{Sr}$ and $^{87}\text{Sr}/^{86}\text{Sr}$ values in the palaeo-waters of the South Lagoon. The Sr isotope composition profiles of the paleo-South Lagoon were complemented by radiocarbon (^{14}C), ^{210}Pb and pollen based geochronological models. Overall, $^{87}\text{Sr}/^{86}\text{Sr}$ and Mg/Sr data suggest that over the past ca. two millennia the South Lagoon had never been a purely marine environment but rather hosted brackish waters (with modelled minimum salinities ranging from ~6 and 23 PSU) which had a significant mass fraction (up to 60%) of Sr sourced from continental waters. Moreover, Rayleigh and equilibrium modelling of $\delta^{88/86}\text{Sr}$ suggested that the South Lagoon became over time more efficient in removing Sr and thus carbon into authigenic carbonates, which is likely related to its progressively more ‘evaporitic character’ and shift from a brackish to hypersaline lagoon system. Such purported brackish palaeo-lagoon waters are in stark contrast with the present-day hypersaline conditions (>70 PSU) characteristic of the South Lagoon, which are conditions posing major environmental and water management concerns.

5.1 Introduction

Palaeo-environmental reconstructions using sedimentary archives can offer valuable information on past physico-chemical conditions in coastal systems, which are essential for designing strategies for

future ecosystem management in the face of anthropogenic and global climate change impacts (Dearing et al., 2006; Velez et al., 2018). Water bodies in lagoons and estuaries, especially in semi-arid to arid regions such as South Australian, are extremely sensitive to ongoing impacts of climate change and human activities, which can lead to widespread problems such as ecosystem degradation, eutrophication, hypersalinity, hypoxia/anoxia and changing mineral saturation state of coastal waters (Bennett et al., 2001; Halpern et al., 2008). Specifically, local carbonate dynamics (i.e., dissolution vs precipitation of calcite and aragonite minerals) plays an important role in the inorganic carbon cycling in coastal systems, which might act as an important sink for carbon (via in-situ CaCO_3 precipitation) to mitigate the effects of atmospheric CO_2 emissions (Bauer et al., 2013 and references therein; Macreadie et al., 2017).

Radiogenic strontium (Sr) isotope tracer (i.e., $^{87}\text{Sr}/^{86}\text{Sr}$ ratio) has been used for decades as a geochemical tracer for calcium (due to similar charge and ionic radius of Ca^{2+} and Sr^{2+} ions), providing valuable insights and constrains on present-day and past sources of these alkaline earth metals (and by inference also waters) in terrestrial, marine and coastal systems. Particularly, $^{87}\text{Sr}/^{86}\text{Sr}$ is useful for tracing continental vs. marine water sources associated with weathering of different types of bedrock geology, where the difference in age and Rb content of continental and oceanic crust causes different radiogenic ^{87}Sr excess produced by radioactive decay of ^{87}Rb . In addition, specific $^{87}\text{Sr}/^{86}\text{Sr}$ signature of waters and/or calcifying fluids is also directly recorded in precipitated biogenic or inorganic carbonate minerals/shells, which thus acts as natural archives allowing to trace for past changes in Sr sources and water provenance in carbonate-producing depositional systems (see Fig. 1) (Holmden et al., 1997; Anadón et al., 2002; Porcelli and Baskaran, 2012). Unlike $^{87}\text{Sr}/^{86}\text{Sr}$ which is relatively insensitive to mass-dependent kinetic and equilibrium isotope fractionation, the stable Sr isotope tracer (denoted as $\delta^{88/86}\text{Sr}$) is particularly sensitive to carbonate precipitation and dissolution processes governed by these mass-dependent isotope fractionation effects, thus allowing a better tracing and quantification of local carbonate cycling in various depositional environments (cf., Krabbenhöft et al., 2010; Pearce et al., 2015; Fruchter et al., 2016). Recent pioneering studies on $\delta^{88/86}\text{Sr}$ (Raddatz et al., 2013;

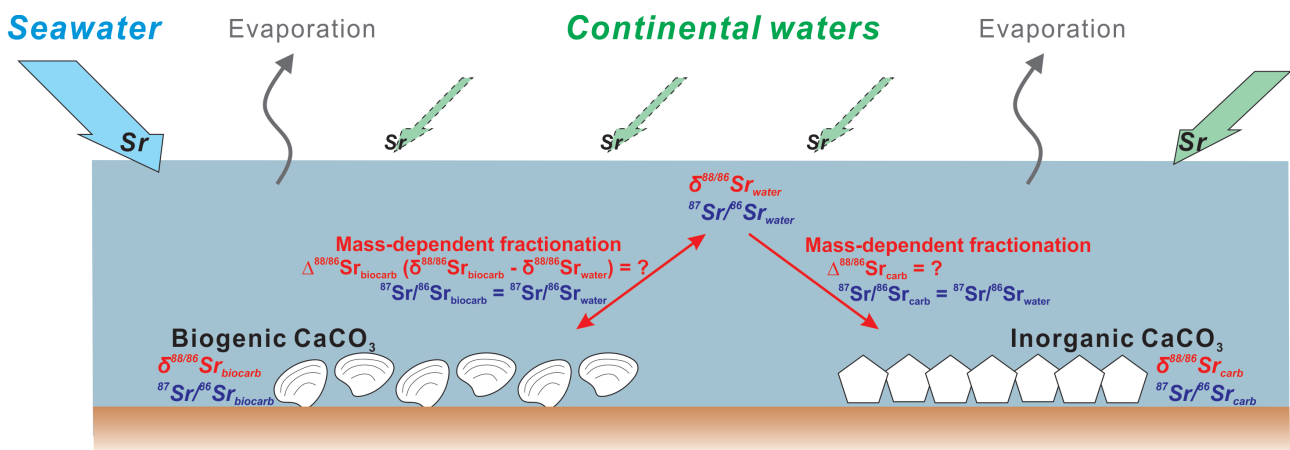


Figure 1: Schematic diagram of Sr cycling and isotope fractionation between carbonates and water in coastal systems.

Vollstaedt et al., 2014; Fruchter et al., 2016 and 2017) found a relatively constant offset ($\Delta^{88/86}\text{Sr}$) between $\delta^{88/86}\text{Sr}$ values of biogenic skeletal carbonates (e.g., bivalves, brachiopods, belemnites and corals) and ambient water/seawater. On average, this offset ($\Delta^{88/86}\text{Sr} = \delta^{88/86}\text{Sr}_{\text{biocarb}} - \delta^{88/86}\text{Sr}_{\text{water}}$) was around -0.2‰ and is relatively insensitive to various environmental parameters such as temperature, saturation states and pH of the fluid, thus providing a potential ‘new tool’ for the reconstruction of the $\delta^{88/86}\text{Sr}$ signature of palaeo-water based on analysis of fossil biogenic or inorganic carbonates (Fig. 1).

The Ramsar-listed Coorong is an elongated estuarine lagoon located at the terminus of the River Murray and Murray-Darling Basin in South Australia (Settre and Wheeler, 2017; Aldridge et al., 2019). The unique geomorphology divides the Coorong into North and South Lagoons by a narrow channel at Parnka Point (Fig. 2), forming a mixing zone of Southern Ocean seawater with various continental water sources (Gibbs et al., 2019). During the decades since intensification of European settlement in the region in the 1950s, changes in land use for agriculture and over extraction of fresh water from the Murray-Darling Basin has deteriorated the Coorong ecosystem and water quality of the lagoon. These effects are particularly pronounced in the geomorphologically restricted South Lagoon, causing hypersalinity and eutrophication problems (Krull et al., 2009, McKirdy et al., 2010; Reeves et al., 2015; Brookes et al., 2018; Aldridge et al., 2019). Currently suggested interventions to restore the water conditions of the hypersaline South Lagoon include increasing freshwater inflows (i.e., River Murray environmental flow provisions, barrage operations, and increase flows from the South East via the Salt Creek at the southern end of the Coorong) and increasing seawater inflow (i.e., Murray Mouth dredging) into the Coorong (Mosley et al., 2020). To advise decision-making on future water management strategies, palaeo-environmental studies are often important and relevant to identify ‘pre-impact’ environmental conditions (Dearing et al., 2006). Previous studies on the palaeo-environment of the Coorong were mostly based on direct observations of fossil invertebrates and algae assemblages, sedimentation, complemented by $\delta^{13}\text{C}$ and $\delta^{15}\text{N}$ data, which all seem to suggest that the South Lagoon was much less saline in the past (Krull et al., 2009; McKirdy et al., 2010; Reeves et al., 2015; Haynes et al., 2019). However, as many observed fossil species could tolerate a wide range of salinities, there remains a lack of confidence in these interpretations of palaeo-salinity changes, and thus more work and innovative applications of palaeo-environmental tracers is needed.

This study is the first one that examines the feasibility of a short-lived aragonitic *Arthritica helmsi* bivalve shells (Chamberlayne et al., 2020) as a suitable archive of paleo-lagoon water Sr isotope composition in the Coorong by comparing $^{87}\text{Sr}/^{86}\text{Sr}$ and $\delta^{88/86}\text{Sr}$ data in living shells and ambient lagoon waters. We then apply this calibration to reconstruct the $^{87}\text{Sr}/^{86}\text{Sr}$ and $\delta^{88/86}\text{Sr}$ evolution of the South lagoon waters based on the Sr isotope analyses of fossil shells collected from two sediment cores, which were radiocarbon dated (yielding age up to ~2400 years ago). Finally, quantitative interpretations of past water source mixing, salinity changes and local carbonate fluxes in the South Lagoon were attempted based on the multi-tracer ($^{87}\text{Sr}/^{86}\text{Sr}$, $\delta^{88/86}\text{Sr}$ and Mg/Sr) elemental and isotope

mass-balance mixing models. The acquired results and interpretations should be of interest and benefit also for future water management strategies to improve the water quality of the Coorong lagoon system.

5.2 Material and methods

5.2.1 Modern sample collection and field measurements

Pairs of modern water and *A. helmsi* shell samples were collected from four sites along the Coorong North Lagoon (labelled as 1-4 in Fig. 2) in 2018 by Chamberlayne et al. (2021, in review) and in 2020 by Woolston (2020). Unfortunately, no *A. helmsi* shells were found in the South Lagoon due to the hypersaline and oxygen-depleted waters. The GPS location of each sampling site was recorded, and water temperature and salinity were measured in the field using a Hanna Instruments HI-98194 multiparameter probe. For the 2020 sampling campaign these parameters were measured in the field using a YSI ProDSS multi-parameter water quality meter. These data and sampling locations are listed in Table A.1, Appendix A.

At each site, a water sample was collected from the surface of the lagoon with an acid-cleaned HDPE bottle, and 5-10 individual *A. helmsi* shells were collected from the sediment water interface. The collected water samples were stored at 4°C. Elemental concentrations (Mg and Sr) of water and shell samples were adopted from Woolston (2020). Elemental concentrations (Mg, Ca, Sr and Ba) of water samples were taken from Chamberlayne et al., (2021, in review).

5.2.2 Sediment core collection

The sediment core C18 was collected at the main channel of the South Lagoon 5 km southeast of Parnka Point (Fig. 2) in early autumn 2005 by Prof. John Tibby and his team (for details see also Haynes et al., 2019). Core collection was conducted with a piston corer, following the approach detailed in Chambers and Cameron (2001) using a 50 mm wide PVC pressure pipe. The collected sediment was ~130 cm in length and collected from water depth of 0.6 m. The pipe was capped at both ends, sealed with tape to limit exposure to air and transported for a long-term storage using refrigerated facilities and a cold room at the University of Adelaide. The sediment core was subsampled using a 'continuous' ~1 cm sampling step or interval, and collected sample horizons were subsequently freeze-dried at -55°C for 24 hours (see also Chamberlayne, 2015). A total of 73 sub-samples (i.e., 1-cm interval samples) from dried sediment fractions were selected from the core for further analyses and the fossil shells collection (Table B.3, Appendix B.1).

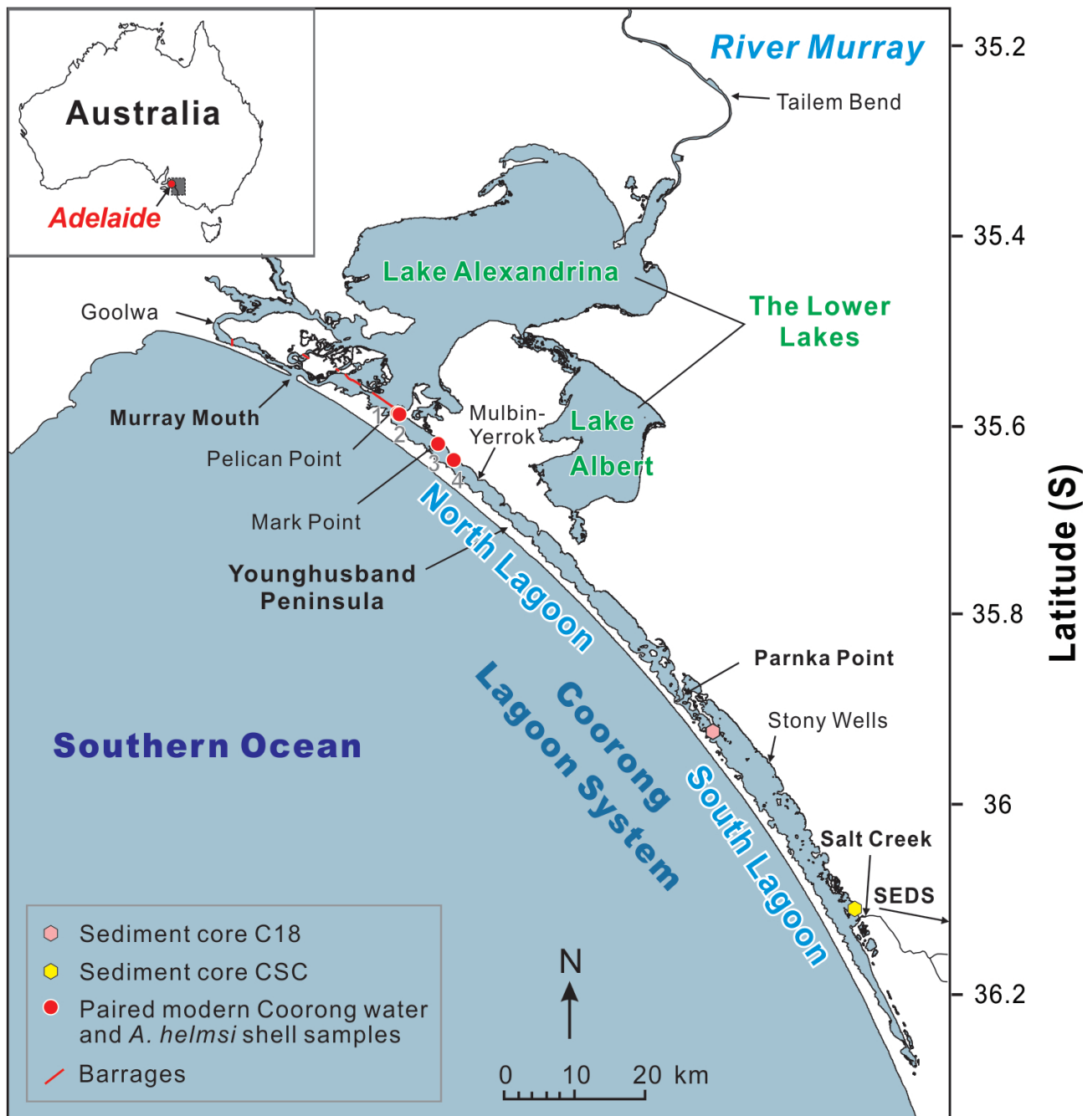


Figure 2: Map of the Coorong region with the sampling sites. The solid red lines represent the five barrages. Note that the numbers next to the paired modern Coorong water and *A. helmsi* shell samples are site numbers from north to South, which are listed together with their coordinates and sampling dates in the Appendix (Table A.1).

The second sediment core CSC in this study was collected from the South Lagoon near Salt Creek (Fig. 2) in June 2019 by Bronwyn Gillanders and her team. The core collection was conducted using manual hammering of a 75 mm PVC pipe that was inserted into the sediment. The collected core was ~80 cm long and sampled from water depth of ~0.3 m. The core was sealed and transported vertically back to University of Adelaide and stored in a cold room. A total of 13 sub-samples (i.e., 1-cm fractions) of sediment were sliced and collected along the length of the core for further analyses (Table

B.2, Appendix B.1). These sub-sample sediment fractions were then oven-dried at 60°C for 24 hours.

Both sediment cores were investigated for lithology and organic materials, including biogenic skeletal carbonates. Schematic lithostratigraphy diagrams for both sediment cores can be found in Fig. 4.

5.2.3 Water and shell sample preparation

Water samples collected in 2018 were filtered through 0.2 µm cellulose nitrate filters and acidified to 2% with nitric acid. The 2020 water sample was filtered through a 0.45µm cellulose nitrate membrane filter.

From each of the sub-samples from the cores (n = 90, i.e., 73 from C18 and 13 from CSC), approximately 20 pieces of *A. helmsi* shells were picked for the analysis of elemental concentrations (Table B.3, Appendix B.1). 20 out of the 73 sub-samples from core C18 selected from various depths and all 13 sub-samples from core CSC were selected for Sr isotope analyses (Table B.5, Appendix B.3). Additional 3 to 5 pieces of *A. helmsi* shells were picked from sub-samples of core C18 for the purpose of radiocarbon ¹⁴C dating done at ANSTO facilities.

The shells collected from selected sediment fractions were first cleaned from any visible impurities such as attached clays and/or sediment particles using a soft brush and deionised water. Subsequently, these pre-clean shells were further purified following the steps or cleaning protocols of Zaky et al. (2015), which include (i) immersing shells in 10% H₂O₂ for three days, (ii) ultrasonic cleaning for 60 seconds, (iii) dissolving the outer surface of shells with 0.27M HCl for approximately 30s, followed by drying. Between each step, the shells were rinsed with deionised water three times.

Cleaned shells for radiocarbon ¹⁴C dating collected from the core C18 were weighed prior to analysis and dating, and cleaned shells for elemental concentration and the Sr isotope analyses were also weighed and acid digested using single-distilled 0.2M HNO₃.

5.2.4 Geochronological methods

Geochronological models for the two sediment cores C18 and CSC were built using the software “Bacon” in R (Blaauw and Christen, 2011). For C18, the age model was based on ¹⁴C ages of *A. helmsi* shell samples from C18 (n = 17) supported by the first appearance of the exotic *Pinus radiata* pollen (~1955AD). For CSC, a single ¹⁴C age from a bulk carbonate sample was derived (Table B.4, Appendix B.2). The radiocarbon ¹⁴C dating of shells and carbonate sample were performed using Accelerator Mass Spectrometry (AMS) facilities at the Waikato Dating Laboratory in New Zealand and the Australian Nuclear Science and Technology Organisation (ANSTO, Lucas Heights, Sydney),

(details in Appendix D.2). The acquired ^{14}C ages of shells from the upper part of C18 core were systematically older than the known arrival date of the exotic pollen *P. radiata*. This age difference is identified as the “reservoir effect”, likely linked to the incorporation of older dissolved carbon into the shells sourced from the weathering of surrounding limestones and/or transported into the lagoon via local groundwater inputs (Geyh et al., 1998). It is assumed that such ‘reservoir effect’ causes a constant age offset of shells in both cores, which can be calculated following the method described in Barr et al. (2014). Specifically, the ^{210}Pb -derived age of the exotic *Pinus* pollen was first converted to ^{14}C age using the Southern Hemisphere ^{14}C calibration curve (Hogg et al., 2013), then subtracted from the acquired ^{14}C age of shells from closest depth in the core C18. Such age offset, estimated to be around ~ 816 years, was calculated by Chamberlayne (2021, thesis in preparation) and applied for the ‘reservoir effect’ correction before Bacon modelling of both cores. The chronostratigraphic diagrams of both cores developed from Bacon age-depth model are presented in Fig. B.1, Appendix B.2.

5.2.5 Elemental concentration analyses of water and shell samples

Elemental concentration analyses were performed at Adelaide Microscopy Centre, University of Adelaide, with an Agilent 8900x inductively coupled plasma-mass spectrometer (ICP-MS/MS).

Specifically, for three water samples (122w, 149w and 151w, Table B. 1, Appendix B.1) collected in 2018, the plasma conditions for ICP MS/MS were: RF power 1550W, sample depth 10 mm and total Ar carrier gas flow rate 1.05 L/min, with a Micro Mist nebuliser and Scott Type spray chamber. The collision cell (MS/MS) was run in He mode (4 mL/min He gas flow) for the majority of elements (Mg, Sr and Ba). Ca was analysed with oxygen (30% flow rate) in the collision cell and the MO^+ reaction products measured: $^{44}\text{Ca} \rightarrow ^{44}\text{Ca}^{16}\text{O}$ at mass 60. On-line addition of indium was used as the internal standard. A series of mixed element calibration solutions (10, 50, 100, 200, 300, 500, 1000 ppb) were used for quantification. The IAPSO seawater standard was used as a quality control standard. Samples were diluted with ultra-pure water acidified to 2% with nitric acid by a factor of 10, 20, 40, 50, 80, 100 or 120 times depending on sample salinity. 15% of samples were analysed in triplicate, the mean precision for triplicate samples was $<1\%$ for Mg and Sr; 1.8% for Ca; and 5.2 % for Ba.

For 3 modern shell samples (122s, 149s and 151s, Table B. 3, Appendix B.1) collected in 2018 from and 73 fossil shell samples from the core C18, the plasma conditions of the ICP-MS/MS instrument were: RF power 1550W, sample depth 10 mm and Ar carrier gas flow rate 0.95 L/min and Ar make up gas 0.1 L/min, with a Micro Mist nebuliser and Scott Type spray chamber. The collision cell (MS/MS) was run in He mode (4 mL/min He gas flow) for the following elements: Mg, Al, P, K, Ca, Mn, Fe, Co, Ni, Zn, Sr, Cd and Ba. Phosphorus, Ca and Fe were analysed in Oxygen mode (0.45 ml/min) and the MO^+ reaction products measured for each element: $^{31}\text{P} \rightarrow ^{31}\text{P}^{16}\text{O}$ measured at mass 47; $^{44}\text{Ca} \rightarrow ^{44}\text{Ca}^{16}\text{O}$ at mass 60; and $^{56}\text{Fe} \rightarrow ^{56}\text{Fe}^{16}\text{O}$ at mass 72. Boron and potassium were also measured in

the oxygen (O₂) mode but measured (not as reaction products) at masses 11 and 39 amu respectively. On-line addition of indium (In) was used as the internal element standard for instrumental drift correction and data normalisation. The above-mentioned multi-element calibration solutions were used for data calibration and quantification, and standard solution and samples were diluted with 2% v/v HNO₃. The sample introduction system was rinsed in two stages with 5% and 2% HNO₃ between each analysis. Typical analytical error was on the order of ca. 5%.

Finally, the Mg and Sr concentrations in a water sample (COOR-50) and modern/fossil shell samples (COOR-50-P and COOR-50-W) were collected as the complementary data in 2020, from shell samples extracted from the core CSC and measured by Woolston (2020), following the same ICP MS/MS methods as described above (Table B.2, Appendix B.1).

5.2.6 $^{87}\text{Sr}/^{86}\text{Sr}$ and $\delta^{88/86}\text{Sr}$ analyses via thermal ionisation mass spectrometry

Samples of filtered waters and dissolved shells were analysed for $^{87}\text{Sr}/^{86}\text{Sr}$ and $\delta^{88/86}\text{Sr}$ by thermal ionisation mass spectrometry (TIMS) using a Phoenix Isotopx instrument at the Metal Isotope Group (MIG) and Mawson Analytical Spectrometry Services (MASS) facilities at the University of Adelaide. In core C18, fossil shell samples yielding consistent Ca and Sr concentration data from 20 sediment fractions were analysed via TIMS and double-spike approach. Specifically, the Sr isotope analyses of shells from both cores followed the procedures described in Shao et al. (2021) for both stable ($\delta^{88/86}\text{Sr}$) and radiogenic ($^{87}\text{Sr}/^{86}\text{Sr}$) strontium isotope analyses. In order to apply the ^{87}Sr - ^{84}Sr double spike method to analyse the $\delta^{88/86}\text{Sr}$ in an unknown sample, two aliquots from each sample (each containing about 500 ng of Sr) were taken from a stock sample solution, where one aliquot was spiked with the ^{87}Sr - ^{84}Sr double spike solution (composition described in Appendix of Shao et al., 2021), aiming for an optimal ‘sample to spike’ ratio ($^{84}\text{Sr}_{\text{sp}}/^{84}\text{Sr}_{\text{sa}}$ ratios) close to 20 (mean = 20.5, 2SEM = 0.4, n=53). Prior to the TIMS analysis, the Sr fractions from each sample and standard were purified from the sample ‘matrix’ using a 600 μL Micro Bio-Spin separation column filled with Sr-specific resin (Eichrom Sr-SPS), and such purified Sr fractions were then loaded on single non-zone-refined rhenium (Re) filaments (see Shao et al., 2021).

For stable Sr isotopes, all data measured in this study are reported as $\delta^{88/86}\text{Sr}$, expressed in per mil (‰), where $^{88}\text{Sr}/^{86}\text{Sr}$ ratio of an unknown sample is normalised relative to SRM987 standard, according to the following equation:

$$\delta^{88/86}\text{Sr} = \left[\left(\frac{^{88}\text{Sr}/^{86}\text{Sr}}{^{88}\text{Sr}/^{86}\text{Sr}} \right)_{\text{sample}} / \left(\frac{^{88}\text{Sr}/^{86}\text{Sr}}{^{88}\text{Sr}/^{86}\text{Sr}} \right)_{\text{SRM987}} - 1 \right] \times 1000 \quad (\text{Eq. 1})$$

The total procedural Sr blanks determined via ^{84}Sr isotope dilution ranged from 6 to 214 picograms (pg), with an average value of 55 pg (2SEM = 29 pg, n=14), corresponding to less than 0.1% of a total

Sr originating from the analysed sample (500 ng).

Following the analytical procedures described above, the long-term average $^{87}\text{Sr}/^{86}\text{Sr}$ and $\delta^{88/86}\text{Sr}$ values and uncertainties of standards in this study were, respectively, 0.709249 ± 0.000004 (2SEM, $n=25$) and $0.000 \pm 0.008\text{‰}$ (2SEM, $n=23$) for SRM987 standard; 0.709173 ± 0.000005 (2SEM, $n=9$) and $0.390 \pm 0.012\text{‰}$ (2SEM, $n=8$) for IAPSO seawater; and 0.709174 ± 0.000004 (2SEM, $n=11$) and $0.204 \pm 0.011\text{‰}$ (2SEM, $n=11$) for JCP-1 carbonate standard. The analysed $^{87}\text{Sr}/^{86}\text{Sr}$ and $\delta^{88/86}\text{Sr}$ in the Coorong waters and shell samples are listed in Tables B.5 and B.6, Appendix B.3.

5.3 Results and discussion

5.3.1 $^{87}\text{Sr}/^{86}\text{Sr}$ and $\delta^{88/86}\text{Sr}$ variations in modern shells and water samples

To use the fossil shells of *A. helmsi* as a suitable archive of the paleo-lagoon waters in Coorong and their Sr isotope evolution over time, we compared $^{87}\text{Sr}/^{86}\text{Sr}$ and $\delta^{88/86}\text{Sr}$ in living *A. helmsi* shells to ambient water samples collected simultaneously at sites 1-4 from the Coorong North Lagoon (labelled in Fig. 2). Taking into account that *A. helmsi* bivalve species has a lifespan of ca. 1 year (Chamberlayne et al., 2020), the $^{87}\text{Sr}/^{86}\text{Sr}$ and $\delta^{88/86}\text{Sr}$ signatures of North Lagoon waters collected in 2018-2019 (data from Chapter 4) were also considered as these represent an annual variation of Sr isotope water composition in the North Lagoon (Fig. 3). According to previous studies (e.g., Holmden et al., 1997; Schmitz and Andreasson, 2001; Fruchter et al., 2017), it is expected that the shells would have identical $^{87}\text{Sr}/^{86}\text{Sr}$ signature to their ambient water. However, the $^{87}\text{Sr}/^{86}\text{Sr}$ in modern shells of *A. helmsi* (0.70930 ± 0.00010 , 2SD, $n = 4$) was higher than the ambient water samples (0.70923 ± 0.00013 , 2SD, $n = 4$) as well as the North Lagoon water samples from 2018-2019 (0.70923 ± 0.00005 , 2SD, $n = 16$, data from Chapter 4) (Fig. 3A). On the other hand, the $\delta^{88/86}\text{Sr}$ differences between modern shells and ambient water samples ($\Delta^{88/86}\text{Sr} = \delta^{88/86}\text{Sr}_{\text{shell}} - \delta^{88/86}\text{Sr}_{\text{water}}$) were similar and rather constant among all four sampling sites in the North Lagoon, giving an average $\Delta^{88/86}\text{Sr}$ of -0.104‰ , with 2SD of 0.030‰ ($n = 4$), (Fig. 3B). This apparently constant $\Delta^{88/86}\text{Sr}$ value agrees with previous studies on stable Sr isotope fractionation between carbonates and fluids (Raddatz et al., 2013; Fruchter et al., 2016 and 2017), although the latter reported larger absolute $\Delta^{88/86}\text{Sr}$ values closer to -0.20‰ . These differences in observed $\Delta^{88/86}\text{Sr}$ magnitudes might be species dependent as observed between coccolithophores and seawater by Stevenson et al. (2014).

As to the above-mentioned inconsistency between $^{87}\text{Sr}/^{86}\text{Sr}$ of modern shells and ambient North Lagoon waters, one possibility is that it could be caused by more radiogenic (i.e., ^{87}Sr enriched) local sediment pore waters or fluid (as modern shells were collected from top sediment) due to the presence of detrital silicate minerals within the sediment that might have locally shifted $^{87}\text{Sr}/^{86}\text{Sr}$ of porewaters or bottom lagoon waters to higher and more radiogenic values (cf., Lerouge et al.,

2010), where the latter could be then reflected in analysed shells. Therefore, one cannot completely rule out that those more radiogenic $^{87}\text{Sr}/^{86}\text{Sr}$ values of modern shells (compared to ambient or seasonal water samples) could be an artefact of more radiogenic Sr in local sediment pore fluids (compared to typical lagoon waters), where the former could be then imparted into the Sr isotope composition of shells growing within the sediment, even though our cleaning and leaching procedure aimed to minimise the effects of detrital contamination. On the other hand, such plausible detrital mineral contamination effects and/or pore water related effects are not expected to impact significantly $\delta^{88/86}\text{Sr}$ of shells, as unlike for $^{87}\text{Sr}/^{86}\text{Sr}$ tracer, silicate minerals have $\delta^{88/86}\text{Sr}$ close to that of carbonates and/or natural waters (Krabbenhöft et al., 2010; Moynier et al., 2010; Charlier et al., 2012). Alternatively, our North Lagoon water samples from 2018-2019 might have missed some

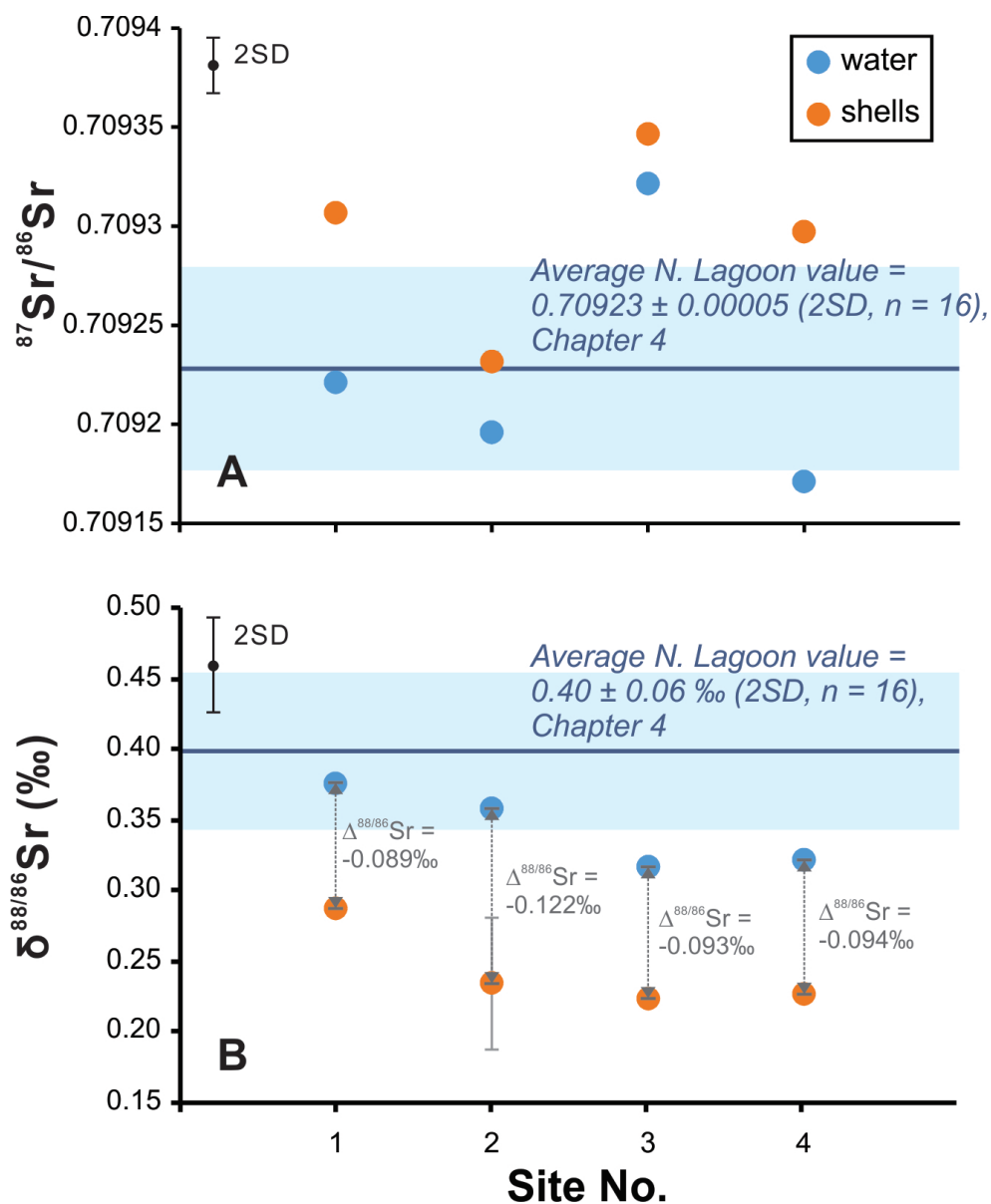


Figure 3: Comparison of $^{87}\text{Sr}/^{86}\text{Sr}$ and $\delta^{88/86}\text{Sr}$ signatures in *A. helmsi* shells and their ambient water from four sites of the Coorong (labelled as 1-4 in Fig. 2). The dark blue band represents average value of 2018-2019 North Lagoon samples from Chapter 4, with 2SD variation indicated by the light blue rectangle.

major freshwater input events (i.e., barrage outflows) into the lagoon, which will supply continental waters with higher $^{87}\text{Sr}/^{86}\text{Sr}$, where the latter would be then reflected in $^{87}\text{Sr}/^{86}\text{Sr}$ of shells, but missed in our seasonal water sampling data. Due to the above uncertainties, we also calculated alternative $\Delta^{88/86}\text{Sr}$ values using $\delta^{88/86}\text{Sr}$ of shell samples and the average North Lagoon water value ($\delta^{88/86}\text{Sr} = 0.40\text{‰}$, Chapter 4), and the corresponding $\Delta^{88/86}\text{Sr}$ varies from -0.167‰ to -0.115‰ , with an average $\Delta^{88/86}\text{Sr}$ value of -0.160‰ (2SD = 0.059‰ , $n = 4$). In this study, the observed $\Delta^{88/86}\text{Sr}$ values in both scenarios above for *A. helmsi* and ambient lagoon water of are further discussed below and used to reconstruct the $\delta^{88/86}\text{Sr}$ of palaeo-lagoon waters from the measured $\delta^{88/86}\text{Sr}$ in fossil shells, and their $^{87}\text{Sr}/^{86}\text{Sr}$ were used as a direct record of palaeo-water $^{87}\text{Sr}/^{86}\text{Sr}$ composition; although caution needs to be taken regarding possible detrital and/or pore water related effects.

5.3.2 Geochronology, $^{87}\text{Sr}/^{86}\text{Sr}$ and $\delta^{88/86}\text{Sr}$ evolution of the South Lagoon waters

Based on our radiocarbon and pollen dating, the sedimentary record of core C18 spans up to ~ 1755 cal. years before present (BP), and core CSC up to ~ 2407 cal. yrs BP (where 0 cal. yr BP = 1950 AD, Hughen et al., 2004) (for details see Fig. 4, and data from Table B.4 and Fig. B.1, Appendix B.2). Although the timeframes of the two cores are not identical and the core CSC has only one ^{14}C date (Table B.4, Appendix B.2), there is a significant proportion of time overlap that allows comparison of reconstructed palaeo-lagoon water $^{87}\text{Sr}/^{86}\text{Sr}$ and $\delta^{88/86}\text{Sr}$ data and temporal trends between these two cores.

Due to the above-discussed uncertainties related to $\Delta^{88/86}\text{Sr}$ parameter and its fidelity to directly reconstruct the $\delta^{88/86}\text{Sr}$ of palaeo-lagoon waters based on analysis of fossil shells, a number of plausible scenarios and interpretations should be discussed. For example, assuming an average $\Delta^{88/86}\text{Sr}$ of -0.160‰ , the reconstructed $\delta^{88/86}\text{Sr}$ data of South Lagoon palaeo-water from cores C18 ($0.44 \pm 0.05\text{‰}$, 2SD, $n = 20$) and CSC ($0.45 \pm 0.06\text{‰}$, 2SD, $n = 13$) are overall comparable to the present-day $\delta^{88/86}\text{Sr}$ of this hypersaline South Lagoon waters ($0.43 \pm 0.07\text{‰}$, 2SD, $n = 15$), which would suggest that this part of the Coorong Lagoon had always been carbonate-oversaturated and likely hypersaline as it is in the present day. However, such conclusion is at odds with previous studies of the palaeo-environmental conditions in the South Lagoon based on observations of sediment organic matter, fossil invertebrates and algae assemblages, which all seems to suggest that the South Lagoon was much less saline in the past (Krull et al., 2009; McKirdy et al., 2010; Reeves et al., 2015; Haynes et al., 2019). Hence, in the following sections, a plausible $\Delta^{88/86}\text{Sr}$ value of -0.104‰ is used instead for the reconstruction of $\delta^{88/86}\text{Sr}$ of palaeo-water in the South Lagoon.

Overall, the modern South Lagoon waters are slightly higher in both $^{87}\text{Sr}/^{86}\text{Sr}$ (0.70926 ± 0.00003 , 2SD, $n = 15$) and $\delta^{88/86}\text{Sr}$ ($0.43 \pm 0.07\text{‰}$, 2SD, $n = 15$) compared to reconstructed palaeo-waters from

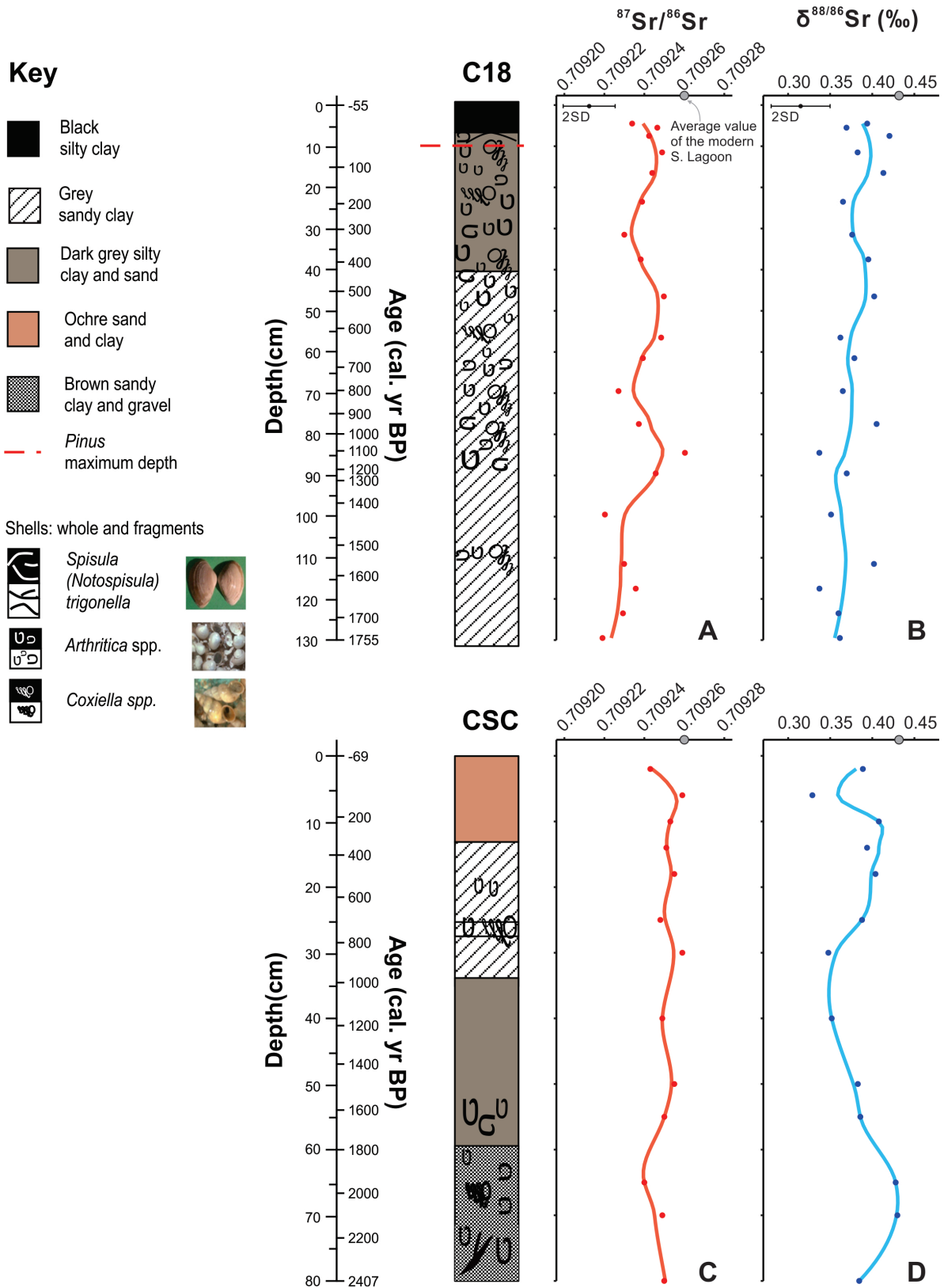


Figure 4: Geochronology, lithostratigraphy and Sr isotope signatures ($^{87}\text{Sr}/^{86}\text{Sr}$ and $\delta^{88/86}\text{Sr}$) of palaeo-waters from cores C18 (A, B) and CSC (C, D) calculated from contemporary *A. helmsi* shell samples using their measured $^{87}\text{Sr}/^{86}\text{Sr}$ and $\Delta^{88/86}\text{Sr}$ ($\delta^{88/86}\text{Sr}_{\text{shell}} - \delta^{88/86}\text{Sr}_{\text{water}} = -0.104\text{‰}$). Grey dots are average values of Sr isotope signatures of the modern South Lagoon (data from Shao et al., 2018 and 2021).

both cores (C18 data: $^{87}\text{Sr}/^{86}\text{Sr} = 0.70924 \pm 0.00002$, $\delta^{88/86}\text{Sr} = 0.38 \pm 0.05\text{‰}$, 2SD, $n = 20$; and CSC data: $^{87}\text{Sr}/^{86}\text{Sr} = 0.70925 \pm 0.00001$, $\delta^{88/86}\text{Sr} = 0.39 \pm 0.06\text{‰}$, 2SD, $n = 13$, Fig. 4).

Also, the $^{87}\text{Sr}/^{86}\text{Sr}$ of palaeo-water inferred for the South Lagoon from both cores are generally similar, and systematically higher than that of the Southern Ocean seawater (0.70917, Chapter 4). In detail, core C18 data exhibited a slightly increasing trend of $^{87}\text{Sr}/^{86}\text{Sr}$ from ~ 0.70922 (dated at 1755 cal. yr BP) to ~ 0.70925 in modern times (data from Chapter 4). In addition, there were transient periods of relatively lower $^{87}\text{Sr}/^{86}\text{Sr}$ palaeo-waters in C18 dated at ~ 300 , ~ 800 and ~ 1400 cal. yr BP. However, $^{87}\text{Sr}/^{86}\text{Sr}$ data from the core CSC seem less variable (0.70925 ± 0.00001 , 2SD, $n = 13$), which might be related to closer proximity of this core location to Salt Creek input. In summary, these results strongly suggest that the South Lagoon had never been a purely marine environment for the last ~ 2400 years, and continental water inputs have played an important role in the overall Sr isotope budget of the lagoon.

As to stable Sr isotopes, the reconstructed $\delta^{88/86}\text{Sr}$ of South Lagoon palaeo-water from cores C18 ($0.38 \pm 0.05\text{‰}$, 2SD, $n = 20$) and CSC ($0.39 \pm 0.06\text{‰}$, 2SD, $n = 13$) are comparable to each other and also to that of the Southern Ocean (0.39‰ , see data in Chapter 4). In C18, the evolution of $\delta^{88/86}\text{Sr}$ palaeo-water showed a similar and slightly increasing trend through time (as $^{87}\text{Sr}/^{86}\text{Sr}$ data showed) ranging from $\sim 0.35\text{‰}$ at the bottom of the core to $\sim 0.40\text{‰}$ at the top. Interestingly, the $\delta^{88/86}\text{Sr}$ palaeo-water signatures from CSC showed slightly larger variations, ranging from lower values of $\sim 0.33\text{--}0.35\text{‰}$ at ~ 100 cal. yr BP and 800-1200 cal. yr BP, to highest values of $\sim 0.43\text{‰}$ recorded between 2100 and 1900 cal. yr BP, assuming that the latter age estimates are linearly correlated with depths along CSC. The highest palaeo-lagoon water values of $\sim 0.43\text{‰}$ were comparable to the present-day $\delta^{88/86}\text{Sr}$ signatures found in hypersaline South Lagoon ($0.43 \pm 0.07\text{‰}$, 2SD, $n = 15$, Shao et al., 2021 and Chapter 4), which implies that the southern end of the South Lagoon might had experienced a period of authigenic carbonate formation, similar to those occurring at present-day.

5.3.3 Water source mixing and palaeo-salinity reconstruction of the South Lagoon waters via a coupled $^{87}\text{Sr}/^{86}\text{Sr}$ and Mg/Sr approach

To apportion the water sources (seawater vs. continental waters) and estimate the salinity of the paleo-waters in the South Lagoon based on the analysis of fossil shells from the two cores, we employed the elemental and isotope mass balance approach (Holmden et al., 1997; Shao et al., 2018) using $^{87}\text{Sr}/^{86}\text{Sr}$ and Mg/Sr tracers (Fig. 5). Note that Mg and Sr both behave conservatively across the Coorong lagoon (see Fig. D.1, Appendix in Chapter 4) and were measured in fossil shells from both cores (Tables B.2 and B.3, Appendix B.1), thus Mg/Sr was used as a water source tracer. Since Salt Creek (SC) and groundwater (GW) were the two most important continental water sources to the South Lagoon (Chapter 4), theoretical mixing lines were built between these water sources and

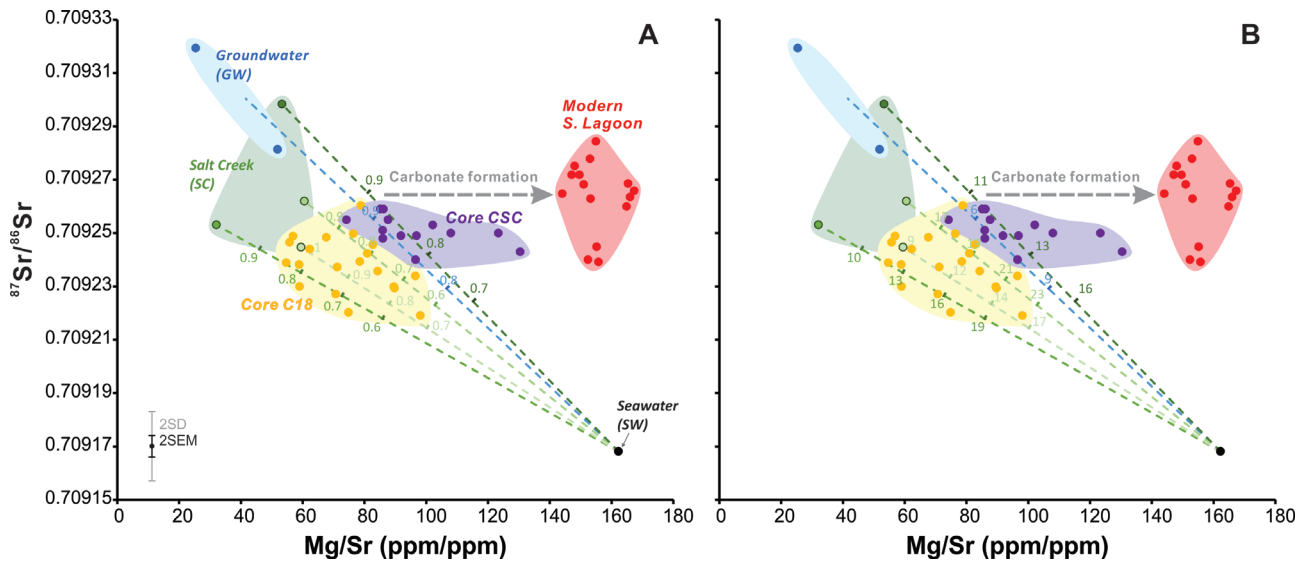


Figure 5: Cross-plots of $^{87}\text{Sr}/^{86}\text{Sr}$ vs. Mg/Sr in palaeo-waters from cores C18 and CSC calculated from contemporary *A. helmsi* shell samples and the modern South Lagoon (data from Shao et al., 2021 and Chapter 4). The dashed lines represent theoretical mixing lines between Southern Ocean seawater and continental water sources (i.e., groundwater, Salt Creek water) (data from Shao et al., 2021 and Chapter 4). The numbers on the mixing lines represent calculated (A) mass fraction of continental water and (B) salinity in the water mixture.

Southern Ocean seawater using $^{87}\text{Sr}/^{86}\text{Sr}$ vs. Mg/Sr cross-plots. In order to reconstruct the Mg/Sr of the paleo-water in the South Lagoon, the distribution coefficient for Mg/Sr ($D_{\text{Mg}/\text{Sr}} = (\text{Mg}/\text{Sr}_{\text{shell}}) / (\text{Mg}/\text{Sr}_{\text{water}})$) had to be determined. Accordingly, the average and representative $D_{\text{Mg}/\text{Sr}}$ (0.00079) was calculated from the four pairs of the modern shells and ambient water samples (Tables B.1 and 2, Appendix B.1) and used in this study (Table B.7, Appendix B.4). Due to seasonal variations in local water composition, especially for brackish continental waters from Salt Creek (described in detail in Chapter 4), we constructed a “mixing triangle” rather than a single “mixing line” where the former reflects the seasonal variability of local water sources to the South Lagoon (see Fig. 5).

Assuming that the $^{87}\text{Sr}/^{86}\text{Sr}$ of past continental water sources into the Coorong (during the deposition of fossil shells) had similar $^{87}\text{Sr}/^{86}\text{Sr}$ as the present-day sources, the reconstructed paleo-water signatures in the South Lagoon from the core C18 plotted almost completely within the calculated “mixing triangle” (Fig. 5). This indicates that the palaeo-lagoon water at this site was a mixture of seawater (SW) and Salt Creek (SC), thus representing a simple two-component SW- SC mixing, and/or alternatively the SW-GW (groundwater) mixing (Fig. 5). The mass fraction of Salt Creek water and/or groundwater contribution into the palaeo-lagoon water (i.e., mixture) was estimated to be approximately 0.6-1 (60 to 100%) and 0.8-0.9 (80 to 90%) for SW-SC and SW-GW mixing scenarios, respectively (see ‘fraction numbers’ next to dashed mixing lines in Fig. 5A). Importantly, based on $\delta^{88}\text{Sr}/^{86}\text{Sr}$ data from fossil shells (Fig. 4B), the palaeo-lagoon water at C18 site was likely less evaporated and not significantly affected by authigenic carbonate formation compared to the present-day hypersaline and supersaturated South Lagoon (details discussed in Chapter 4), therefore yielded brackish palaeo-salinities that ranged from ~6 PSU (GW-SW mixing) up to ~23 PSU (SC-SW mix-

ing) (see ‘fraction numbers’ next to dashed mixing lines in Fig. 5B).

Interestingly, the reconstructed paleo-waters from South Lagoon at CSC site only partially plots within the abovementioned “mixing triangle”, as some samples plot to the right (see purple circles in Fig. 5) thus suggesting an impact of carbonate formation. This might be related to its proximity to Salt Creek input which supplies highly alkaline and oversaturated brackish waters into the South Lagoon (discussed in Chapter 4), which could thus promote local carbonate precipitation. For those CSC palaeo-water samples that plot within the theoretical “mixing triangle”, the calculated mass fractions of continental water inputs range from 0.8-0.9 (80 to 90%) for both mixing scenarios (SW-SC and SW-GW) with a corresponding palaeo-salinity range of 6-17 PSU (Fig. 5), which is consistent with the estimates from C18 core.

Overall, except for potential periods of higher carbonate formation and likely evaporation at CSC site, the paleo-lagoon waters from the South Lagoon had predominantly brackish salinities (ca. 6 to 23PSU) with significant contributions (i.e.. mass fractions up to 60%) of continental waters from Salt Creek and/or local groundwater inputs. Such reconstructed and generally brackish palaeo-salinity was thus in stark contrast with the present-day and permanently hypersaline conditions in the South Lagoon.

5.3.4 Evolution of $^{87}\text{Sr}/^{86}\text{Sr}$ and $\delta^{88/86}\text{Sr}$ in palaeo-waters of the South Lagoon: Evidence for temporal changes in water source mixing and local carbonate cycling

Understanding temporal changes in water sources and authigenic carbonate formation in the Coorong lagoon is important as these phenomena are closely linked to palaeo-climate variations via processes such as freshwater discharge (i.e., wetter and cooler climate) and/or increase in water salinity and thus carbonate saturation state (i.e., dry and hotter climate).

Importantly, the first-order estimates of past continental water discharge as well as changes in local carbonate fluxes (i.e., aragonite/calcite precipitation vs. dissolution) in the South Lagoon can be made with the aid of the $^{87}\text{Sr}/^{86}\text{Sr}$ and $\delta^{88/86}\text{Sr}$, respectively. Accordingly, the fossil shell-based reconstructions of palaeo-lagoon water $^{87}\text{Sr}/^{86}\text{Sr}$ and $\delta^{88/86}\text{Sr}$ signatures and their evolution over the last ~2000 years (Figs. 5 and 6) can shed more light on the above climate-related processes. Reconstructed palaeo-water Sr isotope data acquired from two cores (C18 and CSC) show generally comparable trends and ranges, however the major difference in data lies in the $^{87}\text{Sr}/^{86}\text{Sr}$ signatures, as $\delta^{88/86}\text{Sr}$ values largely overlap between both sites (Fig. 6). Specifically, some samples or palaeo-water signatures from C18 yielded low $\delta^{88/86}\text{Sr}$ (~0.35‰) and also relatively low $^{87}\text{Sr}/^{86}\text{Sr}$ values (~0.70922), whereas the palaeo-waters from CSC site yielded higher and relatively constant $^{87}\text{Sr}/^{86}\text{Sr}$ values scattering around ~0.70927, which overlap with the $^{87}\text{Sr}/^{86}\text{Sr}$ of the Salt Creek input (Fig. 6). Such differences

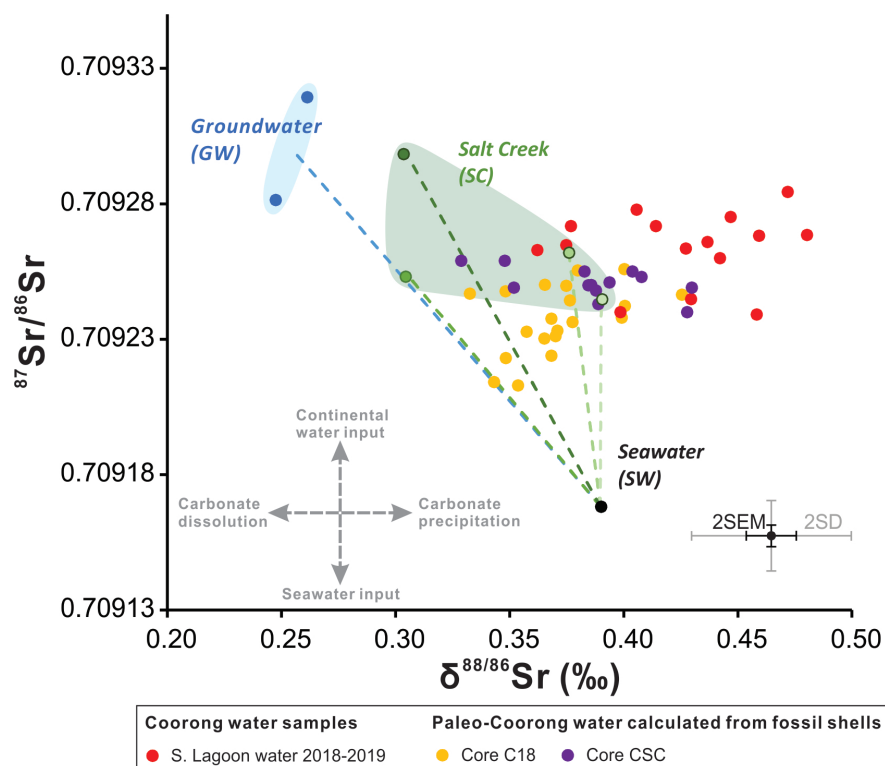


Figure 6: Cross-plots of $^{87}\text{Sr}/^{86}\text{Sr}$ vs. $\delta^{88/86}\text{Sr}$ in palaeo-waters from cores C18 and CSC calculated from contemporary *A. helmsi* shell samples and the modern South Lagoon (data from Shao et al., 2021 and Chapter 4). The dashed lines represent theoretical mixing lines between Southern Ocean seawater and continental water sources (i.e., groundwater, Salt Creek water) (data from Shao et al., 2021 and Chapter 4).

in $^{87}\text{Sr}/^{86}\text{Sr}$ between C18 and CSC sites can be interpreted as evidence for spatial variability in the palaeo-South Lagoon water composition, likely reflecting relatively higher proportion of the continental inputs (potentially Salt Creek) at site CSC and more marine influence (or less continental influence) at site C18 near Parnka Point. Interestingly, the samples or palaeo-water signatures from C18 showing relatively low $\delta^{88/86}\text{Sr}$ and $^{87}\text{Sr}/^{86}\text{Sr}$ were also the oldest ones in the core (before ~1400 cal. yrs BP, Figs. 4 and 6). The younger samples from C18 show progressively higher $\delta^{88/86}\text{Sr}$ and $^{87}\text{Sr}/^{86}\text{Sr}$ that overlap with CSC data and were also closer to the modern South Lagoon waters (Fig. 6). This in turn suggests that the South Lagoon became more spatially ‘isotopically homogenised’ and more dominated by continental water inputs (i.e., reduced seawater inputs) over the last two millennia, which seems to be also supported by progressively increasing Ba/Ca ratio of fossil shells (Fig. C.1, Appendix C) and the fact that Ba/Ca ratio of continental waters is systematically and significantly higher than that of seawater (cf. Gillanders and Munro, 2012).

5.3.5 Quantifying local carbonate output through time in the Coorong South Lagoon

Burial of dissolved inorganic carbon (DIC) into carbonate sediments is a poorly constrained process in the present-day and ancient coastal systems that also impact the global carbon cycle, thus needs

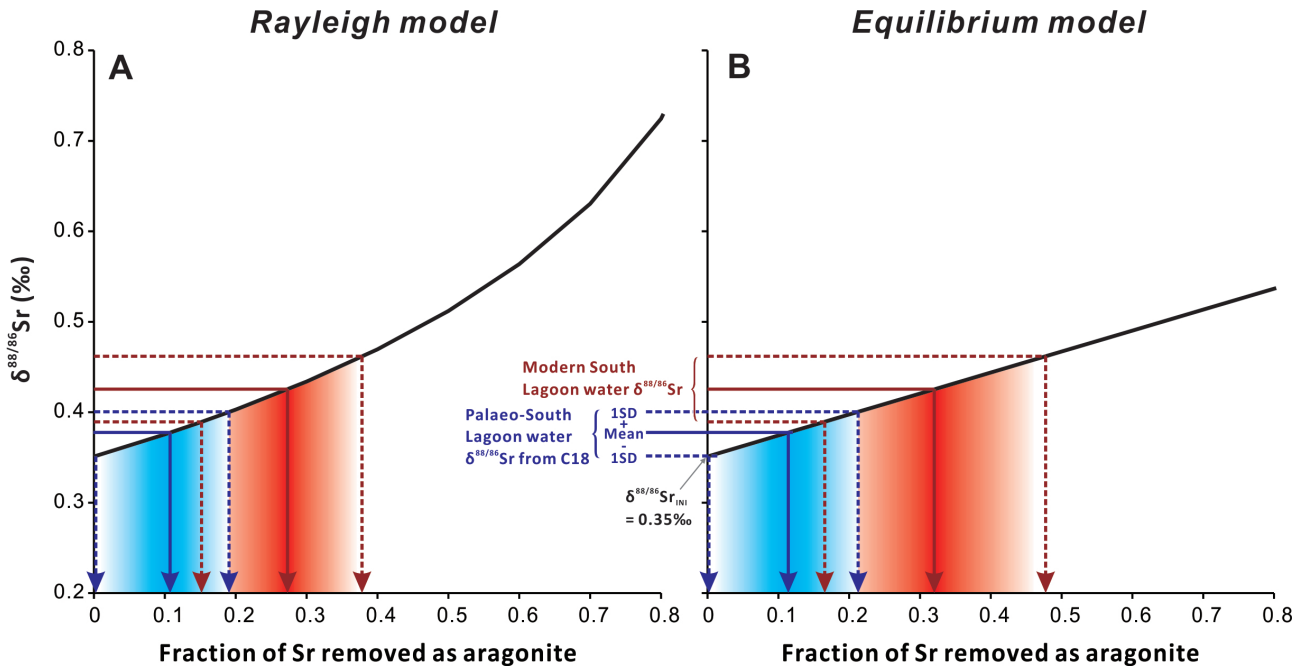


Figure 7: Plots showing modelled $\delta^{88/86}\text{Sr}$ trends in the South Lagoon waters as a function of Sr fraction removed from the lagoon waters as aragonite, where the initial value ($\delta^{88/86}\text{Sr}_{\text{INI}} = 0.35\text{‰}$) representing the fresher periods of the palaeo-South Lagoon. (A) The Rayleigh model; (B) the equilibrium model. The ending $\delta^{88/86}\text{Sr}$ values consider both palaeo- and modern South Lagoon (with $\pm 1\text{SD}$) scenarios, with blue (palaeo) and red (modern) shaded areas projecting the possible fraction of Sr removal.

to be better quantified, especially given that the South Lagoon was an efficient sink or DIC (Shao et al., 2018). Specifically, our data from sediment cores, especially C18, indicate that over the last ~ 2400 years the South Lagoon shifted from one characterised by less intense carbonate deposition associated with ‘brackish and less evaporitic’ conditions (reflected by lower $\delta^{88/86}\text{Sr}$ in palaeo-water of $\sim 0.35\text{‰}$ from older samples of core C18) towards a modern system dominated by hypersaline waters and higher $\delta^{88/86}\text{Sr}$ values (average = 0.43‰) (Fig. 6). The relative amount of Sr that were removed from the South Lagoon as CaCO_3 (mainly Sr-rich aragonite) (i) within the ‘palaeo’ period of the past two millennia and (ii) compared to the modern times can be calculated using simple Rayleigh and equilibrium Sr isotope models (see also Shao et al., 2021). Specifically, the models assume that (i) the South Lagoon behaves as a ‘closed system’ (i.e., Rayleigh) and (ii) the Sr isotope signatures of both input and output fluxes remained relatively constant over time (i.e., equilibrium), respectively. Considering the spatial and temporal variability of $\delta^{88/86}\text{Sr}$ in the (i) paleo- (data from core C18) and (ii) modern South Lagoon (data from Chapter 4), for each scenario, three horizontal lines representing the average $\delta^{88/86}\text{Sr}$, and $\pm 1\text{SD}$ envelopes, were used as ending values in Rayleigh and equilibrium models (Fig. 7).

Overall, the Rayleigh and equilibrium models suggest a temporal shift in the South Lagoon from ‘no detectable’ Sr removal ($<20\%$) in the palaeo-lagoon (i.e., oldest C18 data) to more efficient and larger removal of Sr into carbonate minerals (aragonite) in modern lagoon system, with calculated magnitudes of Sr removal up to $\sim 37\%$ or 47% (for the Rayleigh and Equilibrium models, respective-

ly, (Fig. 7). The average estimate for Sr removal in the present-day South Lagoon is ~30%, which is systematically higher than the average for palaeo-lagoon data from C18 core that suggest a much smaller average Sr removal of only ~10%. Importantly, these findings and differences also suggest that the South Lagoon became over time more efficient in removing Sr and thus carbon (CO_3^{2-}) into authigenic carbonates, which is likely related to its progressively more ‘evaporitic character’ and temporal shift from a ‘brackish’ to ‘hypersaline’ lagoon system.

5.4 Conclusions

Calibration of radiogenic and stable Sr isotopes ($^{87}\text{Sr}/^{86}\text{Sr}$ and $\delta^{88/86}\text{Sr}$) in living species of *Arthritica helmsi* bivalve shells along with ambient water samples from the Coorong lagoon, demonstrate the feasibility to reconstruct past Sr isotope signatures of palaeo-lagoon waters using shells as archives. Specifically, an ‘offset’ in $\delta^{88/86}\text{Sr}$ between a shell and water ($\Delta^{88/86}\text{Sr} = \delta^{88/86}\text{Sr}_{\text{shell}} - \delta^{88/86}\text{Sr}_{\text{water}} = -0.104\%$) has to be applied to reconstruct the stable Sr isotope composition and temporal $\delta^{88/86}\text{Sr}$ evolution of palaeo-lagoon waters based on the analysis of fossil shells preserved in two sediment cores (C18 and CSC) from the South Lagoon of the Coorong. In contrast, the $^{87}\text{Sr}/^{86}\text{Sr}$ signatures of shell samples were directly used as $^{87}\text{Sr}/^{86}\text{Sr}$ of lagoon water, thus not being impacted by mass-dependent fractionation as $\delta^{88/86}\text{Sr}$. Importantly, our reconstructed Sr isotope data of paleo-waters suggest that the South Lagoon had never been a purely marine environment (i.e., dominated by seawater inputs from the Southern Ocean) over the last ~2400 years, but was rather dominated by continental water inputs and in fact $^{87}\text{Sr}/^{86}\text{Sr}$ signature of palaeo-lagoon waters was similar to the modern South Lagoon system (~0.70926). In other words, continental water input from sources such as Salt Creek and/or local groundwater must have, and still does today, played an important role in supplying fresh water and dissolved Sr^{2+} ions to the South Lagoon. Specifically, our elemental and isotope mass balance modelling based on $^{87}\text{Sr}/^{86}\text{Sr}$ and Mg/Sr tracers indicate that the fraction continental water sources in the paleo-South Lagoon was at least 60%, and the estimated palaeo-salinity ranged between 6 and 23 PSU. This points to an originally ‘brackish’ South Lagoon that must have progressively evolved to the present-day hypersaline (~70-100 PSU) conditions. Finally, our stable Sr isotope data and Rayleigh modelling of local carbonate output suggest that the average Sr removal in present-day South Lagoon via carbonate (mostly aragonite) deposition is about 30%, which is systematically higher than average estimates for palaeo-lagoon data (from C18 core) that suggest a much smaller carbonate Sr removal of only ~10%. These findings and modelling results thus indicate that the South Lagoon became over time more efficient in removing Sr, and therefore also inorganic carbon (CO_3^{2-}), into precipitated CaCO_3 (mainly aragonite), thus acting as a net ‘sink’ for the local coastal carbon cycle.

Acknowledgements

This work was supported by the Healthy Coorong Healthy Basin (HCHB) program, and partly supported by the Environment Institute of the University of Adelaide. We also acknowledge the financial support for the Centre for Accelerator Science at ANSTO through the Australian National Collaborative Research Infrastructure Strategy (NCRIS) (ANSTO portal No. 12390). This study is part of the Ph.D. research of YS, supported by an Adelaide Graduate Research Scholarship, and funding from the CRC LEME Regolith Science Scholarship via Cooperative Research Centre for Landscape Environments and Mineral Exploration (CRC LEME) Regolith Science Scholarship. Sampling of sediment core C18 was performed under the Upper South-East Program - Coorong Sub-Program, Historical Water Quality Assessment - Coring research permit No. Y24952 – 1; sampling of modern water and shells in the Coorong National Park in 2018 were collected under Ministerial Exemption #ME9902752. Prof. John Tibby is acknowledged for the access to C18 core and samples of fossil shells used in this study. Technical and laboratory assistance was provided by David Bruce (University of Adelaide), which is greatly appreciated, especially regarding the maintenance of TIMS and clean laboratory facilities.

References

- Aldridge, K., Mosley, L. M. and Oliver, R. (2019) Water Quality of the Coorong, Lower Lakes and Murray Mouth. In *Natural history of the Coorong, Lower Lakes, and Murray Mouth region (Yarluwar-Ruwe)* (eds. L. M. Mosley, Q. Ye, S. Shepherd, S. Hemming, and R. Fitzpatrick) University of Adelaide Press on behalf of the Royal Society of South Australia, Adelaide. pp. 253-270.
- Anadón, P., Gliozzi, E. and Mazzini, I. (2002) Paleoenvironmental reconstruction of marginal marine environments from combined paleoecological and geochemical analyses on ostracods. *GEOPHYSICAL MONOGRAPH-AMERICAN GEOPHYSICAL UNION* **131**, 227-248.
- Barr, C., Tibby, J., Gell, P., Tyler, J., Zawadzki, A. and Jacobsen, G. E. (2014) Climate variability in south-eastern Australia over the last 1500 years inferred from the high-resolution diatom records of two crater lakes. *Quaternary Science Reviews* **95**, 115-131.
- Bauer, J. E., Cai, W. J., Raymond, P. A., Bianchi, T. S., Hopkinson, C. S. and Regnier, P. A. (2013) The changing carbon cycle of the coastal ocean. *Nature* **504**, 61-70.
- Bennett, E. M., Carpenter, S. R. and Caraco, N. F. (2001) Human impact on erodable phosphorus and eutrophication: a global perspective: increasing accumulation of phosphorus in soil threatens rivers, lakes, and coastal oceans with eutrophication. *BioScience* **51**, 227-234.

Blaauw, M. and Christen, J. A. (2011) Flexible paleoclimate age-depth models using an autoregressive gamma process. *Bayesian analysis* **6**, 457-474.

Brookes, J., Dalby, P., Dittmann, S., O'Connor, J., Paton, D., Quin, R., Rogers, D., Waycott, M. and Ye, Q. (2018) *Recommended actions for restoring the ecological character of the South Lagoon of the Coorong*. Goyder Institute for Water Research Technical Report Series No. 18/04, Adelaide, South Australia. ISSN: 1839-2725.

Chamberlayne, B. K. (2015) *Late Holocene seasonal and multicentennial hydroclimate variability in the Coorong Lagoon, South Australia: evidence from stable isotopes and trace element profiles of bivalve molluscs*. (Honours (Geology)), The University of Adelaide, Adelaide.

Chamberlayne, B. K., Tyler, J. J. and Gillanders, B. M. (2020) Environmental controls on the geochemistry of a short-lived bivalve in Southeastern Australian estuaries. *Estuaries and Coasts*, 1-16.

Chamberlayne, B.K. (2021). *Oxygen isotope and elemental ratios in waters and bivalves as tracers of hydrological change in modern and ancient waters of the Coorong Lagoons, South Australia* (Unpublished PhD thesis). University of Adelaide, Adelaide.

Chamberlayne, B. K., Tyler, J. J., Gillanders, B. M. (2021) Elemental concentrations of waters and bivalves across a salinity gradient in the Coorong Lagoons, South Australia: Implications for palaeo-environmental studies. *Estuarine, Coastal and Shelf Science*, in review.

Chambers, J. W. and Cameron, N. G. (2001) A rod-less piston corer for lake sediments; an improved, rope-operated percussion corer. *Journal of Paleolimnology* **25**, 117-122.

Charlier, B. L. A., Nowell, G. M., Parkinson, I. J., Kelley, S. P., Pearson, D. G. and Burton, K. W. (2012) High temperature strontium stable isotope behaviour in the early solar system and planetary bodies. *Earth and Planetary Science Letters* **329**, 31-40.

Dearing, J. A., Battarbee, R. W., Dikau, R., Larocque, I., & Oldfield, F. (2006). Human–environment interactions: learning from the past.

Fruchter, N., Eisenhauer, A., Dietzel, M., Fietzke, J., Böhm, F., Montagna, P., Stein, M., Lazar, B., Rodolfo-Metalpa, R. and Erez, J. (2016) $^{88}\text{Sr}/^{86}\text{Sr}$ fractionation in inorganic aragonite and in corals. *Geochimica et Cosmochimica Acta* **178**, 268-280.

Fruchter, N., Lazar, B., Nishri, A., Almogi-Labin, A., Eisenhauer, A., Shlevin, Y. B. E. and Stein, M. (2017) $^{88}\text{Sr}/^{86}\text{Sr}$ fractionation and calcite accumulation rate in the Sea of Galilee. *Geochimica et Cosmochimica Acta* **215**, 17-32.

Geyh, M. A., Schotterer, U. and Grosjean, M. (1997) Temporal changes of the ^{14}C reservoir effect in

lakes. *Radiocarbon* **40**, 921-931.

Gibbs, M., Joehnk, K., Webster, I. and Heneker, T. (2019) Hydrology and Hydrodynamics of the Lower Lakes, Coorong and Murray Mouth. In *Natural history of the Coorong, Lower Lakes, and Murray Mouth region (Yarluwar-Ruwe)* (eds. L. M. Mosley, Q. Ye, S. Shepherd, S. Hemming, and R. Fitzpatrick) University of Adelaide Press on behalf of the Royal Society of South Australia, Adelaide. pp. 197-216.

Gillanders, B. M. and Munro, A. R. (2012) Hypersaline waters pose new challenges for reconstructing environmental histories of fish based on otolith chemistry. *Limnology and Oceanography* **57**, 1136-1148.

Halpern, B. S., Walbridge, S., Selkoe, K. A., Kappel, C. V., Micheli, F., D'Agrosa, C., Bruno, J. F., Casey, K. S., Ebert, C., Fox, H. E., Fujita, R., Heinemann, D., Lenihan, H. S., Madin, E. M. P., Perry, M. T., Selig, E. R., Spalding, M., Steneck, R. and Watson, R. (2008). A global map of human impact on marine ecosystems. *Science* **319**, 948-952.

Haynes, D., Tibby, J., Fluin, J. and Skinner, R. (2019) Palaeolimnology of the Lower Lakes and Coorong Lagoon. In *Natural history of the Coorong, Lower Lakes, and Murray Mouth region (Yarluwar-Ruwe)* (eds. L. M. Mosley, Q. Ye, S. Shepherd, S. Hemming, and R. Fitzpatrick) University of Adelaide Press on behalf of the Royal Society of South Australia, Adelaide. pp. 122-143.

Hogg, A.G., Hua, Q., Blackwell, P.G., Niu, M., Buck, C.E., Guilderson, T.P., Heaton, T.J., Palmer, J.G., Reimer, P.J., Reimer, R.W., Turney, C.S.M., Zimmerman, S.R.H. (2013). SHCal13 Southern Hemisphere calibration, 0–50,000 years cal BP. *Radiocarbon* **55**, 1889-1903.

Holmden, C., Creaser, R. A. and Muehlenbachs, K. (1997). Paleosalinities in ancient brackish water systems determined by $^{87}\text{Sr}/^{86}\text{Sr}$ ratios in carbonate fossils: a case study from the Western Canada Sedimentary Basin. *Geochimica et Cosmochimica Acta* **61**, 2105-2118.

Hughen, K. A., Baillie, M. G., Bard, E., Beck, J. W., Bertrand, C. J., Blackwell, P. G., Buck, C. E., Burr, G. S., Cutler, K. B., Damon, P. E., Edwards, R. L., Fairbanks, R. G., Michael Friedrich, M., Guilderson, T. P., Kromer, B., McCormac, G., Manning, S., Bronk Ramsey, C.,

Krabbenhöft, A., Eisenhauer, A., Böhm, F., Vollstaedt, H., Fietzke, J., Liebetrau, V., Augustin, N., Peucker-Ehrenbrink, B., Müller, M. N., Horn, C., Hansen, B. T., Nolte, N. and Wallmann, K. (2010) Constraining the marine strontium budget with natural strontium isotope fractionations ($^{87}\text{Sr}/^{86}\text{Sr}^*$, $\delta^{88/86}\text{Sr}$) of carbonates, hydrothermal solutions and river waters. *Geochimica et cosmochimica acta* **74**, 4097-4109.

Krull, E., Haynes, D., Lamontagne, S., Gell, P., McKirdy, D., Hancock, G., McGowan, J. and Smernik,

R. (2009) Changes in the chemistry of sedimentary organic matter within the Coorong over space and time. *Biogeochemistry* **92**, 9-25.

Lerouge, C., Gaucher, E. C., Tournassat, C., Négrel, P., Crouzet, C., Guerrot, C., Gautier, A., Michel, P., Vinsot, A. and Buschaert, S. (2010) Strontium distribution and origins in a natural clayey formation (Calloviaian-Oxfordian, Paris Basin, France): A new sequential extraction procedure. *Geochimica et Cosmochimica Acta* **74**, 2926-2942.

Macreadie, P. I., Serrano, O., Maher, D. T., Duarte, C. M. and Beardall, J. (2017) Addressing calcium carbonate cycling in blue carbon accounting. *Limnology and Oceanography Letters* **2**, 195-201.

McKirdy, D. M., Thorpe, C. S., Haynes, D. E., Grice, K., Krull, E. S., Halverson, G. P. and Webster, L. J. (2010) The biogeochemical evolution of the Coorong during the mid-to late Holocene: An elemental, isotopic and biomarker perspective. *Organic Geochemistry* **41**, 96-110.

Moynier, F., Agranier, A., Hezel, D. C. and Bouvier, A. (2010) Sr stable isotope composition of Earth, the Moon, Mars, Vesta and meteorites. *Earth and Planetary Science Letters* **300**, 359-366.

Mosley, L. M., Priestley, S., Brookes, J., Dittmann, S., Farkaš, J., Farrell, M., Ferguson, A. J., Gibbs, M., Hipsey, M., Huang, J., Lam-Gordillo, O., Simpson, S. L., Teasdale, P. R., Tyler, J. J., Waycott, M., Welsh, D. T. (2020) *Coorong water quality synthesis with a focus on the drivers of eutrophication*. Goyder Institute for Water Research Technical Report Series No. 20/10.

Pearce, C. R., Parkinson, I. J., Gaillardet, J., Charlier, B. L., Mokadem, F. and Burton, K. W. (2015) Reassessing the stable ($\delta^{88/86}\text{Sr}$) and radiogenic ($^{87}\text{Sr}/^{86}\text{Sr}$) strontium isotopic composition of marine inputs. *Geochimica et Cosmochimica Acta* **157**, 125-146.

Porcelli, D. and Baskaran, M. (2012) An overview of isotope geochemistry in environmental studies. *Handbook of environmental isotope geochemistry*, 11-32.

Raddatz, J., Liebetrau, V., Rüggeberg, A., Hathorne, E., Krabbenhöft, A., Eisenhauer, A., Böhm, F., Vollstaedt, H., Fietzke, J., López Correa, M., Freiwald, A. and -Chr.Dullo, W., (2013) Stable Sr-isotope, Sr/Ca, Mg/Ca, Li/Ca and Mg/Li ratios in the scleractinian cold-water coral *Lophelia pertusa*. *Chemical geology* **352**, 143-152.

Reeves, J. M., Haynes, D., García, A. and Gell, P. A. (2015) Hydrological change in the Coorong Estuary, Australia, past and present: Evidence from fossil invertebrate and algal assemblages. *Estuaries and coasts* **38**, 2101-2116.

Settre, C. M. and Wheeler, S. A. (2017) A century of intervention in a Ramsar wetland—the case of the Coorong, Lower Lakes and Murray Mouth. *Australasian Journal of Environmental Management* **24**, 163-183.

Shao, Y., Farkaš, J., Holmden, C., Mosley, L., Kell-Duivesteyn, I., Izzo, C., Reis-Santos, P., Tyler, J., Törber, P., Frýda, J., Taylor, H., Haynes, D., Tibby, J. and Gillanders, B.M. (2018) Calcium and strontium isotope systematics in the lagoon-estuarine environments of South Australia: Implications for water source mixing, carbonate fluxes and fish migration. *Geochimica et Cosmochimica Acta* **239**, 90-108.

Shao, Y., Farkaš, J., Mosley, L., Tyler, J., Wong, H., Chamberlayne, B., Raven, M., Samanta, M., Holmden, C., Gillanders, B.M., Kolevica, A., Eisenhauer, A. (2021) Impact of salinity and carbonate saturation on stable Sr isotopes ($\delta^{88/86}\text{Sr}$) in a lagoon-estuarine system. *Geochimica et Cosmochimica Acta* **293**, 461-476. doi: <https://doi.org/10.1016/j.gca.2020.11.014>

Schmitz, B. and Andreasson, F. P. (2001) Air humidity and lake $\delta^{18}\text{O}$ during the latest Paleocene–earliest Eocene in France from recent and fossil fresh-water and marine gastropod $\delta^{18}\text{O}$, $\delta^{13}\text{C}$, and $^{87}\text{Sr}/^{86}\text{Sr}$. *Geological Society of America Bulletin* **113**, 774-789.

Stevenson, E. I., Hermoso, M., Rickaby, R. E., Tyler, J. J., Minoletti, F., Parkinson, I. J., Mokadem, F. and Burton, K. W. (2014) Controls on stable strontium isotope fractionation in coccolithophores with implications for the marine Sr cycle. *Geochimica et Cosmochimica Acta* **128**, 225-235.

Velez, M. I., Conde, D., Lozoya, J. P., Rusak, J. A., García-Rodríguez, F., Seitz, C., Harmon, T., Perillo, G. M. E., Escobar, J. and Vilardy, S. P. (2018) Paleoenvironmental reconstructions improve ecosystem services risk assessment: case studies from two coastal lagoons in South America. *Water* **10**, 1350.

Vollstaedt, H., Eisenhauer, A., Wallmann, K., Böhm, F., Fietzke, J., Liebetrau, V., Krabbenhöft, A., Farkaš, J., Tomašových, A., Raddatz, J. and Veizer, J. (2014) The Phanerozoic $\delta^{88/86}\text{Sr}$ record of seawater: New constraints on past changes in oceanic carbonate fluxes. *Geochimica et cosmochimica acta* **128**, 249-265.

Woolston, Z. (2020) *A coupled radiogenic ($^{87}\text{Sr}/^{86}\text{Sr}$) and stable ($\delta^{88/86}\text{Sr}$) strontium isotope approach to reconstruct past changes in water mixing and salinity in the Coorong Lagoon, South Australia.* (Honours (Environmental Geoscience)), The University of Adelaide, Adelaide.

Zaky, A. H., Brand, U. and Azmy, K. (2015) A new sample processing protocol for procuring seawater REE signatures in biogenic and abiogenic carbonates. *Chemical Geology* **416**, 36-50.

CHAPTER 6

**Conclusions and implications for
future work**

Chapter 6.

Conclusions and implications for future work

This thesis endeavoured to calibrate selected alkaline earth metals (Ca and Sr) and their isotope tracers including $\delta^{44/40}\text{Ca}$, $\delta^{88/86}\text{Sr}$ and $^{87}\text{Sr}/^{86}\text{Sr}$ with respect to (i) water mixing, (ii) salinity and (iii) carbonate saturation in coastal waters of a semi-arid lagoon-estuary environment in South Australia – the Coorong, Lower Lakes and Murray Mouth (CLLMM) estuary. This coastal system exhibits large natural gradients in (i) water salinity ranging from fresh to hypersaline (>100 PSU) and (ii) carbonate saturation states of waters (i.e., undersaturated to oversaturated) (Fernandes and Tanner, 2009; Gillanders and Munro, 2012), thus providing an ideal ‘natural laboratory’ to study and calibrate the above alkaline earth metal isotope tracers with respect to these water parameters. In addition, a multi-proxy approach using $\delta^{88/86}\text{Sr}$, $^{87}\text{Sr}/^{86}\text{Sr}$ and Mg/Sr ratio was applied to fossil carbonate shells from two sediment cores to reconstruct the palaeo-hydrology, salinity and local carbonate cycling in the Coorong South Lagoon over the past ~2400 years. The analysed sediment cores were also dated using radiocarbon (^{14}C) geochronology. The outcomes of this thesis do not only provide advanced knowledge on the present-day and past water source mixing phenomena in the CLLMM, as well as the local carbonate cycling in the Coorong, but are also beneficial for future environmental and water management strategies for this unique lagoon-estuarine system.

6.1 Calibrating $\delta^{44/40}\text{Ca}$ and $\delta^{88/86}\text{Sr}$ tracers in a semi-arid coastal system with respect to water salinity and carbonate saturation

In chapter 2 and 3, we discovered similar increasing trends of $\delta^{44/40}\text{Ca}$ and $\delta^{88/86}\text{Sr}$ in water samples from the CLLMM with increasing water salinity and CaCO_3 (aragonite and calcite) saturation indices (SI) of the studied coastal waters. Based on the results from chapters 2-4, the North Lagoon waters are typical marine to brackish (with salinities of 15-35 PSU) and generally supersaturated with respect to carbonate minerals (SI \approx 0 to 0.5), while the South Lagoon waters are hypersaline (70-120 PSU) and slightly more oversaturated (SI \approx 1). Also, both stable calcium ($\delta^{44/40}\text{Ca}$) and strontium ($\delta^{88/86}\text{Sr}$) tracers in the Coorong lagoon waters become progressively more positively fractionated (i.e., yielding higher and more positive values) across a transect from the marine-like North Lagoon towards the hypersaline and highly oversaturated South Lagoon. A comparison and cross-plotting of $\delta^{44/40}\text{Ca}$ and $\delta^{88/86}\text{Sr}$ data from the CLLMM system revealed a strong coupling and correlation between these two metal isotope proxies, which follows a theoretical mass-dependent fractionation trend (Böhm et al., 2012), suggesting that both $\delta^{44/40}\text{Ca}$ and $\delta^{88/86}\text{Sr}$ in this semi-arid coastal system are predominantly

controlled by carbonate dissolution vs precipitation processes. Chapter 4 provides a new perspective and insights on the seasonal variations and environmental controls on $\delta^{88/86}\text{Sr}$ and $^{87}\text{Sr}/^{86}\text{Sr}$ variability in the CLLMM waters sampled in 2018-2019, and the influence of water source mixing, salinity and carbonate saturation on the chemistry and stable/radiogenic Sr isotope composition of studied coastal waters. Overall, water salinity showed the strongest positive correlation with $\delta^{88/86}\text{Sr}$ data especially in the Coorong lagoon, suggesting some control of increased dissolved ion concentrations, and thus carbonate saturation on stable Sr isotope tracers in the lagoon. In addition, $\delta^{88/86}\text{Sr}$ data from selected sites in the South Lagoon also suggest that an increased alkalinity input likely supply from the Salt Creek, may have also acted as a 'trigger' or precondition for in-situ carbonate (predominantly aragonite) precipitation.

6.2 Water source mixing and local carbonate cycling in the present-day Coorong Lagoons

Chapter 2 confirmed a very distinctive geochemistry and Ca and Sr isotope characteristics of the North versus South Coorong Lagoons. Specifically, radiogenic Sr isotope data ($^{87}\text{Sr}/^{86}\text{Sr}$) showed that the North Lagoon waters are mainly sourced from the Southern Ocean (~ 0.70917), with transient and short-lived freshwater inputs sourced from the River Murray and Lower Lakes via barrage outflow (~ 0.711 - 0.712) and/or from local groundwater discharge (~ 0.70930). In contrast, the hypersaline South Lagoon waters (with salinity up to ~ 120 PSU) are basically highly evaporated brackish waters (with $\sim 45\%$ contribution originally from continent-derived freshwaters), which were further modified by progressive evaporation and in-situ carbonate formation as reflected by their non-marine $^{87}\text{Sr}/^{86}\text{Sr}$ and $\delta^{44/40}\text{Ca}$ signatures. The importance of continent-derived freshwaters across the entire Coorong lagoon system was also confirmed by $^{87}\text{Sr}/^{86}\text{Sr}$ data in the otoliths, but the interpretation of the latter data is complicated by fish migration processes within the lagoon. In addition, Rayleigh and equilibrium modelling of both $\delta^{44/40}\text{Ca}$ (Chapter 2) and $\delta^{88/86}\text{Sr}$ (Chapter 3) data from the Coorong lagoons revealed that ~ 35 to 45% of the dissolved Ca^{2+} in the South Lagoon has been removed as CaCO_3 (mostly as aragonite), which in turn confirms that the South Lagoon acts as a net sink for the dissolved inorganic carbon (DIC). In addition, $^{87}\text{Sr}/^{86}\text{Sr}$ and $\delta^{88/86}\text{Sr}$ datasets from the CLLMM waters collected over four seasons in 2018-2019 (Chapter 4) revealed the importance of brackish and highly alkaline Salt Creek water input into the South Lagoon, supplying alkalinity during winter time, thus facilitating later carbonate precipitation during summer season when temperature and evaporation rates were higher, promoting carbonate oversaturation. The Chapter 4 also points out that seasonal carbonate dynamics in the South Lagoon can lead to increased (~ 25 - 30% fraction) Sr removal from the lagoon waters into carbonate (aragonite) minerals, reflected as highly positively fractionated $\delta^{88/86}\text{Sr}$ values in lagoon waters of up to 0.48% , thus significantly higher than seawater and/or local Salt Creek water input.

Finally, Chapter 4 found a significant spatial variations in elemental and Sr isotope composition of groundwater samples collected along the Coorong, where the ones sampled near the North Lagoon were generally fresher and had lower $^{87}\text{Sr}/^{86}\text{Sr}$, while groundwaters collected near the South Lagoon were more saline, and with higher $^{87}\text{Sr}/^{86}\text{Sr}$ values, which might be related to longer residence times or ‘ages’ of these particular groundwaters and their prolonged interactions with the local subsurface granitic basement (Barnett, 2019).

6.3 Reconstructions of palaeo-hydrology, salinity and water source mixing history in the Coorong South Lagoon

A suitable carbonate archive is essential for reliable reconstructions of palaeo-environmental conditions in marine, continental and coastal settings. Here we used aragonitic shells of small bivalve species *Arthritica helmsi* living in the present-day North Lagoon, and fossils of this shell species sampled from sediment cores in the Coorong South Lagoon (Chapter 5). In general, $^{87}\text{Sr}/^{86}\text{Sr}$ signatures of biogenic carbonates are usually considered as a direct ‘proxy’ for palaeo-water $^{87}\text{Sr}/^{86}\text{Sr}$ signature. However for stable Sr isotope tracer ($\delta^{88/86}\text{Sr}$), the reconstructions are complicated by species-specific ‘offsets’ which thus need to be constrained. Pioneering studies (e.g., Raddatz et al., 2013; Vollstaedt et al., 2014; Fruchter et al., 2016 and 2017) revealed that such $\delta^{88/86}\text{Sr}$ offset between biogenic skeletal carbonates (e.g., bivalves, brachiopods, belemnites and corals) and local water ($\Delta^{88/86}\text{Sr} = \delta^{88/86}\text{Sr}_{\text{carb}} - \delta^{88/86}\text{Sr}_{\text{water}}$) was species-dependent but relatively constant at about -0.1 to -0.2 ‰, and also not much sensitive to environmental conditions such as temperature, saturation states and pH. In Chapter 5 we analysed $\delta^{88/86}\text{Sr}$ of aragonitic shells *A. helmsi* collected alive from the Coorong North Lagoon, along with local and ambient lagoon waters. The results confirmed a relatively constant ‘offset’ ($\Delta^{88/86}\text{Sr} = \delta^{88/86}\text{Sr}_{\text{carb}} - \delta^{88/86}\text{Sr}_{\text{water}}$) of about -0.104‰. These experimental data and calibrations done in the present-day Coorong lagoon, thus formed the basis for reconstructions of the Sr isotope variations of palaeo-lagoon waters in the Coorong South Lagoon based on the analysis of fossil *A. helmsi* shells. Specifically, results from $\delta^{88/86}\text{Sr}$ as well as other tracers such as $^{87}\text{Sr}/^{86}\text{Sr}$ and Mg/Sr ratios measured in fossil shells from two sediment cores revealed that the South Lagoon received at least 60% of Sr from continental inputs over the past ~2400 years, with the estimated minimum salinities between ~5 and 20 PSU, which was thus brackish rather than hypersaline (>70PSU) as in modern times. Such progressive evaporation of South Lagoon waters over time likely also led to increased carbonate saturation of lagoon waters and in-situ carbonate precipitation, as confirmed by elevated $\delta^{88/86}\text{Sr}$ data in modern waters compared to those of the palaeo-waters. Moreover, a Rayleigh modelling of stable Sr isotopes suggest that compared to past, the present-day South Lagoon acts as a sink of dissolved inorganic carbon, with estimated ~30% of Sr entering the lagoon being removed via carbonate (primarily aragonite) mineral precipitation.

6.4 Future recommendations

Overall, the results arising from this thesis provide a novel approach and ‘proof of concept’ for the application of coupled radiogenic and stable Sr as well as stable Ca isotope tracers to constrain the present-day as well as past changes in water sources, salinity and local carbonate dynamics in semi-arid carbonate producing coastal systems. However, there are also a few precautions that needs to be taken into account for future successful applications of these alkaline earth metal isotope tracers in the CLLMM and/or other lagoon-estuarine systems. Firstly, when applying Ca and Sr isotopes in tandem, one parameter to be aware of is that due to relative mass difference between these two elements, the observed $\delta^{88/86}\text{Sr}$ variations in nature are systematically smaller compared to $\delta^{44/40}\text{Ca}$ variations, thus requiring a high-precision analytical methods for $\delta^{88/86}\text{Sr}$ measurements. Secondly, and this is specific to the CLLMM, the fact that groundwaters collected along the Coorong lagoon have very similar geochemical and isotope characteristics as the Salt Creek brackish waters (which are thus probably also partly fed by groundwaters) causes problems and certain limitations for an effective detection of groundwater inputs into the Coorong lagoon using Ca and Sr isotope tracers. Therefore, future studies that aim to evaluate and quantify groundwater inputs into the Coorong lagoon system should employ some alternative and more specialised groundwater tracing methods, such as those utilising radium and/or radon isotopes (Cerdà-Domènech et al., 2017; Duque et al., 2019) to further advance our understanding of the role of groundwater in the CLLMM estuary. Finally, when calibrating alkaline earth metal isotope tracers for biogenic carbonates to be used as archives for palaeo-water reconstructions, more systematic collection and analysis of species of interest (i.e., present-day shells) and ambient waters at a particular sampling site would be desirable. Ideally, such data could be collected throughout the lifespan of the calcifying organism, considering that biogenic carbonates are affected by ‘vital effects’ which might thus change with time due to (i) ontogenesis of the organism and related changes in biocalcification, and/or linked to (ii) local environmental conditions and spatial/temporal variations in the representative isotope signatures of ambient waters controlled by rather dynamic hydrology and water source mixing processes in the lagoon-estuarine systems.

References

Barnett, S. (2019) Hydrogeology of the Lower Lakes and Coorong Region. In *Natural history of the Coorong, Lower Lakes, and Murray Mouth region (Yarluwar-Ruwe)* (eds. L. M. Mosley, Q. Ye, S. Shepherd, S. Hemming, and R. Fitzpatrick) University of Adelaide Press on behalf of the Royal Society of South Australia, Adelaide. pp. 217-226.

Böhm, F., Eisenhauer, A., Tang, J., Dietzel, M., Krabbenhöft, A., Kisakürek, B. and Horn, C. (2012)

Strontium isotope fractionation of planktic foraminifera and inorganic calcite. *Geochimica et Cosmochimica Acta* **93**, 300-314.

Cerdà-Domènech, M., Rodellas, V., Folch, A. and Garcia-Orellana, J. (2017) Constraining the temporal variations of Ra isotopes and Rn in the groundwater end-member: Implications for derived SGD estimates. *Science of the total environment* **595**, 849-857.

Duque, C., Knee, K. L., Russoniello, C. J., Sherif, M., Risha, U. A. A., Sturchio, N. C. and Michael, H. A. (2019) Hydrogeological processes and near shore spatial variability of radium and radon isotopes for the characterization of submarine groundwater discharge. *Journal of Hydrology* **579**, 124192.

Fernandes, M. and Tanner, J. E. (2009) Hypersalinity and phosphorus availability: the role of mineral precipitation in the Coorong lagoons of South Australia. CSIRO: Water for a Healthy Country National Research Flagship and South Australian Research and Development Institute (Aquatic Sciences).

Fruchter, N., Eisenhauer, A., Dietzel, M., Fietzke, J., Böhm, F., Montagna, P., Stein, M., Lazar, B., Rodolfo-Metalpa, R. and Erez, J. (2016) $^{88}\text{Sr}/^{86}\text{Sr}$ fractionation in inorganic aragonite and in corals. *Geochimica et cosmochimica acta* **178**, 268-280.

Fruchter, N., Lazar, B., Nishri, A., Almogi-Labin, A., Eisenhauer, A., Shlevin, Y. B. E. and Stein, M. (2017) $^{88}\text{Sr}/^{86}\text{Sr}$ fractionation and calcite accumulation rate in the Sea of Galilee. *Geochimica et Cosmochimica Acta* **215**, 17-32.

Gillanders, B. M. and Munro, A. R. (2012) Hypersaline waters pose new challenges for reconstructing environmental histories of fish based on otolith chemistry. *Limnology and Oceanography* **57**, 1136.

Raddatz, J., Liebetrau, V., Rüggeberg, A., Hathorne, E., Krabbenhöft, A., Eisenhauer, A., Böhm, F., Vollstaedt, H., Fietzke, J., López Correa, M., Freiwald, A. and -Chr.Dullo, W., (2013) Stable Sr-isotope, Sr/Ca, Mg/Ca, Li/Ca and Mg/Li ratios in the scleractinian cold-water coral *Lophelia pertusa*. *Chemical geology* **352**, 143-152.

Vollstaedt, H., Eisenhauer, A., Wallmann, K., Böhm, F., Fietzke, J., Liebetrau, V., Krabbenhöft, A., Farkaš, J., Tomašových, A., Raddatz, J. and Veizer, J. (2014) The Phanerozoic $\delta^{88/86}\text{Sr}$ record of seawater: New constraints on past changes in oceanic carbonate fluxes. *Geochimica et cosmochimica acta* **128**, 249-265.

APPENDICES

Appendix 1

**Published forms of journal articles arising
from chapters 2 and 3**



Calcium and strontium isotope systematics in the lagoon-estuarine environments of South Australia: Implications for water source mixing, carbonate fluxes and fish migration

Yuexiao Shao^{a,*}, Juraj Farkaš^{a,b}, Chris Holmden^c, Luke Mosley^d,
Isaac Kell-Duivesteyn^{a,e}, Christopher Izzo^{d,1}, Patrick Reis-Santos^{d,f},
Jonathan Tyler^a, Philip Törber^{b,a}, Jiří Frýda^b, Holly Taylor^g,
Deborah Haynes^a, John Tibby^h, Bronwyn M. Gillanders^d

^a Department of Earth Sciences and Sprigg Geobiology Centre, School of Physical Sciences, University of Adelaide, Australia

^b Department of Environmental Geosciences, Faculty of Environmental Sciences, Czech University of Life Sciences Prague, Kamýcká 129, Praha – Suchbátka, 165 00, Czech Republic

^c Department of Earth Sciences, University of Saskatchewan, Saskatoon, Canada

^d Department of Ecology and Environmental Science, School of Biological Sciences, University of Adelaide, Australia

^e Institute of Applied Geosciences, Graz University of Technology, Austria

^f MARE – Marine and Environmental Sciences Centre, Faculty of Sciences, University of Lisbon, Portugal

^g School of Earth and Environmental Sciences, University of Wollongong, NSW, Australia

^h Department of Geography, Environment and Population, School of Social Sciences, University of Adelaide, Australia

Received 15 January 2018; accepted in revised form 26 July 2018; Available online 4 August 2018

Abstract

This study uses Ca and Sr isotopes ($\delta^{44/40}\text{Ca}$ and $^{87}\text{Sr}/^{86}\text{Sr}$), coupled with elemental ratios, to better understand the water source apportionment and carbonate output in the Coorong, Lower Lakes and Murray Mouth Estuary, which represents the terminus of Australia's longest river system. The geochemistry of waters in the Coorong (i.e., North and South Lagoon) can be explained by mixing of three major components, including: (i) the Southern Ocean seawater, (ii) local freshwaters, and (iii) hypersaline lagoon waters, the latter significantly modified by ongoing evaporation and carbonate formation. The Sr and Ca isotope composition of the North Lagoon is indistinguishable from that of the Southern Ocean (i.e., normal salinity of ~ 35 PSU), with the exception of transient freshwater input events that can temporarily lower the salinity to brackish levels. Interestingly, our results from the hypersaline South Lagoon (salinity up to ~ 120 PSU) confirmed that the latter is highly evaporated brackish water (with $\geq 40\%$ contribution from continent-derived waters), which has been additionally modified by in-situ carbonate precipitation. Importantly, our Ca isotope and elemental constraints showed that about 15–17% of the dissolved Ca^{2+} in the South Lagoon has been removed as CaCO_3 (primarily as aragonite). This in turn has implications for the local carbonate cycle and blue carbon studies, suggesting that the South Lagoon acts as a net sink for the dissolved inorganic carbon (DIC).

Ca isotope data from the otoliths of smallmouth hardyhead fish species (*Atherinosoma microstoma*) collected in the Coorong indicate that $\delta^{44/40}\text{Ca}$ is primarily controlled by biological processes (i.e., kinetic isotope fractionation effects related to

* Corresponding author.

E-mail address: yuexiao.shao@adelaide.edu.au (Y. Shao).

¹ Current address: Fisheries Research and Development Corporation, Adelaide, Australia.

growth rate), rather than by the Ca isotope composition of local lagoon waters. As to $^{87}\text{Sr}/^{86}\text{Sr}$ in otoliths, the latter confirmed the importance of continent-derived water sources in the Coorong, recorded over the life span of the fish.

Overall, with suitable fossil carbonate archives (e.g., bivalve shells, foraminifera), our calibration of $^{87}\text{Sr}/^{86}\text{Sr}$ and $\delta^{44/40}\text{Ca}$ in the modern hydrological system, with respect to a large salinity gradient (ranging from fresh to hypersaline, i.e., 0 to ~ 120 PSU), implies potential future applications of these isotope tracers in carbonate-producing coastal systems, which include (i) tracing and apportioning different water sources, (ii) quantifying local carbonate outputs, and (iii) reconstructing paleo-salinity changes.

© 2018 Published by Elsevier Ltd.

Keywords: Calcium; Strontium; Isotopes; Water mixing; Carbonate fluxes; Otoliths; PHREEQC

1. INTRODUCTION

Coastal systems such as lagoons and estuaries represent a dynamic interface between terrestrial and marine environments, which provides an essential link between biogeochemical processes operating on the continents and in the oceans. Isotopes have not only been applied as natural tracers in a variety of coastal environments to infer fluxes and biogeochemical pathways of elements, but also used as proxies to reconstruct the recent and past environmental changes in these hydrological systems through studies of local sediment archives and included fossils (e.g., carbonate shells).

Traditionally, stable isotope tracers of light elements, such as $\delta^{13}\text{C}$, $\delta^{18}\text{O}$ and δD , have been used to trace carbon and water sources and understand the degree of water evaporation and paleo-salinity in coastal environments (Tan and Hudson, 1974; Patterson and Walter, 1994; Hendry and Kalin, 1997; Patterson, 1999; Holmden and Hudson, 2003; Wierzbowski and Joachimski, 2007; McKirdy et al., 2010; Gemitzi et al., 2014; Petersen et al., 2016). However, these approaches are often hampered by non-conservative mixing of the above light elements related to gas exchange reactions at the air-water interface, involving water vapor and carbon dioxide. In contrast, traditional radiogenic isotope tracers of heavier metals (e.g., $^{87}\text{Sr}/^{86}\text{Sr}$, $^{143}\text{Nd}/^{144}\text{Nd}$, $^{206}\text{Pb}/^{207}\text{Pb}$) are not sensitive to water-gas exchange processes, but they are still susceptible to non-conservative mixing effects related to local water-sediment interactions (Holmden et al., 1997; Anadón et al., 2002; Holmden and Hudson, 2003; Dickin, 2005; Elderfield, 2006; Frank, 2011). More recent studies have seen increasing applications of stable isotope systems of redox-sensitive elements (Cr, Mo, U), and/or alkali and alkaline earth metals (Li, Mg, Ca, Sr, Ba) as natural tracers of metals and water sources in both marine and terrestrial settings (Baskaran, 2012; Holmden et al., 2012; Fantle and Tipper, 2014; Scheiderich et al., 2015; Wiederhold, 2015; Cao et al., 2016; Teng et al., 2017).

Of particular interest are the isotope studies of geochemically similar alkaline earth metals, such as Sr and Ca, which are the primary focus of this study. These metal isotope tracers (i) are highly abundant and readily soluble in natural waters forming divalent cations, (ii) exhibit both stable and radiogenic isotope variations, and (iii) have biogeochemical pathways closely linked to the global carbon cycle via processes involving precipitation and weathering

of carbonate minerals. Hence, Sr and Ca isotopes are valuable tracers of carbonate weathering/precipitation, water source mixing, as well as biological uptake of these elements by plants and organisms in coastal systems (Holmden et al., 1997; Fantle and DePaolo, 2007; Tang et al., 2008; Holmden and Bélanger, 2010; Holmden et al., 2012; Fantle and Tipper, 2014; Fantle, 2015; Farkaš et al., 2011, 2016; Harouaka et al., 2014, 2016). Importantly, the calcium carbonate (CaCO_3) cycle in coastal systems plays an important role in quantifying the blue carbon budget (i.e., carbon storage capacity) in coastal ecosystems. This in turn is essential for better assessment of global CO_2 input and output fluxes. However, most studies have been only focused on brackish and marine salinities, the hypersaline coastal environments, which receive much more significant effects from water evaporation and induced mineral precipitation, are poorly understood.

Here we illustrate how a novel approach with coupled Sr and Ca isotopes could be used in the carbonate-producing Coorong lagoon system, which has a salinity range from fresh to hypersaline, to distinguish and apportion different water sources, and better constrain the local CaCO_3 cycle, which is currently a poorly constrained component in the global blue carbon studies (Macreadie et al., 2017). Additionally, the Sr and Ca isotope data of fish otoliths (i.e., aragonitic ear-stones) from Coorong are used to infer potential short-term changes in the isotope signatures of local water masses (Gillanders and Munro, 2012). Finally, a broader objective of this study is to explore the possibility of using these isotope tracers, calibrated with respect to salinity in modern settings, to reconstruct paleo-salinity changes in the studied area and/or other carbonate-producing coastal environments from suitable fossil carbonates (e.g., bivalve shells or foraminifera) in local sediment archives.

2. STUDY AREA

The Coorong, Lower Lakes and Murray Mouth Estuary, located on the southeast coast of Australia (Fig. 1), represents a unique mixing zone where continental-sourced freshwaters interact with seawater from the Southern Ocean in the circulation-restricted Coorong, which is a 130-km-long lagoon formed behind a complex of Quaternary- and Holocene-age sand barrier islands and beach dunes (i.e., Youngusband Peninsula, see Fig. 1) (Kjerfve, 1986; Knoppers, 1994). This coastal area is of

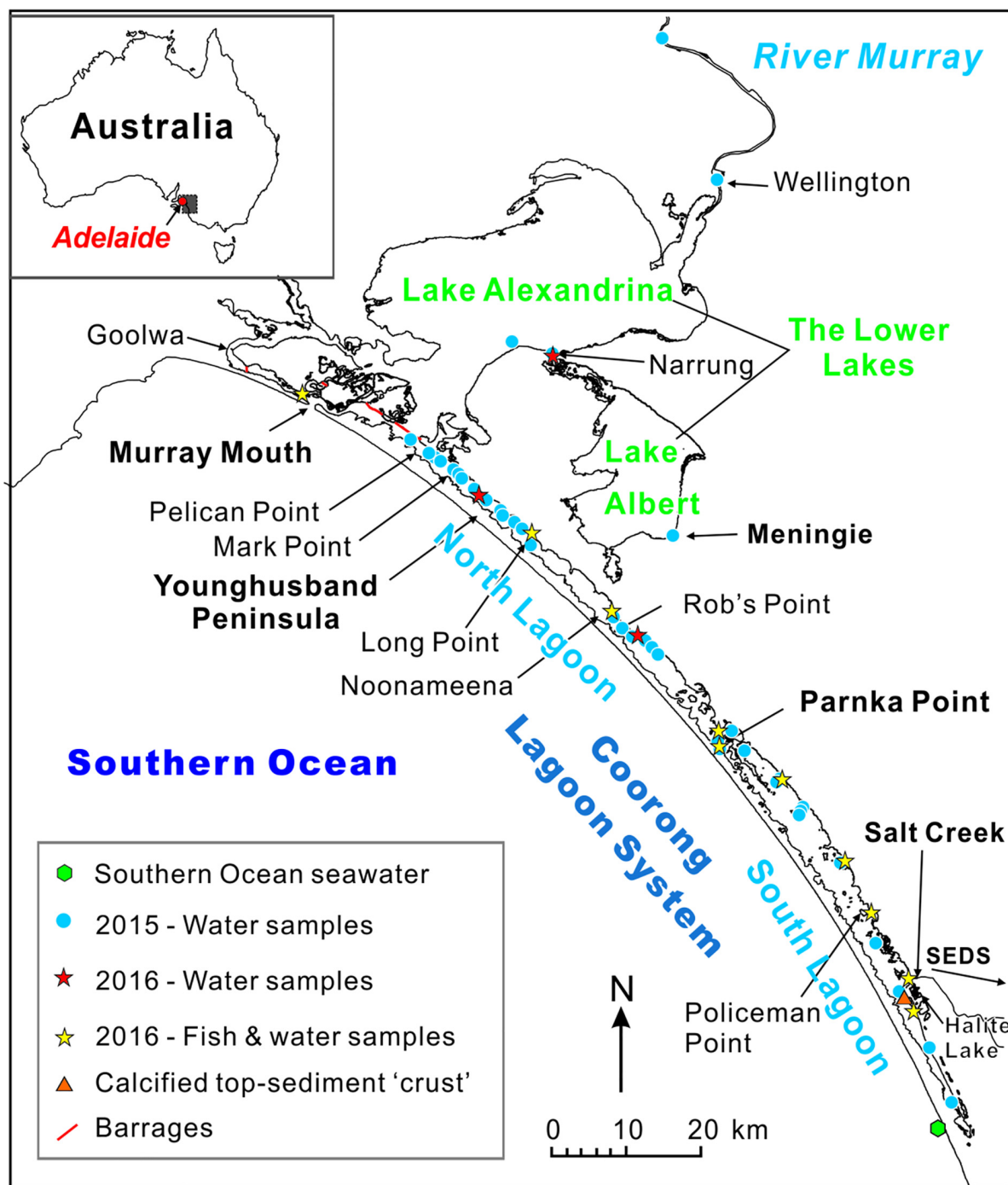


Fig. 1. A map showing the Coorong and Lower Lakes at the terminus of the River Murray in South Australia. Sampling locations for this study are color and symbol coded for sampling years of 2015 (circles) and 2016 (stars). Red bars in North Lagoon between Pelican Point and Goolwa show the locations of barrages. SEDS = the South East drainage system. Note that *the Coorong* refers to the narrow back-barrier lagoon separated from the Southern Ocean by the Younghusband Peninsula; *the Lower Lakes* refer to Lake Alexandrina and Albert; and *the Murray Mouth* refers to the connection of the Coorong to the ocean, locating at the northern end of the lagoon (cf., Webster, 2010). (For interpretation of the references to colour in this figure legend, the reader is referred to the web version of this article.)

particular ecological and environmental importance, being a conservation park for many local species, has also been listed in the Ramsar Convention of wetlands of international importance since 1985 (Webster, 2010).

The Coorong lagoon system acts as a natural 'reservoir' for mixing of different water sources, and it is divided into two sub-lagoons – the North and South Lagoons, with a narrow and shallow (< 1 m depth) connection at Parnka

Point (Fig. 1). The two lagoons have average water levels of ~ 1.2 m and ~ 1.4 m respectively, fluctuating seasonally with an amplitude of approximately 0.8 m to 1 m (Webster, 2010). The North Lagoon receives water inputs from the Southern Ocean via the Murray Mouth at its northern end and occasionally also from the release of freshwater through barrages. The latter separate the Coorong from the Lower Lakes (i.e., Lake Alexandrina and Lake Albert), which are fed by the River Murray (see Fig. 1). Prior to the construction of barrages between 1935 and 1940, water exchange between the Coorong, Lake Alexandrina and the Southern Ocean occurred naturally through the Murray Mouth. Thus, the construction of the barrages effectively isolated the Lower Lakes from the saline waters of the Coorong. This, along with increased extraction of river water for upstream irrigation, has gradually reduced freshwater inputs to the Coorong over the past seven decades (Phillips and Muller, 2006). In addition, the South Lagoon is hydrologically more restricted compared to North Lagoon, and the supply of waters is facilitated either via Parnka Point (i.e., a connection to the North Lagoon), or via Salt Creek that receives freshwater from the South East drainage system (Fig. 1) constructed over the last 150 years (Reid and Mosley, 2016; Mosley et al., 2017). Limited flushing by river outflows and reduced connectivity with the open ocean through the mouth have caused the South Lagoon to become progressively more hypersaline over the last five decades, which is of significant environmental and ecological concern (Haese et al., 2008; Mckirdy et al., 2010; Webster, 2010).

The mean annual rainfall in the studied area is ~ 390 mm with the average annual pan evaporation approximately 1500 mm according to Bureau of Meteorology (Station 023,894 on Hindmarsh Island), based on data from 2003 to 2018. In addition, there is evidence for ongoing and past local groundwater discharge through numerous seeps exposed in the lagoon and along its shorelines. These groundwater inputs are sourced from the Murray Group limestone aquifer, and are manifested by *in situ* carbonate precipitation occurring at the sites of local groundwater discharge in the form of carbonate tufa structures (Von der Borch et al., 1975; Haese et al., 2008; Webster, 2010; Gillanders and Munro, 2012). Proximal to the Coorong, especially the South Lagoon, are a series of shallow inland ephemeral lakes (0.5 m–1 m deep) that are fed by seawater intrusions, rainfall and local groundwater seepage. These lakes contain waters and brines modified by extreme evaporation and freshwater-seawater mixing, which has led to formation of *in-situ* primary dolomite (\pm magnesite), high-Mg calcite, aragonite and halite (Von der Borch et al., 1975). However, these ephemeral lakes are currently not directly connected to the Coorong lagoons. The above-mentioned groundwater discharge is likely not limited only to the Coorong, but the overall impact of groundwater on water quality in this coastal system remains unconstrained. Better knowledge of these processes and local groundwater inputs is of considerable interest and concern, especially with respect to future sustainable water management strategies (Haese et al., 2008; Barnett, 2015).

3. METHODS

3.1. Sample collection and preparation

In total, we collected 31 water samples in 2015, including river water from the channel of the River Murray near Wellington, waters from the Lower Lakes and the Coorong, two samples of local groundwater, as well as a reference ‘seawater’ collected from the Southern Ocean. In 2016/2017, we collected 42 samples in the Coorong area, including 13 water samples from the Coorong and Lower Lakes, 4 rainwater samples in Adelaide area (not shown in Fig. 1), one cemented top-sediment ‘crust’ in the Coorong South Lagoon, and 24 fish specimens across the lagoon. The coordinates of the sampling sites and dates are listed in the Appendix (Table C.1), and see also Fig. 1 for our sampling locations.

Supplementary data associated with this article can be found, in the online version, at <https://doi.org/10.1016/j.gca.2018.07.036>.

3.1.1. Waters and sediment

Representative water samples were collected from the surface of the water bodies by wading, using pre-cleaned 500 mL polypropylene bottles washed with 10% HNO₃. Water temperature, pH, conductivity/salinity, and total dissolved solids (TDS) were measured directly at the sampling sites using a Hanna Instrument HI-98194 multiparameter probe. In addition, two samples of local groundwater were collected via a 12 V Whale inline pump from two separate private wells located near Noonameena. Water samples were filtered through 0.45 μ m cellulose nitrate filters and stored in acid-cleaned 15 mL polypropylene test tubes. All Teflon labware for isotope and elemental analysis was cleaned in 6 M HNO₃ at 170 °C on a hotplate for 48 h, rinsed with deionised water, and then further cleaned in 6 M HCl at 170 °C for 24 h and dried.

Additionally, four rainwater samples were collected about 150 km north of the Coorong in the Adelaide area to determine the representative isotope composition of South Australian atmospheric precipitation, and its possible impact on the isotope signatures observed in the Coorong. Rainwaters were collected from polyethylene (Rain-PT) and a galvanised iron (Rain-IT) tanks, respectively. These ‘bulk’ samples thus represent the long-term average of local rainwaters that accumulated in the tanks over a period of several years. Two more rainwater samples (Rain-A and Rain-B) were collected in August 2016 during storm events using 2L pre-cleaned polypropylene bottles, which thus represent more recent and ‘snap-shot’ samples of the local atmospheric deposition.

A carbonate-cemented top sediment ‘crust’ (ca. 0.5–1 cm thick), which is commonly formed in the Coorong lagoons, was collected from the South Lagoon on March 2017 at a site south of Salt Creek near Halite Lake.

3.1.2. Fish species and otoliths

The smallmouth hardyhead (*Atherinosoma microstoma*, Fig. C.1B, Appendix C), belonging to the Atherinidae

family, generally have a total length of less than 110 mm and an annual life cycle (Gillanders and Munro, 2012; Wedderburn et al., 2014). This species lives usually in shallow estuarine and marine environments (within 2 m of water depth) and feeds on small invertebrates and plankton. The major advantage of using *A. microstoma* in this study is that the species has limited migration patterns (Molsher et al., 1994; Wedderburn et al., 2007, 2008) and also extremely high salinity tolerance (i.e., from 3.3 to 108 PSU; Lui, 1969), which allows sampling of this fish across the entire Coorong and the Murray Mouth (Fig. 1).

Specimens of smallmouth hardyheads were collected by wading in shallow waters using a fine-meshed seine net. Two or three large specimens were selected from each sampling site, weighed and measured for length. Sagittal otoliths were removed under a dissecting microscope, cleaned of adhering tissue in ultrapure water, dried, weighed and transferred to individual 1.5 mL centrifuge tubes. Additionally, two otoliths from the North and South Lagoons (samples C03-03 and C10-03, respectively) were embedded in epoxy resins and polished using fine grit lapping paper until the core was exposed (see also Fig. C.1A, Appendix C), then subsampled using a computer operated micromilling device (Merchantek Micromill Sampler). Each sample comprised the core of the otolith, which represents the early life of the fish, while the edge comprised material laid down shortly before capture and should be representative of the area where fish were collected.

3.2. Elemental and isotope analyses

3.2.1. Elemental concentrations

Elemental concentrations of Ca, Sr, Mg, Ba, Mn, Fe, Na, Zn and Cu in filtered water samples were measured with an Agilent 7500cs solution ICP-MS at Adelaide Microscopy, University of Adelaide. A multi-element standard was used for calibration. The uncertainty for all analyses is $\pm 3\%$ (2 s). The measured elemental concentrations are listed in Table C.3 in the Appendix (see also plots of concentrations against salinity in Fig. C.2, Appendix C).

3.2.2. XRD mineralogical composition analysis

The mineralogical composition of the sediment 'crust' from the South Lagoon was determined using X-Ray diffraction (XRD) adapted from Schreiner (1995) and Martin et al. (2015), performed at the School of Earth and Environmental Sciences, University of Wollongong. The sediment 'crust' sample was dried at 50–60 °C and crushed to $<4 \mu\text{m}$ by hand using an agate mortar and pestle prior to analysis. The sample was then mounted in aluminum holders and placed in a Phillips 1130/90 diffractometer with Spellman DF3 generator set to 1 kW. The mounted sample was loaded and analysed through an automatic sample holder. The 1 kW energy was achieved by setting the diffractometer to 35 kV and 28.8 mA. Then the sample was analysed between 4° and 70° 2-theta at 2° per minute with a step size of 0.02°. Diffraction patterns were produced through a GBC 122 control system and analysed using Traces, UPDSM and SIROQUANT software. The XRD diffraction patterns were calibrated using the quartz

peak at 26.66° 2-theta. The areas between 3.5° and 5.7° 2-theta were excluded as these were subject to background radiation. Peaks within 44.4° and 44.9° 2-theta were removed as they resemble the aluminum peak from the sample holder. The error on the XRD diffraction pattern was assessed by the chi-squared value (χ^2). A χ^2 of 3.52 was obtained. When $\chi^2 = 1$ it is statistically a perfect fit of the observed data to the model, therefore a χ^2 value of 1–5 is acceptable (Schreiner, 1995).

3.2.3. $^{87}\text{Sr}/^{86}\text{Sr}$ and $\delta^{44/40}\text{Ca}$

A total of 76 samples were measured for $^{87}\text{Sr}/^{86}\text{Sr}$, including 48 waters and 28 whole otoliths samples or micro-drilled sections of otoliths. The isotopic measurements were performed by thermal ionisation mass spectrometry (TIMS) using a Phoenix Isotopx instrument at the University of Adelaide. Prior to TIMS analyses, all samples were processed through a chromatographic column to separate the Sr fraction at the University of Adelaide using a semi-automated prepFAST-MC system, with the method adapted from Romaniello et al. (2015). See Section B.1 in Appendix for detailed procedures. Procedural Sr blanks were run in parallel with samples for each batch of samples, and the ^{84}Sr -enriched single spike was used to determine the Sr blanks via an isotope dilution (Lamberty and Pauwels, 1991). These tests confirm that most of the Sr blank was sourced from the chromatographic columns. The total procedural Sr blanks of our method ranged from ~60 to 200 ng, and considering that these represent only ~0.1% of our sample Sr signal, these blanks are negligible. The typical external precision of the $^{87}\text{Sr}/^{86}\text{Sr}$ analyses is better than ± 0.00001 (2 s), and the long-term reproducibility of IAPSO (OSIL) standard is 0.709171 ± 0.00001 (2 s, $n = 13$). Whereas the long-term reproducibility of SRM 987 (NIST) standard is 0.710246 ± 0.000018 (2 s, $n = 36$), which was used to monitor the stability and overall performance of TIMS measurements. For smaller sample sizes (~100 ng), the reproducibility of SRM 987 standard is 0.710247 ± 0.000011 (2 s, $n = 16$), giving a typical external precision of <0.00003 (2 s). Detailed information on sample loading, filament ionisation, and measurement uncertainties is provided in Section B.2 in Appendix B.

A total of 26 samples were analysed for $\delta^{44/40}\text{Ca}$, including 15 water samples, the sediment sample from the South Lagoon and 10 whole otolith samples. Prior to the Ca isotope analysis, all samples were mixed with a ^{43}Ca - ^{42}Ca double-spike and passed through cation exchange columns to purify Ca (Holmden, 2005; Lehn et al., 2013). The isotopic measurements were performed using a double-spike TIMS technique using a Thermo Elemental Triton instrument in the Saskatchewan Isotope Laboratory at the University of Saskatchewan, adapted from Holmden and Bélanger (2010) and Farkaš et al. (2016). The total procedure Ca blank was 80–130 ng, and represents less than 0.1% of Ca originating from a sample (for detailed procedures, refer to Holmden and Bélanger, 2010). The Ca isotope variations presented in this study are expressed in the conventional delta notation (as $\delta^{44/40}\text{Ca}$ values) relative to IAPSO, according to the following relationship: $\delta^{44/40}\text{Ca} = [(^{44}\text{Ca}/^{40}\text{Ca})_{\text{Sample}}/$

$^{44}\text{Ca}/^{40}\text{Ca}_{\text{IAPSO}} - 1] \times 1000$. The typical external precision of the $\delta^{44/40}\text{Ca}$ values is better than $\pm 0.05\text{‰}$ (2 s) (see Table A.1, Appendix A), and the long-term reproducibility of SRM 915b (NIST) standard is $-1.13 \pm 0.03\text{‰}$ (2se, $n = 3$).

3.3. Geochemical modeling of mineral saturations in waters using PHREEQC

The saturation states or indices (SI) of calcite, aragonite, gypsum and dolomite in the Coorong waters were calculated via PHREEQC (Parkhurst and Appelo, 2013), using concentrations of the major cations (Na^+ , Ca^{2+} , Mg^{2+} , K^+) and anions (Cl^- , SO_4^{2-} , DIC), as well as alkalinity, pH and temperature from representative water samples from five different locations across the Coorong (i.e., C02, C03, C06, C10 and C11). However, because the concentrations of Cl^- , SO_4^{2-} , and alkalinity were not measured in our water samples, these parameters had to be inferred indirectly from available historical geochemical data collected in the Coorong from 1998 to 2010 (provided by the Department for Environment, Water and Natural Resources South Australia), using sodium (Na^+) concentrations as a reference element. Based on the local long-term correlation trends between the concentrations of Na and the above ions of interest from historical data (i.e., 1998–2010), we were able to infer the corresponding concentrations of K^+ , Cl^- , SO_4^{2-} , and alkalinity for our water samples (for details see Appendix, Section B.3.1, Table B.2 and Fig. B.1). For PHREEQC modeling, Cl^- was used as the sole anion for charge balancing, with calculated charge balance errors typically $< 5\%$ (2 s). The activity coefficients and Saturation Indices (SI) were calculated using the *Pitzer database* (Parkhurst and Appelo, 2013). To examine potential uncertainty in saturation index (SI) calculations, several simulations were performed varying pH (± 0.2), Ca ($\pm 10\%$), alkalinity ($\pm 10\%$) from measured values. This was based on estimated analytical errors in this range and a lot of the correlations being around 0.9 for derivation of the missing major ion concentrations.

4. RESULTS

All analytical data, including measured $^{87}\text{Sr}/^{86}\text{Sr}$, $\delta^{44/40}\text{Ca}$, and selected elemental concentrations are compiled in Tables A.1 and A.2, in Appendix A. Salinity, $^{87}\text{Sr}/^{86}\text{Sr}$ and $\delta^{44/40}\text{Ca}$ data across the north-south trend of the Coorong, Lower Lakes and River Murray are plotted in Fig. 2 against the latitude of sampling locations to illustrate their spatial variability.

4.1. Spatial variations of salinity in the Coorong

The salinity of the North Lagoon was similar to the adjacent Southern Ocean (~ 35 PSU, i.e., normal seawater). In contrast, the salinity of the South Lagoon increased from ~ 60 PSU around Parnka Point to high values of ~ 120 PSU approaching the southern end (Fig. 2A), reflecting the

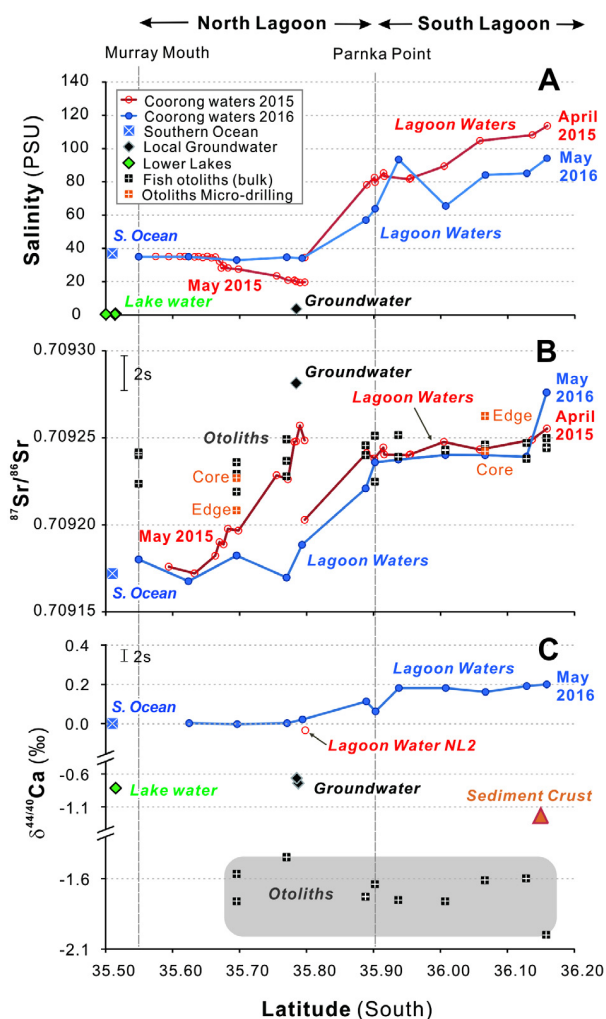


Fig. 2. (A) Salinity profile across the Coorong and Lower Lakes, measured in 2015 and 2016. (B) $^{87}\text{Sr}/^{86}\text{Sr}$ variability in the Coorong, based on samples of waters and otoliths. Note that fish samples (i.e., the otolith providers) were collected only in 2016. Black squares with white cross represent whole otolith $^{87}\text{Sr}/^{86}\text{Sr}$, whereas orange squares with white cross represent $^{87}\text{Sr}/^{86}\text{Sr}$ measured in core and edge material of a single otolith. The Lower Lakes and River Murray samples are too high to be plotted on the scale (see Table A.1 in Appendix). (C) The $\delta^{44/40}\text{Ca}$ in the Coorong and Lower Lakes, based on the water samples (circles), carbonate-cemented top sediment (triangle) and fish otoliths (black squares with white cross). All data were plotted as a function of the geographic latitude for corresponding sampling sites.

geomorphological restriction of the lagoon towards the south. The most obvious difference between 2015 and 2016 data is the decrease in water salinity (from marine to brackish) in 2015 in the central part of the North Lagoon (near Noonameena and extending towards Rob's Point). This brackish event reflects increased freshwater inputs either via barrage outflow from the Lower Lakes or local groundwater seepage, which are scenarios evaluated in the discussion section.

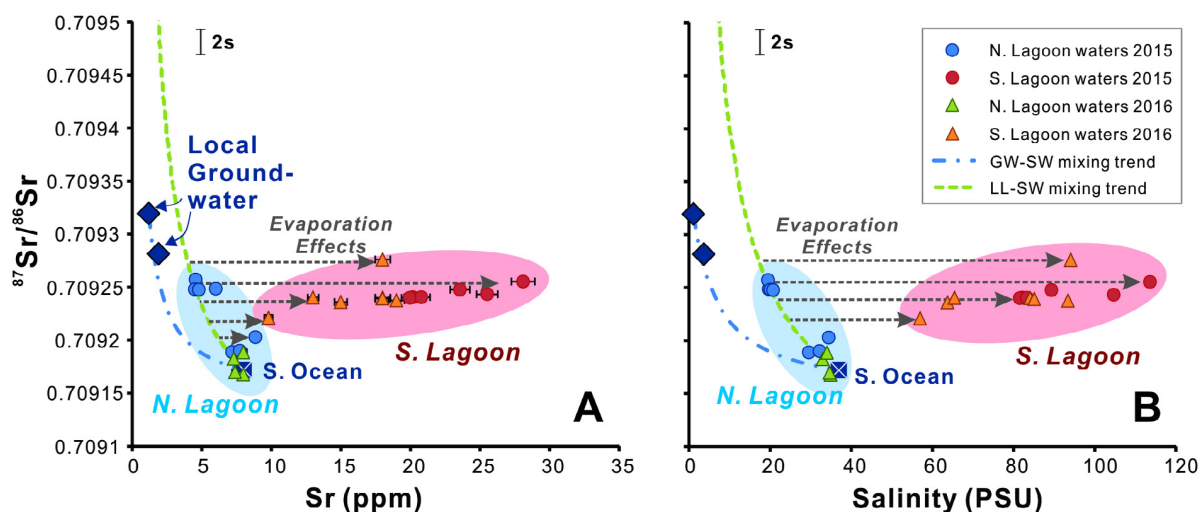


Fig. 3. (A) The theoretical mixing trends for $^{87}\text{Sr}/^{86}\text{Sr}$ versus Sr concentration data, constructed for the mixing of the following end-members: a local groundwater (GW), seawater (SW), and the continental surface freshwaters represented by the Lower Lakes water (noted as LL); plotted along with data acquired from the Coorong water samples. (B) The modeled mixing trends and water data for $^{87}\text{Sr}/^{86}\text{Sr}$ versus Salinity cross-plot. Note that the continental surface freshwater - seawater (LL-SW) mixing trends were truncated due to a very high $^{87}\text{Sr}/^{86}\text{Sr}$ of the continental surface freshwater (represented as 0.710880, see Table 3), which is out of scale. As neither water evaporation nor carbonate precipitation is expected to change the $^{87}\text{Sr}/^{86}\text{Sr}$ of the lagoon waters, the original Sr concentration and salinity can be estimated by projecting the back-projection) of the measured data onto the theoretical mixing trends.

4.2. $^{87}\text{Sr}/^{86}\text{Sr}$ and $\delta^{44/40}\text{Ca}$ variations in waters, sediments and otoliths

4.2.1. Coorong lagoon waters and local groundwater

Excluding the brackish water samples measured in 2015, the average $^{87}\text{Sr}/^{86}\text{Sr}$ of the North Lagoon water was 0.70918 ± 0.00001 (2 s), which is indistinguishable from the average $^{87}\text{Sr}/^{86}\text{Sr}$ of global seawater, 0.70917 ± 0.00002 (2 s, $n = 7$) (see Krabbenhöft et al., 2009, and references therein). In contrast, the brackish waters (Table A.1, Appendix A) yielded 0.70925 ± 0.00001 (2 s), indicating continental water inputs with higher $^{87}\text{Sr}/^{86}\text{Sr}$ than seawater. The groundwater samples yielded an average $^{87}\text{Sr}/^{86}\text{Sr}$ of 0.70930 ± 0.00001 (2 s), which is higher than the brackish water and seawater. The average $^{87}\text{Sr}/^{86}\text{Sr}$ of the hypersaline South Lagoon was $\sim 0.70924 \pm 0.00001$ (2 s) (Fig. 2B), similar to the North Lagoon brackish water, despite their contrasting salinities.

Other continental waters yielded much higher $^{87}\text{Sr}/^{86}\text{Sr}$ values than those illustrated above. Specifically, the River Murray water had a $^{87}\text{Sr}/^{86}\text{Sr}$ of ~ 0.71212 – the highest among waters analysed in this study. Following are the Lower Lakes waters with $^{87}\text{Sr}/^{86}\text{Sr}$ of ~ 0.71094 (Table 3, and Fig. 3A). Samples of local atmospheric precipitation or rainwaters yielded $^{87}\text{Sr}/^{86}\text{Sr}$ ratios ranging between ~ 0.71008 and 0.71154 (Table A.1, Appendix A), indicating a continental influence in the rainwater, most likely due to the presence of dissolved Sr from mineral dust.

The $\delta^{44/40}\text{Ca}$ of lagoon waters generally increased with increasing water salinity (Fig. 2C), with the exception of brackish water (i.e., sample NL2 with salinity ~ 20 PSU) collected from the North Lagoon in 2015. Overall, North Lagoon waters with normal seawater salinities (~ 35 PSU), yielded $\delta^{44/40}\text{Ca}$ values close to 0‰. In contrast,

freshwater samples yielded systematically lower $\delta^{44/40}\text{Ca}$ values, with groundwater at -0.73‰ , and water from the Lower Lakes as low as -0.84‰ . Finally, hypersaline waters from the South Lagoon yielded much higher $\delta^{44/40}\text{Ca}$ values of about $+0.20\text{‰}$, which is thus higher than typical seawater, the latter uniform at $\sim 0\text{‰}$.

4.2.2. Sediment crust from Coorong Lagoon

The carbonate fraction of the sediment crust in the South Lagoon (sample CLS-1, see also XRD data in Table 1) yielded $\delta^{44/40}\text{Ca}$ of $-1.16 \pm 0.03\text{‰}$, which is approximately 1.4‰ lower than the $\delta^{44/40}\text{Ca}$ in the South Lagoon waters. Note that this sample was not analysed for $^{87}\text{Sr}/^{86}\text{Sr}$.

4.2.3. Fish otoliths

The $^{87}\text{Sr}/^{86}\text{Sr}$ of whole fish otoliths vary from ~ 0.70922 in the North Lagoon to up to ~ 0.70925 in the South

Table 1
Relative abundances of mineral phases (determined by XRD) in the top-sediment cemented ‘crust’, sampled in the South Lagoon (south of Salt Creek, near Halite Lake). The CaCO_3 phases, i.e. calcite and aragonite, are highlighted.

Sample ID	CSL-1 (top sediment crust) Depth: 0.5–1 cm	
Mineral phase	% Abundance	% Error
Quartz	18.7	0.3
Dolomite	0.3	0.4
Gypsum	1.1	0.4
Halite	2.9	0.2
Aragonite	64.7	0.7
Calcite	8.9	0.3
Magnesite	1.5	0.6
Ankerite	2.0	0.4

Lagoon (Fig. 2B; see also data in Table A.1, Appendix A). Otolith $^{87}\text{Sr}/^{86}\text{Sr}$ ratios of fish collected from the South Lagoon are very close to the average $^{87}\text{Sr}/^{86}\text{Sr}$ of local lagoon waters. In contrast, $^{87}\text{Sr}/^{86}\text{Sr}$ ratios of otoliths from fish collected in the North Lagoon are higher than the local lagoon waters.

The measured $^{87}\text{Sr}/^{86}\text{Sr}$ from the micro-drilled sections of selected otoliths (orange squares in Fig. 2B, Table A.2 and Fig. C.1 in Appendix) represent early (juvenile = core) and older or more recent (i.e., edge) growth increments, and by inference fish migration patterns and/or changes in $^{87}\text{Sr}/^{86}\text{Sr}$ of local lagoon waters over the lifespan of the fish. Specifically, a sample C03-03 from the North Lagoon shows that the recent $^{87}\text{Sr}/^{86}\text{Sr}$ value (i.e., edge) is lower than the one recorded during fish's early life (i.e., core). In contrast, sample C10-03 from the South Lagoon shows that the recent $^{87}\text{Sr}/^{86}\text{Sr}$ value in otolith (i.e., edge) is higher (~ 0.70926), while the juvenile $^{87}\text{Sr}/^{86}\text{Sr}$ parts of this otolith (i.e., core) yielded $^{87}\text{Sr}/^{86}\text{Sr}$ that is similar to the ambient lagoon waters (~ 0.70924) (Table A.1, Appendix A).

Whole otolith samples yielded $\delta^{44/40}\text{Ca}$ values ranging between -1.46 and -2.00‰ (Fig. 2C and data in Table A.1, Appendix A). There is no obvious correlation between the $\delta^{44/40}\text{Ca}$ values of otoliths and those of local lagoon waters where the fish were captured (Fig. C.4, Appendix C). There is, however, a correlation between

fish/otolith size and $\delta^{44/40}\text{Ca}$ ($R^2 \approx 0.4$, $p < 0.08$, $n = 10$). Specifically, smaller otoliths (i.e., smaller fish) tend to have lower $\delta^{44/40}\text{Ca}$ values (see data in Table A.1, Appendix A).

4.3. XRD analysis of the sediment crust sample

The mineralogy of the sediment 'crust' from the South Lagoon is given in Table 1. Approximately 75% of the sediment crust is composed of carbonate minerals, the latter being mostly aragonite ($\sim 65\%$), with smaller amounts of calcite ($\sim 9\%$), ankerite ($\sim 2\%$) and magnesite ($\sim 1\%$). The non-carbonate component of the sediment is mostly quartz ($\sim 19\%$), with minor amounts of halite ($\sim 3\%$) and gypsum ($\sim 1\%$).

4.4. Mineral saturation (SI) of lagoon waters

PHREEQC modeling shows increasing saturation indices (SI) in the Coorong lagoon waters from north to south with respect to calcite, aragonite, dolomite, and gypsum (Table 2, see also Fig. B2 in Appendix B). Carbonate minerals (CaCO_3 and $\text{CaMg}(\text{CO}_3)_2$) are systematically oversaturated ($\text{SI} > 0$) in waters across the entire Coorong, whereas gypsum ($\text{CaSO}_4 \cdot 2\text{H}_2\text{O}$) is mostly undersaturated ($\text{SI} < 0$) except in the most circulation restricted portions of the South Lagoon where SI is close to 0. The typical uncertainty associated with calculated SI values is $\pm 0.2\text{SI}$ (2 s), which is based on propagation of analytical uncertainties (Table 2).

These PHREEQC modeling results, and predicted minerals formed from local waters, are consistent with the mineralogical data acquired using XRD from the sediment 'crust' sample collected in the South Lagoon (Table 1). The only exception is dolomite, which was not present in the XRD scans, but is predicted to occur. This discrepancy, also referred to as 'dolomite problem', is discussed in more details in the Appendix B.3.2.

5. DISCUSSION

Previous studies (Haese et al., 2008, 2009; Webster, 2010; Gillanders and Munro, 2012; Mosley et al., 2017)

Table 2

A summary with calculated SI values for selected minerals, based on the PHREEQC modelling.

Sample IDs and 2016 sampling sites ^a	Mineral saturation index (SI)			
	Calcite	Aragonite	Dolomite	Gypsum
C02 - Mark Point	0.82	0.67	2.49	-0.69
C03 - Long Point	0.87	0.72	2.6	-0.76
C06 - Parnka Point	1.41	1.26	3.74	-0.38
C10 - Policemans Point	1.44	1.29	3.82	-0.24
C11 - Salt Creek	1.4	1.25	3.75	-0.23

^a The locations of these sampling sites are available in Fig. 1, and for more accurate coordinates see also Table C.1, Appendix C. Note that the estimated error on individual SI values is about $\pm 0.2\text{SI}$ -unit.

Table 3

The Sr, Ca and Na concentrations and isotope compositions of possible end-members for water sources used in our isotope mixing models (data extracted from Tables A.1, A.2, and Table C.4, in Appendix). The data presented for the mixtures are the average values, specific sample IDs refer to Table A.1, Appendix A.

	Sample ID	Salinity (PSU)	Sr (ppm)	Ca (ppm)	Na (ppm)	$^{87}\text{Sr}/^{86}\text{Sr}$	$\delta^{44/40}\text{Ca}$ (‰)
<i>End-members^a</i>							
Seawater/S. Ocean (SW)	SL11	36.9	8.0	414	10,800	0.70917	0.00
Groundwater (GW)	JWP2	1.2	1.3	101	148	0.70932	-0.77
Continental surface freshwater/The Lower Lakes (LL)	C01	0.8	0.5	33	181	0.71088	-0.84
<i>Mixtures</i>							
Brackish North Lagoon waters	-	~ 20	4.9	301	6223	0.70925	-0.04 ^b
The South Lagoon	-	~ 100	23.6	980 ^c	26,769	0.70924	+0.2

^a The possible freshwater (FW) end-members for water source apportioning models are the GW and LL.

^b The $\delta^{44/40}\text{Ca}$ value for the brackish North Lagoon water is from sample NL2, since this is the only one analysed for $\delta^{44/40}\text{Ca}$.

^c Inferred from the cross plots of Ca concentration versus salinity in the Coorong from Gillanders and Munro (2012).

have documented and modeled the spatially and temporally variable character of the surface waters and hydrology of the Coorong, Lower Lakes and Murray Mouth Estuary. This complexity is evident also from the range of salinities in this hydrological system, and further supported by systematic variations observed in our $^{87}\text{Sr}/^{86}\text{Sr}$ and $\delta^{44/40}\text{Ca}$ water data. In this section, we aim to use these two isotope tracers to understand the water source mixing, evaporation and carbonate precipitation in this modern lagoon estuary system, especially the North and South Lagoons. Furthermore, we also discuss here the potential of Sr and Ca isotope proxies to reconstruct the hydrology and paleo-salinity of this lagoon-estuarine system based on the $^{87}\text{Sr}/^{86}\text{Sr}$ and $\delta^{44/40}\text{Ca}$ analysis of suitable carbonate archives.

In order to distinguish between surface and groundwater sources of freshwater in the studied lagoon system, two mixing scenarios – *groundwater-seawater* (GW-SW) and *continental surface freshwater-seawater* (LL-SW) are considered in our models. Specifically, the continental surface freshwaters are represented here by the Lower Lakes water sample (labeled as LL, see Table 3), which has average geochemical characteristics and isotopic compositions of all freshwater samples analysed (i.e., the River Murray, the Lower Lakes and the rainwater). A local groundwater is labeled as GW, and the Southern Ocean seawater is labeled as SW in our models. The elemental concentrations and isotope compositions of these individual water sources (i.e., end-members) and mixtures used in our calculations are listed in Table 3.

5.1. Constraints on water source mixing and evaporation effects

5.1.1. Sr isotope systematics

As obvious from Fig. 2, the similarities in salinities and $^{87}\text{Sr}/^{86}\text{Sr}$ of the North Lagoon waters (~ 35 PSU and ~ 0.70918 , respectively) and the Southern Ocean seawater (37 PSU and 0.70917) indicate that the primary source of water in the North Lagoon is typical seawater. However, samples from May 2015 show brackish salinity (~ 20 PSU) and higher $^{87}\text{Sr}/^{86}\text{Sr}$ in the central part of the North Lagoon (~ 0.70925), pointing to inputs of continentally derived freshwater either from the Lower Lakes (0.71094), and/or local groundwater sources (~ 0.70932) (Table 3). As to the South Lagoon, these waters are systematically more radiogenic ($^{87}\text{Sr}/^{86}\text{Sr} \sim 0.70924$) than typical seawater, indicating inputs of continentally derived Sr and by inference freshwaters. The hypersaline waters of the South Lagoon are thus a product of highly evaporated brackish waters present in this semi-restricted environment.

5.1.2. Evaluation of the water evaporation effects in the Coorong

Before resolving the water source mixing in the studied hydrological system with the aid of Sr and Ca isotopes, it is important to understand the net effect of water evaporation on the chemical and isotope composition of the Coorong waters, since the latter can be significantly altered by these processes. These evaporation effects on Coorong waters are shown in plots of $^{87}\text{Sr}/^{86}\text{Sr}$ ratios against Sr

concentrations and salinity (Fig. 3). The theoretical LL-SW and GW-SW mixing trends (i.e., dashed curves in Fig. 3), not affected by water evaporation, were calculated using the end-member values listed Table 3, and the following elemental and isotopes mass balance equations:

$$\left(\frac{^{87}\text{Sr}}{^{86}\text{Sr}}\right)_{\text{MIX}} M_{\text{MIX}} C_{\text{MIX}} = \left(\frac{^{87}\text{Sr}}{^{86}\text{Sr}}\right)_{\text{FW}} M_{\text{FW}} C_{\text{FW}} + \left(\frac{^{87}\text{Sr}}{^{86}\text{Sr}}\right)_{\text{SW}} M_{\text{SW}} C_{\text{SW}} \quad (1)$$

where M is the mass of water, such that $M_{\text{MIX}} = M_{\text{FW}} + M_{\text{SW}}$, and C is the Sr concentration or salinity of individual end-members and the mixture. The subscripts SW and FW denote seawater and freshwater (i.e., LL or GW for each mixing scenario) respectively, and MIX denotes the theoretical mixture of the two water sources.

$$C_{\text{MIX}} = C_{\text{FW}} X_{\text{FW}} + C_{\text{SW}} (1 - X_{\text{FW}}) \quad (2)$$

where X_{FW} is the mass fraction of freshwater, assigned from 0 to 1.

Accordingly, if the mixtures were formed only by mixing of the above water sources with no impact from evaporation, they should all plot along those theoretical mixing trends.

Overall, Fig. 3 confirmed that the South Lagoon experienced water geochemistry exhibited much higher effects of water evaporation, as the data plot away from theoretical mixing trends, while the North Lagoon was under very limited water evaporation effect. This difference can be explained the specific hydrology of the Coorong, where – the North Lagoon readily exchanges water with the Southern Ocean, thus the evaporation effect is barely accumulates. In contrast, the South Lagoon is highly restricted with limited connectivity to the North Lagoon via Parnka Point (Fig. 1). Furthermore, the brackish North Lagoon water from 2015 plot along the LL-SW mixing trend (Fig. 3), indicating that the primary source of freshwater during this transient brackish event was most likely sourced from the Lower Lakes rather than from local groundwater sources.

5.1.3. Multi-proxy constraints ($\delta^{44/40}\text{Ca}$, $^{87}\text{Sr}/^{86}\text{Sr}$, element/Na) on water source mixing

In order to visualise the water source mixing in the studied hydrological system in a bigger picture while eliminating the cumulative effects of water evaporation, we plot $^{87}\text{Sr}/^{86}\text{Sr}$ and $\delta^{44/40}\text{Ca}$ acquired from the water samples against their element/Na ratios, along with the calculated theoretical mixing trends in Fig. 4.

A close-up view on the data (Fig. 4B) confirms the North Lagoon waters were predominantly derived from the Southern Ocean, with the exception of the ‘brackish event’ from 2015, which reflects temporary freshwater input from the Lower Lakes water over the barrages during a period of high water levels in the River Murray (Mosley, 2016, and reference therein).

Interestingly, the South Lagoon waters also plots along the LL-SW mixing trend (Fig. 4B), suggesting that a

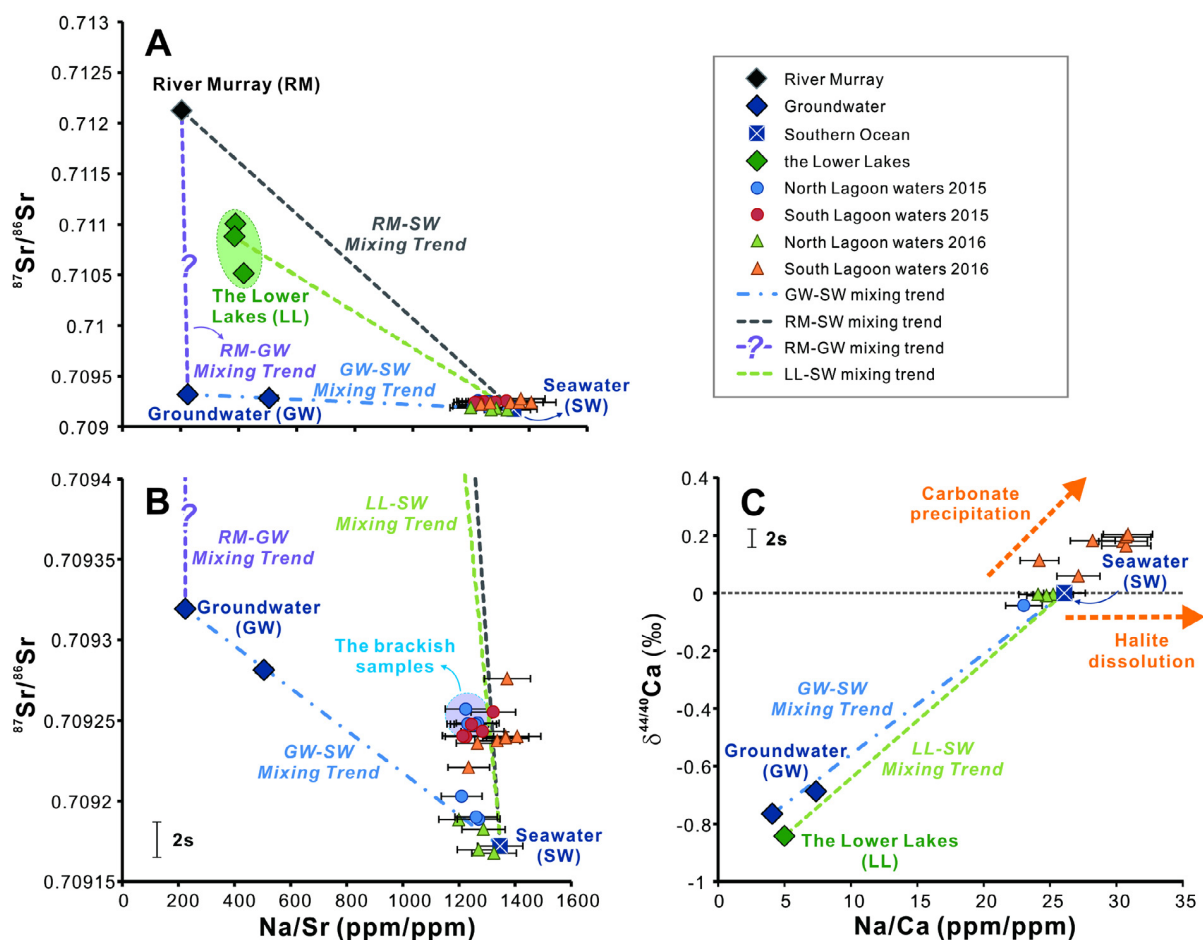


Fig. 4. (A) The modeled mixing lines for $^{87}\text{Sr}/^{86}\text{Sr}$ versus Na/Sr ratio, defined by simple two-component mixings of (i) local groundwater (GW, presumably sourced from the surrounding limestone aquifers) and seawater (SW, i.e., the Southern Ocean), (ii) the Lower Lakes (LL) and seawater (SW), (iii) the River Murray (RM) and seawater (SW), and (iii) the River Murray (RM) and groundwater (GW); plotted together with the Coorong water data. The question mark on the RM-GW mixing trend is added because groundwaters around the Lower Lakes might have different $^{87}\text{Sr}/^{86}\text{Sr}$ to the ones sampled at the Coorong. (B) Truncated Y-axis to a $^{87}\text{Sr}/^{86}\text{Sr}$ value of 0.7094 from (A) to better visualise the water mixing scenarios. (C) The modeled mixing trends for $\delta^{44/40}\text{Ca}$ versus Na/Ca ratio, defined by simple two-component mixings of (i) local groundwater (GW) versus seawater (SW, i.e., the Southern Ocean), and (ii) the Lower Lakes (LL) versus seawater (SW). Dashed arrows indicate anticipated directions/trends for progressive (i) aragonite precipitation, and (ii) halite dissolution, and their expected impact on water chemistry and Ca isotope composition.

continental surface freshwater source with similar chemistry to the Lower Lakes water plays an important role in the water mixing in the South Lagoon. Considering the distance from the barrages and the narrow constriction at Parnka Point, the only way for the Lower Lakes water to enter the South Lagoon is during periods of increased barrage outflow in the North Lagoon, driving increased flow of brackish waters to the South Lagoon. This scenario is consistent with the hydrodynamic study of the Coorong by Webster (2010), showing that water levels and salinity in the North and South Lagoons are closely tied to the barrage outflow regime. However, this does not preclude that other contributions of local sources of freshwater to the South Lagoon are not important, and these might include groundwater seeps and/or surface drainage water inputs from the South East drainage system (Mosley, 2016, see also Fig. 1). More work

is needed to identify and quantify the impact of these alternative freshwater sources, and their $^{87}\text{Sr}/^{86}\text{Sr}$, $\delta^{44/40}\text{Ca}$ and elemental concentrations must be measured.

Additionally, the $\delta^{44/40}\text{Ca}$ vs. Na/Ca diagram (i.e., Fig. 4C) also shows that the South Lagoon waters yielded consistently higher $\delta^{44/40}\text{Ca}$ and Na/Ca ratios than other samples. We interpret this as evidence for ongoing carbonate precipitation in the South Lagoon, mainly in the form of aragonite as suggested by the XRD data (Table 1). Alternatively, the high Na/Ca ratios can be caused by the dissolution of halite (NaCl) transported from nearby ephemeral lakes (e.g., Halite Lake) via runoff during rainfall events or lifted by wind and deposited as halite dust. However, the processes of halite dissolution/addition versus carbonate precipitation will follow different trajectories in the $\delta^{44/40}\text{Ca}$ vs. Na/Ca plot (see dashed arrows in Fig. 4C).

Table 4

The mass fractions of freshwater (X_{FW}) in the brackish North Lagoon waters observed in May 2015, using (i) salinity constraints, (ii) $^{87}\text{Sr}/^{86}\text{Sr}$ and Sr concentration, and (iii) $\delta^{44/40}\text{Ca}$ and Ca concentration.

The mass fraction of freshwater (X_{FW}) ^a		Based on salinity constraints	Based on $^{87}\text{Sr}/^{86}\text{Sr}$ and Sr	Based on $\delta^{44/40}\text{Ca}$ and Ca
Mixing scenarios	LL-SW	47%	44%	39%
	GW-SW	46%	88%	18%

^a The FW components are LL and GW in both mixing scenarios, respectively.

Specifically, halite dissolution only adds Na to the lagoon waters, but does not affect Ca concentrations or $\delta^{44/40}\text{Ca}$ values, which is thus at odds with our data. In contrast, carbonate precipitation is expected to change both parameters, i.e., increasing Na/Ca and $\delta^{44/40}\text{Ca}$, due to removal of Ca^{2+} and light ^{40}Ca isotopes from the lagoon waters, which is a trend that agrees with our water data from the South Lagoon (Fig. 4C).

Interestingly, our results also showed that the Lower Lakes are not a simple mixture of seawater and the River Murray water, as the lake water plot away from a theoretical mixing line for a river water and seawater end-members (RM-SW) (Fig. 4A). The lake waters must thus receive Sr also from additional freshwater source, which could be local groundwater as shown in Fig. 4A, in agreement with observed physical evidence for local groundwater discharge in the Coorong and Lower Lakes (Haese et al., 2008), and/or other small tributary sources from the Eastern Mount Lofty Ranges (Australian Water Environments, Ecological Associates and GHD Pty Ltd., 2011).

5.1.4. Water source mixing and apportionment

Below we use both salinity and elemental/isotope mass balance constraints to quantify the water source mixing and apportionment in the brackish North Lagoon (samples from 2015) and also in typical hypersaline South Lagoon waters.

The mass fraction of freshwater in the brackish North Lagoon can be calculated from the decrease in salinity, using a salinity of 36.9 PSU for seawater (SW), 0.8 PSU for the Lower Lakes water (LL), and 1.2 PSU for groundwater (GW) (Table 3). The LL-SW mixing scenario yields a freshwater fraction of 47% (Table 4), suggesting that seawater was diluted with approximately equal amount of lake water in the North Lagoon in May 2015. A very similar freshwater fraction of 46% is calculated based on salinity data for the alternative GW-SW mixing scenario (Table 4).

To resolve which one of the above scenarios (LL-SW versus GW-SW) is more realistic, and to better quantify the amount and origin of freshwater in the Coorong, one can also use isotope mass balance constraints. These allow to calculate the mass fraction of freshwater (X_{FW}) in the mixture ($X_{FW} = \frac{M_{FW}}{M_{MIX}}$), based on the rearranged Eqs. (1) and (2):

$$X_{FW} = \frac{M_{FW}}{M_{MIX}} = \frac{C_{SW} \left[\left(\frac{^{87}\text{Sr}}{^{86}\text{Sr}} \right)_{MIX} - \left(\frac{^{87}\text{Sr}}{^{86}\text{Sr}} \right)_{SW} \right]}{C_{FW} \left[\left(\frac{^{87}\text{Sr}}{^{86}\text{Sr}} \right)_{FW} - \left(\frac{^{87}\text{Sr}}{^{86}\text{Sr}} \right)_{MIX} \right] + C_{SW} \left[\left(\frac{^{87}\text{Sr}}{^{86}\text{Sr}} \right)_{MIX} - \left(\frac{^{87}\text{Sr}}{^{86}\text{Sr}} \right)_{SW} \right]} \quad (3)$$

Similar approach can be used also for $\delta^{44/40}\text{Ca}$ and Ca concentration data to calculate the mass fractions of freshwater (X_{FW}) in the Coorong.

Importantly, these three different approaches give very similar fractions of freshwater derived from the Lower Lakes, and we therefore conclude that the barrage outflow from the lakes is the major source of freshwater during 2015 brackish event (in agreement with data plotted in Fig. 4B). In contrast, the calculated freshwater fractions for the GW-SW mixing scenario disagree with each other (Table 4), further corroborating that this mixing scenario is not realistic for our data set.

As for the restricted and hypersaline South Lagoon, we cannot use the salinity and $\delta^{44/40}\text{Ca}$ constraints for the calculation of X_{FW} in local lagoon waters due to the impacts from water evaporation and carbonate precipitation processes. Nevertheless, one can use Sr isotope constraints that are not sensitive to these processes, and this approach yields freshwater mass fractions of 41% and 85%, for LL-SW and GW-SW scenarios respectively.

5.2. Carbonate fluxes in the Coorong

5.2.1. Ca isotope systematics

The carbonate fluxes in the Coorong are mainly addressed by the $\delta^{44/40}\text{Ca}$, which is a sensitive indicator of carbonate precipitation, as the latter preferentially incorporates light Ca isotopes in CaCO_3 minerals (Gussone et al., 2005; Fantle and Tipper, 2014; Farkaš et al., 2016). The process of carbonate precipitation can thus explain the systematically higher $\delta^{44/40}\text{Ca}$ values (+0.2‰) relative to Southern Ocean, observed in the hypersaline South Lagoon (Fig. 4C). There might be also minor impact from gypsum formation in the highly evaporated lagoon waters (Von der Borch, 1962; Fernandes and Tanner, 2009; Harouaka et al., 2014), since these Ca-bearing sulfate minerals also preferentially sequester lighter Ca isotopes (Gussone et al., 2005; Harouaka et al., 2014).

In addition, Ca isotopes in coastal waters are also sensitive to freshwater-seawater mixing due to the expected differences in $\delta^{44/40}\text{Ca}$ signatures for these isotopically contrasting water sources (Holmden et al., 2012; Fantle and Tipper, 2014). Such salinity- and water source-controlled behavior of the $\delta^{44/40}\text{Ca}$ is also confirmed by our data (Fig. 5), and a similar pattern has been observed in the published data from the coastal waters of the Florida Bay (Holmden et al., 2012, see cross-symbols in Fig. 5).

A comparison between $\delta^{44/40}\text{Ca}$ and salinity (PSU) in the Coorong waters suggests a systematic coupling between these two variables, expressed as statistically significant positive correlation ($R^2 = 0.974$, $p < 0.05$) (Fig. 5). Taking into account the characteristic $\delta^{44/40}\text{Ca}$ values of different water sources in earth surface environments (cf., Fantle and Tipper, 2014), the observed $\delta^{44/40}\text{Ca}$ variability in the North Lagoon waters (Fig. 5), including the brackish

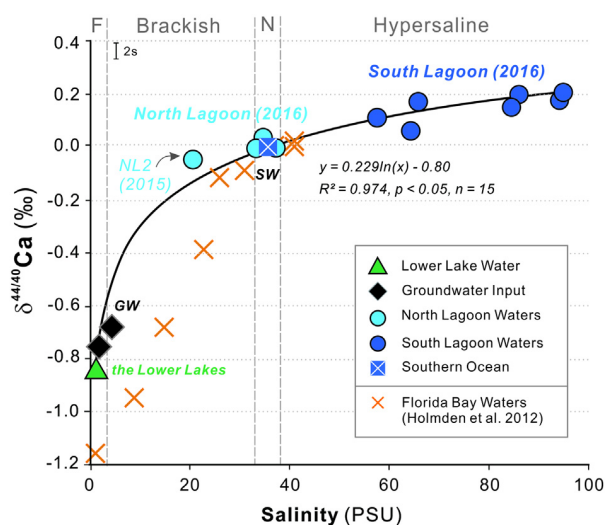


Fig. 5. $\delta^{44/40}\text{Ca}$ of waters from the Coorong, Lower Lakes, and Murray Mouth hydrological system, which cover a wide range of water salinities (i.e., fresh, brackish, marine and hypersaline) and show a logarithmic correlation pattern; complemented by the published data from waters collected in the Florida Bay (Holmden et al., 2012). The following abbreviations are used: F = Freshwater; N = Normal Marine; SW = Seawater; and GW = Groundwater.

sample NL2 from 2015 with slightly lower $\delta^{44/40}\text{Ca}$, can be explained by a mixing between seawater (0.0‰) and continentally derived freshwaters (−0.77 to −0.84‰) (Fig. 5), see also data and the water apportionment calculation in Table 4.

5.2.2. Quantifying the fraction of Ca^{2+} removal in the South Lagoon due to CaCO_3 formation

To further quantify the plausible magnitudes of Ca removal in the South Lagoon, due to local carbonate precipitation, we explore here two approaches or fractionation models that rely on Ca concentration and isotope data measured in the lagoon waters and precipitated CaCO_3 minerals based on data from Table 3.

5.2.2.1. Rayleigh and Equilibrium Ca isotope fractionation models.

Ca isotopes can be used to estimate the fraction of Ca^{2+} removed in the South Lagoon by CaCO_3 precipitation using Rayleigh and/or equilibrium models. These models assume a closed-system behavior of Ca isotopes in a reservoir, which is a reasonable approximation for the highly restricted hydrological setting of the South Lagoon.

To apply these models, one has to constrain the initial $\delta^{44/40}\text{Ca}$ value of the South Lagoon water, which assume no precipitation of CaCO_3 minerals, as a hypothetical starting point for the models. Such initial $\delta^{44/40}\text{Ca}$ can be calculated from theoretical mixing trends for Sr and Ca isotopes in South Lagoon, and the corresponding $^{87}\text{Sr}/^{86}\text{Sr}$ signature measured in the South Lagoon waters, as the latter is not expected to be impacted by carbonate precipitation (for details see Fig. 6). The two hypothetical mixing scenarios, LL-SW and GW-SW, are shown in Fig. 6, each yields very different initial $\delta^{44/40}\text{Ca}$ values: −0.05‰ for the LL-SW,

and −0.44‰ for the GW-SW mixing scenario. In the following calculations, we use both of these initial $\delta^{44/40}\text{Ca}$ values, to illustrate the range of plausible Ca^{2+} removal fractions in the South Lagoon.

The Rayleigh model assumes a finite pool of Ca in the South Lagoon where precipitated carbonate minerals (i.e., product) once formed would not interact with the seawater or lagoon water (i.e., reactant). In such a system, the fractionation of Ca isotopes between the reactant and product can be described by the Rayleigh distillation (Frings et al., 2016), according to the following equation:

$$\delta^{44/40}\text{Ca} = \left[\left(\delta^{44/40}\text{Ca}_{\text{INI}} + 10^3 \right) * \left(1 - f_{\text{CC}} \right)^{\alpha_{\text{CC/SW}} - 1} \right] - 10^3 \quad (4)$$

where $\delta^{44/40}\text{Ca}$ represents the isotope value of a residual unreacted Ca^{2+} pool in the lagoon waters; $\delta^{44/40}\text{Ca}_{\text{INI}}$ is the initial $\delta^{44/40}\text{Ca}$ value derived from Fig. 6; and f_{CC} represents the fraction of Ca that was removed from the measured lagoon waters (i.e., reactant) as CaCO_3 minerals (i.e., product), and solving Eq. (4) gives:

$$f_{\text{CC}} = 1 - \sqrt[\alpha_{\text{CC/SW}}]{\frac{\delta^{44/40}\text{Ca} + 10^3}{\delta^{44/40}\text{Ca}_{\text{INI}} + 10^3}} \quad (5)$$

finally, the parameter $\alpha_{\text{CC/SW}}$ is the Ca isotope fractionation factor between carbonate minerals (CC) and lagoon waters or seawaters (SW) (Frings et al., 2016), calculated by:

$$\alpha_{\text{CC/SW}} = \frac{1 + \frac{\delta^{44/40}\text{Ca}_{\text{CC}}}{1000}}{1 + \frac{\delta^{44/40}\text{Ca}_{\text{MIX}}}{1000}} = \frac{1000 + \delta^{44/40}\text{Ca}_{\text{CC}}}{1000 + \delta^{44/40}\text{Ca}_{\text{MIX}}} \quad (6)$$

where $\delta^{44/40}\text{Ca}_{\text{CC}}$ is the Ca isotope value of the precipitated CaCO_3 mineral, and $\delta^{44/40}\text{Ca}_{\text{MIX}}$ refers to the lagoon water (+0.2‰). According to Gussone et al. (2005), and taking into account the average water temperature in Coorong lagoons of $\sim 17.5^\circ\text{C}$, the $\delta^{44/40}\text{Ca}_{\text{CC}}$ for two CaCO_3 polymorphs of aragonite and calcite would be −1.65‰ and −0.75‰, respectively. These give the $\alpha_{\text{CC/SW}}$ values of ~ 0.9984 for aragonite and ~ 0.9993 for calcite. Based on our isotope measurements of the sediment crust sample (CLS-1) from the South Lagoon, the difference between $\delta^{44/40}\text{Ca}$ of the sediment sample (−1.16‰) and the lagoon waters (+0.20‰) is −1.36‰. This in turn, corresponds to an $\alpha_{\text{CC/SW}}$ value of ~ 0.9986 , in agreement with the predominant aragonite precipitation.

The equilibrium model, on the other hand, describes a system with a finite pool of Ca in which the reactant and products interact and exchange Ca isotopes as carbonates are precipitated (Frings et al., 2016). In this case, the following expression applies for the calculation of the $\delta^{44/40}\text{Ca}$ value in lagoon water as a function of changing f_{CC} parameter (cf., Sigman et al., 2009; Frings et al., 2016):

$$\delta^{44/40}\text{Ca} = \delta^{44/40}\text{Ca}_{\text{INI}} + \varepsilon * f_{\text{CC}} \quad (7)$$

where ε is the fractionation isotope effect, which is related to the abovementioned $\alpha_{\text{CC/SW}}$ based on the following equation:

$$\varepsilon = -10^3 * (\alpha_{\text{CC/SW}} - 1) \quad (8)$$

Accordingly, the f_{CC} can be calculated based on:

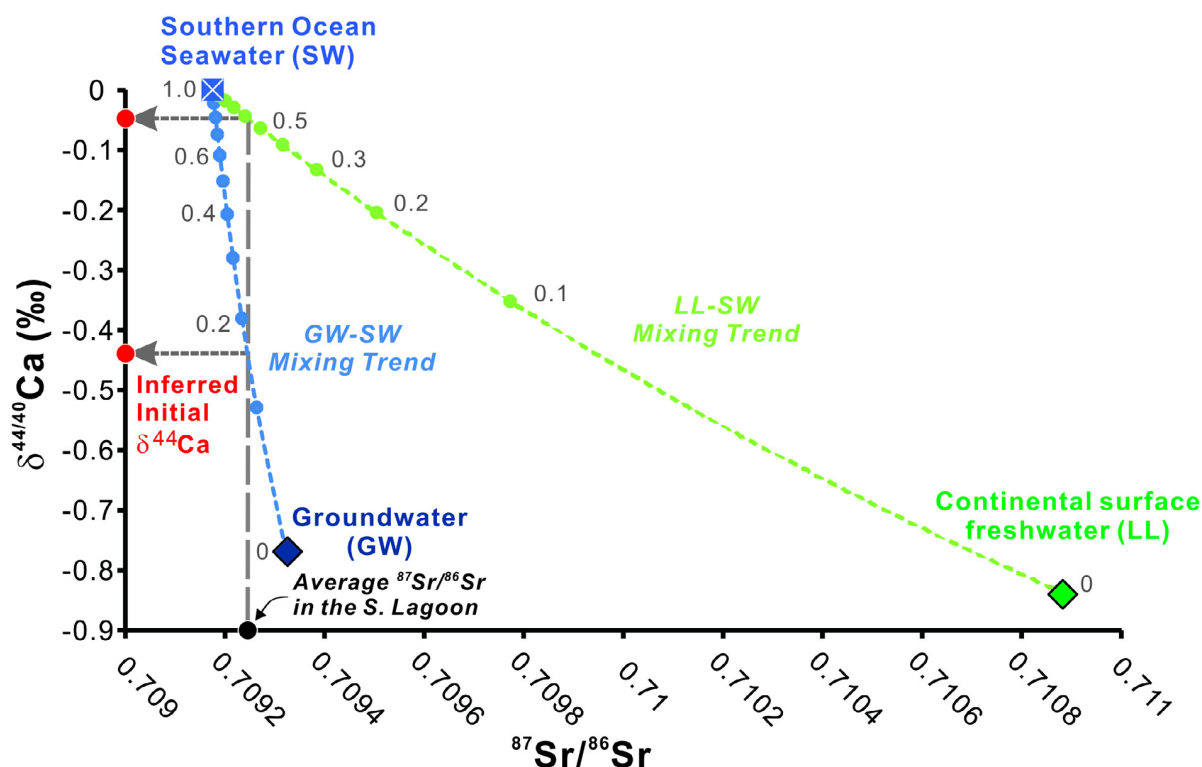


Fig. 6. Theoretical mixing trends for $\delta^{44/40}\text{Ca}$ and $^{87}\text{Sr}/^{86}\text{Sr}$ tracers in the Coorong, calculated for the following end-members: normal seawater (SW), groundwater (GW), and the continental surface freshwater represented by the Lower Lakes water (LL), assuming no evaporation and/or additional carbonate formation in the system. Note that the numbers next to circles represent the calculated fractions of seawater (F_{SW}) in the mixtures; and red circles illustrate the expected 'initial' $\delta^{44/40}\text{Ca}$ of the South Lagoon waters for GW-SW and LL-SW scenarios (based on $^{87}\text{Sr}/^{86}\text{Sr}$ constraints), not impacted by additional carbonate precipitation in the lagoon. (For interpretation of the references to colour in this figure legend, the reader is referred to the web version of this article.)

$$f_{\text{CC}} = \frac{\delta^{44/40}\text{Ca} - \delta^{44/40}\text{Ca}_{\text{INI}}}{-10^3 * (\alpha_{\text{CC/SW}} - 1)} \quad (9)$$

Considering the GW-SW and LL-SW mixing scenarios, the modeled evolution curves for $\delta^{44/40}\text{Ca}$ in the South Lagoon waters based on the two Ca isotope fractionation models above are illustrated in Fig. 7. Based on the measured $\delta^{44/40}\text{Ca}$ of the hypersaline South Lagoon waters (+0.2‰) and the fact that aragonite is the major carbonate precipitate, the calculated fractions of Ca^{2+} removed in the South Lagoon as CaCO_3 (as aragonite) range from ~15% and ~45% (Fig. 7). These estimates are also in general agreement with mass balance calculations based on Ca concentration and salinity and constraints from the carbonate alkalinity of local lagoon waters (see Appendix, Section B.4). Importantly, these supplementary calculations suggest that a more realistic fraction is actually closer to ~15% (rather than 45%), thus points to the importance of LL-SW mixing, or continental freshwater inputs into the South Lagoon.

5.2.3. The local carbon cycling in the Coorong

The quantification of Ca^{2+} removal in the Coorong has also implications for the local carbon cycling, as our data suggest that the hypersaline South Lagoon acts as a sink for the dissolved inorganic carbon (DIC) present in the

lagoon waters, based on the simplified equation for the marine carbonate formation:



Taking the buffering capacity of seawater or seawater-like solutions (Zeebe and Wolf-Gladrow, 2001) into consideration, a large proportion of this liberated CO_2 is actually converted to bicarbonate (HCO_3^-). Specifically, under typical surface ocean conditions that are in contact with the present-day atmospheric CO_2 pressure, the precipitation of 1 mol of CaCO_3 yields only about 0.6 mol of CO_2 (Ware et al., 1992; Elderfield, 2006), with remaining C being converted to dissolved C species (0.4 mol as HCO_3^-), and therefore not released into the atmosphere. Thus, if applicable to the Coorong, this would suggest that with each mole of dissolved Ca^{2+} that is removed as aragonite and/or calcite approximately 1.4 mols of carbon is also fixed in the system (i.e., 1 mol of C in CaCO_3 mineral, and ~0.4 mol of C in the produced HCO_3^- species), with remaining ~0.6 mol being outgassed as CO_2 from the lagoon into the atmosphere. Overall, these theoretical constraints coupled with our Ca isotope data suggest that the South Lagoon acts as a net sink for the dissolved inorganic carbon due to the locally enhanced precipitation of CaCO_3 minerals in the hypersaline and carbonate-oversaturated lagoon waters.

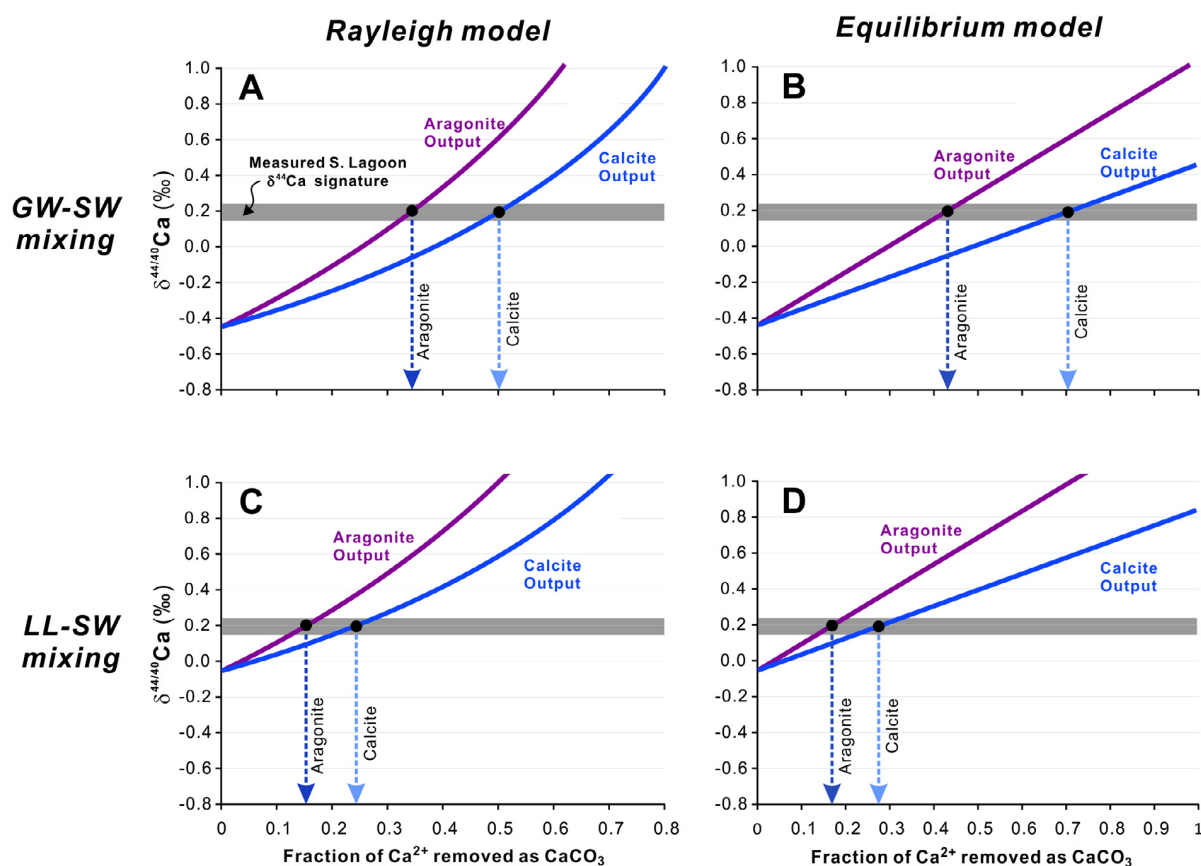


Fig. 7. The groundwater-seawater (GW-SW) and continental surface freshwater-seawater (LL-SW) mixing scenarios for the quantification of Ca^{2+} removal and carbonate output in the South Lagoon: (A) (C) The *Rayleigh model* for Ca isotopes in lagoon waters, driven by increasing carbonate precipitation in the South Lagoon, assuming no interaction between precipitated carbonate (i.e. product) and lagoon waters (i.e., reactant), modeled for *aragonite* and *calcite* carbonate outputs. (B) (D) The *equilibrium model* for the South Lagoon, assuming an exchange and interactions between the product (CaCO_3) and reactant (lagoon waters), modeled for both *aragonite* and *calcite* scenarios. The gray band represents the observed $\delta^{44/40}\text{Ca}$ in the South Lagoon waters.

5.3. Fish migration and otoliths biomineralisation: Insights from Ca and Sr isotopes

5.3.1. $^{87}\text{Sr}/^{86}\text{Sr}$ in otoliths: A time-integrated signature of local water masses?

$^{87}\text{Sr}/^{86}\text{Sr}$ in fish otoliths of migratory species are interpreted as historical records of the movement of individual fish (Chesney et al., 1998; Brennan et al., 2015a, 2015b). As for less mobile species such as *A. microstoma* in the Coorong, the observed $^{87}\text{Sr}/^{86}\text{Sr}$ in otoliths relative to those measured in ambient lagoon waters (Fig. 2B) could be viewed as an integrated signal of the environmental history of local water masses over the entire lifespan of a fish (ca. 1 year period; see Gillanders and Munro, 2012; Wedderburn et al., 2014, and references therein). Accordingly, otolith data indicate that there is an overall higher input of continent-derived freshwater sources with higher $^{87}\text{Sr}/^{86}\text{Sr}$ into the North Lagoon, compared to our estimates that are based only on ‘snap-shot’ sampling of waters performed in 2015 and 2016. Alternatively, our otolith $^{87}\text{Sr}/^{86}\text{Sr}$ data might suggest that fish collected in the North Lagoon have

spent a significant portion of their life in the hypersaline South Lagoon with higher $^{87}\text{Sr}/^{86}\text{Sr}$, and moved to the North Lagoon waters where they were caught and sampled.

We tried to address these questions via micro-drilling selected otoliths for the Sr isotope analysis along the growth increments (i.e., core and edge $^{87}\text{Sr}/^{86}\text{Sr}$ record). Theoretically, the $^{87}\text{Sr}/^{86}\text{Sr}$ of core (i.e., juvenile part) and edge (i.e., more recent) of an otolith should reflect the local water composition of the years 2015 and 2016, respectively, given the fish sampled was large and old enough. However, the core and edge $^{87}\text{Sr}/^{86}\text{Sr}$ of the North Lagoon otolith is constantly higher than the local water, this points to some of the complexities of interpreting otolith $^{87}\text{Sr}/^{86}\text{Sr}$ records in terms of fish migration patterns. Nevertheless, the North Lagoon otolith shows a lower edge $^{87}\text{Sr}/^{86}\text{Sr}$ value than that of the otolith core, this trend matches the observed temporal decline in local water $^{87}\text{Sr}/^{86}\text{Sr}$ over one year (from 2015 to 2016). On the other hand, the core and edge $^{87}\text{Sr}/^{86}\text{Sr}$ pattern acquired from another larger otolith (sample C10-03), collected from the South Lagoon, showed an opposite trend where the $^{87}\text{Sr}/^{86}\text{Sr}$ value from the edge is higher than

the core (see Fig. 2B), perhaps suggesting that the former was inherited from the highly radiogenic waters present at the southern-most end of the lagoon.

5.3.2. $\delta^{44/40}\text{Ca}$ in otoliths: The role of ‘kinetics’ and biomineralisation

The lack of correlation between the $\delta^{44/40}\text{Ca}$ of otoliths and local lagoon waters indicates that biomineralisation processes rather than water mixing and/or fish migration are primarily responsible for the otoliths’ Ca isotope composition. However, as light Ca isotopes are preferentially incorporated during otolith biomineralisation, the $\delta^{44/40}\text{Ca}$ of otoliths might be potentially used to infer changes in otoliths growth rates. To better visualise the fractionation of Ca isotopes in the otoliths relative to ambient lagoon waters, the fractionation factor Δ is used here, and this parameter reflects the difference between $\delta^{44/40}\text{Ca}$ of otolith and local waters at the same sampling site. In Fig. 8, we plot the Ca isotope fractionation factor, Δ (otolith-water), as a function of the fish size parameters, including (i) fish body length, and (ii) the otolith’s weight.

Otolith size is proportional to fish body length ($R^2 = 0.8914$, $p < 0.05$) (Fig. 8A), but data also indicate the large (more mature) fish yield smaller fractionations (i.e. less negative Δ) in otoliths. In contrast, small (juvenile) fish yielded larger fractionations (i.e. more negative Δ) ($R^2 = 0.44$, $p < 0.08$, $n = 10$) (Fig. 8B and C). This correlation between the fish/otolith size (or weight) and the Δ values likely reflect kinetic Ca isotope fractionation effects, where juvenile fish otoliths grows at faster rates during early life stages, thus preferentially incorporating lighter Ca isotopes, therefore producing larger isotope fractionations (Tang et al., 2008; Fantle and Tipper, 2014; AlKhatib and Eisenhauer, 2017).

Although further validation is required, our $\delta^{44/40}\text{Ca}$ data from otoliths suggest an overall strong biological control related to growth rate effects. As elemental/Ca concentration patterns in fish otoliths are also related to the latter biological processes (Grønkvær, 2016; Izzo et al., 2018), future Ca isotopes studies coupled with elemental proxies might help to differentiate signals originating from (i) biological processes (i.e., changes in growth or precipitation rates of otoliths), and those imparted by (ii) distinct water

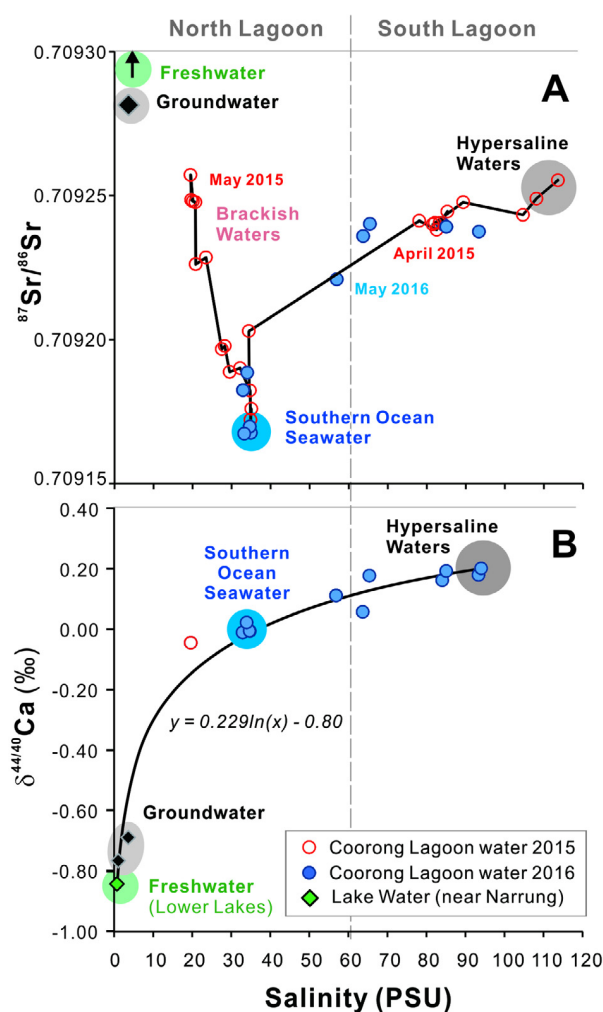


Fig. 9. Summary charts illustrating water mixing trends in the Coorong hydrological system: (A) $^{87}\text{Sr}/^{86}\text{Sr}$ versus salinity plot showing the main end-members and water sources; note that the Lower Lake and River Murray samples were too high to be plotted on the scale. (B) $\delta^{44/40}\text{Ca}$ versus salinity plot for the main end-members and studied water samples. The three colored circles represent the main end-member or water sources: (i) the local groundwater, (ii) normal seawater, and (iii) hypersaline lagoon waters.

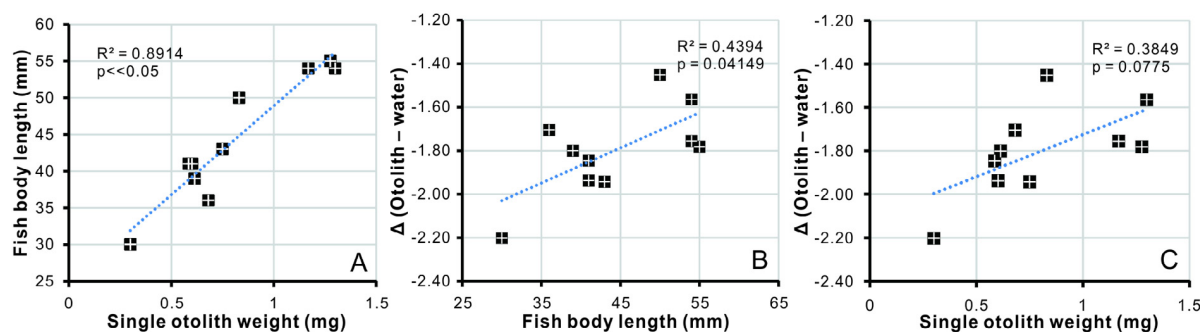


Fig. 8. Correlations of fish size parameters (i.e. fish body length and single otoliths weight) with otoliths $\delta^{44/40}\text{Ca}$ values: (A) Fish body length vs. single otoliths weight; (B) Fractionation factor Δ of $\delta^{44/40}\text{Ca}$ between otoliths and lagoon water of the same sampling site vs. fish body lengths; (C) Fractionation factor Δ vs. single otoliths weight. In chart (B) and (C), $\delta^{44/40}\text{Ca}$ for sites C07, C08 and C09 in South Lagoon were estimated by linear interpolation of $\delta^{44/40}\text{Ca}$ values measured in waters from the most proximal sites, and Δ values were then calculated.

masses with unique elemental and isotope signatures (i.e., fish migration signal).

5.4. Implications for paleo-salinity reconstructions of lagoon-estuarine environments based on coupled $^{87}\text{Sr}/^{86}\text{Sr}$ and $\delta^{44/40}\text{Ca}$

To illustrate the potential of the above isotope proxies for paleo-studies, we plot here $^{87}\text{Sr}/^{86}\text{Sr}$ and $\delta^{44/40}\text{Ca}$ of waters against their respective salinities (from 0 to ~120 PSU, Fig. 9). This approach shows the potential and limitations of these isotope proxies for paleo-salinity studies of the Coorong, Lower Lakes, and Murray Mouth Estuary.

As shown in Fig. 9A, the Coorong have three major water components, which are (i) normal marine waters, (ii) fresh/brackish waters, and (iii) the chemically/isotopically evolved hypersaline lagoon waters, the last type was present primarily in the South Lagoon. Solely based on $^{87}\text{Sr}/^{86}\text{Sr}$, one can distinguish less radiogenic ‘normal marine waters’ from more radiogenic waters impacted by continental water sources. However, the Sr isotope data cannot distinguish between the brackish and the hypersaline lagoon waters, as both yielded equally high $^{87}\text{Sr}/^{86}\text{Sr}$, plot above the typical Southern Ocean seawater (Fig. 9A). Importantly, this inability of Sr isotopes, can be resolved with the application of $\delta^{44/40}\text{Ca}$ (Fig. 9B), because the hypersaline waters have systematically positive $\delta^{44/40}\text{Ca}$ of up to $+0.20\text{‰}$, compared to normal seawater ($0.00 \pm 0.05\text{‰}$), while the freshwater sources yielded very negative $\delta^{44/40}\text{Ca}$ as low as $-0.84 \pm 0.03\text{‰}$ (Fig. 9B).

Thus, with analyses in suitable carbonate archives, a multi-proxy approach combining both $^{87}\text{Sr}/^{86}\text{Sr}$ and $\delta^{44/40}\text{Ca}$ tracers can be used to reconstruct paleo-salinity changes in the Coorong over geological time. Moreover, this approach should be generally applicable to other carbonate-producing coastal lagoon-estuarine environments and their salinity reconstructions.

6. CONCLUSIONS

The Sr and Ca isotopes applied in this study illustrate that the Coorong hydrological system has three major water components, including: (i) local freshwaters (i.e., River Murray and groundwater), (ii) the Southern Ocean seawater, and (iii) hypersaline lagoon waters, the latter additionally modified by ongoing evaporation, and in-situ carbonate precipitation.

The $\delta^{44/40}\text{Ca}$, $^{87}\text{Sr}/^{86}\text{Sr}$ and salinity data from the North Lagoon waters are basically indistinguishable from those in the Southern Ocean (i.e., normal seawater), with the exception of transient freshwater input events, such as the one documented in May 2015. The latter had caused a shift to more brackish salinity (~20 PSU) in parts of the lagoon, which based on our isotope constraints was a consequence of ‘trapped’ barrage outflow sourced from the Lower Lakes, with some although minor contributions from local groundwater. Interestingly, the South Lagoon hypersaline waters are much more complex in terms of their origins and mixing histories, and our mass balance constraints showed that they are basically highly evaporated brackish

waters (with $\geq 40\%$ contribution from originally continent-derived waters), and their chemistries have been additionally modified via ongoing carbonate precipitation. These processes, i.e., the CaCO_3 formation and inputs of continent-derived Sr, have led to a systematic shift of the South Lagoon waters to higher $\delta^{44/40}\text{Ca}$ and $^{87}\text{Sr}/^{86}\text{Sr}$ values relative to the Southern Ocean seawater. Based on the Ca isotope constraints (i.e., *Rayleigh* and *equilibrium* models), the plausible fraction of the Ca removed in the South Lagoon due to in-situ carbonate precipitation (mostly as aragonite) is about 15–17% of the original Ca pool present in the lagoon. This in turn has implications for the blue carbon studies and local C cycling in the South Lagoon, suggesting that the latter acts as a net sink for the dissolved inorganic carbon (DIC), due to the ongoing CaCO_3 formation.

Ca isotope data from smallmouth hardyhead (*Atherinosoma microstoma*), indicate that $\delta^{44/40}\text{Ca}$ in otoliths is primarily controlled by biological process (i.e., the kinetic growth rate effects). Thus future Ca isotopes studies on otoliths coupled with trace-element data might help to differentiate ‘signals’ originating from (i) biological processes (i.e., changes in growth rates of otoliths), and those imparted by (ii) distinct water masses with unique elemental and isotope signatures (i.e., fish migration signal). Additionally, the $^{87}\text{Sr}/^{86}\text{Sr}$ record of otoliths confirmed the importance of continent-derived water sources to the Coorong over the life span of the fish.

Overall, our calibration of $^{87}\text{Sr}/^{86}\text{Sr}$ and $\delta^{44/40}\text{Ca}$ based on two sets of data mainly from 2015 and 2016 proxies provides spatial variations of water chemistry in the modern Coorong hydrological system, with respect to salinity and CaCO_3 saturation. Further studies focusing on temporal variations are necessary for a more complete understanding of the modern hydrology of Coorong. Nevertheless, such multi-proxy approach combining Sr and Ca isotopes measured in suitable fossil carbonate archives (e.g., bivalve shells, foraminifera) could potentially be used to (i) trace and apportion different water sources, (ii) quantify local carbonate output, and/or (ii) to reconstruct paleo-salinity changes at our study site, or other carbonate-producing lagoon-estuarine environments.

ACKNOWLEDGMENTS

This project was supported by the Czech Science Foundation (GACR grant No. 17-18120S), the Environment Institute and a start-up grant of the University of Adelaide to JF; and via the Australian Research Council to BMG (ARC grant No. DP110100716, FT100100767). Additional support from the Base-Line Earth project (grant No. 643084) funded by European Commission via the Marie Curie (ITN MC) grant under Horizon 2020 program, and the ARC Linkage project (ARC grant No. LP160101353) are also acknowledged. Fundação para a Ciência e Tecnologia via UID/MAR/04292/2013 and the SFRH/BPD/95784/2013 grant awarded to PRS also supported this work. This study is part of the Ph.D. research of YS, supported by Adelaide Graduate Research Scholarship and the CRC Landscape Environments and Mineral

Exploration (LEME) Regolith Science Supplementary Scholarship (year 2018).

The sampling in the Coorong National Park was performed under the Department for Environment, Water and Natural Resources (DEWNR) research permit No. Q26018-5. The water quality data provided by the DEWNR is gratefully acknowledged. Technical and laboratory assistance of David Bruce and Tony Hall at University of Adelaide is greatly appreciated, especially regarding the training sessions, and the maintenance of TIMS and clean laboratory facilities. We also thank Aoife McFadden for her assistance with the elemental analyses by ICP-MS at the Adelaide Microscopy Centre. Finally, Prof. Justin Brookes at the University of Adelaide is acknowledged for his assistance with obtaining water samples in the North Lagoon.

REFERENCES

- AlKhatib M. and Eisenhauer A. (2017) Calcium and strontium isotope fractionation during precipitation from aqueous solutions as a function of temperature and reaction rate; II. Aragonite. *Geochim. Cosmochim. Acta* **209**, 320–342.
- Anadón P., Gliozzi E. and Mazzini I. (2002) Paleoenvironmental reconstruction of marginal marine environments from combined paleoecological and geochemical analyses on ostracods. *Geophys. Monograph-Am. Geophys. Union* **131**, 227–248.
- Australian Water Environments, Ecological Associates and GHD Pty Ltd. (2011). Environmental water delivery: River Murray—Coorong, Lower Lakes and main channel below Lock 1. Prepared for Commonwealth Environmental Water, Department of Sustainability, Environment, Water, Population and Communities. ISBN: 978-1-921733-37-6.
- Barnett, S. (2015) Assessment of the groundwater resources in the non-prescribed areas of the South Australian Murray-Darling Basin, DEWNR Technical report 2015/09, Government of South Australia, Department of Environment, Water and Natural Resources, Adelaide. ISBN: 978-1-922255-47-1.
- Baskaran M. (2012) *Handbook of Environmental Isotope Geochemistry*. Springer, Heidelberg, p. 951, Springer-Verlag, Berlin. ISBN: 3642106366.
- Brennan S. R., Fernandez D. P., Zimmerman C. E., Cerling T. E., Brown R. J. and Wooller M. J. (2015a) Strontium isotopes in otoliths of a non-migratory fish (slimy sculpin): Implications for provenance studies. *Geochim. Cosmochim. Acta* **149**, 32–45.
- Brennan S. R., Zimmerman C. E., Fernandez D. P., Cerling T. E., McPhee M. V. and Wooller M. J. (2015b) Strontium isotopes delineate fine-scale natal origins and migration histories of Pacific salmon. *Sci. Adv.* **1**, e1400124.
- Cao Z., Siebert C., Hathorne E. C., Dai M. and Frank M. (2016) Constraining the oceanic barium cycle with stable barium isotopes. *Earth Planet. Sci. Lett.* **434**, 1–9.
- Chesney E. J., McKee B. M., Blanchard T. and Chan L. H. (1998) Chemistry of otoliths from juvenile menhaden Brevoortia patronus: evaluating strontium, strontium: calcium and strontium isotope ratios as environmental indicators. *Mar. Ecol. Prog. Ser.*, 261–273.
- Dickin A. P. (2005) *Radiogenic Isotope Geology*. Cambridge University Press, p. 508, ISBN 0521823161.
- Elderfield H. (2006) *The oceans and Marine Geochemistry, Vol. 6, Treatise on Geochemistry*. Elsevier-Perigamon, Oxford.
- Fantle M. S. and DePaolo D. J. (2007) Ca isotopes in carbonate sediment and pore fluid from ODP Site 807A: the Ca 2+(aq)-calcite equilibrium fractionation factor and calcite recrystallization rates in Pleistocene sediments. *Geochim. Cosmochim. Acta* **71**, 2524–2546.
- Fantle M. S. and Tipper E. T. (2014) Calcium isotopes in the global biogeochemical Ca cycle: Implications for development of a Ca isotope proxy. *Earth Sci. Rev.* **129**, 148–177.
- Fantle M. S. (2015) Calcium isotopic evidence for rapid recrystallization of bulk marine carbonates and implications for geochemical proxies. *Geochim. Cosmochim. Acta* **148**, 378–401.
- Farkaš J., Déjeant A., Novák M. and Jacobsen S. B. (2011) Calcium isotope constraints on the uptake and sources of Ca²⁺ in a base-poor forest: a new concept of combining stable (^{844/42}Ca) and radiogenic (εCa) signals. *Geochim. Cosmochim. Acta* **75**, 7031–7046.
- Farkaš J., Frýda J. and Holmden C. (2016) Calcium isotope constraints on the marine carbon cycle and CaCO₃ deposition during the late Silurian (Ludfordian) positive δ¹³C excursion. *Earth Planet. Sci. Lett.* **451**, 31–40.
- Fernandes M. and Tanner J. E. (2009) Hypersalinity and phosphorus availability: the role of mineral precipitation in the Coorong lagoons of South Australia. *CSIRO Water for a Healthy Country*.
- Frank M. (2011) Geochemical proxies for ocean circulation and weathering inputs: Radiogenic isotopes of Nd, Pb, Sr, Hf, and Os. In *IOP Conf. Series: Earth and Environmental Science* **14**, 1–7. IOP Publishing. <https://doi.org/10.1088/1755-1315/14/1/012010>.
- Frings P. J., Clymans W., Fontorbe G., Christina L. and Conley D. (2016) The continental Si cycle and its impact on the ocean Si isotope budget. *Chem. Geol.* **425**, 12–36.
- Gemitzi A., Stefanopoulos K., Schmidt M. and Richnow H. H. (2014) Seawater intrusion into groundwater aquifer through a coastal lake-complex interaction characterised by water isotopes ²H and ¹⁸O. *Isot. Environ. Health Stud.* **50**, 74–87.
- Gillanders B. M. and Munro A. R. (2012) Hypersaline waters pose new challenges for reconstructing environmental histories of fish based on otolith chemistry. *Limnol. Oceanogr.* **57**, 1136.
- Grønkvær P. (2016) Otoliths as individual indicators: a reappraisal of the link between fish physiology and otolith characteristics. *Mar. Freshw. Res.* **67**, 881–888.
- Gussone N., Boehm F., Eisenhauer A., Dietzel M., Heuser A., Teichert B. M. and Dullo W. C. (2005) Calcium isotope fractionation in calcite and aragonite. *Geochim. Cosmochim. Acta* **69**, 4485–4494.
- Haese R. R., Gow L., Wallace L. and Brodie R. S. (2008) Identifying groundwater discharge in the Coorong (South Australia). *AUSGEO News* **91**, 1–6.
- Haese R. R., Wallace L. and Murray E. J. (2009) Nutrient sources, water quality, and biogeochemical processes in the Coorong, South Australia. *Geosci. Australia*.
- Harouaka K., Eisenhauer A. and Fantle M. (2014) Experimental investigation of Ca isotope fractionation during abiotic gypsum precipitation. *Geochim. Cosmochim. Acta* **129**, 157–176.
- Harouaka K., Mansor M., Macalady J. L. and Fantle M. S. (2016) Calcium isotopic fractionation in microbially mediated gypsum precipitates. *Geochim. Cosmochim. Acta* **184**, 114–131.
- Hendry J. P. and Kalin R. M. (1997) Are oxygen and carbon isotopes of mollusc shells reliable palaeosalinity indicators in marginal marine environments? A case study from the Middle Jurassic of England. *J. Geol. Soc.* **154**, 321–333.
- Holmden C., Creaser R. A. and Muehlenbachs K. (1997) Paleosalinities in ancient brackish water systems determined by ⁸⁷Sr/⁸⁶Sr ratios in carbonate fossils: A case study from the Western Canada Sedimentary Basin. *Geochim. Cosmochim. Acta* **61**, 2105–2118.

- Holmden C. and Hudson J. D. (2003) $^{87}\text{Sr}/^{86}\text{Sr}$ and Sr/Ca investigation of Jurassic molluscs from Scotland: Implications for paleosalinities and the Sr/Ca ratio of seawater. *Geol. Soc. Am. Bull.* **115**, 1249–1264.
- Holmden C. (2005) Measurement of $\delta^{44}\text{Ca}$ using a ^{43}Ca - ^{42}Ca double-spike TIMS technique. In Summary of Investigations 2005, Vol. 1, Saskatchewan Geological Survey, Sask. Industry Resources, Misc. Rep. 2005-1, CD-ROM, Paper A-4, 7p.
- Holmden C. and Bélanger N. (2010) Ca isotope cycling in a forested ecosystem. *Geochim. Cosmochim. Acta* **74**, 995–1015.
- Holmden C., Papanastassiou D. A., Blanchon P. and Evans S. (2012) $\delta^{44/40}\text{Ca}$ variability in shallow water carbonates and the impact of submarine groundwater discharge on Ca-cycling in marine environments. *Geochim. Cosmochim. Acta* **83**, 179–194.
- Izzo C., Reis-Santos P. and Gillanders B. M. (2018) Otolith chemistry does not just reflect environmental conditions: A meta-analytic evaluation. *Fish. Fish.* **1–14**. <https://doi.org/10.1111/faf.12264>.
- Kjerfve B. (1986) Comparative oceanography of coastal lagoons. In *Estuarine Variability* (ed. D. A. Wolf). Academic Press, New York, USA, pp. 63–81.
- Knoppers B. (1994) Aquatic primary production in coastal lagoons. *Elsevier Oceanography Ser.* **60**, 243–286.
- Krabbenhöft A., Fietzke J., Eisenhauer A., Liebetrau V., Böhm F. and Vollstaedt H. (2009) Determination of radiogenic and stable strontium isotope ratios ($^{87}\text{Sr}/^{86}\text{Sr}$; $\delta^{88/86}\text{Sr}$) by thermal ionization mass spectrometry applying an $^{87}\text{Sr}/^{84}\text{Sr}$ double spike. *J. Anal. At. Spectrom.* **24**, 1267–1271.
- Lamberty A. and Pauwels J. (1991) How to correct for blanks in isotope dilution mass spectrometry. *Int. J. Mass Spectrom. Ion Processes* **104**, 45–48.
- Lehn G. O., Jacobson A. D. and Holmden C. (2013) Precise analysis of Ca isotope ratios ($\delta^{44/40}\text{Ca}$) using an optimized ^{43}Ca - ^{42}Ca double-spike MC-TIMS method. *Int. J. Mass Spectrom.* **351**, 69–75.
- Lui L. C. (1969) Salinity tolerance and osmoregulation of Taeniomenbers microstomus (Gunther, 1861), (Pisces: Mugiliformes: Atherinidae) from Australian salt lakes. *Mar. Freshw. Res.* **20**, 157–162.
- Macreadie P. I., Serrano O., Maher D. T., Duarte C. M. and Beardall J. (2017) Addressing calcium carbonate cycling in blue carbon accounting. *Limnol. Oceanogr. Lett.* **2**, 195–201.
- Martin A. N., Dosseto A. and Kinsley L. P. (2015) Evaluating the removal of non-detrital matter from soils and sediment using uranium isotopes. *Chem. Geol.* **396**, 124–133.
- McKirdy D. M., Thorpe C. S., Haynes D. E., Grice K., Krull E. S., Halverson G. P. and Webster L. J. (2010) The biogeochemical evolution of the Coorong during the mid-to late Holocene: an elemental, isotopic and biomarker perspective. *Org. Geochem.* **41**, 96–110.
- Molsher R. L., Geddes M. C. and Paton D. C. (1994) Population and reproductive ecology of the small-mouthed hardyhead *Atherinosoma microstoma* (Günther) (Pisces: Atherinidae) along a salinity gradient in the Coorong, South Australia. *Trans. Royal Soc. South Australia* **118**, 207–216.
- Mosley L. M. (2016) *Barrage Release Optimisation Trial August 2015: Assessment of Environmental Outcomes and Achievement of Management Objectives*. University of Adelaide, South Australia.
- Mosley L. M., Hamilton B., Busch B., Hipsey M. and Taylor B. (2017) Assessment and modelling of the effects of the 2013–2016 Morella Basin releases on Coorong water quality. Report to the Department of Environment, Water and Natural Resources (DEWNR). University of Adelaide, South Australia.
- Parkhurst D. L. and Appelo C. A. J. (2013) Description of input and examples for PHREEQC version 3: a computer program for speciation, batch-reaction, one-dimensional transport, and inverse geochemical calculations. U.S. Geological Survey Techniques and Methods, book 6, chap. A43, p. 497; Available at <http://pubs.usgs.gov/tm/06/a43>.
- Patterson W. P. and Walter L. M. (1994) Depletion of ^{13}C in seawater ΣCO_2 on modern carbonate platforms: Significance for the carbon isotopic record of carbonates. *Geology* **22**, 885–888.
- Patterson W. P. (1999) Oldest isotopically characterized fish otoliths provide insight to Jurassic continental climate of Europe. *Geology* **27**, 199–202.
- Petersen S. V., Tabor C. R., Lohmann K. C., Poulsen C. J., Meyer K. W., Carpenter S. J., Erickson J. M., Matsunaga K. K., Smith S. Y. and Sheldon N. D. (2016) Temperature and salinity of the Late Cretaceous Western Interior Seaway. *Geology* **44**, 903–906.
- Phillips B. and Muller K. (2006) Ecological character of the Coorong, Lakes Alexandrina and Albert wetland of international importance. Department for Environment and Heritage.
- Reid R. J. and Mosley L. M. (2016) Comparative contributions of solution geochemistry, microbial metabolism and aquatic photosynthesis to the development of high pH in ephemeral wetlands in South East Australia. *Sci. Total Environ.* **542**, 334–343.
- Romaniello S., Field M., Smith H., Gordon G., Kim M. and Anbar A. D. (2015) Fully automated chromatographic purification of Sr and Ca for isotopic analysis. *J. Anal. At. Spectrom.* **30**, 1906–1912.
- Scheiderich K., Amini M., Holmden C. and Francois R. (2015) Global variability of chromium isotopes in seawater demonstrated by Pacific, Atlantic, and Arctic Ocean samples. *Earth Planet. Sci. Lett.* **423**, 87–97.
- Schreiner W. N. (1995) A standard test method for the determination of RIR values by X-ray diffraction. *Powder Diffr.* **10**, 25–33.
- Sigman, D. M., Karsh, K. L. and Casciotti, K. L. (2009) Ocean process tracers: nitrogen isotopes in the Ocean. In *Encyclopedia of Ocean Sciences 2nd Ed* (eds. J. H. Steele, K. K. Turekian and S. A. Thorpe). Elsevier ScienceDirect, Amsterdam. <https://doi.org/10.1016/B978-012374473-9.00632-9>.
- Tan F. C. and Hudson J. D. (1974) Isotopic studies on the palaeoecology and diagenesis of the Great Estuarine Series (Jurassic) of Scotland. *Scott. J. Geol.* **10**, 91–128.
- Tang J., Dietzel M., Böhm F., Köhler S. J. and Eisenhauer A. (2008) $\text{Sr}^{2+}/\text{Ca}^{2+}$ and $^{44}\text{Ca}/^{40}\text{Ca}$ fractionation during inorganic calcite formation: II. Ca isotopes. *Geochim. Cosmochim. Acta* **72**, 3733–3745.
- Teng F. Z., Dauphas N. and Watkins J. M. (2017) Non-traditional stable isotopes: retrospective and prospective. *Rev. Mineral. Geochem.* **82**, 1–26.
- Von der Borch C. C. (1962) Sedimentary carbonate deposits of the Coorong area, South Australia (Doctoral dissertation).
- Von der Borch C. C., Lock D. E. and Schwebel D. (1975) Groundwater formation of dolomite in the Coorong region of South Australia. *Geology* **3**, 283–285.
- Ware J. R., Smith S. V. and Reaka-Kudla M. L. (1992) Coral reefs: sources and sinks of atmospheric CO_2 ? *Coral Reefs* **11**, 127–130.
- Webster I. T. (2010) The hydrodynamics and salinity regime of a coastal lagoon—The Coorong, Australia—Seasonal to multi-decadal timescales. *Estuar. Coast. Shelf Sci.* **90**, 264–274.
- Wedderburn S. D., Walker K. F. and Zampatti B. P. (2007) Habitat separation of *Craterocephalus* (Atherinidae) species and populations in off-channel areas of the lower River Murray, Australia. *Ecol. Freshw. Fish* **16**, 442–449.

- Wedderburn S. D., Walker K. F. and Zampatti B. P. (2008) Salinity may cause fragmentation of hardyhead (Teleostei: Atherinidae) populations in the River Murray, Australia. *Mar. Freshw. Res.* **59**, 254–258.
- Wedderburn S. D., Barnes T. C. and Hillyard K. A. (2014) Shifts in fish assemblages indicate failed recovery of threatened species following prolonged drought in terminating lakes of the Murray-Darling Basin, Australia. *Hydrobiologica* **730**, 179–190.
- Wiederhold J. (2015) Metal stable isotope signatures as tracers in environmental geochemistry. *Environ. Sci. Technol.* **49**, 2606–2624.
- Wierzbowski H. and Joachimski M. (2007) Reconstruction of late Bajocian-Bathonian marine palaeoenvironments using carbon and oxygen isotope ratios of calcareous fossils from the Polish Jura Chain (central Poland). *Palaeogeogr. Palaeoclimatol. Palaeoecol.* **254**, 523–540.
- Zeebe R. and Wolf-Gladrow D. (2001) CO₂ in Seawater: Equilibrium, Kinetics, Isotopes. Elsevier Oceanography Series 65 Amsterdam, 346.

Associate editor: Andrew D. Jacobson



Impact of salinity and carbonate saturation on stable Sr isotopes ($\delta^{88/86}\text{Sr}$) in a lagoon-estuarine system

Yuexiao Shao^{a,*}, Juraj Farkaš^{a,b}, Luke Mosley^c, Jonathan Tyler^a, Henri Wong^d,
Briony Chamberlayne^a, Mark Raven^g, Moneesha Samanta^a, Chris Holmden^e,
Bronwyn M. Gillanders^c, Ana Kolevica^f, Anton Eisenhauer^f

^a Department of Earth Sciences, School of Physical Sciences, University of Adelaide, Australia

^b Department of Environmental Geosciences, Czech University of Life Sciences, Prague, Czech Republic

^c Department of Ecology and Evolutionary Biology, School of Biological Sciences, University of Adelaide, Australia

^d Australian Nuclear Science and Technology Organisation, Sydney, Australia

^e Department of Earth Sciences, University of Saskatchewan, Saskatoon, Canada

^f GEOMAR, Helmholtz Centre for Ocean Research Kiel, Wischhofstr, Germany

^g The Commonwealth Scientific and Industrial Research Organisation, Adelaide, Australia

Received 19 May 2020; accepted in revised form 13 November 2020; Available online 24 November 2020

Abstract

Local carbonate cycling in lagoon-estuarine systems, involving processes such as inorganic and biogenic carbonate precipitation/dissolution, represents an important but poorly constrained component of the coastal carbon budget. This study investigates the sensitivity of stable Sr isotope tracer ($\delta^{88/86}\text{Sr}$) with respect to carbonate saturation and salinity of local waters in the Coorong, Lower Lakes and Murray Mouth (CLLMM) estuary in South Australia. The CLLMM has an extensive range of salinity from fresh to hypersaline (from ~ 0 to over 100 PSU), with corresponding variations in water chemistry and major ion composition that in turn controls mineral saturation states, and thus CaCO_3 precipitation/dissolution in local waters. Here we use the novel $\delta^{88/86}\text{Sr}$ tracer in tandem with the more established radiogenic Sr isotope ratio ($^{87}\text{Sr}/^{86}\text{Sr}$), where the latter is a robust proxy for Sr sources and thus water provenance. We also produced a geochemical (PHREEQC) model of calcium carbonate (CaCO_3) saturation changes across this unique lagoon-estuarine system.

The results indicate a systematically increasing trend of $\delta^{88/86}\text{Sr}$ (from $\sim 0.25\text{‰}$ to $\sim 0.45\text{‰}$) with increasing salinity and CaCO_3 (aragonite, calcite) saturation indices of the coastal waters, which in turn suggest an overall control of carbonate dissolution/precipitation processes on the stable Sr isotope composition in the CLLMM system. This was further corroborated by Ca isotope data ($\delta^{44/40}\text{Ca}$) published previously on the same samples from the Coorong, as well as a quantitative simulation of local carbonate removal in the lagoon based on Rayleigh modelling and Sr isotope data.

Overall, our results confirm that a coupled Sr isotope approach (combining $^{87}\text{Sr}/^{86}\text{Sr}$ and $\delta^{88/86}\text{Sr}$) can be used to constrain not only the main water sources (continental versus marine Sr) but also local CaCO_3 dissolution/precipitation processes, and thus inorganic carbon and coastal carbonate cycling in the CLLMM system. Finally, this coupled $\delta^{88/86}\text{Sr}$ and $^{87}\text{Sr}/^{86}\text{Sr}$ approach can be potentially applied to fossil carbonate archives to reconstruct paleo-hydrology and salinity changes in the CLLMM and/or other carbonate-producing coastal systems.

© 2020 Elsevier Ltd. All rights reserved.

Keywords: Stable Sr isotopes; Lagoon-estuarine system; Carbonate saturation; Salinity; Water mixing; PHREEQC

* Corresponding author at: Room 46, Mawson Laboratories,
The University of Adelaide, North Terrace, SA 5005, Australia
E-mail address: yuexiao.shao@adelaide.edu.au (Y. Shao).

1. INTRODUCTION

Lagoon-estuarine systems represent unique coastal environments at the land-ocean interface that are ecologically important and highly productive, in particular for fisheries. Moreover, temperate and arid lagoon-estuarine systems are regarded as some of the most degraded ecosystems due to their susceptibility to salinisation and eutrophication from anthropogenic effects, as well as their sensitivity to climate change induced perturbations (Anthony et al., 2009; Glamore et al., 2016; Warwick et al., 2018). These dynamic environments typically involve complex interactions of hydrological, geochemical, and biological processes and water source mixing phenomena, resulting in variable salinities, mineral saturation states and chemical/isotopic composition. These in turn are critical parameters for the calcium carbonate (CaCO_3) cycling in marine and coastal regions, representing an important but currently poorly constrained component of the global carbon cycle, including the coastal 'blue carbon' budget (i.e., the carbon storage capacity of vegetated coastal systems, Macreadie et al., 2017). For instance, inorganic carbonate precipitation due to evaporation releases CO_2 to the atmosphere and increasing atmospheric CO_2 levels and exchange with surface waters leads to coastal ocean acidification and affects the local carbon storage (Zeebe and Wolf-Gladrow, 2001). Thus, detailed studies into C and CaCO_3 cycling in lagoon-estuarine systems, especially in arid environments, is of high importance and remains a priority.

Stable isotopes of elements such as H, C, N, O and S in the oceans, continental waters and/or sediment archives have been used successfully to trace the Earth's surface processes and to reconstruct paleo-environmental conditions in both marine and terrestrial systems (Hoefs, 2018 and references therein). However, to constrain the local CaCO_3 budget and carbonate precipitation/dissolution processes in coastal systems, more robust and direct tracers for inorganic C cycling are needed. Novel isotope tracers of alkali and alkaline earth metals such as stable calcium ($\delta^{44/40}\text{Ca}$) and magnesium ($\delta^{26}\text{Mg}$) isotopes have the potential to resolve and quantify some aspects of the marine carbonate cycle, and implications for the present and past Ca, Mg, and C budgets and elemental cycling in the oceans (Tipper et al., 2006; Farkaš et al., 2007; 2016; Holmden et al., 2012; de Souza et al., 2010; Chao et al., 2013, 2015; Shalev et al., 2018).

Strontium (Sr) is geochemically similar to calcium (Ca) with an identical charge (+2) and similar ionic radius (Finch and Allison, 2007; Menadakis et al., 2009; de Souza et al., 2010). As an indirect tracer of the oceanic Ca cycling and marine carbonate budget, the Sr isotopes offer a perspective that is different but complementary to that of Ca isotope studies. The most notable difference is the larger (and thus easier to measure) range in variations of the radiogenic Sr isotope (^{87}Sr) abundance in most terrestrial materials, compared to fairly limited radiogenic ^{40}Ca excess observed in natural waters and carbonates (Caro et al., 2010). Applications of the $^{87}\text{Sr}/^{86}\text{Sr}$ tracer for hydrological and ecosystem studies have thus been established for decades as a sensitive tool for investigations of

Sr provenance in both terrestrial and marine environments (Holmden et al., 1997; Capo et al., 1998; Bullen and Bailey, 2005; de Souza et al., 2010; Farkaš et al., 2011; Chao et al., 2013; 2015; Pearce et al., 2015). Modern seawater has a relatively homogeneous $^{87}\text{Sr}/^{86}\text{Sr}$ ratio (~ 0.7092) due to the long oceanic residence time of Sr in global oceans compared with the mixing time of seawater ($\sim 1\text{ka}$) (2.5 Ma, Hodell et al., 1990; Vollstaedt et al., 2014). However, at the interface between continental and marine environments, which is the subject of this study, the variation in seawater $^{87}\text{Sr}/^{86}\text{Sr}$ can be considerably larger, due to the release of radiogenic ^{87}Sr into coastal waters from the weathering of the continental crust (Kuznetsov et al., 2012).

Variations of stable Sr isotopes (expressed as $\delta^{88/86}\text{Sr}$) in marine and terrestrial Earth-surface environments can be used as a complementary isotope tracer to better constrain the global Sr cycle and its main input and output fluxes (Krabbenhöft et al., 2010; de Souza et al., 2010; Raddatz et al., 2013; Chao et al., 2013; 2015; Stevenson et al., 2014; Vollstaedt et al., 2014; Pearce et al., 2015; Fruchter et al., 2016). Carbonate minerals such as calcite and aragonite preferentially incorporate light isotopes of Sr and thus, their $\delta^{88/86}\text{Sr}$ values are lower than the dissolved Sr in the waters from which they formed (Krabbenhöft et al., 2009; Vollstaedt et al., 2014). Thus, carbonate precipitation in the oceans, coastal marine environments and/or lakes drives the $\delta^{88/86}\text{Sr}$ of seawater or local lagoon/lake waters to higher values, while carbonate dissolution has an opposite effect (Krabbenhöft et al., 2009; Fruchter et al., 2017). The stable Sr isotope variations resulting from these processes are quite small in nature, on the order of about 0.1–0.2 per mil (‰), which thus requires precise and accurate measurement of $\delta^{88/86}\text{Sr}$ (Andrews et al., 2016; Shalev et al., 2017; Fruchter et al., 2016 and, 2017).

Reconnaissance studies show that the stable Sr isotopes are fractionated by similar processes to those that fractionate Ca isotopes (Böhm et al., 2012; Stevenson et al., 2014; Vollstaedt et al., 2014; Fruchter et al., 2016; 2017). Therefore $\delta^{88/86}\text{Sr}$, similar to $\delta^{44/40}\text{Ca}$, can be also used to identify water sources, carbonate precipitation/dissolution or chemical kinetics of CaCO_3 formation in natural waters (cf., Krabbenhöft et al., 2009; Alkhatib and Eisenhauer, 2017), but with the advantage of simultaneously analysing the radiogenic ^{87}Sr component (i.e., $^{87}\text{Sr}/^{86}\text{Sr}$).

In this study, we present high-precision $\delta^{88/86}\text{Sr}$ measurements ($\pm 0.03\text{‰}$, 2SD) of waters and carbonates from a lagoon-estuarine system in South Australia – the Coorong, Lower Lakes and Murray Mouth (CLLMM) estuary (Fig. 1). In the CLLMM system, a wide variation in: (i) water salinity (from fresh to hypersaline), (ii) carbonate saturation states and (iii) redox conditions (from oxic to sub-oxic/anoxic) combine to create a 'natural laboratory' for testing the behaviour and sensitivity of geochemical and isotopic tracers to the above physico-chemical parameters of coastal waters. The main objective of this study is to calibrate and assess the sensitivity of the $\delta^{88/86}\text{Sr}$ tracer in the CLLMM to changes in salinity, carbonate saturation state, and CaCO_3 precipitation/dissolution; and to compare these findings to previous work done on stable Ca isotopes ($\delta^{44/40}\text{Ca}$) analysed in the same samples (see Shao et al.,

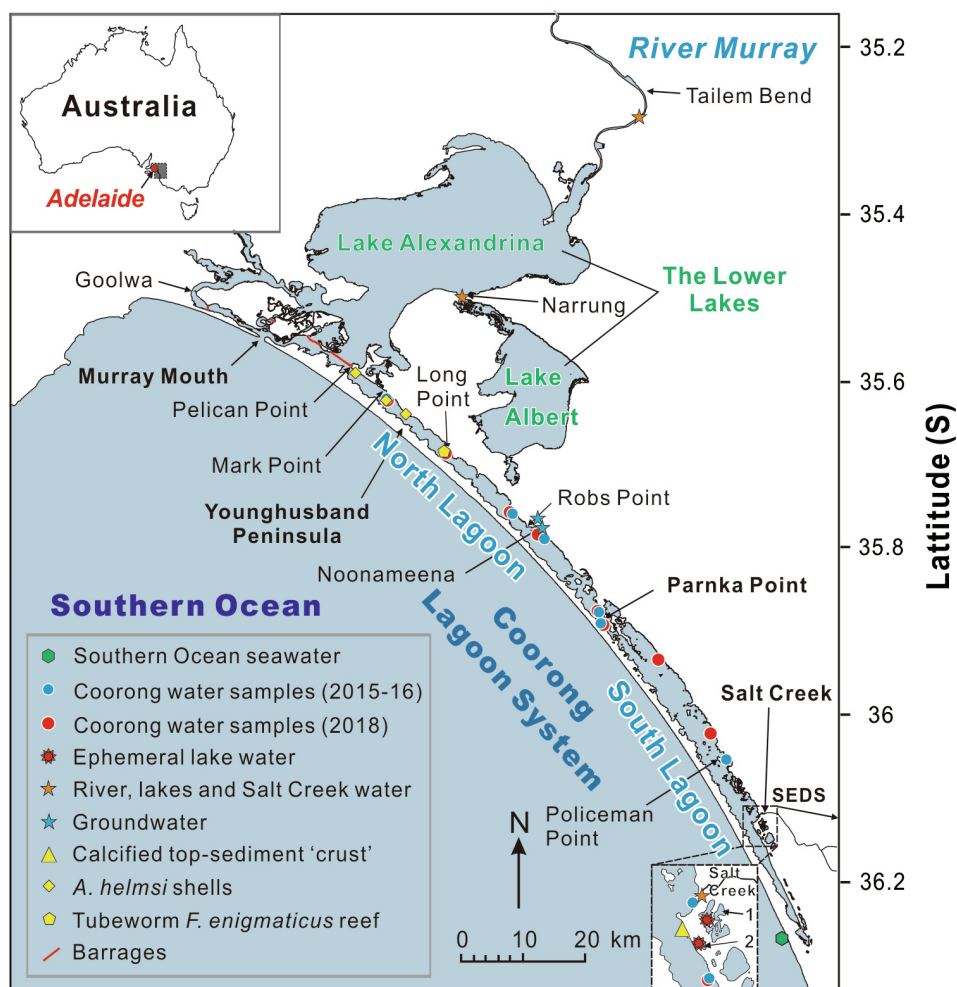


Fig. 1. Map of the Coorong, Lower Lakes and Murray Mouth (CLLMM) estuary with the representative sampling sites for waters and carbonates. The inset represents a magnified view near Salt Creek. Note that “1” = Milne Lake, and “2” = Halite Lake; coordinates and sampling dates for all samples analysed are listed in the Appendix (Tables A.1 and 2). SEDS = South East Drainage System.

2018). We also discuss the potential of a coupled $^{87}\text{Sr}/^{86}\text{Sr}$ and $\delta^{88/86}\text{Sr}$ approach for palaeo-hydrological and salinity reconstructions in the CLLMM and/or other coastal marine, lagoon and freshwater systems based on Sr isotope analysis of fossil carbonate archives.

2. STUDY AREA

The CLLMM forms a unique coastal system in South Australia (Fig. 1), located at the terminus of the River Murray and Murray-Darling Basin, which is Australia’s largest river system. Due to its specific geomorphology and hydrology, waters of the CLLMM range from freshwater (~ 0 PSU) to hypersaline (>100 PSU) (Gillanders and Munro, 2012), accompanied by ongoing CaCO_3 precipitation and seasonal groundwater discharge events (Haese et al., 2008; Fernandes and Tanner, 2009). These phenomena are particularly prominent in the Coorong, which is a semi-restricted and elongated lagoon that runs parallel to the coast of the Southern Ocean, divided at a narrow connection (i.e., Parnka Point) that separates the North and South Lagoons (Fig. 1). The North Lagoon receives water inputs from the

Southern Ocean via the Murray Mouth and occasionally also from the River Murray via the Lower Lakes, from which discharge is regulated by a series of barrages (Fig. 1). The South Lagoon is hydrologically more restricted compared to the North Lagoon, and in recent decades, the lagoon water has become increasingly hypersaline, ecologically impoverished, and locally anoxic due to reduced flow of freshwater from the South East Drainage System (SEDS) via Salt Creek (see Fig. 1) (Reeves et al., 2015; Brookes et al., 2018; Mosley et al., 2019). These environmental changes and habitat deterioration have hampered the establishment of benthic calcifying communities, such as bivalves and foraminifera that would normally produce biogenic carbonates in the South Lagoon. At present, it is more common to find biogenic carbonates in the North Lagoon where the salinity is lower (close to typical seawater), including bivalves, foraminifera and tubeworm species (Dittmann et al., 2009; Chamberlayne et al., 2019). In contrast, inorganic carbonate precipitates in the form of crusts and carbonate tufa are now commonly forming in the hypersaline South Lagoon (Haese et al., 2008), and these are predominantly composed of aragonite ($\sim 87\%$) and

calcite (~12%), complemented by minor occurrences of gypsum (~1%) (Von der Borch et al., 1975; Shao et al., 2018). Unlike abundant carbonate precipitation, the impact of gypsum formation on the Coorong water chemistry and its isotope composition is believed to be minor and transient, as gypsum precipitation in the South Lagoon is only evident during summer (i.e., December to February, in S. Hemisphere) when salinity is > 3.5 times that of normal seawater (i.e., >120 PSU, see Lazar et al., 1983; Fernandes and Tanner, 2009).

3. MATERIAL AND METHODS

3.1. Sample description

In this study, samples were divided into groups 1 to 3 according to time of collection and analytical purposes (Fig. 1).

Group 1 originates from the previous study of Shao et al. (2018), including Coorong lagoon waters (n = 8), Lower Lakes waters (n = 1) and local groundwaters (n = 2) all collected in 2015 and 2016, and a sample of calcified aragonitic top-sediment crust collected in 2017. All these water samples were previously measured for major/trace element concentrations and stable Ca isotopes ($\delta^{44/40}\text{Ca}$), and the sediment crust sample was analysed for mineralogy via X-ray diffraction (XRD), (data from Shao et al., 2018).

Group 2 consists of newly collected samples, including waters from the River Murray (n = 1), Salt Creek (n = 1) and two ephemeral lakes (Milne Lake and Halite Lake; n = 2), which were all collected in August 2018 (for details see Fig. 1). Biogenic carbonate samples from the North Lagoon include (i) *Arthritica helmsi* bivalve shell samples (n = 3) collected alive in January and May 2018 (Fig. B.2 in the Appendix), and (ii) a sample of carbonate precipitates produced by the tubeworm *Ficopomatus enigmaticus*, which typically forms small ‘reefs’ or colonies, collected near Long Point in August 2018 (Fig. B.3 in the Appendix). *A. helmsi* is an aragonitic micro bivalve that is short-lived with a lifespan of ca. 1 year (Dittmann et al., 2009; Chamberlayne et al., 2019). The Serpulid tubeworms (*F. enigmaticus*), which produces calcitic skeletal carbonates (see XRD analysis in Table B.5, Appendix B.3), is believed to be an invasive species that is currently found in the North Lagoon all year round with a natural lifespan of ca. 20–24 months (Dittmann et al., 2009).

Group 3 consists of water samples (n = 12) collected from the CLLMM in May 2018; data from these water samples were used for PHREEQC modelling of mineral saturation states. Sample site information and locations for all the above samples of waters and carbonates are listed in Appendix A (see Tables A.1 and 2).

3.2. Field measurements and sample preparation of waters and carbonates

For water samples collected in 2018 (i.e., Groups 2 and 3), temperature and salinity were measured in the field

using a YSI ProDSS multi-parameter water quality meter, with location recorded by GPS at each sampling site (Tables A.1 and 2, Appendix A). The water samples were filtered through 0.45 μm cellulose nitrate membrane filters to remove particulate matter and other impurities, and the filtered waters were refrigerated at 4 °C and stored in acid-cleaned HDPE bottles before alkalinity, elemental concentrations and isotopic analyses were undertaken. For pH measurements, unfiltered water samples were collected simultaneously in acid-cleaned HDPE bottles with minimum headspace to avoid creation of air bubbles and loss of CO_2 , and samples were stored and refrigerated at 4 °C before pH measurements.

The dried, powdered and homogenised calcified sediment crust (CLS-1) and tubeworm carbonate reef (CW2w) were analysed for mineralogy via XRD with a PANalytical X’Pert Pro Multi-purpose Diffractometer as described in Appendix B.4. Afterwards, the powdered samples were reacted with 0.5 M acetic acid in a Teflon vial on a hotplate at 45 °C for 24 hours to dissolve the carbonate fraction (Palchan et al., 2013), which was used for subsequent elemental and isotope analyses after centrifugation. A total of 5 to 10 shells from living specimens of *A. helmsi* (Sample IDs: 122 s, 149 s and 151 s) were collected and extracted from top sediments from the North Lagoon (see Table A.1 in the Appendix for sample locations). Shells were then rinsed with DI water, cleaned in 10% H_2O_2 overnight, rinsed in an ultrasonic bath, leached in 0.27 M HCl for ~1 minute (to remove attached clays and coatings), dried and weighed, and then completely dissolved in 5% HNO_3 in preparation for elemental concentration analysis (described in Appendix B.2), and follow up $^{87}\text{Sr}/^{86}\text{Sr}$ and $\delta^{88/86}\text{Sr}$ analyses.

3.3. Coupled $^{87}\text{Sr}/^{86}\text{Sr}$ and $\delta^{88/86}\text{Sr}$ analyses via TIMS

Samples of filtered waters, dissolved biogenic carbonates, and a sediment crust (i.e., groups 1 and 2) were all analysed for $^{87}\text{Sr}/^{86}\text{Sr}$ and $\delta^{88/86}\text{Sr}$ by thermal ionisation mass spectrometry (TIMS) using a Phoenix Isotopx instrument at the Metal Isotope Group (MIG) facility at the University of Adelaide. In order to apply the ^{87}Sr - ^{84}Sr double spike method to analyse the $\delta^{88/86}\text{Sr}$ in an unknown sample, two aliquots each containing about 500 ng of Sr were taken from a stock sample solution, where one aliquot was spiked with the ^{87}Sr - ^{84}Sr double spike solution, resulting ‘spike to sample’ ratios (i.e., $^{84}\text{Sr}_{\text{sp}}/^{84}\text{Sr}_{\text{sa}}$) ranging from ~10 to ~32 (details in Appendix C.4). Afterwards, the Sr fraction from each sample was purified from the sample ‘matrix’ using a 600 μL Micro Bio-Spin separation columns filled with Sr-specific resin (Eichrom Sr-SPS) following procedures in Appendix C.1. The pure Sr fractions were then loaded on single non-zone-refined rhenium filaments before TIMS analyses. For each ‘batch’ of TIMS analyses (i.e., one analytical session), which contain both spiked and unspiked samples, these were run in parallel with two SRM987 standards (one at the beginning and one at the end of analytical session). In addition, an IAPSO seawater or JCP-1 carbonate standard were analysed in each ‘batch’,

depending on whether waters or carbonate samples were analysed (i.e., IAPSO was used for the former and JCP-1 for the latter).

For stable Sr isotopes, all data measured in this study are reported as a conventional delta notation ($\delta^{88/86}\text{Sr}$), expressed in per mil (‰), where $^{88}\text{Sr}/^{86}\text{Sr}$ ratio of an unknown sample is normalised relative to SRM987 standard, according to the following equation:

$$\delta^{88/86}\text{Sr} = \left[\frac{(^{88}\text{Sr}/^{86}\text{Sr})_{\text{sample}}}{(^{88}\text{Sr}/^{86}\text{Sr})_{\text{SRM987}}} - 1 \right] \times 1000 \quad (1)$$

Specifically, $\delta^{88/86}\text{Sr}$ values of unknown samples (and IAPSO and JCP-1 standards) were normalised to the average of two SRM987 standards analysed in the same ‘batch’ or analytical session. This approach was used to correct any session-to-session drifts, which were quantified by monitoring SRM987 (see Appendix, Fig C.2B), following the approach adopted by previous studies focused on high-precision Sr isotope analyses (Krabbenhöft et al., 2009; Andrews et al., 2016; Andrews and Jacobson, 2017, Shalev et al., 2017).

The total procedural Sr blanks (details in Appendix C.3) ranged from 19 to 211 pictograms (pg) Sr, with an average value of 72 pg (2SEM = 20 pg, $n = 30$), determined by an isotope dilution (ID) technique using an ^{84}Sr -enriched single spike, amounting to less than 0.1% of Sr from the analysed samples (see below). In addition, the ^{85}Rb ion beam during TIMS analyses was lower than 1×10^{-4} V for all analysed samples, and therefore the isobaric interference from ^{87}Rb was negligible, but an on-line correction for Rb on mass 87 was performed for all samples.

To determine $\delta^{88/86}\text{Sr}$, both spiked and unspiked samples were analysed by TIMS using a static multicollection routine. Typically, a ^{88}Sr beam with a magnitude of about 5–6 V was attained, and ^{84}Sr , ^{85}Rb , ^{86}Sr , ^{87}Sr , and ^{88}Sr isotope beams were collected over 200 cycles (10 cycles for 20 blocks, with 30 s baseline and 8 s peak integrations), with a total analytical time of ca. 1 hour. From these collected data, the following isotope ratios were calculated: $^{88}\text{Sr}/^{84}\text{Sr}$, $^{86}\text{Sr}/^{84}\text{Sr}$, $^{87}\text{Sr}/^{84}\text{Sr}$ and $^{88}\text{Sr}/^{86}\text{Sr}$, which in turn were used to calculate the ‘double-spike corrected’ $^{88}\text{Sr}/^{86}\text{Sr}$ ratios, and thus $\delta^{88/86}\text{Sr}$ (see Eq. (1)). Any procedural and/or instrumental isotope fractionation effects were corrected using an iterative $^{87}\text{Sr}/^{84}\text{Sr}$ double spike correction algorithm (i.e., double-spike correction) adapted from Heuser et al. (2002) and Samanta et al. (2016) using the Sr isotopic ratios measured above.

To obtain high-precision $^{87}\text{Sr}/^{86}\text{Sr}$ ratios, unspiked sample aliquots were re-run on the TIMS using a multi-dynamic peak-hopping method (details see Appendix C.2). In this approach, a typical ^{88}Sr beam of 5–6 V was attained, and the following isotope ratios were collected: $^{87}\text{Sr}/^{86}\text{Sr}$, $^{86}\text{Sr}/^{88}\text{Sr}$ and $^{84}\text{Sr}/^{86}\text{Sr}$, using a method consisting of 100 cycles (20 cycles for 5 blocks), with 30 s of baseline and 10 s peak integrations. Instrumental mass-dependent fractionation effects were corrected via an internal normalisation, using an exponential law and assuming $^{86}\text{Sr}/^{88}\text{Sr}$ of 0.1194 as a normalising ratio (Nier, 1938), which allowed calculation of the corrected $^{87}\text{Sr}/^{86}\text{Sr}$ ratios.

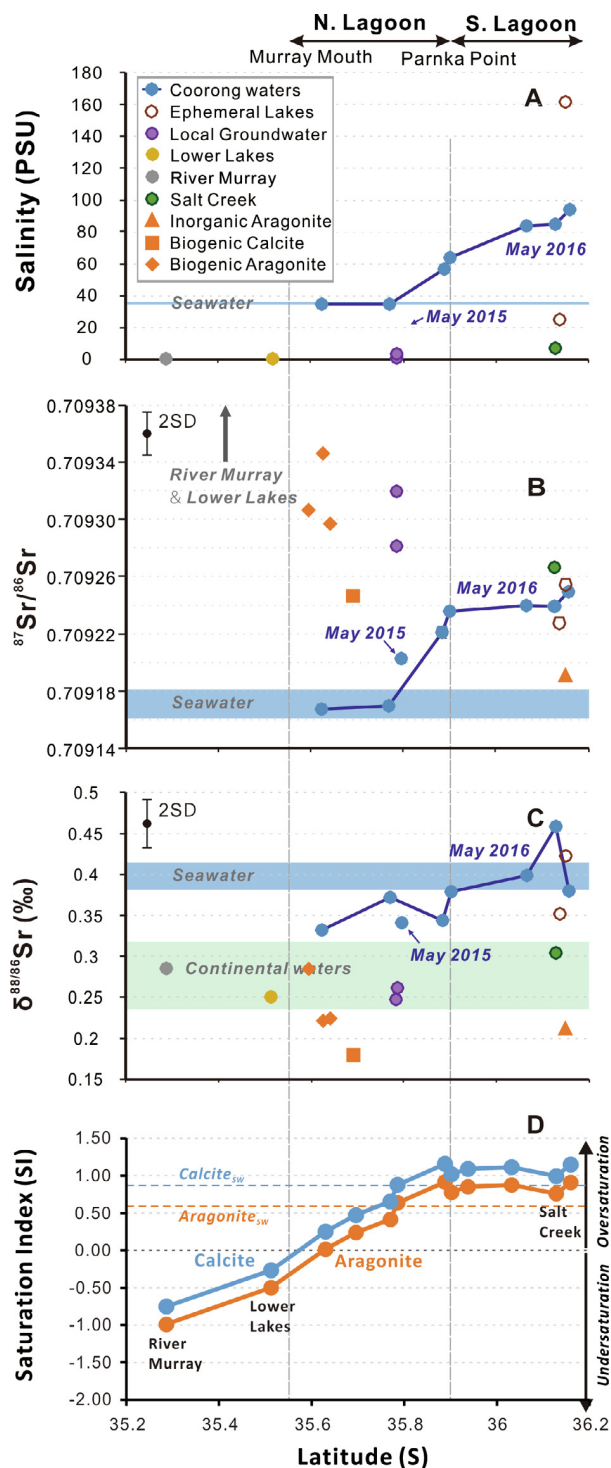
Following the analytical procedures described above, the long-term average $^{87}\text{Sr}/^{86}\text{Sr}$ and $\delta^{88/86}\text{Sr}$ values and

uncertainties of standards in this study were 0.709248 ± 0.000004 (2SEM, $n = 30$) and $0.000 \pm 0.005\text{‰}$ (2SEM, $n = 29$) for SRM987 (Fig. C.2, Appendix), 0.709172 ± 0.000005 (2SEM, $n = 8$) and $0.395 \pm 0.009\text{‰}$ (2SEM, $n = 10$) for IAPSO seawater (Fig. C.3, Appendix), and 0.709174 ± 0.000006 (2SEM, $n = 7$) and $0.198 \pm 0.014\text{‰}$ (2SEM, $n = 7$) for JCP-1 carbonate (Fig. C.3, Appendix). These $^{87}\text{Sr}/^{86}\text{Sr}$ and $\delta^{88/86}\text{Sr}$ results of the above standards (SRM987, IAPSO, JCP-1) acquired during the course of this study agree well with the published data from these standards, where the SRM987 reported $^{87}\text{Sr}/^{86}\text{Sr} = 0.710252 \pm 0.000001$ (2SEM, $n = 94$) and $\delta^{88/86}\text{Sr} = 0.000 \pm 0.004\text{‰}$ (2SEM, $n = 77$) (Andrews et al., 2016), the IAPSO reported $^{87}\text{Sr}/^{86}\text{Sr} = 0.709168 \pm 0.000007$ (2SEM, $n = 10$) (Krabbenhöft et al., 2009) and $\delta^{88/86}\text{Sr} = 0.396 \pm 0.005\text{‰}$ (2SEM, $n = 54$) (Andrews et al., 2016), and the JCP-1 reported $^{87}\text{Sr}/^{86}\text{Sr} = 0.709172 \pm 0.000004$ (2SEM, $n = 32$) and $\delta^{88/86}\text{Sr} = 0.193 \pm 0.004\text{‰}$ (2SEM, $n = 32$) (Vollstaedt et al., 2014). In this study, $^{87}\text{Sr}/^{86}\text{Sr}$ and $\delta^{88/86}\text{Sr}$ analyses of unknown samples were performed only once, if the measurements of standards (SRM987, IAPSO and JCP-1) within the same batch were within 2SD of their long-term values. Detailed discussion on the accuracy and precision of $^{87}\text{Sr}/^{86}\text{Sr}$ and $\delta^{88/86}\text{Sr}$ data on standards is available in Appendix C.4 (see Figs C.2 and C.3).

3.4. Geochemical / PHREEQC modelling of mineral saturation state in waters

The saturation indices (SI) for calcite and aragonite in waters from the CLLMM hydrological system, sampled in May 2018 (Group 3), were calculated using the geochemical model PHREEQC (available at <https://www.usgs.gov/software/phreeqc-version-3>), following the approach detailed in Shao et al. (2018). To ensure that the May 2018 samples represent the water chemistry of May 2016 samples, where the latter account for the majority of the key analyses ($^{87}\text{Sr}/^{86}\text{Sr}$ and $\delta^{88/86}\text{Sr}$), comparison of salinity and major cations between the two sets of samples were made in Appendix E.1. Briefly, the following parameters were used as input data for PHREEQC modelling: temperature, concentrations of the main cations and anions (Tables A.2, B.1 and 2 in Appendix) and high-precision laboratory alkalinity and pH measurements (described in Appendix B.3). The Pitzer database was used since it is suited for high salinity solutions (Parkhurst and Appelo, 2013). As a comparison to the water samples, the SI values of these carbonates in typical seawater were also calculated based on data from Nordstrom et al. (1979). According to the PHREEQC manual by Parkhurst and Appelo (2013), when modelling with PHREEQC, individual element concentrations can be adjusted within their uncertainty limits to achieve charge balance or equilibrium with a pure phase. Such an approach was thus used in this study, where Cl⁻ concentration data were used as a reference element for charge balance calculations.

Additionally, alternative calculation of SI values for calcite and aragonite were estimated using the CO2SYS program (Lewis and Wallace, 1998). The comparison of these



two modelling methods PHREEQC and CO2SYS showed good agreement (Appendix E.3).

4. RESULTS

The salinity, $^{87}\text{Sr}/^{86}\text{Sr}$ and $\delta^{88/86}\text{Sr}$ values of the Coorong waters all displayed systematically increasing trends

from the North to the South Lagoon (Fig. 2A–C). The salinity and $^{87}\text{Sr}/^{86}\text{Sr}$ of North Lagoon waters were similar to that in typical seawater (35 PSU and ~ 0.70917 , respectively). However, $\delta^{88/86}\text{Sr}$ of the North Lagoon waters yielded slightly lower values (0.35‰) than typical seawater that is homogenous at $0.395 \pm 0.016\text{‰}$ (Krabbenhöft et al., 2010; and data from this study). In contrast, hypersaline waters (~ 90 PSU) in the more restricted South Lagoon yielded higher $^{87}\text{Sr}/^{86}\text{Sr}$ of ~ 0.70924 ; and their $\delta^{88/86}\text{Sr}$ values were quite variable, ranging from 0.40 to 0.45‰, with an average of $\sim 0.42\text{‰}$. The latter were slightly but systematically higher than the $\delta^{88/86}\text{Sr}$ of present-day seawater (Fig. 2A–C). The analysis of the continental waters (i.e., River Murray, Lower Lakes, and Salt Creek) with fresh to brackish salinities, yielded $^{87}\text{Sr}/^{86}\text{Sr}$ ratios ranging from ~ 0.70925 in Salt Creek up to ~ 0.71206 in the River Murray (Fig. 2B), and their $\delta^{88/86}\text{Sr}$ were systematically lower than those of the lagoon waters and/or seawater, ranging from 0.25 to 0.30‰ with an average of $\sim 0.27\text{‰}$ (Fig. 2C).

All carbonate samples including carbonate crust and biogenic skeletal carbonates, yielded variable $^{87}\text{Sr}/^{86}\text{Sr}$ ranging from ~ 0.70919 to ~ 0.70935 , which were higher than typical seawater (0.70917). Biogenic calcite and aragonite samples from the North Lagoon (i.e., tubeworm and bivalve skeletal carbonates, respectively) yielded higher $^{87}\text{Sr}/^{86}\text{Sr}$ (> 0.70924) than the local lagoon waters (~ 0.70917); while the inorganic aragonite sample (i.e., carbonate crust) collected in the South Lagoon had a lower $^{87}\text{Sr}/^{86}\text{Sr}$ (0.709192) than the local lagoon waters (~ 0.70924) (Fig. 2B). In contrast, $\delta^{88/86}\text{Sr}$ of all carbonate samples including inorganic and biogenic carbonates were relatively less variable, ranging from $\sim 0.18\text{‰}$ to $\sim 0.28\text{‰}$ (Fig. 2C). Also, these $\delta^{88/86}\text{Sr}$ values overlapped with each other within 2SD error (Fig. D.5 in Appendix D.4). These $\delta^{88/86}\text{Sr}$ values are thus all lower than the local lagoon waters, corresponding to Sr isotope difference between the $\delta^{88/86}\text{Sr}$ of local waters and carbonate minerals of 0.1 to 0.20‰ (see Fig. 2C).

Waters from two ephemeral lakes in the Coorong region with very different salinities (i.e., brackish Milne Lake and hypersaline Halite Lake; Fig. 2A) yielded $^{87}\text{Sr}/^{86}\text{Sr}$ ratios similar to the South Lagoon waters (~ 0.70924). The

Fig. 2. (A) Salinity profile across the CLLMM hydrological system, plotted as a function of latitude (adopted from Shao et al., 2018). (B) Radiogenic Sr isotope ratios ($^{87}\text{Sr}/^{86}\text{Sr}$) of local waters and carbonates. Note that water samples from River Murray (RM) and Lower Lakes (LL) plot out of scale and thus are not shown, and their $^{87}\text{Sr}/^{86}\text{Sr}$ were 0.712055 and 0.710880 respectively. (C) Stable Sr isotope values ($\delta^{88/86}\text{Sr}$) of local waters and carbonates normalised to SRM987 standard. Blue rectangles illustrate typical seawater salinity and Sr isotope compositions, based on the long-term analyses of IAPSO seawater standard (for details see Table 1). (D) The saturation indices (SI) of calcite (blue) and aragonite (orange) in waters from the CLLMM, modelled by PHREEQC for water samples collected in May 2018. The SI values of calcite and aragonite in typical surface seawater (Nordstrom et al., 1979) are shown as blue and orange dashed lines, respectively.

Table 1
Stable and radiogenic Sr isotope composition ($\delta^{88/86}\text{Sr}$ and $^{87}\text{Sr}/^{86}\text{Sr}$), and stable Ca isotope variations ($\delta^{44/40}\text{Ca}$), in the samples, with associated sampling location/area, date and water salinity. Note that reported $\delta^{44/40}\text{Ca}$ data are from Shao et al. (2018). 2SEM is the external precision for repeated analyses with size n; but when n is not given, 2SEM is internal precision of a single analysis of the sample through 200 cycles for $\delta^{88/86}\text{Sr}$, and 100 cycles for $^{87}\text{Sr}/^{86}\text{Sr}$.

Area	Sampling date	Salinity (PSU)	$\delta^{88/86}\text{Sr}$ ($\%_{\text{CSRM987}}$)	2SEM	$\delta^{44/40}\text{Ca}$ ($\%_{\text{IAPSO}}$)	2SEM	$^{87}\text{Sr}/^{86}\text{Sr}$	2SEM
<i>Samples</i>								
RMW	Aug 31, 2019	0.22	0.286	0.016			0.712055	0.000004
C01	May 16, 2016	0.80	0.250	0.011	-0.84	0.03	0.710880	0.000009
JWP2	June 25, 2015	1.15	0.261	0.017	-0.77	0.03	0.709319	0.000003
	(Groundwater)							
BWP2	June 25, 2015	3.66	0.247	0.012	-0.69	0.03	0.709281	0.000003
	(Groundwater)							
SCW	Aug 31, 2019	7.18	0.304	0.013	N/A	N/A	0.709253	0.000004
ELW1	Aug 31, 2019	24.99	0.352	0.018	N/A	N/A	0.709236	0.000004
ELW2	Aug 31, 2019	161.86	0.423	0.016	N/A	N/A	0.709248	0.000004
C02	May 16, 2016	34.98	0.332	0.017	0.00	0.03	0.709168	0.000003
C04	May 16, 2016	34.67	0.372	0.016	0.00	0.05	0.709170	0.000003
NL2	May 15, 2015	19.69	0.341	0.019	-0.04	0.03	0.709203	0.000003
C06	May 16, 2016	63.73	0.378	0.018	0.06	0.03	0.709236	0.000003
C07	May 16, 2016	56.97	0.397	0.012	0.11	0.03	0.709221	0.000004
C10	May 16, 2016	84.10	0.399	0.019	0.16	0.03	0.709240	0.000003
C11	May 16, 2016	85.10	0.458	0.017	0.19	0.03	0.709239	0.000003
C12	May 16, 2016	94.10	0.428	0.012	0.20	0.03	0.709245	0.000004
SL11	April 10, 2015	36.97	N/A	N/A	N/A	N/A	0.709172	0.000003
122s	Jan 18, 2018	N/A	0.222	0.012	N/A	N/A	0.709346	0.000004
149s	May 5, 2018	N/A	0.224	0.012	N/A	N/A	0.709297	0.000004
151s	May 5, 2018	N/A	0.285	0.012	N/A	N/A	0.709307	0.000004
CW2w	Aug 31, 2018	N/A	0.181	0.014	N/A	N/A	0.709246	0.000003
CLS-1 ¹	Mar 5, 2017	N/A	0.211	0.011 (n = 3)	-1.16	0.03	0.709192	0.000009 (n = 3)
<i>Standards</i>								
IAPSO	N/A	35.00	0.395	0.009 (n = 10)	0.00	N/A	0.709172	0.000005 (n = 8)
JCP-1	N/A	N/A	0.198	0.014 (n = 7)	N/A	N/A	0.709174	0.000006 (n = 7)

¹ The $\delta^{88/86}\text{Sr}$ and $^{87}\text{Sr}/^{86}\text{Sr}$ of CLS-1 was the average of 3 analyses with different double spike to sample ratios (Appendix C.4, Table C.4). The $\delta^{44/40}\text{Ca}$ of CLS-1 was from Shao et al. (2018).

$\delta^{88/86}\text{Sr}$ value of the brackish Milne Lake (salinity = 25 PSU) was similar to the North Lagoon waters ($\sim 0.35\text{‰}$), while the hypersaline Halite Lake (162 PSU) yielded a much higher $\delta^{88/86}\text{Sr}$ value that was close to the South Lagoon waters ($\sim 0.42\text{‰}$).

The results from PHREEQC modelling showed that the saturation indices (SI) of aragonite and calcite in the Coorong lagoon waters increased from just saturated (SI ≈ 0) in the north part of the lagoon, to slightly oversaturated conditions (SI > 0) near Parnka Point (see data in Fig. 2D). In the hypersaline South Lagoon, the SI values showed systematic oversaturation with relatively stable SI values of ~ 1 , which were slightly higher than those found in the typical surface seawater of the nearby Southern Ocean (Fig. 2D). In contrast, continental waters including the Murray River and Lower Lakes, both yielded systematically undersaturated SI values of -0.25 to -1 (Fig. 2D), apart from the Salt Creek fresh/brackish waters that were oversaturated (SI ≈ 0.7) with respect to calcium carbonate.

5. DISCUSSION

The Coorong lagoon waters are natural mixtures of different water sources including Southern Ocean seawater (SW), local groundwater (GW), River Murray (RM) and Lower Lakes (LL) freshwaters, and the fresh-to-brackish

Salt Creek water (SC). These water sources also represent theoretical end-members for isotope mass balance calculations of the local Sr cycle in the lagoon, and water mixing and carbonate precipitation/dissolution processes in the Coorong. Specifically, the GW-SW and LL-SW mixing scenarios were discussed in Shao et al. (2018) using $^{87}\text{Sr}/^{86}\text{Sr}$, $\delta^{44/40}\text{Ca}$ data and elemental concentrations (e.g., Sr, Na/Sr and Na/Ca ratios). In Appendix D.1, similar mixing models were established using $^{87}\text{Sr}/^{86}\text{Sr}$, Mg/Ca and Mg/Na ratios of waters from the CLLMM, with the addition of Salt Creek. Interestingly, Salt Creek can be explained by GW-SW mixing (see Fig. D1 in Appendix), and the latter input (Salt Creek) was also considered a direct source of freshwater/brackish water input into the Coorong by previous studies (Mosley, 2016). Moreover, based on $^{87}\text{Sr}/^{86}\text{Sr}$ and Mg/Na tracers, the latter mixing scenario (GW-SW) was also observed as dominant mixing scenario for the Coorong lagoon water samples, in contrast to LL-SW mixing (Fig. D1B in Appendix). Nevertheless, the analysed water samples are only ‘snapshots’ of the CLLMM’s hydrological system, and more systematic and seasonal studies are needed to validate the above observations and interpretations.

Unlike $^{87}\text{Sr}/^{86}\text{Sr}$ tracer, the $\delta^{88/86}\text{Sr}$ can be used as an index for carbonate precipitation vs. dissolution, similar to the way $\delta^{44/40}\text{Ca}$ tracer has been used in the CLLMM

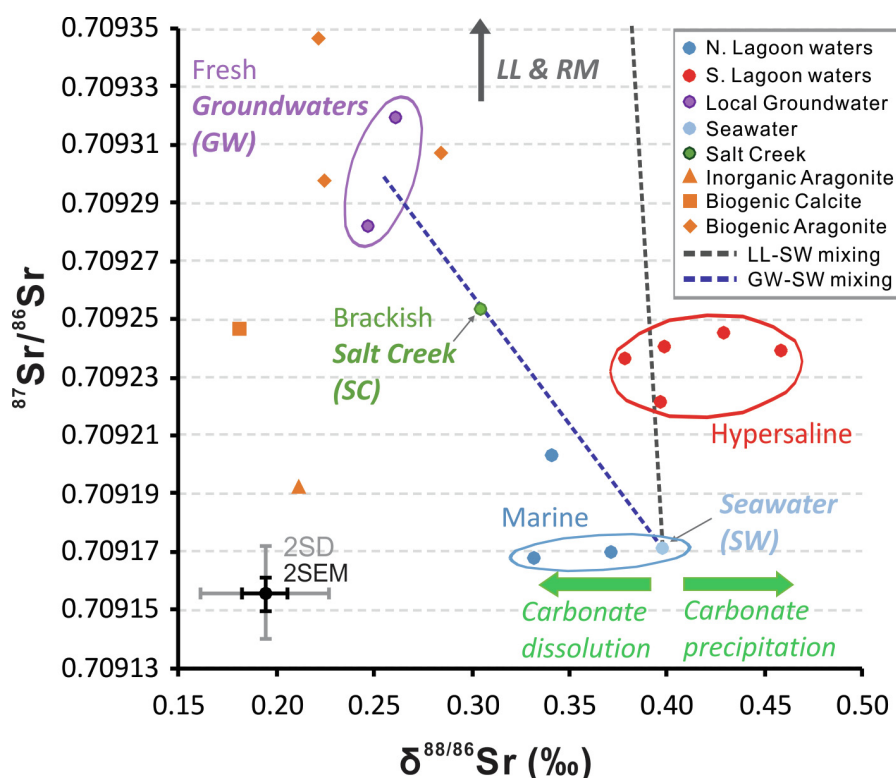


Fig. 3. A cross-plot of $^{87}\text{Sr}/^{86}\text{Sr}$ vs. $\delta^{88/86}\text{Sr}$ values of waters and carbonates from the CLLMM. Note that the following abbreviations are used: LL = the Lower Lakes, RM = River Murray, GW = Groundwater, and SW = seawater). The dashed lines represent theoretical mixing lines for two water-source mixing scenarios (LL-SW and GW-SW). Green arrows illustrate expected shifts in $\delta^{88/86}\text{Sr}$ of local waters due to possible carbonate dissolution or precipitation in the Coorong. The 2SD and 2SEM errors were based on long-term IAPSO and JCP-1 standard measurements (see Appendix C.4).

system by [Shao et al. \(2018\)](#), to provide more advanced understanding of (i) local carbonate fluxes, and (ii) water source mixing in the Coorong.

5.1. Water source mixing and local carbonate cycling: Insights from $^{87}\text{Sr}/^{86}\text{Sr}$ and $\delta^{88/86}\text{Sr}$

$^{87}\text{Sr}/^{86}\text{Sr}$ and $\delta^{88/86}\text{Sr}$ of the samples from CLLMM ([Fig. 3](#)) confirmed that the North Lagoon waters with typical marine salinities of about 35 PSU were primarily sourced from seawater/Southern Ocean, as indicated by their marine $^{87}\text{Sr}/^{86}\text{Sr}$ ratios (~ 0.70917 , [Fig. 2B](#)). However, the generally lower $\delta^{88/86}\text{Sr}$ in North Lagoon waters indicates possible carbonate dissolution in comparison to seawater ([Fig. 3](#)), which is in agreement with the lower SI values for calcite/aragonite documented in the North Lagoon waters compared to typical seawater ([Fig. 2D](#)). This is possibly caused by occasional input of continental waters such as Murray River and Lower Lakes, which yielded highly undersaturated SI values of -0.25 to -1 ([Fig. 2D](#)), as expected for typical freshwaters, but such inputs are not detectable in $^{87}\text{Sr}/^{86}\text{Sr}$ data.

The influence of continental waters and seawater mixing in the South Lagoon was confirmed by their generally higher and non-marine $^{87}\text{Sr}/^{86}\text{Sr}$ values of ~ 0.70924 . In terms of $\delta^{88/86}\text{Sr}$, the South Lagoon waters yielded 0.1 to 0.15% higher $\delta^{88/86}\text{Sr}$ than expected from a theoretical GW-SW mixing line (i.e., the interception of the horizontal line indicating the average $^{87}\text{Sr}/^{86}\text{Sr}$ in the South Lagoon and the GW-SW mixing line, [Fig. 3](#)). Although, these South Lagoon waters plot along the LL-SW mixing line ([Fig. 3](#)), it was not likely that the lake water was a major source as discussed in Appendix D.1. The Salt Creek water plots on the GW-SW mixing line, gave $^{87}\text{Sr}/^{86}\text{Sr}$ similar to the hypersaline South Lagoon, but its $\delta^{88/86}\text{Sr}$ was detectably lower ($\sim 0.1\%$) than ambient South Lagoon waters ([Fig. 3](#)), which was likely impacted by groundwater sourced from carbonate aquifers ([Reid and Mosley, 2016](#)), thus inherited low $\delta^{88/86}\text{Sr}$ from these carbonates. The importance of groundwater to Salt Creek water chemistry was also confirmed in Appendix D.1.

Overall, these data and observations led to several possible explanations with respect to plausible water sources and internal CaCO_3 cycling in the South Lagoon. One explanation is that the lagoon waters could be a mixture of local groundwater (GW) and seawater (SW), which is in agreement with purportedly significant local groundwater discharges to the Coorong proposed by [Haese et al. \(2008\)](#) and [Barnett \(2015\)](#). Alternatively, the brackish Salt Creek input could be the main source of water and Sr into the South Lagoon. In this case, we propose that high degree of water evaporation has caused oversaturation with respect to calcium carbonates, leading to progressive shifts to higher $\delta^{88/86}\text{Sr}$ in South lagoon waters ([Fig. 3](#)) due to carbonate precipitation ([Shao et al., 2018](#)). According to [Reid and Mosley \(2016\)](#), the waters in Salt Creek are supplied mostly from a local carbonate aquifer, with waters that are high in carbonate ions/alkalinity and pH (≥ 8.5),

which was also confirmed by our data (see Table B.4, Appendix). This is consistent with the observed carbonate oversaturation in the Salt Creek waters (SI between 0.5 and 1, [Fig. 2D](#)). Consequently, the inflow of such alkalinity-charged waters might further promote the precipitation of carbonates in the South Lagoon, and thus its shifts to higher $\delta^{88/86}\text{Sr}$, especially near the inflow of Salt Creek waters into the lagoon (see the sample C11, $\delta^{88/86}\text{Sr} = \sim 0.45\%$, [Fig. 2C](#) and 3).

With respect to the carbonate samples (e.g., aragonitic shells and the crust), instead of providing an instant ‘snap shot’ of $^{87}\text{Sr}/^{86}\text{Sr}$ and $\delta^{88/86}\text{Sr}$ signals, which is the case for the local lagoon waters, the Sr isotope composition of carbonates rather reflects a long-term integrated signal of Sr inputs and local processes over a period of shell growth and/or formation of the inorganic carbonate crust. The $^{87}\text{Sr}/^{86}\text{Sr}$ recorded in the samples of biogenic skeletal carbonates (bivalves and tubeworm reef) yielded ratios ranging from ~ 0.70925 to ~ 0.70935 , which are higher than local North Lagoon waters (~ 0.70917) and closer to (i) South Lagoon waters and/or (ii) local continent-derived water sources (e.g., groundwater, Salt Creek waters). These observations thus suggest that the formation of the above biogenic minerals was affected by increased inputs from the River Murray and Lower Lakes due to higher barrage release to the North Lagoon, e.g. during 2016 ([Mosley, 2016](#)), increased groundwater recharge, or accompanied by potential overflow of the South Lagoon waters into the North Lagoon.

In contrast, in the South Lagoon, the closer-to-marine $^{87}\text{Sr}/^{86}\text{Sr}$ ratios of a local inorganic carbonate precipitate (i.e., aragonite-rich crust) suggests that the South Lagoon has been receiving higher inputs of marine Sr in the past, likely via infiltration of seawater from the Southern Ocean into the Coorong. Importantly, the $\delta^{88/86}\text{Sr}$ of the inorganic aragonite crust, which was considered the main carbonate precipitate formed in the South Lagoon, yielded a value that is $\sim 0.2\%$ lower than the present day lagoon waters or typical seawater ([Fig. 2C](#)). This agrees with a typical stable Sr isotope fractionation between aragonite and a solution from laboratory experiments and/or natural systems (cf., [Fruchter et al., 2016](#); [Vollstaedt et al., 2014](#); [Alkhatib and Eisenhauer, 2017](#)). However, the difference in $\delta^{88/86}\text{Sr}$ values between biogenic carbonate (i.e., bivalve shells and tubeworm reefs) and local brackish waters in the North Lagoon is smaller, ranging between 0.10 and 0.15% ([Fig. 2C](#)), thus less than that observed in typical marine environments ($\sim 0.2\%$, [Fruchter et al., 2016](#) and references therein). Nevertheless, due to the limited number of carbonate samples analysed in this study, and potential short term variability in $\delta^{88/86}\text{Sr}$ of local lagoon waters, the magnitude and exact mechanisms responsible for the stable Sr isotope fractionation between waters and biogenic/inorganic carbonates in the Coorong lagoon is difficult to assess and quantify at this stage. In summary, our limited data suggest that the difference between $\delta^{88/86}\text{Sr}$ of local carbonate minerals and lagoon waters in the Coorong is approximately 0.1 to 0.2% .

5.2. Links between $\delta^{88/86}\text{Sr}$ and salinity/carbonate saturation of waters in the CLLMM

According to Von der Borch et al. (1975) and Fernandes and Tanner (2009), aragonite and calcite are the major carbonate precipitates in the Coorong, while gypsum precipitation occurs only seasonally (in summer season) but is generally insignificant. Moreover, our data suggest that carbonate precipitation (aragonite, calcite), rather than gypsum formation is the main control of $\delta^{88/86}\text{Sr}$ fractionation in the Coorong (see also Appendix D.2). Therefore, the following discussion and modelling only involves processes related to carbonates.

Overall, our data from the CLLMM support a general coupling between $\delta^{88/86}\text{Sr}$ and salinity (Fig. 4A), as well as aragonite/calcite saturation index (SI) of the waters (Fig. 4, see also SI data in Fig. 2D). In detail, CaCO_3 undersaturated freshwaters yielded $\delta^{88/86}\text{Sr}$ as low as $\sim 0.25\text{‰}$, brackish/marine waters plot around 0.35‰ , and the oversaturated hypersaline lagoon waters gave positively fractionated $\delta^{88/86}\text{Sr}$ values up to $\sim 0.45\text{‰}$, thus higher than a normal seawater that is homogeneous at 0.40‰ .

Among these lower salinity continental waters, the Salt Creek brackish water was exceptionally oversaturated with respect to CaCO_3 with SI about 0.7 (Fig. 4B), which may explain its slightly higher $\delta^{88/86}\text{Sr}$ of 0.30‰ compared to the rest of freshwaters (Fig. 4A); likely linked to the high alkalinity of the Salt Creek waters that should promote in-situ carbonate precipitation (Reid and Mosley, 2016; Shalev et al., 2017). A similar process involving ongoing carbonate formation can also explain significantly high $\delta^{88/86}\text{Sr}$ values (in excess of 0.4‰ and thus higher than normal seawater) observed in the hypersaline waters of the South Lagoon (90 PSU), and/or in the ephemeral Halite Lake waters with salinity of about 160 PSU (Fig. 4A). In summary, our results and previous studies (Krabbenhöft

et al., 2010; Fruchter et al., 2016; Shalev et al., 2017) suggest that carbonate formation/dissolution processes are the main drivers of the stable Sr isotope composition in natural waters, and the observed $\delta^{88/86}\text{Sr}$ variations in the CLLMM.

Interestingly, the results also suggest that the carbonate saturation in South lagoon waters reached a ‘plateau’ with aragonite SI values of ~ 0.7 (slightly higher than that of typical surface seawater), but the $\delta^{88/86}\text{Sr}$ values of local hypersaline waters is more variable. To further understand this spatial variation of $\delta^{88/86}\text{Sr}$ in the South Lagoon waters (ranging from $\sim 0.38\text{‰}$ to $\sim 0.45\text{‰}$, Fig. 4), which seems to scatter at SI of around ~ 1 , one should bear in mind that there are also numerous other factors such as (i) temperature, (ii) precipitation rate, (iii) biological Sr removal, and (iv) local water chemistry that may additionally affect stable Sr isotope fractionation in the lagoon or other near-surface environments, as documented by previous studies (Rüggeberg et al., 2008; Raddatz et al., 2013; Stevenson et al., 2014; AlKhatib and Eisenhauer, 2017).

Although carbonate saturation, rather than water salinity, seems to be the main driver of stable Sr isotope composition observed in the CLLMM waters, the tight link between these two parameters in the studied hydrological system suggests that there is potential to use $\delta^{88/86}\text{Sr}$ (complemented by $^{87}\text{Sr}/^{86}\text{Sr}$) to distinguish among (i) fresh/brackish, (ii) marine, and (iii) hypersaline waters in the CLLMM (Fig. 3).

5.3. Coupling between $\delta^{88/86}\text{Sr}$ and $\delta^{44/40}\text{Ca}$ in the CLLMM water samples

Shao et al. (2018) showed the sensitivity of stable Ca isotopes ($\delta^{44/40}\text{Ca}$) to local carbonate saturation of waters in the CLLMM, which can be simulated via a Rayleigh fractionation model. Similar properties were observed for

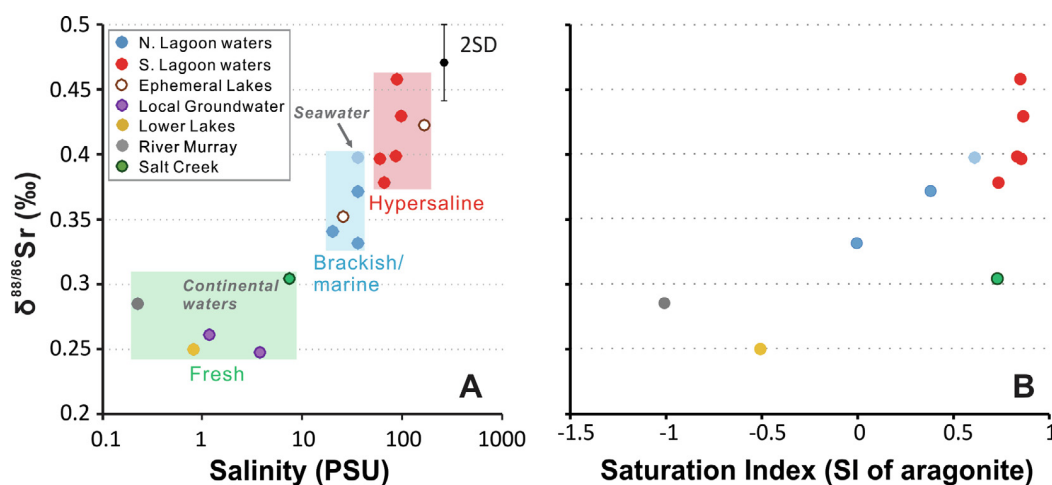


Fig. 4. (A) $\delta^{88/86}\text{Sr}$ values of water samples from the CLLMM, plotted against their respective salinities, ranging from fresh to hypersaline, with source data listed in Table 1. (B) $\delta^{88/86}\text{Sr}$ values of water samples from the CLLMM plotted against their respective aragonite saturation indices (SI values) based on PHREEQC modelling of water data collected in May 2018. Note that based on XRD analysis of local sediments, inorganic aragonite precipitates (i.e., carbonate crusts) represent the main carbonate mineralogy in the South Lagoon.

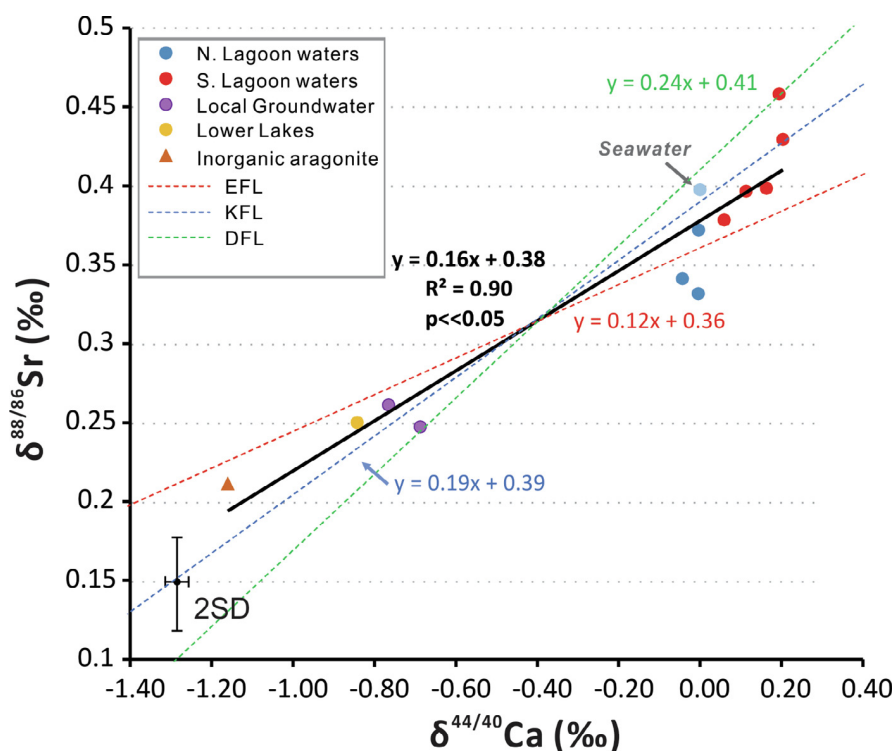


Fig. 5. A cross-plot of $\delta^{88/86}\text{Sr}$ vs. $\delta^{44/40}\text{Ca}$ (normalised to IAPSO seawater) values in waters and the inorganic aragonitic carbonate crust (CLS-1) from the CLLMM hydrological system. The straight black line represents a line of best fit for the data, which can be written as a linear function. Note that $\delta^{44/40}\text{Ca}$ data are from Shao et al. (2018). The three dashed lines represent theoretical fractionation lines for equilibrium (EFL), chemical kinetic (KFL), and diffusional kinetic (DFL) fractionation mechanisms.

$\delta^{88/86}\text{Sr}$ in this study as illustrated by data in Fig. 4 and discussed in the Section 5.2. Moreover, the $\delta^{88/86}\text{Sr}$ and $\delta^{44/40}\text{Ca}$ data from the same waters and carbonates collected in the CLLMM hydrological system exhibit a statistically significant positive correlation ($R^2 = 0.90$, P value $\ll 0.05$, $n = 13$) (Fig. 5). This further corroborates common causative mechanism(s) for stable Sr and Ca isotope fractionation in the CLLMM linked to the dissolution/precipitation of carbonates.

Specifically, we discuss three common fractionation mechanisms – equilibrium (eq), chemical kinetic (kin), and diffusional kinetic (diff) fractionation, and their influence on $^{88}\text{Sr}/^{86}\text{Sr}$ and $^{44}\text{Ca}/^{40}\text{Ca}$ isotope fractionation. Following the studies of Young et al. (2002) and Böhm et al. (2012), one can calculate the slope or a ratio (β) for the $\Delta^{88/86}\text{Sr}_{(\text{carb-aq})}$ vs. $\Delta^{44/40}\text{Ca}_{(\text{carb-aq})}$ relationship for the above three main fractionation mechanisms (equilibrium, kinetic, and diffusional) using the equations below:

$$\beta_{\text{eq}} = (87.906^{-1} - 85.909^{-1}) / (43.955^{-1} - 39.963^{-1}) = 0.12 \quad (2)$$

$$\beta_{\text{kin}} = \log(\mu_{\text{Sr}(\text{h})} / \mu_{\text{Sr}(\text{l})}) / \log(\mu_{\text{Ca}(\text{h})} / \mu_{\text{Ca}(\text{l})}), \quad (3)$$

where $\mu_{i(\text{h})}$ and $\mu_{i(\text{l})}$ represent reduced masses for the heavy and light isotopes of element i , respectively, calculated as $\mu_i = M \cdot m_i / (M + m_i)$, and M is the mass of the molecules contributing to the reacting complex bonded to the element of interest. The equation was calculated with $M = 108.1$

amu for $(\text{H}_2\text{O})_6$, $M = 144.1$ amu for $(\text{H}_2\text{O})_8$ and the respective atomic strontium and calcium isotope masses. Based on these values and parametrisation, the $\beta_{\text{kin}} = 0.19$

Finally, the slope or β_{diff} for the diffusional kinetic fractionation for stable Sr and Ca isotopes is calculated based on:

$$\beta_{\text{diff}} = \log(87.906/85.909) / \log(43.955/39.963) = 0.24 \quad (4)$$

These β values, reflecting the slopes for theoretical mass-dependent fractionation lines (EFL, KFL and DFL) are illustrated in Fig. 5, and plotted along with $\delta^{88/86}\text{Sr}$ and $\delta^{44/40}\text{Ca}$ data from the CLLMM. Interestingly, the slope for the latter data yielded a value of 0.16, thus plotting between KFL (slope = 0.19) and EFL (slope = 0.12), suggesting that both chemical kinetic and equilibrium fractionation processes were responsible for the observed stable Sr and Ca isotope variations measured in the CLLMM data.

Nevertheless, there are also some differences between stable Sr and Ca isotope data from the CLLMM. Specifically, the $\delta^{88/86}\text{Sr}$ of certain North Lagoon waters were slightly lower than that of the seawater (see also Section 5.1, Figs. 3 and 2D), while $\delta^{44/40}\text{Ca}$ data did not show such discrepancy (Fig. 5 and Shao et al., 2018). In addition, $\delta^{88/86}\text{Sr}$ of hypersaline South Lagoon waters varied from close to seawater values of ca. 0.38‰ up to ~ 0.45 ‰ (see Fig. 2C), but the $\delta^{44/40}\text{Ca}$ of these samples were consistently higher than that of a typical seawater (i.e. Southern Ocean and/or North Lagoon waters). These slight differences in the

behaviour of $\delta^{88/86}\text{Sr}$ and $\delta^{44/40}\text{Ca}$ tracers in the Coorong lagoon might be a result of (i) different concentrations and thus residence times of Sr and Ca in the lagoon, impacting the response of their isotope tracers to perturbations, (ii) higher uptake of Sr into aragonite relative to calcite and associated isotope effects, and different solubilities of these carbonate minerals in water, and finally also perhaps due to (iii) variable precipitation rates of carbonates in the lagoon and their comparably different influence on stable Ca and Sr isotopes (Fruchter et al., 2016; 2017;; Alkhatib and Eisenhauer, 2017). Overall, both isotope tracers, $\delta^{88/86}\text{Sr}$ and $\delta^{44/40}\text{Ca}$, suggest that the most saline and oversaturated lagoon waters had experienced highest net removal of light Sr and Ca isotopes from lagoon waters into precipitating carbonates (Figs. 3, 5 and Shao et al., 2018).

5.4. Quantifying carbonate removal in the Coorong via $\delta^{88/86}\text{Sr}$ and Rayleigh modelling

Given that both $\delta^{88/86}\text{Sr}$ and $\delta^{44/40}\text{Ca}$ tracers are controlled by similar fractionation processes, one should be able to quantify the net removal of Sr^{2+} from waters in the South Lagoon driven by ongoing carbonate (mainly aragonite) precipitation using stable Sr isotopes (as done previously for Ca isotopes, Shao et al., 2018). These processes can be quantified via Rayleigh and equilibrium isotope fractionation models (Frings et al., 2016; and Shao et al., 2018), which allow simulation of $\delta^{88/86}\text{Sr}$ variations in lagoon waters as a function of carbonate precipitation. In this case, only the GW/SC-SW (groundwater/Salt Creek-seawater) mixing scenario is shown in the models, since it is dominant in the Coorong for our samples as discussed in the beginning of Section 5 and Appendix D.1.

The Rayleigh model assumes no interaction between precipitated carbonate (i.e. product) and lagoon waters (i.e., reactant). In this case, the stable Sr isotope fractionation (α) between a local lagoon water (i.e., reactant) and precipitated carbonate mineral (i.e., product) controls the $\delta^{88/86}\text{Sr}$ signature of the water based on the following equation:

$$\delta^{88/86}\text{Sr} = \left[(\delta^{88/86}\text{Sr}_{\text{INI}} + 10^3) * (1 - f_{\text{CC}})^{(\alpha_{\text{CC}} - 1)} \right] - 10^3 \quad (5)$$

where $\delta^{88/86}\text{Sr}$ represents the Sr isotope composition of a residual unreacted Sr pool in the lagoon; f_{CC} represents the fraction of Sr^{2+} that was removed as aragonite (i.e., product); the $\delta^{88/86}\text{Sr}_{\text{INI}}$, or the initial Sr isotope composition of lagoon water (with no carbonate precipitation, i.e., $f_{\text{CC}} = 0$) is set at different values in our models for different scenarios. Specifically, the expected $\delta^{88/86}\text{Sr}_{\text{INI}}$ value (equals 0.32‰) can be inferred from the theoretical mixing lines as shown in Fig. D.4, Appendix D.3 using the $^{87}\text{Sr}/^{86}\text{Sr}$ of lagoon water.

The parameter α_{CC} is the Sr isotope fractionation factor between the lagoon water and precipitated CaCO_3 (i.e., aragonite, denoted as subscript CC), the latter calculated by:

$$\alpha_{\text{CC}} = \frac{1 + \frac{\delta^{88/86}\text{Sr}_{\text{CC}}}{1000}}{1 + \frac{\delta^{88/86}\text{Sr}_{\text{MIX}}}{1000}} = \frac{1000 + \delta^{88/86}\text{Sr}_{\text{CC}}}{1000 + \delta^{88/86}\text{Sr}_{\text{MIX}}} \quad (6)$$

where $\delta^{88/86}\text{Sr}_{\text{CC}}$ is the stable Sr isotope signature of the precipitated CaCO_3 mineral (0.21‰), and $\delta^{88/86}\text{Sr}_{\text{MIX}}$ refers to the lagoon water (0.42‰), based on data from the studied CLLMM system (see Fig. 3). Accordingly, the specific α_{CC} (i.e., stable Sr isotope fractionation factor) calculated for the Coorong water-carbonate system has a value of 0.9998.

In contrast with the Rayleigh model, the equilibrium model considers interactions and an isotope exchange (i.e., equilibration) between the product and reactant (Frings et al., 2016); and the evolution of $\delta^{88/86}\text{Sr}$ in lagoon waters due to aragonite precipitation based on this model can be calculated using the following equation (Frings et al., 2016; Shao et al., 2018):

$$\delta^{88/86}\text{Sr} = \delta^{88/86}\text{Sr}_{\text{INI}} + \varepsilon * f_{\text{CC}} \quad (7)$$

where $\delta^{88/86}\text{Sr}_{\text{INI}}$ is the same as that mentioned above; and ε is the fractionation isotope effect, which is related to the abovementioned α_{CC} based on:

$$\varepsilon = -10^3 * (\alpha_{\text{CC}} - 1) \quad (8)$$

Results of both models (Fig. 6) suggest that the fraction of Sr removed from the South Lagoon as aragonite, ranges from 35% to 45% (for Rayleigh and Equilibrium models, respectively). Given that the Sr/Ca ratio of the South Lagoon waters (and precipitated aragonite) is relatively constant (see Table B.1, Fig. B.1 in Appendix, and data in Shao et al., 2018), and the typical Sr partition coefficient K_d of marine aragonite, defined as $K_d^{\text{ar}} = \frac{(\text{Sr}/\text{Ca})_{\text{ar}}}{(\text{Sr}/\text{Ca})_{\text{fluid}}}$, is ~ 1 (Gaetani and Cohen, 2006), it is reasonable to assume that the fraction of Sr removed from the lagoon is proportional to the fraction of Ca that has been removed into CaCO_3 . Indeed, our $\delta^{88/86}\text{Sr}$ data and modelling suggest that the South Lagoon acts as a net sink for CaCO_3 , which is in agreement with Shao et al. (2018) who used $\delta^{44/40}\text{Ca}$ to generate a similar estimate of 35–45% Ca removal by aragonite precipitation in the South Lagoon.

5.5. Coupled $^{87}\text{Sr}/^{86}\text{Sr}$ and $\delta^{88/86}\text{Sr}$ approach for paleo-hydrology and salinity reconstructions

Plotting the main water sources in $^{87}\text{Sr}/^{86}\text{Sr}$ vs. salinity plots (see data and legend in Fig. 7A) revealed that the traditional $^{87}\text{Sr}/^{86}\text{Sr}$ tracer can help to distinguish (i) a normal seawater (with typical marine $^{87}\text{Sr}/^{86}\text{Sr}$ of ~ 0.70917) from (ii) non-marine water sources impacted by continental weathering and thus higher and more radiogenic $^{87}\text{Sr}/^{86}\text{Sr}$ (typically > 0.7092), the latter originating from surficial freshwaters (rivers, streams) and/or subsurface groundwaters. However, as illustrated in Fig. 7A, the $^{87}\text{Sr}/^{86}\text{Sr}$ tracer cannot faithfully distinguish between (i) fresh and (ii) hypersaline water sources in the studied CLLMM system, as both have been affected by continental waters and thus have overlapping and non-marine $^{87}\text{Sr}/^{86}\text{Sr}$ ratios. In contrast, $\delta^{88/86}\text{Sr}$ values of CLLMM waters, impacted by carbonate dissolution/precipitation processes, correlate

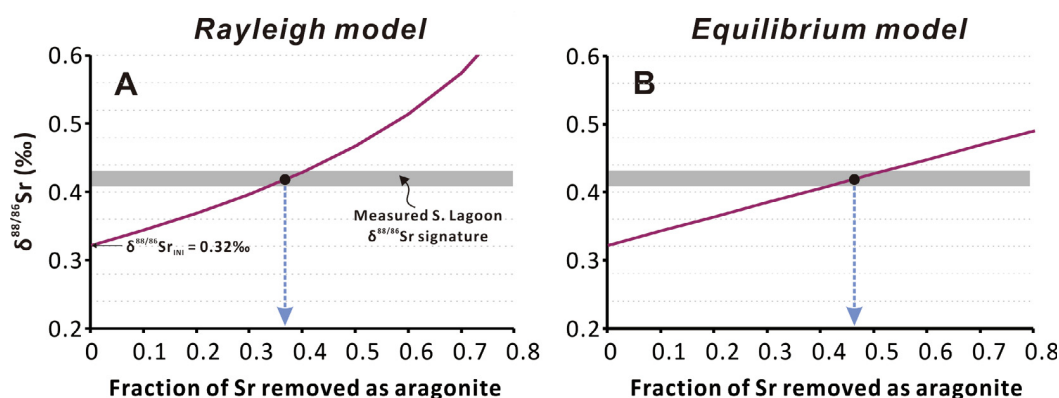


Fig. 6. Plots showing modelled $\delta^{88/86}\text{Sr}$ trends in the South Lagoon waters as a function of Sr fraction removed from the lagoon waters as aragonite. (A) The Rayleigh model; (B) the equilibrium model. The grey band represents the measured $\delta^{88/86}\text{Sr}$ variations in the South Lagoon waters, and coloured line illustrate GW/SC-SW (groundwater/Salt Creek-seawater) mixing scenario for $\delta^{88/86}\text{Sr}_{\text{INI}}$ of 0.32‰.

strongly with the salinity (Fig. 7B) and to some degree also with calcite/aragonite saturation (SI) of CLLMM waters (Fig. 4B). Based on these observations, fresh and undersaturated CLLMM waters yielded low $\delta^{88/86}\text{Sr}$, while hypersaline and oversaturated waters have systematically higher $\delta^{88/86}\text{Sr}$ values. Accordingly, a coupled Sr isotope approach that combines $\delta^{88/86}\text{Sr}$ and $^{87}\text{Sr}/^{86}\text{Sr}$ traces could be applied to other carbonate-producing lagoon-estuarine systems or coastal settings worldwide, such as the Florida Bay (Fig. 7C, Holmden et al., 2012). Moreover, if the observed difference between $\delta^{88/86}\text{Sr}$ of local carbonate minerals and present-day lagoon water in the Coorong has been constant through time, then such a coupled approach combining $^{87}\text{Sr}/^{86}\text{Sr}$ and $\delta^{88/86}\text{Sr}$ analysis of fossil carbonates can be used to reconstruct paleo-hydrology and water source mixing, and by inference paleo-salinity, in the past CLLMM system.

6. CONCLUSIONS

This study shows that $\delta^{88/86}\text{Sr}$ of the waters from the Coorong, Lower Lakes and Murray Mouth estuary in South Australia exhibit a generally increasing trend with increasing carbonate saturation and salinity of local waters. Specifically, the hypersaline waters in the Coorong lagoon have the highest $\delta^{88/86}\text{Sr}$ up to 0.45‰ due to ongoing carbonate formation (i.e., higher than typical seawater at 0.40 ± 0.016 ‰), while freshwaters (river, groundwater, and lake water) yielded systematically lower $\delta^{88/86}\text{Sr}$ values (as low as 0.25‰), likely linked to carbonate dissolution that supplies light Sr from continental weathering of carbonate rocks. This study also revealed a statistically significant positive correlation between stable Sr and Ca isotope data in waters across the CLLMM, where both tracers $\delta^{88/86}\text{Sr}$ (this study) and $\delta^{44/40}\text{Ca}$ (Shao et al., 2018) seem to be controlled by common underlying mechanisms, following equilibrium and kinetic fractionation linked to carbonate dissolution/precipitation processes. The latter process was further quantified by PHREEQC modelling of carbonate saturation in local CLLMM waters. The estimates of Sr removal in the Coorong using Rayleigh and

equilibrium models based on $\delta^{88/86}\text{Sr}$ data is 35–45%, which provided similar results as the Ca removal calculated based on $\delta^{44/40}\text{Ca}$ data (Shao et al., 2018). Both $\delta^{88/86}\text{Sr}$ and $\delta^{44/40}\text{Ca}$ tracers indicate that the South Lagoon acts as a net sink for dissolved inorganic C due to ongoing CaCO_3 precipitation, mostly as aragonite, which readily forms in hypersaline and oversaturated local lagoon waters. Thus, the results of this study suggest that $\delta^{88/86}\text{Sr}$ can be used as an alternative or complementary proxy to $\delta^{44/40}\text{Ca}$ to constrain the local carbon cycling and CaCO_3 dissolution/precipitation processes in coastal systems, with potential application in studying ocean acidification and coastal carbon cycling. Finally, the coupled approach based on stable and radiogenic Sr isotopes ($^{87}\text{Sr}/^{86}\text{Sr}$ and $\delta^{88/86}\text{Sr}$), presented in this study, can be also applied to ancient carbonates, with potential for paleo-hydrology and salinity reconstructions of the CLLMM and/or other carbonate producing coastal and lagoon-estuarine systems.

Declaration of Competing Interest

The authors declare that they have no known competing financial interests or personal relationships that could have appeared to influence the work reported in this paper.

ACKNOWLEDGEMENTS

This work was supported by the Project Coorong (HCHB – Healthy Coorong Healthy Basin program) and the Czech Science Foundation (GACR grant No. 17-18120S), and additional support from the Environment Institute of the University of Adelaide as well as an ARC Linkage project (LP160101353) are also acknowledged. This study is part of the Ph.D. research of YS, supported by an Adelaide Graduate Research Scholarship, ANSTO research portal (No. 11642), and funding from the CRC LEME Regolith Science Scholarship via Cooperative Research Centre for Landscape Environments and Mineral Exploration (CRC LEME) Regolith Science Scholarship.

The sampling in the Coorong National Park was performed under the Department for Environment and Water

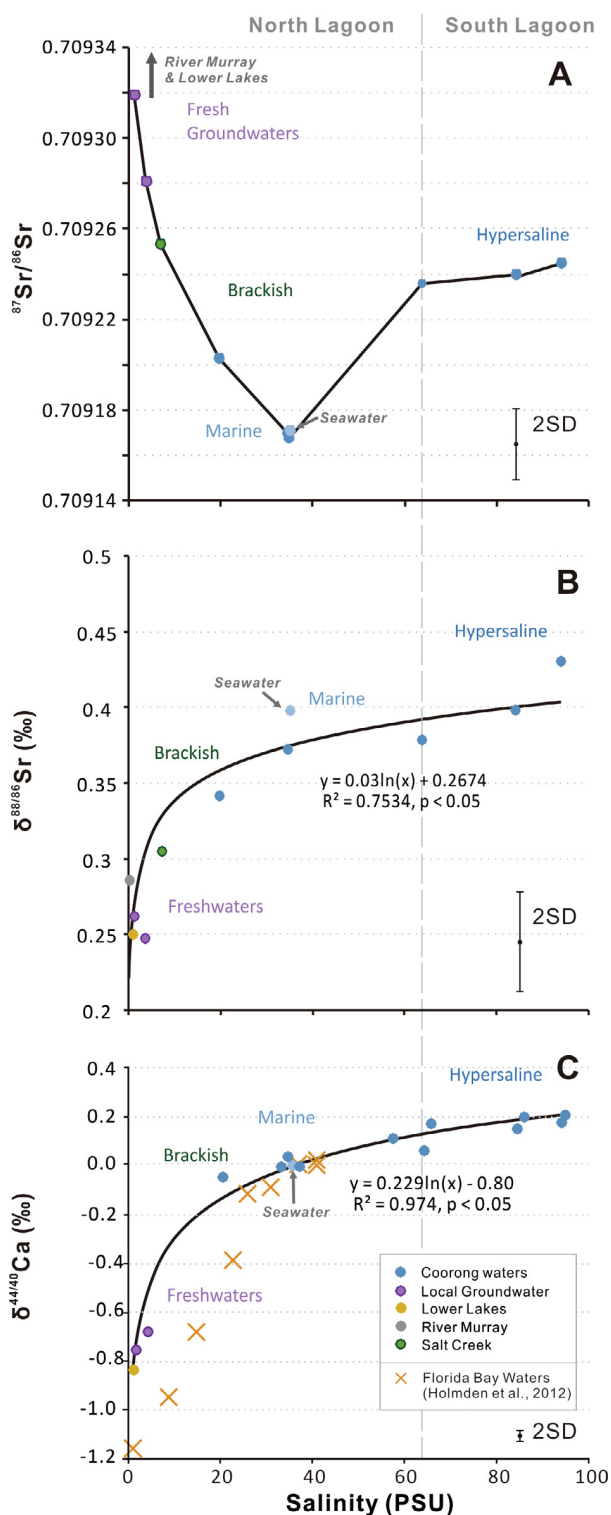


Fig. 7. (A) $^{87}\text{Sr}/^{86}\text{Sr}$ of main water sources in the CLLMM, plotted against their water salinities (in PSU). (B) $\delta^{88/86}\text{Sr}$ vs. salinity of main water sources in the CLLMM. (C) $\delta^{44/40}\text{Ca}$ vs. salinity of main water sources in the CLLMM (data from Shao et al., 2018) and Florida Bay (data from Holmden et al., 2012). The dashed lines represent theoretical mixing trends for two water-source mixing scenarios (LL-SW and GW-SW) calculated by isotope mass balance.

(DEW) research permit No. U26745-1. The living bivalve shell samples were collected under the Primary Industries and Regions South Australia Ministerial Exemption number 9902844. The water quality data provided by the DEW is gratefully acknowledged. Technical and laboratory assistance provided by David Bruce at University of Adelaide is greatly appreciated, especially regarding the training sessions, and the maintenance of TIMS and clean laboratory facilities. We also thank Sima Bargrizen and Flynn Watson for their assistance with pH and alkalinity analyses at the University of Adelaide.

APPENDIX A. SUPPLEMENTARY MATERIAL

Supplementary data to this article can be found online at <https://doi.org/10.1016/j.gca.2020.11.014>.

REFERENCES

- AlKhatib M. and Eisenhauer A. (2017) Calcium and strontium isotope fractionation during precipitation from aqueous solutions as a function of temperature and reaction rate; II. Aragonite. *Geochim. Cosmochim. Acta* **209**, 320–342.
- Andrews M. G. and Jacobson A. D. (2017) The radiogenic and stable Sr isotope geochemistry of basalt weathering in Iceland: role of hydrothermal calcite and implications for long-term climate regulation. *Geochim. Cosmochim. Acta* **215**, 247–262.
- Andrews M. G., Jacobson A. D., Lehn G. O., Horton T. W. and Craw D. (2016) Radiogenic and stable Sr isotope ratios ($^{87}\text{Sr}/^{86}\text{Sr}$, $\delta^{88/86}\text{Sr}$) as tracers of riverine cation sources and biogeochemical cycling in the Milford Sound region of Fiordland, New Zealand. *Geochim. Cosmochim. Acta* **173**, 284–303.
- Anthony A., Atwood J., August P., Byron C., Cobb S., Foster C., Fry C., Gold A., Hagos K., Heffner L., Kellogg D. Q., Lellis-Dibble K., Opaluch J. J., Oviatt C., Pfeiffer-Herbert A., Rohr N., Smith L., Smythe T., Swift J. and Vinhateiro N. (2009) Coastal lagoons and climate change: ecological and social ramifications in U.S. Atlantic and Gulf coast ecosystems. *Ecol. Soc.* **14**, 8.
- Barnett, S. (2015) Assessment of the groundwater resources in the non-prescribed areas of the South Australian Murray-Darling Basin, DEWNR Technical report 2015/09, Government of South Australia, Department of Environment, Water and Natural Resources, Adelaide. ISBN: 978-1-922255-47-1.
- Brookes, J., Dalby, P., Dittmann, S., O'Connor, J., Paton, D., Quin, R., Rogers, D., Waycott, M. and Ye, Q. (2018) Recommended actions for restoring the ecological character of the South Lagoon of the Coorong. Goyder Institute for Water Research Technical Report Series No. 18/04, Adelaide, South Australia. ISSN: 1839-2725.
- Bullen T. D. and Bailey S. W. (2005) Identifying calcium sources at an acid deposition-impacted spruce forest: a strontium isotope, alkaline earth element multi-tracer approach. *Biogeochemistry* **74**, 63–99.
- Böhm F., Eisenhauer A., Tang J., Dietzel M., Krabbenhöft A., Kisakürek B. and Horn C. (2012) Strontium isotope fractionation of planktic foraminifera and inorganic calcite. *Geochim. Cosmochim. Acta* **93**, 300–314.
- Capo R. C., Stewart B. W. and Chadwick O. A. (1998) Strontium isotopes as tracers of ecosystem processes: theory and methods. *Geoderma* **82**, 197–225.

- Caro G., Papanastassiou D. A. and Wasserburg G. J. (2010) ^{40}K - ^{40}Ca isotopic constrains on oceanic calcium cycle. *Earth Planet. Sci. Lett.* **296**, 124–132.
- Chamberlayne B. K., Tyler J. J. and Gillanders B. M. (2019) Environmental Controls on the Geochemistry of a Short-Lived Bivalve in Southeastern Australian Estuaries. *Estuaries Coasts*, 1–16.
- Chao H. C., You C. F., Liu H. C. and Chung C. H. (2013) The origin and migration of mud volcano fluids in Taiwan: Evidence from hydrogen, oxygen, and strontium isotopic compositions. *Geochim. Cosmochim. Acta* **114**, 29–51.
- Chao H. C., You C. F., Liu H. C. and Chung C. H. (2015) Evidence for stable Sr isotope fractionation by silicate weathering in a small sedimentary watershed in southwestern Taiwan. *Geochim. Cosmochim. Acta* **165**, 324–341.
- de Souza G. F., Reynolds B. C., Kiczka M. and Bourdon B. (2010) Evidence for mass-dependent isotopic fractionation of strontium in a glaciated granitic watershed. *Geochim. Cosmochim. Acta* **74**, 2596–2614.
- Dittmann S., Rolston A., Bengler S. N. and Kupriyanova E. K. (2009) Habitat requirements, distribution and colonisation of the tubeworm *Ficopomatus enigmaticus* in the Lower Lakes and Coorong. Report for the South Australian Murray-Darling Basin Natural Resources Management Board, Adelaide, p. 99.
- Farkaš J., Böhm F., Wallmann K., Blenkinsop J., Eisenhauer A., Van Geldern R., Munnecke A., Voigt S. and Veizer J. (2007) Calcium isotope record of Phanerozoic oceans: Implications for chemical evolution of seawater and its causative mechanisms. *Geochim. Cosmochim. Acta* **71**, 5117–5134.
- Farkaš J., Déjeant A., Novák M. and Jacobsen S. B. (2011) Calcium isotope constraints on the uptake and sources of Ca^{2+} in a base-poor forest: a new concept of combining stable ($\delta^{44}/^{42}\text{Ca}$) and radiogenic (ϵ_{Ca}) signals. *Geochim. Cosmochim. Acta* **75**, 7031–7046.
- Farkaš J., Frýda J. and Holmden C. (2016) Calcium isotope constraints on the marine carbon cycle and CaCO_3 deposition during the late Silurian (Ludfordian) positive $\delta^{13}\text{C}$ excursion. *Earth Planet. Sci. Lett.* **451**, 31–40.
- Fernandes, M., and Tanner, J. E. (2009) Hypersalinity and phosphorus availability: the role of mineral precipitation in the Coorong lagoons of South Australia. CSIRO: Water for a Healthy Country National Research Flagship and South Australian Research and Development Institute (Aquatic Sciences).
- Finch A. A. and Allison N. (2007) Coordination of Sr and Mg in calcite and aragonite. *Mineral. Mag.* **71**, 539–552.
- Frings P. J., Clymans W., Fontorbe G., Christina L. and Conley D. (2016) The continental Si cycle and its impact on the ocean Si isotope budget. *Chem. Geol.* **425**, 12–36.
- Fruchter N., Eisenhauer A., Dietzel M., Fietzke J., Böhm F., Montagna P., Stein M., Lazar B., Rodolfo-Metalpa R. and Erez J. (2016) $^{88}\text{Sr}/^{86}\text{Sr}$ fractionation in inorganic aragonite and in corals. *Geochim. Cosmochim. Acta* **178**, 268–280.
- Fruchter N., Lazar B., Nishri A., Almogi-Labin A., Eisenhauer A., Shlevin Y. B. E. and Stein M. (2017) $^{88}\text{Sr}/^{86}\text{Sr}$ fractionation and calcite accumulation rate in the Sea of Galilee. *Geochim. Cosmochim. Acta* **215**, 17–32.
- Gaetani G. A. and Cohen A. L. (2006) Element partitioning during precipitation of aragonite from seawater: a framework for understanding paleoproxies. *Geochim. Cosmochim. Acta* **70**, 4617–4634.
- Gillanders B. M. and Munro A. R. (2012) Hypersaline waters pose new challenges for reconstructing environmental histories of fish based on otolith chemistry. *Limnol. Oceanogr.* **57**, 1136.
- Glamore, W. C., Rayner, D. S. and Rahman, P. F. (2016) Estuaries and climate change. Technical Monograph prepared for the National Climate Change Adaptation Research Facility. Water Research Laboratory of the School of Civil and Environmental Engineering, UNSW.
- Haese R. R., Gow L., Wallace L. and Brodie R. S. (2008) Identifying groundwater discharge in the Coorong (South Australia). *AUSGEO news* **91**, 1–6.
- Heuser A., Eisenhauer A., Gussone N., Bock B., Hansen B. T. and Nögler T. F. (2002) Measurement of calcium isotopes ($\delta^{44}\text{Ca}$) using a multicollector TIMS technique. *Int. J. Mass Spectrom.* **220**, 385–397.
- Hodell D. A., Mead G. A. and Mueller P. A. (1990) Variation in the strontium isotopic composition of seawater (8 Ma to present): Implications for chemical weathering rates and dissolved fluxes to the oceans. *Chem. Geol.: Isotope Geosci. Section* **80**, 291–307.
- Hoefs J. (2018) Isotope fractionation processes of selected elements. In *Stable Isotope Geochemistry*. Springer, Cham, pp. 53–227.
- Holmden C., Creaser R. A. and Muehlenbachs K. (1997) Paleosalinities in ancient brackish water systems determined by $^{87}\text{Sr}/^{86}\text{Sr}$ ratios in carbonate fossils: a case study from the Western Canada Sedimentary Basin. *Geochim. Cosmochim. Acta* **61**, 2105–2118.
- Holmden C., Papanastassiou D. A., Blanchon P. and Evans S. (2012) $\delta^{44}/^{40}\text{Ca}$ variability in shallow water carbonates and the impact of submarine groundwater discharge on Ca-cycling in marine environments. *Geochim. Cosmochim. Acta* **83**, 179–194.
- Krabbenhöft A., Fietzke J., Eisenhauer A., Liebetrau V., Böhm F. and Vollstaedt H. (2009) Determination of radiogenic and stable strontium isotope ratios ($^{87}\text{Sr}/^{86}\text{Sr}$; $\delta^{88/86}\text{Sr}$) by thermal ionization mass spectrometry applying an $^{87}\text{Sr}/^{84}\text{Sr}$ double spike. *J. Anal. At. Spectrom.* **24**, 1267–1271.
- Krabbenhöft A., Eisenhauer A., Böhm F., Vollstaedt H., Fietzke J., Liebetrau V., Augustin N., Peucker-Ehrenbrink B., Müller M. N., Horn C., Hansen B. T., Nolte N. and Wallmann K. (2010) Constraining the marine strontium budget with natural strontium isotope fractionations ($^{87}\text{Sr}/^{86}\text{Sr}^*$, $\delta^{88/86}\text{Sr}$) of carbonates, hydrothermal solutions and river waters. *Geochim. Cosmochim. Acta* **74**, 4097–4109.
- Kuznetsov A. B., Semikhatov M. A. and Gorokhov I. M. (2012) The Sr isotope composition of the world ocean, marginal and inland seas: Implications for the Sr isotope stratigraphy. In *Stratigraphy and Geological Correlation*. Pleiades Publishing Ltd., pp. 501–515.
- Lazar B., Starinsky A., Katz A., Sass E. and Ben-Yaakov S. (1983) The carbonate system in hypersaline solutions: alkalinity and CaCO_3 solubility of evaporated seawater. *Limnol. Oceanogr.* **28**, 978–986.
- Lewis, E. and Wallace, D. (1998) Program developed for CO_2 system calculations (No. ORNL/CDIAC-105). Brookhaven National Lab., Dept. of Applied Science, Upton, NY (United States); Oak Ridge National Lab., Carbon Dioxide Information Analysis Center, TN (United States).
- Macreadie P. I., Serrano O., Maher D. T., Duarte C. M. and Beardall J. (2017) Addressing calcium carbonate cycling in blue carbon accounting. *Limnol. Oceanogr. Lett.* **2**, 195–201.
- Menadakis M., Maroulis G. and Koutsoukos P. G. (2009) Incorporation of Mg^{2+} , Sr^{2+} , Ba^{2+} and Zn^{2+} into aragonite and comparison with calcite. *J. Math. Chem.* **46**, 484.
- Mosley L. M. (2016) Barrage release optimisation trial August 2015: assessment of environmental outcomes and achievement of management objectives. University of Adelaide, South Australia.
- Mosley L. M., Ye Q., Shepherd S., Hemming S. and Fitzpatrick R. (2019) Natural history of the Coorong, Lower Lakes. *and*

- Murray Mouth region (Yarluwar-Ruwe)*. University of Adelaide Press on behalf of the Royal Society of South Australia.
- Nier A. O. (1938) The isotopic constitution of strontium, barium, bismuth, thallium and mercury. *Phys. Rev.* **5**, 275–278.
- Nordstrom D. K., Plummer L. N., Wigley T. M. L., Wolery T. J., Ball J. W., Jenne E. A., Bassett R. L., Crerar D. A., Florence T. M., Fritz B., Hoffman M., Holdren, Jr., G. R., Lafon G. M., Mattigod S. V., McDuff R. E., Morel F., Reddy M. M., Sposito G. and Thraillkill J. (1979) A comparison of computerized chemical models for equilibrium calculations in aqueous systems. In *Chemical Modeling in Aqueous Systems* (ed. E. A. Jenne). American Chemical Society, Washington, pp. 857–892.
- Palchan D., Stein M., Almogi-Labin A., Erel Y. and Goldstein S. L. (2013) Dust transport and synoptic conditions over the Sahara-Arabia deserts during the MIS6/5 and 2/1 transitions from grain-size, chemical and isotopic properties of Red Sea cores. *Earth Planet. Sci. Lett.* **382**, 125–139.
- Parkhurst, D. L. and Appelo, C. A. J. (2013) Description of input and examples for PHREEQC version 3: a computer program for speciation, batch-reaction, one-dimensional transport, and inverse geochemical calculations (No. 6-A43). US Geological Survey.
- Pearce C. R., Parkinson I. J., Gaillardet J., Charlier B. L., Mokadem F. and Burton K. W. (2015) Reassessing the stable ($\delta^{88/86}\text{Sr}$) and radiogenic ($^{87}\text{Sr}/^{86}\text{Sr}$) strontium isotopic composition of marine inputs. *Geochim. Cosmochim. Acta* **157**, 125–146.
- Raddatz J., Liebetrau V., Rüggeberg A., Hathorne E., Krabbenhöft A., Eisenhauer A., Böhm F., Vollstaedt H., Fietzke J., López Correa M., Freiwald A. and Chr. Dullo W. (2013) Stable Sr-isotope, Sr/Ca, Mg/Ca, Li/Ca and Mg/Li ratios in the scleractinian cold-water coral *Lophelia pertusa*. *Chem. Geol.* **352**, 143–152.
- Reeves J. M., Haynes D., García A. and Gell P. A. (2015) Hydrological change in the Coorong Estuary, Australia, past and present: Evidence from fossil invertebrate and algal assemblages. *Estuaries Coasts* **38**, 2101–2116.
- Reid R. J. and Mosley L. M. (2016) Comparative contributions of solution geochemistry, microbial metabolism and aquatic photosynthesis to the development of high pH in ephemeral wetlands in South East Australia. *Sci. Total Environ.* **542**, 334–343.
- Rüggeberg A., Fietzke J., Liebetrau V., Eisenhauer A., Dullo W. C. and Freiwald A. (2008) Stable strontium isotopes ($\delta^{88/86}\text{Sr}$) in cold-water corals—a new proxy for reconstruction of intermediate ocean water temperatures. *Earth Planet. Sci. Lett.* **269**, 570–575.
- Samanta M., Ellwood M. J. and Mortimer G. E. (2016) A method for determining the isotopic composition of dissolved zinc in seawater by MC-ICP-MS with a ^{67}Zn – ^{68}Zn double spike. *Microchem. J.* **126**, 530–537.
- Shalev N., Gavrieli I., Halicz L., Sandler A., Stein M. and Lazar B. (2017) Enrichment of ^{88}Sr in continental waters due to calcium carbonate precipitation. *Earth Planet. Sci. Lett.* **459**, 381–393.
- Shalev N., Farkaš J., Fietzke J., Novak M., Schuessler J., Pogge von Strandmann P. and Torber P. (2018) Mg isotope interlaboratory comparison of reference materials from earth-surface low-temperature environments. *Geostand. Geoanal. Res.* **42**, 205–221.
- Shao Y., Farkaš J., Holmden C., Mosley L., Kell-Duiveststein I., Izzo C., Reis-Santos P., Tyler J., Törber P., Frýda J., Taylor H., Haynes D., Tibby J. and Gillanders B. M. (2018) Calcium and strontium isotope systematics in the lagoon-estuarine environments of South Australia: Implications for water source mixing, carbonate fluxes and fish migration. *Geochim. Cosmochim. Acta* **239**, 90–108.
- Stevenson E. I., Hermoso M., Rickaby R. E., Tyler J. J., Minoletti F., Parkinson I. J., Mokadem F. and Burton K. W. (2014) Controls on stable strontium isotope fractionation in coccolithophores with implications for the marine Sr cycle. *Geochim. Cosmochim. Acta* **128**, 225–235.
- Tipper E. T., Galy A., Gaillardet J., Bickle M. J., Elderfield H. and Carder E. A. (2006) The magnesium isotope budget of the modern ocean: Constraints from riverine magnesium isotope ratios. *Earth Planet. Sci. Lett.* **250**, 241–253.
- Vollstaedt H., Eisenhauer A., Wallmann K., Böhm F., Fietzke J., Liebetrau V., Krabbenhöft A., Farkaš J., Tomašových A., Raddatz J. and Veizer J. (2014) The Phanerozoic $\delta^{88/86}\text{Sr}$ record of seawater: New constraints on past changes in oceanic carbonate fluxes. *Geochim. Cosmochim. Acta* **128**, 249–265.
- Von der Borch C. C., Lock D. E. and Schwebel D. (1975) Groundwater formation of dolomite in the Coorong region of South Australia. *Geology* **3**, 283–285.
- Warwick R. M., Tweedley J. R. and Potter I. C. (2018) Microtidal estuaries warrant special management measures that recognise their critical vulnerability to pollution and climate change. *Mar. Pollut. Bull.* **135**, 41–46.
- Young E. D., Galy A. and Nagahara H. (2002) Kinetic and equilibrium mass-dependent isotope fractionation laws in nature and their geochemical and cosmochemical significance. *Geochim. Cosmochim. Acta* **66**, 1095–1104.
- Zeebe R. E. and Wolf-Gladrow D. (2001) *CO₂ in seawater: equilibrium, kinetics, isotopes*, No. 65. Gulf Professional Publishing.

Associate editor: Andrew D. Jacobson

Appendix 2

Appendices for Chapter 2 - Calcium and strontium isotope systematics in the lagoon-estuarine environments of South Australia: Implications for water source mixing, carbonate fluxes and fish migration

Table A.1. $^{87}\text{Sr}/^{86}\text{Sr}$ and $\delta^{44/40}\text{Ca}$ data (with temperatures, salinities and pH) for water samples and otoliths. For detailed sampling locations and dates, see Table C.1 in Appendix C.

Sample ID	Area	Water temperature (°C)	Salinity (PSU)	pH	$^{87}\text{Sr}/^{86}\text{Sr}$ (2s error < 0.00001)	$\delta^{44/40}\text{Ca} \pm 2s$ (in ‰, normalized to IAPSO)
Coorong water samples						
M13	Murray Mouth	18.00	35.00		0.709180	
C02	North Lagoon	15.14	34.98	8.38	0.709168	0.00 ± 0.03
C03	North Lagoon	14.50	32.96	8.50	0.709182	-0.01 ± 0.03
C04	North Lagoon	15.28	34.67	8.75	0.709170	0.00 ± 0.05
C05	North Lagoon	16.01	34.05	9.06	0.709189	0.02 ± 0.05
C07	NL-SL connection	16.10	56.97	8.96	0.709221	0.11 ± 0.03
C06	NL-SL connection	15.15	63.73	9.03	0.709236	0.06 ± 0.03
C08	South Lagoon	17.95	93.40	8.80	0.709237	0.18 ± 0.03
C09	South Lagoon	17.07	65.45	8.83	0.709240	0.18 ± 0.04
C10	South Lagoon	18.30	84.10	8.78	0.709240	0.16 ± 0.03
C11	South Lagoon	17.70	85.10	8.75	0.709239	0.19 ± 0.03
C12	South Lagoon	16.50	94.10	8.77	0.709276	0.20 ± 0.03
SL9	South Lagoon		113.60	7.90	0.709255	
SL8	South Lagoon		108.10	8.46	0.709249	
SL7	South Lagoon		104.65	8.00	0.709243	
SL6	South Lagoon		89.35	8.00	0.709248	
SL5C	South Lagoon		82.10	8.05	0.709241	
SL5B	South Lagoon		81.55	8.06	0.709240	
SL4B	South Lagoon		83.30	8.12	0.709240	
SL4A	South Lagoon		85.30	8.06	0.709244	
SL2	South Lagoon		78.10	8.48	0.709241	
SL1B	South Lagoon		82.55	8.08	0.709238	
NL1	North Lagoon		34.44	7.27	0.709203	
NL2 ¹	North Lagoon		19.69	8.08	0.709248	-0.04 ± 0.03

Appendix A: Tables of Results

NL3 ¹	North Lagoon		19.50	8.09	0.709257	
NL4 ¹	North Lagoon		20.09	8.14	0.709248	
NL5 ¹	North Lagoon		20.75	8.13	0.709248	
NLB4	North Lagoon		29.53	7.86	0.709189	
NLB5	North Lagoon		32.19	7.81	0.709190	
NL6	North Lagoon		20.82	8.03	0.709226	
NL7	North Lagoon		23.47	7.92	0.709228	
NLB1	North Lagoon		27.51	7.87	0.709197	
NLB3	North Lagoon		28.26	7.88	0.709198	
NLB6	North Lagoon		34.73	7.70	0.709182	
NLB11	North Lagoon		34.87	7.71	0.709172	
NLB15	North Lagoon		35.07	7.78	0.709176	
Groundwater samples						
JWP2	North Lagoon		1.15	7.29	0.709319	-0.77 ± 0.03
BWP2	North Lagoon		3.66	7.95	0.709281	-0.69 ± 0.03
The Lower Lakes samples						
C01	Lower Lakes con- nection	15.17	0.80		0.710880	-0.84 ± 0.03
LL1	Lake Albert		1.29	8.57	0.710515	
LL2	Lake Alexandrina		0.43	8.2	0.711006	
LL3	Lower Lakes con- nection		0.35	8.14	0.711134	
Murray River sample						
MR1	River Murray		0.15	7.49	0.712124	
Seawater sample						
SL11	Southern Ocean		36.97	7.72	0.709172	
Rainwater samples						
Rain-IT (galvanized iron tank)	Adelaide				0.710413	

Rain-PT (polyethylene tank)	Adelaide				0.710085	
Rain-A Sr	Adelaide				0.711210	
Rain-B Sr	Adelaide				0.711537	
Sediment sample						
CLS-1 ²	South Lagoon					-1.16 ± 0.03
Whole fish otoliths samples						
M13-01	Murray Mouth		35.00		0.709224	
M13-02	Murray Mouth		35.00		0.709242	
M13-14	Murray Mouth		35.00		0.709240	
C03-02	North Lagoon		32.96		0.709219	-1.76 ± 0.03
C03-04	North Lagoon		32.96		0.709236	-1.57 ± 0.03
C03-05	North Lagoon		32.96		0.709229	
C04-01	North Lagoon		34.67		0.709249	-1.46 ± 0.04
C04-02	North Lagoon		34.67		0.709228	
C04-03	North Lagoon		34.67		0.709237	
C07-01	South Lagoon		56.97		0.709246	
C07-02	South Lagoon		56.97		0.709240	-1.73 ± 0.04
C06-02	South Lagoon		63.73		0.709225	-1.65 ± 0.02
C06-04	South Lagoon		63.73		0.709251	
C08-01	South Lagoon		93.40		0.709252	-1.76 ± 0.02
C08-03	South Lagoon		93.40		0.709239	
C09-01	South Lagoon		65.45		0.709243	-1.76 ± 0.03
C09-02	South Lagoon		65.45		0.709243	
C10-01	South Lagoon		84.10		0.709245	-1.62 ± 0.03
C10-05	South Lagoon		84.10		0.709246	
C11-01	South Lagoon		85.10		0.709238	-1.61 ± 0.03
C11-03	South Lagoon		85.10		0.709247	
C12-01	South Lagoon		94.10		0.709250	-2.00 ± 0.03

C12-02	South Lagoon		94.10		0.709245	
C12-03	South Lagoon		94.10		0.709244	

¹ Brackish water samples in the North Lagoon.

² The Ca concentration for this sediment sample is 254894 ppm.

Table A.2. ⁸⁷Sr/⁸⁶Sr data from micro-drilled otoliths sections, presented as measurements with 2 standard errors. For detailed sampling locations and dates, see Table C.1 in Appendix C.

Sample ID	sample weight (mg)	Sr (ng)	⁸⁷ Sr/ ⁸⁶ Sr (2s error < 0.00003)
C03-03 edge	0.07	70	0.709208
C03-03 core	0.065	65	0.709227
C10-03 edge	0.022	22	0.709262
C10-03 core	0.139	139	0.709242

Appendix B: Details of research protocols and supplementary modeling

B.1. Chromatographic purification – semi-automatic sample purification method for Sr via prepFAST

Firstly, a total procedural blank of the element of interest (i.e., Sr) was determined via isotope dilution, as it is desirable and important that the blank is less than 0.1% of the total amount of Sr loaded and originating from the sample. The volumes of water to be loaded was calculated based on Sr concentration results from solution ICP-MS, so that each sample contains about 1000 ng of Sr (see Table C.2, Appendix C), which is optimal as our typical procedural Sr blank on prepFAST-MC was about 0.1 ng (i.e., about 0.01% of total Sr from the sample).

For bulk Sr isotope analyses, one otolith per pair from each fish sample was analysed. The whole otolith was dissolved in 100 μL of 15 M HNO_3 in a clean 7 mL round-bottomed PFA teflon vial, if the amount of Sr in the otolith was above 1000 ng (see Table C.3 in Appendix C), only a half of the dissolved otolith solution was used. The otolith solution was then dried and re-dissolved with 1 mL of 2 M HNO_3 . Micro-drilled otolith samples were directly dissolved with 1 mL of 2 M HNO_3 since these samples were in powder form.

All vials of samples in 2 M HNO_3 solutions were labelled and transferred to the operation desk and autosampler unit of the prepFAST-MC system. The same number of clean 7 mL PFA vials were labelled and located in the rack to collect purified Sr from each sample.

The sample purification method for Sr was adapted from Romaniello et al. (2015). As listed in Table B.1, five reagents were used in the method, but instead of 10 mL of Sr solution, only 6 mL were collected, and the remaining 4 mL were discarded since there was very little Sr left in the sample after 6 mL of acid elution, as tested by Romaniello et al. (2015) on BCR-2 basalt, IAPSO seawater, CUE-0001 llama bone, and NIST-1400 bone ash.

Table B.1. Chromatographic steps for the automated separation of Sr by 1 mL ESI Sr–Ca column. Modified from Romaniello et al. (2015).

Step	Purpose	Volume	Reagents
1	Condition column	10 mL	2 M HNO_3 + 1 wt% H_2O_2
2	Load sample	1 mL	2 M HNO_3
3	Elute sample matrix (not collected)	10 mL	2 M HNO_3 + 1 wt% H_2O_2
4	Elute Sr (collected)	6 mL	6 M HNO_3
5	Elute Sr (not collected)	4 mL	6 M HNO_3
6	Elute Ca (not collected)	10 mL	12 M HNO_3

7	Elute REEs, Hf, Cd, U and wash the column	10mL	1M HF
---	---	------	-------

Once the method and purification procedure were finished, the column was stored in 2 M HNO₃ + 1 wt% H₂O₂. The collected Sr solutions were evaporated with a drop of 0.5 M H₃PO₄ was added into each vial to prevent the purified Sr crystal from escaping.

B.2. Further Details on TIMS analyses for Sr isotopes

For each sample, the loading process detailed below was followed. Solutions were dropped on parafilm before pipetting and loading.

Filament Loading Protocol:

Centre filaments with non-zone-refined Re ribbon was used, no inner or outer filaments were used.

1. Load 1 µL 1 M H₃PO₄ and evaporate at 0.5-0.8 A.
2. Load 0.5 µL Bircks Solution and evaporate at 0.5 A.
3. Load ~500ng Sr in 1 µL Bircks Solution and dry at 0.5 A.
4. Gradually increase to ~1 A, but reduce current if load starts to spread.
5. Over about 1 minute, increase to 1.8 A, and leave for 1 minute.
6. Heat to just red for several seconds, estimated at ~2.3-2.4 A.
7. Turn down the current and fix the filament onto the magazine, record sample names and details, corresponding to the position of the filaments.

Sample Heating Routine - Building of Ion Beams:

In the mass spectrometer, the ionisatoin (centre) filament current was ramped slowly to 2.3 A in 30 minutes, then the current was turned up slowly to ~3.1-3.3 A, resulting in an ionisation temperature of ~1350-1400 °C and a target ion beam (⁸⁸Sr) intensity of ~5-6 A.

B.3. PHREEQC Modelling

B.3.1. Quantification of Mineral Saturation

To calculate the saturation indices of the three calcium minerals for 2016 lagoon water samples,

the concentrations of Cl^- , K^+ and SO_4^{2-} , and alkalinity for these samples had to be calculated. The linear correlations of these parameters with Na concentration based on the 1998 to 2010 Coorong laboratory data were established as shown below (see Fig. B.1), and the values of the needed input parameters for PHREEQC modelling of mineral saturation states (for 2016 water samples) were calculated accordingly; for details on input data see also Table B.2.

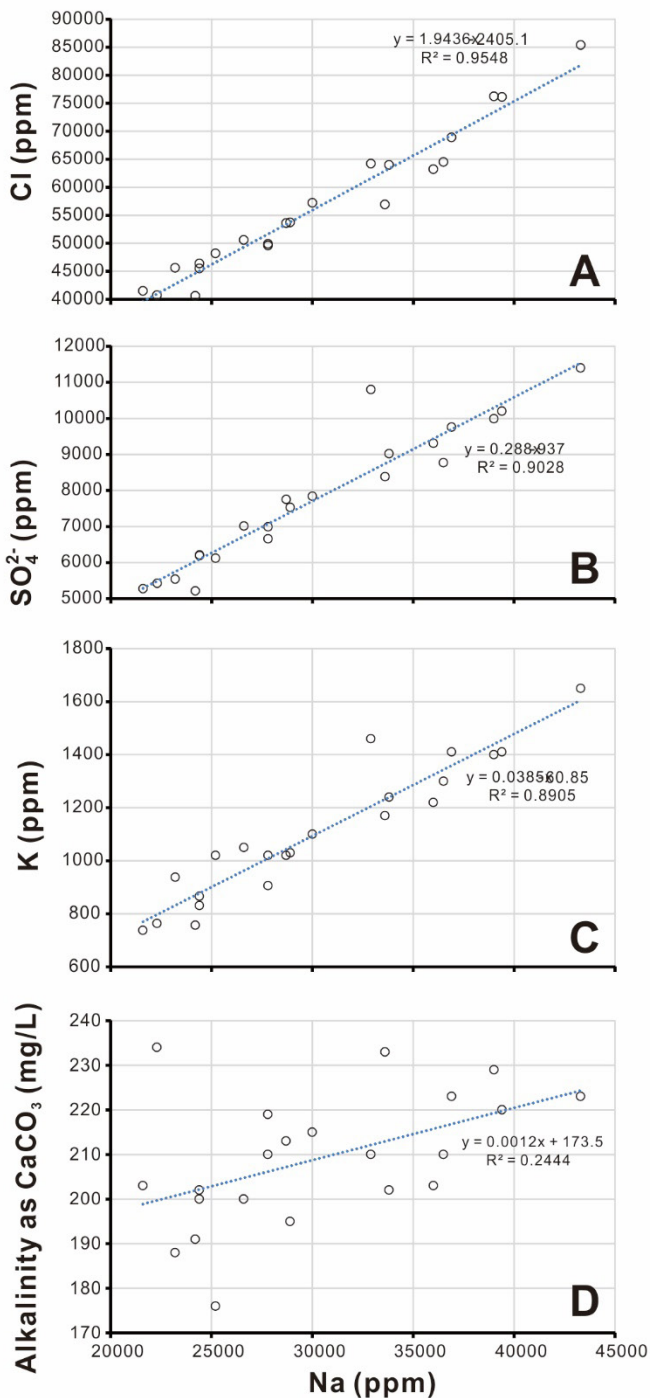


Figure B.1: Charts of linear correlations of Cl^- , K^+ and SO_4^{2-} concentrations, and alkalinity with Na^+

concentration at Policeman Point based on the 1998 to 2010 Coorong laboratory data.

Table B.2. Correlations of Cl^- , K^+ and SO_4^{2-} , and alkalinity with Na concentration based on the 1998 to 2010 Coorong data, and calculated parameter values used in the PHREEQC modeling.

2016 Sampling sites	X (Na^+ concentrations, ppm)	Equations	R^2	Y (Calculated concentrations, ppm; or alkalinity)
Cl^-				
C02 Mark Point	10377.8	$y = 1.7875x + 623.9$	0.992	19174.3
C03 Long Point	9448.5	$y = 1.8466x + 371.78$	0.9839	17819.3
C06 Parnka Point	19981.0	$y = 1.7902x + 1763.1$	0.9786	37533.1
C10 Policeman Point	25442.0	$y = 1.9436x - 2405.1$	0.9548	47043.9
C11 Salt Creek	25689.7	$y = 1.6676x + 4789.4$	0.9756	47629.6
SO_4^{2-}				
C02 Mark Point	10377.8	$y = 0.272x - 128.93$	0.9899	2693.8
C03 Long Point	9448.5	$y = 0.2772x - 224.04$	0.9904	2395.1
C06 Parnka Point	19981.0	$y = 0.2627x - 138.1$	0.8938	5110.9
C10 Policeman Point	25442.0	$y = 0.288x - 937$	0.9028	6390.3
C11 Salt Creek	25689.7	$y = 0.2088x + 1367.6$	0.8809	6731.6
K^+				
C02 Mark Point	10377.8	$y = 0.0379x - 0.8088$	0.9594	756.5
C03 Long Point	9448.5	$y = 0.038x - 1.9569$	0.9448	964.8
C06 Parnka Point	19981.0	$y = 0.0368x - 9.1425$	0.9024	936.2
C10 Policeman Point	25442.0	$y = 0.0385x - 60.85$	0.8905	338.7
C11 Salt Creek	25689.7	$y = 0.0356x + 10.15$	0.9446	346.5
Alkalinity as CaCO_3 (mg/L)				
C02 Mark Point	10377.8	$y = 0.0024x + 109.07$	0.3039	134.0
C03 Long Point	9448.5	$y = 0.0034x + 99.799$	0.3626	131.9
C06 Parnka Point	19981.0	$y = 0.0018x + 141.28$	0.5966	177.2
C10 Policeman Point	25442.0	$y = 0.0012x + 173.5$	0.2444	204.0

C11 Salt Creek	25689.7	$y = 0.0015x + 159.18$	0.5618	197.7
----------------	---------	------------------------	--------	-------

In the input file, all the input parameters for the selected five 2016 samples were then entered in the created spreadsheet in the SOLUTION_SPREAD block (Table B.3).

Table B.3. Input data used for PHREEQC SI calculations, with PHREEQC calculated density based on salinity.

Sam- ple	Alka- linity (mg/L as CaCO ₃)	Ca (mg/L)	Cl (mg/L)	Mg (mg/L)	K (mg/L)	Na (mg/L)	SO4 (mg/L)	pH	Temp (°C)	Density (g·cm ⁻³)	Sa- linity (PSU)
C02	134	383	19174	1275	339	10378	2694	8.28	15.14	1.02201	34.98
C03	132	337	17819	1162	347	9448	2395	8.4	14.50	1.01987	32.96
C06	177	652	37533	2409	756	19981	5111	8.86	15.15	1.04407	63.73
C10	204	814	47044	3027	965	25442	6390	8.68	18.30	1.05663	84.10
C11	198	803	47630	3107	936	25690	6732	8.65	17.70	1.05742	85.10

The output file, i.e., the calculated mineral saturation indices (SI) were automatically generated after the input stimulations were run, and the essential results of our PHREEQC modelling are summarised in Table 2.

B.3.2. Graphical representation of saturation states (SI) of major Ca-bearing minerals

The PHREEQC calculations confirmed systematic oversaturation (SI > 0) of calcium carbonate minerals in the lagoon waters across the entire Coorong, and both calcite and aragonite show progressive oversaturation towards the South Lagoon (see Fig. B.2A), which follows the generally increasing trend of water salinity. Similar trend is also observed for another Ca-bearing mineral, gypsum (CaSO₄·2H₂O), however the latter is undersaturated (SI < 0) throughout most of the lagoon with the exception of the southern most parts of the Coorong where gypsum approaches saturation (SI ≈ 0) in local hypersaline waters (see Fig. B.2A).

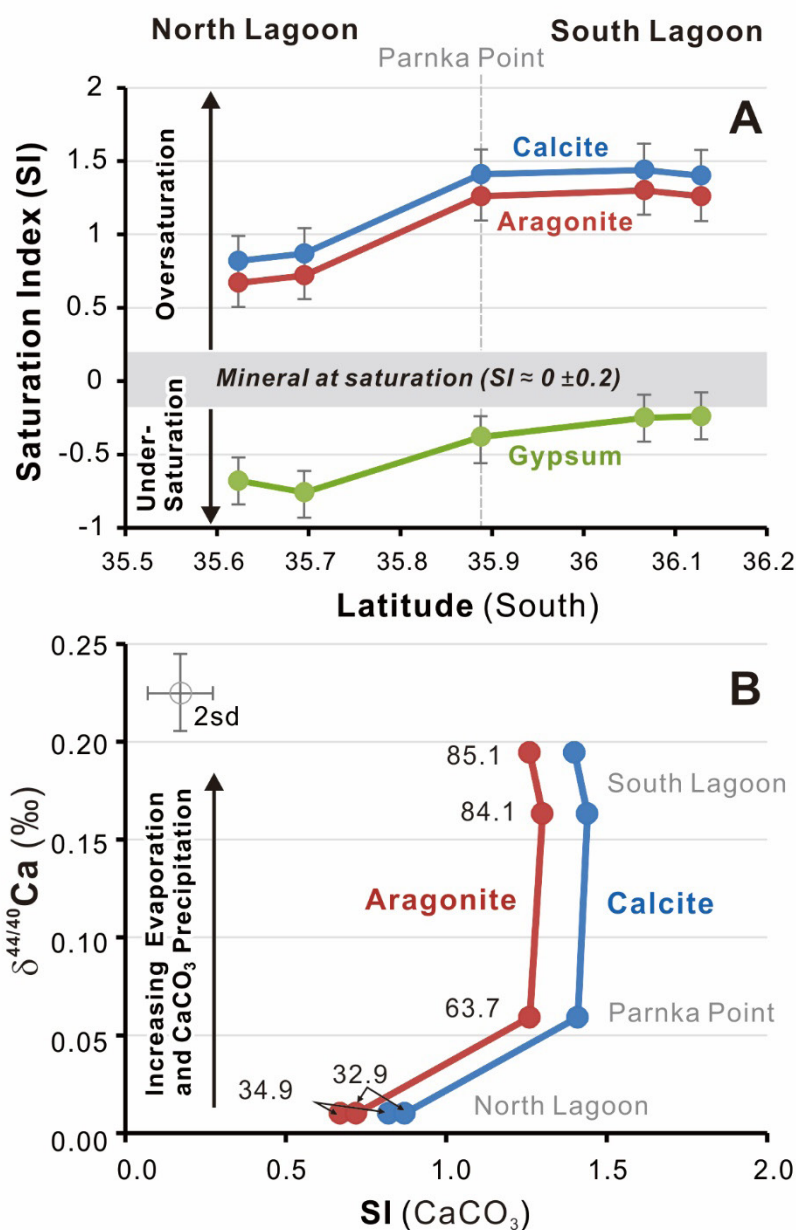


Figure B.2: (A) Saturation index (SI) profiles for calcite, aragonite and gypsum across the Coorong modeled by PHREEQC, based on water chemistry data of selected samples (see Table 2). Data shown as circles. The solid color-coded lines represent the SI trends for these main three Ca-bearing minerals. (B) Measured $\delta^{44/40}\text{Ca}$ signatures of the five water samples selected for the PHREEQC modeling (see Table 2). The numbers plotted next to color-coded lines represent the measured salinities (in PSU) for individual samples.

Interestingly, the $\delta^{44/40}\text{Ca}$ of the South Lagoon waters become progressively heavier with increasing

salinity, while our data in Fig. B.2 indicate that the corresponding SI for CaCO_3 are basically kept constant and oversaturated at around 1.2 for aragonite, and ~ 1.4 for calcite in waters with salinities above ~ 65 PSU (Fig. B.2B). These results thus suggest that more Ca^{2+} (and by inference also dissolved inorganic carbon (DIC)) has been removed as CaCO_3 from the South Lagoon waters that have higher salinities. Unlike SI data that basically reflect the ‘current status’ of water carbonate chemistry and mineral saturation at a specific site, the Ca isotope signatures of lagoon waters record an integrated signal reflecting the ‘history’ of the net removal of dissolved Ca^{2+} (and DIC) species from waters at a particular site, due to the ongoing and/or past precipitation of CaCO_3 .

Finally, the PHREEQC modeling results for dolomite ($\text{CaMg}(\text{CO}_3)_2$) indicate its high oversaturation (with $\text{SI} > 2.5$) and thus ubiquitous precipitation from the Coorong waters, simply due to the excess of Ca^{2+} , Mg^{2+} and CO_3^{2-} ions in local waters. This is at odds with our observations and XRD data that clearly show almost no dolomite (i.e., $\sim 0.3 \pm 0.4\%$, see data in Table 2). This can be reconciled by taking into account (i) the high dehydration energy for Mg^{2+} ions (cf., Arvidson and Mackenzie, 1999; Mackenzie and Andersson, 2013), and (ii) the effect of dissolved sulfate anions (SO_4^{2-}) present in lagoon waters, as both of these parameters are known to act as efficient inhibitors for the precipitation of dolomite directly from seawater and/or seawater-derived fluids at typical surface temperatures (Arvidson and Morse, 2013; Mackenzie and Andersson, 2013).

B.4. Additional constraints to the magnitudes of Ca removal in the South Lagoon

B.4.1. Ca concentration and salinity

Based on the water source apportionment calculation in 5.1.4, the mass fraction of continental surface freshwater (X_{LL}) in the South Lagoon mixture is 41%. Given the Ca concentrations and salinities of the continental surface freshwater (33 ppm, 1 PSU) and seawater (414 ppm, 37 PSU), the Ca concentration and salinity of the mixture (i.e., the South Lagoon water before evaporation) are calculated to be 258 ppm and 22 PSU. Considering the typical salinity of the South Lagoon to be ~ 100 PSU, the concentration factor is ~ 4.5 . Therefore, the theoretical Ca concentration in the South Lagoon water (i.e. not considering CaCO_3 precipitation) is calculated to be ~ 1161 ppm. However, the realistic Ca concentration of the South Lagoon water at salinity of ~ 100 PSU is ~ 980 ppm (Table 3; Gillanders and Munro, 2012) and Fig. C.2. The fraction of the removed Ca which accounts for CaCO_3 precipitation is $(1 - 980/1161) \times 100\% \approx 16\%$.

B.4.2. Carbonate alkalinity

According to the fact that for every mole of Ca is precipitated as CaCO_3 , 2 moles of alkalinity are

removed from the water (i.e. 1 mole of CO_3^{2-}) (Lazar et al., 1983; Wojtowicz, 2001). The Ca concentration and the alkalinity (as CaCO_3) of the South Lagoon water are ~ 980 ppm (Table 3; Gillanders and Munro, 2012) and ~ 200 mg/L (Table B.2 and/or Fig. B.1) respectively, hence the fraction of Ca to be removed as CaCO_3 is calculated to be $< 11\%$ in the South Lagoon based on the available alkalinity.

But given that (i) both the Ca concentration and alkalinity data were inferred or extrapolated, (ii) the uncertainties carried along from the PHREEQC modelling (see section B.3.2), (iii) the ion concentration data in Table B.3 shows increasing Ca/alkalinity ratio towards the South Lagoon, suggesting potential non-stoichiometric effects during water evaporation in the South Lagoon due to the higher amount of Ca present relative to alkalinity in the source waters, and (iv) water input from the Salt Creek and/or groundwater discharge could add additional alkalinity to the South Lagoon, as observed by Reid and Mosley (2016), suggesting existing seasonal variations of CaCO_3 fluxes. Therefore, this calculation only provides a rough estimate of the magnitude of Ca removal in the South Lagoon at the time of sampling.

Appendix C: Supplementary Tables and Figures

Table C.1. Table with the sampling locations, coordinates, and sampling dates.

Sample ID ¹	Area	Position	Sampling Date	Latitude (degree South)	Longitude (degree East)
Coorong Lagoon water samples					
M13	Murray Mouth		April 28, 2016	35.55	138.88
C02	North Lagoon	Mark Point	May 16, 2016	35.62	139.08
C03	North Lagoon	Long Point	May 16, 2016	35.70	139.16
C04	North Lagoon	Noonameena	May 16, 2016	35.77	139.27
C05	North Lagoon	Rob's Point	May 16, 2016	35.79	139.32
C07	NL-SL connection	Parnka Point North	May 16, 2016	35.89	139.40
C06	NL-SL connection	Parnka Point	May 16, 2016	35.90	139.40
C08	South Lagoon	The end of Field Road	May 16, 2016	35.94	139.49
C09	South Lagoon	1.5 km south to the end of Woods Well Road	May 16, 2016	36.01	139.56
C10	South Lagoon	Policemen's Point	May 16, 2016	36.07	139.60
C11	South Lagoon	Salt Creek	May 16, 2016	36.13	139.64
C12	South Lagoon	1 km south of Pipe Clay Lake	May 16, 2016	36.16	139.65
SL9	South Lagoon	Site near Halite Lake	April 10, 2015	36.16	139.65
SL8	South Lagoon	Pelet/Milne Lake (Ephemeral Lake)	April 10, 2015	36.14	139.65
SL7	South Lagoon	Policeman Point	April 10, 2015	36.06	139.59
SL6	South Lagoon	Woods Well	April 10, 2015	36.01	139.55
SL5C	South Lagoon	Seawater further from seepage site	April 10, 2015	35.96	139.50
SL5B	South Lagoon	Seawater close to seepage	April 10, 2015	35.95	139.50
SL4B	South Lagoon	Lagoon widest part	April 10, 2015	35.92	139.46
SL4A	South Lagoon	Lagoon widest part	April 10, 2015	35.91	139.46
SL1B	South Lagoon	Parnka Point	April 10, 2015	35.90	139.40
SL2	South Lagoon	Parnka Point	April 10, 2015	35.89	139.41
NL1	North Lagoon	Rob's Point	April 10, 2015	35.80	139.32

Appendix 2

NL2	North Lagoon	Near Robs Point	May 15, 2015	35.80	139.32
NL3	North Lagoon	North of Robs Point ~1.5km	May 15, 2015	35.79	139.31
NL4	North Lagoon	Near Emohruo	May 15, 2015	35.78	139.30
NL5	North Lagoon	North of NL4 ~1.5km	May 15, 2015	35.78	139.29
NL6	North Lagoon	Noonameena	May 15, 2015	35.77	139.27
NL7	North Lagoon	Near Camp Coorong	May 15, 2015	35.76	139.26
NLB1	North Lagoon	Northern North Lagoon, boat sample	May 15, 2015	35.70	139.16
NLB3	North Lagoon	Northern North Lagoon, boat sample	May 15, 2015	35.68	139.15
NLB4	North Lagoon	Northern North Lagoon, boat sample	May 15, 2015	35.68	139.14
NLB5	North Lagoon	Northern North Lagoon, boat sample	May 15, 2015	35.67	139.13
NLB6	North Lagoon	Northern North Lagoon, boat sample	May 15, 2015	35.66	139.12
NLB11	North Lagoon	Northern North Lagoon, boat sample	May 15, 2015	35.63	139.07
NLB15	North Lagoon	Northern North Lagoon, boat sample	May 15, 2015	35.59	139.02
Groundwater samples					
JWP2	North Lagoon (Groundwater)	Near Noonameena		35.79	139.31
BWP2	North Lagoon (Groundwater)	Near Noonameena		35.78	139.30
Lower Lakes, river and seawater samples					
C01	Lower Lakes connection	Narrung	May 16, 2016	35.51	139.19
LL1	Lake Albert	Jetty on Lake Albert in Meningie	May 15, 2015		
LL2	Lake Alexandrina		May 15, 2015	35.51	139.13
LL3	Lower Lakes Connection	Narrung	May 15, 2015	35.51	139.19
MR1	Murray River	Wellington ferry crossing	May 15, 2015	35.33	139.39

Appendix 2

SL11	Southern Ocean	Open Ocean seawater	April 10, 2015	36.29	139.70
Sediment sample					
CLS-1	South Lagoon	Near Halite Lake in the Coorong	Mar 5, 2017	36.15	139.64
Rainwater samples					
Rain-IT (galvanized iron tank)	South Australia	10 km north to coastline	Sept. 13, 2016		
Rain-PT (polyethylene tank)	South Australia	10 km north to coastline	Sept. 13, 2016		
Rain-A Sr	South Australia	10 km north to coastline	Aug. 29-30, 2016		
Rain-B Sr	South Australia	10 km north to coastline	Aug. 29-30, 2016		

¹refers to IDs of waterbody samples, fish/otoliths samples collected at the same location are labelled and referred in the main text as “waterbody sample ID-XX”, where XX is the code for the fish.

Table C.2. Measured fish sample parameters. Minimum Sr content in otoliths samples, calculated based on otoliths weights and the minimum concentration of Sr, which is about 1000 ppm (Doubleday et al., 2013).

Sample ID	Fish body length (mm)	Fish weight (g)	Single otolith weight (mg)	Minimum Sr in a single otolith (ng)
M13-01	51	0.74	0.954	954
M13-02	56	1.02	1.162	1162
M13-14	61	1.53	1.317	1317
C03-02	54	1.10	1.169	1169
C03-03	69	2.52	1.495	1495
C03-04	54	1.28	1.300	1300
C03-05	55	1.18	1.197	1197
C04-01	50	0.79	0.831	831
C04-02	41	0.49	0.595	595
C04-03	47	0.73	0.865	865
C07-01	35	0.27	0.481	481
C07-02	41	0.41	0.586	586
C06-02	36	0.42	0.682	682
C06-04	40	0.40	0.634	634
C08-01	41	0.45	0.602	602
C08-03	36	0.28	0.513	513
C09-01	43	0.53	0.750	750

Appendix 2

C09-02	36	0.33	0.515	515
C10-01	55	1.39	1.277	1277
C10-03	68	2.13	2.139	2139
C10-05	48	0.90	1.048	1048
C11-01	39	0.43	0.614	614
C11-03	34	0.36	0.633	633
C12-01	30	0.19	0.300	300
C12-02	29	0.15	0.305	305
C12-03	28	0.15	0.301	301

Table C.3. Elemental concentrations (in ppm) of waterbody samples and standard seawater IAPSO (OSIL) measured by solution ICP-MS.

Sample name	Salinity (PSU)	Na	Mg	Al	Ca	Ti	Cr	Mn	Fe	Cu	Zn	Sr	Ba
MR1*	0.15	27.5			10.1							0.13	
LL2	0.43	125.9	21.1	0.0020	35.2	0.45	0.00024	0.00026	0.009	0.0105	0.0027	0.32	0.0558
C01	0.80	181.2	29.9	0.0045	33.1	0.63	0.00047	0.00068	0.014	0.0061	0.0136	0.48	0.0752
JWP2*	1.15	147.4			101.1							1.34	
LL1	1.29	369.5	58.6	0.0042	46.5	0.61	0.00027	0.00031	0.019	0.0277	0.0051	0.88	0.0980
BWP2*	3.66	460.7			149.7							2.12	
NL3	19.50	5582.5	676.4	0.0101	213.3	1.76	0.00087	0.00034	0.047	0.0031	0.0031	4.56	0.0197
NL2	19.69	7721.3	946.8	0.0119	301.0	6.89	0.00189	0.00185	0.059	0.0076	0.0038	6.05	0.0172
NL4	20.09	5552.4	681.2	0.0140	201.9	5.29	0.00124	0.00069	0.048	0.0027	0.0044	4.51	0.0195
NL5	20.75	6034.8	732.6	0.0131	205.9	7.90	0.00280	0.00060	0.056	0.0026	0.0112	4.80	0.0206
NLB4	29.53	9120.4	1117.9	0.0028	313.9	0.96	0.00200	0.00162	0.062	0.0059	0	7.18	0.0165
NLB5	32.19	9760.4	1192.0	0	402.4	1.75	0.00148	0.00163	0.065	0.0049	0	7.74	0.0127
C03	32.96	9448.5	1162.3	0	336.5	7.21	0.00212	0.00123	0.067	0.0028	0.0068	7.56	0.0086
C05	34.05	9945.7	1216.6	0	382.5	1.23	0.00130	0.00560	0.067	0.0015	0	8.42	0.0113
NL1	34.44	10715.9	1298.4	0.0265	355.9	8.28	0.00165	0.00049	0.074	0.0026	0.0043	8.86	0.0213
C04	34.67	10129.6	1247.9	0.0009	367.2	4.39	0.00176	0.00355	0.073	0.0024	0.0376	8.10	0.0095
OSIL	35.00	11333.6	1374.6	0.0098	390.4	2.09	0.02781	0.00177	0.181	0.0023	0.0462	8.86	0.0028
C02	34.98	10377.8	1275.1	0.0213	382.9	8.75	0.00567	0.00726	0.084	0.0035	0.0576	8.16	0.0083
C07	56.97	12821.8	1567.9	0.0025	445.8	2.37	0.00206	0.00053	0.084	0.0021	0	10.57	0.0194
C06	63.73	19981.0	2409.1	0.0150	652.3	3.17	0.00268	0.00255	0.131	0.0027	0	16.15	0.0268
C09	65.45	19792.3	2407.1	0.0011	638.6	3.22	0.00256	0.00353	0.128	0.0035	0.0067	15.87	0.0265

SL5B	81.55	24432.5	2936.4	0	780.5	2.74	0.00238	0.00104	0.160	0.0049	0	19.95	0.0255
SL5C	82.10	24479.1	2905.5	0.0092	798.1	4.27	0.00245	0.00127	0.169	0.0051	0.0006	20.16	0.0264
SL4B	83.30	25223.6	3067.7	0	795.6	3.80	0.00233	0.00095	0.166	0.0062	0	20.78	0.0252
C10	84.10	25442.0	3026.6	0.0027	814.4	6.10	0.00399	0.00837	0.183	0.0075	0.0023	19.87	0.0294
C11	85.10	25689.7	3106.6	0.0217	802.7	3.26	0.00440	0.01049	0.170	0.0072	0.0414	19.95	0.0298
SL6	89.35	29316.3	3537.0	0.0130	883.5	3.69	0.00297	0.00081	0.196	0.0058	0.0013	23.56	0.0272
C08	93.40	13428.0	1653.0	0.0064	433.5	6.53	0.00361	0.01886	0.176	0.0054	0.0023	11.16	0.0304
C12	94.10	26618.3	3204.0	0.0038	810.5	5.85	0.00577	0.00484	0.174	0.0044	0	20.65	0.0290
SL7	104.65	32761.2	3962.2	0.0231	986.1	6.09	0.00305	0.00336	0.205	0.0083	0.0031	25.51	0.0275
SL8	108.10	36897.0	2698.3	0.0052	441.5	5.13	0.00516	0.00036	0.033	0.0086	0.0005	58.11	0.0479
SL9	113.60	37147.4	4373.1	0.0259	1066.3	13.62	0.00318	0.00136	0.235	0.0111	0.0053	28.09	0.0300
SL11	36.97	10800.0			414.0							8.02	

*Measurements from Kell-Duivestein (2015).

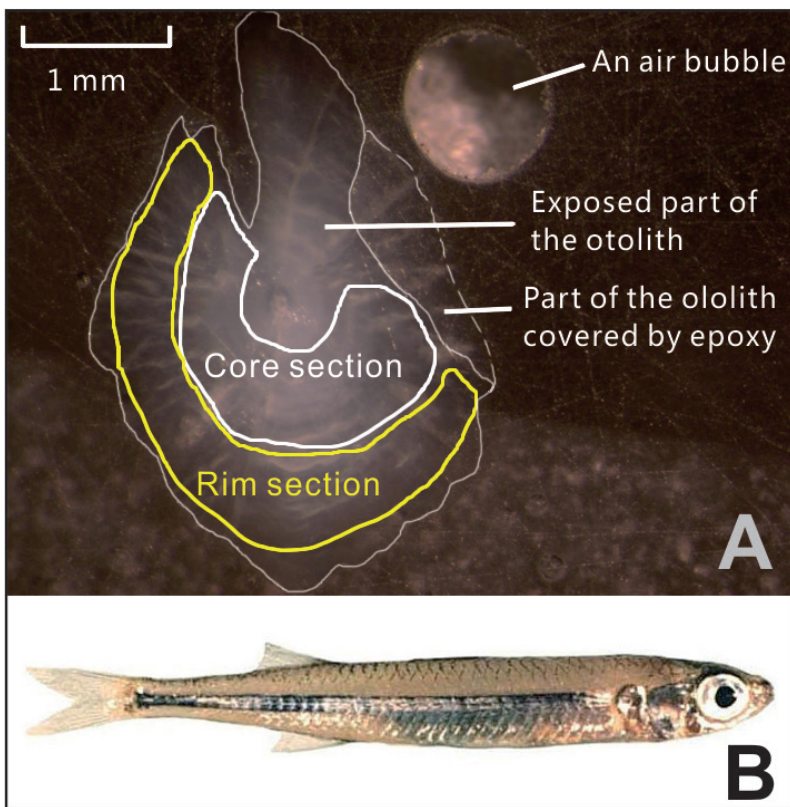
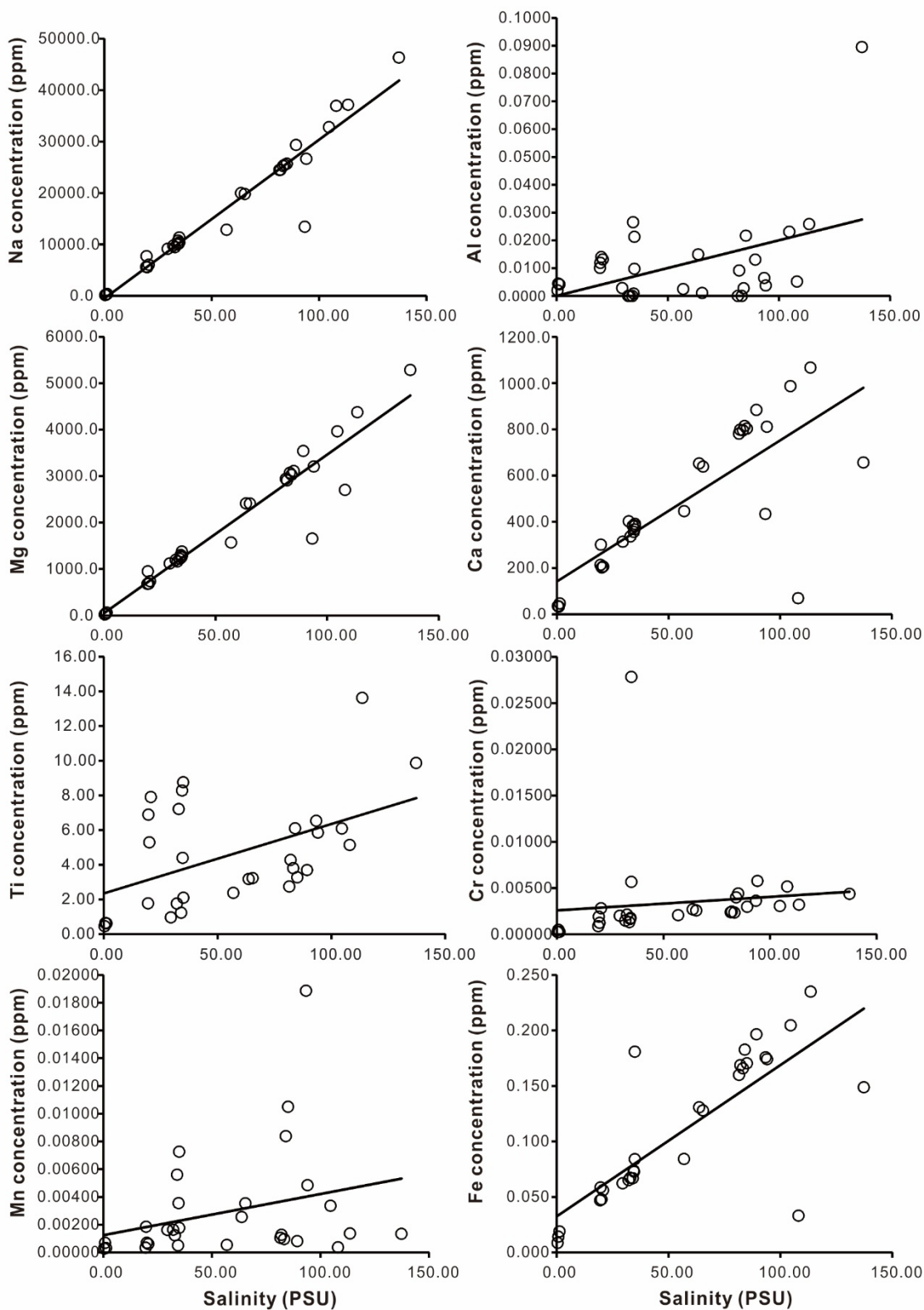


Figure C.1: (A) Photo of otolith sample C03-03 embedded in epoxy and polished, with micro-drilling section patterns on the exposed part of the otolith indicated. (B) Image of a mature fish specimen of *Atherinosoma microstoma* (body length ca. 10 cm).



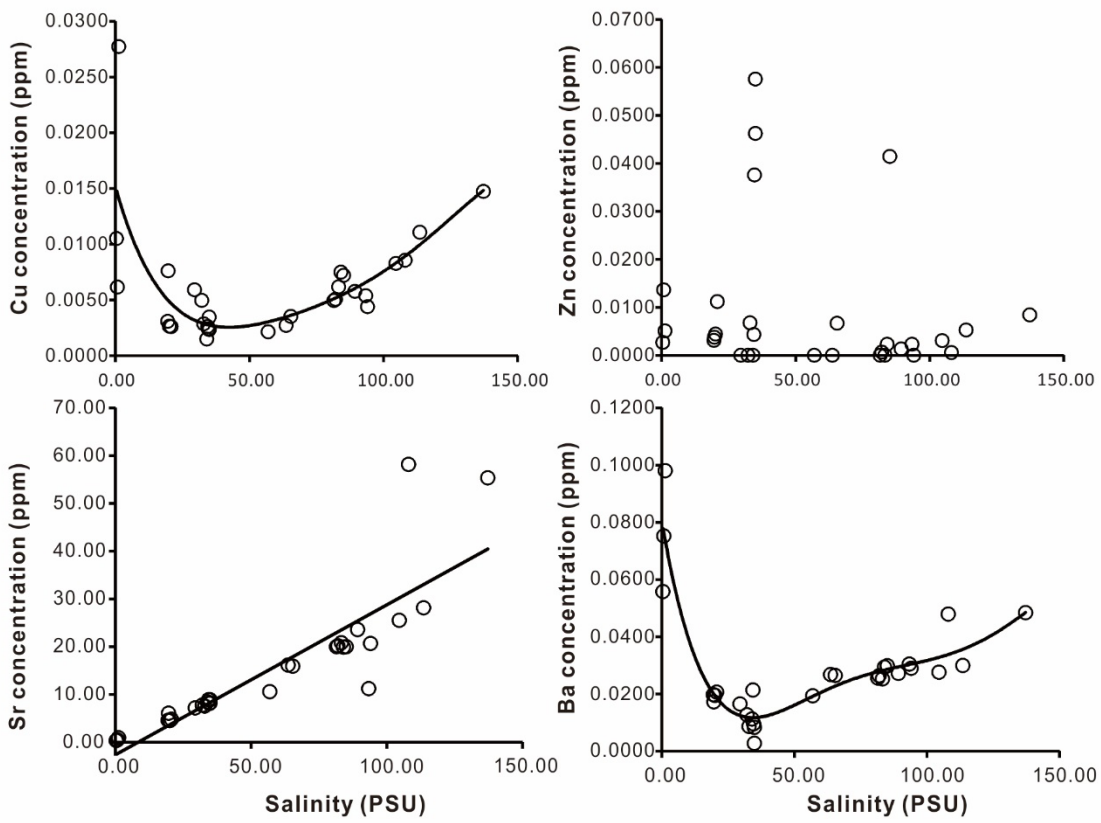


Figure C.2: Elemental concentrations (ppm) vs. salinity (PSU) for waterbody samples collected in May 2016.

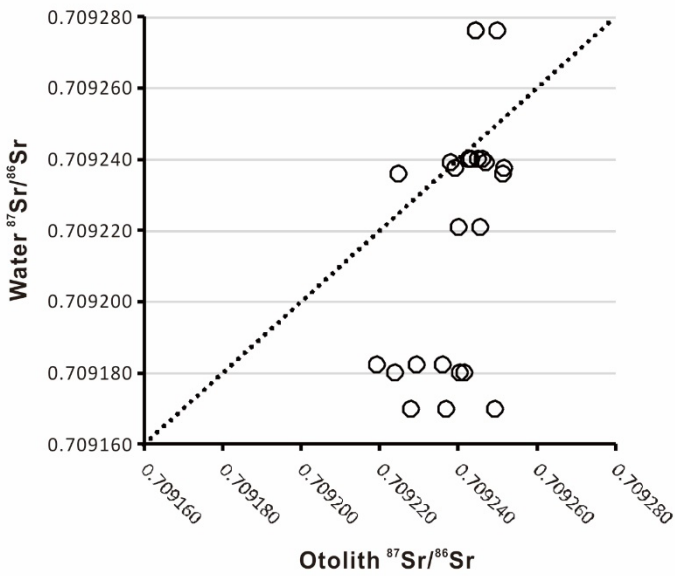


Figure C.3: $^{87}\text{Sr}/^{86}\text{Sr}$ in the Coorong waters vs. $^{87}\text{Sr}/^{86}\text{Sr}$ in fish otoliths (sampled in 2016).

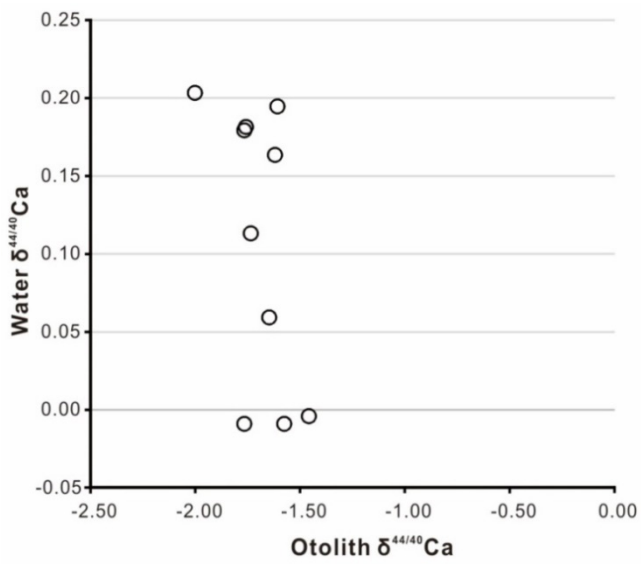


Figure C.4: $\delta^{44/40}\text{Ca}$ in the Coorong waters and fish otoliths (sampled in 2016).

References

- Arvidson, R. S., and Mackenzie, F. T. (1999) Dolomite Problem: control of precipitation kinetics by temperature and saturation state. *American Journal of Science* **229**, 257-288.
- Arvidson, R. S., and Morse, J. W. (2013) Formation and diagenesis of carbonates. In: Mackenzie F. T. (Ed.) *Treatise on Geochemistry: Sediments, Diagenesis and Sedimentary Rocks*. Vol. 9, 2nd Edition, Elsevier-Pergamon, Oxford.
- Doubleday, Z. A., Harris, H. H., Izzo, C. and Gillanders, B. M. (2013) Strontium randomly substituting for calcium in fish otolith aragonite. *Analytical Chemistry* **86**, 865-869.
- Gillanders, B. M. and Munro, A. R. (2012) Hypersaline waters pose new challenges for reconstructing environmental histories of fish based on otolith chemistry. *Limnology and Oceanography* **57**, 1136.
- Lazar, B., Starinsky, A., Katz, A., Sass, E. and Ben-Yaakov, S. (1983) The carbonate system in hypersaline solutions: alkalinity and CaCO₃ solubility of evaporated seawater. *Limnology and Oceanography* **28**, 978-986.
- Mackenzie, F. T., and Andersson, A. J. (2013) The Marine Carbonate System and Ocean Acidification during Phanerozoic Time. *Geochemical Perspectives*, **2**, p. 227.
- Kell-Duivesteyn, I. (2015) Tracing the groundwater inputs and water-mass mixing in the Coorong lagoons (South Australia) using strontium isotopes. (Honours (Geology/Geophysics)), The University of Adelaide, Adelaide.
- Reid, R. J. and Mosley, L. M. (2016) Comparative contributions of solution geochemistry, microbial metabolism and aquatic photosynthesis to the development of high pH in ephemeral wetlands in South East Australia. *Science of The Total Environment* **542**, 334-343.
- Romaniello, S., Field, M., Smith, H., Gordon, G., Kim, M. and Anbar, A. D. (2015) Fully automated chromatographic purification of Sr and Ca for isotopic analysis. *Journal of Analytical Atomic Spectrometry* **30**, 1906-1912.
- Wojtowicz, J. A. (2001) Calcium carbonate precipitation potential. *Journal of the Swimming Pool and Spa Industry* **2**, 51-57.

Appendix 3

**Appendices for Chapter 3 - Impact of salinity
and carbonate saturation on stable Sr
isotopes ($\delta^{88/86}\text{Sr}$) in a lagoon-estuarine system**

Appendix A. Sampling site information

Table A.1. Table of sampling locations, GPS coordinates, water temperature, salinity and sampling dates, associated with samples analysed for Sr isotopes (i.e., groups 1-2) of the main manuscript. The following abbreviations are used: NL = North Lagoon, and SL = South Lagoon.

Sample ID	Area	Location	Temperature (°C)	Salinity (PSU)	Sampling Date	Latitude (degree South)	Longitude (degree East)
Coorong Lagoon water samples							
C02	North Lagoon	Mark Point	15.1	34.98	May 16, 2016	35.62	139.08
C04	North Lagoon	Near Robs Point	15.3	34.67	May 16, 2016	35.77	139.27
NL2	North Lagoon	Noonameena		19.69	May 15, 2015	35.80	139.32
C07	NL-SL connection	Parnka Point North	16.1	56.97	May 16, 2016	35.89	139.40
C06	NL-SL connection	Parnka Point	15.2	63.73	May 16, 2016	35.90	139.40
C10	South Lagoon	Policemen's Point	18.3	84.10	May 16, 2016	36.07	139.60
C11	South Lagoon	Salt Creek	17.7	85.10	May 16, 2016	36.13	139.64
C12	South Lagoon	1 km south to Milne Lake/ Pipe Clay Lake	16.5	94.10	May 16, 2016	36.16	139.65
Groundwater samples							
JWP2	North Lagoon (Groundwater)	Near Noonameena		1.15	June 25, 2015	35.79	139.31
BWP2	North Lagoon (Groundwater)	Near Noonameena		3.66	June 25, 2015	35.78	139.30
Continental water and seawater samples							
RMW	River Murray	Near Tailem Bend	12.1	0.22	Aug 31, 2018	35.29	139.45
C01	The Lower Lakes connection	Narrung	15.2	0.80	May 16, 2016	35.51	139.19
SCW	Salt Creek	East side of Princes Hwy	15.9	7.18	Aug 31, 2018	36.13	139.65
SL11	Southern Ocean	End of 42 Mile Crossing		36.97	April 10, 2015	36.29	139.70
Ephemeral Lakes							
ELW1	Milne Lake/ Pipe Clay Lake	Along Scenic Dr/Loop Rd	17.2	24.99	Aug 31, 2018	36.14	139.64
ELW2	Halite Lake	Along Scenic Dr/Loop Rd	18.0	161.86	Aug 31, 2018	36.15	139.64
Carbonate samples							

Appendix 3

122s	North Lagoon (<i>A. helmsi</i> shells)	Mark Point			Jan 18, 2018	35.63	139.08
149s	North Lagoon (<i>A. helmsi</i> shells)	~3km SE to Mark Point			May 5, 2018	35.65	139.10
151s	North Lagoon (<i>A. helmsi</i> shells)	Pelican Point			May 5, 2018	35.60	139.03
CW2w	North Lagoon (tubeworm <i>Ficopomatus enigmaticus</i> formed reef)	Long Point			Aug 31, 2018	35.70	139.16
CLS-1	South Lagoon (sediment crust)	Near Halite Lake in the Coorong			Mar 5, 2017	36.15	139.64

Table A.2. Table of sampling locations, GPS coordinates, water temperature, salinity and sampling dates of waters used for PHREEQC (Figs. 2D and D.2) and CO2SYS modelling of mineral saturation (Fig. D.2). The following abbreviations are used: NL = North Lagoon, and SL = South Lagoon.

Sample ID	Area	Location	Temperature (°C)	Salinity (PSU)	Sampling Date	Latitude (degree South)	Longitude (degree East)
Coorong Lagoon water samples							
CA1	North Lagoon	Mark Point	14.6	27.56	May 24, 2018	35.63	139.08
CW1	North Lagoon	Mark Point	12.0	31.66	Aug 31, 2018	35.63	139.08
CA2	North Lagoon	Long point	14.6	32.53	May 24, 2018	35.70	139.16
CW2	North Lagoon	Long point	13.8	44.98	Aug 31, 2018	35.70	139.16
CA3	North Lagoon	Near Robs Point	15.5	38.29	May 24, 2018	35.77	139.27
CW3	North Lagoon	Near Robs Point	14.0	51.29	Aug 31, 2018	35.77	139.27
CA4	North Lagoon	Noonamena	15.7	44.09	May 24, 2018	35.79	139.30
CW4	North Lagoon	Noonamena	15.6	55.51	Aug 31, 2018	35.79	139.30
CA6	NL-SL connection	Parnka Point North	16.3	61.39	May 24, 2018	35.89	139.40

Appendix 3

CA5	NL-SL connection	Parnka Point	15.7	62.93	May 24, 2018	35.90	139.40
CW5	NL-SL connection	Parnka Point	15.1	58.51	Aug 31, 2018	35.90	139.40
CA7	South Lagoon	Field Rd	15.3	69.54	May 24, 2018	35.94	139.49
CW7	South Lagoon	Field Rd	16.4	57.62	Aug 31, 2018	35.94	139.49
CA8	South Lagoon	Jacks Point	15.3	76.90	May 24, 2018	36.03	139.57
CW8	South Lagoon	Jacks Point	16.6	60.65	Aug 31, 2018	36.03	139.57
CA9	South Lagoon	South to Salt Creek	15.5	90.83	May 24, 2018	36.16	139.65
CW9	South Lagoon	South to Salt Creek	15.3	58.51	Aug 31, 2018	36.16	139.65
Continental water and seawater samples							
RMA	River Murray	Near Tailem Bend	15.2	0.21	May 24, 2018	35.29	139.45
RMW	River Murray	Near Tailem Bend	12.1	0.22	Aug 31, 2018	35.29	139.45
LLA	The Lower Lakes connection	Narrung	14.0	0.50	May 24, 2018	35.51	139.19
SCA	Salt Creek	Salt Creek	14.7	7.66	May 24, 2018	36.13	139.65
SCW	Salt Creek	Salt Creek	15.9	7.18	Aug 31, 2018	36.13	139.65

Appendix B. Elemental and cation/anion compositions of waters and carbonates

B.1 Elemental concentrations analyses of water samples

The concentrations of selected dissolved cations (Al, B, Ca, Fe, K, Mg, Mn, Na, P, S, Si and Sr) in filtered water samples collected in 2018 (i.e., Group 3) were measured using a Thermo Fisher iCAP 7600 ICP-AES at the Australian Nuclear Science and Technology Organisation (ANSTO). All elemental concentrations were determined against calibration standards with element concentrations ranging from 0.01 - 10 ppm and up to 500 ppm for Ca, K, Mg and Na. All standards were prepared from certified 1000 ± 3 ppm single element National Institute of Standards and Technology (NIST) standards in 3% v/v Merck Suprapure Nitric acid. A certified ‘cocktail’ of multi-element NIST standard from another supplier was run at the beginning of each analytical session as another independent quality control. A set of standards was added after every 20th sample throughout the analysis session to monitor instrument drift. All samples and standards were spiked with 1 ppm of In and Rh for internal standard correction. Samples with concentrations over the instrument calibration range were diluted with 3% v/v HNO₃ and reanalysed. A separate rinse containing 0.25 ml of 1% v/v Triton X-100 in 5 L of 1% HNO₃ was used for rinsing between standards and samples. The typical uncertainty for all analyses was $\pm 5\%$ (2SD).

The concentrations of dissolved anions (F⁻, Cl⁻, NO₂⁻, Br⁻, NO₃⁻, SO₄²⁻, I⁻ and PO₄³⁻) in filtered water samples collected in 2018 were measured using a Dionex ICS-2100 Ion Chromatograph (IC) with a KOH eluant generator, an auto-suppressor and temperature controlled conductivity detector coupled to a 4 mm AS19 guard and AS19 analytical column at ANSTO. Samples were diluted with Type I ultra-pure water.

Concentrations were determined against calibration standards ranging from 0.01 ppm to 100 ppm for F⁻, NO₂⁻, Br⁻, NO₃⁻, I⁻, PO₄³⁻ and up to 500ppm for Cl⁻ and SO₄²⁻. All standards were prepared from certified 1000 ± 3 ppm (except for NO₂⁻, which is certified for 1000 ± 12 ppm) single element NIST traceable standards with type I ultra-pure water. A certified ‘cocktail’ or multi-element NIST standard from HPS (High Purity Standards) was run at the beginning of each analytical session as another independent quality control. The typical uncertainty for all analyses was $\pm 5\%$. The measured elemental concentrations in waters, including main cations and anions, are listed in Tables B.1 and B.2 below.

Table B.1. Elemental concentrations of dissolved cations in waters analysed by ICP-AES in ppm (mg/L). For water salinity and sampling site information see also Table A.2. The typical uncertainty of measurements for this study was $\pm 5\%$ (2SD).

Water samples											
ID	B	Ca	Fe	K	Mg	Mn	Na	P	S	Si	Sr
RMA	0.05	12.75	<0.005	3.96	8.415	<0.001	43.4	<0.01	6.1	0.8	0.16
L1A	0.1	24.27	<0.005	8.86	20.843	<0.001	126	0.01	14.9	0.1	0.32
CA1	2.85	221	<0.005	230	693	0.006	5792	0.03	649	0.3	4.38
CA2	3.82	290	<0.005	310	966	0.007	7663	0.03	820	0.7	6.05
CA3	4.81	360	<0.005	387	1206	0.027	9819	0.04	964	0.2	7.84
CA4	5.69	411	<0.005	454	1400	0.009	11671	0.05	1147	0.2	9.34
CA6	8.37	578	<0.005	670	2126	0.049	17500	0.09	1700	0.8	13.5
CA5	8.3	585	<0.005	676	2120	0.006	17302	0.08	1744	0.6	13.6
CA7	9.9	697	<0.005	819	2531	0.07	20383	0.09	2064	1.3	16.5
CA8	11.92	759	0.008	918	2833	0.033	22743	0.1	2319	1.5	18.3
CA9	13.84	860	0.011	1061	3127	0.004	26006	0.12	2783	1.9	21.1
SCA	1.03	31.8	<0.005	45.90	140	<0.001	1413	0.03	129	2.6	2.63
RMW	0.04	10.7	0.116	3.54	9.4	<0.001	57.5	0.02	7.6	0.8	0.15
CW1	4.6	329	<0.005	361	1115	0.005	9260	0.11	944	0.4	7.28
CW2	6.49	467	<0.005	513	1623	0.007	13482	0.09	1288	0.2	10.5
CW3	7.43	532	<0.005	596	1891	0.011	15195	0.07	1477	0.2	12.2
CW4	7.94	553	<0.005	628	1952	0.025	15902	0.22	1587	0.4	12.9
CW5	8.49	580	<0.005	666	2078	<0.001	16938	0.18	1701	0.9	13.6
CW7	8.11	568	<0.005	653	2034	0.002	16715	0.27	1630	1.2	13.6
CW8	8.78	616	<0.005	718	2181	<0.001	17755	0.26	1762	1.6	14.8
ELW1	5.52	27.6	0.007	252	607	<0.001	7926	0.16	466	1.0	19.0
ELW2	22.2	120	<0.005	1200	3570	0.011	51152	0.17	3640	0.3	11.1
CW9	8.58	566	<0.005	684	2064	0.002	17322	0.17	1685	1.8	14.3
SCW	1.18	98.4	<0.005	54.3	245	<0.001	2067	0.06	217	4.9	7.66
Standards and certified values											

ID	B	Ca	Fe	K	Mg	Mn	Na	P	S	Si	Sr
IAPSO measured#	5.4	406.5		418	1310		10600		965.5	0.8	8.1
IAPSO published values*	4.5	412		399	1290		10770		904	2.8	7.9
IV-ICPMS-71A (10ppm) measured	9.73	9.74	10.19	9.37	9.76	9.67	9.58	9.58	9.61		9.80
IV-ICPMS-71A certified values	9.99	9.99	9.99	10.00	9.99	9.99	9.99	9.99	9.99		9.99
±	0.06	0.04	0.04	0.04	0.04	0.04	0.04	0.04	0.05		0.04
IV-ICPMS-71B (10ppm) measured										11.74	
IV-ICPMS-71B certified values										10.00	
±										0.06	

The typical uncertainty of the IAPSO standard for this study was $\pm 5\%$ (2SD).

* Source: Summerhayes, C. P., and Thorpe, S. A., 1996 : *Oceanography An Illustrated Guide*, Chapter 11, 165-181.

Table B.2. Concentrations (ppm) of main dissolved anions in waters analysed by IC. For more details on water salinity and sampling sites see also data in Table A.2. The typical uncertainty of measurements for this study was $\pm 5\%$ (2SD).

Water samples										
ID	F ⁻	Cl ⁻	NO ₂ ⁻	Br ⁻	NO ₃ ⁻	SO ₄ ²⁻	I ⁻	PO ₄ ³⁻		
RMA	0.18	71.57	<0.01	0.20	0.63	18.23	<0.05	<0.5		
LLA	0.23	239.23	<0.01	0.74	<0.5	43.7	<0.05	<0.5		
CA1	<5	12167	<1	38.4	<50	1931	<5	<50		

CA2	<5	16559	<1	54.2	<50	2342	<5	<50
CA3	<5	19126	<1	62.2	<50	2802	<5	<50
CA4	<5	22712	<1	74.7	<50	3280	<5	<50
CA6	<5	37430	<1	123.3	<50	5161	<5	<50
CA5	<5	38109	<1	124.8	<50	5410	<5	<50
CA7	<5	42413	<1	138.0	<50	5887	<5	<50
CA8	<5	58235	<1	174.1	<50	7253	<5	<50
CA9	<5	61703	<1	178.3	<50	7769	<5	<50
SCA	0.8	2584	<0.1	5.99	<5	397	<0.5	<5
RMW	0.23	100	0.04	0.26	<0.5	23	<0.05	<0.5
CW1	<5	18579	<1	59.80	<50	2587	<5	<50
CW2	<5	26367	<1	86.73	<50	3660	<5	<50
CW3	<5	30391	<1	100.32	<50	4201	<5	<50
CW4	<5	39381	<1	128.78	<50	5444	<5	<50
CW5	<5	34089	<1	111.22	<50	4724	<5	<50
CW7	<5	33847	<1	110.96	<50	4689	<5	<50
CW8	<5	37877	<1	123.01	<50	5246	<5	<50
ELW1	<5	14835	<1	26.23	<50	1301	<5	<50
ELW2	<5	102918	<1	154.95	<50	9950	<5	<50
CW9	<5	37475	<1	120.47	<50	5188	<5	<50
SCW	1.7	4105	<0.1	10.62	<5	652	<0.5	<5
Standards and certified values								
ID	F-	Cl-	NO₂⁻	Br-	NO₃⁻	SO₄²⁻	I-	PO₄³⁻
IAPSO measured#	1	19050		67		2655	0.05	
IAPSO published values*	1.3	19354		67				
IC-1 Solution A (5ppm) measured	4.97	4.97		4.89	5.87	4.83		4.80
IC-1 Solution A (5ppm) certified values	5.00	5.00		5.00	5.00	5.00		5.00
±	0.05	0.05		0.05	0.05	0.05		0.05

IC-1 Solution B (5ppm) measured			4.63						
IC-1 Solution B (5ppm) certified values			5.00						
±			0.10						

The typical uncertainty of the IAPSO standard for this study was $\pm 5\%$ (2SD).

* Source: Summerhayes, C. P., and Thorpe, S. A., 1996 : *Oceanography An Illustrated Guide*, Chapter 11, 165-181.

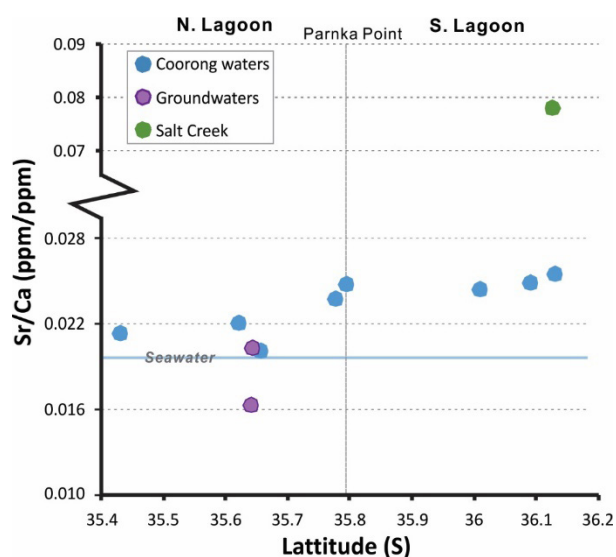


Figure B.1: Elemental Sr/Ca ratios (ppm/ppm) in waters displayed in Figs. 2A, B, C of the main manuscript (for more details on sampling site information see also Table A.1).

B.2 Elemental concentration analyses of shell samples (*A. helmsi*)

The concentrations of selected elements including: Mg, Al, P, K, Ca, Cr, Mn, Fe, Co, Sr and Ba from shells of *A. helmsi* (sample IDs: 122s, 149s and 151s) were measured using an Agilent 7500cs solution ICP-MS at Adelaide Microscopy, University of Adelaide, following the method from Shao et al. (2018). The concentrations of the above elements in the shells are reported in Table B.3 below.

Table B.3. Major and trace elemental concentrations (in ppm) of bivalve shells (*A. helmsi*) analysed via solution ICP-MS. The sampling site information of these shells is listed in Table A.1.

Sample ID	Mg	Al	P	K	Ca	Cr	Mn	Fe	Co	Sr	Ba
122s	144	2.09	13.60	18.17	270011	0.08	10.95	13.44	0.04	1238	11.25
149s	201	1.40	28.21	24.47	395291	0.04	12.33	23.30	0.06	1797	12.87
151s	171	0.91	22.85	22.85	393066	0.05	22.34	10.90	0.06	1661	17.21

B.3 Alkalinity and pH of waters

Traditional glass electrode measurements of estuarine and hypersaline waters using conventional water quality probes can lead to large and unquantifiable errors (Bargrizan et al., 2017; Nand and Ellwood, 2018; Mosley and Liss, 2020). Moreover, pH buffers used for calibrating traditional elec-

trodes have much lower ionic strength compared to hypersaline waters (Loucaides et al., 2017). Thus, to ensure that the pH of collected water samples was not compromised by the above effects, we employed state-of-the-art laboratory based spectrophotometric methods for the measurement of alkalinity and pH of water samples (listed in Table A.2, Appendix A), which were analysed in the laboratory right after sample collection. The pH was spectrophotometrically determined from unfiltered water samples using meta-Cresol Purple, following Loucaides et al. (2017), which is specifically suited for Coorong water conditions that are extended to hypersaline salinity range (>100 PSU). Such procedure provides precision of 0.001-0.004 pH unit and uncertainty no more than 0.010-0.020 pH unit. However, for the purposes of a comparison of pH measurements, the acquired laboratory based spectrophotometric pH measurements are compared to field based pH data acquired by a conventional portable pH probe (YSI ProDSS meter), for samples collected in May 2018 (for details see data in Table B.4 below, and also Figure D.3).

The alkalinity was also determined spectrophotometrically following acid addition using the method of Nand and Ellwood (2018) to pH of 3.5 with 0.1M HCl. The measurements were performed in the laboratory shortly after the collection of water samples, which were transported to the lab on ice and in the dark. A set of Seawater Certified Reference Materials (supplied by Prof. Andrew Dickson, Scripps Institution of Oceanography) were also measured for pH and alkalinity with each batch of samples, and these standards gave results within certified values. The measured alkalinity and pH data from collected samples are listed below in the Table B.4. For the purposes of comparison, pH measurements made spectrophotometrically on the total pH scale were converted to the NBS pH scale using the equations of Dickson (1990), and Lewis and Wallace (1998), and the latter NBS pH scale was used in the PHREEQC modelling (Appendix D). Note that this conversion (from Total to NBS scale) might be affected by additional errors, especially in hypersaline waters where sulphate and proton equilibrium constants are more uncertain compared to typical seawater.

Table B.4. Spectrophotometric laboratory based pH data (Lab pH) and alkalinity data measured in waters collected in May and August 2018, along with conventional field-based measurements (Probe pH). For more details on water salinity and sampling site information see also Table A.2.

Sample ID	Lab pH (total scale)	Lab pH (NBS scale)	Probe pH (NBS scale)	Total Alkalinity ($\mu\text{mol/kg}$)
RMA	7.86	8.03	8.41	444
LLA	7.79	7.99	8.22	1001
CA1	7.72	8.08	7.87	971
CA2	7.92	8.29	8.22	895
CA3	7.95	8.31	8.15	1071
CA4	8.08	8.43	8.31	1277

CA6	8.03	8.50	8.28	1686
CA5	8.21	8.32	8.51	1750
CA7	7.98	8.25	8.26	2056
CA8	7.99	8.23	8.25	2064
CA9	7.96	8.16	8.26	2192
SCA	8.88	9.22	9.14	2022
RMW	7.46	7.64	N/A	571
CW1	7.77	8.18	N/A	2530
CW2	8.08	8.46	N/A	2929
CW3	7.93	8.29	N/A	3360
CW4	8.01	8.33	N/A	3728
CW5	8.05	8.37	N/A	3968
CW7	7.99	8.30	N/A	4286
CW8	8.00	8.28	N/A	4320
CW9	8.00	8.31	N/A	4424
SCW	8.57	8.87	N/A	7410

B.4 Mineralogical XRD analysis of the tubeworm carbonate sample

The X-ray Diffraction (XRD) analysis of the tubeworm carbonate sample (CW2w) was performed at the Commonwealth Scientific and Industrial Research Organisation (CSIRO), Australia. Briefly, small sub-samples of the carbonate material were hand ground in an agate mortar and pestle before being lightly pressed onto silicon low background sample holders for XRD analysis. XRD patterns were recorded with a PANalytical X'Pert Pro Multi-purpose Diffractometer using Fe filtered Co K α radiation, automatic divergence slit, 2° anti-scatter slit and fast X'Celerator Si strip detector. The diffraction patterns were recorded from 3 to 80° in steps of 0.017° 2 theta with a 0.5 second counting time per step for an overall counting time of approximately 35 minutes.

Qualitative analysis was performed on the XRD data using in-house XPLOT and HighScore Plus (from PANalytical) search/match software. Semi-quantitative analysis was performed on the XRD data using the commercial package SIROQUANT from Sietronics Pty Ltd. The results below were normalised to 100%, and hence do not include estimates of unidentified or amorphous materials.

Table B.5. Semi-quantitate (in wt.%) mineralogical XRD analysis of a 'bulk' carbonate (sample CW2w) represented by a colony of tubeworm (*F. enigmaticus*) carbonate reefs. The sampling site information is provided in Table A.1.

Sample ID	Quartz	Mg-Calcite	Aragonite	Halite
-----------	--------	------------	-----------	--------

CW2w	6	84	4	6
------	---	----	---	---



Figure B.2: An indicative photo of aragontic shells of *Arthritica helmsi* micro-bivalve (size of ca. 2.5 mm). Image by J. Trausel, Natural History Museum Rotterdam.



Figure B.3: An indicative photo of colony of calcitic tubeworm *Ficopomatus enigmaticus* reef (size ca. 50 mm). Image by J. Farkaš, Department of Earth Sciences, University of Adelaide.

Appendix C. Sr isotope analysis – Sample preparation and TIMS measurements

C.1 Column chemistry – Purification of Sr prior to the isotope analysis

Aliquots of samples and standards containing ca. 500 ng of Sr, dissolved in a nitric acid in 7 mL Teflon vials, were evaporated to dryness at $\leq 140^\circ\text{C}$. Note that the double-spiked samples were evaporated on a separate hotplate from the unspiked samples to avoid possible cross-contamination. To purify the Sr fraction from a sample matrix for isotope analyses, the procedure described in Table C.1 below was followed.

Table C.1. Purification of Sr using Micro Bio-Spin column procedure.

Step	Description
1	Remove columns from 1M HNO ₃ storage container and rinse 3 times with DI water
2	Fill 1/3 column space each with Eichrom Sr-SPS resin.
3	Wash resin and column with 3mL of single-distilled 8M HNO ₃ .
4	Wash resin and column with 3mL of DI water.
5	Wash resin and column with 3mL of single-distilled 8M HNO ₃ .
6	Wash resin and column with 3mL of DI water.
7	Wash resin and column with 3mL of single-distilled 8M HNO ₃ .
8	Load evaporated sample in 1mL of single-distilled 8M HNO ₃ .
9	Wash resin and column 5 times with 1mL of single-distilled 8M HNO ₃ .
10	Collect Sr with 6mL of 0.05M HNO ₃ , remove the purified Sr solution from the column.
11	Add a drop of 0.5 M H ₃ PO ₄ to the Sr solution to prevent the purified Sr from escaping.
12	Evaporate the Sr solution at $\leq 140^\circ\text{C}$ on hotplate.
13	Add 0.5mL of 15M HNO ₃ and 0.25 mL of 30% H ₂ O ₂ to oxidise any organics, and cap vials and heat at 110°C for at least 5 hours.
14	Evaporate the Sr solution at $\leq 140^\circ\text{C}$ on hotplate.

After the column chemistry procedure, the sample or purified Sr fractions were ready to be loaded on filaments and analysed on TIMS, as described in more details in the following section.

C.2 Mass Spectrometry and TIMS analytical procedures

All samples, standards, and blanks that went through column chemistry were loaded on single degassed Rhenium filaments following the procedure used in Shao et al. (2018), and placed into a magazine ready for TIMS analysis, which included both $\delta^{88/86}\text{Sr}$ and $^{87}\text{Sr}/^{86}\text{Sr}$ data collection using different analytical methods (for details see below).

In this study, $\delta^{88/86}\text{Sr}$ were analysed via a ‘static’ analytical method and corrected for any instrumental and/or procedural Sr isotope fractionation effects using the ^{87}Sr - ^{84}Sr double spike technique (Krabbenhöft et al., 2009). The $^{87}\text{Sr}/^{86}\text{Sr}$ ratios were analysed via a conventional ‘dynamic’ analytical

method to further improve the accuracy of Sr isotope analyses and to keep the method consistent with previously published $^{87}\text{Sr}/^{86}\text{Sr}$ data from CLMMS reported in Shao et al. (2018).

The differences in a precision and reproducibility of $^{87}\text{Sr}/^{86}\text{Sr}$ data collected by ‘static’ versus ‘dynamic’ methods (applied to the SRM987 standard) are illustrated in Fig. C.1 below, see also Andrews et al. (2016). Generally, the ‘static’ method tends to produce slightly less precise $^{87}\text{Sr}/^{86}\text{Sr}$ data with larger errors and more pronounced session-to-session drifts, compared to the ‘dynamic’ method (see Fig. C.1). However, due to longer analytical times of the latter, and the fact that the ‘static’ approach allowed to achieve sufficient precision on $\delta^{88/86}\text{Sr}$ data with the abovementioned 2SD errors of $\pm 0.03\%$ or better, we applied the more efficient ‘static’ mode for the $\delta^{88/86}\text{Sr}$ analyses, but the ‘dynamic’ approach was used for determination of high-precision $^{87}\text{Sr}/^{86}\text{Sr}$ data.

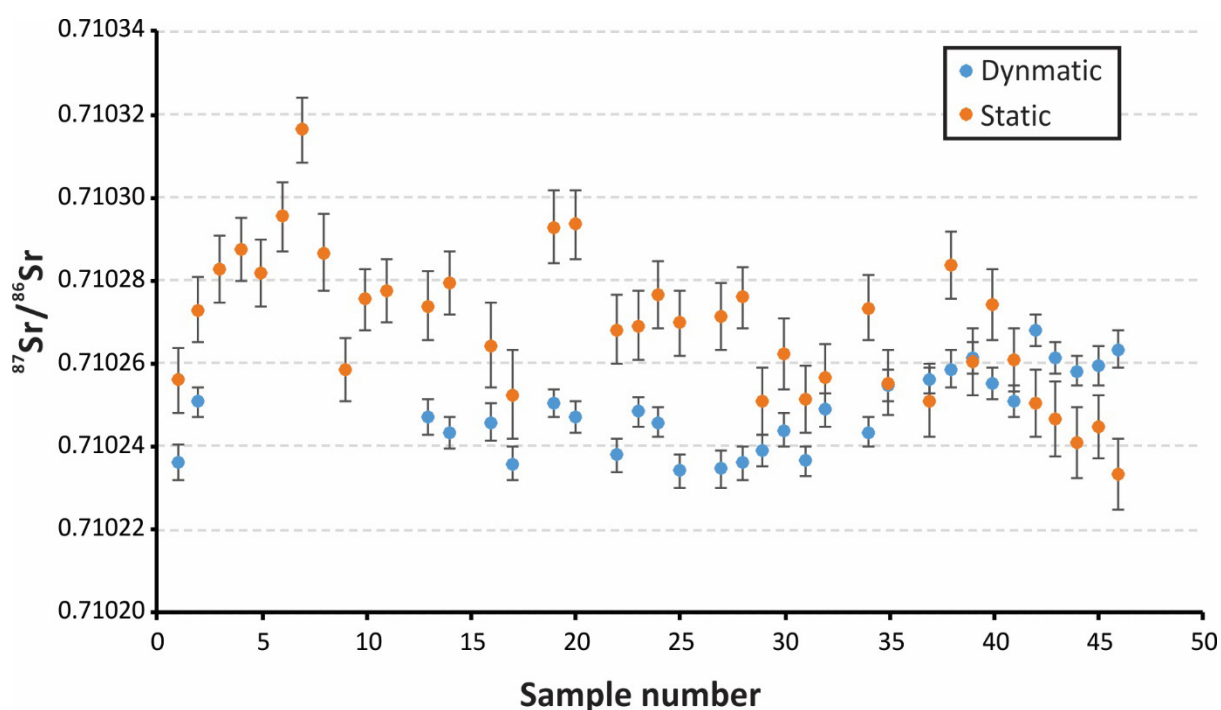


Figure C.1: A comparison of internally normalised $^{87}\text{Sr}/^{86}\text{Sr}$ ratios of SRM987 standards measured via ‘static’ and ‘dynamic’ analytical methods using TIMS. The error bars on the symbols represent internal precision (2SE) for individual runs.

C.3 Procedural Sr blank analyses

To determine the total procedural Sr blanks during the sample processing, including dissolution, evaporation, column chemistry and filament loading processes, we used an isotope dilution technique and an ^{84}Sr -enriched single spike. Such procedural blank runs were added to each batch of samples processed through columns and analysed via TIMS. Briefly, a drop of DI water was added into a 7

mL Teflon vial and one drop of 0.1 M H_3PO_4 , and an additional drop of ^{84}Sr -enriched single spike was also added to the vial and weighed on a 5-digit balance. After that, the Sr blank went through column chemistry and TIMS analyses in parallel with each batch of samples and standards.

C.4 The Sr double-spike method

In order to apply the ^{87}Sr - ^{84}Sr double spike method to analyse the $^{88}\text{Sr}/^{86}\text{Sr}$ ratios (and thus $\delta^{88/86}\text{Sr}$) in an unknown sample, one has to perform two separate analyses or runs via TIMS, where one run is on a ‘spiked’ sample and the other on its ‘un-spiked’ aliquote (cf. Krabbenhöft et al., 2009). The ^{87}Sr - ^{84}Sr double spike solution was prepared at GEOMAR (Kiel, Germany) with a total Sr concentration of 0.0090mg/g, and its respective Sr isotope composition as determined by TIMS at University of Adelaide is provided below in Table C.2.

Table C.2. Sr isotope composition of the ^{87}Sr - ^{84}Sr double spike solution analysed by TIMS IsotopX.

Isotope ratio	Mean Value	2SD (n = 4)
$^{86}\text{Sr}/^{84}\text{Sr}$	0.0099866	0.000020
$^{88}\text{Sr}/^{84}\text{Sr}$	0.0833956	0.000350
$^{87}\text{Sr}/^{84}\text{Sr}$	0.9352386	0.002940
$^{88}\text{Sr}/^{86}\text{Sr}$	8.3508519	0.017260

Table C.3. $^{84}\text{Sr}_{\text{sp}}/^{84}\text{Sr}_{\text{sa}}$ ratios of the samples from the CLLMM, with associated $\delta^{88/86}\text{Sr}$ values and corresponding dates of TIMS analysis. Note the carbonate sample ‘CLS-1’ was analysed three times with the different $^{84}\text{Sr}_{\text{sp}}/^{84}\text{Sr}_{\text{sa}}$. 2SEM is the external precision for repeated analyses with size n; but when n is not given, 2SEM is internal precision of a single analysis of the sample through 200 cycles for $\delta^{88/86}\text{Sr}$, and 100 cycles for $^{87}\text{Sr}/^{86}\text{Sr}$.

Sample	Area	Date analysed	$\delta^{88/86}\text{Sr}$ (‰ _{SRM987})	2SEM	$^{84}\text{Sr}_{\text{sp}}/^{84}\text{Sr}_{\text{sa}}$
RMW	River Murray	Dec 2018	0.286	0.016	21.4
C01	Lower Lakes	Nov 2018	0.250	0.011	31.9
JWP2	North Lagoon (Groundwater)	Nov 2018	0.261	0.017	19.9
BWP2	North Lagoon (Groundwater)	Nov 2018	0.247	0.012	20.9
SCW	Salt Creek	Dec 2019	0.304	0.013	21.3
ELW1	Milne Lake/ Pipe Clay Lake	Dec 2018	0.352	0.018	20.0
ELW2	Halite Lake	Dec 2018	0.423	0.016	20.8
C02	North Lagoon	Aug 2018	0.332	0.017	21.2
C04	North Lagoon	Nov 2018	0.372	0.016	18.9

NL2	North Lagoon	Aug 2018	0.341	0.019	19.9
C06	NL-SL connection	Aug 2018	0.378	0.018	18.3
C07	NL-SL connection	Jan 2020	0.397	0.012	24.2
C10	South Lagoon	Aug 2018	0.399	0.019	22.4
C11	South Lagoon	Aug 2018	0.458	0.017	22.3
C12	South Lagoon	Jan 2020	0.429	0.012	21.1
CLS-1a	South Lagoon	Jan 2019	0.203	0.012	18.0
CLS-1b	South Lagoon	Jan 2019	0.222	0.018	10.0
CLS-1c	South Lagoon	Jan 2020	0.209	0.013	19.3

All samples analysed and presented in the study yielded close to optimal ‘spike to sample’ ratios (i.e., $^{84}\text{Sr}_{\text{sp}}/^{84}\text{Sr}_{\text{sa}}$) ranging from ~ 10 to ~ 32 , where most of the samples gave the $^{84}\text{Sr}_{\text{sp}}/^{84}\text{Sr}_{\text{sa}}$ ratio close to 20 (Table C.3), with is found to be the optimal spiking ratio according to Krabbenhöft et al. (2009) and our testing, considering the specific isotope composition of our ^{87}Sr - ^{84}Sr double spike. In order to test the accuracy and robustness of the $\delta^{88/86}\text{Sr}$ data presented in this study within the above range of spiking conditions (i.e., variability in $^{84}\text{Sr}_{\text{sp}}/^{84}\text{Sr}_{\text{sa}}$ ratios in sample-spike mixtures), we performed a simple ‘spike to sample’ test analysis on SRM987 standard that was doped with variable amount of the ^{87}Sr - ^{84}Sr double spike. Specifically, different amounts of the double spike solution were added to the SRM987 standard to obtain a set of samples (i.e., sample-spike mixtures) with variable $^{84}\text{Sr}_{\text{sp}}/^{84}\text{Sr}_{\text{sa}}$ ratios ranging from ~ 8 to ~ 36 (see Fig. C1), thus representing ‘underspiked’ to ‘overspiked’ conditions, respectively (regarding ~ 20 as the ‘optimal’ $^{84}\text{Sr}_{\text{sp}}/^{84}\text{Sr}_{\text{sa}}$). The acquired $\delta^{88/86}\text{Sr}$ data from the SRM987 standard, plotted as a function of variable $^{84}\text{Sr}_{\text{sp}}/^{84}\text{Sr}_{\text{sa}}$ are plotted in Fig. C.2. Some spiking tests (marked as grey dots in Fig. C.2) were performed during the initial stages of the project in March 2018, when our TIMS method and analysis was still being optimised, and thus prior to the main analytical work done on the CLLMM samples that commenced in August 2018 and lasted until January 2020 (see data in Table C.3).

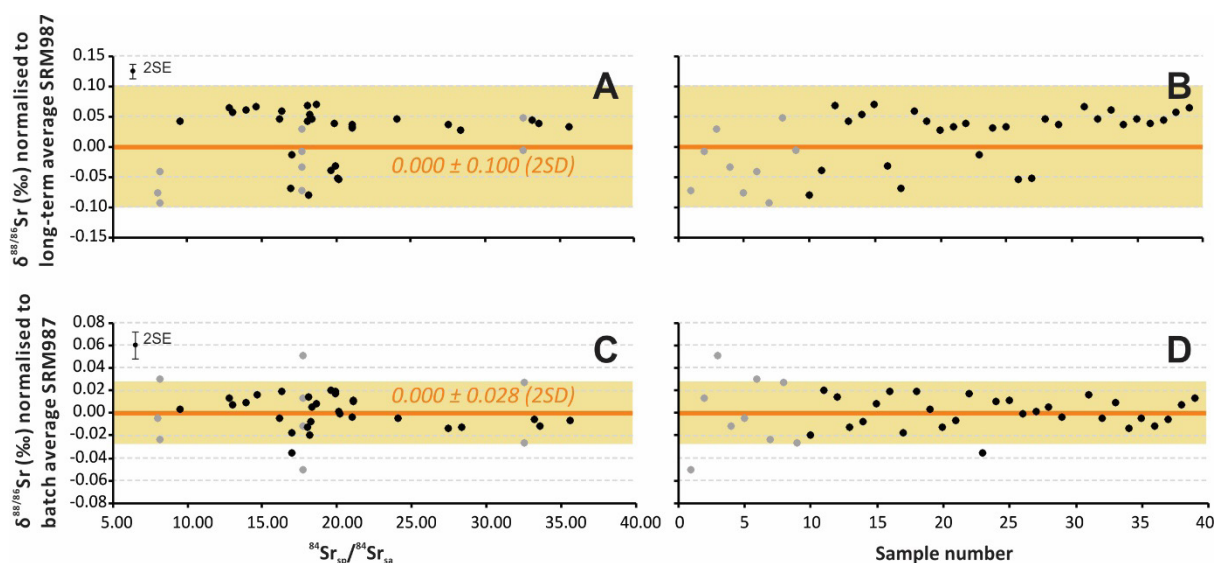


Figure C.2: $\delta^{88/86}\text{Sr}$ values of SRM987 standard normalised to its **long-term average** value and plotted as a function of (A) variable ‘spike to sample’ ratios ranging from ~ 8 to ~ 36 ; and (B) the number of analyses performed during the spiking experiment and sample analyses. $\delta^{88/86}\text{Sr}$ values of SRM987 normalised to its **batch average value** calculated from the same ‘batch’ or analytical session, plotted against (C) variable $^{84}\text{Sr}_{\text{sp}}/^{84}\text{Sr}_{\text{sa}}$ ratios, and (D) the number of analyses during the spiking experiment and sample analyses. Note that the grey dots represent SRM987 standard data from the early experimental runs done in March 2018, and black dots are from later analysis of SRM987 performed during August 2018 and January 2020, when most of the samples were analysed. The average $\delta^{88/86}\text{Sr}$ value of SRM987 (i.e., equals to 0 ‰) is shown as the orange horizontal line, and their representative $\pm 2\text{SD}$ error envelopes are depicted as beige rectangles, and in (C) and (D), they grey dots were excluded in 2SD calculation. The error bars in the top left corners of the individual plots (A and C) illustrates the typical internal precision (2SE) for individual analyses of 200 cycles (i.e., black/grey dots).

Importantly, within the investigated range the $^{84}\text{Sr}_{\text{sp}}/^{84}\text{Sr}_{\text{sa}}$ ratio there is no obvious influence of the latter on the absolute values of $\delta^{88/86}\text{Sr}$ measurements as $\delta^{88/86}\text{Sr}$ of SRM987 normalised to its long-term average do not show any trend with increasing $^{84}\text{Sr}_{\text{sp}}/^{84}\text{Sr}_{\text{sa}}$ ratio (Fig. C.2A). Moreover, a carbonate sample CLS-1 was analysed three times under different spiking conditions, with $^{84}\text{Sr}_{\text{sp}}/^{84}\text{Sr}_{\text{sa}}$ ratios ranging from ~ 10 to 19, and regardless of these different conditions its $\delta^{88/86}\text{Sr}$ values all agree within error of $\pm 0.030\text{‰}$, 2SD (for details see data in Table C.3, sample: CLS-1a, b and c).

Each ‘batch’ or analytical session always contained two SRM987 standards, loaded on separate filaments, which were measured at the beginning and the end of the session along with unknown samples from CLLMM run in that batch. These standard runs were used to assess and correct any session-to-session bias and in-session drifts in collected Sr isotope data, as occasionally the measured and calculated $\delta^{88/86}\text{Sr}$ values of SRM987 showed a slight long-term drift (Fig C.2B), which was also observed in previous studies focused on high-precision Sr isotope analyses (Krabbenhöft et al., 2009; Andrews et al., 2016, Shalev et al., 2017). The in-session drifts in $\delta^{88/86}\text{Sr}$ of SRM987, on the other hand, tend to be quite limited (see an error envelope of $\pm 0.03\text{‰}$ in Fig. C.2D), which reflect $\delta^{88/86}\text{Sr}$ normalised to the average $^{88}\text{Sr}/^{86}\text{Sr}$ of SRM987 from the same batch. Therefore, to account for the session-to-session drift in measured $\delta^{88/86}\text{Sr}$ values of standards and samples, they were all normalised to the average $\delta^{88/86}\text{Sr}$ of SRM987 runs acquired from the same batch (i.e., the same TIMS analytical session). The validity of such normalisation was also corroborated by analyses of IAPSO seawater and/or JCP-1 carbonate standards, which were also added to each batch, to test and monitor the accuracy and reproducibility of the acquired data (see results in Fig. C.3A and B). As most of the samples in the study were analysed for their $\delta^{88/86}\text{Sr}$ only once (i.e., in one analytical session on TIMS), their external reproducibility (2SD) is based on the long-term 2SD errors of measured and bias/drift-correct data of IAPSO and JCP-1 standards which are on the order of $\pm 0.03\text{‰}$ (2SD) for $\delta^{88/86}\text{Sr}$ (see Fig

C3, A and B), and for their $^{87}\text{Sr}/^{86}\text{Sr}$ ratios the error is ± 0.000016 (Fig C3, C and D).

Although the early measurements done in March 2018 (see grey circles in Fig. C.2) shows relatively larger variations in normalised $\delta^{88/86}\text{Sr}$ data, which is likely related to the fact that our analytical technique was not yet as refined and precise during this early stage of the project; but the observed session-to-session bias and in-session drifts became smaller (see black circles in Fig. C.2D and F) with increasing experience of the operator and gradual improvements in our analytical technique, sample loading procedures and the tuning/running conditions of TIMS.

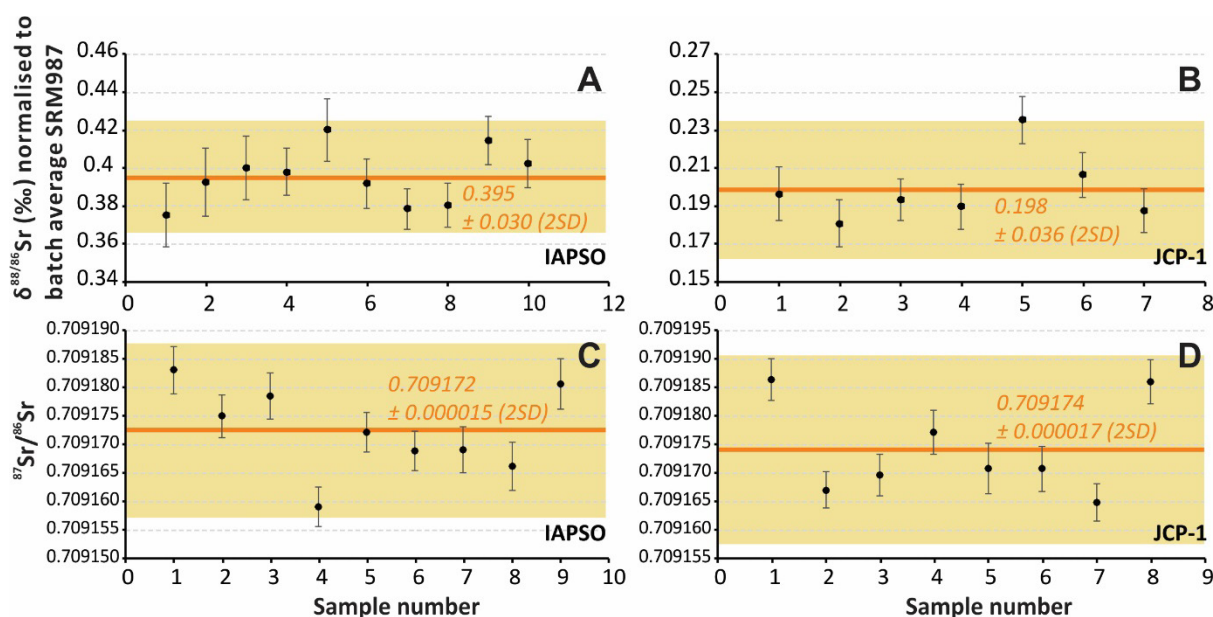


Figure C.3: $\delta^{88/86}\text{Sr}$ values of IAPSO (A) and JCP-1 (B) standards normalised to the average SRM987 of the same batch of analyses, and $^{87}\text{Sr}/^{86}\text{Sr}$ ratios of IAPSO (C) and JCP-1 (D) standards normalised to a fixed $^{86}\text{Sr}/^{88}\text{Sr}$ ratio of 0.1194. The long-term average of the standard and its representative $\pm 2\text{SD}$ errors are shown, respectively, as an orange horizontal line and a beige rectangle. The error bars on the dots (black dots) represent internal precision (2SE) of individual runs of the standards.

Table C.4. $^{87}\text{Sr}/^{86}\text{Sr}$ and $\delta^{88/86}\text{Sr}$ values of individual IAPSO and JCP-1 standards analysed by TIMS and corrected for session-to-session drift. 2SEM is the external precision for repeated analyses with size n; but when n is not given, 2SEM is internal precision of a single analysis of the sample through 200 cycles for $\delta^{88/86}\text{Sr}$, and 100 cycles for $^{87}\text{Sr}/^{86}\text{Sr}$.

Individual standards	Time analysed	$^{87}\text{Sr}/^{86}\text{Sr}$	2SEM	$\delta^{88/86}\text{Sr}$ ($\%_{\text{SRM987}}$)	2SEM	$^{84}\text{Sr}_{\text{sp}}/^{84}\text{Sr}_{\text{sa}}$
IAPSO						

Appendix 3

A	May 2018			0.375	0.017	19.39
B	May 2018	0.709183	0.000004	0.392	0.018	19.57
C	Aug 2018			0.400	0.017	25.27
D	Nov 2018	0.709175	0.000004	0.398	0.012	20.54
E	Dec 2018	0.709178	0.000004	0.420	0.017	21.20
F	May 2019	0.709159	0.000003	0.392	0.013	20.70
G	Jun 2019	0.709172	0.000003	0.378	0.011	25.14
H	Jul 2019	0.709169	0.000003	0.380	0.011	20.11
I	Jul 2019	0.709169	0.000004	0.414	0.013	17.15
J	Sep 2019	0.709166	0.000004			
K	Dec 2019	0.709181	0.000004	0.402	0.013	22.18
Average		0.709172	0.000005 (n=8)	0.395	0 . 0 0 9 (n=10)	
Published literatures		0 . 7 0 9 1 6 8 (Krabbenhöft et al., 2009)	0.000007 (n=10)	0.396 (Andrews et al., 2016)	0 . 0 0 5 (n=54)	
JCP-1						
A	Jun 2019	0.709167	0.000003	0.196	0.014	18.65
B	Jul 2019	0.709170	0.000004	0.181	0.013	19.17
C	Jul 2019	0.709177	0.000004	0.193	0.011	24.22
D	Sep 2019	0.709171	0.000004	0.189	0.012	21.80
E	Oct 2019	0.709171	0.000004	0.235	0.012	20.37
F	Oct 2019	0.709165	0.000003	0.206	0.012	22.89
G	Dec 2019	0.709186	0.000004	0.187	0.012	26.43
Average		0.709174	0.000006 (n=7)	0.198	0 . 0 1 4 (n=7)	
Published literatures		0 . 7 0 9 1 7 2 (Vollstaedt et al., 2014)	0.000004 (n=32)	0.193 (Vollstaedt et al., 2014)	0 . 0 0 4 (n=32)	

Appendix D. Supporting models using Sr isotopes and elemental concentrations

D.1 Apportioning water sources through $^{87}\text{Sr}/^{86}\text{Sr}$ and elemental ratio tracers

In order to visualise the influence of multiple processes (i.e., water source mixing, evaporation and mineral precipitation) on the water chemistry of the Coorong, we plot $^{87}\text{Sr}/^{86}\text{Sr}$ of Coorong lagoon waters along with main water sources (as described in Discussion section) against their elemental concentrations, or Mg/Ca and Mg/Na ratios (see Fig. D.1 below), complemented also by theoretical mixing lines using Sr isotope mass balance (i.e., GW-SW, SC-SW and LL-SW mixing scenarios).

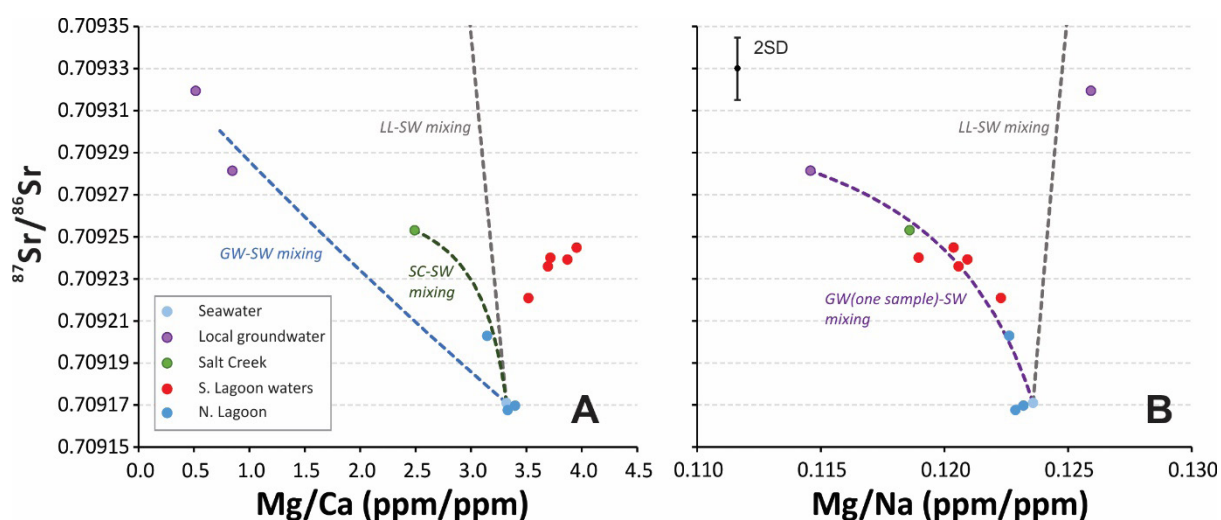


Figure D.1: Cross-plots of $^{87}\text{Sr}/^{86}\text{Sr}$ vs. (A) Mg/Ca and (B) Mg/Na of waters from the CLLMM. Note that the following abbreviations are used: LL = the Lower Lakes, SC = Salt Creek, GW = Groundwater and SW = seawater). The dashed lines represent theoretical mixing lines for water-source mixing scenarios.

Based on Von der Borch et al. (1975) and also XRD data from Shao et al. (2018), dolomite precipitation in the Coorong lagoons is limited or very low, therefore Mg concentration in the Coorong lagoon waters should be conservative (i.e., not affected by dolomite formation). Thus Mg/Na ratio is used as a conservative tracer. Also, while $^{87}\text{Sr}/^{86}\text{Sr}$ of the Coorong waters were controlled by water source mixing, horizontal increase of Mg/Ca in the Coorong waters (specifically, the South Lagoon) compared with the theoretical mixing lines was a result of Ca loss (i.e., CaCO_3 precipitation) (Fig. D.1A). In contrast, North Lagoon samples showed no signal of the latter process.

Plotting $^{87}\text{Sr}/^{86}\text{Sr}$ of the samples against ratios of two conservative elements (e.g. Mg/Na) is a complementary method to identify the water sources and their mixing in the Coorong. Interestingly, while one groundwater sample seemed to be a mixture of seawater and lake waters nearby and had little influence to the Coorong water chemistry, the other groundwater sample mixing with seawater can

explain the geochemistry of the Salt Creek, which also directly flows into the Coorong South Lagoon. Therefore, the Coorong (especially the South Lagoon) waters are likely mixtures of seawater, groundwater and Salt Creek drainage water, the GW/SC-SW mixing scenario is thus the only one used in the Rayleigh model (section 5.4)

D.2 Evidence of CaCO_3 precipitation through $\delta^{88/86}\text{Sr}$ and elemental concentrations

Precipitation of CaCO_3 , predominantly aragonite and minor amount of calcite, causes mass-dependent fractionation of $\delta^{88/86}\text{Sr}$ in South Lagoon water samples. However, gypsum ($\text{CaSO}_4 \cdot 2\text{H}_2\text{O}$) precipitation in the South Lagoon, although not significant by quantity, could in theory also cause further fractionation of $\delta^{88/86}\text{Sr}$. Therefore, the dependence of $\delta^{88/86}\text{Sr}$ on CaCO_3 and $\text{CaSO}_4 \cdot 2\text{H}_2\text{O}$ precipitation needs more critical assessment, which can be observed through plotting $\delta^{88/86}\text{Sr}$ of water samples against their (i) Sr/Ca ratio and (ii) SO_4^{2-} concentration (Fig. D.2).

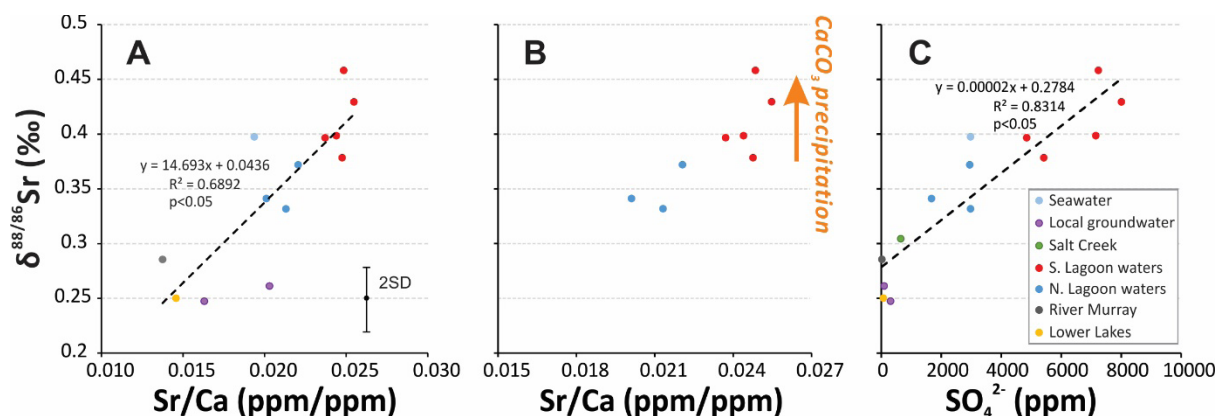


Figure D.2: Cross-plots of $\delta^{88/86}\text{Sr}$ vs. (A) Sr/Ca of waters from the CLLMM, (B) Sr/Ca of waters from the Coorong only, and (C) SO_4^{2-} of waters from the CLLMM. The dashed black line represents a line of best fit for the data, which can be written as a linear function.

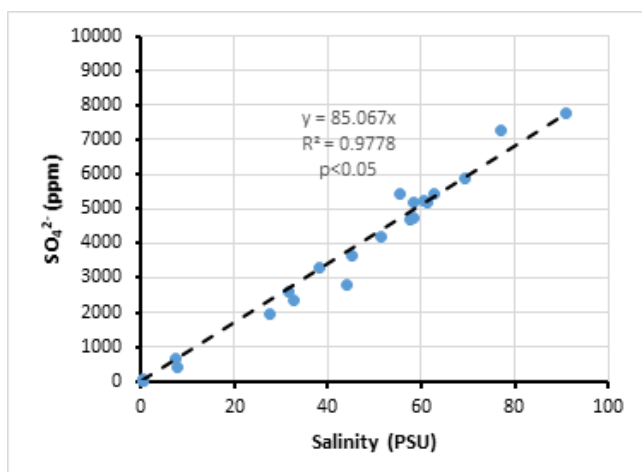


Figure D.3: SO_4^{2-} concentration of waters from the CLLMM sampled in May and August 2018. The dashed black line represents a line of best fit for the data, which can be written as a linear function.

The typical Sr partition coefficient K_d of marine aragonite, defined as $K_d^{\text{ar}} = (\text{Sr}/\text{Ca})_{\text{ar}} / (\text{Sr}/\text{Ca})_{\text{fluid}}$, is around 0.8 to 1.2, depending on temperature (Gaetani and Cohen, 2006); in contrast, the K_d of gypsum (K_d^{gy}) is only ~ 0.18 (Butler, 1973). As a result, aragonite precipitation is the main sink or output flux of Sr from the Coorong lagoon, and it should also keep the Sr/Ca ratio in the South Lagoon waters relatively constant as with carbonate (aragonite) precipitation not only Sr but also Ca is removed simultaneously. However, $\delta^{88/86}\text{Sr}$ should increase due to enhanced carbonate/aragonite precipitation, and such ‘trend’ or behavior of $\delta^{88/86}\text{Sr}$ is indicated in the data in Fig. D.2B. Note the different trend of $\delta^{88/86}\text{Sr}$ vs. Sr/Ca for South Lagoon waters (with an active carbonate precipitation) in comparison to North Lagoon waters. Gypsum precipitation, on the other hand, reduces SO_4^{2-} concentration and thus SO_4^{2-} should not be conservative if gypsum is actively forming at significant rates in the lagoon, which however is not observed in our data (Fig. D.3). In agreement, a strong correlation ($R^2 = 0.83$, $p < 0.05$) was found between $\delta^{88/86}\text{Sr}$ and SO_4^{2-} concentrations and salinity for all waters from the CLLMM (Fig. D.2C), and no different trends or ‘offsets’ from that correlation (e.g. that could be linked to purported CaSO_4 precipitation) are seen in data from North and South Lagoon samples. Therefore, we conclude that gypsum precipitation had no significant impact on $\delta^{88/86}\text{Sr}$ variation observed in waters from the South Lagoon.

D.3 Constraints on $\delta^{88/86}\text{Sr}_{\text{INI}}$ parameter from the Sr isotope mass balance calculations

To derive the $\delta^{88/86}\text{Sr}_{\text{INI}}$ value (i.e., initial Sr isotope composition) for GW/SC-SW mixing scenario in the Rayleigh and equilibrium models (section 5.4), firstly we calculated the theoretical $\delta^{88/86}\text{Sr}$ and $^{87}\text{Sr}/^{86}\text{Sr}$ of the water mixture following the Sr mass balance equations D.1 and D.2, shown below:

$$I_{MIX} = I_{FW} X_{FW} C_{FW} / C_{MIX} + I_{SW} (1 - X_{FW}) C_{SW} / C_{MIX} \quad (\text{Eq. D.1})$$

$$C_{MIX} = C_{FW} X_{FW} + C_{SW} (1 - X_{FW}) \quad (\text{Eq. D.2})$$

where is the ‘initial’ Sr isotope composition ($^{87}\text{Sr}/^{86}\text{Sr}$ or $\delta^{88/86}\text{Sr}$); C is the Sr concentration of individual end-members and the mixture; and X_{FW} is the mass fraction of freshwater, assigned from 0 to 1. The subscripts SW and FW denote respectively seawater and freshwater (where the latter can be GW = Grounwater, or SC = Salt Creek), and MIX denotes the theoretical mixture of the two water sources.

When plotting the theoretical mixing lines in the $^{87}\text{Sr}/^{86}\text{Sr}$ and $\delta^{88/86}\text{Sr}$ cross plot (modified from Fig. 3), for the above mixing scenario (i.e., GW/SC-SW), the $\delta^{88/86}\text{Sr}_{INI}$ value (0.32‰) can be derived from such mixing lines using the representative $^{87}\text{Sr}/^{86}\text{Sr}$ value measured in the South Lagoon waters (~ 0.70924) (Fig. D.4).

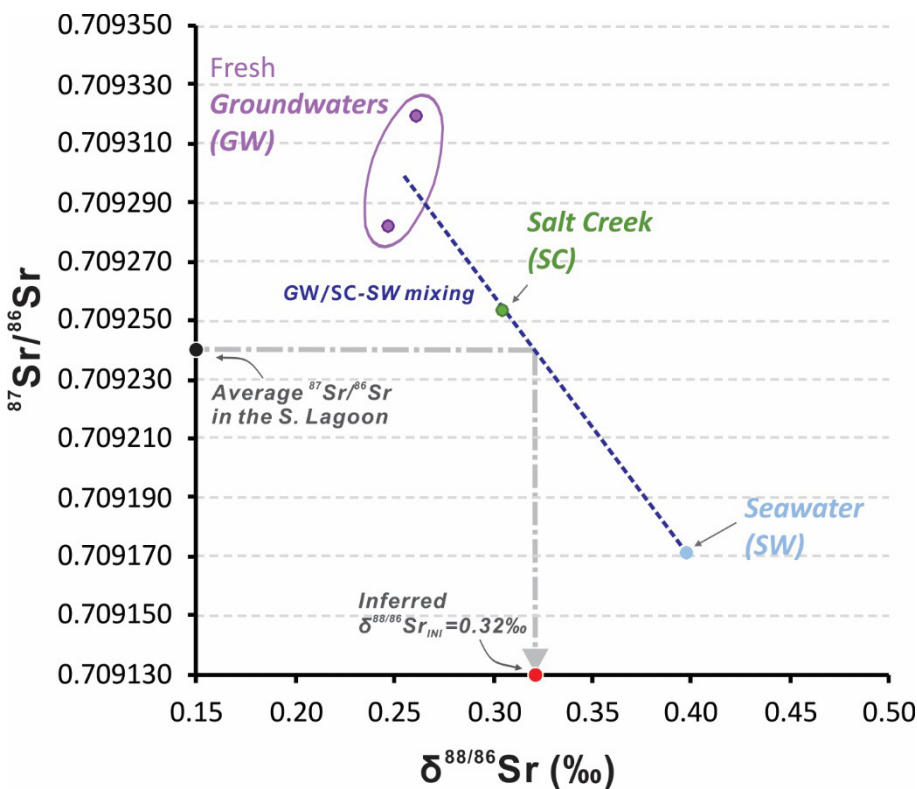


Figure D.4: Theoretical mixing trend for $^{87}\text{Sr}/^{86}\text{Sr}$ and $\delta^{88/86}\text{Sr}$ in the CLLMM for GW/SC-SW scenario. Note that the red circles illustrate the expected or derived ‘initial’ $\delta^{88/86}\text{Sr}$ value of the South Lagoon waters (constrained based on $^{87}\text{Sr}/^{86}\text{Sr}$ data), not impacted by carbonate precipitation in the lagoon.

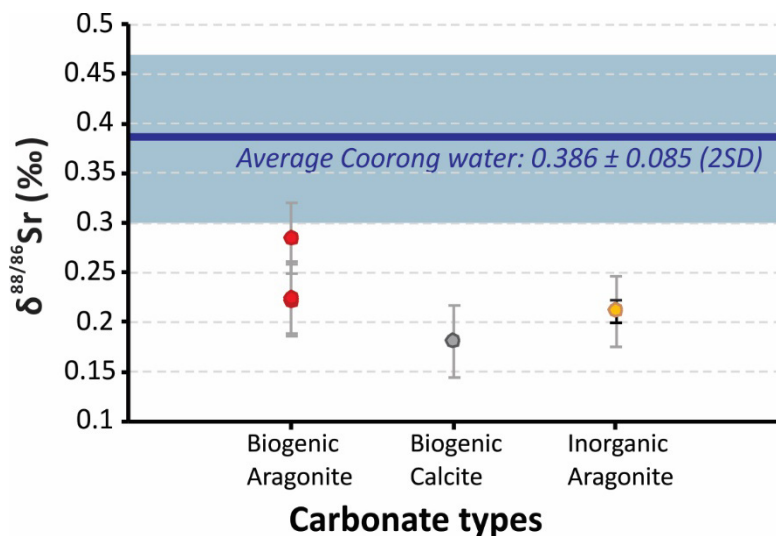
D.4 $\delta^{88/86}\text{Sr}$ values of carbonate samples

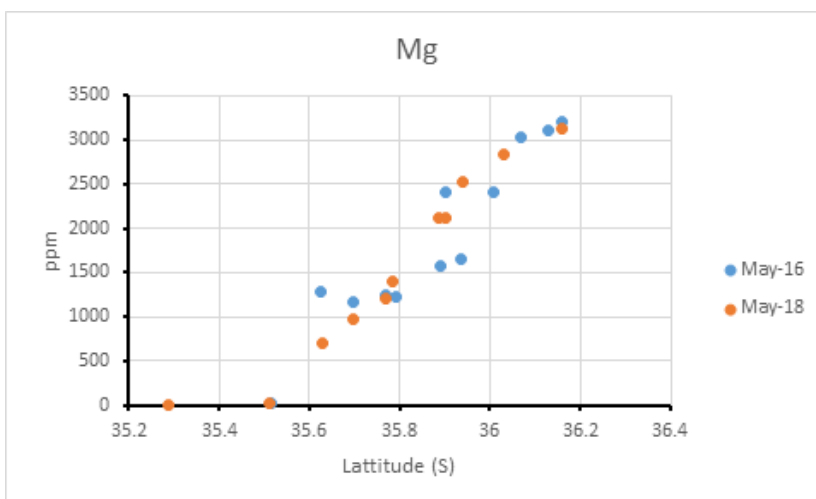
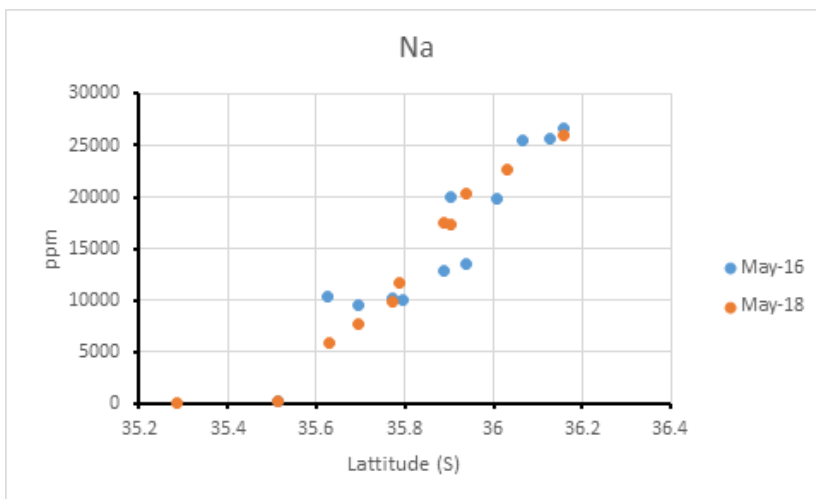
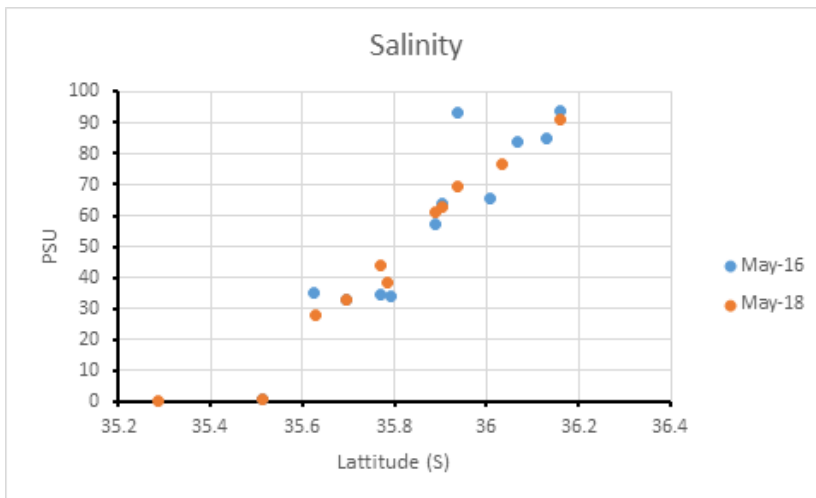
Figure D.5: $\delta^{88/86}\text{Sr}$ of collected carbonates in the Coorong lagoon, plotted along with the average $\delta^{88/86}\text{Sr}$ of Coorong lagoon waters (calculated by averaging the average North and South Lagoon samples associated with samples from Figs. 1 and 2) and their 2SD represented as the dark blue horizontal line and light blue rectangle respectively. The biogenic aragonite data were analysed from three *Arthritica helmsi* shells, the biogenic calcite is represented by a tubeworm (*Ficopomatus enigmaticus*) forming abundant colonies or ‘reefs’ especially in the North lagoon (sample: CW2w), and the inorganic aragonite/carbonate sample represents the top sediment ‘crust’ (CLS-1) collected in the South Lagoon; described in more details in Shao et al. (2018). Note that the grey error bars are the 2SD from JCP-1 measurements (see Fig. C.2B, Appendix C.1), and the black error bar is the 2SEM (n=3), for multiple measurements of the sample CLS-1 (Table. 1).

Appendix E. PHREEQC modelling and analyses of waters for the calculation of mineral saturation states

E.1 Source data for PHREEQC modelling

All water samples collected in May 2018 were analysed for cations and anions concentrations, alkalinity, pH (see Tables B.1-4) and temperatures (see Table A.2), as described in section 2.5. These parameters were used as source data for PHREEQC modelling and calculation of accurate and representative mineral saturation indices (SI) of local CLLMM waters presented in Fig. 2D in the main manuscript. Importantly, geochemical modelling of mineral saturation states relies on accurate measurement of the above parameters as input data, and this is a major improvement of the PHREEQC model in this study compared to the one presented in Shao et al. (2018). The latter study utilised for PHREEQC modelling alkalinity and anion concentrations inferred from historical geochemical data collected in the Coorong, as the actual samples or collected waters (from May 2016) were not analysed for these parameters, and pH was measured in situ by a conventional glass electrode or portable pH probe (for details see Shao et al., 2018).

The Coorong water samples collected in May 2016 however account for majority of results presented in this study (Fig. 2A-C), and these waters were also measured for $\delta^{44/40}\text{Ca}$ values (see Shao et al., 2018), which could be thus directly compared with $\delta^{88/86}\text{Sr}$ data generated by this study (Fig. 5). To verify that SI values acquired from May 2018 water samples are comparable to SI values from May 2016 samples, it is necessary to check that the water samples from the above two sample sets (May 2016 and 2018) yielded comparable water chemistry data, and thus calculated mineral saturation indices. Accordingly, in Fig. E.1, we compare the salinity and available major cation concentration data between the samples collected in May 2016 (analysed via ICP-MS, data from Shao et al., 2018) and those from May 2018. Importantly, results from these two datasets show consistent results and high degree of correlation, thus providing confidence that May 2018 samples used for PHREEQC modelling can be used for calculation of representative local saturation state of waters in the Coorong lagoon.



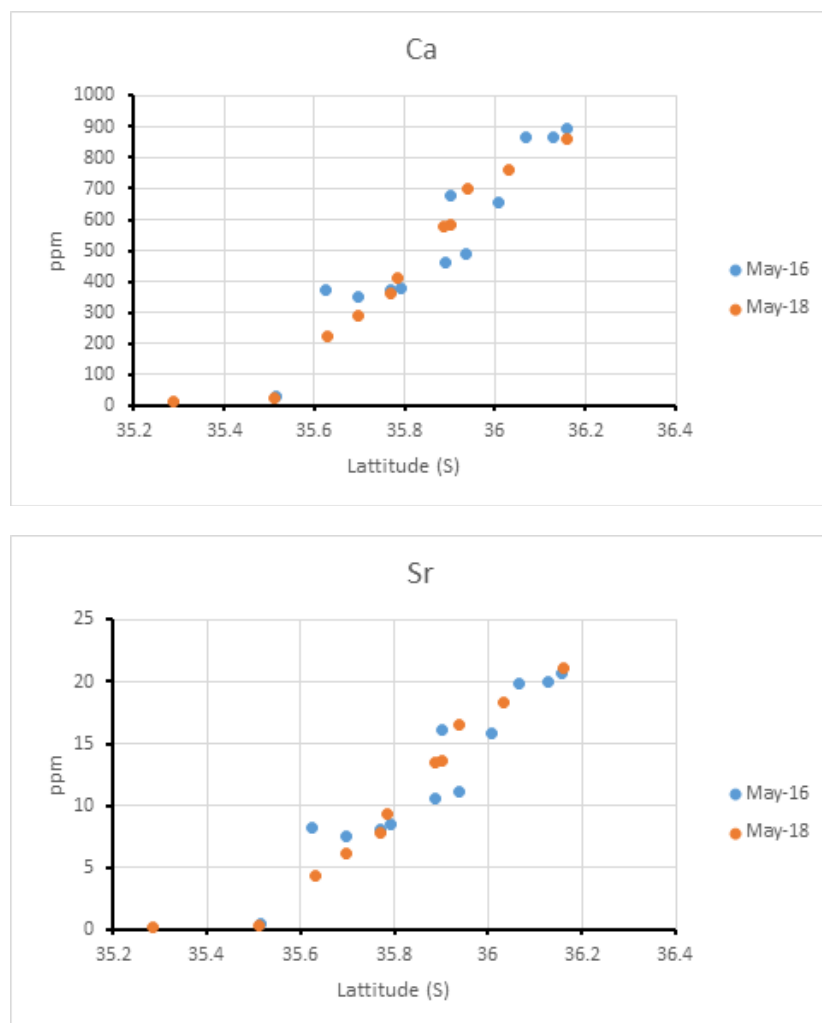


Figure E.1: Salinity (PSU) and major cation concentrations (ppm) of waters collected in May 2016 (data from Shao et al., 2018) and May 2018 from the Coorong lagoon plotted as a function of latitude.

E.2 Saturation Indices (SI) based on laboratory-based (lab pH) and field-based pH (probe pH) measurements

To ensure the PHREEQC SI model using the lab spectrophotometric pH measurements is representative of the water chemistry at the time of sampling, we compare SI values for several minerals (aragonite, calcite and gypsum) modelled by PHREEQC using laboratory-based (spectrophotometric) and field-based probe pH measurements, where the latter were performed in-situ during sample collection in the Coorong lagoons and Murray Mouth Estuary (Fig. E.2).

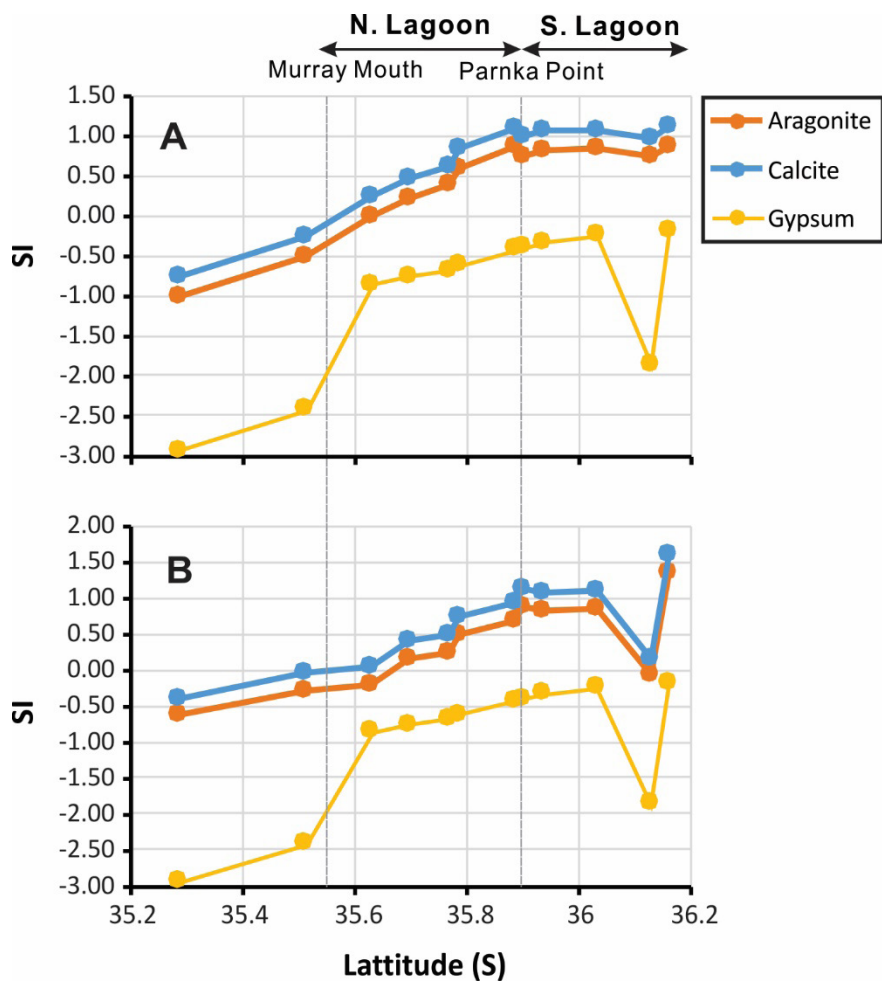


Figure E.2: PHREEQC SI values for May 2018 samples produced using (A) the laboratory-based spectrophotometric pH data and (B) probe pH data acquired directly in the field during collection.

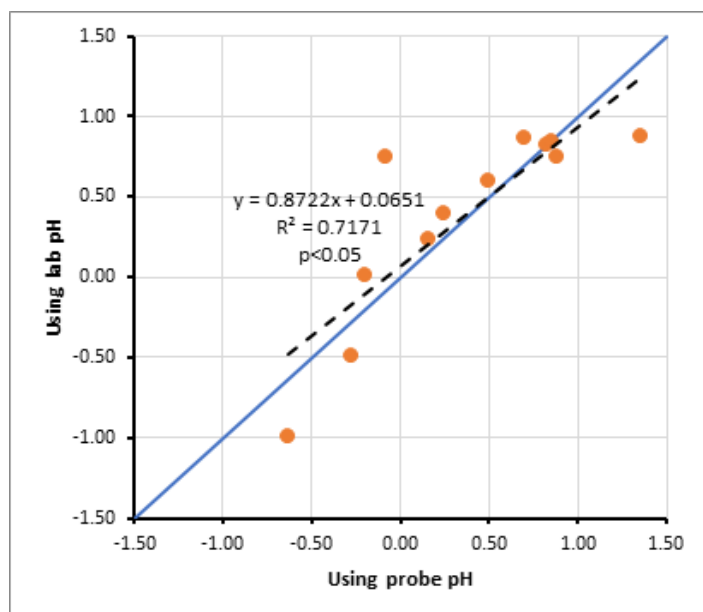


Figure E.3: PHREEQC SI values of aragonite for May 2018 samples produced using laboratory spectrophotometric pH vs. probe pH measurements, the latter collected directly in the field. The blue solid line represents a 1:1 line.

Overall, data in Fig. E.3 show the PHREEQC modelling for SI value based on lab and probe pH measurements agree with each other and show a moderate correlation ($R^2 = 0.71$, $p < 0.05$), following closely the 1:1 correlation line. This in turn confirms that in general, the pH measurements acquired by laboratory-based and field-based methods are comparable to each other, but in this study, we adopt the laboratory-based pH measurements due to the abovementioned limitation of traditional pH probe for hypersaline solutions.

E.3 Saturation Indices (SI) calculated via PHREEQC vs. CO2SYS

The saturation indices (SI) of aragonite and calcite, which were modelled through PHREEQC, were also calculated alternatively with the CO2SYS program (Lewis and Wallace, 1998). The CO2SYS program contains a selection of pH scales (described in Dickson, 1984) compared with PHREEQC which uses the NBS scale. In this case, the total hydrogen ion concentration scale is selected based on the scale used in the spectrophotometric pH (Table B.4) and alkalinity measurements.

According to Lewis and Wallace (1998), the CO2SYS program calculates the saturation states as Ω , which is defined as

$$\Omega = [\text{CO}_3^{2-}][\text{Ca}^{2+}]/K_{\text{sp}}$$

Where $[\text{CO}_3^{2-}]$ and $[\text{Ca}^{2+}]$ are concentrations of carbonate and calcium respectively, and K_{sp} is the solubility product constant of the mineral.

Then SI can be then calculated using the following relationship:

$$\text{SI} = \log \Omega$$

To calculate the Ω values for aragonite and calcite in the CO2SYS, the following input parameters: (i) water salinity (PSU), (ii) temperature ($^{\circ}\text{C}$), (iii) total P and total Si ($\mu\text{mol/kg}$ seawater) – calculated by

$$\text{concentration in mg/L (from Table B.1)/atomic mass} \times 1000$$

were filled in the ‘input conditions’ section; and (i) total alkalinity ($\mu\text{mol/kg}$ seawater) and (ii) pH (total scale) were filled in the ‘data’ section. The values for the above parameters used in the CO2SYS modelling can be found in tables in Appendix B.

Finally, in Fig. E.4 below we compare the SI values for aragonite and calcite (for 2018 water samples). calculated via PHREEQC and CO2SYS, to further evaluate the validity of our SI data, and to compare these two modelling approaches for the calculation of mineral saturation states in hypersaline conditions such as those in the Coorong lagoon.

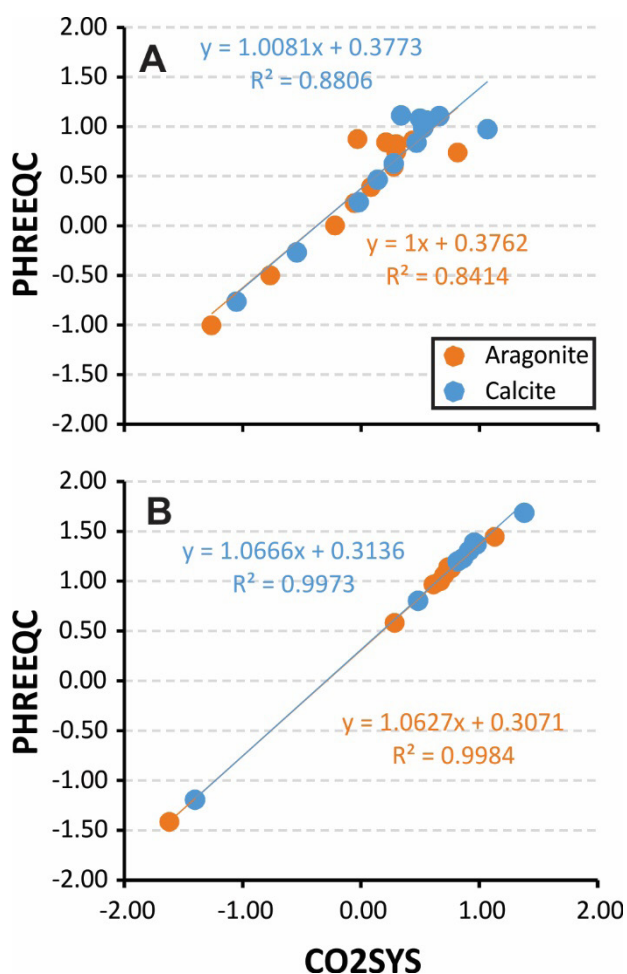


Figure E.4: Comparison of SI values of aragonite and calcite in Coorong water samples collected in (A) May 2018 and (B) Aug 2018, modelled via PHREEQC and CO2SYS approaches (see also Table A.2 for more details on these water samples).

This comparison revealed that the CO2SYS produces similar SI values of calcite and aragonite compared to PHREEQC when the water salinity is below ~60 PSU (August 2018 samples, see Fig. E.4.B), given that the CO2SYS has a computation error of 3% for the Ω parameter (Chou et al., 2013). However, the calculated SI values from these two approaches differ when the water salinity is higher (e.g., the South Lagoon water samples from May 2018, see Fig. E.4.A), which is likely because the CO2SYS program is mainly designed for waters with normal marine salinities (Lewis and Wallace, 1998), while in PHREEQC model (with the Pitzer database) can also deal with hypersaline waters and very high ionic strengths (Parkhurst and Appelo, 2013; Lassin et al., 2017; Hörbrand et al., 2018).

References

- Andrews, M. G., Jacobson, A. D., Lehn, G. O., Horton, T. W. and Craw, D. (2016) Radiogenic and stable Sr isotope ratios ($^{87}\text{Sr}/^{86}\text{Sr}$, $\delta^{88/86}\text{Sr}$) as tracers of riverine cation sources and biogeochemical cycling in the Milford Sound region of Fiordland, New Zealand. *Geochimica et Cosmochimica Acta* **173**, 284-303.
- Bargrivan, S., Smernik, R. J. and Mosley, L. M. (2017) Development of a spectrophotometric method for determining pH of soil extracts and comparison with glass electrode measurements. *Soil Science Society of America Journal* **81**, 1350-1358.
- Butler, G. P. (1973) Strontium geochemistry of modern and ancient calcium sulphate minerals. In *The Persian Gulf* (pp. 423-452). Springer, Berlin, Heidelberg.
- Chamberlayne, B. K., Tyler, J. J. and Gillanders, B. M. (2019) Environmental Controls on the Geochemistry of a Short-Lived Bivalve in Southeastern Australian Estuaries. *Estuaries and Coasts*, 1-16.
- Chou, W. C., Gong, G. C., Hung, C. C. and Wu, Y. H. (2013) Carbonate mineral saturation states in the East China Sea: present conditions and future scenarios. *Biogeosciences* **10**, 6453-6467.
- Dickson, A. G. (1984) pH scales and proton-transfer reactions in saline media such as sea water. *Geochimica et Cosmochimica Acta* **48**, 2299-2308.
- Dickson, A. G. (1990) Standard potential of the reaction: $\text{AgCl (s)} + 1/2\text{H}_2\text{(g)} = \text{Ag (s)} + \text{HCl (aq)}$, and the standard acidity constant of the ion HSO_4^- in synthetic sea water from 273.15 to 318.15 K. *The Journal of Chemical Thermodynamics* **22**, 113-127.
- Gaetani, G. A. and Cohen, A. L. (2006) Element partitioning during precipitation of aragonite from seawater: a framework for understanding paleoproxies. *Geochimica et Cosmochimica Acta* **70**, 4617-4634.
- Hörbrand, T., Baumann, T. and Moog, H. C. (2018) Validation of hydrogeochemical databases for problems in deep geothermal energy. *Geothermal Energy* **6**, 20.
- Krabbenhöft, A., Fietzke, J., Eisenhauer, A., Liebetrau, V., Böhm, F. and Vollstaedt, H. (2009) Determination of radiogenic and stable strontium isotope ratios ($^{87}\text{Sr}/^{86}\text{Sr}$; $\delta^{88/86}\text{Sr}$) by thermal ionization mass spectrometry applying an $^{87}\text{Sr}/^{84}\text{Sr}$ double spike. *Journal of Analytical Atomic Spectrometry* **24**, 1267-1271.
- Lamberty, A. and Pauwels, J. (1991) How to correct for blanks in isotope dilution mass spectrometry. *International Journal of Mass Spectrometry and Ion Processes* **104**, 45-48.
- Lassin, A., André, L. and Lach, A. (2017) Considerations about the building of a thermodynamic da-

tabase for the chemical description of highly saline systems. *Procedia Earth and Planetary Science* **17**, 304-307.

Lewis, E. and Wallace, D. (1998) *Program developed for CO₂ system calculations* (No. ORNL/CDI-AC-105). Brookhaven National Lab., Dept. of Applied Science, Upton, NY (United States); Oak Ridge National Lab., Carbon Dioxide Information Analysis Center, TN (United States).

Loucaides, S., R erolle, V. M., Papadimitriou, S., Kennedy, H., Mowlem, M. C., Dickson, A. G., Gledhill, M. and Achterberg, E. P. (2017) Characterization of meta-Cresol Purple for spectrophotometric pH measurements in saline and hypersaline media at sub-zero temperatures. *Scientific reports* **7**, 2481.

Mosley, L. M. and Liss P. S. (2020) Particle aggregation, pH changes and metal behaviour during estuarine mixing; review and integration. *Marine and Freshwater Research* **71**, 300–310. <https://doi.org/10.1071/MF19195>

Nand, V. and Ellwood, M. J. (2018) A simple colorimetric method for determining seawater alkalinity using bromophenol blue. *Limnology and Oceanography: Methods* **16**, 401-410.

Parkhurst, D. L. and Appelo, C. A. J. (2013) Description of input and examples for PHREEQC version 3: a computer program for speciation, batch-reaction, one-dimensional transport, and inverse geochemical calculations (No. 6-A43). US Geological Survey.

Shalev, N., Gavrieli, I., Halicz, L., Sandler, A., Stein, M. and Lazar, B. (2017) Enrichment of ⁸⁸Sr in continental waters due to calcium carbonate precipitation. *Earth and Planetary Science Letters* **459**, 381-393.

Shao, Y., Farkaš, J., Holmden, C., Mosley, L., Kell-Duivestien, I., Izzo, C., Reis-Santos, P., Tyler, J., T rber, P., Fr yda, J., Taylor, H., Haynes, D., Tibby, J. and Gillanders, B.M. (2018) Calcium and strontium isotope systematics in the lagoon-estuarine environments of South Australia: Implications for water source mixing, carbonate fluxes and fish migration, *Geochimica et Cosmochimica Acta* **239**, 90-108.

Von der Borch, C. C., Lock, D. E. and Schwebel, D. (1975) Ground-water formation of dolomite in the Coorong region of South Australia. *Geology* **3**, 283-285.

Appendix 4

**Appendices for Chapter 4 - Seasonal
carbonate cycling and water source mixing in
a semi-arid coastal lagoon-estuarine system:
Insights from stable strontium isotopes
($\delta^{88/86}\text{Sr}$)**

Appendix A. Sampling site information

Table A.1. Table of sampling locations, GPS coordinates, water temperature, salinity and sampling dates. The following abbreviations are used: NL = North Lagoon, SL = South Lagoon. Except groundwater samples, all sample IDs are formatted as A+B (+number), where A is the waterbody being sampled (C = the Coorong, RM = River Murray, LL = the Lower Lakes, SC = Salt Creek, SW = seawater), B is the season (S, Hemisphere) in which the sample was collected (Su = summer, S = spring, W = winter, A = autumn), and a number is added at the end when multiple samples were collected in the same waterbody in the each trip.

Sample ID	Area	Location	Temperature (°C)	Salinity (PSU)	Sampling Dates (dd/mm/yy)	Latitude (degree South)	Longitude (degree East)
Coorong water samples							
CSu1	North Lagoon	Mark Point	21.5	30.05	07-08/3/19	35.63	139.08
CSu2	North Lagoon	Long point	19.8	37.24	07-08/3/19	35.70	139.16
CSu3	North Lagoon	Noonamena	23.6	56.88	07-08/3/19	35.77	139.27
CSu4	North Lagoon	Near Robs Point	24.6	66.21	07-08/3/19	35.79	139.30
CSu5	NL-SL connection	Panaka Point	21.3	83.79	07-08/3/19	35.90	139.40
CSu7	South Lagoon	North of Stony Wells/Field Rd	24.1	105.78	07-08/3/19	35.94	139.49
CSu8	South Lagoon	Jacks Point	24.7	103.51	07-08/3/19	36.03	139.57
CSu9	South Lagoon	Salt Creek south	19.8	100.43	07-08/3/19	36.16	139.65
CS1	North Lagoon	Mark Point	24.7	32.56	07/12/18	35.63	139.08
CS2	North Lagoon	Long point	24.3	38.89	07/12/18	35.70	139.16
CS3	North Lagoon	Noonamena	24.9	60.64	07/12/18	35.77	139.27
CS4	North Lagoon	Near Robs Point	24.8	70.08	07/12/18	35.79	139.30
CS6	NL-SL connection	Panaka Point North	27.2	85.66	07/12/18	35.89	139.40
CS5	NL-SL connection	Panaka Point	25.9	85.71	07/12/18	35.90	139.40
CS7	South Lagoon	North of Stony Wells/Field Rd	26.9	80.42	07/12/18	35.94	139.49
CS8	South Lagoon	Jacks Point	26.3	74.48	07/12/18	36.03	139.57
CS9	South Lagoon	Salt Creek south	27.3	68.18	07/12/18	36.16	139.65
CW1	North Lagoon	Mark Point	12	31.66	31/08/18	35.63	139.08
CW2	North Lagoon	Long point	13.8	44.98	31/08/18	35.70	139.16

CW3	North Lagoon	Noonamena	14	51.29	31/08/18	35.77	139.27
CW4	North Lagoon	Near Robs Point	15.6	55.51	31/08/18	35.79	139.30
CW5	NL-SL connection	Parka Point	15.1	58.51	31/08/18	35.90	139.40
CW7	South Lagoon	North of Stony Wells/Field Rd	16.4	57.62	31/08/18	35.94	139.49
CW8	South Lagoon	Jacks Point	16.6	60.65	31/08/18	36.03	139.57
CW9	South Lagoon	Salt Creek south	15.3	58.51	31/08/18	36.16	139.65
CA1	North Lagoon	Mark Point	14.6	27.56	24/05/18	35.63	139.08
CA2	North Lagoon	Long point	14.6	32.53	24/05/18	35.70	139.16
CA3	North Lagoon	Noonamena	15.5	44.09	24/05/18	35.77	139.27
CA4	North Lagoon	Near Robs Point	15.7	38.29	24/05/18	35.79	139.30
CA6	NL-SL connection	Parka Point North	16.3	61.39	24/05/18	35.89	139.40
CA5	NL-SL connection	Parka Point	15.7	62.93	24/05/18	35.90	139.40
CA7	South Lagoon	North of Stony Wells/Field Rd	15.3	69.54	24/05/18	35.94	139.49
CA8	South Lagoon	Jacks Point	15.3	76.9	24/05/18	36.03	139.57
CA9	South Lagoon	Salt Creek south	15.5	90.83	24/05/18	36.16	139.65
Groundwater samples							
GWN	North Lagoon	North to Noonamena	20.7	1.83	11-12/04/19	35.74	139.25
GWR	North Lagoon	Near Robs Point, beach, drilled	22.3	17.39	11-12/04/19	35.79	139.30
GWP	South Lagoon	South to Parka Point, beach, drilled	20.6	19.67	11-12/04/19	35.91	139.46
GWSW	South Lagoon	Near Stony Wells	16.9	10.45	11-12/04/19	35.95	139.54
GWWW2	South Lagoon	Near Woods Well, inland		8.54	11-12/04/19	35.99	139.57
GWWW	South Lagoon	Near Woods Well	14.8	18.08	11-12/04/19	35.99	139.55
GWWW3	South Lagoon	Near Woods Well, beach, drilled	19.5	15.70	11-12/04/19	35.99	139.54
JWP2	North Lagoon	Near Robs Point		1.15	25/06/15	35.79	139.31
BWP2	North Lagoon	Near Robs Point		3.66	25/06/15	35.78	139.30
Continental water and seawater samples							

RMSu	River Murray	Near Taillem Bend	22.2	0.14	07-08/3/19	35.29	139.45
RMS	River Murray	Near Taillem Bend	22.4	0.20	07/12/18	35.29	139.45
RMW	River Murray	Near Taillem Bend	12.1	0.22	31/08/18	35.29	139.45
RMA	River Murray	Near Taillem Bend	15.2	0.21	24/05/18	35.29	139.45
LSu	the Lower Lakes	Lakes Alexandrina-Albert connection	19.9	0.47	07-08/3/19	35.51	139.19
LS	the Lower Lakes	Lakes Alexandrina-Albert connection	23.6	0.48	07/12/18	35.51	139.19
LA	the Lower Lakes	Lakes Alexandrina-Albert connection	14.0	0.50	24/05/18	35.51	139.19
SCSu	Salt Creek	East side of Princes Hwy	17.8	14.55	07-08/3/19	36.13	139.65
SCS	Salt Creek	East side of Princes Hwy	24.2	90.8	07/12/18	36.13	139.65
SCW	Salt Creek	East side of Princes Hwy	15.9	7.18	31/08/18	36.13	139.65
SCA	Salt Creek	East side of Princes Hwy	14.7	7.66	24/05/18	36.13	139.65
SWSu	Southern Ocean	End of 42 Mile Crossing	22.0	36.97	07-08/3/19	36.29	139.70

Appendix B. Supplementary results

B.1 Elemental concentrations of waters

Table B.1. Elemental concentrations of dissolved cations in waters analysed by ICP-AES in ppm (mg/L). For water salinity and sampling site information see also Table A.2. The typical uncertainty of measurements for this study was $\pm 5\%$ (2SD).

Water samples											
ID	B	Ca	Fe	K	Mg	Mn	Na	P	S	Si	Sr
RMSu	0.03	8.57	0.33	2.65	6.36	<0.005	34.42	<0.05	4.90	1.80	0.10
LLLSu	0.09	26.87	<0.005	7.92	20.65	<0.005	120.29	<0.05	16.20	0.20	0.31
CSu-1	4.83	358.26	<0.05	349.24	1086.43	<0.05	9238.12	<0.5	888.10	<1	6.54
CSu-2	6.14	434.69	<0.05	447.66	1334.12	<0.05	11370.08	<0.5	1120.40	<1	8.11
CSu-3	9.63	620.95	<0.05	676.38	2103.42	0.07	17433.43	<0.5	1805.90	<1	12.80
CSu-4	11.05	722.11	<0.05	791.46	2400.86	<0.05	19893.11	<0.5	2103.40	<1	15.21
CSu-5	14.62	891.38	<0.05	1003.07	3020.11	0.07	27155.45	<0.5	2489.10	1.40	18.53
CSu-7	18.24	1075.76	<0.05	1288.27	3896.09	<0.05	35269.50	<0.5	3224.60	<1	23.47
CSu-8	18.09	1040.71	<0.05	1293.74	3754.88	<0.05	33878.00	<0.5	3172.80	1.10	22.78
CSu-9	17.46	996.45	<0.05	1242.83	3745.32	<0.05	32517.45	<0.5	3046.30	1.20	22.39
SCSu	2.39	76.16	0.02	109.78	459.77	<0.005	4576.90	0.20	412.70	11.90	7.60
SWSu	6.05	403.87	<0.005	424.40	1294.73	<0.005	10895.01	<0.05	1093.40	<0.1	7.98
RMS	0.05	11.58	0.19	3.15	8.52	<0.005	51.54	0.07	7.90	2.20	0.14
LLLS	0.09	27.58	<0.005	8.21	20.58	<0.005	121.51	<0.05	16.10	0.40	0.31
CS-1	5.30	389.04	<0.05	383.63	1208.12	0.07	9860.41	<0.5	962.20	<1	7.03
CS-2	6.44	443.87	<0.05	468.28	1425.77	<0.05	11936.39	<0.5	1176.20	<1	8.81
CS-3	9.83	645.25	<0.05	711.22	2223.95	0.09	18131.15	<0.5	1915.60	1.10	13.87
CS-4	11.49	741.59	<0.05	841.61	2538.24	0.10	21877.28	<0.5	2296.30	1.80	16.13
CS-6	14.45	892.73	<0.05	1008.50	3138.74	<0.05	29848.01	<0.5	2558.10	2.30	19.15
CS-5	14.57	922.48	<0.05	1079.42	3187.53	<0.05	26355.18	<0.5	2898.10	2.40	20.12
CS-7	13.26	779.42	<0.05	917.14	2820.65	<0.05	26276.50	<0.5	2287.50	1.00	17.06
CS-8	12.35	757.50	<0.05	903.73	2638.49	<0.05	23059.00	<0.5	2432.50	<1	17.22
CS-9	11.37	676.25	<0.05	801.52	2422.74	<0.05	20866.86	<0.5	2195.30	<1	16.05
SCS	1.78	82.77	0.01	75.73	315.13	<0.005	2758.24	0.09	229.90	12.60	5.30
RMW	0.04	10.69	0.12	3.54	9.41	<0.001	57.48	0.02	7.60	0.80	0.15
CW-1	4.60	329.17	<0.005	361.22	1115.08	0.01	9260.33	0.11	943.70	0.40	7.28

CW-2	6.49	467.12	<0.005	513.31	1623.44	0.01	13482.09	0.09	1287.70	0.20	10.48
CW-3	7.43	532.40	<0.005	595.66	1891.50	0.01	15195.14	0.07	1477.20	0.20	12.21
CW-4	7.94	552.83	<0.005	628.12	1951.95	0.03	15902.06	0.22	1586.50	0.40	12.87
CW-5	8.49	580.24	<0.005	666.36	2078.02	<0.001	16938.16	0.18	1701.20	0.90	13.58
CW-7	8.11	568.42	<0.005	652.83	2034.26	0.00	16714.61	0.27	1629.80	1.20	13.60
CW-8	8.78	616.31	<0.005	717.88	2181.24	<0.001	17755.25	0.26	1762.10	1.60	14.83
CW-9	8.58	566.43	<0.005	683.63	2064.34	0.00	17322.44	0.17	1685.20	1.80	14.33
SCW	1.18	98.44	<0.005	54.26	245.14	<0.001	2067.10	0.06	217.40	4.90	7.66
MRA	0.05	12.75	<0.005	3.96	8.42	<0.001	43.40	<0.01	6.10	0.80	0.16
LLA	0.10	24.27	<0.005	8.86	20.84	<0.001	126.15	0.01	14.90	0.10	0.32
CA-1	2.85	220.90	<0.005	230.39	693.21	0.01	5792.33	0.03	649.20	0.30	4.38
CA-2	3.82	290.29	<0.005	309.51	965.50	0.01	7663.11	0.03	819.60	0.70	6.05
CA-3	4.81	359.96	<0.005	387.16	1206.37	0.03	9818.68	0.04	963.80	0.20	7.84
CA-4	5.69	410.75	<0.005	453.68	1400.05	0.01	11670.56	0.05	1146.80	0.20	9.34
CA-6	8.37	578.47	<0.005	669.85	2125.83	0.05	17500.14	0.09	1699.80	0.80	13.49
CA-5	8.30	585.13	<0.005	676.18	2120.29	0.01	17301.95	0.08	1744.10	0.60	13.61
CA-7	9.90	697.23	<0.005	819.16	2530.52	0.07	20382.57	0.09	2064.20	1.30	16.54
CA-8	11.92	759.11	0.01	917.68	2832.58	0.03	22742.79	0.10	2319.10	1.50	18.28
CA-9	13.84	859.72	0.01	1060.84	3126.66	0.00	26005.84	0.12	2783.30	1.90	21.12
SCA	1.03	31.81	<0.005	45.90	140.27	<0.001	1412.62	0.03	129.30	2.60	2.63
GWF	0.49	71.37	0.02	94.53	61.45	0.95	256.09	6.97	32.10	14.80	1.97
GWN	0.30	115.68	<0.005	19.91	46.07	0.02	264.98	0.10	48.10	8.60	1.09
GWR	2.87	336.12	0.01	183.44	681.56	0.19	5060.27	0.17	659.80	7.60	9.52
GWP	4.55	339.67	0.01	204.62	873.80	0.22	7922.82	0.38	791.00	10.10	17.94
GWSW	2.28	318.89	0.07	171.40	421.34	0.14	4341.30	5.16	414.40	18.10	7.77
GWWW2	1.22	418.29	0.02	88.00	338.44	<0.005	3827.50	0.57	526.70	0.10	4.38
GWWW	3.08	330.57	0.02	163.75	808.64	<0.005	6623.39	0.14	683.80	0.20	14.49
GWWW3	2.56	238.14	0.01	187.04	590.09	0.13	5316.29	0.10	465.60	9.70	9.99
Standards and certified values											
ID	B	Ca	Fe	K	Mg	Mn	Na	P	S	Si	Sr

IAPSO measured#	5.4	406.5		418	1310		10600		965.5	0.8	8.1
IAPSO published values*	4.5	412		399	1290		10770		904	2.8	7.9
IV-ICPMS-71A (10ppm) measured	9.73	9.74	10.19	9.37	9.76	9.67	9.58	9.58	9.61		9.80
IV-ICPMS-71A certified values	9.99	9.99	9.99	10.00	9.99	9.99	9.99	9.99	9.99		9.99
±	0.06	0.04	0.04	0.04	0.04	0.04	0.04	0.04	0.05		0.04
IV-ICPMS-71B (10ppm) measured										11.74	
IV-ICPMS-71B certified values										10.00	
±										0.06	

The typical uncertainty of the IAPSO standard for this study was $\pm 5\%$ (2SD).

* Source: Summerhayes, C. P., and Thorpe, S. A., 1996 : *Oceanography An Illustrated Guide*, Chapter 11, 165-181.

Table B.2. Concentrations (ppm) of main dissolved anions in waters analysed by IC. For more details on water salinity and sampling sites see also data in Table A.2. The typical uncertainty of measurements for this study was $\pm 5\%$ (2SD).

Water samples											
ID	F ⁻	Cl ⁻	NO ₂ ⁻	Br ⁻	NO ₃ ⁻	SO ₄ ²⁻	I ⁻	PO ₄ ³⁻			
RMSu	0.12	59.00	0.11	13.90	0.15	7.50	<0.05	<5			
LLLsu	0.24	220.00	0.31	43.30	0.66	6.30	<0.05	<5			
CSu1	2.30	17900.00	22.60	2450.00	59.80	17.10	<5	<500			
CSu2	2.46	24600.00	31.10	3350.00	83.70	16.60	<5	<500			

CSu3	2.89	34000.00	45.30	4650.00	114.00	51.90	<5	<500
CSu4	2.88	39800.00	54.40	5450.00	133.00	30.20	<5	<500
CSu5	3.52	50300.00	73.80	7310.00	178.00	24.70	<5	<500
CSu7	3.95	63600.00	94.50	9610.00	227.00	44.00	<5	<500
CSu8	4.74	62600.00	95.10	9370.00	222.00	41.30	<5	<500
CSu9	4.78	61300.00	92.40	9120.00	214.00	39.10	<5	<500
SCSu	2.06	7620.00	11.80	1180.00	20.40	5.70	4.94	<50
SWSu	<0.1	20600.00	14.50	3430.00	86.20	22.30	5.95	<50
RMS	0.11	91.00	0.14	22.10	0.24	0.10	<0.05	<5
LLLS	0.48	223.00	0.31	43.40	0.68	0.20	<0.05	<5
CS1	2.19	19500.00	22.90	2670.00	67.50	<10	<5	<500
CS2	2.25	23400.00	31.70	3210.00	78.10	12.20	<5	<500
CS3	2.67	36400.00	46.50	11400.00	124.00	<10	<5	<500
CS4	3.85	42600.00	57.50	5880.00	144.00	17.30	<5	<500
CS6	4.28	50400.00	67.30	7290.00	178.00	<10	<5	<500
CS5	2.95	49900.00	68.50	6940.00	167.00	<10	<5	<500
CS7	4.01	47200.00	73.60	7330.00	177.00	<10	<5	<500
CS8	4.03	44800.00	60.80	6200.00	148.00	20.00	<5	<500
CS9	3.85	41100.00	55.10	5680.00	137.00	11.50	<5	<500
SCS	1.60	4760.00	7.63	694.00	13.00	<1	3.79	<50
RMW	0.23	99.87	0.04	0.26	<0.5	22.78	<0.05	<0.5
CW1	<5	18578.58	<1	59.80	<50	2587.40	<5	<50
CW2	<5	26366.79	<1	86.73	<50	3660.37	<5	<50
CW3	<5	30391.31	<1	100.32	<50	4201.22	<5	<50
CW4	<5	39380.69	<1	128.78	<50	5443.99	<5	<50
CW5	<5	34089.12	<1	111.22	<50	4723.80	<5	<50
CW7	<5	33846.60	<1	110.96	<50	4689.47	<5	<50
CW8	<5	37877.03	<1	123.01	<50	5245.63	<5	<50
CW9	<5	37474.62	<1	120.47	<50	5188.24	<5	<50
SCW	1.72	4105.03	<0.1	10.62	<5	652.22	<0.5	<5

MRA	0.18	71.57	<0.01	0.20	0.63	18.23	<0.05	<0.5
L/A	0.23	239.23	<0.01	0.74	<0.5	43.67	<0.05	<0.5
CA1	<5	12167.17	<1	38.35	<50	1930.81	<5	<50
CA2	<5	16558.59	<1	54.16	<50	2341.75	<5	<50
CA3	<5	19126.08	<1	62.19	<50	2802.18	<5	<50
CA4	<5	22712.21	<1	74.65	<50	3280.30	<5	<50
CA6	<5	37430.06	<1	123.26	<50	5161.25	<5	<50
CA5	<5	38109.14	<1	124.81	<50	5409.59	<5	<50
CA7	<5	42413.08	<1	138.00	<50	5886.99	<5	<50
CA8	<5	58235.17	<1	174.11	<50	7253.18	<5	<50
CA9	<5	61702.52	<1	178.34	<50	7768.63	<5	<50
SCA	0.82	2584.39	<0.1	5.99	<5	396.84	<0.5	<5
GW _F	2.91	467.00	3.79	89.30	2.36	25.00	1.70	<5
GW _N	0.34	527.00	0.80	141.00	2.00	4.80	<0.05	<5
GW _R	0.72	10700.00	15.40	1720.00	36.40	6.40	<0.5	<50
GW _P	0.97	15300.00	18.70	2310.00	49.70	10.70	1.98	<50
GW _{SW}	<0.1	7790.00	12.80	1280.00	26.30	2.30	0.98	<50
GW _{WW2}	<0.1	6820.00	10.90	1590.00	20.40	7.00	1.41	<50
GW _{WW}	1.06	13500.00	17.60	1950.00	39.50	1.40	1.14	<50
GW _{WW3}	1.60	11000.00	15.00	1390.00	34.20	5.60	0.70	<50
Standards and certified values								
ID	F⁻	Cl⁻	NO₂⁻	Br⁻	NO₃⁻	SO₄²⁻	F⁻	PO₄³⁻
IAPSO measured#	1	19050		67		2655		
IAPSO published values*	1.3	19354		67			0.05	
IC-1 Solution A (5ppm) measured	4.97	4.97		4.89	5.87	4.83		4.80
IC-1 Solution A (5ppm) certified values	5.00	5.00		5.00	5.00	5.00		5.00
±	0.05	0.05		0.05	0.05	0.05		0.05
IC-1 Solution B (5ppm) measured			4.63					

IC-1 Solution B (5ppm) certified values				5.00						
±				0.10						

The typical uncertainty of the IAPSO standard for this study was $\pm 5\%$ (2SD).

* Source: Summerhayes, C. P., and Thorpe, S. A., 1996 : *Oceanography An Illustrated Guide*, Chapter 11, 165-181.

B.2 Alkalinity and pH of waters

Table B.3. Spectrophotometric laboratory-based pH data and alkalinity data measured in waters collected 2018 and 2019. For more details on water salinity and sampling site information see also Table A.1. For the purposes of comparison, pH measurements made spectrophotometrically on the total pH scale were converted to the NBS pH scale using the equations of Dickson (1990), and Lewis and Wallace (1998), and the latter NBS pH scale was used in the PHREEQC modelling (section 3.6).

Sample ID	Lab pH (total scale)	Lab pH (NBS scale)	Alkalinity (mg CaCO ₃ /L)
RMSu	7.22	7.28	22
LLSu	7.19	7.29	89
CSu1	8.28	8.57	129
CSu2	8.06	8.37	118
CSu3	7.81	8.03	170
CSu4	7.69	7.84	160
CSu5	7.62	7.75	158
CSu7	7.45	7.48	180
CSu8	7.62	7.65	188
CSu9	7.61	7.71	194
SCSu	7.85	8.15	500
SWSu	7.90	8.19	116
RMS	7.10	7.16	24
LLS	7.25	7.31	90
CS1	7.62	7.87	122
CS2	7.72	7.98	129
CS3	7.75	7.93	168
CS4	7.55	7.68	180
CS6	7.47	7.51	178
CS5	7.61	7.67	181
CS7	7.31	7.37	164
CS8	7.44	7.54	196
CS9	7.74	7.86	212
SCS	8.13	8.32	454
RMW	7.46	7.64	29
CW1	7.77	8.18	126
CW2	8.08	8.46	146
CW3	7.93	8.29	168
CW4	8.01	8.33	186
CW5	8.05	8.37	198
CW7	7.99	8.30	214
CW8	8.00	8.28	216
CW9	8.00	8.31	221

SCW	8.57	8.87	370
RMA	7.86	8.03	44
LLA	7.79	7.99	100
CA1	7.72	8.08	97
CA2	7.92	8.29	89
CA3	7.95	8.31	107
CA4	8.08	8.43	128
CA6	8.21	8.50	169
CA5	8.03	8.32	175
CA7	7.98	8.25	206
CA8	7.99	8.23	206
CA9	7.96	8.16	219
SCA	8.88	9.22	202
GWN	8.01	8.17	223
GWR	7.74	7.99	325
GWP	7.50	7.77	419
GWSW	8.05	8.35	745
GWWW2	7.53	8.01	227
GWWW	7.98	8.34	289
GWWW3	7.65	7.92	443

B.3 Results of Sr isotope ratios ($^{87}\text{Sr}/^{86}\text{Sr}$ and $\delta^{88/86}\text{Sr}$) of all water samples

Table B.4. Radiogenic and stable Sr isotope composition ($^{87}\text{Sr}/^{86}\text{Sr}$ and $\delta^{88/86}\text{Sr}$) of the samples, with associated sampling location/area, date and water salinity. Note that 2SEM is the external precision for repeated analyses with size n; but when n is not given, 2SEM is internal precision of a single analysis of the sample through 200 cycles for $\delta^{88/86}\text{Sr}$, and 100 cycles for $^{87}\text{Sr}/^{86}\text{Sr}$.

Sample ID	Area	Sampling date (dd/mm/yy)	Salinity (PSU)	$^{87}\text{Sr}/^{86}\text{Sr}$	2SEM	$\delta^{88/86}\text{Sr}$ (‰ _{SRM987})	2SEM
Coorong water samples							
CSu1	North Lagoon	07-08/3/19	30.05	0.709212	0.000004	0.402	0.014
CSu2	North Lagoon	07-08/3/19	37.24	0.709212	0.000004	0.371	0.013
CSu3	North Lagoon	07-08/3/19	56.88	0.709236	0.000004	0.388	0.013
CSu4	North Lagoon	07-08/3/19	66.21	0.709247	0.000004	0.388	0.013
CSu5	NL-SL connection	07-08/3/19	83.79	0.709251	0.000004	0.427	0.013
CSu7	South Lagoon	07-08/3/19	105.78	0.709246	0.000004	0.427	0.013
CSu8	South Lagoon	07-08/3/19	103.51	0.709243	0.000003	0.442	0.011
CSu9	South Lagoon	07-08/3/19	100.43	0.709249	0.000004	0.437	0.014

Appendix 4

CS1	North Lagoon	07/12/18	32.56	0.709198	0.000005	0.399	0.013
CS2	North Lagoon	07/12/18	38.89	0.709244	0.000004	0.322	0.013
CS3	North Lagoon	07/12/18	60.64	0.709255	0.000005	0.416	0.013
CS4	North Lagoon	07/12/18	70.08	0.709252	0.000004	0.429	0.013
CS6	NL-SL connection	07/12/18	85.66	0.709250	0.000004	0.436	0.013
CS5	NL-SL connection	07/12/18	85.71	0.709251	0.000004	0.428	0.013
CS7	South Lagoon	07/12/18	80.42	0.709269	0.000004	0.480	0.014
CS8	South Lagoon	07/12/18	74.48	0.709263	0.000004	0.362	0.013
CS9	South Lagoon	07/12/18	68.18	0.709268	0.000004	0.459	0.013
CW1	North Lagoon	31/08/18	31.66	0.709245	0.000004	0.387	0.016
CW2	North Lagoon	31/08/18	44.98	0.709238	0.000004	0.390	0.013
CW3	North Lagoon	31/08/18	51.29	0.709238	0.000005	0.406	0.013
CW4	North Lagoon	31/08/18	55.51	0.709263	0.000003	0.394	0.013
CW5	NL-SL connection	31/08/18	58.51	0.709254	0.000004	0.402	0.013
CW7	South Lagoon	31/08/18	57.62	0.709258	0.000004	0.414	0.013
CW8	South Lagoon	31/08/18	60.65	0.709258	0.000004	0.377	0.013
CW9	South Lagoon	31/08/18	58.51	0.709250	0.000004	0.375	0.012
CA1	North Lagoon	24/05/18	27.56	0.709190	0.000003	0.401	0.012
CA2	North Lagoon	24/05/18	32.53	0.709179	0.000003	0.427	0.012
CA3	North Lagoon	24/05/18	44.09	0.709207	0.000003	0.399	0.013
CA4	North Lagoon	24/05/18	38.29	0.709211	0.000003	0.448	0.012
CA6	NL-SL connection	24/05/18	61.39	0.709252	0.000003	0.409	0.013
CA5	NL-SL connection	24/05/18	62.93	0.709245	0.000003	0.415	0.012
CA7	South Lagoon	24/05/18	69.54	0.709253	0.000003	0.406	0.014
CA8	South Lagoon	24/05/18	76.9	0.709259	0.000004	0.472	0.013
CA9	South Lagoon	24/05/18	90.83	0.709250	0.000003	0.447	0.013
Groundwater samples							
GWN	North Lagoon	11-12/04/19	1.83	0.709283	0.000004	0.260	0.013
GWR	North Lagoon	11-12/04/19	17.39	0.709231	0.000004	0.288	0.012
GWP	South Lagoon	11-12/04/19	19.67	0.709382	0.000004	0.294	0.014
GWSW	South Lagoon	11-12/04/19	10.45	0.709368	0.000004	0.299	0.013
GWWW2	South Lagoon	11-12/04/19	8.54	0.709348	0.000004	0.321	0.013
GWWW	South Lagoon	11-12/04/19	18.08	0.709333	0.000004	0.341	0.012
GWWW3	South Lagoon	11-12/04/19	15.7	0.709319	0.000004	0.347	0.014
JWP2	North Lagoon	25/06/15	1.15	0.709319	0.000003	0.261	0.017
BWP2	North Lagoon	25/06/15	3.66	0.709281	0.000003	0.247	0.012
Continental water and seawater samples							
RMSu	River Murray	07-08/3/19	0.14	0.712060	0.000004	0.290	0.016

RMS	River Murray	07/12/18	0.2	0.711918	0.000004	0.266	0.012
RMW	River Murray	31/08/18	0.22	0.712055	0.000004	0.286	0.016
RMA	River Murray	24/05/18	0.21	0.711933	0.000003	0.302	0.012
LLSu	the Lower Lakes	07-08/3/19	0.47	0.711415	0.000003	0.252	0.012
LLS	the Lower Lakes	07/12/18	0.48	0.711356	0.000004	0.300	0.014
LLA	the Lower Lakes	24/05/18	0.5	0.711310	0.000004	0.341	0.014
SCSu	Salt Creek	07-08/3/19	14.55	0.709262	0.000004	0.376	0.011
SCS	Salt Creek	07/12/18	90.8	0.709245	0.000004	0.391	0.014
SCW	Salt Creek	31/08/18	7.18	0.709253	0.000004	0.304	0.013
SCA	Salt Creek	24/05/18	7.66	0.709298	0.000003	0.304	0.016
SWSu	S o u t h e r n Ocean	07-08/3/19	36.97	0.709168	0.000005	0.390	0.012

Appendix C. Supporting evidence of water chemistry in the Coorong

C.1. Influence of storm events, barrage outflows and Salt Creek discharges on Coorong water salinities and levels

Agencies of South Australian Government has been monitoring the water quality spanning the Coorong since late 90s at multiple sites. Specifically, water level, electric conductivity (EC) and temperature were recorded daily. These data covering the time span of water sampling of this study (1st May 2018 – 1st May 2019) were extracted from five Coorong-Lower Lakes barrages, a Salt Creek regulator and six sites in the North and South Lagoons listed in Table C.1 below.

Table C.1. List of current telemetered water quality monitoring sites in Coorong (note sites in Murray Mouth region excluded). The locations of these sites can be found in Fig. 1 and its caption.

Site No.	Location	Name	Latitude (degree South)	Longitude (degree East)	Instruments
A4261122	Barrage	Goolwa Barrage	35.5242	138.8068	Department for Environment and Water (South Australia) “barrage calculator” based water level sensor measurements, known flow rating curves, and number of barrage gates open.
A4261204	Barrage	Mundoo Barrage	35.5341	138.9098	
A4261205	Barrage	Boundary Creek Barrage	35.5502	138.9557	
A4261206	Barrage	Ewe Island Barrage	35.5569	138.9776	
A4261207	Barrage	Tauwitchere Barrage	35.5828	139.0189	

Appendix 4

A4261134	North Lagoon	Pelican Point	35.6005	139.0266	Insitu AT200 sensor
A4261135	North Lagoon	Long Point	35.6957	139.1618	Insitu AT200 sensor
A4260572	North Lagoon	Rob's Point	35.7860	139.2951	Insitu AT100 sensor/Shaft Encoder for WL
A4260633	South Lagoon	Parnka Point	35.9020	139.3956	Greenspan EC/Shaft Encoder for WL
A4261209	South Lagoon	Woods Well	36.0102	139.5294	Aquamonix EC/Shaft Encoder for WL
A4261165	South Lagoon	NW Snipe Island	36.1087	139.6083	AT100 sensor/Shaft Encoder for WL
A2390568	Salt Creek	Salt Creek Outlet	36.1248	139.6535	

For the purpose of comparison, EC (mS/cm) was converted to salinity (PSU) using the equation from Mosley et al. (2020), which is:

$$\text{Salinity} = -7 \times 10^{-6} \text{EC}^3 + 0.003 \text{EC}^2 + 0.5865 \text{EC} \quad (\text{Eq. C.1})$$

The calculated salinity data are shown in Figs. C.2-4.

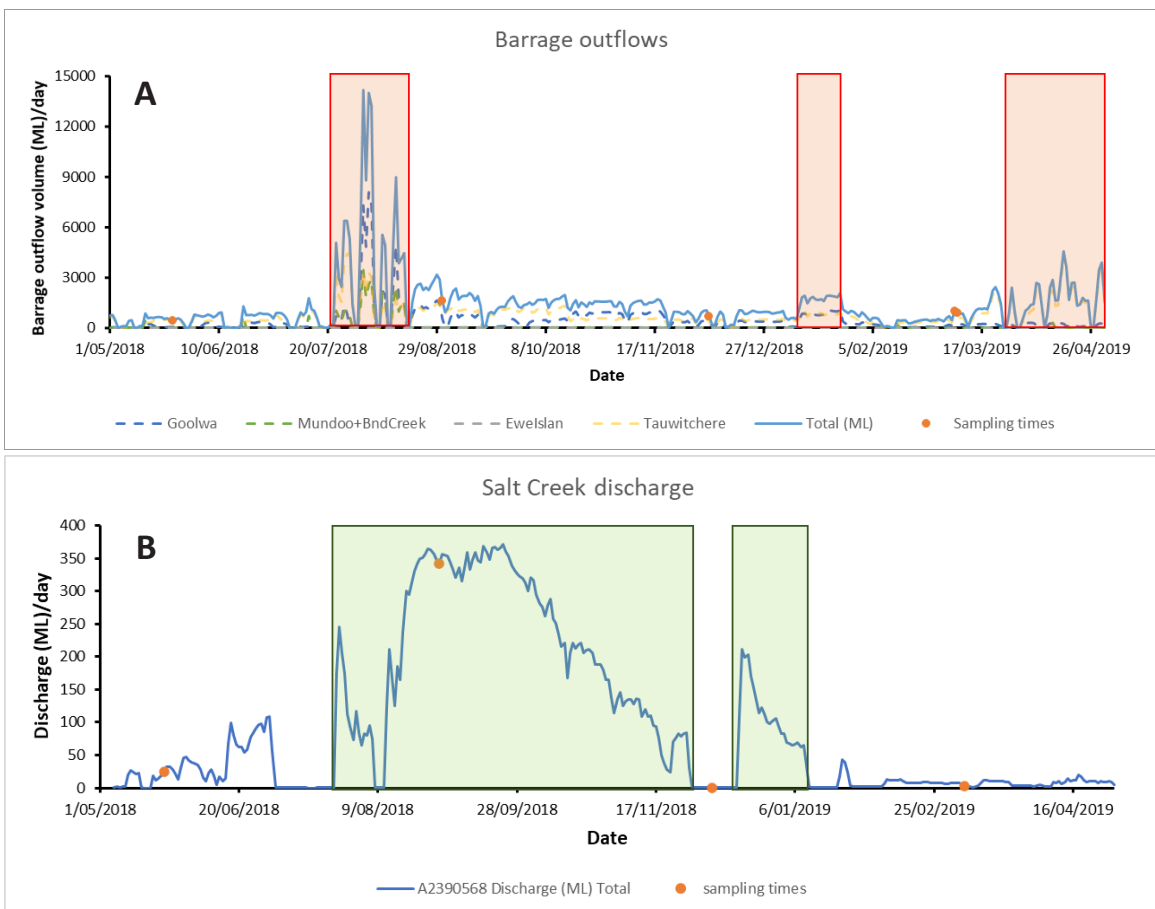


Figure C.1: Daily record of (A) Barrage outflow (into the Coorong), and (B) Salt Creek discharge from 1st May 2018 to 1st May 2019. The red rectangles mark times of high barrage outflows, and green rectangles mark times of high Salt Creek discharge.

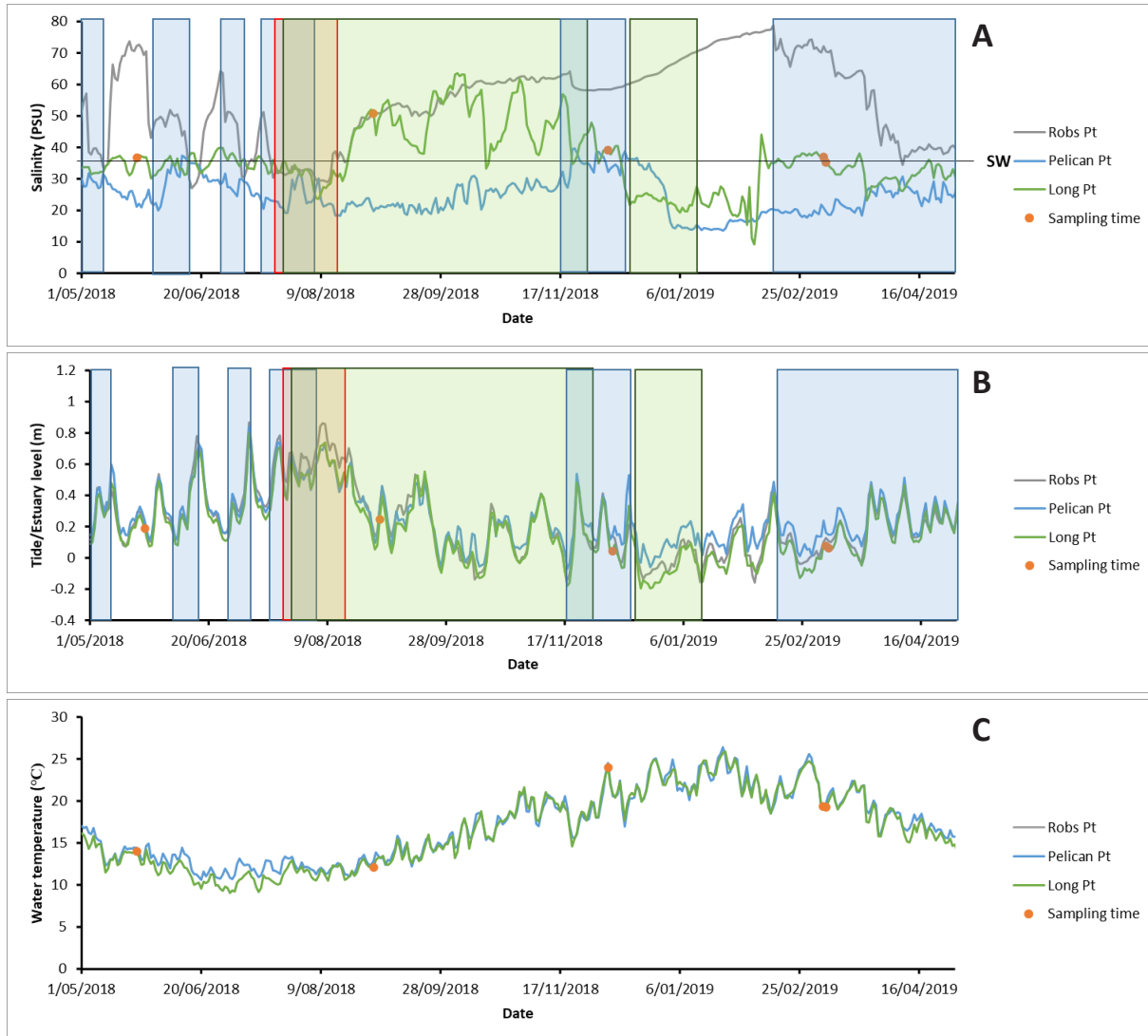


Figure C.2: Daily record of (A) water salinity (calculated from Eq. C.1), (B) water level relative to Australian Height Datum (AHD) and (C) water temperature (°C) of North Lagoon monitoring sites (i.e., Pelican Point, Long Point and Robs Point) from 1st May 2018 to 1st May 2019. The blue rectangles mark deduced storm events based on convergence of salinities at all sites towards seawater (SW) value (36 PSU), the latter is marked as a black horizontal line in (A). The red rectangles mark times of high barrage outflows, and green rectangles mark times of high Salt Creek discharge, referred from Fig. C.1.

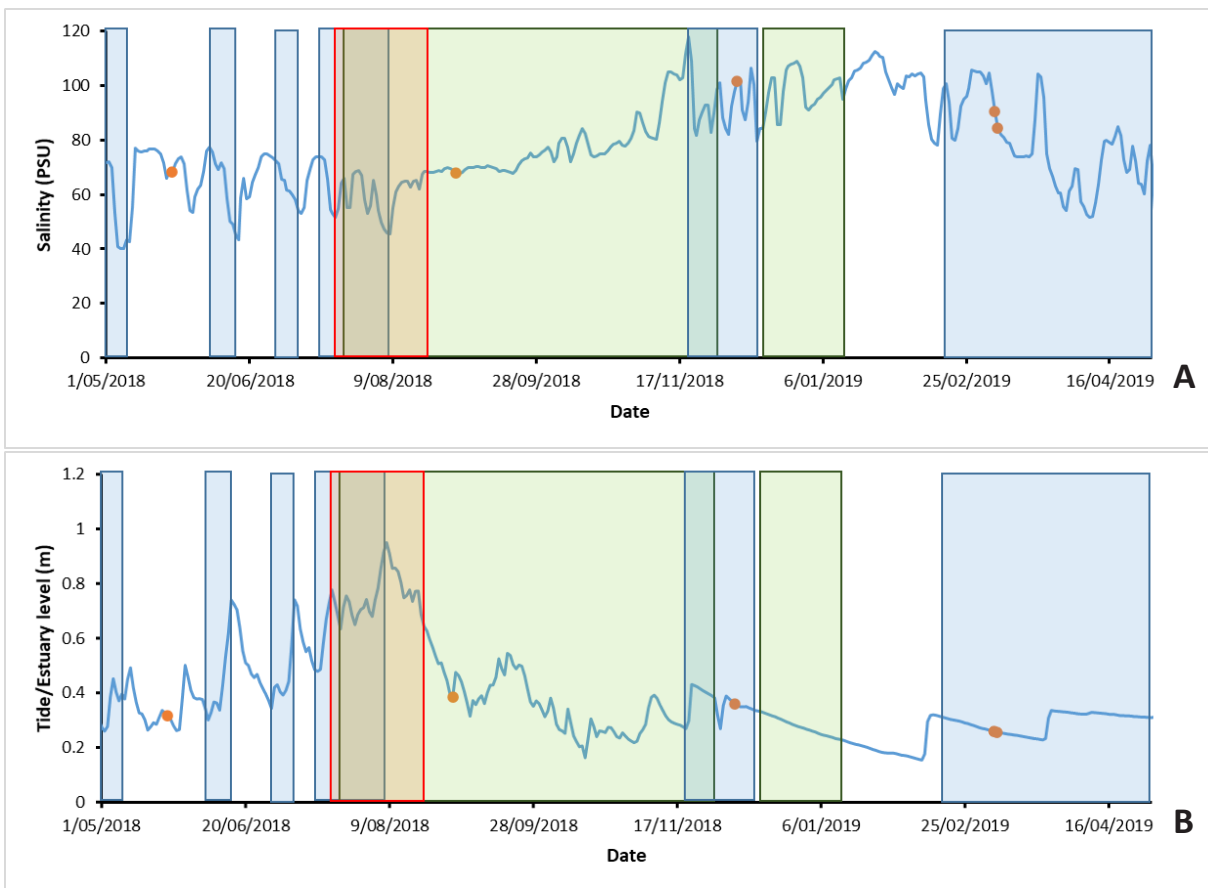
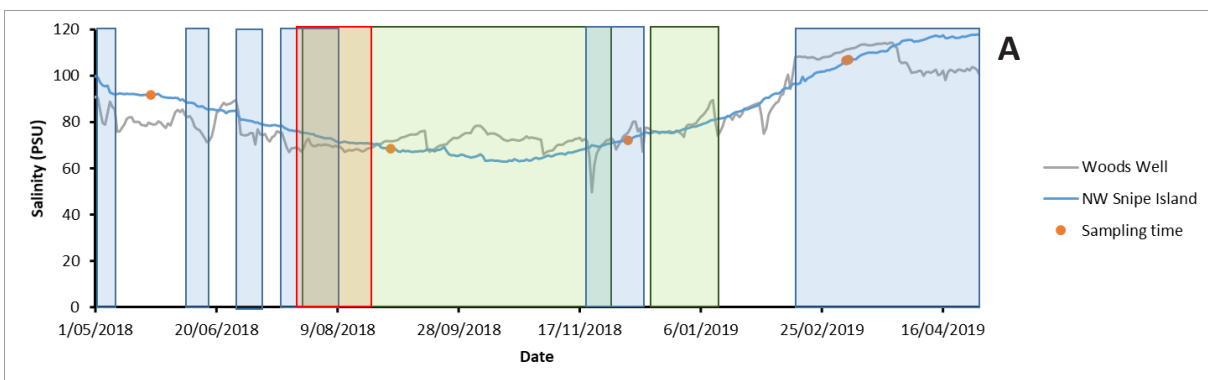


Figure C.3: Daily record of (A) water salinity (calculated from Eq. C.1), (B) water level relative to Australian Height Datum (AHD) and (C) water temperature ($^{\circ}\text{C}$) of Parnka Point monitoring sites from 1st May 2018 to 1st May 2019. The orange dots represent sampling times. The blue rectangles mark deduced storm events based on convergence of salinities at all sites towards seawater (SW) value (36 PSU), the latter is marked as a black horizontal line in (A). The red rectangles mark times of high barrage outflows, and green rectangles mark times of high Salt Creek discharge, referred from Fig. C.1.



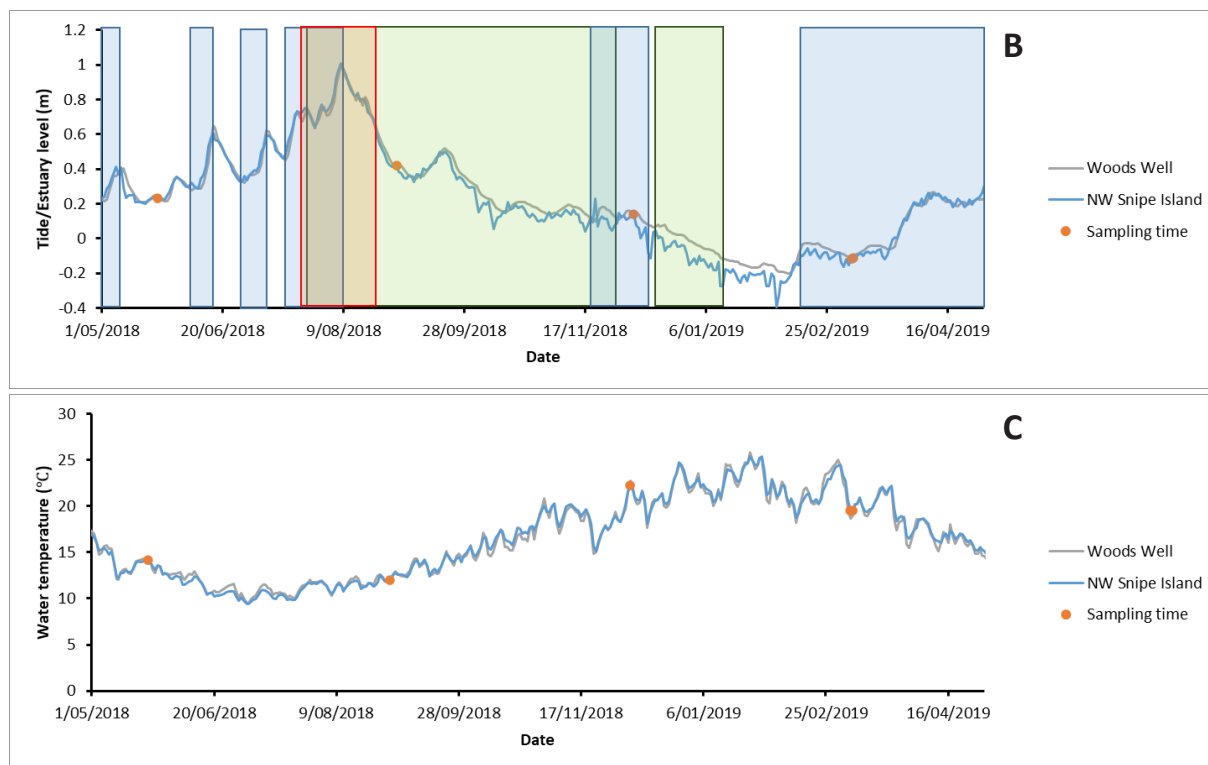


Figure C.4: (A) water salinity (calculated from Eq. C.1), (B) water level relative to Australian Height Datum (AHD) and (C) water temperature (°C) of South Lagoon monitoring sites (i.e., Woods Well and NW Snipe Island) from 1st May 2018 to 1st May 2019. The blue rectangles mark deduced storm events based on convergence of salinities at all sites towards seawater (SW) value (36 PSU), the latter is marked as a black horizontal line in (A). The red rectangles mark times of high barrage outflows, and green rectangles mark times of high Salt Creek discharge, referred from Fig. C.1.

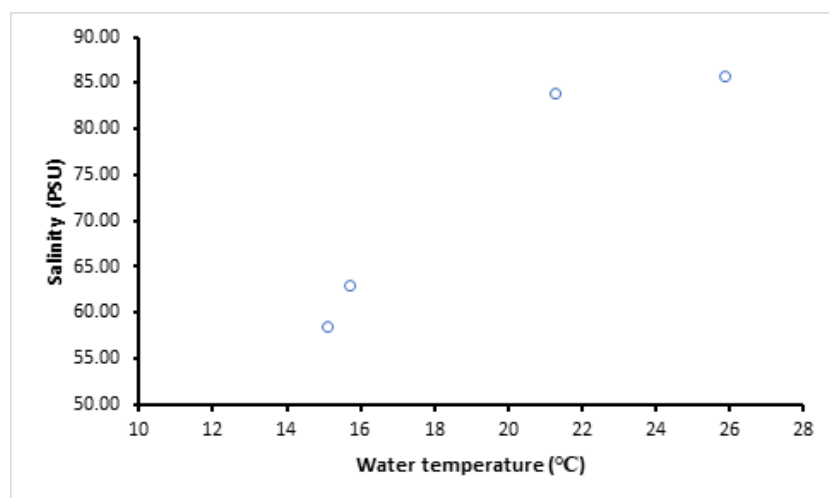


Figure C.5: Water salinity (PSU) vs. water temperature (°C) at the Parnka Point during 2018-2019 sampling times.

Seawater, barrage outflows (i.e., River Murray and Lower Lakes water input into the North Lagoon) and Salt Creek discharges have significant impact on the salinity profile of the Coorong, and therefore account for most of the water sources to the Coorong. According to Mosley et al. (2020), water level of the Coorong is mainly controlled by wind/storm events. Barrage outflows and seawater can be pushed towards the North Lagoon by storm events (e.g., on 10th August 2015 recorded by Mosley, 2016) or strong winds.

Although there is no measurement of seawater input volume into the Coorong, it can be deduced that from Figs. C.2-4 that major storm events, labelled by blue rectangles, happened frequently during the first time of sampling (24 May 2018) and until early August 2018 and pushed seawater throughout the Coorong. This is because seawater has a typical salinity of 35PSU, storm events bringing in seawater can thus be observed as temporary convergence of salinity towards 35PSU in all monitoring sites (Figs. C.2A, C.3A and C.4A), and a rapid increase in water levels.

Barrage outflows constantly existed throughout the sampling period at a 1000s ML/day scale and were especially high during late July – mid August 2018 (Fig. C.1A). However, there was no obvious decrease in salinity in the North Lagoon sites during this period, possibly due to lack of storm events. Despite of that, the barrage outflows were able to constantly reach the Pelican Point as the local salinity were mostly lower than seawater (35PSU) except when seawater entered the North Lagoon pushed by storms.

In the South Lagoon, the water level receives much more influence from seasonal cycles of evaporation (i.e., high evaporation in summer and low evaporation in winter) and variations of water exchange with the North Lagoon (Gibbs et al., 2018), which can also be observed in Fig. C.4B. The Salt Creek, although has minimal impact on the water level of South Lagoon, it significantly lowers water salinity and increase water export to the North Lagoon (Mosley et al., 2017). From 1st May 2018 to 1st May 2019, the major Salt Creek discharge into the South Lagoon spanned from late July to the end of November 2018 (Fig. C.1B). Consequently, the salinities of the South Lagoon monitoring sites decreased ~20PSU spontaneously (Fig. C.4A). The salinity of Parnka Point showed an opposite trend (Fig. C.3A) due to the South Lagoon water pushed northwards by the Salt Creek discharge. Such trend of salinity increase was also observed in Robs Point in the North Lagoon, but not further north (i.e., Long Point and Pelican Point) (Fig. C.2A).

C.2. The driving mechanisms of the aragonite saturation indices in the Coorong

The saturation indices of aragonite (SI_{arag}) is defined as

$$SI_{\text{arag}} = \log(IAP_{\text{arag}}/K_{\text{sp}}) = \log[(a_{\text{Ca}^{2+}(\text{actual})} \times a_{\text{CO}_3^{2-}(\text{actual})}) / (a_{\text{Ca}^{2+}(\text{eq})} \times a_{\text{CO}_3^{2-}(\text{eq})})] \quad (\text{Eq. C.2})$$

Where the equilibrium constant (K_{sp}) is calculated by the product of ion activities at equilibrium (a_{eq}), and IAP (Ion Activity Product) has the same form as K_{sp} but calculated with actual ion activities (a_{actual}).

In the semi-confined Coorong lagoon, changing in supplies of Ca^{2+} and alkalinity (i.e., carbonate species) is highly responsible for SI_{arag} fluctuations. Furthermore, water temperature and pressure also drive the SI_{arag} by affecting the solubility of CO_2 and therefore CO_3^{2-} concentration. However, in shallow pools like the Coorong, the water pressure is relatively constant. We hereby look for relationships between SI_{arag} of the Coorong water samples and the parameters above and explore the main controls on SI_{arag} in the Coorong.

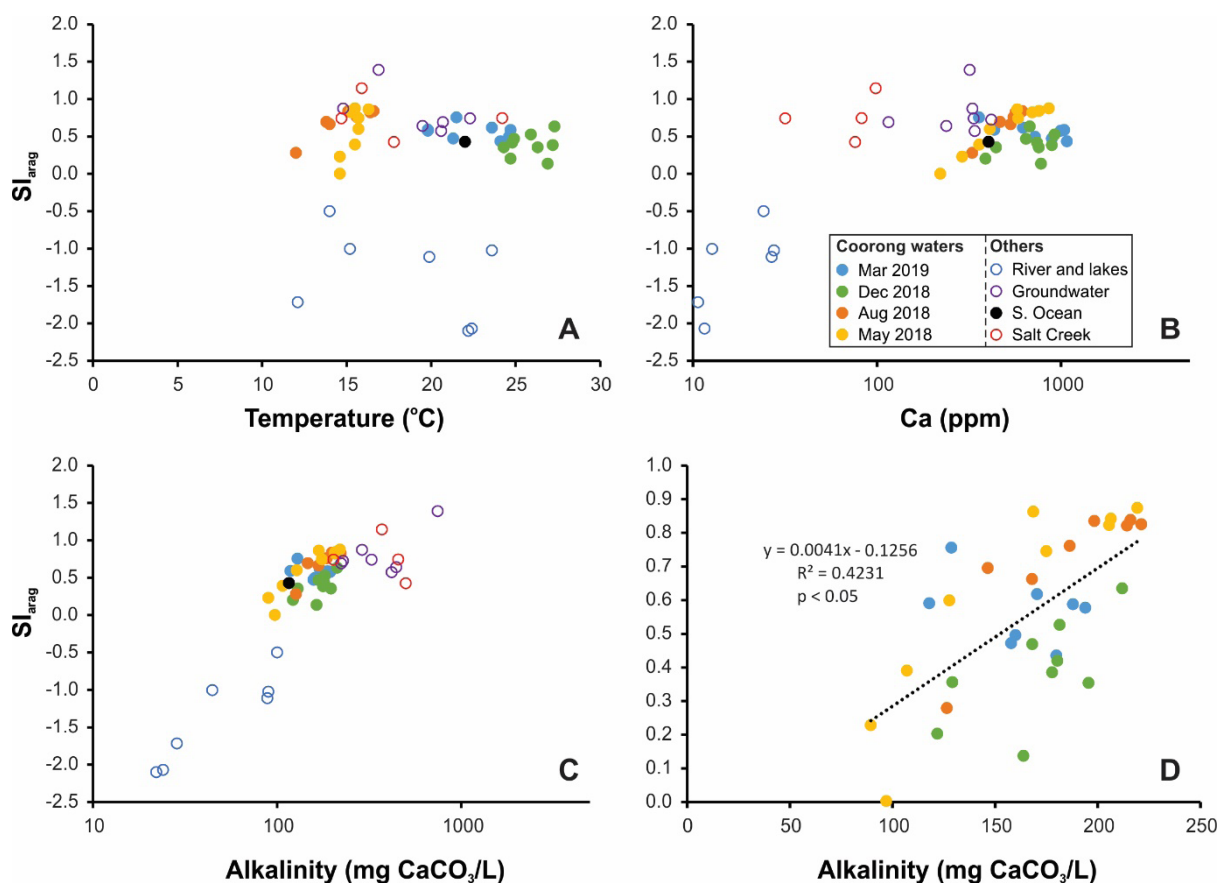


Figure C.6: The saturation indices of aragonite (SI_{arag}) of water samples in the CLLMM system vs. (A) water temperature ($^{\circ}\text{C}$), (B) Ca^{2+} concentration (log scale), (C) alkalinity (mg CaCO_3/L) (log scale) and (D) SI_{arag} of water samples in the Coorong only vs. alkalinity (mg CaCO_3/L).

It is not difficult to see that neither water temperature nor Ca^{2+} concentration had strong correlation to SI_{arag} in the Coorong or CLLMM (Fig. C.5A and B), and the latter seem to be dependent on the amount of alkalinity available to form CaCO_3 (Fig. C.5C and D). Specifically, SI_{arag} of water samples in the Coorong has a moderate and positive correlation with their alkalinity (Fig. C.5D).

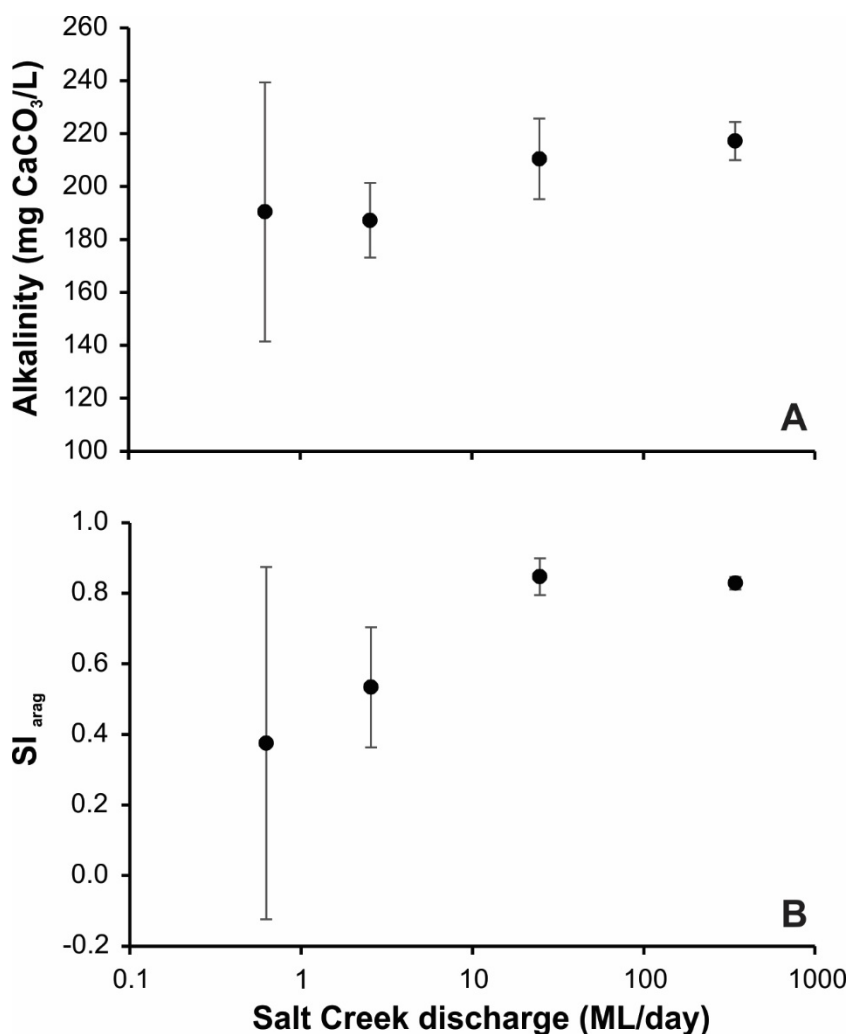


Figure C.7: Average values of (A) Alkalinity (mg CaCO_3/L) and (B) saturation indices of aragonite (SI_{arag}) of South Lagoon water samples (#7-9 in Fig. 2) vs. Salt Creek discharge (ML/day) on the date of sampling (log scale). The error bars represent 2SD variation of alkalinity and SI_{arag} among South Lagoon samples #7-9 in each sampling time.

Furthermore, alkalinity and SI_{arag} of South Lagoon water samples seems to be positively correlated to the amount of Salt Creek discharge (Fig. C.6), especially the latter (Fig. C.6B). Although this might not be so true for May 2018 samples due to large variation of alkalinity and SI_{arag} (largest 2SD error bars in Fig. C.6A and B) in these samples, it potentially implies that the Salt Creek water, which is high in alkalinity compared to the Coorong (Table B.4, Appendix B.2), is an important source of alkalinity to the South Lagoon, which in turn leads to high SI_{arag} .

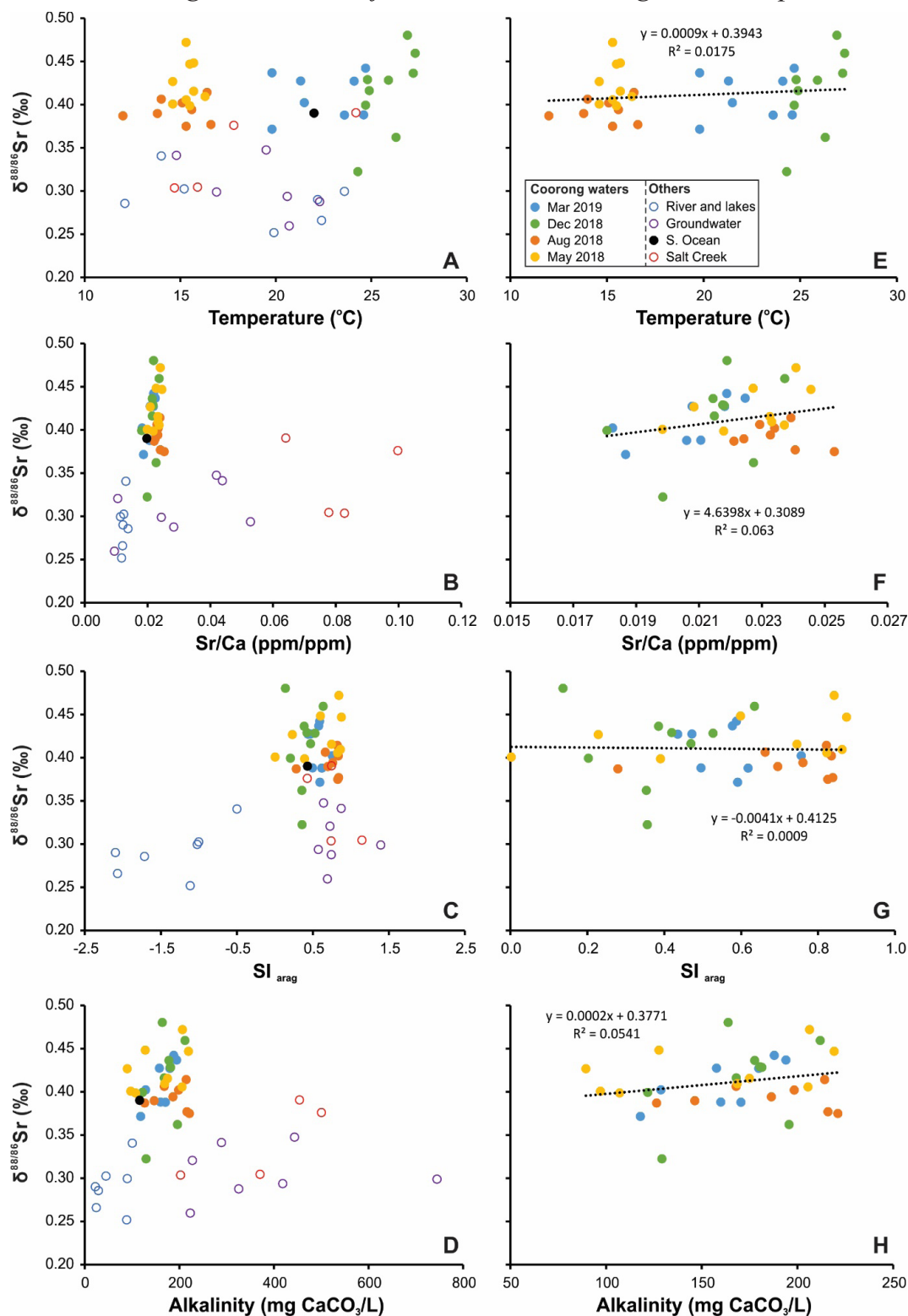
C.3. The driving mechanisms of $\delta^{88/86}\text{Sr}$ in the Coorong water samples

Figure C.8: $\delta^{88/86}\text{Sr}$ of the CLLMM water samples vs. (A) water temperature (°C), (B) Sr/Ca (ppm/ppm), (C) SI_{arag} and (D) alkalinity (mg CaCO_3/L); and $\delta^{88/86}\text{Sr}$ of the Coorong water samples vs. the same parameters (E-H).

Appendix D. Elemental concentrations vs. salinity in the CLLMM

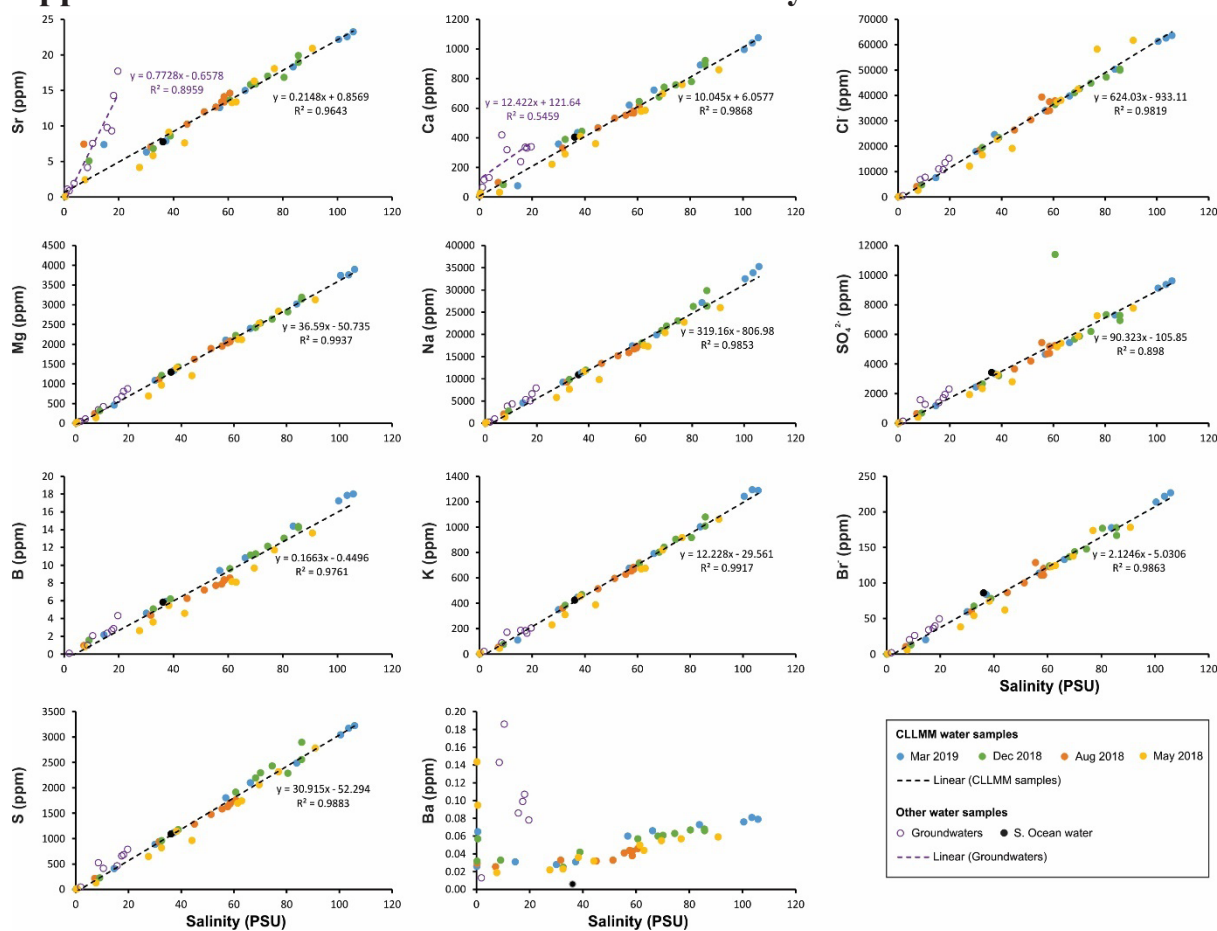


Figure D.1: Concentrations of ions (Sr, Ca, Mg, Na, B, K, S, Ba, Cl⁻, SO₄²⁻ and Br) in CLLMM water samples vs. salinity (PSU).

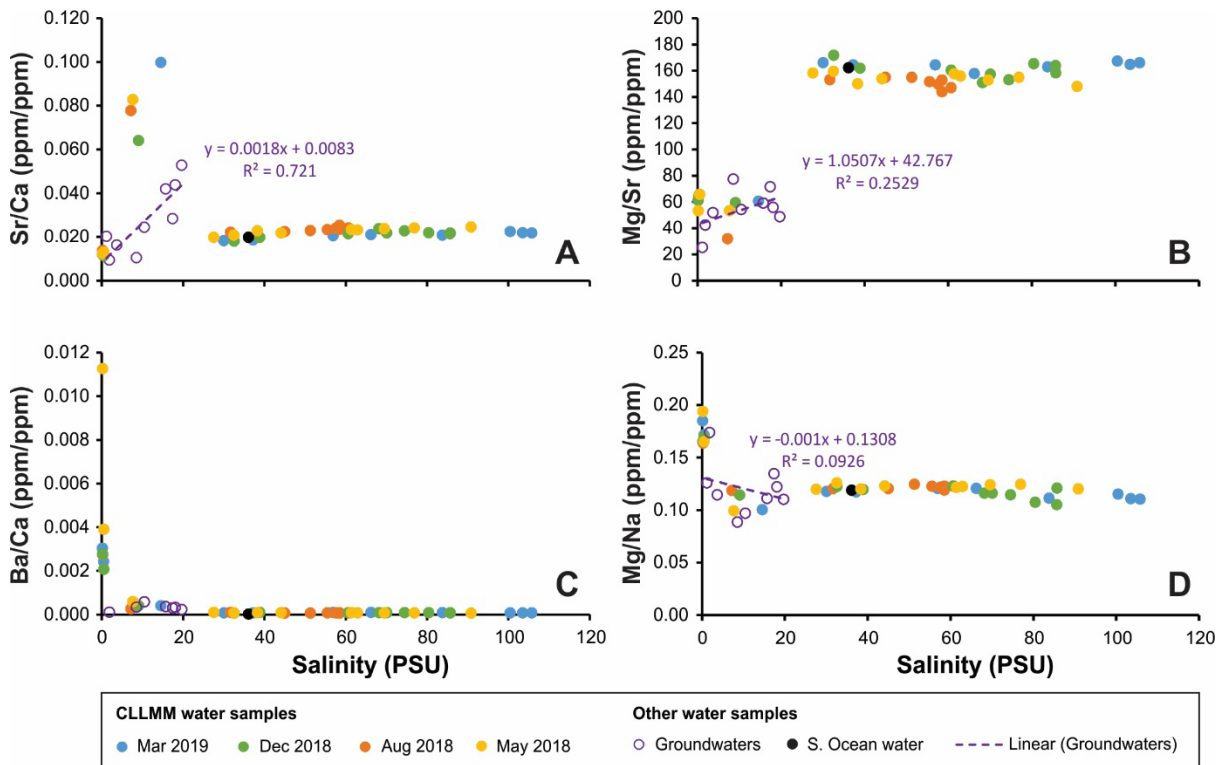


Figure D.2: (A) Sr/Ca (ppm/ppm), (B) Mg/Sr (ppm/ppm), (C) Ba/Ca (ppm/ppm) and (D) Mg/Na (ppm/ppm) of CLLMM water samples vs. salinity (PSU).

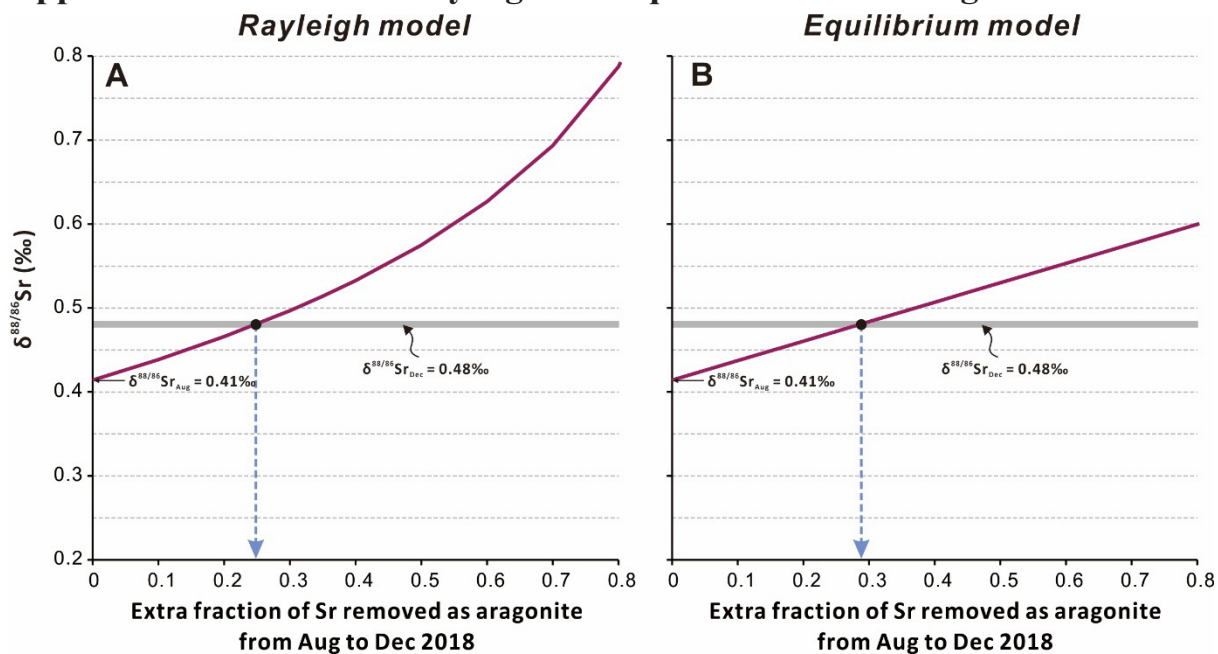
Appendix E. $\delta^{88/86}\text{Sr}$ and Rayleigh and equilibrium modelling

Figure E.1: Plots showing modelled $\delta^{88/86}\text{Sr}$ trends in the site #7 waters as a function of Sr fraction removed from the lagoon waters as aragonite from August to December 2018. (A) The Rayleigh model; (B) the equilibrium model.

References

- Dickson, A. G. (1990) Standard potential of the reaction: $\text{AgCl (s)} + 1/2\text{H}_2 \text{(g)} = \text{Ag (s)} + \text{HCl (aq)}$, and the standard acidity constant of the ion HSO_4^- in synthetic sea water from 273.15 to 318.15 K. *The Journal of Chemical Thermodynamics* **22**, 113-127.
- Gibbs, M., Joehnk, K., Webster, I., and Heneker, T. (2018) Hydrology and Hydrodynamics of the Lower Lakes, Coorong and Murray Mouth. In *Natural history of the Coorong, Lower Lakes, and Murray Mouth region (Yarluwar-Ruwe)* (eds. L. M. Mosley, Q. Ye, S. Shepherd, S. Hemming, and R. Fitzpatrick) University of Adelaide Press on behalf of the Royal Society of South Australia, Adelaide. pp. 197-216.
- Lewis, E. and Wallace, D. (1998) *Program developed for CO₂ system calculations* (No. ORNL/CDI-AC-105). Brookhaven National Lab., Dept. of Applied Science, Upton, NY (United States); Oak Ridge National Lab., Carbon Dioxide Information Analysis Center, TN (United States).
- Mosley, L.M. (2016) Barrage release optimisation trial August 2015; assessment of environmental outcomes and achievement of management objectives. Report to SA Water. University of Adelaide, 23rd March, 2016.
- Mosley, L.M., Hamilton, B., Busch, B., Hipsey, M. and Taylor, B. (2017) Assessment and modelling of the effects of the 2013-2016 Morella Basin releases on Coorong water quality. Report to the Department of Environment, Water and Natural Resources (DEWNR). University of Adelaide, South Australia.
- Mosley L.M., Priestley S., Brookes J., Dittmann S., Farkaš J., Farrell M., Ferguson A.J., Gibbs M., Hipsey M., Huang J., Lam-Gordillo O., Simpson S.L., Teasdale P.R., Tyler J.J., Waycott M., Welsh D.T. (2020) Coorong water quality synthesis with a focus on the drivers of eutrophication. Goyder Institute for Water Research Technical Report Series No. 20/10, Adelaide, South Australia. ISSN: 1839-2725.
- Summerhayes, C. P. and Thorpe, S. A. (1996). Oceanography: an illustrated guide. *Oceanographic Literature Review* **10**, 1068.

Appendix 5

**Appendices for Chapter 5 - Reconstructing
palaeo-hydrology and salinity of the Coorong
lagoon in South Australia based on multi-
tracer analyses ($^{87}\text{Sr}/^{86}\text{Sr}$, $\delta^{88/86}\text{Sr}$ and Mg/Sr)
of fossil carbonate shells**

Appendix A. Sampling site information

A.1 Modern samples and sediment cores

Table A.1. Table of field measurements and locations of paired modern Coorong water and shell samples, including GPS coordinates, water temperature, salinity and sampling dates.

Sample ID	Labelled number on Fig. 2	Collected by	Location	Sampling Dates (dd/mm/yy)	Temperature (°C)	Water salinity (PSU)	Latitude (degree South)	Longitude (degree East)
BB0151	1	Chamber-layne, B.	Near Pelican Point	03/05/18	15.7	23.97	35.598	139.027
COOR-50	2	Woolston, Z.	Near Pelican Point	13/03/20	19.9	31.50	35.598	139.024
BB0122	3	Chamber-layne, B.	Mark Point	18/01/18	33.2	14.49	35.630	139.080
BB0149	4	Chamber-layne, B.	Between Mark Pt and Mulbin Yerrok	03/05/18	15.6	32.58	35.646	139.101

Table A.2. Sampling information of sediment cores C18 and CSC.

Sediment core ID	Collected by	Location	Sampling time	Latitude (degree South)	Longitude (degree East)
C18	Haynes, D.	5 km southeast of Parn-ka Point	March 2005	35.933	139.443
CSC	Foster, N.	Near Salt Creek	June 2019	36.119	139.638

Appendix B. Supplementary results

B.1 Elemental concentrations

Table B.1. Concentrations of major elements of water samples collected in 2018 in ppm (mg/L). For sampling site information see Table A.1. The typical uncertainty of measurements for this study was $\pm 5\%$ (2SD). Data from Chamberlayne et al. (2021, in review)

ID	Mg	Ca	Sr	Ba
2018 water samples				
122w	572.10	205.37	4.53	0.074
149w	1095.11	365.52	8.14	0.036
151w	774.83	303.87	5.77	0.044
Standards and certified values				
IAPSO measured	1160.61	349.85	7.94	0.072
$\pm 2\text{se}$ (n = 2)	17.55	8.74	0.03	0.002
IAPSO published (Summerhayes, and Thorpe, 1996)	1290	412	7.90	0.014
\pm	#	#	#	0.004-0.020

#Variations are determined entirely or largely by those in salinity (Summerhayes and Thorpe, 1996).

Table B.2. Concentrations of major and trace elements in water and shell samples collected in 2020 and fossil shell samples from core CSC in ppm (mg/L). For sampling site information see Table A.1. The typical uncertainty of measurements for this study was $\pm 5\%$ (2SD). Data from Woolston (2020).

ID/Depths (cm) from top of core	Mg	Sr
2020 water sample		
COOR-50	1208.95	7.16
2020 shell sample		
COOR-50s*	282.71	2564.45
Fossil shell samples from core CSC		
2.5-3.5	447.40	4317.51
5.5-6.5	202.90	2963.00
9.5-10.5	508.70	6270.40
13.5-14.5	283.10	4147.20
17.5-18.5	282.00	4782.40
24.5-25.5	230.30	3371.50
29.5-30.5	293.07	4331.18
39.5-40.5	318.50	4364.70
49.5-50.5	334.30	4801.80

 Appendix 5

54.5-55.5	421.10	4908.30
64.5-65.5	344.50	4491.10
69.5-70.5	188.50	2448.20
79-80	228.35	2402.40
Standards and certified values		
JLs-1 measured	3710.01	309.39
JLs-1 published (Geological Survey of Japan)	3720	295
IAPSO measured	1381.44	8.33
± 2se (n = 2)	69.59	0.66
IAPSO published (Summerhayes, and Thorpe, 1996)	1290	7.90
±	#	#

*Results were average measurements of two times analyses from Woolston (2020).

#Variations are determined entirely or largely by those in salinity (Summerhayes and Thorpe, 1996).

Table B.3. Concentrations of major and trace elements in 2018 modern shell samples and fossil shell samples from core C18 in ppm (mg/L). For sampling site information see Table A.1. The typical uncertainty of measurements for this study was $\pm 5\%$ (2SD).

ID/Depths (cm) from top of core	Mg	Al	P	K	Ca	Cr	Mn	Fe	Co	Ni	Zn	Sr	Cd	Ba
Modern shell samples														
122s	144.24	2.09	13.60	18.17	270011.25	0.079	10.95	13.44	0.043	1.78	1.37	1238.61	0.0020	11.25
149s	201.66	1.40	28.21	24.47	395291.92	0.045	12.33	23.30	0.064	1.95	0.34	1797.33	0.0000	12.87
151s	171.69	0.91	22.85	22.85	393066.11	0.049	22.34	10.90	0.058	1.81	0.84	1661.68	0.0000	17.21
Fossil shell samples from core C18														
4-5	188.28	56.39	89.29	59.69	345419.16		19.01					2455.39	0.0106	14.87
5-6	170.08	6.10	63.80	41.27	386338.23		20.91	21.32	0.054	0.82		3838.40	0.0000	23.78
6-7	166.63	17.06	28.70	65.36	384524.94		6.86	13.81				2316.39	0.0000	9.83
7-8	150.26	3.90	28.14	67.19	373207.89		8.11	16.24	0.067	1.12		2336.56	0.0077	11.99
8-9	143.98	1.55	28.73	45.48	403185.12		12.86		0.038	0.51		2635.67	0.0010	16.26
10-11	142.98	2.65	28.65	31.02	367670.80	0.026	11.08	6.47	0.053	1.65		2958.10	0.0000	20.92
11-12	125.95	1.66	25.29	25.44	334297.19	0.033	13.48	8.52	0.044	0.63	0.36	2787.63	0.0022	20.24
12-13	136.57	1.91	30.94	36.36	379355.31		11.63	8.26	0.044	0.55		2782.99	0.0000	20.21
13-14	94.72	0.52	25.98	24.31	287443.53	0.028	12.08	8.34	0.053	1.04		2466.00	0.0011	16.06
14-15	135.35	3.06	29.53	44.52	381465.10		16.20	9.92	0.043	0.68		2644.24	0.0000	18.53
15-16	125.30	0.52	31.67	30.73	335427.11	0.039	13.05	7.72	0.042	0.91		2699.72	0.0006	18.93
16-17	142.31	3.95	32.65	47.93	377104.57	0.051	12.80	10.44	0.049	0.65	0.93	2875.67	0.0011	20.96
17-18	148.48	7.35	29.17	40.21	375423.19		9.75	6.15	0.038	0.62		2675.86	0.0011	17.68
20-21	161.91	2.50	27.19	45.61	387745.85		6.99	5.98	0.043	0.64	1.86	2744.97	0.0000	19.33
21-22	125.09	0.37	21.93	32.56	298842.10		5.33	2.95	0.036	0.44		2160.13	0.0000	16.24
23-24	128.23	1.05	27.73	33.86	366111.91		13.03	4.81	0.045	0.67		2952.39	0.0011	23.00
24-25	95.89	1.22	24.54	22.18	287247.63		10.99	3.84	0.048	0.47		2294.30	0.0011	16.33
25-26	104.91	0.93	28.19	29.08	261112.33		9.75	4.99	0.045	0.52		1939.03	0.0000	12.97
26-27	137.62	218.05	38.74	46.14	397157.69	0.068	18.78	27.67	0.068	0.78		2915.94	0.0000	19.58
27-28	106.70	3.08	31.06	34.60	289324.72	0.029	13.39	8.70	0.046	0.68	0.76	2266.97	0.0000	14.75

28-29	95.99	0.26	27.38	29.53	282351.11	0.027	10.90	7.65	0.036	0.45		2028.38	0.0017	13.33
31-32	127.91	1.97	41.67	37.28	382548.89	0.049	18.29	12.02	0.065	1.00	2.26	2730.45	0.0000	16.89
32-33	154.34	0.46	36.56	28.66	365888.68	0.031	18.15	7.84	0.065	0.75		2844.38	0.0006	18.27
36-37	138.74	1.54	33.79	35.71	380878.11	0.046	19.19	13.86	0.076	0.81	0.91	2628.16	0.0000	18.77
37-38	125.89	0.42	37.76	31.67	345558.55	0.035	16.20	6.50	0.051	0.63		2691.07	0.0022	19.19
38-39	134.71	1.08	37.25	44.40	375055.86	0.047	19.29	6.65	0.055	0.82		2646.86	0.0000	18.24
41-42	168.62	19.36	38.05	39.72	395410.16	0.057	14.46	7.46	0.055	0.77	3.32	2780.90	0.0011	18.88
42-43	132.40		22.73	26.06	284563.04		13.43	2.56	0.036	0.42		2053.16	0.0000	14.33
43-44	168.01	1.76	31.65	43.12	392763.17		16.33	4.98	0.055	0.68		2613.62	0.0054	16.25
45-46	166.32	1.87	31.04	32.56	376797.85	0.024	18.31	4.47	0.051	0.55		2874.05	0.0011	18.67
46-47	178.78	2.33	32.02	36.83	414864.67	0.028	12.11	6.02	0.054	0.92	0.44	2944.53	0.0013	18.57
47-48	115.38	5.73	19.94	31.40	263445.54	0.033	5.39	3.58	0.032	0.74	1.98	1927.45	0.0028	12.55
48-49	134.50	10.07	25.38	27.27	257238.56	0.052	10.48		0.039	0.45	1.44	2182.02	0.0011	14.61
49-50	187.52	8.61	36.79	36.38	400993.85	0.068	13.52	7.49	0.058	0.88	1.76	3108.94	0.0000	20.91
50-51	167.46	4.53	37.19	38.90	398944.74	0.050	10.28	10.23	0.044	0.74		2700.97	0.0011	16.92
52-53	160.06	2.03	42.80	31.78	390324.62	0.069	10.13	11.89	0.067	0.85		2685.63	0.0022	16.19
55-56	152.95	3.70	52.41	34.10	380555.86	0.072	16.06	14.63	0.066	0.95		2966.49	0.0000	18.89
56-57	146.41	2.68	55.56	37.37	414339.94	0.068	11.53	11.48	0.066	1.08	1.33	2721.95	0.0011	17.35
57-58	183.56	4.72	60.12	36.76	437930.11	0.080	15.37	32.10	0.072	1.91	1.78	2925.14	0.0028	18.35
59-60	178.25	3.11	50.31	33.81	399513.01	0.068	20.63	15.43	0.054	0.74		3155.22	0.0011	19.50
61-62	176.82	1.17	53.42	35.60	397463.16	0.057	14.44	7.76	0.055	0.77		2834.15	0.0000	18.57
62-63	169.22	1.51	54.55	40.94	396297.41	0.106	11.82	9.23	0.061	0.96	4.14	2853.75	0.0034	18.33
64-65	173.05	1.53	56.10	41.90	396972.37	0.051	11.86	5.14	0.050	0.74	2.25	2702.34	0.0011	17.32
65-66	170.99	1.29	57.40	34.82	397083.93	0.063	12.34	10.27	0.062	0.79		2888.94	0.0000	19.24
66-67	159.48	1.04	49.13	37.42	381778.55	0.060	12.64	4.47	0.053	0.74		2894.66	0.0000	18.95
69-70	140.81	1.22	59.28	32.68	416295.71	0.073	13.38	10.96	0.089	1.08		2505.35	0.0022	15.21
70-71	115.00	0.53	46.72	21.96	300565.82	0.052	12.85	9.47	0.057	0.62		2253.90	0.0023	14.74
71-72	134.93	0.54	60.55	28.06	378196.07	0.044	15.48	23.43	0.083	0.84		2641.29	0.0006	17.86
73-74	138.10	2.59	80.50	29.97	409304.56	0.065	13.03	33.43	0.085	1.18		2637.81	0.0006	16.76
74-75	126.47	1.85	48.41	22.32	300523.72	0.046	8.25	10.78	0.069	1.13		2057.36	0.0006	13.57

75-76	127.80	0.50	53.73	24.41	319216.38	0.036	16.98	4.87	0.068	0.62		2320.60	0.0011	14.73
77-78	185.97	2.22	68.99	24.02	375603.18	0.039	24.43	7.05	0.069	0.66		3287.43	0.0000	21.81
78-79	186.56	2.07	69.83	31.23	395352.64	0.079	25.49	11.55	0.066	0.92		3253.71	0.0011	21.40
82-83	133.81	1.60	62.87	25.10	308767.15	0.038	9.95	4.85	0.060	0.60		2275.71	0.0017	15.63
84-85	170.82	0.84	68.55	24.58	375632.38	0.053	19.98	5.51	0.074	0.75		2726.24	0.0000	19.21
86-87	141.43	1.21	57.13	27.41	322692.64	0.057	13.42	4.66	0.049	0.89		2126.89	0.0000	15.84
89-90	165.62	4.06	81.63	31.79	414016.93	0.068	13.22	4.92	0.065	0.84		2518.98	0.0000	21.05
92-93	165.24	2.65	75.91	28.79	412334.03	0.109	23.34	8.86	0.092	0.85	0.82	2891.62	0.0011	20.80
94-95	186.04	1.55	75.01	30.35	417699.64	0.104	13.14	7.28	0.096	0.94		2824.52	0.0011	21.54
97-98	153.57	0.81	72.05	23.17	367186.88	0.060	22.10	5.18	0.071	0.71	0.58	2504.63	0.0006	16.80
98-99	178.17	1.24	80.54	30.85	446277.45	0.075	16.00	6.68	0.086	0.85		2692.27	0.0011	17.05
99-100	148.11	1.02	89.80	24.25	407071.18	0.055	13.77	3.66	0.069	0.76		2490.89	0.0012	15.96
103-104	178.38	19.71	116.38	43.64	409298.45	0.278	6.58		0.092	1.53	7.24	2429.61	0.0113	14.88
105-106	230.18	18.02	120.84	97.82	431370.85	0.495	4.95					2356.57	0.0112	12.70
107-108	189.39	4.90	91.86	32.84	432808.65	0.094	12.34	8.56	0.073	1.07	1.65	2527.89	0.0038	16.87
111-112	191.25	1.11	82.90	26.65	420476.04	0.067	15.39	4.87	0.075	1.06		2688.47	0.0000	18.81
112-113	180.28	7.59	80.00	25.35	432891.64	0.132	14.40	11.10	0.093	1.27		2732.01	0.0012	18.29
113-114	192.47	1.88	86.26	27.35	438330.76	0.101	17.73	8.92	0.092	1.11		2766.01	0.0023	18.75
116-117	182.03	5.71	85.52	25.63	415553.01	0.108	16.73	9.92	0.096	1.02		2554.60	0.0012	18.70
117-118	159.67	2.26	78.29	27.42	430615.65	0.186	14.34	12.16	0.134	1.45	3.01	2383.19	0.0000	16.54
123-124	154.71	13.96	106.02	30.04	464341.47	0.123	9.84	5.45	0.077	1.35		2169.67	0.0000	11.82
127-128	187.65	8.33	88.14	26.64	425986.60	0.141	12.77	21.28	0.105	1.13	1.24	2522.26	0.0038	15.30
129-130	177.65	1.19	106.62	30.78	430685.28	0.068	12.19	11.74	0.091	0.87		2277.98	0.0012	13.99
Standards and certified values														
JCp-1 measured	1167.14	131.24		184.05	390245.49	1.80			0.53			6760.31	0.10	10.61
JCp-1 published (Geological Survey of Japan)	972.00		4.10	185.00			1.00	29				7240.00		10.30

*Results were average measurements of two times analyses from Woolston (2020).

±	8.00		0.90	8.00			0.10	2.00					70.00			0.50
---	------	--	------	------	--	--	------	------	--	--	--	--	-------	--	--	------

B.2 Chronological age data and model

Table B.4. Results of ^{14}C and pollen dating on sediment cores. Note that all ages below are shown as years BP (Before Present, 0 yr BP = 1950 AD, Hughen et al., 2004), offset applied age is the age after reservoir effect correction, and calibrated years BP (cal. yr BP) is the final age after Bacon modelling.

Lab ID	Collected and prepared by	Notes	Conventional ^{14}C age	Offset applied age	1 σ error	Depth (cm)	Modelled age (cal. yr BP)
Core C18							
surface			-55	-55	1	0	-55
OZZ021	Shao, Y.	<i>A. helmsi</i> shell sample.	1030	214	30	5.5	-10
OZS803	Chamberlayne, B.	<i>A. helmsi</i> shell sample. Outlier. Not included in calibration	1720	904	25	9.5	33
OZZ022	Shao, Y.	<i>A. helmsi</i> shell sample.	985	169	30	10.5	45
OZZ023	Shao, Y.	<i>A. helmsi</i> shell sample.	985	169	30	16.5	117.5
OZS804	Chamberlayne, B.	<i>A. helmsi</i> shell sample.	985	169	25	20.5	167.5
W k - 24750	Haynes, D.	<i>A. helmsi</i> shell sample. Outlier. Not included in calibration	1584	768	30	30.5	302.5
OZZ024	Shao, Y.	<i>A. helmsi</i> shell sample. Outlier. Not included in calibration	1575	759	35	30.5	302.5
OZS805	Chamberlayne, B.	<i>A. helmsi</i> shell sample.	1320	504	25	45.5	506
OZZ025	Shao, Y.	<i>A. helmsi</i> shell sample.	1505	689	30	55.5	612.5
OZS806	Chamberlayne, B.	<i>A. helmsi</i> shell sample.	1665	849	20	65.5	726
W k - 24751	Haynes, D.	<i>A. helmsi</i> shell sample.	1987	1171	30	82.5	1056.5
OZZ026	Shao, Y.	<i>A. helmsi</i> shell sample.	2235	1419	35	89.5	1262
OZS807	Chamberlayne, B.	<i>A. helmsi</i> shell sample.	2420	1604	25	95.5	1384
OZZ027	Shao, Y.	<i>A. helmsi</i> shell sample.	2365	1549	30	106.5	1494

OZS808	Chamberlayne, B.	<i>A. helmsi</i> shell sample.	2630	1814	25	115.5	1617.5
OZZ026	Shao, Y.	<i>A. helmsi</i> shell sample.	2565	1749	35	122.5	1679
W k - 24752	Haynes, D.	<i>A. helmsi</i> shell sample.	2638	1822	30	129.5	1755
	Haynes, D.	<i>Pinus radiata</i> pollen maximum depth. Not included in calibration. For comparison only	-5	-5		9.5	-5
Core CSC							
surface			-69	-69	1	0	-69
OZY612	Foster, N.	Carbonate from ground sediment	3275	2459	25	80	2407

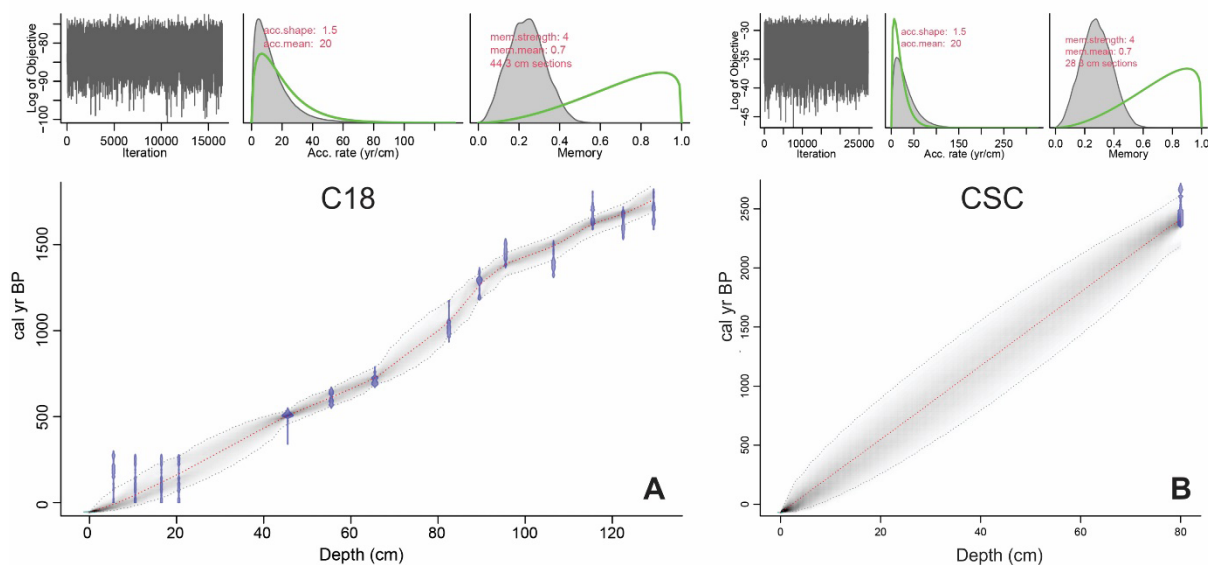


Figure B.1: Chronostratigraphic diagrams of cores (A) C18 (developed by Chamberlayne, 2021, thesis in prep) and (B) CSC. Age-depth models were developed after reservoir effect correction.

B.3 Results of Sr isotope ratios ($^{87}\text{Sr}/^{86}\text{Sr}$ and $\delta^{88/86}\text{Sr}$) of all water and shell samples

Table B.5. Radiogenic and stable Sr isotope composition ($^{87}\text{Sr}/^{86}\text{Sr}$ and $\delta^{88/86}\text{Sr}$) of the modern water and shell samples, with associated sampling location/area and water salinity. Note that 2SEM is the internal precision of a single analysis of the sample through 200 cycles for $\delta^{88/86}\text{Sr}$, and 100 cycles for

$^{87}\text{Sr}/^{86}\text{Sr}$.

ID	Labelled number on Fig. 2	Water salinity (PSU)	$^{87}\text{Sr}/^{86}\text{Sr}$	2SEM	$\delta^{88/86}\text{Sr}$ (‰ _{SRM987})	2SEM
Modern water samples						
122w	3	14.49	0.709322	0.000004	0.315	0.012
149w	4	32.58	0.709171	0.000004	0.319	0.012
151w	1	23.97	0.709221	0.000004	0.373	0.012
COOR-50	2	31.50	0.709196	0.000003	0.355	0.013
Modern shell samples						
122s	3		0.709346	0.000004	0.222	0.012
149s	4		0.709297	0.000004	0.224	0.012
151s	1		0.709307	0.000004	0.285	0.012
COOR-50s*	2		0.709232	0.000003	0.234	0.014

*The result of this sample was the average of two measurements from Woolston (2020), where 2SEM (n = 2) for $^{87}\text{Sr}/^{86}\text{Sr}$ and $\delta^{88/86}\text{Sr}$ were 0.000003 and 0.047‰.

Table B.6. Radiogenic and stable Sr isotope composition ($^{87}\text{Sr}/^{86}\text{Sr}$ and $\delta^{88/86}\text{Sr}$) of the fossil shell samples and calculated $\delta^{88/86}\text{Sr}$ of water of their living time based on $\Delta^{88/86}\text{Sr}$ ($\delta^{88/86}\text{Sr}_{\text{carb}} - \delta^{88/86}\text{Sr}_{\text{water}}$) = -0.104‰ (Fig. 3). Note that 2SEM is the internal precision of a single analysis of the sample through 200 cycles for $\delta^{88/86}\text{Sr}$, and 100 cycles for $^{87}\text{Sr}/^{86}\text{Sr}$, unless elsewhere indicated.

Depths (cm) from top of core	$^{87}\text{Sr}/^{86}\text{Sr}$ shell and water	2SEM	$\delta^{88/86}\text{Sr}$ (‰ _{SRM987}) shell	2SEM	Calculated $\delta^{88/86}\text{Sr}$ (‰ _{SRM987}) of water
Fossil shell samples from core C18					
4-5	0.709234	0.000003	0.290	0.013	0.394
5-6	0.709246	0.000004	0.266	0.013	0.369
7-8	0.709242	0.000003	0.317	0.014	0.420
11-12	0.709249	0.000004	0.279	0.016	0.383
16-17	0.709244	0.000004	0.309	0.012	0.413
23-24	0.709239	0.000004	0.261	0.011	0.365
31-32	0.709230	0.000004	0.272	0.012	0.376
37-38	0.709238	0.000005	0.292	0.012	0.395
46-47	0.709250	0.000004	0.299	0.012	0.402
56-57	0.709248	0.000003	0.258	0.012	0.362
61-62	0.709239	0.000004	0.275	0.011	0.379
69-70	0.709227	0.000004	0.261	0.013	0.365
77-78	0.709237	0.000003	0.301	0.013	0.405
84-85	0.709260	0.000004	0.233	0.013	0.337
89-90	0.709246	0.000004	0.266	0.012	0.370
99-100	0.709220	0.000004	0.247	0.012	0.351

111-112	0.709230	0.000004	0.298	0.013	0.402
117-118	0.709236	0.000004	0.233	0.011	0.337
123-124	0.709229	0.000004	0.256	0.013	0.360
129-130	0.709219	0.000004	0.258	0.012	0.362
Fossil shell samples from core CSC					
2.5-3.5	0.709243	0.000003	0.285	0.012	0.389
5.5-6.5	0.709259	0.000003	0.225	0.014	0.329
9.5-10.5	0.709253	0.000003	0.304	0.012	0.408
13.5-14.5	0.709251	0.000003	0.290	0.016	0.394
17.5-18.5	0.709255	0.000003	0.300	0.011	0.404
24.5-25.5	0.709248	0.000003	0.284	0.020	0.388
29.5-30.5	0.709259	0.000002	0.244	0.014	0.348
39.5-40.5	0.709249	0.000003	0.248	0.017	0.352
49.5-50.5	0.709255	0.000004	0.279	0.012	0.383
54.5-55.5	0.70925	0.000003	0.282	0.013	0.386
64.5-65.5	0.70924	0.000003	0.324	0.013	0.428
69.5-70.5	0.709249	0.000003	0.326	0.013	0.430
79-80*	0.709250	0.000003	0.281	0.014	0.384

*The result of this sample was average of two measurements from Woolston (2020), where 2SEM (n = 2) for $^{87}\text{Sr}/^{86}\text{Sr}$ and $\delta^{88/86}\text{Sr}$ were 0.0000004 and 0.005‰.

B.4 Distribution coefficients between shell and water samples

Table B.7. Calculated distribution coefficients $D_{\text{Mg/Sr}}$ and $D_{\text{Sr/Ca}}$ between modern shells and water samples (data from Tables B.1 and 2).

Site number on Fig. 2	$D_{\text{Mg/Sr}} = (\text{Mg/Sr}_{\text{shell}}) / (\text{Mg/Sr}_{\text{water}})$	$D_{\text{Sr/Ca}} = (\text{Sr/Ca}_{\text{shell}}) / (\text{Sr/Ca}_{\text{water}})$
3	0.00092	0.208
4	0.00083	0.204
1	0.00077	0.223
2	0.00065	N/A
Average	0.00079	0.212
2sd	0.00022 (n = 4)	0.019 (n = 3)

Appendix C. Supporting evidence of palaeo-hydrology of the South Lagoon

C.1. Elemental concentrations

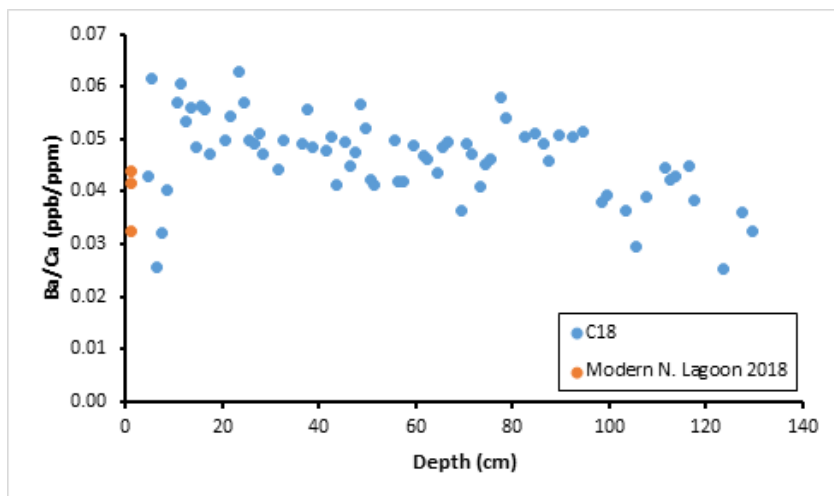


Figure C.1: Ba/Ca ratios in modern shells collected in 2018 ($n = 3$) and shell samples from core C18 vs. core depth (cm). The surface is a depth of 0 cm.

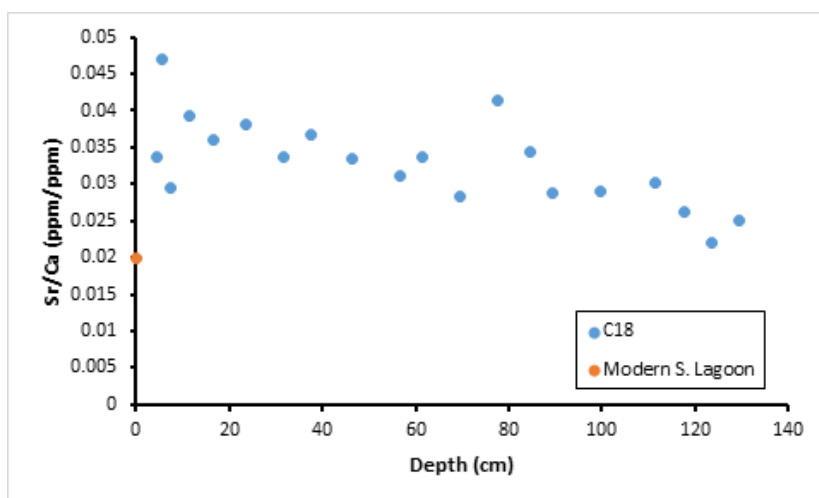


Figure C.2: Sr/Ca ratios in palaeo-South Lagoon water calculated from shell samples from core C18 vs. core depth using $D_{Sr/Ca} = 0.212$ (Table B.8, Appendix B.4), as well as Sr/Ca modern South Lagoon water (Chapter 4).

Appendix D. Details of ^{14}C dating and pollen age

D.1 Pollen age

For core C18, the presence of *Pinus radiata* pollen was found from the surface to a maximum depth of 9.5 cm. The first appearance of pollen of *Pinus radiata*, an exotic species introduced by Europeans, in a core can be used as an approximate marker for year 1955 AD (Gell and Haynes 2005; Krull et al. 2009). This is based on calibration with radionuclide data (^{210}Pb -derived age) of *Pinus* pollen from other cores from the Coorong (Krull et al., 2009).

D.2 ^{14}C dating

^{14}C dating of shell samples ($n = 17$) from the core C18 was performed in three separate analyses spanning multiple years. In 2009, shell samples from 3 sediment fractions (collected by Haynes, Table XXX) were analysed for ^{14}C dating using Accelerator Mass Spectrometry (AMS) at the Waikato Dating Laboratory in New Zealand. The *A. helmsi* shells were cleaned with deionised water and dried in an oven at 40°C. The shells were etched in HCl on the surfaces and pulverised into powder before analyses. ^{14}C ages were calibrated utilising OxCal v.4.0.5 (Bronk Ramsey, 2007), and using the marine curve Marine04 (Hughen et al., 2004) incorporating a ΔR of 84 ± 57 years. This correction was determined from three sites (map number: 382, 390 and 391) (14CHRONO marine reservoir database), which were chosen based on geographical proximity to the study region and the incorporation of the least overall error.

In 2015, additional shell samples from 6 more sediment fractions throughout the core were analysed for ^{14}C dating at the Australian Nuclear Science and Technology Organisation (ANSTO) using the STAR accelerator following the methods described in Chamberlayne (2015). In 2020, 8 more additional shell samples were analysed for ^{14}C dating at ANSTO using the ANTARES AMS facility (Fink et al., 2004). The cleaned shell samples were dissolved in 2 mL 85% H_3PO_4 and heated at 60°C overnight to evolve CO_2 , which was then converted to graphite using the H_2/Fe method (Hua et al., 2001). AMS ^{14}C measurements on the graphite targets were carried out using the Vega 1MV accelerator at ANSTO (Wilcken et al., 2015), with a typical precision of 0.30–0.40%. ^{14}C measurements were normalised to NBS Oxalic acid I (HOxI) as primary standard and NIST SRM 4990 C (HOxII) as secondary standard (Mann 1983). Raw measurement results were corrected for possible contamination during processing using blank IAEA C1 marble (Rozanski et al. 1990), and assessed for machine background using spectroscopic-grade powdered graphite from Union Carbide Co. Stable carbon isotopic ratios were measured on the graphite targets using an EA-IRMS and the $\delta^{13}\text{C}$ used to correct the measured $^{14}\text{C}/^{13}\text{C}$ values to determine the radiocarbon age. All results are reported as percent modern carbon (pMC) and as conventional radiocarbon ages (yr BP) following the conventions of Stuiver and

Polach (1977).

The sediment core CSC was ^{14}C dated at the Australian Nuclear Science and Technology Organisation (ANSTO, Lucas Heights, Sydney) at each horizon. ~1g of ground sediment was acidified using 2M HCl to remove inorganic carbon then centrifuged at 3,400 rpm for 5 min. The supernatant was then removed, and 2M NaOH was added to the residual pellet and placed in a water bath at 60°C for 1 hr. This was repeated until the supernatant was clear, upon which, 2M HCL was added to remove left over contaminant carbon. Samples were then dried and weighed, and carbon dioxide was isolated via combustion and converted into graphite. This graphite was then analysed using Accelerator Mass Spectrometry (AMS) to measure the amount of ^{14}C present. Unfortunately, due to the high carbonate content at this site, much of the carbon was removed during the acidification step, leaving minimal carbon to complete dating at all horizons. This resulted in only one date being recorded for the whole core which was at ~80cm, yielding an age of 3275 ± 25 yrs BP.

D.3 Bacon age model code in R program

The results of ^{14}C analyses (i.e., conventional ^{14}C ages) and a pollen date were used to derive the age models in “Bacon” – an approach to age-depth modelling that uses Bayesian statistics to reconstruct accumulation histories for deposits, through combining radiocarbon and other dates (Blaauw and Christen, 2011). The R programming code for the Bacon models prepared by Chamberlayne (2021, thesis in prep) is shown below:

```
install.packages('rbacon')
```

```
require(rbacon)
```

```
Bacon("filename", thick=3, d.lab='Depth (cm)',yr.lab='Age (cal yr BP)', d.by = 1,cc = 3, ssize = 8000)
```

References

Blaauw, M. and Christen, J. A. (2011) Flexible paleoclimate age-depth models using an autoregressive gamma process. *Bayesian Analysis* **6**, 457-474.

Chamberlayne, B. K. (2015) *Late Holocene seasonal and multicentennial hydroclimate variability in the Coorong Lagoon, South Australia: evidence from stable isotopes and trace element profiles of bivalve molluscs*. (Honours (Geology)), The University of Adelaide, Adelaide.

Chamberlayne, B.K. (2021). *Oxygen isotope and elemental ratios in waters and bivalves as tracers of hydrological change in modern and ancient waters of the Coorong Lagoons, South Australia* (Unpublished PhD thesis). University of Adelaide, Adelaide.

Chamberlayne, B. K., Tyler, J. J., Gillanders, B. M. (2021) Elemental concentrations of waters and bivalves across a salinity gradient in the Coorong Lagoons, South Australia: Implications for palaeo-environmental studies. *Estuarine, Coastal and Shelf Science*, in review.

Fink, D., Hotchkis, M., Hua, Q., Jacobsen, G., Smith, A. M., Zoppi, U., Child, D., Mifsud, C., van der Gaast, H., Williams, A. and Williams, M. (2004) The ANTARES AMS facility at ANSTO, *Nuclear Instruments and Methods in Physics Research Section B: Beam Interactions with Materials and Atoms* **223-224**, 109-115.

Gell, P. and Haynes, D. (2005) A palaeoecological assessment of water quality change in the Coorong, South Australia. *A report for the Department of Water, Land and Biodiversity Conservation SA*. The University of Adelaide, Adelaide.

Hua Q, Jacobsen G.E, Zoppi U, Lawson E.M, Williams A.A., McGann M.J. 2001. Progress in radiocarbon target preparation at the ANTARES AMS Centre. *Radiocarbon* 432A: 275–82.

Hughen, K. A., Baillie, M. G., Bard, E., Beck, J. W., Bertrand, C. J., Blackwell, P. G., Buck, C. E., Burr, G. S., Cutler, K. B., Damon, P. E., Edwards, R. L., Fairbanks, R. G., Michael Friedrich, M., Guilderson, T. P., Kromer, B., McCormac, G., Manning, S., Bronk Ramsey, C., Reimer, P. J., Reimer, R. W., Remmele, S., Southon, J. R., Stuiver, M., Talamo, S., Taylor, F. W., van der Plicht, J., and Weyhenmeyer, C. E. (2004) Marine04 marine radiocarbon age calibration, 0–26 cal kyr BP. *Radiocarbon* **46**, 1059-1086.

Krull, E., Haynes, D., Lamontagne, S., Gell, P., McKirdy, D., Hancock, G., McGowan, J. and Smernik, R. (2009) Changes in the chemistry of sedimentary organic matter within the Coorong over space and time. *Biogeochemistry* **92**, 9-25.

Mann, W. (1983) An International Reference Material for Radiocarbon Dating*. *Radiocarbon* **25**, 519-527.

Rozanski, K., Stichler, W., Gonfiantini, R., Scott, E. M., Beukens, R. P., Kromer, B. and van Der Plicht, J. (1992) The IAEA 14 C intercomparison exercise 1990. *Radiocarbon* **34**, 506-519.

Stuiver, M. and Polach, A. (1977) Reporting of 14C data. *Radiocarbon* **19**, 355-363.

Summerhayes, C. P. and Thorpe, S. A. (1996). Oceanography: an illustrated guide. *Oceanographic Literature Review* **10**, 1068.

Wilcken, K. M., Hotchkis, M., Levchenko, V., Fink, D., Hauser, T. and Kitchen, R. (2015) From carbon to actinides: a new universal 1MV accelerator mass spectrometer at ANSTO. *Nuclear Instruments and Methods in Physics Research Section B: Beam Interactions with Materials and Atoms* **361**, 133-138.

Woolston, Z. (2020) *A coupled radiogenic ($^{87}\text{Sr}/^{86}\text{Sr}$) and stable ($\delta^{88/86}\text{Sr}$) strontium isotope approach to reconstruct past changes in water mixing and salinity in the Coorong Lagoon, South Australia.* (Honours (Environmental Geoscience)), The University of Adelaide, Adelaide.

Appendix 6

Representative conference abstracts

Goldschmidt 2017, Paris, France. Form: Poster

Calibration of marine Ca and Sr isotope proxies against ‘salinity’ in fresh-to-hypersaline coastal lagoon-estuarine settings of South Australia

Y. Shao^{1,*}, J. Farkaš^{1,2}, C. Holmden³, L. Mosley¹, I. Kell-Duivesteyn^{1,4}, C. Izzo¹, P. Reis-Santos¹, J. Tyler¹, D. Haynes¹, J. Tibby¹, And B. Gillanders¹

*Email (corresponding author): mandy9425@qq.com

¹University of Adelaide, Australia

²Czech University of Life Sciences, Czech Republic

³University of Saskatchewan, Canada

⁴Graz University of Technology, Austria

Abstract

The application of marine Ca and Sr isotope proxies for paleo-seawater studies requires their precise calibration in modern coastal and marine environments. Here we investigate the variability of $\delta^{44/40}\text{Ca}$ and $^{87}\text{Sr}/^{86}\text{Sr}$ proxies (as a function of *salinity*) in natural waters collected from the lagoon-estuarine environments of the Coorong Lagoon and Murray Mouth (CLMM) hydrological system, in South Australia. The latter represents a unique ‘natural laboratory’ for proxy calibration studies, as the salinity in the CLMM system ranges from *fresh* (~0 psu; near the River Murray Mouth), through *normal marine* (~35 psu; in Coorong North Lagoon), to *hypersaline* (up to ~130 psu; in South Lagoon). Our results confirmed that both $\delta^{44/40}\text{Ca}$ and $^{87}\text{Sr}/^{86}\text{Sr}$ proxies in coastal/lagoon waters are sensitive to *salinity* changes due to (i) seawater-freshwater mixing of isotopically distinct waters, and (ii) the input of local groundwaters into the lagoon. In addition, and unlike the radiogenic $^{87}\text{Sr}/^{86}\text{Sr}$ tracer, the $\delta^{44/40}\text{Ca}$ is also sensitive to local carbonate (CaCO_3) precipitation and deposition in the *hypersaline* South Lagoon, where the lagoon waters are highly oversaturated with respect to CaCO_3 minerals. The degree of mineral saturation (i.e., calcite, aragonite, gypsum) across the Coorong Lagoon was quantified using PHREEQC modelling, and the calculated mineral saturation indices (SI) are evaluated with respect to variations in the $\delta^{44/40}\text{Ca}$ of lagoon waters and their salinities.

Specifically, a progressive seawater evaporation in South Lagoon leads to *hypersalinity* and a local oversaturation with respect to main Ca-bearing minerals (i.e., calcite and aragonite, but not gypsum), which in turn impacts the Ca isotope composition of local waters, as these have systematically higher $\delta^{44/40}\text{Ca}$ signatures (compared to *normal seawater*) due to preferential removal of light Ca into CaCO_3 . A simple Rayleigh modelling approach (and also PHREEQC calculations) suggest that about 40 to 55% of the dissolved Ca^{2+} in the South Lagoon was removed as CaCO_3 , which has also implications

for a better understanding of the local carbon cycling and C burial fluxes within the lagoon.

Australian Geoscience Council Convention 2018, Adelaide, Australia. Form: Oral

Stable and radiogenic strontium isotope systematics in hypersaline coastal environments: constraints for paleo-hydrology in the Coorong, South Australia.

Y. Shao¹, J. Farkaš¹, J. Tyler¹, B. M. Gillanders¹, B. Chamberlyane¹, D. Haynes¹

¹University of Adelaide, Adelaide, SA, Australia

Abstract

Strontium (Sr) isotopes have been widely used in large-scale ecosystem and hydrological studies. Specifically, the $^{87}\text{Sr}/^{86}\text{Sr}$ is commonly used for tracing radiogenic processes such as water source mixing, while the newly employed stable $^{88}\text{Sr}/^{86}\text{Sr}$ (noted as $\delta^{88/86}\text{Sr}$) is sensitive to isotope fractionation processes such as carbonate formation. Combining the two isotope signatures in carbonate sediment archives and ambient water adds potential to reconstruct paleo-hydrology in carbonate-producing coastal environments. Importantly, the stable $^{88}\text{Sr}/^{86}\text{Sr}$ has been applied in recent years in coastal environments with fresh to marine salinity conditions, very few studies were conducted in hypersaline environments.

The Coorong hydrological system, located ~100 km southeast to Adelaide, represents a unique 'natural laboratory' to calibrate novel and traditional isotope tracers in due to its unique geomorphology and large salinity gradient in water bodies ranging from fresh to hypersaline (from ~0 PSU to ~120 PSU). This study aims to assess the radiogenic and stable Sr isotope ratios (i.e., $^{87}\text{Sr}/^{86}\text{Sr}$ and $\delta^{88/86}\text{Sr}$) in the Coorong lagoon waters, inorganic carbonates and bivalve shells *Arthritica helmsi* from sediment cores, and hence explore the potential of these isotope tracers to be used to reconstruct the paleo-hydrology in the Coorong throughout the recent thousands of years.

Goldschmidt 2019, Barcelona, Spain. Form: Oral

Calibration of stable strontium isotopes ($\delta^{88/86}\text{Sr}$) with respect to salinity and carbonate saturation in lagoon-estuarine environments

Y. Shao^{1*}, J. Farkaš^{1,2}, L. Mosley¹, H. Wong³, M. Samanta⁴, J. Tyler¹, C. Holmden⁵, B.M. Gil-

landers¹, A. Kolevica⁶, and A. Eisenhauer⁶

¹University of Adelaide, Adelaide, SA5005, Australia (*correspondence: yuexiao.shao@adelaide.edu.au)

² Czech University of Life Sciences, Prague, Kamýcká 129, 165 00 Praha-Suchdol, Czech Republic

³ANSTO – Sydney, NSW 2234, Australia

⁴Australian National University, Canberra, ACT 2601, Australia

⁵University of Saskatchewan, Saskatoon, S7N 5A2, Canada

⁶GEOMAR, Helmholtz Centre for Ocean Research Kiel, Wischhofstr, 24148 Kiel, Germany

Abstract

The novel stable strontium isotope tracer ($\delta^{88/86}\text{Sr}$) has been used to constrain mass-dependent isotope fractionation processes such as carbonate formation/dissolution, where the latter has implications for climate studies related to local C cycling and CO_2 fluxes and thus “blue carbon” studies [1]. More recently, this tracer has also been applied in coastal environments as a paleo-environmental proxy [2][3]. However, there are no systematic studies using stable Sr isotopes conducted in hypersaline lagoon environments in which higher mass of carbonate production is likely to happen. The Coorong hydrological system in South Australia, located ~100 km southeast to Adelaide, represents a unique ‘natural laboratory’ to calibrate the $\delta^{88/86}\text{Sr}$ tracer to salinity changes across a large salinity gradient of local water bodies ranging from fresh to hypersaline (from ~0 to over 100PSU) [4]. Available results confirmed a systematically increasing trend of $\delta^{88/86}\text{Sr}$ in lagoon waters with increasing salinity and carbonate saturation state, also coupled with changes in water $\delta^{44/40}\text{Ca}$ [4]. Based on these observations, we explore the potential of combined radiogenic and stable Sr isotope tracers (i.e., $^{87}\text{Sr}/^{86}\text{Sr}$ and $\delta^{88/86}\text{Sr}$) to reconstruct the paleo-hydrology and salinity variations in the Coorong lagoon system.

[1] Macreadie *et al.* (2017) *Limnology and Oceanography Letters* **2**, 195–201.

[2] Rüggeberg *et al.* (2008) *Earth and Planetary Science Letters* **269**, 570-575.

[3] Fruchter *et al.* (2017) *Geochimica et Cosmochimica Acta* **215**, 17–32

[4] Shao *et al.* (2018) *Geochimica et cosmochimica acta* **239**, 90-108.

AESC 2021, virtual conference 2021. Form: Oral

Insights into palaeo-hydrology of the Coorong Lagoon, South Australia, based on Strontium Isotope Tracers ($^{87}\text{Sr}/^{86}\text{Sr}$ and $\delta^{88/86}\text{Sr}$) in fossil carbonates

Yuexiao Shao^{1,2}, Zara Woolston¹, Juraj Farkaš^{1,2}, Briony Chamberlayne¹, John Tibby³ Deborah Haynes¹, Jonathan Tyler¹

¹Department of Earth Sciences, School of Physical Sciences, University of Adelaide, Australia

²Metal Isotope Group (MIG), University of Adelaide, Australia

³Department of Geography, Environment and Population, School of Social Sciences, University of Adelaide, Australia

Abstract

The Coorong lagoon, as part of the wetland system at the terminus of the River Murray, is recognised not only for its ecological importance but also for its unique geomorphology and salinity gradient that ranges from fresh/brackish (< 35 PSU) in the North Lagoon to hypersaline (> 70 PSU) in the South Lagoon. The lagoon hydrology is controlled by seawater-continental water mixing processes that are traceable via the radiogenic Strontium (Sr) isotopes ($^{87}\text{Sr}/^{86}\text{Sr}$ ratios). The hypersaline South Lagoon, being more geomorphologically restricted, is known for high degree of evaporation, which leads to ongoing calcium carbonate precipitation, which also acts as a sink for dissolved inorganic carbon (DIC) [1]. These processes involving carbonate formation and a local inorganic carbon cycling are traceable via the novel stable Sr isotope ($\delta^{88/86}\text{Sr}$), which is particularly sensitive to mass-dependent isotope fractionation linked to carbonate precipitation/dissolution. Importantly, the South Lagoon has seen dramatic hydrological and ecological changes over the last ~200 years (since the European settlement), which is evident from geochemical and diatom records of the Coorong sediment cores [2], and has implications for water resource management and future strategies for the recovery of local ecosystem to more natural conditions[3]. In order to reconstruct paleo-hydrology of the Coorong before and after the European settlement, this study calibrated the $\delta^{88/86}\text{Sr}$ fractionation between recent aragonitic bivalve shells (*Arthritica helmsi* species) and local water in the modern Coorong lagoon, and a constant difference of $\delta^{88/86}\text{Sr}$ between the shells and the local water $\Delta^{88/86}\text{Sr}$ ($\delta^{88/86}\text{Sr}_{\text{solid}} - \delta^{88/86}\text{Sr}_{\text{water}}$) = -0.92‰ was discovered. Such calibrations, coupled with $^{87}\text{Sr}/^{86}\text{Sr}$ and $\delta^{88/86}\text{Sr}$ analyses of fossil *A. helmsi* shells from a sediment core in the South Lagoon, are complemented by radiocarbon dating and elemental concentration data, to better constrain (i) variability in the mixing of water sources in modern Coorong and over the last ~2500 years; and (ii) to reconstruct palaeo-salinity changes and associated carbonate precipitation/dissolution processes. Primary results based on $^{87}\text{Sr}/^{86}\text{Sr}$ of shells indicated the source of water in the South Lagoon were never purely marine; however, according to $\delta^{88/86}\text{Sr}$ of the shells, the the South Lagoon in the past ~2500 years was probably less evaporated than it has been in recent times (i.e., post European settlement).

[1] Shao et al (2018), *Geochimica et Cosmochimica Acta* **239**, 90-108.

[2] McKirdy *et al.* (2010) *Organic Geochemistry* **41**, 96-110.

[3] Brookes *et al.* (2018). Goyder Institute for Water Research Technical Report Series No. 18/04, Adelaide, South Australia. ISSN: 1839-2725.